Method Development of Ultra-High-Performance Liquid Chromatography with Tandem Mass Spectrometry for Synthetic Oligonucleotides

Dissertation

der Mathematisch-Naturwissenschaftlichen Fakultät

der Eberhard Karls Universität Tübingen

zur Erlangung des Grades eines

Doktors der Naturwissenschaften

(Dr. rer. nat.)

vorgelegt von

Feiyang Li

aus Shenyang/VR China

Tübingen

2024

Gedruckt mit Genehmigung der Mathematisch-Naturwissenschaftlichen Fakultät der Eberhard Karls Universität Tübingen.

Tag der mündlichen Qualifikation:	08.03.2024
Dekan:	Prof. Dr. Thilo Stehle
1. Berichterstatter/-in:	Prof. Dr. Michael Lämmerhofer
2. Berichterstatter/-in:	Prof. Dr. Carolin Huhn

Eigenständigkeitserklärung

Hiermit erkläre ich, dass ich die vorliegende Arbeit selbstständig verfasst und keine anderen als die angegebenen Quellen und Hilfsmittel benutzt habe.

Alle sinngemäß und wörtlich übernommenen Textstellen aus fremden Quellen wurden kenntlich gemacht.

Tübingen, den 24. Januar 2024

Feiyang Li

Table of contents

I. Summary

Synthetic oligonucleotide therapies are on the increase and have emerged as a viable therapeutic approach for gene expression modulation. This family of synthetic nucleic acids includes antisense oligonucleotides (ASOs), which are typically 12 to 30 nucleotides in length and chemically phosphorothioates, aptamers, and RNA interference (RNAi) oligonucleotides. Considering the many clinical trials with oligonucleotide-based drugs, a further growth of this segment of therapeutics can be expected in the future. For pharmaceutical applications in humans and clinical trials, the products must be of high purity. However, many different kinds of oligonucleotide impurities with deleted or extended base sequences (N±1, N±2), base modifications (depurination, deamination) and incomplete cleavage of protection groups are frequently found in raw products of synthetic oligonucleotides. Consequently, appropriate purification methods and assays are necessary for the quality control of the development and production of pharmaceutical grade oligonucleotide therapeutics. In case of liquid chromatography (LC), ion-pair reversed liquid chromatography (IP-RPLC) is the state-of-the-art technology which has been very commonly used since decades. Nevertheless, the usage of highly concentrated ion-pairing reagents like triethylammonium acetate leads to strong ion suppression for the structural analysis of oligonucleotides via mass spectrometry (MS) causing reduced detection limit. Simultaneously, the selectivity of IP-RP is often not sufficient or unsatisfying for oligonucleotides as complex biomacromolecules. Therefore, it is reasonable to find alternative, ideally ion-pair-free LC methods providing selectivity for structurally closely related oligonucleotides which is the main focus of this dissertation. Interesting ion-pair-free applications using some unconventional stationary phases based on cholesterol or polybutylene terephthalate are discussed. Hydrophilic interaction liquid

chromatography (HILIC) as promising alternative for polar analytes was used to enable a detailed impurity profiling for siRNA under the usage of ammonium acetate as mobile phase additives. Besides of one-dimensional LC, several two-dimensional (2D-LC) solutions have also been developed. With 2D-LC, a general platform method was created allowing free choice of any chromatography modes in the first dimension. Problematic effluents like phosphate buffer for anion-exchange chromatography could be removed in the second dimension using a C18 reversed-phase column with methanol as organic modifier and without ion-pair reagent to avoid contamination of the MS system. In another study, the orthogonality between different chromatography methods for siRNA oligonucleotide separations was investigated for a 2D-LC setup. Next, the “best match” was combined for a selective comprehensive 2D-LC experiment leading to increased resolution. At the end, 2D-LC was also used for diastereoselective separations of phosphorothioates. Here, one of the oxygen atoms at the phosphate backbone is exchanged for sulfur introducing a chiral center. With 2D-LC using an amylose-based chiral column in the first dimension and a C18 column in the second dimension, a profoundly extended diastereoselectivity was enabled which cannot be achieved by one-dimensional separations.

II. Zusammenfassung

Synthetische Oligonukleotide als pharmazeutische Wirkstoffe sind auf dem Vormarsch und haben sich als praktikabler therapeutischer Ansatz zur Modulation der Genexpression erwiesen. Zu dieser Familie synthetischer Nukleinsäuren gehören Antisense-Oligonukleotide (ASO), die in der Regel 12 bis 30 Nukleotide lang sind, sowie chemische Phosphorothioate, Aptamere und RNA-Interferenz-Oligonukleotide (RNAi). In Anbetracht der zahlreichen klinischen Versuche ist in Zukunft mit einem weiteren Wachstum von Therapeutika dieser Art zu rechnen. Für pharmazeutische Anwendungen und klinische Versuche müssen die Produkte von hoher Reinheit sein. In den Rohprodukten synthetischer Oligonukleotide finden sich jedoch häufig viele verschiedene Formen von Oligonukleotid-Verunreinigungen mit verkürzten oder verlängerten Basensequenzen (N±1, N±2), Basenmodifikationen (Depurinierung, Desaminierung) und unvollständiger Abspaltung von Schutzgruppen. Daher sind für die Qualitätskontrolle bei der Entwicklung und Herstellung von solchen pharmazeutischen Oligonukleotiden geeignete Reinigung- und Testmethoden erforderlich. Im Falle der Flüssigkeitschromatographie (LC) ist die Ionenpaar-Umkehr-Flüssigkeitschromatographie (IP-RPLC) die bewährte Methode, welche seit Jahrzehnten sehr häufig eingesetzt wird. Die Verwendung hochkonzentrierter Ionenpaar-Reagenzien wie beispielweise Triethylammoniumacetat verursacht jedoch eine starke Ionenunterdrückung bei der Strukturanalyse von Oligonukleotiden mittels Massenspektrometrie (MS), was zu einer reduzierten Nachweisgrenze führt. Gleichzeitig ist die Selektivität der IP-RP für Oligonukleotide als komplexe Biomakromoleküle oft nicht ausreichend oder unbefriedigend. Daher ist es sinnvoll, alternative, idealerweise ionenpaarfreie LC-Methoden zu finden, die Selektivität für strukturell ähnliche Oligonukleotide bieten, was den Schwerpunkt dieser Dissertation

darstellt. Es werden interessante ionenpaar-freie Anwendungen mit unkonventionellen stationären Phasen auf der Basis von Cholesterin oder Polybutylen-Terephthalat diskutiert. Die hydrophile Interaktionsflüssigkeitschromatographie (HILIC) als vielversprechende Alternative für polare Analyten wurde ebenfalls eingesetzt, um ein detailliertes Verunreinigungsprofil für siRNA unter Verwendung von Ammoniumacetat als Additiv für die mobile Phase zu generieren. Neben der eindimensionalen LC wurden auch mehrere zweidimensionale (2D-LC) Lösungen entwickelt. Mit der 2D-LC wurde eine allgemeine Plattform-Methode entworfen, die eine freie Wahl beliebiger Chromatographie in der ersten Dimension erlaubt. Problematische Komponente wie beispielweise Phosphate oder Ionen-Paar-Reagenzien, die in den mobilen Phasen aus der 1. Dimension enthalten sind, konnten in der zweiten Dimension auf einer C18-Phase unter dem Ausschluss von Ionen-Paar-Reagenzien entfernt werden, um eine Kontamination des MS-Systems zu vermeiden. In einer anderen Studie wurde die Orthogonalität zwischen verschiedenen Chromatographie-Methoden für siRNA-Oligonukleotide in einem potentiellen 2D-LC-Setup untersucht. Anschließend wurde die "beste Übereinstimmung" für ein 2D-LC-Experiment kombiniert, was zu einer höheren Auflösung führte. Schließlich wurde die 2D-LC auch für diastereoselektive Trennungen von Phosphorothioaten verwendet. Dabei wird eines der Sauerstoffatome am Phosphatgerüst gegen Schwefel ausgetauscht, wodurch ein chirales Zentrum entsteht. Die Kombination von einer Amylose-basierten, chiralen Säule mit einer C18 Phase in einer 2D-LC Anordnung ermöglicht eine stark erweiterte Diastereoselektivität, die mit eindimensionalen Trennungen nicht erreicht werden kann.

III. List of publications

Publication I

F. Li, X. Su, S. Bäurer, M. Lämmerhofer. Multiple heart-cutting mixed-mode chromatography-reversed-phase 2D-liquid chromatography method for separation and mass spectrometric characterization of synthetic oligonucleotides. *J. Chromatogr. A* 1625 (2020) 461338. DOI: 10.1016/j.chroma.2020.461338

Publication II

F. Li, M. Lämmerhofer. Impurity profiling of siRNA by two-dimensional liquid chromatography-mass spectrometry with quinine carbamate anion-exchanger and ion-pair reversed-phase chromatography. *J. Chromatogr. A* 1643 (2021) 462065. DOI: 10.1016/j.chroma.2021.462065.

Publication III

F. Li, S. Chen, S. Studzińska, M. Lämmerhofer. Polybutylene terephthalate-based stationary phase for ion-pair-free reversed-phase liquid chromatography of small interfering RNA. Part 1: direct coupling with mass spectrometry. *J. Chromatogr. A* 1694 (2023) 463898. DOI: 10.1016/j.chroma.2023.463898.

Publication IV

F. Li, S. Chen, S. Studzińska, M. Lämmerhofer. Polybutylene terephthalate-based stationary phase for ion-pair-free reversed-phase liquid chromatography of small interfering RNA. Part 2: Use for selective comprehensive two-dimensional liquid

chromatography. *J. Chromatogr. A* 1701 (2023) 464069. DOI: 10.1016/j.chroma.2023.464069.

Publication V

S. Studzińska, F. Li, M. Szumski, B. Buszewski, M. Lämmerhofer, Cholesterol Stationary Phase in the Separation and Identification of siRNA Impurities by Two-Dimensional Liquid Chromatography-Mass Spectrometry. *Int. J. Mol. Sci.* (2022) 23, 14960. DOI: 10.3390/ijms232314960.

Publication VI (Manuscript only)

F. Li, C. Knappe, E. Favorat, M. Gao, R. Pell, W. Holkenjans, Two-dimensional reversed phase liquid chromatography of synthetic phosphorothioate oligonucleotides.

Other Publications (not included in this work)

F. Li, R. Karongo, D. Mavridou, J. Horak, A. Sievers-Engler, M. Lämmerhofer, Automated sample preparation with 6-Aminoquinolyl-N-hydroxysuccinimidyl carbamate and iodoacetamide derivatization reagents for enantioselective liquid chromatography tandem mass spectrometry amino acid analysis. *J. Chromatogr. A.* 1708 (**2023**) 464349.

F. Li, S. Chen, S. Studzinska, M. Lämmerhofer, Ionenpaar-freie RPLC-MS von Oligonukleotiden: Anwendung für die Verunreinigungsanalytik von siRNA mithilfe einer Polybutylenterephthalat-basierten Säule. *chrom+food forum*. 04 (**2023**) 44-46.

IV. Author contributions

Publication I

Multiple heart-cutting mixed-mode chromatography-reversed-phase 2D-liquid chromatography method for separation and mass spectrometric characterization of synthetic oligonucleotides.

Feiyang LI
Investigation, Methodology, Formal analysis, Data curation, Visualization, Writing – original draft, Writing – review & editing

Xiaoli SU
Investigation

Dr. Stefanie BÄURER
Writing – review & editing

Prof. Dr. Michael LÄMMERHOFER
Conceptualization, Methodology, Supervision, Writing – review & editing, Resources, Funding acquisition

Publication II

Impurity profiling of siRNA by two-dimensional liquid chromatography-mass spectrometry with quinine carbamate anion-exchanger and ion-pair reversed-phase chromatography.

Feiyang LI
Investigation, Methodology, Formal analysis, Data curation, Visualization, Writing – original draft, Writing – review & editing

Prof. Dr. Michael LÄMMERHOFER
Conceptualization, Methodology, Supervision, Writing – review & editing, Resources, Funding acquisition

Publication III

Polybutylene terephthalate-based stationary phase for ion-pair-free reversed-phase liquid chromatography of small interfering RNA. Part 1: direct coupling with mass spectrometry.

Feiyang LI
Investigation, Methodology, Formal analysis, Data curation, Visualization, Writing – original draft, Writing – review & editing

Shenkai CHEN
Investigation

Prof. Dr. Sylwia STUDZIŃSKA
Supervision, Writing – review & editing

Prof. Dr. Michael LÄMMERHOFER
Conceptualization, Methodology, Supervision, Writing – review & editing, Resources, Funding acquisition

Publication IV

Polybutylene terephthalate-based stationary phase for ion-pair-free reversed-phase liquid chromatography of small interfering RNA. Part 2: Use for selective comprehensive two-dimensional liquid chromatography.

Feiyang LI
Investigation, Methodology, Formal analysis, Data curation, Visualization, Writing – original draft, Writing – review & editing

Shenkai CHEN
Investigation

Prof. Dr. Sylwia STUDZIŃSKA
Supervision, Writing – review & editing

Prof. Dr. Michael LÄMMERHOFER
Conceptualization, Methodology, Supervision, Writing – review & editing, Resources, Funding acquisition

Publication V

Cholesterol Stationary Phase in the Separation and Identification of siRNA Impurities by Two-Dimensional Liquid Chromatography-Mass Spectrometry.

Prof. Dr. Sylwia STUDZIŃSKA
Conceptualization, Methodology, Validation, Investigation, Data curation, Writing- original draft preparation, Writing- review and editing, Visualization

Feiyang LI

Conceptualization, Methodology, Validation, Investigation, Data curation, Writing- original draft preparation, Writing- review and editing, Visualization

Prof. Dr. Michał SZUMSKI
Writing- review and editing

Prof. Dr. Michael LÄMMERHOFER
Conceptualization, Methodology, Validation, Writing- review and editing

Prof. Dr. Bogusław BUSZEWSKI
Writing- review and editing

Publication VI

Two-dimensional reversed phase liquid chromatography of synthetic phosphorothioate oligonucleotides

Feiyang LI
Investigation, Methodology, Formal analysis, Data curation, Visualization, Writing – original draft, Writing – review & editing

Cornelius KNAPPE
Methodology, Formal analysis, Data curation, Visualization, Writing – original draft, Writing – review & editing

Enrico FAVORAT
Investigation

Dr. Mimi GAO, Dr. Reinhard PELL, Dr. Wiebke HOLKENJANS
Writing – review & editing, Resources, Funding

Prof. Dr. Michael LÄMMERHOFER
Conceptualization, Methodology, Supervision, Writing – review & editing, Resources, Funding acquisition

Other Publications

Automated sample preparation with 6-Aminoquinolyl-N-hydroxysuccinimidyl carbamate and iodoacetamide derivatization reagents for enantioselective liquid chromatography tandem mass spectrometry amino acid analysis

Feiyang LI
Investigation, Methodology, Formal analysis, Data curation, Visualization, Writing – original draft, Writing – review & editing

Dr. Ryan KARONGO
Methodology, Formal analysis, Data curation, Writing – review & editing

Despoina MAVRIDOU
Methodology

Dr. Jeannie HORAK
Conceptualization, Methodology, Writing – review & editing

Dr. Adrian ENGLER-SIEVERS
Investigation, Methodology, Writing – review & editing

Prof. Dr. Michael LÄMMERHOFER
Conceptualization, Methodology, Supervision, Writing – review & editing, Resources, Funding acquisition

Ionenpaar-freie RPLC-MS von Oligonukleotiden: Anwendung für die Verunreinigungsanalytik von siRNA mithilfe einer Polybutylenterephthalat-basierten Säule

Feiyang LI
Investigation, Methodology, Formal analysis, Data curation, Visualization, Writing – original draft, Writing – review & editing

Prof. Dr. Michael LÄMMERHOFER
Conceptualization, Methodology, Supervision, Writing – review & editing, Resources, Funding acquisition

V. List of oral presentations

2022: 32nd Doktorandenseminar by German Chemical Society, Online, Germany.

VI. List of poster presentations

2019: Annual Meeting of DPhG (German Pharmaceutical Society), Heidelberg, Germany.

2020: HTC-16, 16th International Symposium on Hyphenated Techniques in Chromatography and Separation Technology, Ghent, Belgium.

2022: HTC-17, 17th International Symposium on Hyphenated Techniques in Chromatography and Separation Technology, Ghent, Belgium.

2022: 33rd International Symposium on Chromatography, Budapest, Hungary.

2023: ANAKON by Austrian Society of Analytical Chemistry, Vienna, Austria.

VII. Abbreviations

DNA	Deoxyribonucleic acid
RNA	Ribonucleic acid
A	Adenine
G	Guanine
C	Cytosine
T	Thymine
U	Uracil
PCR	Polymerase chain reaction
miRNA	microRNA
piRNA	Piwi-interacting RNA
siRNA	small interfering RNA
DMT	Dimethoxytrityl
DCC	Dicyclohexyl carbodiimide
tRNA	Transfer RNA
ASO	Antisense oligonucleotides
RISC	RNA-induced silencing complex
AMD	Age-related mascular degeneration
VEGF	Vascular endothelial growth factor
PEG	Polyethylene glycol
PS	Phosphorothioates
PS2	Phosphorodithioate
MOP	Methoxypropylphosphonate
MP	Methylphosphonate
ON	Oligonucleotide
LNA	Locked nucleic acid
PMO	Phosphorodiamidate morpholino oligomers
GalNAC	*N*-acetylgalactosamine
ASGR1	Asialoglycoprotein receptor 1
LDL	Low-density lipoprotein
HDL	High-density lipoprotein
LC-MS	Liquid chromatography - mass spectrometry
IP	Ion pairing
RPLC	Reversed phase liquid chromatography
IP-RPLC	Ion-pairing reversed phase liquid chromatography
PO	Phosphodiester
TEAA	Triethylammonium acetate
ESI-MS	Electrospray ionization mass spectrometry
TEA	Triethylamine
HFIP	Hexafluoro-2-propanol
HILIC	Hydrophilic interaction liquid chromatography
2D-LC	Two-dimensional liquid chromatography
^{1}D	First dimension

^{2}D	Second dimension
PBT	Polybutylene-terephthalate
AA	Ammonium acetate
AF	Ammonium formate
MMC	Mixed-mode chromatography
AEX	Anion-exchange
TRIS	Tris(hydroxymethyl)aminomethane
NaCl	Sodium chloride
ASM	Active solvent modulation
SPAM	Stationary phase assisted modulation
eq.	Equation
ACN	Acetonitrile
CI	Chemical ionization
EI	Electron ionization
ESI	Electrospray ionization
APCI	Atmospheric-pressure chemical ionization
kV	Kilovolt
MeOH	Methanol
FWHM	Full width half maximum
ppm	Parts per million
RF	Radio frequency
DC	Direct current
TOF	Time of Flight
ns	Nanosecond
EM	Electron multipliers
FC	Faraday cups
C	Coulombs
A	Ampere
NanoSIMS	Nanoscale secondary ion mass spectrometer
MCP	Microchannel plates
EDTA	Ethylenediaminetetraacetic acid
RP/WAX	Reversed-phase/weak anion exchange
UV	Ultraviolet
API	Active pharmaceutical ingredient

VIII. Introduction

1. Synthetic Oligonucleotides

1.1 Structures, properties and functions

Oligonucleotides, both DNA- and RNA-based, are linear polymers consisting of 8-50 nucleotides in various length [1,2]. Just as with DNA and RNA, oligonucleotides are composed of a nitrogenous base, a ribose/deoxyribose sugar and a phosphate group. Regarding the nucleobases, those can be divided into pyrimidine and purine bases. RNA and DNA contain the purine bases A, G and pyrimidine base C. In the case of DNA, the pyrimidine base T is present and will be exchanged by U during the transcription into RNA [2]. Single nucleotides can contain several numbers of phosphate groups resulting in nucleoside tri-, di-, and monophosphates. Nucleotides can be linked to each other in a condensation reaction nucleoside triphosphate by the cleavage of a pyrophosphate to form a phosphodiester bond. Consequently, depending on the position of the phosphate group of the initial or terminal nucleotide, oligonucleotide (also RNA and DNA) strands contain both 5’ and 3’ ends. The 5’ end consists (typically) of a phosphate group which is linked to the 5’ position of the ribose (RNA) or deoxyribose (DNA). At the 3’ end, the ribose or deoxyribose carries (usually) a free OH group at the 3’ position. When it comes to double helix configuration, both strands are arranged antiparallel. The DNA- helix is stabilized by hydrogen bonds formed by complementary base pairing (G-C, A-T or A-U) [3–5]. Besides of complementary hydrogen bonding, π-π interaction between the (adjacent not complementary) nucleobases also plays an important role for the stability of the double helix structure (base stacking) [6,7]. The described structural properties of

oligonucleotide strands are illustrated on **Figure 1**, further structural modification of synthetic oligonucleotides will be discussed in chapter 3.

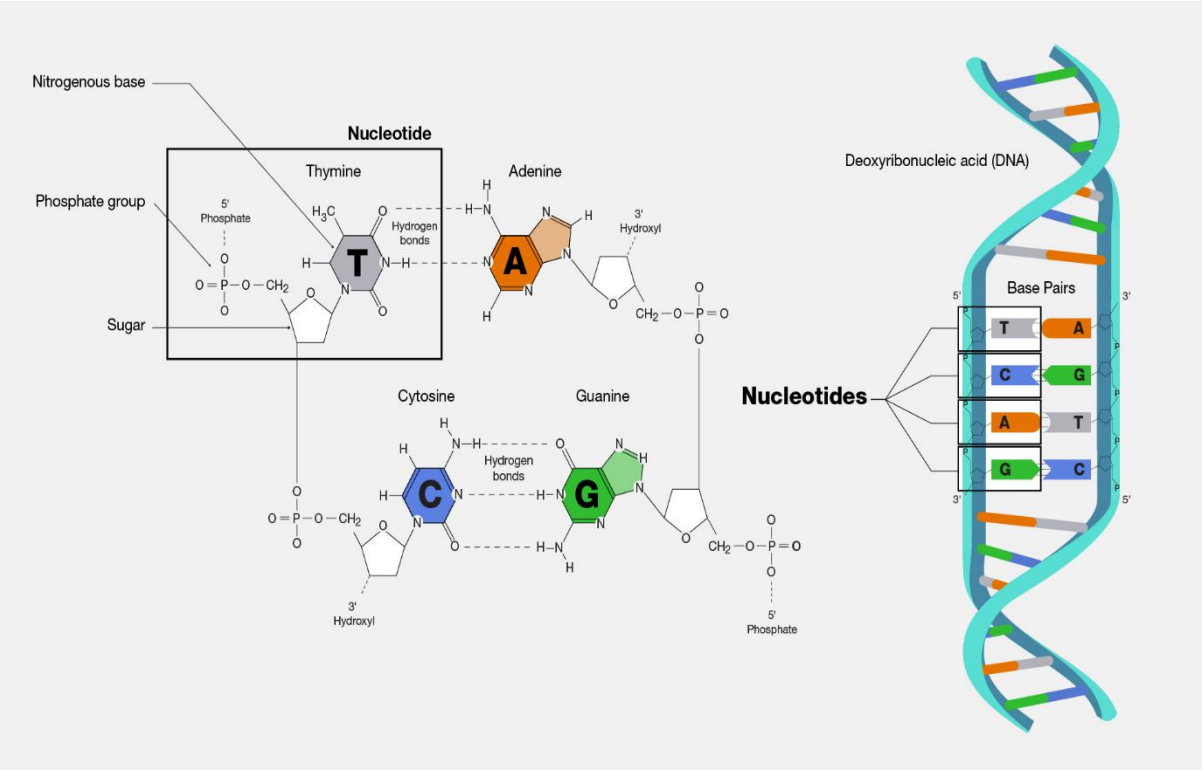

Figure 1. Structural arrangement of nucleotides within nucleic acids. Reprinted from [8]. Permission granted by Elsevier ©.

Because of its high flexibility, synthetic oligonucleotides with any user-specified sequence have been frequently used in different fields of biotechnology like PCR, DNA sequencing, molecular cloning and more. Already in the end of the 90s, *Tavitian, Chardin* and *Touchout* tested different oligonucleotide mixtures focusing on their ability to hybridize 11 cloned members of the ras gene. Two complementary oligonucleotide strands were designed with weak G-T base pairings. After the hybridization, four cDNAs encoding Ras-related proteins were able to be isolated from a brain library [9]. Nowadays, the usage of oligonucleotide for molecular cloning has become a routine technique. *Okasha* and *Samir* aimed to synthesize the gene of Chromogranin using 5

pairs of oligonucleotides [10]. *Jacobs* established a method to take single stranded DNA oligonucleotide with Gibson assembly to augment Golden Gate cloning workflows in process which they called “oligo stitching” [11,12].

For PCR, oligonucleotide between 18 and 30 bases are used as primers. These short single strands are designed with at least part of their sequence being complementary to the 5’ end of the sequence targeted for amplification. Since the introduction of PCR by *Saiki et al.* in 1985, many efforts have been invested into efficient primer design of suitable oligonucleotides for PCR [13–15]. Today, the technique has been established as an essential part of bioanalysis. A huge data bank of oligonucleotide primer is available and can be used for different requirements [16,17].

In nature, oligonucleotides are commonly existing as small RNA molecules like miRNA, siRNA, piRNA and more. miRNA are single-stranded non-coding RNA composed of 21 to 23 nucleotides [18]. Being present in both eukaryotic and prokaryotic cells, miRNA are responsible for RNA silencing and post-transcriptional regulation of gene expression [19]. piRNA contain various length of nucleotides between 21 to 31 nucleotides. Similar to miRNA and siRNA, piRNA has a role in RNA silencing via the formation of a complex with piwi proteins [20]. RNA silencing is a versatile tool for gene expression to suppress the biosynthesis of pathogenic proteins has been more and more brought into the focus. Synthetically generated mimics of those oligonucleotide strands are promising candidates as biopharmaceutical. As vital aspect of this work, more details will be further discussed in chapter 2. But firstly, the chemical backgrounds of the synthesis of oligonucleotide strands will be described in the following chapter.

1.2 Synthesis

The first work of the directed chemical synthesis of an oligonucleotide was published by *Michelson* and *Todd* from 1955 for the preparation of a dithymidinyl nucleotide. Here, the phosphate link between to T nucleotides was synthesized by preparing the 3’ phosphoryl chloride of a 5’ benzyl protected T, using phenylphosphoryl dichloride [21].

In the late 1950’s, *Khorana* introduced two concepts which enabled the synthesis of oligonucleotides more than just a few bases long. The first concept, an on-off protection scheme is still widely used until today for sequential oligonucleotide synthesis. A well-designed protecting group scheme enabling the selective removal of a specific protecting group at the desired time is crucial for an efficient, cyclic, step-wise synthesis of oligonucleotides. The solution *Khorana* offered for the 5’ hydroxyl protection was the usage of a DMT protecting group [22] which can be considered as a milestone achievement for the oligonucleotide synthesis. The combination of good general stability and convenient removal under mild acidic condition is overwhelming in comparison to alternative protection strategies and still very popular until nowadays. The second concept suggested by *Khorana* was the phosphodiester method for oligonucleotide synthesis. This cyclic theme is already very similar to the currently used one with the exception of the addition of oxidation. Instead of phosphoryl chloride as by *Michelson* and *Todd*, this method prepared 3’-phosphates of the 5’-protected nucleosides using phosphorochloridates which were hydrolysed to the phosphomonoester. These 5’-protected nucleosides 3’-phosphates were activated using a condensation reagent like DCC to couple to the 5’-hydroxyl of another 3’-protected nucleoside. This method was also a revolutionary step resulting in a successful synthesis of a 72-mer tRNA molecule [23].

From the beginning of 1960's on, *Letsinger* entered the field of oligonucleotide synthesis and established three major contributions: first, he introduced solid phase chemistry which was originally designed for the synthesis of peptides. Furthermore, the phosphotriester method was developed which was a significant improvement on *Khorana*' s phosphodiester method. And finally, *Letsinger* introduced the P(III) based phosphite-triester method, which can be considered as the preliminary stage of the phosphoramidite method developed by *Marvin Caruthers.* In 1965, *Letsinger* published the first paper describing the soli-phase synthesis of dimer and trimer oligonucleotides using a "popcorn" polymer consisting of a styrene-divinylbenzene polymer as support material. Here, 2'-deoxycytidine was attached through the amine at the 4' position of the base to the support material. The amide bond was then cleaved under basic condition. The 3' hydroxyl of the 2' deoxycytidine was protected with a benzoyl group and the 5' position with a DMT group. After the removal of DMT, the nucleoside bound to the support material can be linked with further building blocks completing the oligonucleotide synthesis [24]. In 1969, *Letsinger* published the first paper describing the phosphotriester method with its key improvement in comparison to the phosphodiester approach considering the branching at the internucleotide phosphate linkage. Here, *Letsinger* used a beta-cyanoethyl to protect the phosphate group. With mesityl sulfonyl chloride and mesityl sulfonyl nitrotriazole, two important activators were found to push the efficiency. With this approach, the chemistry has become so convenient and simple to be reproduced in many labs. The combination of soli-phase methodology with the phosphotriester chemistry enabled the creation of first viable automated and semi-automated DNA synthesizers. With this equipment, the industry was primed for the emerging techniques of gene mapping, PCR and target validation [25].

Based on the phosphotriester method, *Letsinger* developed the phosphite-triester chemistry in the mid-1970's. Until now, the phosphorus always used to have the oxidation state of V for oligonucleotide synthesis, which did not show very high reactivity. With the new phosphite-triester method, *Letsinger* and *Caruthers* used the more reactive phosphorus in the P(III) state leading to a significant reduction of time required for the coupling due to the high reactivity of the nucleoside phosphomonochloridite intermediate [26,27].

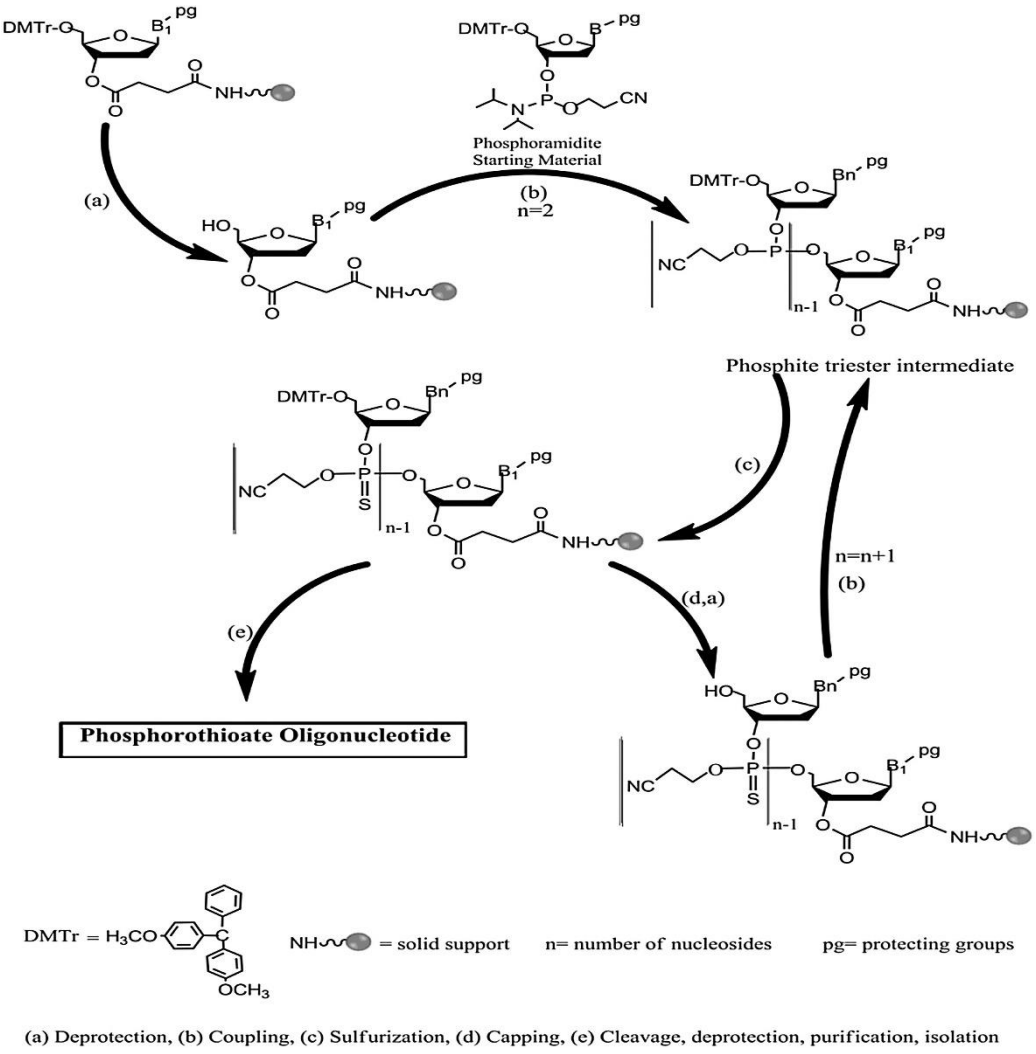

Figure 2. A classic phosphoramidite synthesis cycle for a phosphorothioate oligonucleotide. Reprint from [28], with permission of John Wiley & Sons, Ltd. ©.

Finally, *Caruthers* continued the heritage of *Letsinger* and modified the phosphite-triester method by exchanging one leaving group, a chloride, for another, an amine. With this, the phosphitylated nucleoside intermediate – a phosphoramidite – was able to be isolated as a stable solid and stored for further synthesis. Next, the phosphoramidite will be activated prior to coupling by adding tetrazole as weak acid. This new approach allowed the commercial scale manufacture and distribution of oligonucleotide synthesis reagent. The phosphoramidite-cycle is elegant and simple and has remained nearly unchanged for almost two decades [29,30]. The typical synthesis cycle is composed of several chemical reactions including detritylation, activation and coupling, oxidation, capping, cleavage and deprotection (see **Figure 2**). A brief explanation of each single step is listed below [28]:

- Detritylation is an acid-induced removal of the 5'-DMT protecting group with dichloroacetic acid or trichloroacetic acid solutions to free the 5'-hydroxyl group of the support-bound oligonucleotide.
- Extension of the oligonucleotide strand is realized by coupling to a protected nucleoside phosphoramidite in the presence of the tetrazole to form the phosphite triester intermediate.
- Next, a stabilization will be featured through iodine oxidation and formation of the phosphotriester backbone and afterwards incorporation of a sulfur atom by oxidative sulfurization to yield a phosphorothioate triester using 3*H*-1,2-benzodithiol-3-one-1,1-dioxide (Beaucage reagent).
- The free terminal 5'-hydroxyl groups will be capped to prevent elongation of failure sequences using acetic anhydride in the presence of a tertiary heterocyclic base

- The cycle is now repeated until the desired oligonucleotide sequence is obtained.
- Cleavage and release of the target strand from the solid support with gaseous methylamine or concentrated ammonium hydroxide. Removal of the protecting groups.

2. Oligonucleotide-based therapeutics

As mentioned above, one of the main application fields for synthetic oligonucleotide is their application as biopharmaceutical substances. The use of oligonucleotides as therapeutic agents was first proposed in the late 1970s [31]. After going through many ups and downs in regard to many different obstacles like delivery, stability and specificity, the market for therapeutic oligonucleotides is now rapidly growing [32]. Until today, 44 companies have molecules on the market or in late clinical development (past phase II). These include oligonucleotide-focused biotech companies like Ionis, Alnylam as well as Big Pharma companies like Johnson & Johnson, Roche, Novartis and AstraZeneca. At the beginning of 2022, 93 compounds targeted on gene expression via direct interaction with RNA or DNA are in advanced stages of clinical development (phases II and III). 13 oligonucleotide-based therapeutics obtained approval and one is under regulatory review. 130 phase II or phase III clinical trials involving 80 oligonucleotides are ongoing [32]. In this chapter, some important representatives of the oligonucleotide therapeutic and their action mechanism are going to be discussed. Furthermore, structural modifications to overcome the issues like stability and target affinity are shown as well.

2.1 Antisense oligonucleotide (ASO)

ASOs are short, synthetic, single-stranded oligonucleotides that can alter RNA and reduce, restore or modify protein expression through several distinct mechanisms [33]. At the moment, 9 of 15 FDA-approved oligonucleotide drugs are ASOs. The worldwide firstly FDA-approved oligonucleotide drug called Fomivirsen (1998) was also an ASO [34,35]. Currently, 44 further candidates are in phase II or phase III clinical trials. Depending on their chemistry, target and binding sequence, the main mechanisms of action for ASOs may vary. Here, the most important ones are gene expression

modulation and pre-mRNA splicing [33]. In the case of gene expression, ASOs will be bound to the target RNA via Watson-Crick base pairing forming a partial double strand hybrid which becomes a substrate for nuclease which leads to the degradation of the target mRNA [36,37]. Besides of this, ASOs can also modulate gene expression via steric block of the ribosomal machinery suppressing the translation of the target mRNA [38]. By diseases caused by a toxic RNA gain-of-function mechanism, unexpected expansion of repeated sequences in non-coding regions result in different pathogenic expressions [39]. ASOs are able to bind with high-affinity to those untranslated regions and prevent binding and sequestration of RNA-binding proteins by steric hindrance. In the case of splice-switching strategies, binding of ASOs to intro-exon sequences can destabilize splicing sites resulting in the exclusion or inclusion of particular exons. Malfunctioning genes can be then restored, either by re-establishing the normal reading frame following a pathogenic frame shift, or by excluding mutated segments of DNA. Nusinersen, an ASO developed to enhance inclusion of exon 7 in the survival motor neuron (SMN1) gene is one of the most notable agents with this mechanism of action [40,41]. An overview of further ASOs, either FDA-approved or in clinical trials, are listed on **Table 1**. The described mechanisms of action are illustrated in **Figure 3**.

Table 1. ASOs approved or in clinical development (Status: End 2022, from [32]).

Drug Name	Target Gene	Mode of Action	Therapy Area	Latest Stage of Development	Company
Nusinersen	SMN2	Splicing modulation	Neurology	Marketed	Biogen
Eteplirsen	DMD	Splicing modulation	Muscular disorders	Marketed	Sarepta Therapeutics
Inotersen	TTR	Expression inhibition	Metabolic disorders	Marketed	Akcea Therapeutics
Viltolarsen	DMD	Splicing modulation	Muscular disorders	Marketed	NS Pharma

Casimersen	DMD	Splicing modulation	Muscular disorders	Marketed	Sarepta Therapeutics
Golodirsen	DMD	Splicing modulation	Muscular disorders	Marketed	Sarepta Therapeutics
Mipomersen	APOB	Expression inhibition	Metabolic disorders	Marketed	Kastle Therapeutics
Volanesorsen	APOC3	Expression inhibition	Metabolic disorders	Marketed	Akcea Therapeutics
Fomivirsen	CMV virus IE2	Expression inhibition	Infectious disease	Marketed and withdrawn	Novartis
Aganirsen	IRS1	Expression inhibition	Ophthalmology and metabolic disorders	Phase III	Gene Signal
Alicaforsen	ICAM1	Expression inhibition	Gastrointestinal	Phase III	Atlantic Healthcare
Eplontersen	TTR	Expression inhibition	Metabolic disorders	Phase III	Akcea Therapeutics
ION-363	FUS	Expression inhibition	Neurology	Phase III	Ionis Pharmaceuticals
Olezarsen	APOC3	Expression inhibition	Cardiovascular and metabolic disorders	Phase III	Akcea Therapeutics
Pelacarsen	LPA	Expression inhibition	Cardiovascular and metabolic disorders	Phase III	Novartis
Sepofarsen	CEP290	Splicing modulation	Ophthalmology	Phase III	ProQR Therapeutics
Tofersen	SOD1	Expression inhibition	Neurology	Phase III	Biogen
Tominersen	HTT	Expression inhibition	Neurology	Phase III	Roche
Trabedersen	TGFB2	Expression inhibition	Oncology	Phase III	Oncotelic
Zilganersen	GFAP	Expression inhibition	Neurology	Phase III	Ionis Pharmaceuticals
ASM-8	CCR3 and CSF2RB	Expression inhibition	Respiratory	Phase II	Pharmaxis
Atesidorsen	GHR	Expression inhibition	Hormonal disorders	Phase II	Antisense Therapeutics
ATL-1102	ITGA4	Expression inhibition	Neurology and muscular disorders	Phase II	Antisense Therapeutics
AZD-8233	PCSK9	Expression inhibition	Metabolic disorders	Phase II	AstraZeneca

AZD-8701	FOXP3	Expression inhibition	Oncology	Phase II	AstraZeneca
Bepirovirsen	Viral HBV	Expression inhibition	Infectious disease	Phase II	Ionis Pharmaceuticals
BIIB-080	MAPT	Expression inhibition	Neurology	Phase II	Biogen
Cepadacursen	PCSK9	Expression inhibition	Metabolic disorders	Phase II	Civi Biopharma
Cimderlirsen	GHR	Expression inhibition	Hormonal disorders	Phase II	Ionis Pharmaceuticals
CODA-001	GJA1	Expression inhibition	Ophthalmology	Phase II	Eyevance Pharmaceuticals
Danvatirsen	STAT3	Expression inhibition	Oncology	Phase II	AstraZeneca
Donidalorsen	KLKB1	Expression inhibition	Immunology and infectious disease	Phase II	Ionis Pharmaceuticals
DYN-101	DYN2	Expression inhibition	Muscular disorders	Phase II	Dynacure
GTX-102	UBE2A	Expression inhibition	Neurology	Phase II	GeneTx Biotherapeutics
ION-224	DGAT2	Expression inhibition	Gastrointestinal	Phase II	Ionis Pharmaceuticals
ION-253	Undisclosed	Expression inhibition	Gastrointestinal	Phase II	Johnson & Johnson
ION-464	SNCA	Expression inhibition	Neurology	Phase II	Ionis Pharmaceuticals
ION-541	ATXN2	Expression inhibition	Neurology	Phase II	Ionis Pharmaceuticals
ION-859	LRRK2	Expression inhibition	Neurology	Phase II	Ionis Pharmaceuticals
IONIS-AGTLRx	AGT	Expression inhibition	Cardiovascular	Phase II	Ionis Pharmaceuticals
IONIS-FB-LRx	CFB	Expression inhibition	Genitourinary system and ophthalmology	Phase II	Ionis Pharmaceuticals
IONIS-FXILRx	F11	Expression inhibition	Cardiovascular, hematology, and genitourinary system	Phase II	Ionis Pharmaceuticals
IONIS-GCGRRx	GCGR	Expression inhibition	Metabolic disorders	Phase II	Ionis Pharmaceuticals

IONIS-HBVLRx	Viral HBV	Expression inhibition	Infectious disease	Phase II	Ionis Pharmaceuticals
IONIS-PKKRx	KLKB1	Expression inhibition	Neurology	Phase II	Ionis Pharmaceuticals
IONISAR-2.5Rx	AR	Expression inhibition	Oncology	Phase II	Ionis Pharmaceuticals
IONISENAC-2.5Rx	SCNN1A	Expression inhibition	Respiratory	Phase II	Ionis Pharmaceuticals
IONISTMPRSS-6LRx	TMPRSS6	Expression inhibition	Hematology	Phase II	Ionis Pharmaceuticals
ISTH-0036	TGFB2	Expression inhibition	Ophthalmology	Phase II	Isarna Therapeutics
NS-089	DMD	Splicing modulation	Muscular disorders	Phase II	Nippon Shinyaku
Prexigebersen	GRB2	Expression inhibition	Oncology	Phase II	Bio-Path Holdings
QR-1123	RHO	Expression inhibition	Ophthalmology	Phase II	ProQR Therapeutics
QRX-421a	USH2A	Splicing modulation	Ophthalmology	Phase II	ProQR Therapeutics
Renadirsen	DMD	Splicing modulation	Muscular disorders	Phase II	Daiichi Sankyo
SRP-5051	DMD	Splicing modulation	Muscular disorders	Phase II	Sarepta Therapeutics
STK-001	SCN1A	Splicing modulation	Neurology	Phase II	Stoke Therapeutics
Vupanorsen	ANGPTL3	Expression inhibition	Metabolic disorders	Phase II	Pfizer
WVE-003	HTT	Expression inhibition	Neurology	Phase II	Wave Life Sciences
WVE-004	C9orf72	Expression inhibition	Neurology	Phase II	Wave Life Sciences
WVEN-531	DMD	Splicing modulation	Muscular disorders	Phase II	Wave Life Sciences

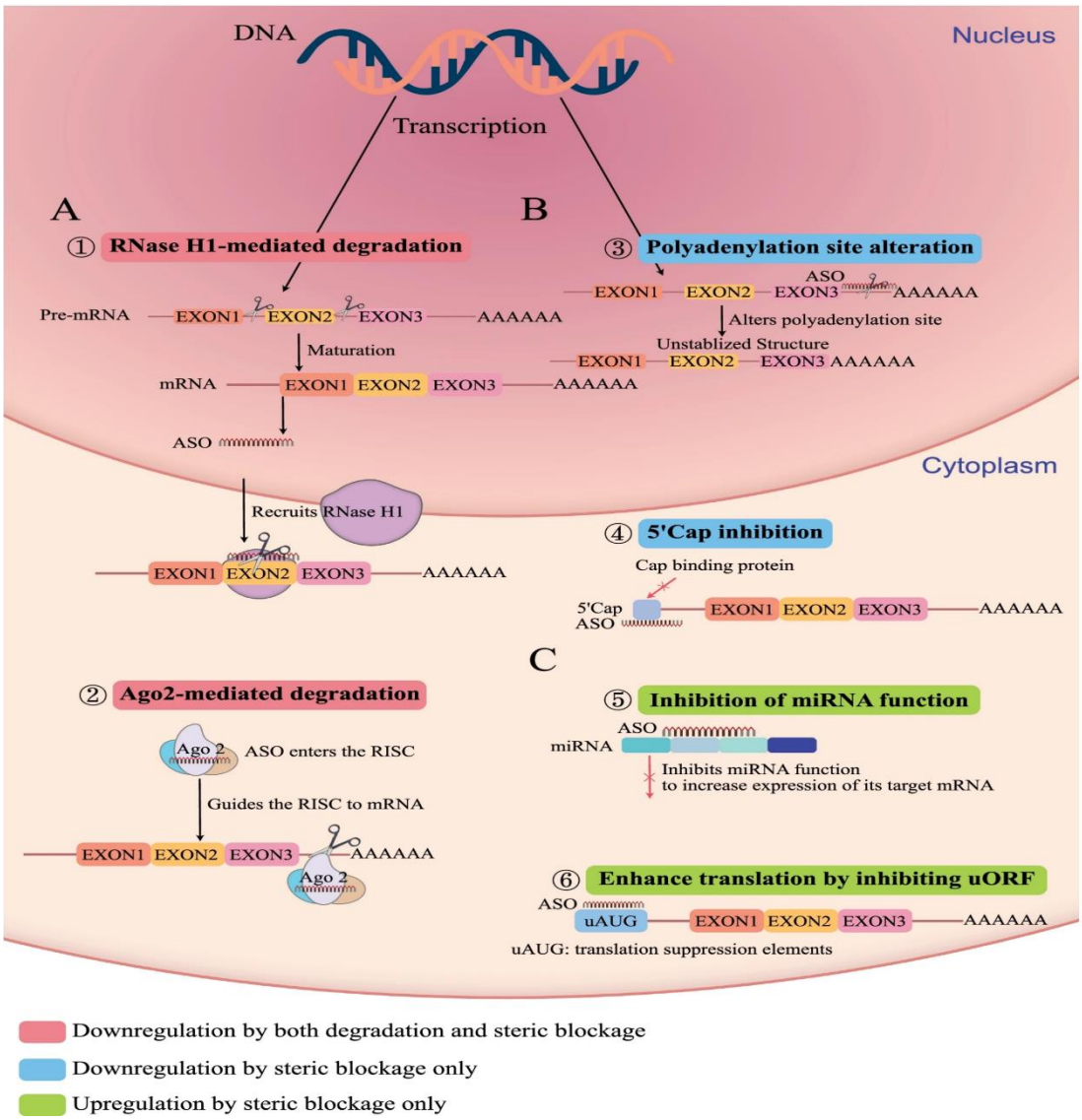

Figure 3. The main mechanisms of ASO. A: Downregulation of degradation and steric blockage on the same time. B: Downregulation by steric blockage only. C: Upregulation by steric blockage. Reprint from [42], permission granted due to open access.

2.2 Small interfering RNA (siRNA)

siRNAs are double-stranded RNA with typically 20-24 base pairs in length. Currently, 4 siRNA as therapeutics are FDA-approved and on the market. 25 further candidates are in phase II or III clinical trials [43]. As ASOs, siRNAs are also able to modulate

gene expression prohibiting the biosynthesis of pathogenic proteins. But siRNAs are operating within the RNA interference pathway [44]. Such a process with the aim to suppress the translation can be generally described as follows:

- The double-strands commonly consisting of a guide- and passenger strand is cleaved by an endo-ribonuclease called Dicer into several fragments [45].
- After the cleavage, the siRNA fragments enter the cell where it gets incorporated into Argonaute protein to form RISC [46].
- As part of the RISC complex, double-stranded siRNAs are now unwound to form single stranded siRNAs.
- The guide strand which is thermodynamically less stable will remain part of the RISC-complex. The passenger strand will be degraded.
- The single guide strand as part of the complex is now able to bind to a complementary target mRNA via Watson-Crick mechanism.
- Captured by this complex, the target mRNA will be cleaved into shorter parts.
- The single parts are now recognized as abnormal by the cell. A degradation of the mRNA is induced. Thus, the silencing is completed and no translation is possible.

The described mechanism above is illustrated in **Figure 4**. From this point of view, siRNA is working similar to miRNA. But siRNAs are able to silence the genes with much higher specificity by cleaving the target mRNA before the translation. Besides of ASO, siRNA is the second driving force for the development of oligonucleotide-based therapeutics. The latest FDA-approved siRNA therapeutic is Lumasiran, a double-stranded siRNA that reduces levels of glycolate oxidase enzyme by targeting HAO 1 mRNA in hepatocytes to treat primary hyperoxaluria type 1 [47]. Further siRNA candidates are listed on **Table 2**.

Table 2. siRNAs approved or in clinical development (Status: End 2022, from [32]).

Drug Name	Target Gene	Mode of Action	Therapy Area	Latest Stage of Development	Company
Patisiran	TTR	Expression inhibition	Metabolic disorders	Marketed	Alnylam Pharmaceuticals
Givosiran	ALAS1	Expression inhibition	Metabolic disorders	Marketed	Alnylam Pharmaceuticals
Inclisiran	PCSK9	Expression inhibition	Cardiovascular and metabolic disorders	Marketed	Novartis
Lumasiran	HAO1	Expression inhibition	Genitourinary system	Marketed	Alnylam Pharmaceuticals
Vutrisiran	TTR	Expression inhibition	Cardiovascular and metabolic disorders	Pre-registration	Alnylam Pharmaceuticals
Fitusiran	SERPINC1	Expression inhibition	Hematology	Phase III	Sanofi
Nedosiran	LDHA	Expression inhibition	Genitourinary system	Phase III	Dicerna Pharmaceuticals
QPI-1007	CASP2	Expression inhibition	Ophthalmology	Phase III	Quark Pharmaceuticals
Teprasiran	TP53	Expression inhibition	Immunology	Phase III	Quark Pharmaceuticals
Tivanisiran	TRPV1	Expression inhibition	Ophthalmology	Phase III	Sylentis
AB-729	HBsAg	Expression inhibition	Infectious disease	Phase II	Arbutus Biopharma
ALNAAT-02	SERPINA1	Expression inhibition	Gastrointestinal and metabolic disorders	Phase II	Alnylam Pharmaceuticals
ARO-HSD	HSD17B13	Expression inhibition	Gastrointestinal	Phase II	Arrowhead Pharmaceuticals
AROANG-3	ANGPTL3	Expression inhibition	Metabolic disorders	Phase II	Arrowhead Pharmaceuticals
AROAPOC-3	APOC3	Expression inhibition	Metabolic disorders	Phase II	Arrowhead Pharmaceuticals
Bamosiran	ADRB2	Expression inhibition	Ophthalmology	Phase II	Sylentis
Belcesiran	SERPINA1	Expression inhibition	Gastrointestinal	Phase II	Dicerna Pharmaceuticals

BMS-986263	SERPINH1	Expression inhibition	Gastrointestinal and respiratory	Phase II	Bristol-Myers Squibb
Cemdisiran	C5	Expression inhibition	Genitourinary system	Phase II	Alnylam Pharmaceuticals
Fazirsiran	SERPINA1	Expression inhibition	Metabolic disorders	Phase II	Arrowhead Pharmaceuticals
JNJ-3989	viral HBV	Expression inhibition	Infectious disease	Phase II	Arrowhead Pharmaceuticals
MT-5745	CHST15	Expression inhibition	Gastrointestinal	Phase II	Mitsubishi Tanabe Pharma
Olpasiran	LPA	Expression inhibition	Cardiovascular	Phase II	Amgen
OLX-101	CTGF	Expression inhibition	Dermatology	Phase II	Hugel/OliX Pharmaceuticals
RG-6346	HBsAg	Expression inhibition	Infectious disease	Phase II	Dicerna Pharmaceuticals
siG-12D-LODER	KRAS	Expression inhibition	Oncology	Phase II	Silenseed
SR-063	AR	Expression inhibition	Oncology	Phase II	Suzhou Ribo Life Sciences
STP-705	PTGS2/TGFB1	Expression inhibition	Oncology and dermatology	Phase II	Sirnaomics
VIR-2218	HBsAg	Expression inhibition	Infectious disease	Phase II	Alnylam Pharmaceuticals
Zilebesiran	AGT	Expression inhibition	Cardiovascular	Phase II	Alnylam Pharmaceuticals

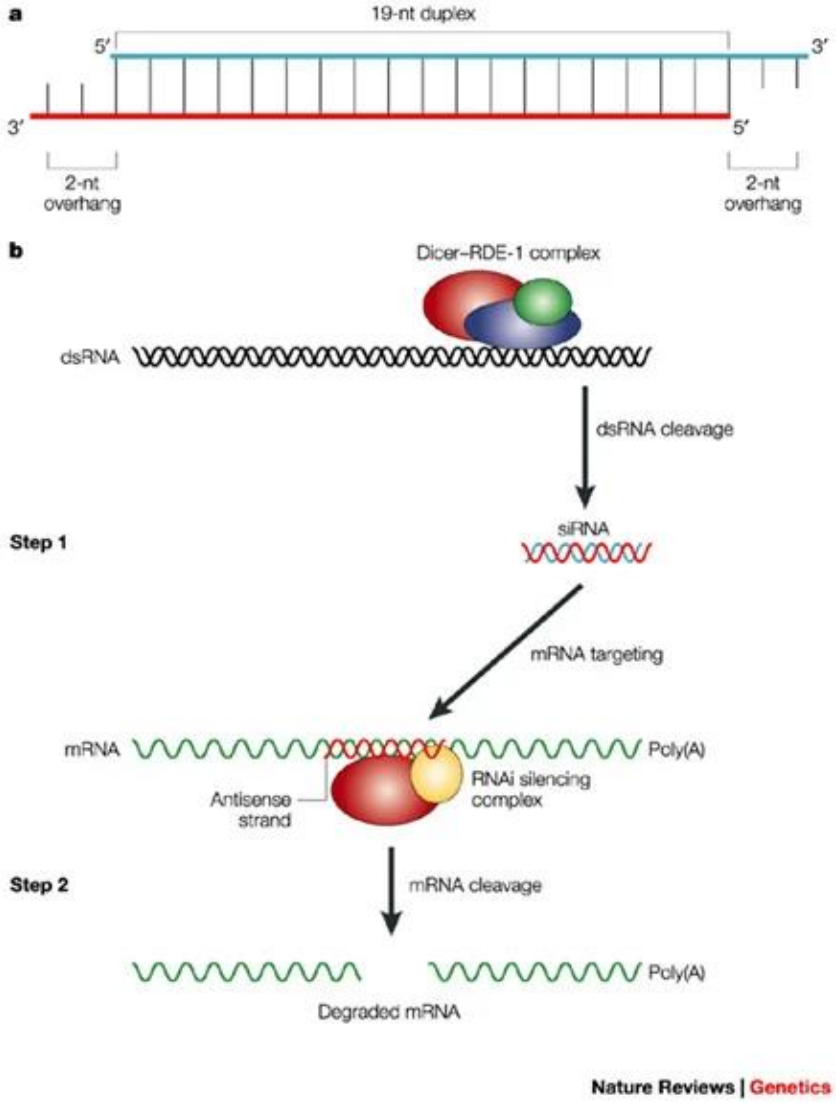

Figure 4. A: Double strand of a 19mer siRNA. B: Mechanism of action for siRNA. Reprint from [48], with permission of Nature Publishing Group ©.

2.3 RNA aptamer

Aptamers are single-stranded oligonucleotides that are designed in defined architectures mimicking monoclonal antibodies, and bind to targets like proteins. Thus, protein-protein interaction can be inhibited realizing therapeutic effects [49]. An aptamers selection process, named Systematic evolution of Ligands by Exponential Enrichment (SELEX), was developed in 1990 by *Tuerk* and *Gold*, and *Ellington* and *Sozstak* [50,51]. Even until today, the SELEX still has been a gold-standard strategy for the generation of aptamers [52]. The conventional SELEX begins with a nucleic acid library containing a random region of the target with 20-60 nucleotides extended by fixed primer regions at both 5' and 3' ends. After the incubation of this randomized library with the target, bound species are partitioned and washed. Next, the desired species will be eluted and isolated. For RNA selections, a reverse transcription is necessary before the amplification via PCR. Followed up by a transcription back into RNA, the "chosen" RNA sequences are ready for the next SELEX round. This selection cycle is repeated several times until the sequence is enriched with the target affinity [52,53]. A brief summary of the SELEX process is visualized in **Figure 5**. Although the fundamental methods of SELEX have not changed for the discovery of aptamers, some critical improvements have been innovated in the way that aptamers can be characterized from the selection process, the target types that can be explored, and the modifications in which aptamers can be applied, expanding the practical applications of aptamers both in vivo and in vitro. In vivo selected aptamers may not be functional in vivo though. Therefore, SELEX based on living animals has been developed as a promising solution. Here, the oligonucleotide library is firstly injected into the animal organism. A target tissue or organ can then be recovered, and the bound oligonucleotide chains are isolated. After the PCR amplification, the SELEX

cycle can be repeated as by classic method for further selection processes. With this, it can be ensured that the chosen aptamer will be compatible with in vivo applications [52,54,55]. As the only FDA-approved aptamer therapeutic, Pegaptanib entered the market in December 2004 for the treatment of noevascular AMD. This aptamer is targeted to the isoform 165 of VEGF, a protein that is responsible for the formation of new blood vessels, one of the reasons for the vision loss associated with AMD. Pegaptanib works as an antagonist to bind VEGF blocking its action leading to reduction of growth of the blood vessels [56].

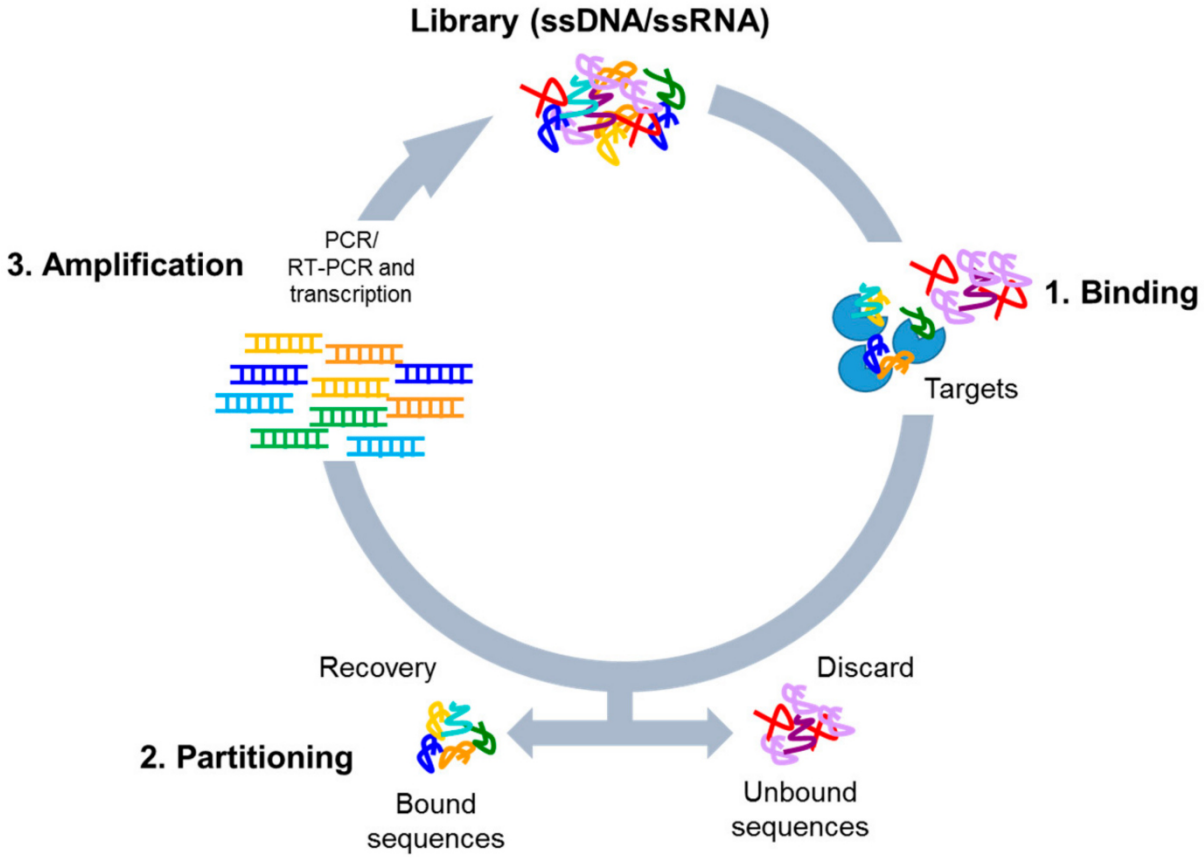

Figure 5. Scheme of SELEX cycle. Reprint from [57], permission granted due to open access.

In comparison to monoclonal antibodies, aptamers benefit from their convenience of generation, low manufacturing cost, little batch-to-batch difference and low immunogenicity [58]. Furthermore, aptamers can be easily modified and adjusted

depending on the therapeutic applications [59]. In general, the structural modifications of oligonucleotide are so important that this will be discussed in a separated chapter coming up.

Despite of its feasibility and flexibility, aptamers also have two main weak points: one is the short half-life of aptamers in vivo, and another drawback is their susceptibility to the hydrolysis of nuclease. Several attempts focusing on either the chemical modification or the conjugation of the aptamer have been published to increase their stability inside human organism [60,61]. But another critical point of aptamer is the toxicity caused by chemical modification or non-specific immune responses. Some of the modified nucleic acids showed strong hepatotoxicity [62]. Also, the formulation of therapeutic aptamers can also be an origin of adverse responses. It has been reported that the PEG moieties lead to serious immune reactions [63]. Further rational designs will be crucial for the future of aptamers as therapeutic class. But the potential of an alternative towards conventional monoclonal antibodies is highly interesting.

3. Structural modification of synthetic oligonucleotides

Synthetic oligonucleotides as gene therapeutics have strongly expanded the possibilities to personalize clinical treatments healing special rare diseases. Still, numerous obstacles at almost all levels from drug design to functional delivery must be overcome to guarantee the safety and treatment efficiency of nucleic-acid-based therapeutics [64]:

- Chemical: adequate half-life and stability must be ensured.
- Cellular: precise targeting of specific cells; ability of entering cells in necessary concentration and crossing biological lipid membranes.
- Immunological: no unexpected, harmful immune response should be induced.
- Clinical: low toxicity, minimal off target affects.

These barriers have been objectives for dedicated research since years. One important strategy is the structural modification of synthetic oligonucleotides. In this chapter, several meaningful approaches will be discussed. I n **Figure 6**, all common structural modifications are summarized and illustrated.

3.1 Chemical modification

3.1.1 Backbone

Non-modified oligonucleotides are linked by phosphodiester bonds which are rapidly cleaved by nuclease attacking [65]. As showed in chapter 2, the usage of suitable sulfurization reagents during the phosphoramidite leads to the synthesis of PS. This modification replaces one nonbridging oxygen of a phosphodiester. The most important advantage of this substitution is that oligonucleotides with PS linkages gain resistance against nuclease degradation [66]. Although PS modifications reduce the binding affinity between the oligonucleotide and its target, it is still a breakthrough

technique that can delay the degradation by a few days [43,67]. Besides of the pharmacological changes induced by PS, the stereochemistry of the oligonucleotides also fundamentally changed. Because of the four different substituents at the phosphorus atom, a new chiral center is obtained leading to two diastereomers: *Rp* and *Sp*. It is reported that PS linkages with the *Sp* configuration are more stable [68]. Furthermore, the performance of siRNA can be remarkably changed by the chirality of PS linkages [43]. Since the number of diastereomers increases by 2^n, this sums up to the formation of about half a million of diastereomeric compounds during the synthesis of a 20-mer. Until nowadays, the majority of the PS modified oligonucleotide is prepared with unselective methods.

In addition, other possibilities to modify the backbone of oligonucleotide to enhance their pharmaceutical properties also have entered the market. Another important approach in this field is the introduction of phosphorodithioate linkages. PS2 linkages are beneficial to increase the affinity between RISC and siRNA [69]. The negatively charged phosphate backbone can also be protected by either methylphosphonate or methoxypropylphosphonate. As a result of this charge neutralization modification, the MOP linkage incorporated at position 2 or 3 from 5'-end of the DNA gap significantly mitigated the hepatotoxicity of ASOs [70]. It is also reported that the negative charge can be neutralized by introducing a peptide nucleic acid. With this modification, the capability to detect certain nucleic acid targets of the oligonucleotides can be improved [71,72].

3.1.2 Nucleobase

Nucleobases are often modified when stronger Watson-Crick base pairing is demanded. Modified nucleobases also lead to higher affinity for the target nucleotides increasing the thermal stability of the duplex formed between the oligonucleotide and

the target. In this way, the activity of the gene-silencing process is enhanced [64]. With the stronger Watson-Crick base pairing, the bonding between the ON and its target RNA becomes so tight that certain splice sites can be hidden, ribosomal assembly will be prevented resulting in inhibition of translation [73]. The tightness of the bonding can also be beneficial to strengthen the 3D structures of ON aptamers [74]. The position 5 of pyrimidines is a frequently selected location for modification [75]. The so called “5-methyl-C” chemistry by attaching a methyl group is a popular strategy for the modification of nucleobases. As described above, base-modifications can intensify the ON-target RNA duplex. This increase of stability is attributed to the stacking of the methyl groups between the nucleobases in the major groove of the duplex. Although, if the substituent in the 5 position becomes too large, the gene silencing process can be negatively affected due to the mismatch of the bulky modification with the RISC [76].

Besides of the “5-methyl-C” chemistry, there are also other possibilities to modify the nucleobases. For instance, the substitution of pseudouridine, 2-thiouridine, N6-methyladenosine, 5-methylcytidine or other base analogs of uridine and cytidine residues are able to make ASOs more resistant towards nuclease degradation [77–79]. It is possible, that the increased affinity of ON-target RNA duplex will lead to undesired off-target effects [64]. This can be reduced by modifying the position 15 of the siRNA passenger strand by introducing a 5-nitroindole leading to strong restriction of its activity, whereas the effectiveness of the guide strand is barely affected. With this strategy, off-target effects can be significantly limited [80]. It is reported that siRNAs containing 5-fluoro-2’-deoxyuridine moieties can suppress targeted gene expression. Furthermore, this modification residue will be released after entering the

cell inducing a series of DNA-damage repair triggering cell death. This can also be considered for siRNA-based cancer therapy [81].

3.1.3 Carbohydrate

Ribose (in case of DNA: Deoxyribose) modifications often are needed to increase the stability against nuclease degradation – the pharmacokinetic half-life can be extended from a matter of days to weeks [82]. The reason for this behaviour is that an electron-withdrawing group on the 2' carbon of ribose can induce the ribose to fold into a conformation which is favourable for duplex formation [83]. Similar as with other forms of modification, increased affinity can also be achieved by carbohydrate chemistry. Hybridization analysis of several 2'-position modifications revealed that not all modifications enhance RNA affinity equally [84]. Via a 2'-*O*-methyl link it is possible to attach a methyl group to the sugar – the mostly utilized chemistry for the carbohydrate modification. Other common modifications include 2'-*O*-methoxyethyl and 2'-fluoro RNA. Highly electronegative fluorine makes the modified siRNAs more readily to adopt a C3'-endo confirmation, providing considerable benefits in binding affinity [67]. Other modification moieties like 2'-*O*-benzyl and 2'-*O*-methyl-4-pyridine were well tolerated when they were incorporated on the guide strand of siRNA in vivo showing comparable activity with the unmodified siRNA in vivo [85]. Additionally, even the whole sugar ring can also undergo modifications resulting in phosphorodiamidate morpholino oligomers. PMOs do not look like classic nucleotides, as the ribose subunit has been exchanged with a morpholine subunit. PMOs are uncharged at physiological pH and are not substrates of RNase H. Therefore, they are used to block RNA splicing or translation [34,86].

3.1.4 Bridging

The sugar residues can also contain modifications which “lock” the nucleotide into its C3’-endo (north) conformation. By bridging the 2’-*O* to the C4’ with a methylene linkage, the duplex stabilization can be strongly increased gaining better affinity of base pairing [43]. This kind of locked nucleic acid has been effectively used in siRNAs and other nucleic acid based therapeutics [87]. Data have shown that the incorporation of LNAs increases the DNA melting temperature up to 8 °C per LNA [88]. Because of the advantages of LNAs, many more bicyclic and even tricyclic analogs, including ethyl-bridged nucleic acids, constrained ethyl nucleic acids and tricyclo-DNA, have been designed and modified into RNA or DNA strands with success [43,89,90]. Tricyclo-DNA has three additional carbon atoms between C5’ and C3’ that enhance binding of the ON to target RNA. The tricyclo-DNA has shown antisense therapeutic potential in mice in the liver and other tissues, such as the kidney and heart [83,88,91]

3.2 Bioconjugation

Apart from chemical modification, another main strategy to modify ONs in order to adjust its property is the bioconjugation. The delivery potential of ASOs and siRNAs can be enhanced through direct covalent conjugation of various moieties that promote intracellular uptake, target the drug to specific cells/tissues or reduce clearance from the circulation [92]. Because its distinct, homogeneous and single-component constitution of molecular entities with precise stoichiometry, bioconjugates are able to be synthesized in high-scaling amount with well-defined pharmacokinetic properties [92]. In the case of siRNAs, conjugation to the 5’ end of the guide strand is often avoided as this terminal phosphate makes problematic contacts with the side chain residues within the RISC for interference activity [93]. Conjugation to the passenger

strand is always preferred so as not to limit the on-target silencing activity of the guide strand, and, not surprisingly, to minimize the off-target effects. A common mechanism of bioconjugates for ONs is the promotion of interactions between the conjugate and its corresponding cell surface receptor protein, leading to internalization by receptor-mediated endocytosis [94]. Classical bioconjugates applicated for ON modification are peptides, aptamers, antibodies, lipids and GalNAc [95–98].

3.2.1 GalNAc

GalNAc is a carbohydrate moiety that binds to the highly liver-expressed asialoglycoprotein receptor 1 with high affinity and facilitates the uptake of ASOs or SiRNAs into hepatocytes by endocytosis [99–101]. ASGR1 is very highly expressed in the liver, and is rapidly recycled to the cell membrane, making it an ideal receptor for effective liver-targeted delivery [92]. A dissociation of the receptor and oligonucleotide conjugate occurs during acidification of the endosome, where the GalNAc moiety is subsequently subject to enzymatic degradation that liberates the oligonucleotide [100,102]. Traditionally, a triantennary GalNAc structure is used as the conjugated moiety, although there are other structural variants [101]. Early structure-activity studies revealed that tetravalent and trivalent ligands exhibit orders of magnitude higher affinity than monovalent and bivalent ASGPR when the spacing is about 20 Å. Thus, trivalent or tetravalent GalNAc moieties are covalently conjugated to siRNA with a proprietary linker structure [95,103]. Supported by GalNAc conjugation, ASO potency was increased by 30-fold in human patients [104]. This tendency makes GalNAc conjugation to one of the leading strategies for delivering experimental oligonucleotide drugs currently in the development, given its high liver silencing potential, small size relative to nanoparticle complexes and low cost of synthesis [92].

3.2.2 Lipid

Lipid molecules have been covalently conjugated to siRNAs and antagomir ASOs to empower the delivery capacity. siRNAs with a cholesterol conjugation to the 3’ end of the passenger strand have been utilized for hepatic gene silencing and to silence myostatin in murine skeletal muscle after systemic delivery [105,106]. It is also reported that siRNAs which are conjugated to vitamin E are able to induce potent silencing in mouse liver. Here, the lipid moiety was conjugated to the 5’ end of the passenger strand of a Dicer substrate siRNA 27/29mer duplex. After endocytosis, the siRNA is cleaved by Dicer so as to generate the mature active silencing trigger and to cleave off the target [107]. The in vivo activity of lipid-conjugated siRNAs depends on their ability to bind to lipoprotein as HDL and LDL in the circulation hijacking the endogenous system for lipid transport and uptake. Pre-assembly between cholesterol siRNAs and purified HDL particles performed stronger gene silencing in comparison to cholesterol siRNAs alone [94]. Also, lipoprotein particle pre-assembly also showed influence on siRNA biodistribution: with LDL, siRNA was exclusively taken up by the

liver. In the case of HDL, siRNA again was primarily taken up by the liver, but also by kidney and small intestine [94].

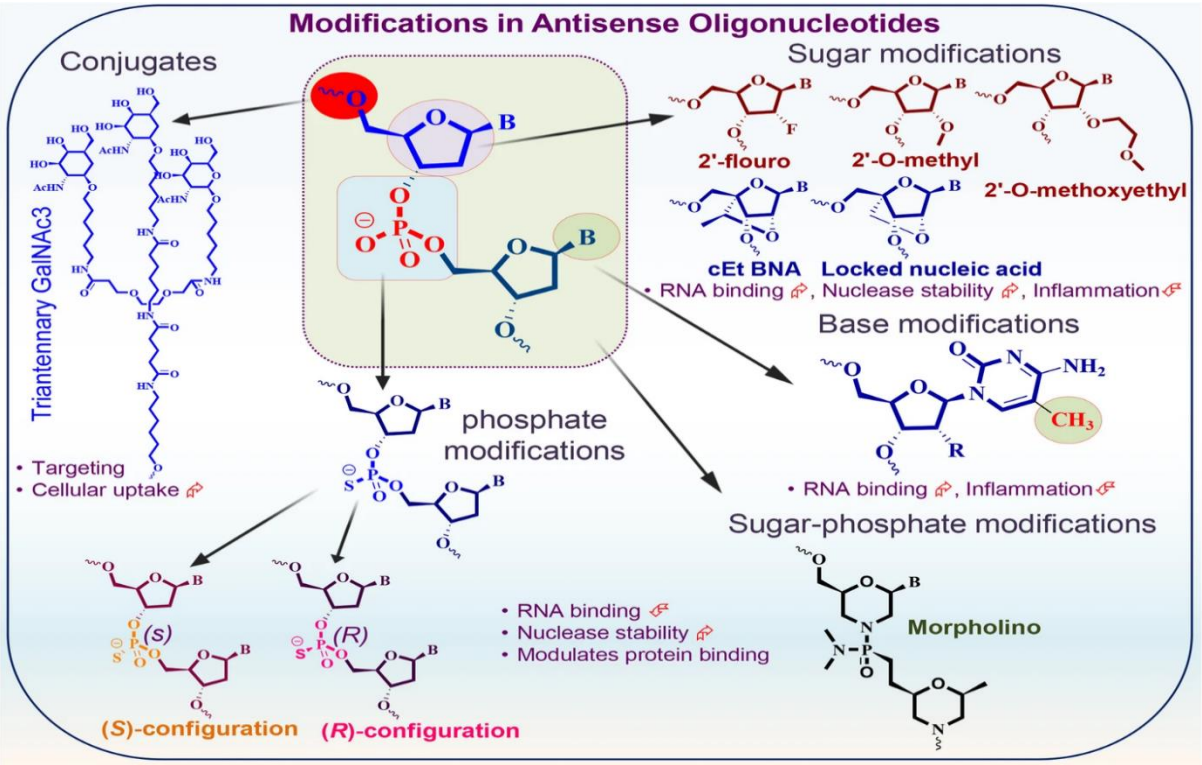

Figure 6. A graphical overview of common chemical modifications for synthetic oligonucleotides. Reprint from [108], permission granted due to open access.

4. Liquid chromatography for synthetic oligonucleotides

As described in the chapters before, the synthesis and chemical modifications of artificial oligonucleotides are complex, which require many manufacturing steps resulting in a plethora of (usually early eluting) impurities [109]. The first group of those impurities are commonly formed due to coupling failures during the synthesis via phosphoramidite coupling. In this way, numerous failure sequences may be produced lacking one or more nucleotides (n-1 mer, n-2 mer etc.), from the target sequence n. In a typical synthesis circle, the reactions start at the 3' end and proceed to completion at the 5' end. Because of that fact, the failure sequences formed under these mechanisms will have nucleotides missing from the 5' end terminating in a hydroxyl group [110]. Another major mechanism leading to impurities is the abasic cleavage originated from depurination [111]. The possible impurity species produced under this mechanism contain the original 5' end, but have lost its original 3' end at the purine position and may contain various 3' terminal groups [110]. Further familiar impurity species are phosphodiester impurity in PS ONs due to incomplete sulfurization and possible side reaction related to the reagent used [112]. Similar as by depurination, other different types of impurities can occur at the base residues, such as deamination and oxidation at guanine. For conjugated oligonucleotides like GalNac constructs, it is possible that one of the GalNAc sugars can be lost because of hydrolysis or ammonolysis [113]. The need to identify this wide spectrum of impurity species has increased constantly. Both regulatory authorities and pharmaceutical industries are demanding for sufficient analytical methods to face this challenge. In that regard, LC-MS has been proved as capable and reliable tool for oligonucleotide analysis. In the following chapters, different approaches of liquid chromatography for ON separation will be discussed.

4.1 Ion-pair reversed liquid chromatography

Owing to their unique physiochemical properties, LC-MS method development for ONs can be challenging. ONs are more polar than other biomolecules with similar molecular weight due to their phosphate backbone leading to extremely difficult retention on conventional reversed-phase column [114]. Over the last 20 years, the use of IP reagents has been the solution to compensate the lack of retention power [112]. The IP agent is an ion species selected so that it has an opposite charge to the ONs and is able to form a molecular association with it allowing the bonding to stationary phase (C18) [115]. A scheme of the interaction mechanism is visualized on **Figure 7**.

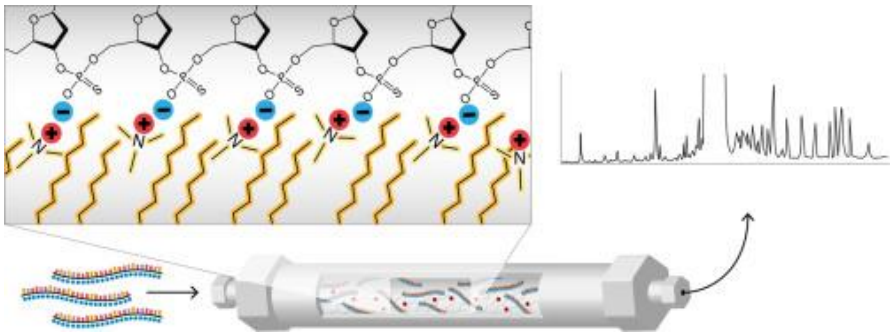

Figure 7. An illustration to describe the interactions between the stationary phase, ion-pairing reagent and the oligonucleotides. After the adsorption of ion-pairing reagents with the stationary phase, a retention of ONs has been enabled. Reprint from [116], permission granted due to open access.

Gilar and *Neue* investigated various chromatographic parameters to achieve maximal peak capacity for model 15- to 60-mer ONs. Surprisingly, a limited gain in resolution was evidenced when using longer columns, which was not proportional to column length. To reach higher resolution, a suitable adjustment of the gradient slope seems to be much more crucial and effective [117,118]. Furthermore, the particle size should be minimized to reduce undesired peak broadening effect because of the slow mass transfer of ONs [119]. Considering of pore size, *Close et al.* compared RPLC silica-

based columns packed with porous particles and concluded that pore size of the packing materials should be matched to the analytes. Shorter ON strands were better separated on columns with smaller pore size and vice versa [120]. Besides of C18, which is not surprisingly the predominantly used stationary phase for IP-RPLC, C4, C8, phenyl, fluoro and cyano stationary phases have been also possible column candidates [121]. Nevertheless, chain length only has a limited effect on the separation power of ONs. It has been reported that the use of C4 over C18 columns did not show significant advantages for the separation of common deaminated and N-1 impurities from the original ON strand [112,121,122]. Phenyl-based stationary phases were used for the separation PO/PS siRNAs from lipids [123]. Due to additional pi-pi interactions, stronger retention between siRNAs and lipids were observed. In this work, we also introduced an aromatic-rich stationary phase for the separation of siRNAs, even without the presence of IP, please see **Publication III and IV**.

As mentioned above, IP agents must be added in the mobile phases to implement retention of ONs on RPLC columns. Commonly used IP agents are listed in **Table 3**. “100 mM TEAA” has been frequently used as “standard condition” for IP-RPLC in the past, although the high concentration is problematic for ESI-MS detection because of pronounced ion-suppression [124]. This effect was attributed to the preferential evaporation of TEA, leaving acetic acid in the droplets and reducing the ionization efficiency of the dissolved ONs [112,125]. To overcome this drawback, *Apffel* proposed the use of HFIP in 1997 [125]. This discovery has fundamentally changed the IP-RPLC of ONs, even until today. IP-RPLC with HFIP is still the golden standard method for ON separations. Due to the lower boiling point of HFIP in comparison to acetic acid, the ionization process can be significantly increased leading to 20- to 100-fold stronger MS signal intensity [126]. HFIP has not only proven to be more MS

friendly, several studies also demonstrated that a combination of TEA with HFIP was also more efficient for the chromatographic separation of ONs compared to TEAA [112]. A notable obstacle using HFIP is its insolubility in acetonitrile, thus limiting the choice of the organic mobile phase to protic solvents such as methanol.

Despite of its advantages, IP-RPLC with HFIP still uses TEA. As like all the other alkylamines, TEA will lead to permanent decontamination of ionization sources. Therefore, MS instruments must be dedicated limiting method development. To avoid the usage of IP, other LC approaches for ON separation are on the rise.

Table 3. Overview of commonly used IP reagents and mobile phase additives, respectively [127].

Name	Accurate MW (g/mol)	Formula	Boiling point (°C)	Log P	Log D
Acetic acid	60.021	$C_2H_4O_2$	118	-0.223	-3.753
Hexafluoroisopropanol	168.001	$C_3H_2F_6O$	58.2	1.451	-1.545
Diethylamine	73.089	$C_4H_{11}N$	55.5	0.521	-2.721
Triethylamine	101.12	$C_6H_{15}N$	89.3	1.261	-2.241
Diisopropylamine	101.12	$C_6H_{15}N$	84	1.354	-1.888
Diisopropylethylamine	129.152	$C_8H_{19}N$	127	2.094	-1.408
Butylamine	73.098	$C_4H_{11}N$	78	0.698	-2.335
Dimethylbutylamine	101.12	$C_6H_{15}N$	106	1.514	-1.987
Tripropylamine	143.167	$C_9H_{21}N$	156	2.828	-0.673
Dibutylamine	129.152	$C_8H_{19}N$	159	2.455	-0.787

Hexylamine	101.12	$C_6H_{15}N$	131	1.588	-1.446
Dicyclohexylamine	181.183	$C_{12}H_{23}N$	255.8	3.406	0.164
Octylamine	129.152	$C_8H_{19}N$	176	2.477	-0.556
Dihexylamine	185.214	$C_{12}H_{27}N$	193.5	4.233	0.991
Tributylamine	185.214	$C_{12}H_{27}N$	214	4.162	0.661

4.2 Ion-pair free reversed liquid chromatography

The usage of alkylamines leads to persistent contamination of the ion source. Consequently, the strong background signal of the residual IP agents will negatively affect the detection limit for other target analytes in subsequent use of the non-dedicated mass spectrometers for other applications. Since the removal of IP agents is time consuming and not always successful, an abandonment would be favourable. The most frequently used method to that regard is the HILIC which will be discussed in chapter 4.3. Here, the ion-pair free RPLC is going to be presented. Since the IP-RPLC has been dominating in the last two decades, absence of IP agents for RPLC of was never seriously considered as an alternative strategy. The only notable publication in the history was from 1979, when *McFarland* and *Borer* used a C18-based silica as stationary phase to separate homologous series of the mononucleotide oligomers with ammonium acetate only. Without any IP agents in the mobile phases, this method showed sufficient retention- and resolution power to distinguish the various homo-oligonucleotide mixtures containing 20 oligomers (from 1-mer to 20-mer) [128]. Besides of this attempt, no further approaches in this direction have been undertaken ever since. Nevertheless, the reasons for this trend are obvious. The separation of minor complex homologous mixtures by *McFarland* could only be

considered as a model attempt. Real oligonucleotide samples are much more complicated, of higher molecular mass combined with higher polarity. Without IP agents, the lacking retention power could lead to reduced selectivity. In view of this fact, the success of HFIP/TEA has been so overwhelming that a focus on method development of IP-free RP for ONs has not been pursued.However, the situation changed, both HPLC instruments and HPLC columns have been remarkably improved. With the new generation of techniques, it is reasonable to believe that continuous efforts for IP-free RP might pay off. And indeed, in this work, we successfully discovered numerous approaches for oligonucleotide separation using ammonium acetate or formate as buffer. In **Publication I and II**, an Agilent ZORBAX Eclipse Plus C18 column was used in a 2D-LC setup as online desalting tool. With this stationary phase, DNA oligonucleotides were retained with 10 mM ammonium acetate as buffer and methanol as organic modifier. Meanwhile, highly polar phosphate residues from the first dimension were eluted at void time enabling a free choice of LC modes in ^{1}D including MS-incompatible conditions. The special chemistry of doubly endcapping the packing material strongly leads to maximum deactivation of the silica surface reducing secondary interactions. Nevertheless, a retention of ONs was still possible. And since the surface activity is minimized, the obtained peaks of the ONs were superiorly sharp which was beneficial for upcoming MS-detection.

As briefly mentioned above, another different stationary phase which contains a plethora of π-systems has been tested under IP-free RP conditions. In **Publication III and IV**, this stationary phase based on polybutylene-terephthalate (PBT) selector ligand was able to separate a series of impurity products from two complementary siRNA strands. Due to its unique chemical structure, the ONs could be retained without

IP agents. A mix of pi-pi interactions, dipole interactions, hydrogen-bonding and lipophilic interactions created sufficient retention power providing surprising selectivity.

Eventually, in **Publication V**, a cholesterol-based stationary phase was also successfully applied for impurity profiling of siRNAs without the presence of any IP agents. As with PBT, the mixed nature of this selector ligand established retention of the ONs under RP conditions.

4.3 Hydrophilic interaction liquid chromatography

Nowadays, HILIC has been proven as capable separation tool for the analysis of polar compounds. The beginning of HILIC is marked by *Alpert* in 1990 when he succeed separating oligothymidylic acids (but also peptides) with different chain lengths on a polyhydroxyethyl A column using a TEA/phosphate buffer [129]. The final mechanism of HILIC is still not fully explored, the consensus is that retention occurs primarily due to the partitioning of the analyte between the organic-rich mobile phase and aqueous layer on the surface of the stationary phase. Furthermore, electrostatic and hydrogen-bonding interactions may also be present, the postulated mechanism is illustrated in **Figure 8** [130]. Related to the LC-MS detection of ONs, the most important benefit of HILIC is the higher amount of volatile organic solvent in the mobile phase providing higher MS intensity. Besides of that, the absence of IP agents is possible to retain ONs due to the mechanism described above. In the last past years, several attempts using different HILIC stationary phases (amide-based, zwitterionic, diol) to separate target ONs (RNA-based, DNA-based, modified etc.) were reported [131–134]. Numerous groups have reported about different chromatographic factors which do have impact on ON analysis. Regardless of salt types and concentrations, a general HILIC retention order was observed: duplexed RNA > DNA oligonucleotide > PS-modified DNA oligonucleotide [135]. PS modifications showed the lowest HILIC

retention in this series because of the higher hydrophobicity comparing to phosphate backbone, with the displacement of oxygen with the less electronegative sulfur [136]. On diol-column, weaker elution strength of AF in comparison to AA was indicated, since the analyte retention is more attributed to the pH rather than ionic strength of the mobile phase [132,135]. On some amide-column as BEH Amide of Waters, this trend is opposed: AF-containing mobile phases showed slightly stronger elution strength because of its stronger character as counterion. As far as the ion strength concerns, the retention factor k elevated with increased salt concentrations, consistent with previous findings made on various HILIC stationary phases [132,137,138]. This observation can be interpreted as a sign of dominating solvation/distribution process for the retention mechanism which is responsible for HILIC [130]. Higher salt concentrations lead to expansion of the aqueous layer adsorbed on the stationary phase surface, more solvated salt ions accumulate in this layer will make it “thicker” causing higher retention power.

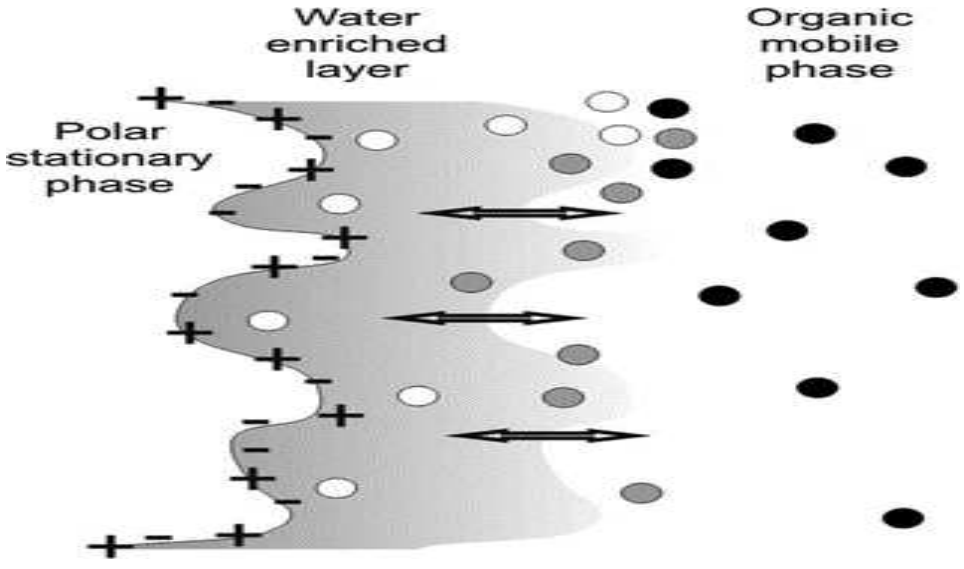

Figure 8. Overview of HILIC principle. White cycle: hydrophilic analyte; grey cycle: semi-hydrophilic; black cycle: hydrophobic analyte. Reprint from [139], with permission of Springer Nature ©.

The effect of pH values is negligible for HILIC. Lower pH value causes peak tailing, whereas higher pH value leads to more symmetrical peak profile. Although, the alterations of mobile phase pH did not have obvious effects on LC peak resolution

To obtain higher peak capacity and enhanced resolution power, respectively, higher column temperatures are beneficial due to reduced non-specific interactions that may arise from internal hydrogen bonding [140]. On the other hand, higher column temperature also decreases UV responses during the detection [141]. Additionally, higher column temperature could result in reduction of the water layer, thereby modulating the partition of the analytes and consequently the retention behaviour [142]. Column temperature is a sensitive factor which must be taken in account carefully depending on the analytical targets.

4.4 Mixed-mode liquid chromatography

ON are complex biomacromolecules consisting of multiple functional moieties and domains like pentose, dipolar carbonyl groups, aromatic systems and all the possible modifications. Because of this structural inconsistency, it is obvious that a single retention mechanism would not generate best selectivity to achieve maximal resolution power. A combination of multiple retention modes to cover as many ON functional groups as possible could be beneficial. For this reason, MMC with two and more dominant retention mechanisms also has been considered as valuable strategy for ON separation. The first attempt was reported by *Crowther et al.* from 1983. Here, both octyl- and 3-chloropropyldimethylmono-chlorosilane ligands were bonded, after which the chloro groups were converted into quaternary amines by nucleophilic substitution with benzyldimethylamine. The resulting reversed-phase anion exchanger

required high concentrated phosphate buffer as counter ion for proper elution. Despite of this harsh elution condition, the separation power was improved in comparison to conventional IP-RP or AEX alone [143]. Due to the negative charges of ONs, the usage of AEX is understandable. In combination with a hydrophobic linker, this kind of mixed-mode stationary phase has been the favourite choice for the separation of ONs. *Biba et al*. used various commercial MMC columns based on this constellation (C18+anion exchange moiety) to separate short RNA oligonucleotides. One of the analysed mixtures was composed of RNA ONs which only differed in the sequence of two nucleotides. With AEX and IP-RP alone, these isomers were not able to be separated from each other. For IP-RP, the hydrophobicity of these isomers was too similar. For AEX, the overall charge-charge interaction of the isomers is nearly identical. But by using the mixed-mode stationary phase, both retention mechanisms were activated causing significant change of selectivity. With 2 M NaCl as counterion, the isomers were separated with well-formed peak shape. An adjustment of counterion by using 200 mM TEAA diminished the resolution since the peaks become much broader due to strong ionic interaction [122]. *Zimmermann et al.* assembled a mixed-mode column with surface-bonded *N*-11-undecenyl-3-aminoquinuclidine based on 5 µm thiol-silica. It features a lipophilic alkyl strand for hydrophobic interaction, a quinuclidinium moiety for ionic interactions and polar embedded groups for polar retention increments, most notably an amide group for hydrogen bonding. The interaction mechanism of MMC is illustrated in **Figure 9** on the base of this stationary phase. Above pH 7, the quaternary nitrogen at the centre of the quinuclidinium moiety will be deprotonated. Under this circumstance, combined with phosphate buffer as counterion and acetonitrile as organic modifier, N-1, N-2 and N-3 standards representing the most relevant impurities in synthetic ONs were eluted and separated.

By increasing the particle pore size from 100 Å to 200 Å, the surface area was lowered by factor of about 2 per unit mass enabling the reduction of necessary buffer concentration by a factor of 2. Nevertheless, selectivity and resolution were not compromised by the reduction of the surface area, because the selector coverage per square meter was essentially identical [144].

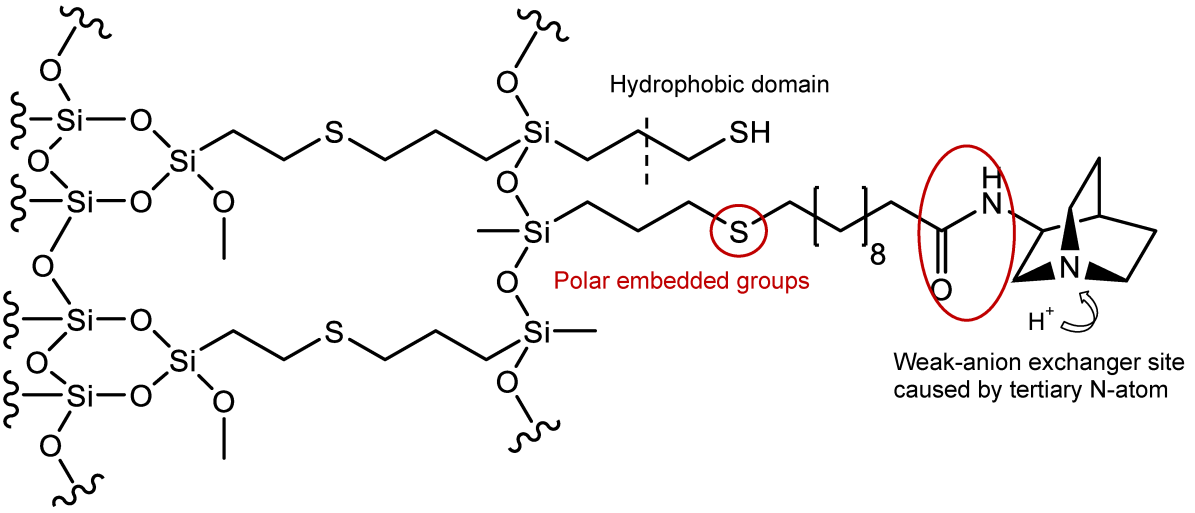

Figure 9. Chemical structure and interaction sites of the stable-bond polymeric reversed-phase/weak anion-exchange mixed mode (Poly-RP/WAX) stationary phase. Reprint from [145].

MMC has been proved as realistic alternative for the separation of ONs showing useful and interesting properties. But because of the strong ionic character, most of the MMC stationary phases must be operated under extremely harsh elution conditions such as highly concentrated bromide, chloride or phosphate salts which are definitely MS-incompatible since they will directly precipitate inside the ion source. This has been the limiting factor of MMC for the analysis of ON. To overcome this, 2D-LC system can be considered as a solution implementing a further separation dimension working under MS compatible conditions. The chromatographic strength of MMC will be remained and MS detection becomes possible. This and more about 2D-LC in general will be discussed in the next chapter.

5. Two-Dimensional Liquid chromatography for synthetic oligonucleotides

2D-LC is a versatile tool to deal with complex analytes by increasing the peak capacity significantly within an acceptable time [146]. Since the first trials in the 1970s, the technique of 2D-LC has been further improved and become more and more commercially mature. Meanwhile, 2D-LC is emerging as one of the most exciting and essential tools for efficient, high quality biopharmaceutical analysis - including synthetic oligonucleotides [147].

As seen by MMC, multiple retention mechanisms are beneficial for the separation of ONs due to its complex structural composition. With 2D-LC, it is possible to target on different regions of interaction in both dimensions by combining two complementary chromatographic mechanisms leading to enhanced selectivity. To characterize the complementary behaviours of stationary phases, *orthogonality* can be calculated as quantitative parameter in various ways with obtained chromatographic results. This will be discussed in chapter 5.3. Complementary separation mechanisms can be combined in different 2D-LC modes which are presented in chapter 5.1. Although, a combination is also not always possible, since certain constellations are not compatible to each other. Sometimes, this “mismatch” can be compensated via 2D modulations. This technical aspect will be shown in chapter 5.2. Finally, some 2D-LC applications examples for ONs are going to be briefly discussed in chapter 5.4.

5.1 Different Modes

In general, there are two main categories of 2D-LC separation: offline and online separations. By offline 2D-LC, fractions of ^{1}D effluent are collected in containers like vials or well plates, and transferred to a second separation later. For online

approaches, effluents from the first dimension are storage in a sample loop which is part of the 2D-LC system such that the fraction never leaves this flow path before being injected into the ^{2}D. Here, we want to focus on the online separations.

The basic idea of 2D-LC is to combine two different chromatographic separations aiming on two different properties of the analytes (e.g. size vs charge). Today, this concept can be straightforwardly executed as illustrated in **Figure 10**. It visualizes a contemporary 2D-LC system consisting of two “separated” 1D-LC systems which are connected by an interface – in this case, a 10-port / 5-position valve.

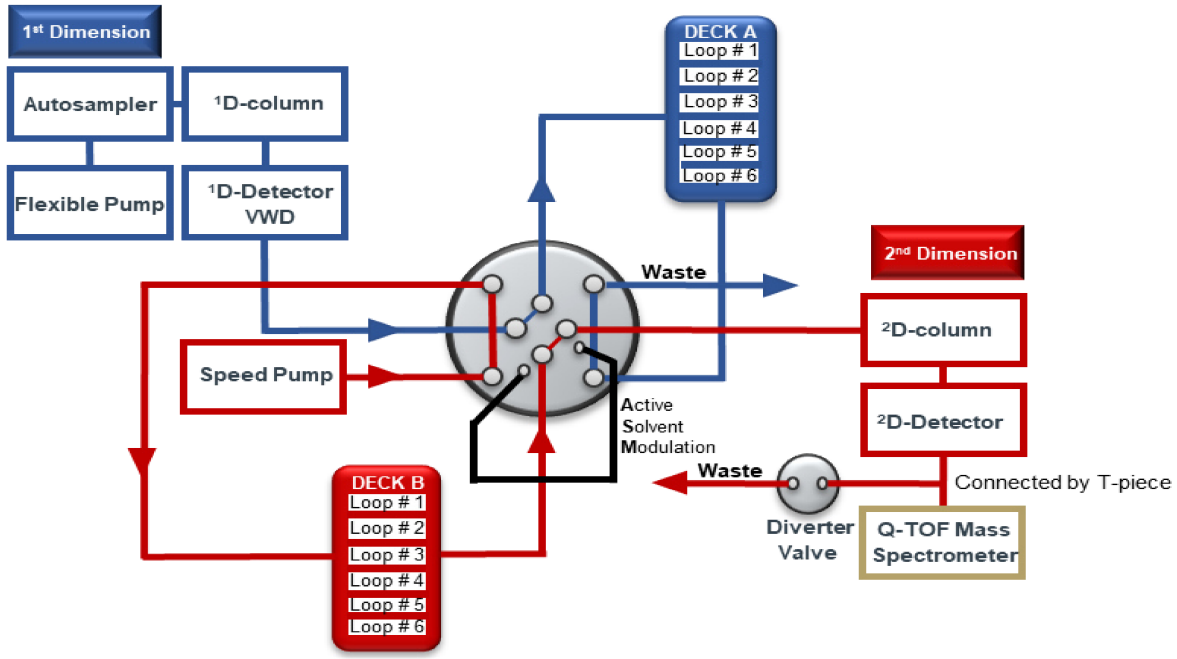

Figure 10. A conventional instrumental setup of a 2D-LC system. Reprint from [145].

2D-LC valve is the key component of the whole 2D-LC system conducting its flow path by valve switches between 2 positions. As illustrated in **Figure 11**, two positions are available to direct the flow path. In position A, the effluent from ^{1}D column flows through the sample loop fixed to the valve, and the outlet of the flow path is connected to waste. When analytes of interests are about to exit the waste-side, the valve is rotated to position B connecting the sample loop to the ^{2}D flow path leading to displacement of the collected fraction of ^{1}D effluent into the ^{2}D column. There are

different modes to transfer “analytes of interests” via 2D-LC which will be described as follows. A graphical summary of those modes can be found in **Figure 12**.

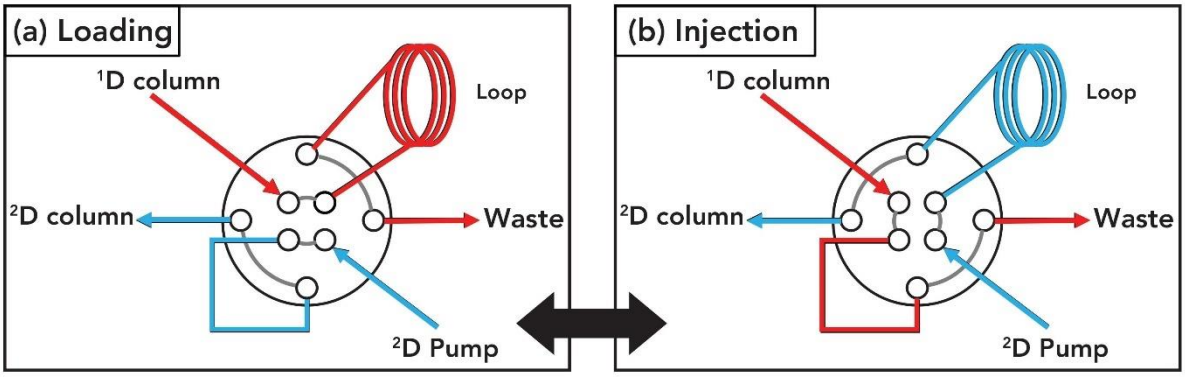

Figure 11. Visualization of 2D-LC flow paths directed by a commonly used 2D-LC valve. Reprint from [148], permission granted by Multimedia Pharma Sciences, LLC..

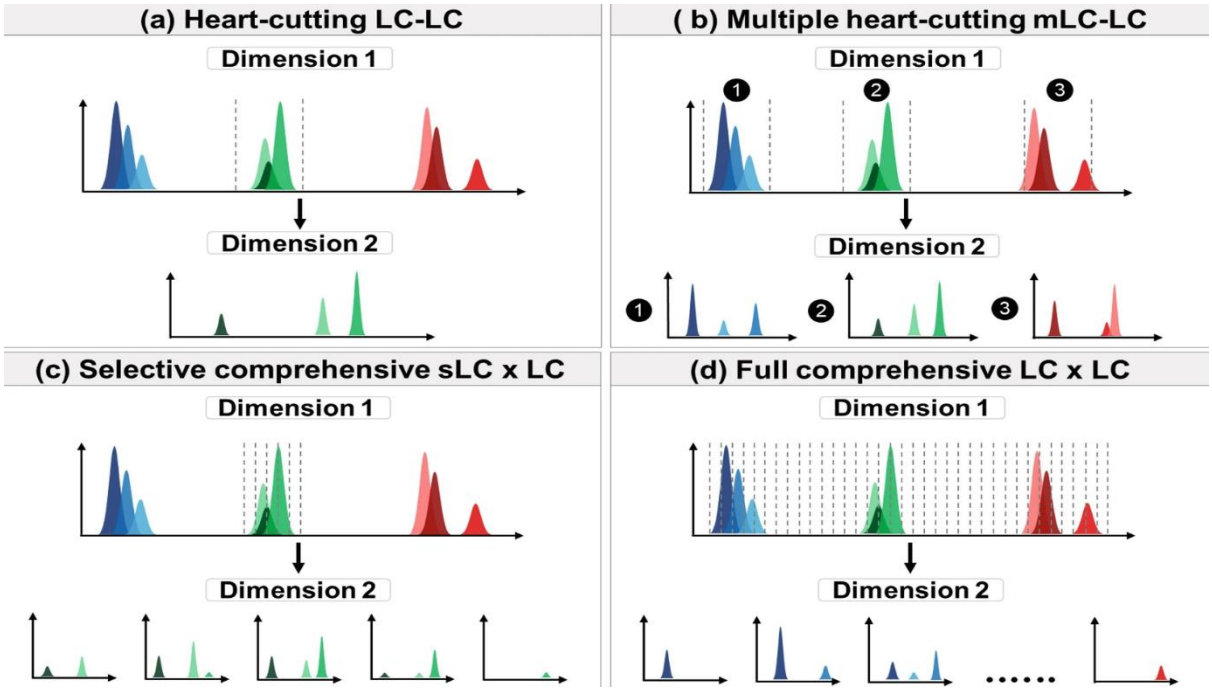

Figure 12. All four possible 2D-LC modes in graphical depiction. A: Heart-cutting; B: Multiple heart-cutting; C: selective comprehensive; D full comprehensive. Reprint from [149], with permission of Springer Nature ©.

Single Heartcut 2D-LC (*LC-LC*)

Here, a single fraction of ¹D effluent containing the particular analytes of interest is transferred into the ²D for further separation or, as mentioned above, for “desalting” to

remove undesired buffer components (see **Publication I, II**). LC-LC is the simplest mode of online 2D-LC, both in terms of execution and interpretation of the results [150].

Multiple Heartcut 2D-LC (*mLC-LC)*

Mechanistically identical to LC-LC, mLC-LC is needed if several peaks of particular interest eluting in different regions of the ^{1}D separation are transferred to a ^{2}D and separated by a complementary retention mechanism. Theoretically, if the analytes elute in parts of the ^{1}D separation that are very far apart in time, simply repeating the single heartcut operations will be sufficient. Although, if the regions of interest become closer in time, there will be no sufficient time to complete the ^{2}D separation of the ^{1}D fraction before the upcoming fraction from ^{1}D must already be collected. To overcome this, *Zhang* and co-workers developed an advent of LC-LC: multiple heartcutting 2D-LC [151]. The main idea of mLC-LC is to temporarily store the ^{1}D effluents in a sampling loop or sorbent cartridge until the ^{2}D separation of the prior ^{1}D effluent fraction is finished. The biggest advantage of mLC-LC is its straightforward implementation, greater flexibility in method development and relative independence of ^{2}D separation speed.

Selective Comprehensive 2D-LC (*sLC×LC*)

Although mLC-LC is very versatile and straightforward in its method development, there is a major drawback caused by limited coverage of the ^{1}D separation for ^{2}D analysis. The problem of mLC-LC is that not the entire chromatogram is covered. This is solved by full comprehensive LCxLC, however, is technically more challenging to implement. However, often it is not necessary to cover the entire chromatogram. For example, if only a critical part of a chromatogram is of particular interest, e.g. a main API peak under which minor impurities might be covered, comprehensive sampling of

a particular part of the 1D chromatogram is sufficient and easier to implement with a multiple heartcutting interface (see Fig 10). For this propose, *Stoll* developed the sLC×LC approach in 2012 [152]. sLC×LC is an effective way to fractionate a specific part of the ^{1}D chromatogram containing analytes of interest into several small adjacent fractions rather than a single heart curt of a specific peak (see **Publication IV, V**, **Figure 13**). For example, if a small impurity is coeluted in the tailing edge of a main API peak, a single heartcut taken in the peak maximum would not detect this impurity in the ^{2}D. If the entire peak is sampled by a series of adjacent cuts this impurity would be detected on at least one of the sampled fractions. Selective comprehensive LC×LC is therefore valuable for impurity profiling of APIs.

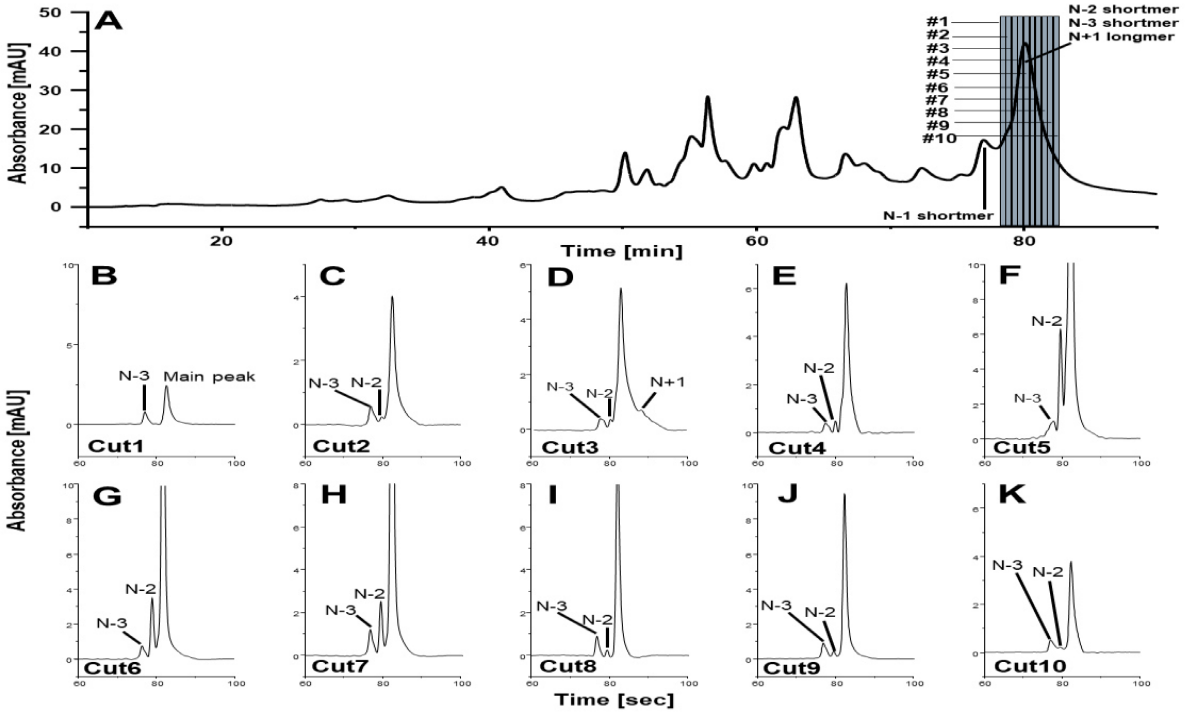

Figure 13. The 1D UV chromatogram and the UV-chromatograms of the selective comprehensive 2D-LC experiment for the antisense of Patisiran. Reprint from **Publication IV** [153].

Fully Comprehensive 2D-LC (*LC×LC*)

In the case of LC×LC, a comprehensive profile of the analyte should be obtained. The ^{1}D effluent will be fractionated at regular intervals across the entire part of the ^{1}D separation. With LC×LC, the sampling of the first separation is unbiased and can be enabled with minimal information about the ^{1}D peak pattern. However, the LC×LC method development is much more challenging and time-consuming in comparison to heartcutting approaches because the ^{2}D separation time for each fraction of ^{1}D effluent is directly linked to the rate at which the ^{1}D is sampled leading to difficult interdependencies between the conditions used for the ^{1}D and ^{2}D separations. A specific problem arising from this interdependency is the undersampling problem. Analytes, which were separated by the ^{1}D column are collected in a single fraction of the effluent and mixed back together upon transfer to the ^{2}D separation. If the ^{2}D column is not able to separate them again, the resolution will be lost.

5.2 Incompatibility and modulation

As described in the chapter above, the key process of 2D-LC is the transfer of ^{1}D effluent into the ^{2}D. This can cause “incompatibility issues”. For both LC-LC and LC×LC, the order in which the both dimensions are combined is crucial, since the ^{1}D effluent detrimentally affects the ^{2}D separation when incompatible solvent systems are combined [154]. The worst-case scenario would be a complete immiscibility between two mobile phase pairs which is easily avoided with common sense. Much more challenging are the more-subtle incompatibilities occurring during the method development. A possible factor which can lead to incompatibility issue is the mismatch of viscosity between two solvent systems. Here, a low viscosity ^{2}D mobile phase can

penetrate a high-viscosity injection plug at the 2D-LC interface. This effect is known as viscous fingering and cause peak deformation or peak splitting [155].

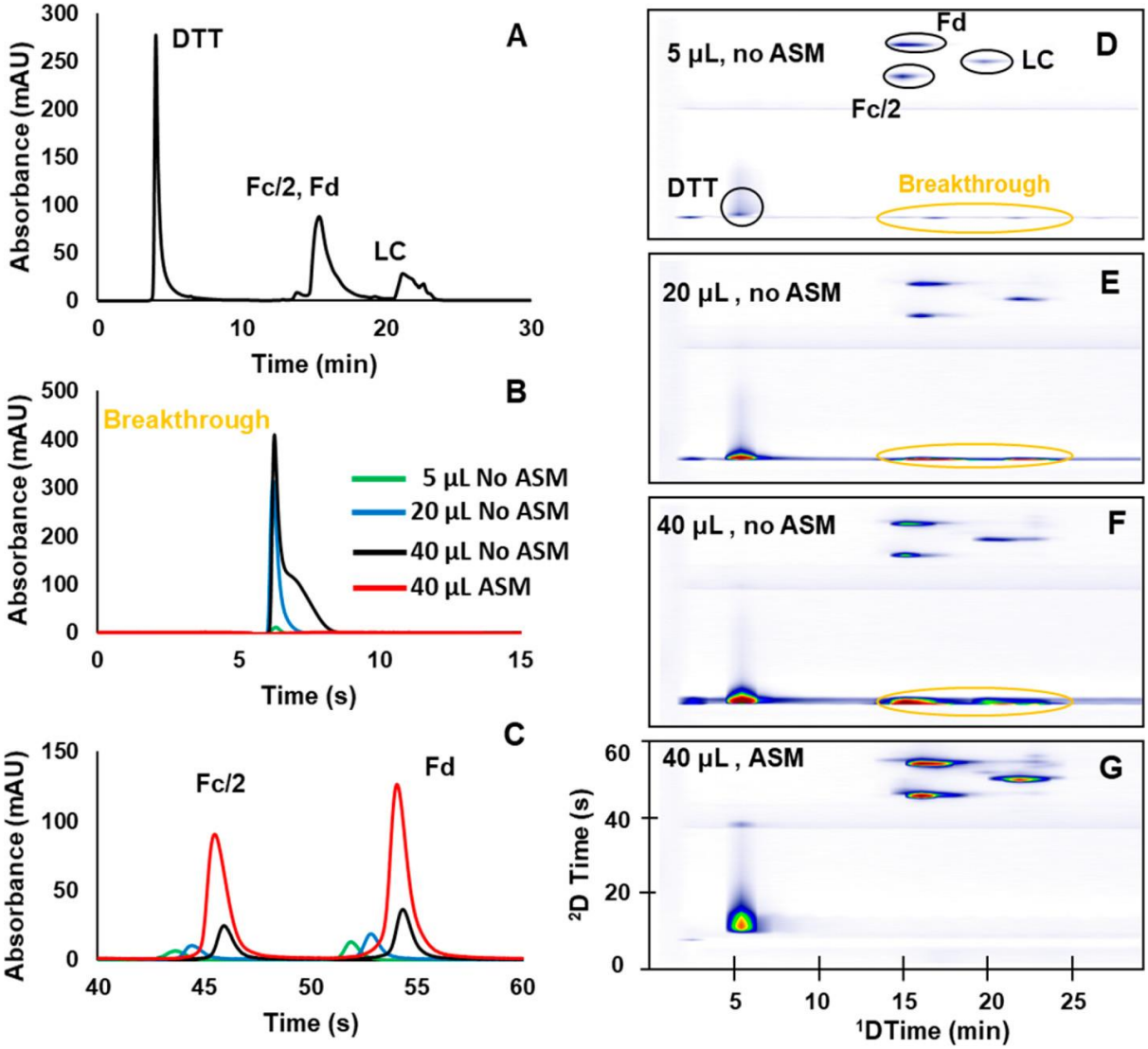

Figure 14. The results of 2D-LC experiments for therapeutic antibodies published by *Guillarme et al.* [156]. On B, C, D, E, F, breakthrough effect at the beginning of the ^{2}D run are clearly indicated which was suppressed by the usage of ASM. Reprint from [156], with permission of American Chemical Society ©.

Another very relevant source for incompatibility issue is the mismatch of solvent strength between two dimensions. According to some reports, this is one of the most commonly occurring problem in most 2D-LC applications [154]. This mismatch arises if the ^{1}D effluent is a strong injection solvent in comparison with the ^{2}D eluent and

phase system, respectively. Hence, the retention mechanism in the second dimension can be disturbed or interaction of the analyte strongly weakened that no retention will be possible. This “breakthrough” effect will lead to immediate peak elution with the dead volume and the real peak at the expected retention time will become much smaller after ^{2}D detection. Such a “breakthrough” is visualized in **Figure 14**.

Solvent mismatch can also be problematic for the lifetime of used ^{2}D columns. For IEX, high concentrated salt buffer and critically high pH values are commonly used. Both circumstances are dangerous for conventional ^{2}D reversed-phase separation because silica-based columns will rapidly degrade under these conditions [157].

In order to achieve optimal separation performance, incompatibility issues must be avoided. Generally, this is addressed by making modifications to the modulation process. Instead of “normal” valve switches between position A and B for effluent transfer, some “actions in-between” can be implemented. This kind of active modulation can significantly reduce incompatibility issues and also lead to a concentration of the analyte band prior to injection in the second dimension, thus increasing the detection sensitivity. There are a few techniques to realize active modulation, here, the *active-solvent modulation* is going to be described in details due to its widespread application.

ASM was firstly reported by *Stoll et al.* in 2017 [158]. The mechanical concept of ASM is illustrated in **Figure 15**. For this approach, two ports are added to a typical 8-port / 2-position valve used as 2D-LC interface, along with a bypass capillary. Consequently, with these additional ports, two rotational positions are added, too. In position 1 and 3 as shown on **Figure 15**, all of the ^{1}D effluent passes through one of the loops and all of the ^{2}D mobile phases passes through the other loop. Thus, previously collected ^{1}D

effluent were transferred into the ^{2}D column. With the new additional positions 2 and 4, the flow from the ^{2}D pump is split into two parts, one goes through the loop and another one bypasses the loop acting as a diluent for the transferred fraction from the ^{1}D effluent. The chromatographical benefit is visualized in **Figure 14B** and **14G**. With increasing transfer volume from the ^{1}D, ASM was necessary to avoid breakthrough effects. In consequence of that, Fc/2, Fd and LC effluents from the first dimension were all sufficiently retained and separated in the second dimension.

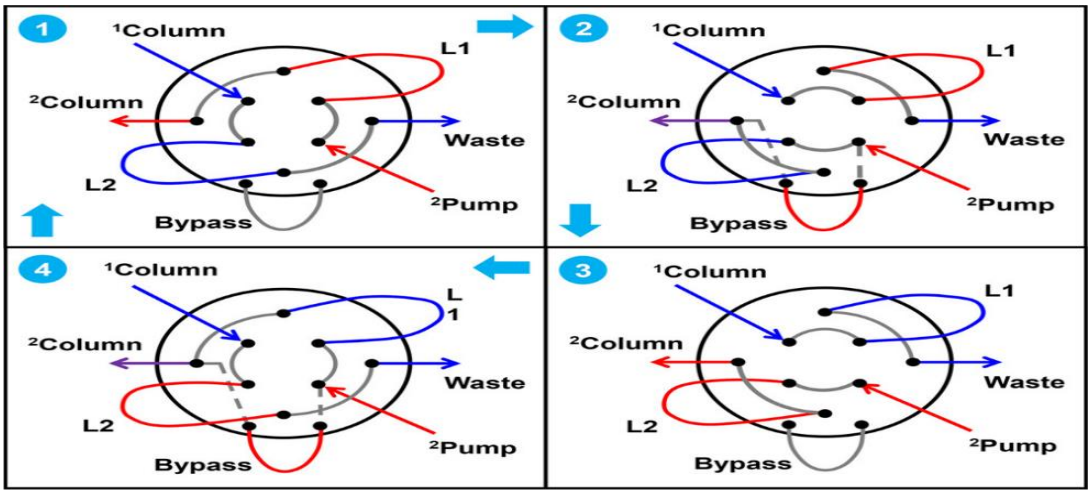

Figure 15. Four different valve configurations of ASM. Reprint from [158], with permission of American Chemical Society ©.

Another popular active-modulation strategy is the usage of trapping columns. Typically, guard columns containing a stationary phase similar to that of the ^{2}D are used as trapping columns. Firstly, reported by *Vonk et al.*, this technique has been referred to as SPAM [159]. As the ^{1}D effluent is sampled by the modulator, the analytes of interests will be trapped in the guard column, whereas the ^{1}D solvent directly leaves the system into waste. After the valve switching, the trapped analytes will be eluted by the ^{2}D mobile phases as sharp, concentrated bands. A schematic illustration of SPAM is shown on **Figure 16**.

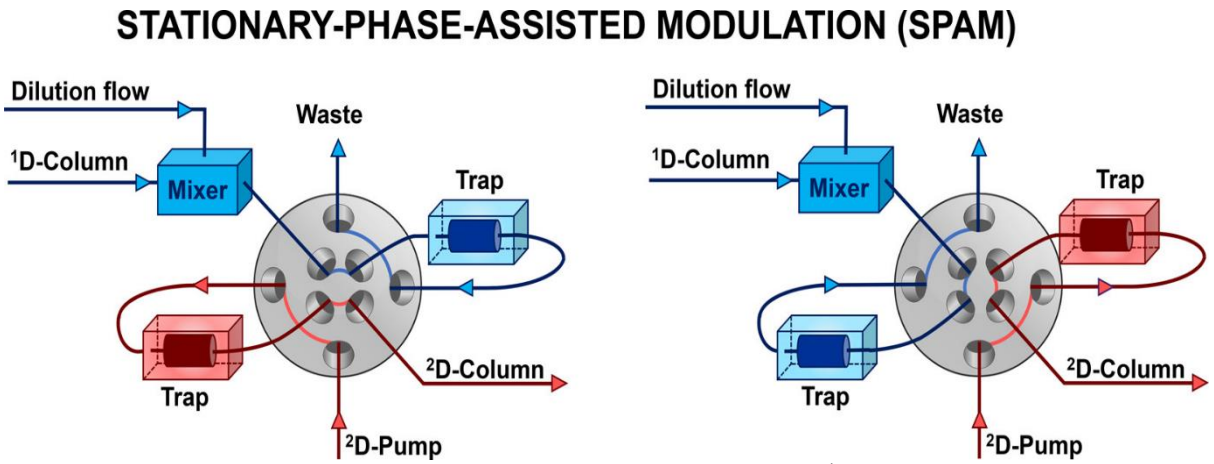

Figure 16. 2D-LC valve equipped with SPAM interface. ^{1}D effluent can be trapped before transferring into the ^{2}D. If necessary, the modulator is able to further dilute the effluents for better compatibility in the ^{2}D. Reprint from [154], permission granted due to open access.

5.3 Orthogonality

As mentioned before, 2D-LC separations are based on efficient separations systems considering stationary and mobile phase displaying strongly different selectivity in each dimension [160]. *Schoenmakers et al.* defined “orthogonality” for the separation science as follows: “orthogonality of two dimensions of separation exists when the retention mechanisms in these dimensions can be considered as statistically independent” [161]. *Pellett et al.* described orthogonality in a more practical way. Orthogonal separation should fulfil two conditions. First, the selectivity in the ^{2}D should significantly vary from the ^{1}D, allowing isolating “new” peaks from coelution in the first dimension. Furthermore, the resulting orthogonal separation should provide baseline resolution. To evaluate orthogonality in an appropriate way, several calculation metrics have been developed. The coefficient of determination R^2 of a linear regression was often used to evaluate the orthogonality between two LC methods [162]. However, it is not well describing orthogonality and therefore two other well established

approaches were applied for this work (**Publication IV**): the bin counting method originally suggested by Gilar et al. [162,163] and the Asterisk method proposed by Camenzuli and Schoenmakers [164]. For this reason, these two metrics will be presented in detail. In order to calculate the orthogonality, normalized retention times ($t_{normalized,i}$) of the analytes between two distinct LC methods are necessary. For this purpose, $t_{normalized,i}$ is defined in accordance to eq. 1 as:

$$\boldsymbol{t_{normalized,i}} = \frac{\boldsymbol{t_{R,i} - t_{min}}}{\boldsymbol{t_{max} - t_{min}}} \qquad \text{(eq. 1)}$$

wherein $t_{R,i}$ is the retention time of the respective species, t_{max} and t_{min} represent the retention times of the most and least retained species.

For the bin counting method by Gilar et al. [162,163], the normalized retention times (according to eq. 1) of two considered dimensions are plotted in the two-dimensional space. The 2D-space is then divided into a geometric distribution of equally spaced "bins". A hypothetical separation of 100 analytes can be divided into 10×10 = 100 bins. Depending on the coverage rate of the bins with the data points of $t_{normalized,\ i}$, it is possible to quantify the orthogonality between two dimensions with the formula of eq. 2:

$$\boldsymbol{O} = \frac{\sum \boldsymbol{bins} - \sqrt{\boldsymbol{P_{max}}}}{\boldsymbol{0.63 P_{max}}} \qquad \text{(eq.2)}$$

wherein *O* is defined as orthogonality. $\sum$ *bins* stands for the total number of bins containing data points. P_{max} is the sum of all bins. The *O* values vary between 0 and 1. Expressed as percent, 100% would stand for a theoretical, full orthogonality i.e. each bin is occupied by 1 data point [162].

Secondly, the so-called asterisk calculation was applied to quantify the orthogonality rate between two different LC-methods [164]. Here, a series of equations describing

the standard deviation of the peaks around four lines which cross the separation space (two orthogonal ones Z_1, and Z_2 corresponding to ^{1}D and ^{2}D, respectively, as well as two diagonal ones Z_- and Z_+ from left bottom to right top corners and left top to right bottom corners, respectively) were used to calculate the Z-parameters as described in detail in eqs 1-9 in ref. [164]. These Z-parameters were then used in a combined equation (eq. 3) defining the orthogonality, known as the A_0 [164].

$$A_0 = \sqrt{Z_- Z_+ Z_1 Z_2} \qquad \text{(eq.3)}$$

Besides of those possibilities, there are other useful methods to calculate orthogonality like the capacity dimension algorithm by Schure or nearest neighbours metric by Nowik. Here, the orthogonality is considered as the quality of peak dispersion in normalized separation space, which is characterized by two factors describing the population of distances between nearest neighbours: the length of distances and the degree of similarity of all lengths. Orthogonality grows with the increase of both factors [160,165]. Furthermore, Jacova et al. and Mommers and van der Wal introduced a critical discussion and some improvements related to surface coverage methods which can be considered as advanced measure of complementary retention behaviour [166,167].

5.4 Applications

In the last years, with the rise of ONs as biopharmaceuticals, numerous interesting 2D-LC applications for oligonucleotide analysis have been reported. *Thayer et al.* identified the location of the linkage in a RNA isomer using a bio-compatible LC system which was equipped with a fraction-collecting autosampler and a column selection valve. The authors reported the use of the phosphodiesterase-II enzyme to cleave 2'-5' linkages to identify the location of the linkage in the isomer. The setup allowed the

purification and the desalting of the AEX fraction for the on-line characterization of the enzymatic digests by MS [168]. However, it is important to point out that this was an offline approach of 2D-LC. The first full-comprehensive online 2D-LC/MS method (HILIC×IP-RP) was developed by *Li et al.* for the characterization of di- to deca-PO ONs. For this study, SPAM was applied as modulation technique. ^{1}D HILIC effluent containing target ONs were trapped on the C18 cartridge by using an aqueous make-up flow to retain and focus the ^{1}D effluent on the ^{2}D RPLC column head. With this constellation, an overall chromatographic peak capacity of 500 was achieved [169]. *Roussis et al.* combined ^{1}D AEX, IP-RP or RPLC with ^{2}D IP-RP in a heartcutting setup for the characterization of PO and PS ON impurities. To store ^{1}D effluent, trapping columns were used instead of loops due to the limitation of loop volume (40 µL). This sLC-LC setup allowed the separation of the dithioate impurity resulting from the substitution of an oxygen atom by sulphur atom in a dimethoxytrityl PS ON [170]. *Zhang and Goyon* established a mLC-LC 2D-LC method to characterize ASO impurities by combining IP-RP and AEX in ^{1}D with HILIC in ^{2}D. The highlight of this work was the fact that with HILIC in the ^{2}D, both online desalting and complementary selectivity were provided. Eventually, with the HILIC in ^{2}D, critical components from ^{1}D like IP-agents or phosphate buffer can be removed providing additional resolution power on the same time [112]. In this work, 2D-LC application of ONs plays a crucial role. We presented different 2D-LC approaches including online desalting via mLC-LC (**Publication I+II**), orthogonality study (**Publication IV**) and enhancing resolution power via mLC-LC or sLC×LC (**Publication IV+V**) which all also have been briefly mentioned in the chapters before.

6. Mass spectrometry for synthetic oligonucleotides

Nowadays, enabled by modern LC techniques, chromatographic separation for both analytical and preparative scales of synthetic ONs can be executed on a high level fulfilling multiple demands. This has been extensively discussed in the main chapters above. But for a complete structural characterization of the isolated species, further hyphenations are mandatory. For this purpose, the usage of MS is one of the most widely used techniques for biomedical applications of ONs [171]. Due to its significance, the MS in general will be discussed in the next chapters considering its theoretical and technical background. Additionally, the particularities of oligonucleotide MS will be explained: ONs as biomacromolecule generate characteristic MS spectra which are not straightforward to interpret. Also, factors affecting the LC-MS efficiency of ONs will be addressed. Finally, some possibilities of software supported data processing of ON MS will be presented. Because of its size and structural complexity, the interpretation of MS spectra for ONs can be very challenging and time consuming. To simplify this process, several computer-based approaches have been published.

6.1 Ionization

At the beginning of MS analysis, analytes must be converted to ionized gas-phase species before entering the mass analyser. There are many types of ionization techniques available with advantages and disadvantages. A classic method which has been frequently used is the EI which was developed by *Dempster* [172]. Another common approach is the CI, firstly postulated by *Field* [173]. In contrast of EI, CI is considered a “soft ionization” because after ionization, the original molecular mass generally stays intact [174]. EI causes as “hard ionization” extensive fragmentation of the molecular ion which mostly disappeared after the ionization. Despite of the popularity for both CI and EI, they are not applicable for LC-MS: in order to be coupled

with LC, the ionization process must occur under atmospheric pressure. Therefore, APCI and ESI are commonly used [175,176]. In this work, all MS measurements were accomplished with ESI as ionization technique. Hence, ESI process will be explained in details.

Although the complete ESI process is complex, it can be summarized as the following steps: by application of high voltage to the spray capillary (e.g. 2.5-6.0 kV), charged droplets will be produced from electrolyte dissolved in solvent; shrinkage of droplet by solvent evaporation caused by the application of a nebulising gas (e.g. nitrogen) and eventually disintegration due to an increase of surface charge density and a decrease of the droplet radius. The electric field strength within the charged droplet will finally reach a critical point enabling the ions at the surface of the droplets to be released into the gas phase; formation of ions and ion clusters from the disintegrated droplets; extraction of the ions into the mass analyser. Here, the emitted ions are collected by a sampling skimmer cone and are then accelerated into the mass analyser [177,178]. The ESI process is illustrated on **Figure 17**.

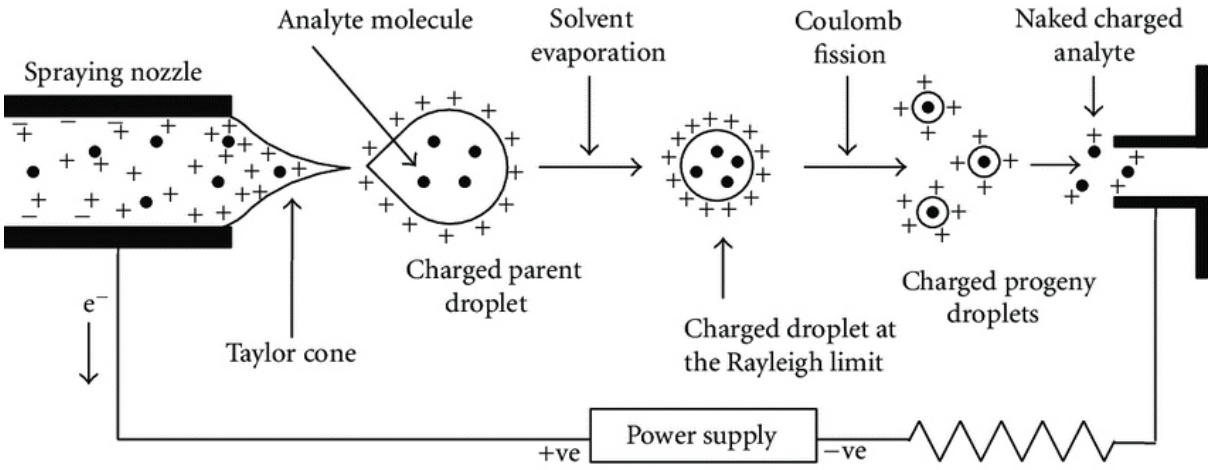

Figure 17. Schematic illustration of the ESI process. Reprint from [179], permission granted due to open access.

Despite of this simplified overview of the ESI process, there are still some other important aspects which should be mentioned. The dissolving of analytes and electrolytes in solution is the step in the whole procedure. Frankly speaking, the solubility is determined by the solute' s capacity to reorient solvent molecules (loss of entropy) and disrupt solvent-solvent interactions (loss of enthalpy) [177]. Next, the solution is passed through the spray capillary which is held at high voltage. Charged ions (+ or -) in the solution are repelled away from the capillary by charge separation forming a Taylor cone [180]. The cone forms when ions attempting to reach the counter electrode are obstructed by the presence of solvent. Following jet expansion of the charged liquid into a spray plume, Droplets enriched in charge will develop. The magnitude of the electric field needed for charged droplet formation is defined as a function of the onset voltage (V_{on}), the radius of the capillary (r_c), the distance to the counter electrode (d) and the surface tension of the solution (γ), as shown in eq. 3:

$$V_{on} \approx 2 \times 10^5 (\gamma r_c)^{1/2} \ln(\frac{4d}{r_c}) \qquad \text{(eq. 3)}$$

It is documented that nonaqueous solvents like ACN or MeOH require a substantially lower potential for droplet formation due to the lower surface tension in comparison to water, which is one of the main reasons for using hydro-organic solvent mixes to accomplish more effective ionization [181]. After the formation of charged droplets, they begin to move through the source chamber toward the counter electrode. During this migration, as briefly described before, the droplets diminish in size owing to a combination of solvent evaporation induced by the convective forces of air molecules in the atmospheric pressure chamber and droplet disintegration caused by the coulombic repulsion of charges at the droplet surface overcoming the force of surface tension attempting to hold the droplet together. The evaporation rate of the solvents

depends on the vapor pressure of the solvent favouring organic solvent with higher volatility [182]. On the other hand, the droplet disintegration is described by the Rayleigh equation:

$$Q_R^2 = 64\pi^2\varepsilon_0\gamma R_R^3 \qquad \text{(eq. 4)}$$

With Q_R as the Coulombs charge on the droplet surface which is just enough to overcome surface, ε_0 as the permittivity of vacuum and R_R as size of the droplet. For water, this value is three times larger in comparison to organic solvents such as ACN, implying that (for a given droplet volume) a charged water droplet may carry substantially more charge than a charged MeOH or ACN droplet before decomposition occurs. In other words, droplets based polar organic solvents dissolve faster, but droplets based on water must lose volume through evaporation before approaching Rayleigh instability.

To summarize, the involvement of the solvent in the ESI process is unquestionably critical. The solvent acts as a dissolving medium for the analytes and electrolytes in the system (related to the dielectric constant of the solvent). It offers conductance for the migration of charge, not only in the production of charged droplets, but also in the formation of charged ions and electrostatically bonded non-covalent complex or adduct ions. Droplet size, droplet desolvation and droplet disintegration are all determined by physicochemical properties of the solvent like density, viscosity, surface tension and vapor pressure. At last, the interaction of all of these processes and conditions results in the release of a gas phase ion. Thus, whether addressing ionization from a low aqueous or nonaqueous liquid, the complete process must be examined, from sample introduction to ion formation. Specific effects are also relevant dependent on experimental characteristics such as applied voltage, nebulizer gas flow

rate, solution flow rate and the distance between the spray capillary and counter electrode [177].

6.2 Mass analyser

After leaving the ion source, ionized species pass through mass analyser and are separated according to their mass-to-charge ratio. The dynamics of charged particles under electric and magnetic fields in vacuum is determined by Lorentz force law and Newton's second law of motion (non-relativistic case, ion velocity much lower than speed of light):

$$F = Q(E + v \times B) \quad \text{(eq. 5)}$$

$$F = ma \quad \text{(eq. 6)}$$

With F as the force applied to the ion, m as the mass of the ion, a as the acceleration, Q as the ion charge, E as the electric field and v $\times$ B as the vector cross product of the ion velocity and the magnetic field. Equating the aforementioned formulas for the ion' s force results in:

$$\left(\frac{m}{Q}\right) a = E + v \times B \quad \text{(eq. 7)}$$

This different equation is the standard equation of motion for charged particles. It specifies the particle' s velocity in space and time in terms of m/Q when combined with the initial conditions of the particles. As a result, mass spectrometer may be thought of as "mass-to-charge'" spectrometers. Consequently, the dimensionless m/z is commonly used, where z denotes the number of elementary charges on the ion. This metric, known informally as the mass-to-charge ratio, represents the ratio of the mass number and the charge number, z.

There are many different types of mass analysers that use static or dynamic fields, magnetic or electric fields, but they all follow the principle of the differential equation above. Each analyser has advantages and disadvantages. For tandem mass spectrometry (MS/MS), two or more mass analysers are used in combination. An overview considering several important parameters of the currently commercial MS analysers is listed in **Table 4** below.

Table 4 Overview of different MS analysers [183].

Mass analyzer	Mass resolution (at FWHM)	Mass accuracy (ppm)	Sensitivity	m/z range	MS/MS capability
Ion Trap	1000-1500	100 - 1000	Picomole	200 - 4000	MS^n
Linear Ion Trap	2000	100 - 500	Femtomole	200 - 4000	MS^n
Triple Quadrupole	1000	100 - 1500	Attomole	50 - 4000	MS/MS
Time of Flight	10 000 - 20 000	5 - 50	Femtomole	no upper limit	n/a
Tandem Time of Flight	10 000 - 40 000	5 - 50	Femtomole	no upper limit	MS/MS
Quadrupole Time of Flight	10 000 - 40 000	5 - 50	Attomole	no upper limit	MS/MS
Fourier-transform Ion Cyclotron Resonance	50 000 - 800 000	1 - 2	Femtomole	200 - 4000	MS^n
Linear Ion Trip Orbitrap	50 000 - 500 000	<5	Femtomole	200 - 4000	MS^n

In this study, all MS experiments were carried out on TripleTOF 5600+ from Sciex equipped with one quadrupole time of flight analyser. Hence, the operation principle of quadrupole and time of flight will be explained in details.

Quadrupole

Quadrupole is made up of four rods or electrodes that are positioned opposite to one another. As the ions pass through the quadrupole, they are filtered based on their m/z

value. The RF and DC voltages applied to the electrodes define the m/z value transmitted by the quadrupole. These voltages provide an oscillating electric field that acts as a bandpass filter, allowing the desired mass to charge value to be passed along. The RF voltage rejects or transmits ions based on their m/z value by concentrating them in various planes. The four electrodes are connected in pairs and the RF is applied between them. Depending on the polarity of the electrodes, the electric field is altered and the ions are focused in either horizontal or vertical plane. As the ions pass through the mass analyser, the quadrupole field continues to alternate. This leads the ions to go through a complicated sequence of movements, resulting in a three-dimensional wave. By selecting a suitable RF, the quadrupole functions as a high pass filter transmitting high m/z ions and rejecting low m/z ions. Because low m/z ions accelerate at a faster pace, their trajectory have a larger amplitude. If the amplitude is large enough, the ions will collide with electrodes and will not be able to reach the detector. A DC voltage is also applied to the electrodes functioning as a low pass filter to reject high m/z ions. The mobility of the low m/z ions is dominated by the RF potential due to their fast response to changing RF fields. Each time the RF potential changes polarity, the course of low m/z ions can be stabilized by fast refocusing. However, high m/z ions do not refocus as rapidly during the RF cycle. The DC potential has a bigger impact on their trajectory, and they gradually drift away from the quadrupole's centre. At the end, they will be too far off-axis to arrive the detector. Finally, the combination of RF- and DC potentials only allow the transmission of selected m/z values [184]. All ions above or below the value set will be rejected. An illustration of quadrupole is shown in **Figure 18**.

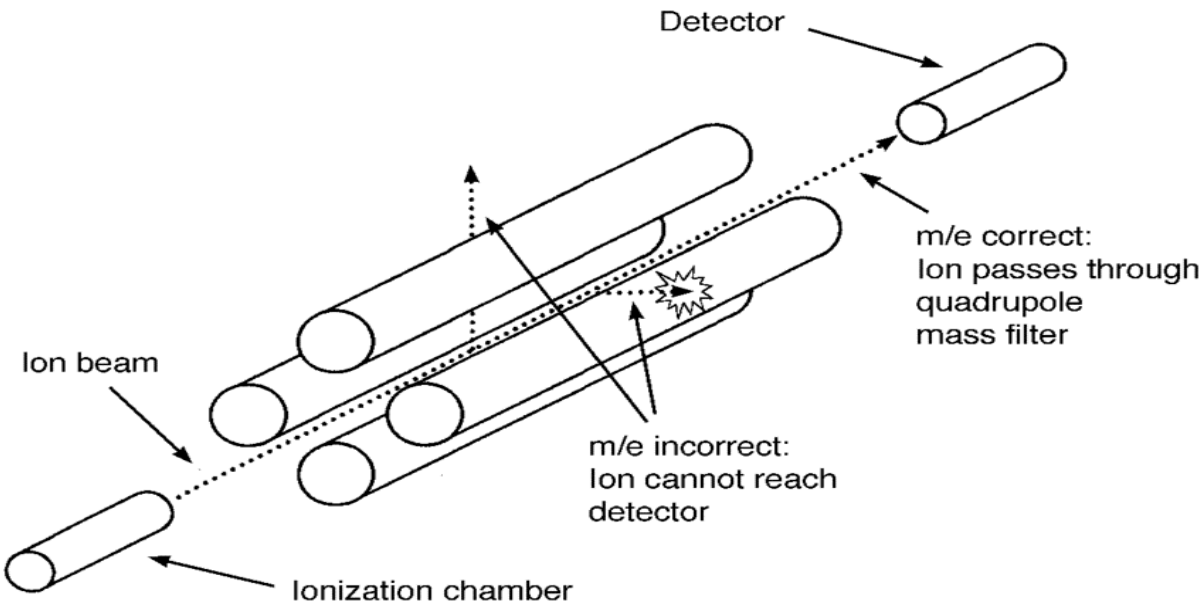

Figure 18. A graphical illustration of an ion beam passing through the quadrupole. Reprint from [185], permission granted due to open access.

Time of Flight

As ions travel down a flight tube, the TOF mass analyser separates them in time. This is a straightforward technique that operates on set voltages and does not require a magnetic field. TOF mass analysers have a high transmission efficiency, no upper m/z limit, low detection limits and quick scan rates. A packet of ions is created in the source of a TOF analyser by a very rapid (ns) ionization pulse. An electric field (usually 2-25 kV) generated between the backing plate and the acceleration grid speeds up these ions into the flight tube. All of the ions have the same kinetic energy since they are all driven across the same distance by the same force. Because velocity (v) is proportional to kinetic energy (E_{kin}), eq. 8 demonstrates that lighter ions with lower mass (m) will move faster.

$$E_{kin} = \frac{1}{2}mv^2 \qquad \text{(eq.8)}$$

The kinetic energy is determined by the instrument's acceleration voltage (V) and the ion's charge (e × z). The velocity of an ion (v) as a function of acceleration voltage and m/z value is given by rearranging equation 8:

$$v = \sqrt{\frac{2V \times e}{m/z}} \qquad \text{(eq. 9)}$$

After accelerating, the ions enter the flight tube. Ions move through this field-free zone at the velocity attained during acceleration. They collide with a detector at the end of the flight tube. According to eq. 9, it is obvious that ions with low m/z will reach the detector much faster. The mass spectrum is obtained by measuring the detector signal as a function of time for each pulse of ions produced in the source region [186]. An overview of the TOF mechanism is illustrated on **Figure 19**.

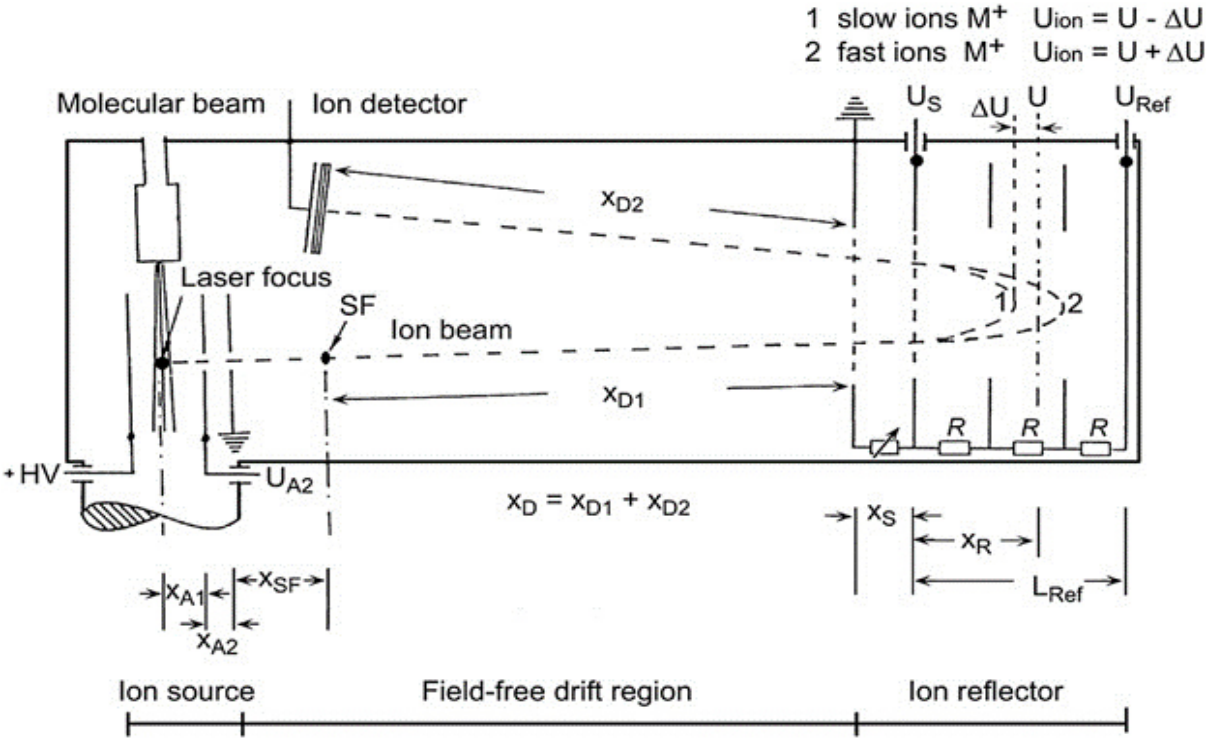

Figure 19. Schematic overview of a matrix-assisted laser desorption/ionization TOF analyser. Reprint from [187], with permission of John Wiley and Sons ©.

6.3 Detection

The type of detector used to convert a current of mass ions into digital signals is a critical component of all mass spectrometry systems [188]. Different detectors are utilized based on criteria such as dynamic range, spatial information retention, noise, and mass analyser appropriateness. Electron multipliers (EM), Faraday cups (FC), photomultiplier conversion dynodes, and array detectors are examples of regular usage.

Electron Multipliers

The fact that EM detectors are noiseless and can count single ions when correctly calibrated is a huge benefit. An EM is essentially a serial connection of discrete metal plates known as dynodes that amplifies an ion current by a factor of ~10^8 into a detectable current of electrons. The initial conversion dynode stops a single secondary ion from entering the EM. The impact energy is dissipated in part by the expulsion of electrons from the dynode material, which creates an electrical charge. A cascade mechanism ejects more electrons via succeeding dynodes. The accumulated charge is sensed as a voltage pulse at the last dynode. The channeltron is another form of detector that is widely used and closely connected to the EM. Instead of a series of discrete metal plates for dynodes, it is made out of a single continuous curved surface that simulates the cascade effect employed in discrete dynode electron multipliers for signal amplification [189].

Faraday Cups

FC detectors are simple devices with low cost. Its most important advantage towards EM is the capacity to detect high ion current. Principally, a hollow conducting electrode is linked to ground through a high resistance. Ions striking the collector produce a flow

of electrons from ground through the resistor, amplifying the potential drop across the resistor. A single ion has an elementary charge of 1.6 x 10^{-19} C. As a result, a count rate of 1 × 10^{6} c/s would lead to a cumulative current of 1.6 x 10^{-13} A. The amplifier must be able to detect a potential decrease of 16 mV even with a resistance as high as 1011 W connected to ground. Therefore, the measurements of lower current will become challenging since thermal and electrical noise in the resistor and amplifier circuits has a significant impact on precision [190].

Photomultiplier conversion dynode

In a photomultiplier conversion dynode detector, ions first hit a dynode, causing electron emission. Next, the emitted electrons will arrive a phosphor screen, releasing photons. The photons are then sent via the multiplier, where amplification happens in a cascade manner, similar to the electron multiplier. The key benefit of employing photons is that the multiplier component of the detector may be kept sealed in a vacuum, reducing contamination and prolonging the detector's lifetime significantly [191].

Array detectors

The first detector which was applied for the MS was an array detector. Ever since, this technique has been further developed based on different principles. Nowadays, many array detectors pursuing various functional mechanisms are in usage. But in general, all array detectors can be summarized into two major categories: those which are position sensitive and those which are able to detect multiple ions with varying m/z simultaneously.

To detect both low and high m/z ions, the array detector is constructed by combining EM and FC. In the case of isotope determination, the most abundant isotope can be

detected by EM, whereas weaker abundant isotope causing low ion current can be more efficiently detected by FC [192]. Another way to realize the detection of multiple m/z ions is to use a multicollection system consists of many EMs and/or FCs. An interesting application for this purpose is the nanoscale secondary ion mass spectrometer (NanoSIMS) with 6 moveable and 1 fixed EM detectors, allowing simultaneous investigation of 7 distinct masses [193].

For position sensitive detections, up to 10^6 microscopic glass channels, each 5-50 mm in diameter, are connected with each other in a honeycomb-type array, so-called microchannel plates (MCP). Each single channel acts as a continuous-dynode EM, and a series of MCPs can be connected in series to intensify the ion current. Due to the restricted localization of each single channel, second electrons will form certain defined “tracks”. And because of this circumstance, MCP is able to generate spatial resolution providing a distribution of the final electron cloud [194].

6.4 MS-Spectra of oligonucleotides

A typical ESI-TOF MS spectrum of an oligonucleotide generated under HILIC can be found in **Figure 20A**. Due to the multiple negatively charged phosphate backbones, ESI-MS for ONs is mostly carried out under negative mode. As visualized in **Figure 20A**, the mass spectra of ONs always consists of a series of multiple deprotonated molecules with different charge states which is conventionally defined as $[M\text{-}nH]^{n-}$. The distribution of those charge states can be manipulated by adjusting pH value, organic modifier, mobile phase additives and various ion source parameters [195]. *Johnson et al.* investigated ASO via ESI-MS and evaluated the influence of pH values on the MS outcomes. With higher pH, the signal intensity of both 3- and 4- charge states significantly increased in comparison to both higher and lower charge states. Furthermore, the ratio of both charge states has become more equally [196]. It has

also been reported that a reduction of the buffer concentration might be beneficial for increasing abundance of lower charge states [197]. To reduce the intensity of "undesired" charge states, *Muddiman et al.* suggested to combine acetic acid with piperidine and imidazole. Under this condition, higher charge states vanished leading to more abundant charge state 3- [198]. In **Figure 20B**, one of the charge states is illustrated enlarged showing the isotopic distribution in form of an envelope.

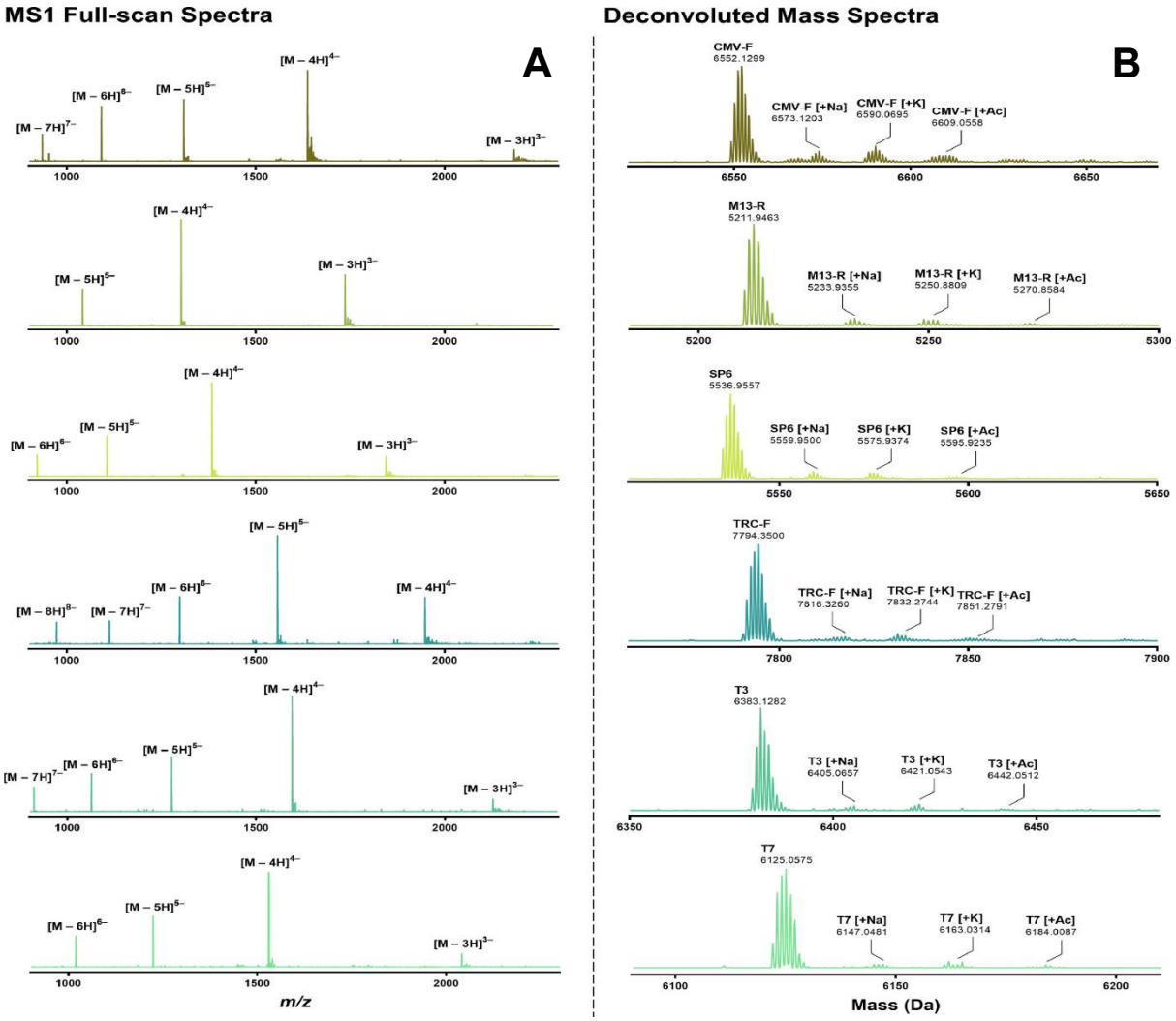

Figure 20. Mass spectra of six different ONs under HILIC. A: MS1 full scan spectra, multiple charge states are illustrated. B: Deconvoluted mass spectra. Different adducts are indicated. Reprint from [135], permission granted due to open access.

Another interesting MS phenomenon for ONs is the presence of "cation adducts" caused by the exchange of H^+ in the phosphate or phosphorothioate groups for Na^+

and K^+. These exchange adducts are frequently observed and even multiple exchange ions as like $[M\text{-}mH+mNa+nH]^{n+}$ or $[M\text{-}mH+mNa\text{-}nH]^{n-}$ can occur (**Figure 20B**). The H^+-$alkali^+$ exchange is omnipresent and poses a challenge due to the reduced detection limit [199,200]. In general, the degree of exchange correlates with the length of the ONs and phosphorothioated ONs tend to stronger presence of those exchange ions [195]. But due to its negative influence towards MS sensitivity, H^+-$alkali^+$ exchange ions must not occur in high degrees. For this purpose, the usage of imidazole and piperidine as mobile phase additives has been proved as advantageous [198]. *Deguchi et al.* featured a post column addition of imidazole in ACN to the eluents during a chromatographic run which leads to enhanced MS sensitivity [201]. *Hail et al.* used EDTA to reduce the formation of exchange ions by trapping the alkali ions competitively [202].

For valid characterization of ONs, tandem MS is mandatory. Here, collision induced dissociation will lead to a complex pattern consisting of numerous fragment ions. *McLuckey et al.* firstly postulated a nomenclature to describe them: fragments formed from the 5' end are defined as *a, b, c* or *d* fragments, depending on the position of the dissociation. Fragments originating from 3' end are labelled as *w, x, y* or *z* fragments (**Figure 21**) [203,204]. It is evident that precursor ions with higher charge states are predominantly fragmented into a few low m/z fragment ions, whereas precursor ions at lower charge states are more stable leading to higher m/z fragment ions [205,206].

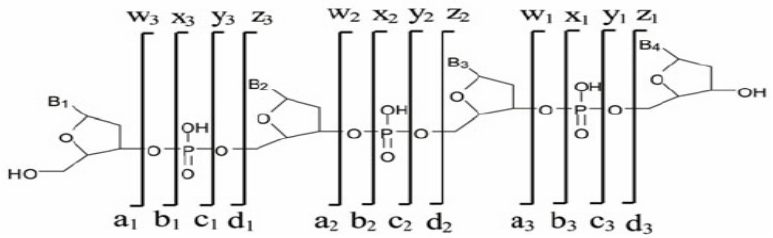

Figure 21. Fragmentation pattern of oligonucleotides postulated by *McLuckey* [203]. Reprint from [207], with permission from Springer Nature ©.

6.5 Software supported data processing

As described in the last chapters, MS spectra of ONs are very complex considering many different aspects. Not surprisingly, the data processing can also be time consuming and complicated: an ON strand with 21 nucleotides can be fragmentated into more than 200 000 species. Hence, a manual interpretation is not possible and must be supported by digital solutions. Today, numerous well-known vendors already offer commercial software packages to analyse oligonucleotide MS. Most of them are designed for automated RNA/DNA sequencing based on MS/MS data. Nevertheless, the licenses are quite expensive. Fortunately, several research groups developed different software packages for oligonucleotide MS which are cost-free accessible.

Table 5 Overview of several published open source solutions for data processing of oligonucleotide MS.

Name	Development group	Function	Publication	Status
Ariadne	RIKEN Center for Sustainable Resource Science, Japan	Open source data base; RNA identification via tandem MS	[208]	ONLINE
RoboOligo	Limbach Group, University of Cincinnati, USA	Software; RNA/DNA oligo identification via tandem MS; de novo sequencing enabled	[209]	Free Download, Version 0.9.5.0
OMA/OPA	Schürch Group, University of Bern, Switzerland	Java Application; RNA/DNA oligo identification/confirmation via tandem MS; sequence must be known	[210]	Free Download

Nakayama et al. used a self-developed analyser program named *Ariadne* to identify an unknown RNA component in a tRNA mixture [208]. Ariadne is a web-based database search engine identifying RNA by two evaluation steps of tandem MS data.

The program initially compares the experimental MS/MS results to those calculated from a candidate nucleotide sequence in a DNA/RNA sequence database. Next, the candidate sequences are mapped for all RNA entries in the database. Each entry is scored based on the number of appearances of the candidate sequences to identify a specific RNA. A graphical summary of the principle of Ariadne is illustrated in **Figure 22** [208].

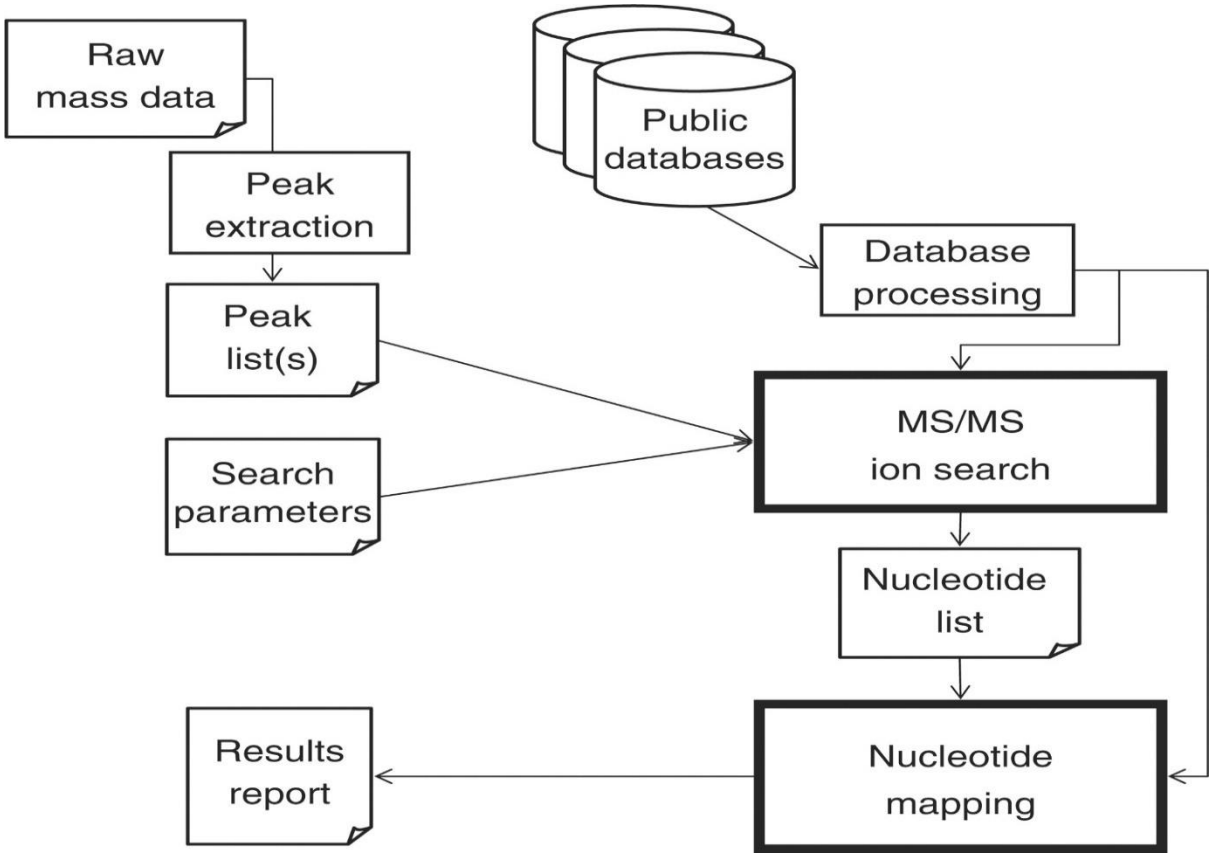

Figure 22. Schematic diagram of the Ariadne web search program. Reprint from [208], with permission of Oxford University Press ©.

A huge problem with the usage of Ariadne is the limitation of the database which is only available for *Saccharomyces cerevisiae*, *Schizosaccharomyces pombe*, *Mus musculus* and *Homo sapiens* [208]. Thus, de novo sequencing is not possible. To

overcome this, the *Limbach Group* developed *RoboOligo* [209]. It is an interactive software for the robust analysis of data generated by tandem MS of ONs. This program is able to feature automated de novo sequencing via the local search paradigm. Additionally, manual sequencing with real-time spectrum labelling and cumulative intensity scoring is also one of the main functions. Lastly, a hybrid approach which combines the user intuition of manual sequencing with the high-throughput sampling of automated de novo sequencing is also available. In **Figure 23**, the algorithm for the de novo sequencing is illustrated [209]. In this study, RoboOligo has been frequently used for data processing.

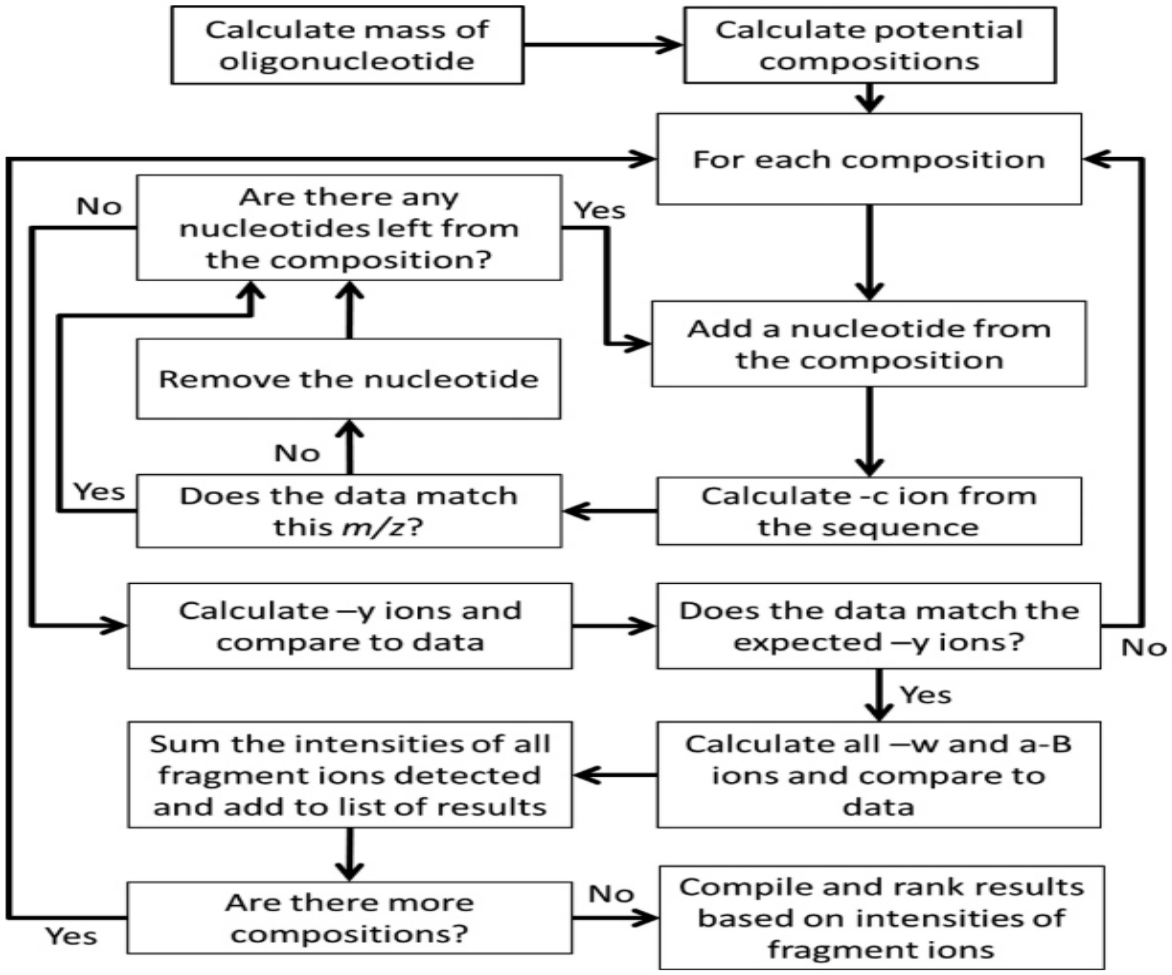

Figure 23. Schematic illustration of the algorithm for de novo sequencing with RoboOligo. Reprint from [209], with permission of Oxford University Press ©.

Another software package named OMA/OPA (Oligonucleotide mass assembler/Oligonucleotide peak analyser) which was used in this study was published by *Schürch* [210]. This platform-independent program is able to calculate all theoretically possible fragments of a known in advance specified sequence and annotates it to an experimental spectrum. The library of building blocks and further modifications for ONs can be expanded individually enabling the inclusion of many structural variations. In our works, OPA/OMA has been applied in combination with RoboOligo to increase the precision of the final characterization of detected ONs [210].

7 List of figures

Figure 9. Chemical structure and interaction sites of the stable-bond polymeric reversed-phase/weak anion-exchange mixed mode (Poly-RP/WAX) stationary phase. Reprint from [145].

Figure 10. A conventional instrumental setup of a 2D-LC system. Reprint from [145].

Figure 11. Visualization of 2D-LC flow paths directed by a commonly used 2D-LC valve. Reprint from [148], permission granted by Multimedia Pharma Sciences, LLC..

Figure 12. All four possible 2D-LC modes in graphical depiction. A: Heart-cutting; B: Multiple heart-cutting; C: selective comprehensive; D full comprehensive. Reprint from [149], with permission of Springer Nature ©.

Figure 13. The 1D UV chromatogram and the UV-chromatograms of the selective comprehensive 2D-LC experiment for the antisense of Patisiran. Reprinted from Publication IV [153].

Figure 14. The results of 2D-LC experiments for therapeutic antibodies published by *Guillarme et al.* [156]. On B, C, D, E, F, breakthrough effect at the beginning of the ^{2}D run are clearly indicated which was suppressed by the usage of ASM. Reprint from [156], with permission of American Chemical Society ©.

Figure 15. Four different valve configurations of ASM. Reprint from [158], with permission of American Chemical Society ©.

Figure 16. 2D-LC valve equipped with SPAM interface. ^{1}D effluent can be trapped before transferring into the ^{2}D. If necessary, the modulator is able to further dilute the effluents for better compatibility in the ^{2}D. Reprint from [154], permission granted due to open access.

8 List of tables

9 References

[1] R. Lakhia, A. Mishra, V. Patel, Chapter 7 - Manipulation of renal gene expression using oligonucleotides, in: T.B.T.-M. in C.B. Weimbs (Ed.), Methods Kidney Cell Biol. - Part B, Academic Press, 2019: pp. 109–120. https://doi.org/https://doi.org/10.1016/bs.mcb.2019.05.006.

[2] S. Sinha, C. Jeyaseelan, G. Singh, T. Munjal, D. Paul, Chapter 8 - Spectroscopy—Principle, types, and applications, in: A.K. Bhatt, R.K. Bhatia, T.C.B.T.-B.B. for B. and B. Bhalla (Eds.), Academic Press, 2023: pp. 145–164. https://doi.org/https://doi.org/10.1016/B978-0-12-816109-8.00008-8.

[3] A. Travers, G. Muskhelishvili, DNA structure and function, FEBS J. 282 (2015) 2279–2295. https://doi.org/10.1111/febs.13307.

[4] G.L. Conn, D.E. Draper, RNA structure, Curr. Opin. Struct. Biol. 8 (1998) 278–285. https://doi.org/https://doi.org/10.1016/S0959-440X(98)80059-6.

[5] S. Minchin, J. Lodge, Understanding biochemistry: Structure and function of nucleic acids, Essays Biochem. 63 (2019) 433–456. https://doi.org/10.1042/EBC20180038.

[6] M. Albrecht, Artificial molecular double-stranded helices, Angew. Chemie - Int. Ed. 44 (2005) 6448–6451. https://doi.org/10.1002/anie.200501472.

[7] C.R. Martinez, B.L. Iverson, Rethinking the term “pi-stacking,” Chem. Sci. 3 (2012) 2191–2201. https://doi.org/10.1039/c2sc20045g.

[8] E. Bano, L. Fradetal, M. Ollivier, J.-H. Choi, V. Stambouli, Chapter 9 - SiC Nanowire-Based Transistors for Electrical DNA Detection, in: S.E.B.T.-S.C.B. (Second E. Saddow (Ed.), Elsevier, 2016: pp. 261–310. https://doi.org/https://doi.org/10.1016/B978-0-12-802993-0.00009-5.

[9] N. Touchot, P. Chardin, A. Tavitian, Four additional members of the ras gene superfamily isolated by an oligonucleotide strategy: molecular cloning of YPT-related cDNAs from a rat brain library., Proc. Natl. Acad. Sci. U. S. A. 84 (1987) 8210–8214. https://doi.org/10.1073/pnas.84.23.8210.

[10] H. Okasha, S. Samir, Synthesis and molecular cloning of antimicrobial peptide chromogranin A N-46 gene using conventional PCR, Gene Reports. 18 (2020) 100571. https://doi.org/https://doi.org/10.1016/j.genrep.2019.100571.

[11] J. De Saeger, M. Vermeersch, C. Gaillochet, T.B. Jacobs, Simple and Efficient Modification of Golden Gate Design Standards and Parts Using Oligo Stitching, ACS Synth. Biol. 11 (2022) 2214–2220. https://doi.org/10.1021/acssynbio.2c00072.

[12] S. Marillonnet, R. Grützner, Synthetic DNA Assembly Using Golden Gate Cloning and the Hierarchical Modular Cloning Pipeline, Curr. Protoc. Mol. Biol. 130 (2020). https://doi.org/10.1002/cpmb.115.

[13] R.K. Saiki, S. Scharf, F. Faloona, K.B. Mullis, G.T. Horn, H.A. Erlich, N. Arnheim, Enzymatic amplification of beta-globin genomic sequences and restriction site analysis for diagnosis of sickle cell anemia. 1985.,

Biotechnology. 24 (1992) 476–480.

[14] H. Telenius, N.P. Carter, C.E. Bebb, M. Nordenskjöld, B.A.J. Ponder, A. Tunnacliffe, Degenerate oligonucleotide-primed PCR: General amplification of target DNA by a single degenerate primer, Genomics. 13 (1992) 718–725. https://doi.org/10.1016/0888-7543(92)90147-K.

[15] J. Vincent, H. Gurling, G. Melmer, Oligonucleotides as Short as 7-Mers Can Be Used for PCR Amplification, DNA Cell Biol. 13 (1994) 75–82. https://doi.org/10.1089/dna.1994.13.75.

[16] M.C. Arias, D. Silvestre, F.D.O. Francisco, R. Weinlich, W.S. Sheppard, An oligonucleotide primer set for PCR amplification of the complete honey bee mitochondrial genome, Apidologie. 39 (2008) 475–480. https://doi.org/10.1051/apido:2008024.

[17] T. Narihiro, Y. Sekiguchi, Oligonucleotide primers, probes and molecular methods for the environmental monitoring of methanogenic archaea, Microb. Biotechnol. 4 (2011) 585–602. https://doi.org/10.1111/j.1751-7915.2010.00239.x.

[18] D. Green, T. Dalmay, T. Chapman, Microguards and micromessengers of the genome, Heredity (Edinb). 116 (2016) 125–134. https://doi.org/10.1038/hdy.2015.84.

[19] A. Qureshi, N. Thakur, I. Monga, A. Thakur, M. Kumar, VIRmiRNA: a comprehensive resource for experimentally validated viral miRNAs and their targets, Database (Oxford). 2014 (2014) 1–10. https://doi.org/10.1093/database/bau103.

[20] M.C. Siomi, K. Sato, D. Pezic, A.A. Aravin, PIWI-interacting small RNAs: The vanguard of genome defence, Nat. Rev. Mol. Cell Biol. 12 (2011) 246–258. https://doi.org/10.1038/nrm3089.

[21] A.M. Michelson, A.R. Todd, Nucleotides part XXXII. Synthesis of a dithymidine dinucleotide containing a 3′: 5′-internucleotidic linkage, J. Chem. Soc. (1955) 2632–2638. https://doi.org/10.1039/JR9550002632.

[22] M. Smith, D.H. Rammler, I.H. Goldberg, H.G. Khorana, Studies on Polynucleotides. XIV. Specific Synthesis of the C3-C5 Interribonucleotide Linkage. Synthesis of Uridyly-(3’-5’)-Uridine and Uridylyl- (3’-5’)-Adenosine, J. Am. Chem. Soc. 931 (1961) 1959–1961.

[23] K.L. Agarwal, H. Büchi, M.H. Caruthers, N. Gupta, H.G. Khorana, K. Kleppe, A. Kumar, E. Ohtsuka, U.L. Rajbhandary, J.H. Van De Sande, V. Sgaramella, H. Weber, T. Yamada, Total synthesis of the gene for an alanine transfer Ribonucleic acid from Yeast, Nature. 227 (1970) 27–34. https://doi.org/10.1038/227027a0.

[24] R.L. Letsinger, V. Mahadevan, Oligonucleotide Synthesis on a Polymer Support1,2, J. Am. Chem. Soc. 87 (1965) 3526–3527. https://doi.org/10.1021/ja01093a058.

[25] R.L. Letsinger, K.K. Ogilvie, Synthesis of oligothymidylates via phosphotriester intermediates, J. Am. Chem. Soc. 91 (1969) 3350–3355.

[26] R.L. Letsinger, J.L. Finnan, G.A. Heavner, W.B. Lunsford, Nucleotide chemistry. XX. Phosphite coupling procedure for generating internucleotide links, J. Am. Chem. Soc. 97 (1975) 3278–3279. https://doi.org/10.1021/ja00844a090.

[27] R.L. Letsinger, W.B. Lunsford, Synthesis of thymidine oligonucleotides by phosphite triester intermediates, J. Am. Chem. Soc. 98 (1976) 3655–3661. https://doi.org/10.1021/ja00428a045.

[28] N.M. El Zahar, N. Magdy, A.M. El-Kosasy, M.G. Bartlett, Chromatographic approaches for the characterization and quality control of therapeutic oligonucleotide impurities, Biomed. Chromatogr. 32 (2018). https://doi.org/10.1002/bmc.4088.

[29] M.D. Matteucci, M.H. Caruthers, Synthesis of deoxyoligonucleotides on a polymer support, J. Am. Chem. Soc. 103 (1981) 3185–3191. https://doi.org/10.1021/ja00401a041.

[30] S.L. Beaucage, M.H. Caruthers, Deoxynucleoside phosphoramidites-A new class of key intermediates for deoxypolynucleotide synthesis, Tetrahedron Lett. 22 (1981) 1859–1862. https://doi.org/10.1016/S0040-4039(01)90461-7.

[31] M.L. Stephenson, P.C. Zamecnik, Inhibition of Rous sarcoma viral RNA translation by a specific oligodeoxyribonucleotide, Proc. Natl. Acad. Sci. U. S. A. 75 (1978) 285–288. https://doi.org/10.1073/pnas.75.1.285.

[32] L. Moumné, A.C. Marie, N. Crouvezier, Oligonucleotide Therapeutics: From Discovery and Development to Patentability, Pharmaceutics. 14 (2022). https://doi.org/10.3390/pharmaceutics14020260.

[33] C. Rinaldi, M.J.A. Wood, Antisense oligonucleotides: The next frontier for treatment of neurological disorders, Nat. Rev. Neurol. 14 (2018) 9–22. https://doi.org/10.1038/nrneurol.2017.148.

[34] S.T. Crooke, J.L. Witztum, C.F. Bennett, B.F. Baker, RNA-Targeted Therapeutics, Cell Metab. 27 (2018) 714–739. https://doi.org/10.1016/j.cmet.2018.03.004.

[35] G. Walsh, Biopharmaceutical benchmarks 2018, Nat. Biotechnol. 36 (2018) 1136–1145. https://doi.org/10.1038/nbt.4305.

[36] K.A. Majorek, S. Dunin-Horkawicz, K. Steczkiewicz, A. Muszewska, M. Nowotny, K. Ginalski, J.M. Bujnicki, The RNase H-like superfamily: New members, comparative structural analysis and evolutionary classification, Nucleic Acids Res. 42 (2014) 4160–4179. https://doi.org/10.1093/nar/gkt1414.

[37] H. Wu, W.F. Lima, H. Zhang, A. Fan, H. Sun, S.T. Crooke, Determination of the Role of the Human RNase H1 in the Pharmacology of DNA-like Antisense Drugs, J. Biol. Chem. 279 (2004) 17181–17189. https://doi.org/10.1074/jbc.M311683200.

[38] B.F. Baker, S.S. Lot, T.P. Condon, S. Cheng-Flournoy, E.A. Lesnik, H.M. Sasmor, C.F. Bennett, 2'-O-(2-methoxy)ethyl-modified anti-intercellular adhesion molecule 1 (ICAM-1) oligonucleotides selectively increase the ICAM-1 mRNA level and inhibit formation of the ICAM-1 translation initiation complex

in human umbilical vein endothelial cells, J. Biol. Chem. 272 (1997) 11994–12000. https://doi.org/10.1074/jbc.272.18.11994.

[39] A.F. Klein, E. Gasnier, D. Furling, Gain of RNA function in pathological cases: Focus on myotonic dystrophy, Biochimie. 93 (2011) 2006–2012. https://doi.org/10.1016/j.biochi.2011.06.028.

[40] S. Bajan, G. Hutvagner, RNA-Based Therapeutics: From Antisense Oligonucleotides to miRNAs, Cells. 9 (2020) 137. https://doi.org/10.3390/cells9010137.

[41] M.A. Havens, M.L. Hastings, Splice-switching antisense oligonucleotides as therapeutic drugs, Nucleic Acids Res. 44 (2016) 6549–6563. https://doi.org/10.1093/nar/gkw533.

[42] S. Huang, X.-Y. Hao, Y.-J. Li, J. Wu, D.-X. Xiang, S. Luo, Nonviral delivery systems for antisense oligonucleotide therapeutics, Biomater. Res. 26 (2022) 49. https://doi.org/10.1186/s40824-022-00292-4.

[43] B. Hu, L. Zhong, Y. Weng, L. Peng, Y. Huang, Y. Zhao, X.J. Liang, Therapeutic siRNA: state of the art, Signal Transduct. Target. Ther. 5 (2020). https://doi.org/10.1038/s41392-020-0207-x.

[44] T. Tuschl, S.M. Elbashir, J. Harborth, W. Lendeckel, A. Yalcin, K. Weber, Duplexes of 21-nucleotide RNAs mediate RNA interference in cultured mammalian cells, Nature. 411 (2001) 494–498. www.nature.com.

[45] K.F. Tang, H. Ren, The role of dicer in DNA damage repair, Int. J. Mol. Sci. 13 (2012) 16769–16778. https://doi.org/10.3390/ijms131216769.

[46] A.J. Pratt, I.J. MacRae, The RNA-induced silencing complex: A versatile gene-silencing machine, J. Biol. Chem. 284 (2009) 17897–17901. https://doi.org/10.1074/jbc.R900012200.

[47] MHRA, Early Access to Medicines Scheme – Treatment protocol – Information for healthcare professionals, (2017) 20. http://www.gmc-uk.org/mobile/14327.

[48] M.T. McManus, P.A. Sharp, Gene silencing in mammals by small interfering RNAs, Nat. Rev. Genet. 3 (2002) 737–747. https://doi.org/10.1038/nrg908.

[49] A.D. Keefe, S. Pai, A. Ellington, Aptamers as therapeutics, Nat. Rev. Drug Discov. 9 (2010) 537–550. https://doi.org/10.1038/nrd3141.

[50] A.D. Ellington, J.W. Szostak, In vitro selection of RNA molecules that bind specific ligands, Nature. 346 (1990) 818–822. https://doi.org/10.1038/346818a0.

[51] C. Tuerk, L. Gold, Systematic Evolution of Ligands by Exponential Enrichment: RNA Ligands to Bacteriophage T4 DNA Polymerase, Science (80-.). 249 (1990) 505–510. https://doi.org/10.1126/science.2200121.

[52] S. Ni, Z. Zhuo, Y. Pan, Y. Yu, F. Li, J. Liu, L. Wang, X. Wu, D. Li, Y. Wan, L. Zhang, Z. Yang, B.T. Zhang, A. Lu, G. Zhang, Recent Progress in Aptamer Discoveries and Modifications for Therapeutic Applications, ACS Appl. Mater. Interfaces. 13 (2021) 9500–9519. https://doi.org/10.1021/acsami.0c05750.

[53] D. O'Connell, A. Koenig, S. Jennings, B. Hicke, H.L. Han, T. Fitzwater, Y.F. Chang, N. Varki, D. Parma, A. Varki, Calcium-dependent oligonucleotide antagonists specific for L-selectin., Proc. Natl. Acad. Sci. 93 (1996) 5883–5887. https://doi.org/10.1073/pnas.93.12.5883.

[54] J. Mi, Y. Liu, Z.N. Rabbani, Z. Yang, J.H. Urban, B.A. Sullenger, B.M. Clary, In vivo selection of tumor-targeting RNA motifs, Nat. Chem. Biol. 6 (2010) 22–24. https://doi.org/10.1038/nchembio.277.

[55] J.M. Healy, S.D. Lewis, M. Kurz, R.M. Boomer, K.M. Thompson, C. Wilson, T.G. McCauley, Pharmacokinetics and Biodistribution of Novel Aptamer Compositions, Pharm. Res. 21 (2004) 2234–2246. https://doi.org/10.1007/s11095-004-7676-4.

[56] E.W.M. Ng, D.T. Shima, P. Calias, E.T. Cunningham, D.R. Guyer, A.P. Adamis, Pegaptanib, a targeted anti-VEGF aptamer for ocular vascular disease, Nat. Rev. Drug Discov. 5 (2006) 123–132. https://doi.org/10.1038/nrd1955.

[57] S. Catuogno, C.L. Esposito, Aptamer Cell-Based Selection: Overview and Advances, Biomedicines. 5 (2017). https://doi.org/10.3390/biomedicines5030049.

[58] Y. Zhang, B.S. Lai, M. Juhas, Recent advances in aptamer discovery and applications, Molecules. 24 (2019). https://doi.org/10.3390/molecules24050941.

[59] F. He, N. Wen, D. Xiao, J. Yan, H. Xiong, S. Cai, Z. Liu, Y. Liu, Aptamer-Based Targeted Drug Delivery Systems: Current Potential and Challenges, Curr. Med. Chem. 27 (2018) 2189–2219. https://doi.org/10.2174/0929867325666181008142831.

[60] K.D. Kovacevic, J.C. Gilbert, B. Jilma, Pharmacokinetics, pharmacodynamics and safety of aptamers, Adv. Drug Deliv. Rev. 134 (2018) 36–50. https://doi.org/https://doi.org/10.1016/j.addr.2018.10.008.

[61] S. Ni, H. Yao, L. Wang, J. Lu, F. Jiang, A. Lu, G. Zhang, Chemical Modifications of Nucleic Acid Aptamers for Therapeutic Purposes, Int. J. Mol. Sci. 18 (2017). https://doi.org/10.3390/ijms18081683.

[62] A.D. Burdick, S. Sciabola, S.R. Mantena, B.D. Hollingshead, R. Stanton, J.A. Warneke, M. Zeng, E. Martsen, A. Medvedev, S.S. Makarov, L.A. Reed, J.W. Davis II, L.O. Whiteley, Sequence motifs associated with hepatotoxicity of locked nucleic acid—modified antisense oligonucleotides, Nucleic Acids Res. 42 (2014) 4882–4891. https://doi.org/10.1093/nar/gku142.

[63] A.M. Lincoff, R. Mehran, T.J. Povsic, S.L. Zelenkofske, Z. Huang, P.W. Armstrong, P.G. Steg, C. Bode, M.G. Cohen, C. Buller, P. Laanmets, M. Valgimigli, T. Marandi, V. Fridrich, W.J. Cantor, B. Merkely, J. Lopez-Sendon, J.H. Cornel, J.D. Kasprzak, M. Aschermann, V. Guetta, J. Morais, P.R. Sinnaeve, K. Huber, R. Stables, M.A. Sellers, M. Borgman, L. Glenn, A.I. Levinson, R.D. Lopes, V. Hasselblad, R.C. Becker, J.H. Alexander, Effect of the REG1 anticoagulation system versus bivalirudin on outcomes after percutaneous coronary intervention (REGULATE-PCI): A randomised clinical

trial, Lancet. 387 (2016) 349–356. https://doi.org/10.1016/S0140-6736(15)00515-2.

[64] J.P. Bost, H. Barriga, M.N. Holme, A. Gallud, M. Maugeri, D. Gupta, T. Lehto, H. Valadi, E.K. Esbjörner, M.M. Stevens, S. El-Andaloussi, Delivery of Oligonucleotide Therapeutics: Chemical Modifications, Lipid Nanoparticles, and Extracellular Vesicles, ACS Nano. 15 (2021) 13993–14021. https://doi.org/10.1021/acsnano.1c05099.

[65] E. Urban, C.R. Noe, Structural modifications of antisense oligonucleotides, Farmaco. 58 (2003) 243–258. https://doi.org/10.1016/S0014-827X(03)00022-3.

[66] S.D. Putney, S.J. Benkovic, P.R. Schimmel, A DNA fragment with an alpha-phosphorothioate nucleotide at one end is asymmetrically blocked from digestion by exonuclease III and can be replicated in vivo., Proc. Natl. Acad. Sci. 78 (1981) 7350–7354. https://doi.org/10.1073/pnas.78.12.7350.

[67] A. Khvorova, J.K. Watts, The chemical evolution of oligonucleotide therapies of clinical utility, Nat. Biotechnol. 35 (2017) 238–248. https://doi.org/10.1038/nbt.3765.

[68] N. Iwamoto, D.C.D. Butler, N. Svrzikapa, S. Mohapatra, I. Zlatev, Di.W.Y. Sah, Meena, S.M. Standley, G. Lu, L.H. Apponi, M. Frank-Kamenetsky, J.J. Zhang, C. Vargeese, G.L. Verdine, Control of phosphorothioate stereochemistry substantially increases the efficacy of antisense oligonucleotides, Nat. Biotechnol. 35 (2017) 845–851. https://doi.org/10.1038/nbt.3948.

[69] W.S. Marshall, M.H. Caruthers, Phosphorodithioate DNA as a Potential Therapeutic Drug, Science (80-.). 259 (1993) 1564–1570. https://doi.org/10.1126/science.7681216.

[70] M.T. Migawa, W. Shen, W. Brad Wan, G. Vasquez, M.E. Oestergaard, A. Low, C.L. De Hoyos, R. Gupta, S. Murray, M. Tanowitz, M. Bell, J.G. Nichols, H. Gaus, L. Xue-Hai, E.E. Swayze, S.T. Crooke, P.P. Seth, Site-specific replacement of phosphorothioate with alkyl phosphonate linkages enhances the therapeutic profile of gapmer ASOs by modulating interactions with cellular proteins, Nucleic Acids Res. 47 (2019) 5465–5479. https://doi.org/10.1093/nar/gkz247.

[71] Z. Zeng, S. Han, W. Hong, Y. Lang, F. Li, Y. Liu, Z. Li, Y. Wu, W. Li, X. Zhang, Z. Cao, A Tat-conjugated Peptide Nucleic Acid Tat-PNA-DR Inhibits Hepatitis B Virus Replication In Vitro and In Vivo by Targeting LTR Direct Repeats of HBV RNA, Mol. Ther. - Nucleic Acids. 5 (2016) e295. https://doi.org/10.1038/mtna.2016.11.

[72] R.P. Singh, B.-K. Oh, J.-W. Choi, Application of peptide nucleic acid towards development of nanobiosensor arrays, Bioelectrochemistry. 79 (2010) 153–161. https://doi.org/https://doi.org/10.1016/j.bioelechem.2010.02.004.

[73] G.F. Deleavey, M.J. Damha, Designing Chemically Modified Oligonucleotides for Targeted Gene Silencing, Chem. Biol. 19 (2012) 937–954. https://doi.org/https://doi.org/10.1016/j.chembiol.2012.07.011.

[74] W. Li, X. Lan, Aptamer Oligonucleotides: Novel Potential Therapeutic Agents

in Autoimmune Disease, Nucleic Acid Ther. 25 (2015) 173–179. https://doi.org/10.1089/nat.2014.0529.

[75] P. Herdewijn, Heterocyclic Modifications of Oligonucleotides and Antisense Technology, Antisense Nucleic Acid Drug Dev. 10 (2000) 297–310. https://doi.org/10.1089/108729000421475.

[76] M. Terrazas, E.T. Kool, RNA major groove modifications improve siRNA stability and biological activity, Nucleic Acids Res. 37 (2009) 346–353. https://doi.org/10.1093/nar/gkn958.

[77] K. Karikó, H. Muramatsu, F.A. Welsh, J. Ludwig, H. Kato, S. Akira, D. Weissman, Incorporation of pseudouridine into mRNA yields superior nonimmunogenic vector with increased translational capacity and biological stability, Mol. Ther. 16 (2008) 1833–1840. https://doi.org/10.1038/mt.2008.200.

[78] M.S.D. Kormann, G. Hasenpusch, M.K. Aneja, G. Nica, A.W. Flemmer, S. Herber-Jonat, M. Huppmann, L.E. Mays, M. Illenyi, A. Schams, M. Griese, I. Bittmann, R. Handgretinger, D. Hartl, J. Rosenecker, C. Rudolph, Expression of therapeutic proteins after delivery of chemically modified mRNA in mice, Nat. Biotechnol. 29 (2011) 154–157. https://doi.org/10.1038/nbt.1733.

[79] B.R. Anderson, H. Muramatsu, B.K. Jha, R.H. Silverman, D. Weissman, K. Karikó, Nucleoside modifications in RNA limit activation of 2′-5′- oligoadenylate synthetase and increase resistance to cleavage by RNase L, Nucleic Acids Res. 39 (2011) 9329–9338. https://doi.org/10.1093/nar/gkr586.

[80] J. Zhang, J. Zheng, C. Lu, Q. Du, Z. Liang, Z. Xi, Modification of the siRNA Passenger Strand by 5-Nitroindole Dramatically Reduces its Off-Target Effects, ChemBioChem. 13 (2012) 1940–1945. https://doi.org/10.1002/cbic.201200349.

[81] S.Y. Wu, T.M. Chen, W.H. Gmeiner, E. Chu, J.C. Schmitz, Development of modified siRNA molecules incorporating 5-fluoro-2′- deoxyuridine residues to enhance cytotoxicity, Nucleic Acids Res. 41 (2013) 4650–4659. https://doi.org/10.1093/nar/gkt120.

[82] R.S. Geary, D. Norris, R. Yu, C.F. Bennett, Pharmacokinetics, biodistribution and cell uptake of antisense oligonucleotides, Adv. Drug Deliv. Rev. 87 (2015) 46–51. https://doi.org/https://doi.org/10.1016/j.addr.2015.01.008.

[83] C.I. Edvard Smith, R. Zain, Therapeutic oligonucleotides: State of the art, Annu. Rev. Pharmacol. Toxicol. 59 (2019) 605–630. https://doi.org/10.1146/annurev-pharmtox-010818-021050.

[84] B.P. Monia, E.A. Lesnik, C. Gonzalez, W.F. Lima, D. McGee, C.J. Guinosso, A.M. Kawasaki, P.D. Cook, S.M. Freier, Evaluation of 2‘-modified oligonucleotides containing 2‘-deoxy gaps as antisense inhibitors of gene expression, J. Biol. Chem. 268 (1993) 14514–14522. https://doi.org/https://doi.org/10.1016/S0021-9258(19)85268-7.

[85] D.M. Kenski, G. Butora, A.T. Willingham, A.J. Cooper, W. Fu, N. Qi, F. Soriano, I.W. Davies, W.M. Flanagan, SiRNA-optimized modifications for enhanced in vivo activity, Mol. Ther. - Nucleic Acids. 1 (2012) e5. https://doi.org/10.1038/mtna.2011.4.

[86] J. SUMMERTON, D. WELLER, Morpholino Antisense Oligomers: Design, Preparation, and Properties, Antisense Nucleic Acid Drug Dev. 7 (1997) 187–195. https://doi.org/10.1089/oli.1.1997.7.187.

[87] J.S. Jepsen, M.D. Sørensen, J. Wengel, Locked Nucleic Acid: A Potent Nucleic Acid Analog in Therapeutics and Biotechnology, Oligonucleotides. 14 (2004) 130–146. https://doi.org/10.1089/1545457041526317.

[88] U. Christensen, N. Jacobsen, V.K. Rajwanshi, J. Wengel, T. Koch, Stopped-flow kinetics of locked nucleic acid (LNA) - Oligonucleotide duplex formation: Studies of LNA-DNA and DNA-DNA interactions, Biochem. J. 354 (2001) 481–484. https://doi.org/10.1042/0264-6021:3540481.

[89] K. Morita, C. Hasegawa, M. Kaneko, S. Tsutsumi, J. Sone, T. Ishikawa, T. Imanishi, M. Koizumi, 2′-O, 4′-C-Ethylene-bridged nucleic acids (ENA) with nuclease-resistance and high affnity for RNA, Nucleic Acids Symp. Ser. 1 (2001) 241–242. https://doi.org/10.1093/nass/1.1.241.

[90] P.P. Seth, G. Vasquez, C.A. Allerson, A. Berdeja, H. Gaus, G.A. Kinberger, T.P. Prakash, M.T. Migawa, B. Bhat, E.E. Swayze, Synthesis and Biophysical Evaluation of 2′,4′-Constrained 2′O-Methoxyethyl and 2′,4′-Constrained 2′O-Ethyl Nucleic Acid Analogues, J. Org. Chem. 75 (2010) 1569–1581. https://doi.org/10.1021/jo902560f.

[91] S. Murray, D. Ittig, E. Koller, A. Berdeja, A. Chappell, T.P. Prakash, M. Norrbom, E.E. Swayze, C.J. Leumann, P.P. Seth, reduce scavenger receptor B1 mRNA in hepatic and extra-hepatic tissues — a comparative study of oligonucleotide length , design and chemistry, 40 (2012) 6135–6143. https://doi.org/10.1093/nar/gks273.

[92] T.C. Roberts, R. Langer, M.J.A. Wood, Advances in oligonucleotide drug delivery, Nat. Rev. Drug Discov. 19 (2020) 673–694. https://doi.org/10.1038/s41573-020-0075-7.

[93] N.T. Schirle, I.J. MacRae, The Crystal Structure of Human Argonaute2, Science (80-.). 336 (2012) 1037–1040. https://doi.org/10.1126/science.1221551.

[94] C. Wolfrum, S. Shi, K.N. Jayaprakash, M. Jayaraman, G. Wang, R.K. Pandey, K.G. Rajeev, T. Nakayama, K. Charrise, E.M. Ndungo, T. Zimmermann, V. Koteliansky, M. Manoharan, M. Stoffel, Mechanisms and optimization of in vivo delivery of lipophilic siRNAs, Nat. Biotechnol. 25 (2007) 1149–1157. https://doi.org/10.1038/nbt1339.

[95] J.K. Nair, J.L.S. Willoughby, A. Chan, K. Charisse, M.R. Alam, Q. Wang, M. Hoekstra, P. Kandasamy, A. V Kel'in, S. Milstein, N. Taneja, J. O'Shea, S. Shaikh, L. Zhang, R.J. van der Sluis, M.E. Jung, A. Akinc, R. Hutabarat, S. Kuchimanchi, K. Fitzgerald, T. Zimmermann, T.J.C. van Berkel, M.A. Maier, K.G. Rajeev, M. Manoharan, Multivalent N-Acetylgalactosamine-Conjugated siRNA Localizes in Hepatocytes and Elicits Robust RNAi-Mediated Gene Silencing, J. Am. Chem. Soc. 136 (2014) 16958–16961. https://doi.org/10.1021/ja505986a.

[96] A. Eguchi, B.R. Meade, Y.-C. Chang, C.T. Fredrickson, K. Willert, N. Puri, S.F.

Dowdy, Efficient siRNA delivery into primary cells by a peptide transduction domain–dsRNA binding domain fusion protein, Nat. Biotechnol. 27 (2009) 567–571. https://doi.org/10.1038/nbt.1541.

[97] J.O. McNamara, E.R. Andrechek, Y. Wang, K.D. Viles, R.E. Rempel, E. Gilboa, B.A. Sullenger, P.H. Giangrande, Cell type–specific delivery of siRNAs with aptamer-siRNA chimeras, Nat. Biotechnol. 24 (2006) 1005–1015. https://doi.org/10.1038/nbt1223.

[98] E. Song, P. Zhu, S.-K. Lee, D. Chowdhury, S. Kussman, D.M. Dykxhoorn, Y. Feng, D. Palliser, D.B. Weiner, P. Shankar, W.A. Marasco, J. Lieberman, Antibody mediated in vivo delivery of small interfering RNAs via cell-surface receptors, Nat. Biotechnol. 23 (2005) 709–717. https://doi.org/10.1038/nbt1101.

[99] K.K. Ray, U. Landmesser, L.A. Leiter, D. Kallend, R. Dufour, M. Karakas, T. Hall, R.P.T. Troquay, T. Turner, F.L.J. Visseren, P. Wijngaard, R.S. Wright, J.J.P. Kastelein, Inclisiran in Patients at High Cardiovascular Risk with Elevated LDL Cholesterol, N. Engl. J. Med. 376 (2017) 1430–1440. https://doi.org/10.1056/NEJMoa1615758.

[100] T.P. Prakash, M.J. Graham, J. Yu, R. Carty, A. Low, A. Chappell, K. Schmidt, C. Zhao, M. Aghajan, H.F. Murray, S. Riney, S.L. Booten, S.F. Murray, H. Gaus, J. Crosby, W.F. Lima, S. Guo, B.P. Monia, E.E. Swayze, P.P. Seth, Targeted delivery of antisense oligonucleotides to hepatocytes using triantennary N-acetyl galactosamine improves potency 10-fold in mice, Nucleic Acids Res. 42 (2014) 8796–8807. https://doi.org/10.1093/nar/gku531.

[101] T.S. Zimmermann, V. Karsten, A. Chan, J. Chiesa, M. Boyce, B.R. Bettencourt, R. Hutabarat, S. Nochur, A. Vaishnaw, J. Gollob, Clinical Proof of Concept for a Novel Hepatocyte-Targeting GalNAc-siRNA Conjugate, Mol. Ther. 25 (2017) 71–78. https://doi.org/https://doi.org/10.1016/j.ymthe.2016.10.019.

[102] A.D. Springer, S.F. Dowdy, GalNAc-siRNA Conjugates: Leading the Way for Delivery of RNAi Therapeutics, Nucleic Acid Ther. 28 (2018) 109–118. https://doi.org/10.1089/nat.2018.0736.

[103] M.M. Janas, M.K. Schlegel, C.E. Harbison, V.O. Yilmaz, Y. Jiang, R. Parmar, I. Zlatev, A. Castoreno, H. Xu, S. Shulga-Morskaya, K.G. Rajeev, M. Manoharan, N.D. Keirstead, M.A. Maier, V. Jadhav, Selection of GalNAc-conjugated siRNAs with limited off-target-driven rat hepatotoxicity, Nat. Commun. 9 (2018) 723. https://doi.org/10.1038/s41467-018-02989-4.

[104] N.J. Viney, J.C. van Capelleveen, R.S. Geary, S. Xia, J.A. Tami, R.Z. Yu, S.M. Marcovina, S.G. Hughes, M.J. Graham, R.M. Crooke, S.T. Crooke, J.L. Witztum, E.S. Stroes, S. Tsimikas, Antisense oligonucleotides targeting apolipoprotein(a) in people with raised lipoprotein(a): two randomised, double-blind, placebo-controlled, dose-ranging trials, Lancet. 388 (2016) 2239–2253. https://doi.org/https://doi.org/10.1016/S0140-6736(16)31009-1.

[105] D. Jones, Silencing the sceptics, Nat. Rev. Drug Discov. 3 (2004) 997. https://doi.org/10.1038/nrd1588.

[106] T. Khan, H. Weber, J. DiMuzio, A. Matter, B. Dogdas, T. Shah, A. Thankappan, J. Disa, V. Jadhav, L. Lubbers, L. Sepp-Lorenzino, W.R. Strapps, M. Tadin-Strapps, Silencing Myostatin Using Cholesterol-conjugated siRNAs Induces Muscle Growth, Mol. Ther. - Nucleic Acids. 5 (2016) e342. https://doi.org/https://doi.org/10.1038/mtna.2016.55.

[107] K. Nishina, T. Unno, Y. Uno, T. Kubodera, T. Kanouchi, H. Mizusawa, T. Yokota, Efficient In Vivo Delivery of siRNA to the Liver by Conjugation of α-Tocopherol, Mol. Ther. 16 (2008) 734–740. https://doi.org/https://doi.org/10.1038/mt.2008.14.

[108] P. Khan, J.A. Siddiqui, I. Lakshmanan, A.K. Ganti, R. Salgia, M. Jain, S.K. Batra, M.W. Nasser, RNA-based therapies: A cog in the wheel of lung cancer defense, Mol. Cancer. 20 (2021) 54. https://doi.org/10.1186/s12943-021-01338-2.

[109] D. Capaldi, A. Teasdale, S. Henry, N. Akhtar, C. den Besten, S. Gao-Sheridan, M. Kretschmer, N. Sharpe, B. Andrews, B. Burm, J. Foy, Impurities in Oligonucleotide Drug Substances and Drug Products, Nucleic Acid Ther. 27 (2017) 309–322. https://doi.org/10.1089/nat.2017.0691.

[110] S.G. Roussis, I. Cedillo, C. Rentel, Automated determination of early eluting oligonucleotide impurities using ion-pair reversed-phase liquid chromatography high resolution-mass spectrometry, Anal. Biochem. 595 (2020) 113623. https://doi.org/10.1016/j.ab.2020.113623.

[111] T. Suzuki, S. Ohsumi, K. Makino, Mechanistic studies on depurination and apurinic site chain breakage in oligodeoxyribonucleotides, Nucleic Acids Res. 22 (1994) 4997–5003. https://doi.org/10.1093/nar/22.23.4997.

[112] A. Goyon, K. Zhang, Characterization of antisense oligonucleotide impurities by ion-pairing reversed-phase and anion exchange chromatography coupled to HILIC/MS using a versatile 2D-LC setup, Anal. Chem. (2020). https://doi.org/10.1021/acs.analchem.0c00114.

[113] D. Capaldi, K. Ackley, D. Brooks, J. Carmody, K. Draper, R. Kambhampati, M. Kretschmer, D. Levin, J. McArdle, B. Noll, R. Raghavachari, I. Roymoulik, B.P. Sharma, R. Thürmer, F. Wincott, Quality Aspects of Oligonucleotide Drug Development: Specifications for Active Pharmaceutical Ingredients, Drug Inf. J. 46 (2012) 611–626. https://doi.org/10.1177/0092861512445311.

[114] A. Liu, M. Cheng, Y. Zhou, P. Deng, Bioanalysis of Oligonucleotide by LC–MS: Effects of Ion Pairing Regents and Recent Advances in Ion-Pairing-Free Analytical Strategies, Int. J. Mol. Sci. 23 (2022). https://doi.org/10.3390/ijms232415474.

[115] S.C. Moldoveanu, V. David, Chapter 5 - Retention Mechanisms in Different HPLC Types, in: S.C. Moldoveanu, V.B.T.-E. in M.H.S. David (Eds.), Elsevier, 2013: pp. 145–190. https://doi.org/https://doi.org/10.1016/B978-0-12-385013-3.00005-7.

[116] T. Fornstedt, M. Enmark, Separation of therapeutic oligonucleotides using ion-pair reversed-phase chromatography based on fundamental separation science, J. Chromatogr. Open. 3 (2023) 100079.

https://doi.org/https://doi.org/10.1016/j.jcoa.2023.100079.

[117] M. Gilar, U.D. Neue, Peak capacity in gradient reversed-phase liquid chromatography of biopolymers. Theoretical and practical implications for the separation of oligonucleotides, J. Chromatogr. A. 1169 (2007) 139–150. https://doi.org/10.1016/j.chroma.2007.09.005.

[118] U.D. Neue, Peak capacity in unidimensional chromatography, J. Chromatogr. A. 1184 (2008) 107–130. https://doi.org/10.1016/j.chroma.2007.11.113.

[119] M. Gilar, K.J. Fountain, Y. Budman, U.D. Neue, K.R. Yardley, P.D. Rainville, R.J. Russell, J.C. Gebler, Ion-pair reversed-phase high-performance liquid chromatography analysis of oligonucleotides: Retention prediction, J. Chromatogr. A. 958 (2002) 167–182. https://doi.org/10.1016/S0021-9673(02)00306-0.

[120] E.D. Close, A.O. Nwokeoji, D. Milton, K. Cook, D.M. Hindocha, E.C. Hook, H. Wood, M.J. Dickman, Nucleic acid separations using superficially porous silica particles, J. Chromatogr. A. 1440 (2016) 135–144. https://doi.org/https://doi.org/10.1016/j.chroma.2016.02.057.

[121] S.G. Roussis, M. Pearce, C. Rentel, Small Alkyl Amines as Ion-Pair Reagents for the Separation of Positional Isomers of Impurities in Phosphate Diester Oligonucleotides, (n.d.).

[122] M. Biba, E. Jiang, B. Mao, D. Zewge, J.P. Foley, C.J. Welch, Factors influencing the separation of oligonucleotides using reversed-phase/ion-exchange mixed-mode high performance liquid chromatography columns, J. Chromatogr. A. 1304 (2013) 69–77. https://doi.org/10.1016/j.chroma.2013.06.050.

[123] L. Li, J.P. Foley, R. Helmy, Simultaneous separation of small interfering RNA and lipids using ion-pair reversed-phase liquid chromatography, J. Chromatogr. A. 1601 (2019) 145–154. https://doi.org/https://doi.org/10.1016/j.chroma.2019.04.061.

[124] B. Chen, S.F. Mason, M.G. Bartlett, The effect of organic modifiers on electrospray ionization charge-state distribution and desorption efficiency for oligonucleotides, J. Am. Soc. Mass Spectrom. 24 (2013) 257–264. https://doi.org/10.1007/s13361-012-0509-5.

[125] A. Apffel, J.A. Chakel, S. Fischer, K. Lichtenwalter, W.S. Hancock, Analysis of oligonucleotides by HPLC-electrospray ionization mass spectrometry, Anal. Chem. 69 (1997) 1320–1325. https://doi.org/10.1021/ac960916h.

[126] K.J. Fountain, M. Gilar, J.C. Gebler, Analysis of native and chemically modified oligonucleotides by tandem ion-pair reversed-phase high-performance liquid chromatography/electrospray ionization mass spectrometry, Rapid Commun. Mass Spectrom. 17 (2003) 646–653. https://doi.org/10.1002/rcm.959.

[127] M. Donegan, J.M. Nguyen, M. Gilar, Effect of ion-pairing reagent hydrophobicity on liquid chromatography and mass spectrometry analysis of oligonucleotides, J. Chromatogr. A. 1666 (2022) 462860. https://doi.org/10.1016/j.chroma.2022.462860.

[128] G. McFarland, P.N. Borer, Separation of oligo-RNA by reverse-phase HPLC, Nucleic Acids Res. 7 (1979) 1067–1080. https://doi.org/10.1093/nar/7.4.1067.

[129] A.J. Alpert, Hydrophilic-interaction chromatography for the separation of peptides, nucleic acids and other polar compounds, J. Chromatogr. A. 499 (1990) 177–196. https://doi.org/https://doi.org/10.1016/S0021-9673(00)96972-3.

[130] B. Buszewski, S. Noga, Hydrophilic interaction liquid chromatography (HILIC)—a powerful separation technique, Anal. Bioanal. Chem. 402 (2012) 231–247. https://doi.org/10.1007/s00216-011-5308-5.

[131] H. Lardeux, D. Guillarme, V. D'Atri, Comprehensive evaluation of zwitterionic hydrophilic liquid chromatography stationary phases for oligonucleotide characterization, J. Chromatogr. A. 1690 (2023). https://doi.org/10.1016/j.chroma.2023.463785.

[132] P.A. Lobue, M. Jora, B. Addepalli, P.A. Limbach, Oligonucleotide analysis by hydrophilic interaction liquid chromatography-mass spectrometry in the absence of ion-pair reagents, J. Chromatogr. A. 1595 (2019) 39–48. https://doi.org/10.1016/j.chroma.2019.02.016.

[133] A. Demelenne, M.-J. Gou, G. Nys, C. Parulski, J. Crommen, A.-C. Servais, M. Fillet, Evaluation of hydrophilic interaction liquid chromatography, capillary zone electrophoresis and drift tube ion-mobility quadrupole time of flight mass spectrometry for the characterization of phosphodiester and phosphorothioate oligonucleotides, J. Chromatogr. A. 1614 (2020) 460716. https://doi.org/https://doi.org/10.1016/j.chroma.2019.460716.

[134] A.M. Abdullah, C. Sommers, J. Hawes, J.D. Rodriguez, K. Yang, Tandem mass spectrometric sequence characterization of synthetic thymidine-rich oligonucleotides, J. Mass Spectrom. 57 (2022). https://doi.org/10.1002/jms.4819.

[135] M. Huang, X. Xu, H. Qiu, N. Li, Analytical characterization of DNA and RNA oligonucleotides by hydrophilic interaction liquid chromatography-tandem mass spectrometry, J. Chromatogr. A. 1648 (2021) 462184. https://doi.org/10.1016/j.chroma.2021.462184.

[136] L. Gong, Analysis of oligonucleotides by ion-pairing hydrophilic interaction liquid chromatography/electrospray ionization mass spectrometry, Rapid Commun. Mass Spectrom. 31 (2017) 2125–2134. https://doi.org/10.1002/rcm.8004.

[137] S. Studzińska, F. Łobodziński, B. Buszewski, Application of hydrophilic interaction liquid chromatography coupled with mass spectrometry in the analysis of phosphorothioate oligonucleotides in serum, J. Chromatogr. B. 1040 (2017) 282–288. https://doi.org/https://doi.org/10.1016/j.jchromb.2016.11.001.

[138] A. Kilanowska, B. Buszewski, S. Studzińska, Application of hydrophilic interaction liquid chromatography coupled with tandem mass spectrometry for the retention and sensitivity studies of antisense oligonucleotides, J. Chromatogr. A. 1622 (2020) 461100.

https://doi.org/https://doi.org/10.1016/j.chroma.2020.461100.

[139] P.H. Jensen, S. Mysling, P. Højrup, O.N. Jensen, Glycopeptide Enrichment for MALDI-TOF Mass Spectrometry Analysis by Hydrophilic Interaction Liquid Chromatography Solid Phase Extraction (HILIC SPE) BT - Mass Spectrometry of Glycoproteins: Methods and Protocols, in: J.J. Kohler, S.M. Patrie (Eds.), Humana Press, Totowa, NJ, 2013: pp. 131–144. https://doi.org/10.1007/978-1-62703-146-2_10.

[140] Z. Hao, B. Xiao, N. Weng, Impact of column temperature and mobile phase components on selectivity of hydrophilic interaction chromatography (HILIC), J. Sep. Sci. 31 (2008) 1449–1464. https://doi.org/https://doi.org/10.1002/jssc.200700624.

[141] A. Goyon, P. Yehl, K. Zhang, Characterization of therapeutic oligonucleotides by liquid chromatography, J. Pharm. Biomed. Anal. 182 (2020) 113105. https://doi.org/10.1016/j.jpba.2020.113105.

[142] Y. Guo, N. Bhalodia, B. Fattal, I. Serris, Evaluating the Adsorbed Water Layer on Polar Stationary Phases for Hydrophilic Interaction Chromatography (HILIC), Separations. 6 (2019). https://doi.org/10.3390/separations6020019.

[143] J.B. Crowther, S.D. Fazio, R.A. Hartwick, High-performance liquid chromatographic separation of oligonucleotides and other nucleic acid constituents on multifunctional stationary phases, J. Chromatogr. A. 282 (1983) 619–628. https://doi.org/https://doi.org/10.1016/S0021-9673(00)91639-X.

[144] A. Zimmermann, R. Greco, I. Walker, J. Horak, A. Cavazzini, M. Lämmerhofer, Synthetic oligonucleotide separations by mixed-mode reversed-phase/weak anion-exchange liquid chromatography, J. Chromatogr. A. 1354 (2014) 43–55. https://doi.org/10.1016/j.chroma.2014.05.048.

[145] F. Li, X. Su, S. Bäurer, M. Lämmerhofer, Multiple heart-cutting mixed-mode chromatography-reversed-phase 2D-liquid chromatography method for separation and mass spectrometric characterization of synthetic oligonucleotides, J. Chromatogr. A. 1625 (2020) 461338. https://doi.org/https://doi.org/10.1016/j.chroma.2020.461338.

[146] D.R. Stoll, P.W. Carr, Two-Dimensional Liquid Chromatography: A State of the Art Tutorial, Anal. Chem. 89 (2017) 519–531. https://doi.org/10.1021/acs.analchem.6b03506.

[147] X. Wang, S. Buckenmaier, D. Stoll, The growing role of two-dimensional LC in the biopharmaceutical industry, J. Appl. Bioanal. 3 (2017) 120–126. https://doi.org/10.17145/jab.17.015.

[148] D.R. Stoll, Troubleshooting for Two-Dimensional Liquid Chromatography (2D–LC): Breakthrough in the Second Dimension, LCGC North Am. 38 (2020) 597–600. https://www.chromatographyonline.com/view/troubleshooting-for-2-dimensional-liquid-chromatography-breakthrough-in-the-second-dimension.

[149] S. Chapel, F. Rouvière, M. Sarrut, S. Heinisch, Two-Dimensional Liquid Chromatography Coupled to High-Resolution Mass Spectrometry for the Analysis of ADCs BT - Antibody-Drug Conjugates: Methods and Protocols, in:

L.N. Tumey (Ed.), Springer US, New York, NY, 2020: pp. 163–185. https://doi.org/10.1007/978-1-4939-9929-3_11.

[150] D.R. Stoll, P.W. Carr, Multi-dimensional Liquid Chromatography: Principles, Practice, and Applications, CRC Press, 2022.

[151] K. Zhang, Y. Li, M. Tsang, N.P. Chetwyn, Analysis of pharmaceutical impurities using multi-heartcutting 2D LC coupled with UV-charged aerosol MS detection, J. Sep. Sci. 36 (2013) 2986–2992. https://doi.org/10.1002/jssc.201300493.

[152] S.R. Groskreutz, M.M. Swenson, L.B. Secor, D.R. Stoll, Selective comprehensive multi-dimensional separation for resolution enhancement in high performance liquid chromatography. Part I: Principles and instrumentation, J. Chromatogr. A. 1228 (2012) 31–40. https://doi.org/https://doi.org/10.1016/j.chroma.2011.06.035.

[153] F. Li, S. Chen, S. Studzińska, M. Lämmerhofer, Polybutylene terephthalate-based stationary phase for ion-pair-free reversed-phase liquid chromatography of small interfering RNA. Part 1: Direct coupling with mass spectrometry, J. Chromatogr. A. 1694 (2023) 463898. https://doi.org/https://doi.org/10.1016/j.chroma.2023.463898.

[154] B.W.J. Pirok, D.R. Stoll, P.J. Schoenmakers, Recent Developments in Two-Dimensional Liquid Chromatography: Fundamental Improvements for Practical Applications, Anal. Chem. 91 (2019) 240–263. https://doi.org/10.1021/acs.analchem.8b04841.

[155] J. Samuelsson, R.A. Shalliker, T. Fornstedt, Viscosity contrast effects in analytical scale chromatography - Evidence and impact, Microchem. J. 130 (2017) 102–107. https://doi.org/https://doi.org/10.1016/j.microc.2016.08.007.

[156] D.R. Stoll, D.C. Harmes, G.O. Staples, O.G. Potter, C.T. Dammann, D. Guillarme, A. Beck, Development of Comprehensive Online Two-Dimensional Liquid Chromatography/Mass Spectrometry Using Hydrophilic Interaction and Reversed-Phase Separations for Rapid and Deep Profiling of Therapeutic Antibodies, Anal. Chem. 90 (2018) 5923–5929. https://doi.org/10.1021/acs.analchem.8b00776.

[157] E.S. Talus, K.E. Witt, D.R. Stoll, Effect of pressure pulses at the interface valve on the stability of second dimension columns in online comprehensive two-dimensional liquid chromatography, J. Chromatogr. A. 1378 (2015) 50–57. https://doi.org/https://doi.org/10.1016/j.chroma.2014.12.019.

[158] D.R. Stoll, K. Shoykhet, P. Petersson, S. Buckenmaier, Active Solvent Modulation: A Valve-Based Approach to Improve Separation Compatibility in Two-Dimensional Liquid Chromatography, Anal. Chem. 89 (2017) 9260–9267. https://doi.org/10.1021/acs.analchem.7b02046.

[159] R.J. Vonk, A.F.G. Gargano, E. Davydova, H.L. Dekker, S. Eeltink, L.J. de Koning, P.J. Schoenmakers, Comprehensive Two-Dimensional Liquid Chromatography with Stationary-Phase-Assisted Modulation Coupled to High-Resolution Mass Spectrometry Applied to Proteome Analysis of Saccharomyces cerevisiae, Anal. Chem. 87 (2015) 5387–5394.

https://doi.org/10.1021/acs.analchem.5b00708.

[160] W. Nowik, S. Héron, M. Bonose, M. Nowik, A. Tchapla, Assessment of two-dimensional separative systems using nearest-neighbor distances approach. Part 1: Orthogonality aspects, Anal. Chem. 85 (2013) 9449–9458. https://doi.org/10.1021/ac4012705.

[161] P. Schoenmakers, P. Marriott, J. Beens, Nomenclature and conventions in comprehensive multidimensional chromatography, LCGC Eur. 25 (2003) 1–4.

[162] M. Gilar, P. Olivova, A.E. Daly, J.C. Gebler, Orthogonality of separation in two-dimensional liquid chromatography, Anal. Chem. 77 (2005) 6426–6434. https://doi.org/10.1021/ac050923i.

[163] M. Gilar, J. Fridrich, M.R. Schure, A. Jaworski, Comparison of orthogonality estimation methods for the two-dimensional separations of peptides, Anal. Chem. 84 (2012) 8722–8732. https://doi.org/10.1021/ac3020214.

[164] M. Camenzuli, P.J. Schoenmakers, A new measure of orthogonality for multi-dimensional chromatography, Anal. Chim. Acta. 838 (2014) 93–101. https://doi.org/10.1016/j.aca.2014.05.048.

[165] M.R. Schure, The dimensionality of chromatographic separations, J. Chromatogr. A. 1218 (2011) 293–302. https://doi.org/10.1016/j.chroma.2010.11.016.

[166] J. Jáčová, A. Gardlo, J.M.D. Dimandja, T. Adam, D. Friedecký, Impact of sample dimensionality on orthogonality metrics in comprehensive two-dimensional separations, Anal. Chim. Acta. 1064 (2019) 138–149. https://doi.org/10.1016/j.aca.2019.03.018.

[167] J. Mommers, S. van der Wal, Two metrics for measuring orthogonality for two-dimensional chromatography, J. Chromatogr. A. 1586 (2019) 101–105. https://doi.org/10.1016/j.chroma.2018.11.081.

[168] J.R. Thayer, N. Puri, C. Burnett, M. Hail, S. Rao, Identification of RNA linkage isomers by anion exchange purification with electrospray ionization mass spectrometry of automatically desalted phosphodiesterase-II digests, Anal. Biochem. 399 (2010) 110–117. https://doi.org/https://doi.org/10.1016/j.ab.2009.11.009.

[169] Q. Li, F. Lynen, J. Wang, H. Li, G. Xu, P. Sandra, Comprehensive hydrophilic interaction and ion-pair reversed-phase liquid chromatography for analysis of di- to deca-oligonucleotides, J. Chromatogr. A. 1255 (2012) 237–243. https://doi.org/10.1016/j.chroma.2011.11.062.

[170] S.G. Roussis, I. Cedillo, C. Rentel, Two-dimensional liquid chromatography-mass spectrometry for the characterization of modified oligonucleotide impurities, Anal. Biochem. 556 (2018) 45–52. https://doi.org/https://doi.org/10.1016/j.ab.2018.06.019.

[171] B. Basiri, M.M. Murph, M.G. Bartlett, Assessing the Interplay between the Physicochemical Parameters of Ion-Pairing Reagents and the Analyte Sequence on the Electrospray Desorption Process for Oligonucleotides, J. Am. Soc. Mass Spectrom. 28 (2017) 1647–1656. https://doi.org/10.1007/s13361-

017-1671-6.

[172] A.J. Dempster, LII. The ionization and dissociation of hydrogen molecules and the formation of H 3 , London, Edinburgh, Dublin Philos. Mag. J. Sci. 31 (1916) 438–443. https://doi.org/10.1080/14786440508635520.

[173] F.H. Field, Chemical ionization mass spectrometry, Acc. Chem. Res. 1 (1968) 42–49. https://doi.org/10.1021/ar50002a002.

[174] A. Saitman, Chapter 13 - Overview of Analytical Methods in Drugs of Abuse Analysis: Gas Chromatography/Mass Spectrometry, Liquid Chromatography Combined With Tandem Mass Spectrometry and Related Methods, in: A.B.T.-C.I. in A. and D. of A.T. (Second E. Dasgupta (Ed.), Academic Press, 2019: pp. 157–171. https://doi.org/https://doi.org/10.1016/B978-0-12-815607-0.00013-7.

[175] M. Wilm, Principles of Electrospray Ionization, Mol. Cell. Proteomics. 10 (2011) M111.009407. https://doi.org/https://doi.org/10.1074/mcp.M111.009407.

[176] W.C. Byrdwell, Atmospheric pressure chemical ionization mass spectrometry for analysis of lipids, Lipids. 36 (2001) 327–346. https://doi.org/https://doi.org/10.1007/s11745-001-0725-5.

[177] H.P. Nguyen, K.A. Schug, The advantages of ESI-MS detection in conjunction with HILIC mode separations: Fundamentals and applications, J. Sep. Sci. 31 (2008) 1465–1480. https://doi.org/https://doi.org/10.1002/jssc.200700630.

[178] C.S. Ho, C.W.K. Lam, M.H.M. Chan, R.C.K. Cheung, L.K. Law, L.C.W. Lit, K.F. Ng, M.W.M. Suen, H.L. Tai, Electrospray ionisation mass spectrometry: principles and clinical applications., Clin. Biochem. Rev. 24 (2003) 3–12.

[179] S. Banerjee, S. Mazumdar, Electrospray Ionization Mass Spectrometry: A Technique to Access the Information beyond the Molecular Weight of the Analyte, Int. J. Anal. Chem. 2012 (2012) 282574. https://doi.org/10.1155/2012/282574.

[180] G.I. Taylor, Disintegration of water drops in an electric field, Proc. R. Soc. London. Ser. A. Math. Phys. Sci. 280 (1964) 383–397. https://doi.org/10.1098/rspa.1964.0151.

[181] P. Kebarle, L. Tang, From ions in solution to ions in the gas phase - the mechanism of electrospray mass spectrometry, Anal. Chem. 65 (1993) 972A-986A. https://doi.org/10.1021/ac00070a001.

[182] R.B. Cole, A.K. Harrata, Solvent effect on analyte charge state, signal intensity, and stability in negative ion electrospray mass spectrometry; implications for the mechanism of negative ion formation, J. Am. Soc. Mass Spectrom. 4 (1993) 546–556. https://doi.org/10.1016/1044-0305(93)85016-Q.

[183] V. Cunsolo, V. Muccilli, R. Saletti, S. Foti, Mass spectrometry in food proteomics: a tutorial, J. Mass Spectrom. 49 (2014) 768–784. https://doi.org/https://doi.org/10.1002/jms.3374.

[184] M. Henchman, C. Steel, Understanding the Quadrupole Mass Filter through Computer Simulation, J. Chem. Educ. 75 (1998) 1049. https://doi.org/10.1021/ed075p1049.

[185] J.W. Honour, Benchtop mass spectrometry in clinical biochemistry, Ann. Clin. Biochem. 40 (2003) 628–638. https://doi.org/10.1258/0004563037703672l6.

[186] R.J. Cotter, Time-of-Flight Mass Spectrometry for the Structural Analysis of Biological Molecules, Anal. Chem. 64 (1992) 1027A-1039A. https://doi.org/10.1021/ac00045a726.

[187] U. Boesl, Time-of-flight mass spectrometry: Introduction to the basics, Mass Spectrom. Rev. 36 (2017) 86–109. https://doi.org/https://doi.org/10.1002/mas.21520.

[188] D.. Koppenaal, C.. Barinaga, M. Bonner Denton, P. Sperline, G.. Hieftje, G.. Schilling, F.. Andrade, B. J.H, MS Detectors, Anal. Chem. 77 (2005) 418 A-427 A. https://doi.org/10.1021/ac053495p.

[189] H.H. Tuithof, A.J.H. Boerboom, H.L.C. Meuzelaar, Simultaneous detection of a mass spectrum using a channeltron electron multiplier array, Int. J. Mass Spectrom. Ion Phys. 17 (1975) 299–307. https://doi.org/https://doi.org/10.1016/0020-7381(75)87040-9.

[190] K.L. Brown, G.W. Tautfest, Faraday-Cup Monitors for High-Energy Electron Beams, Rev. Sci. Instrum. 27 (2004) 696–702. https://doi.org/10.1063/1.1715674.

[191] F. Dubois, R. Knochenmuss, R. Zenobi, An ion-to-photon conversion detector for mass spectrometry, Int. J. Mass Spectrom. Ion Process. 169–170 (1997) 89–98. https://doi.org/https://doi.org/10.1016/S0168-1176(97)00210-3.

[192] J.H. Barnes, G.M. Hieftje, Recent advances in detector-array technology for mass spectrometry, Int. J. Mass Spectrom. 238 (2004) 33–46. https://doi.org/https://doi.org/10.1016/j.ijms.2004.08.004.

[193] J. Nuñez, R. Renslow, J.B. Cliff III, C.R. Anderton, NanoSIMS for biological applications: Current practices and analyses, Biointerphases. 13 (2017) 03B301. https://doi.org/10.1116/1.4993628.

[194] M.P. Sinha, M. Wadsworth, Miniature focal plane mass spectrometer with 1000-pixel modified-CCD detector array for direct ion measurement, Rev. Sci. Instrum. 76 (2005) 25103. https://doi.org/10.1063/1.1840291.

[195] M. Greig, R.H. Griffey, Utility of organic bases for improved electrospray mass spectrometry of oligonucleotides, Rapid Commun. Mass Spectrom. 9 (1995) 97–102. https://doi.org/https://doi.org/10.1002/rcm.1290090121.

[196] J.L. Johnson, W. Guo, J. Zang, S. Khan, S. Bardin, A. Ahmad, J.X. Duggan, I. Ahmad, Quantification of raf antisense oligonucleotide (rafAON) in biological matrices by LC-MS/MS to support pharmacokinetics of a liposome-entrapped rafAON formulation, Biomed. Chromatogr. 19 (2005) 272–278. https://doi.org/https://doi.org/10.1002/bmc.450.

[197] G. Dai, X. Wei, Z. Liu, S. Liu, G. Marcucci, K.K. Chan, Characterization and quantification of Bcl-2 antisense G3139 and metabolites in plasma and urine by ion-pair reversed phase HPLC coupled with electrospray ion-trap mass spectrometry, J. Chromatogr. B. 825 (2005) 201–213. https://doi.org/https://doi.org/10.1016/j.jchromb.2005.05.049.

[198] D.C. Muddiman, X. Cheng, H.R. Udseth, R.D. Smith, Charge-state reduction with improved signal intensity of oligonucleotides in electrospray ionization mass spectrometry, J. Am. Soc. Mass Spectrom. 7 (1996) 697–706. https://doi.org/10.1016/1044-0305(96)80516-2.

[199] M. Gilar, A. Belenky, B.H. Wang, High-throughput biopolymer desalting by solid-phase extraction prior to mass spectrometric analysis, J. Chromatogr. A. 921 (2001) 3–13. https://doi.org/https://doi.org/10.1016/S0021-9673(01)00833-0.

[200] C.G. Huber, H. Oberacher, Analysis of nucleic acids by on-line liquid chromatography-mass spectrometry, Mass Spectrom. Rev. 20 (2001) 310–343. https://doi.org/10.1002/mas.10011.

[201] K. Deguchi, M. Ishikawa, T. Yokokura, I. Ogata, S. Ito, T. Mimura, C. Ostrander, Enhanced mass detection of oligonucleotides using reverse-phase high-performance liquid chromatography/electrospray ionization ion-trap mass spectrometry, Rapid Commun. Mass Spectrom. 16 (2002) 2133–2141. https://doi.org/https://doi.org/10.1002/rcm.840.

[202] M.E. Hail, B. Elliott, K. Anderson, High-throughput analysis of oligonucleotides using automated electrospray ionization mass spectrometry, Am. Biotechnol. Lab. 22 (2004) 12–14.

[203] S.A. Mcluckey, G.J. Van Berkel, G.L. Glish, Tandem Mass Spectrometry of Small, Multiply Charged Oligonucleotides, J. Am. Soc. Mass Spectrom. 3 (1992) 60–70. https://doi.org/10.1016/1044-0305(92)85019-G.

[204] S.A. McLuckey, S. Habibi-Goudarzi, Ion trap tandem mass spectrometry applied to small multiply charged oligonucleotides with a modified base, J. Am. Soc. Mass Spectrom. 5 (1994) 740–747. https://doi.org/10.1016/1044-0305(94)80006-5.

[205] P. Deng, X. Chen, G. Zhang, D. Zhong, Bioanalysis of an oligonucleotide and its metabolites by liquid chromatography-tandem mass spectrometry, J. Pharm. Biomed. Anal. 52 (2010) 571–579. https://doi.org/10.1016/j.jpba.2010.01.040.

[206] D.P. Little, T.W. Thannhauser, F.W. McLafferty, Verification of 50- to 100-mer DNA and RNA sequences with high-resolution mass spectrometry., Proc. Natl. Acad. Sci. 92 (1995) 2318–2322. https://doi.org/10.1073/pnas.92.6.2318.

[207] H.D. Flosadóttir, B. Ómarsson, I. Bald, O. Ingólfsson, Metastable decay of DNA components and their compositions – a perspective on the role of reactive electron scattering in radiation damage, Eur. Phys. J. D. 66 (2012) 13. https://doi.org/10.1140/epjd/e2011-20616-y.

[208] H. Nakayama, M. Akiyama, M. Taoka, Y. Yamauchi, Y. Nobe, H. Ishikawa, N. Takahashi, T. Isobe, Ariadne: a database search engine for identification and chemical analysis of RNA using tandem mass spectrometry data, Nucleic Acids Res. 37 (2009) e47–e47. https://doi.org/10.1093/nar/gkp099.

[209] P.J. Sample, K.W. Gaston, J.D. Alfonzo, P.A. Limbach, RoboOligo: Software for mass spectrometry data to support manual and de novo sequencing of post-transcriptionally modified ribonucleic acids, Nucleic Acids Res. 43 (2015)

1–13. https://doi.org/10.1093/nar/gkv145.

[210] A. Nyakas, L.C. Blum, S.R. Stucki, J.L. Reymond, S. Schürch, OMA and OPA - Software-supported mass spectra analysis of native and modified nucleic acids, J. Am. Soc. Mass Spectrom. 24 (2013) 249–256. https://doi.org/10.1007/s13361-012-0529-1.

IX. Objectives of the thesis

The main objective of this thesis was to develop novel LC and LC-MS methods for oligonucleotide separations and characterization. They should complement conventional ion-pair reversed-phase LC (IP-RPLC) based solutions that are nowadays state of the art in oligonucleotide therapeutics analysis. Ion-pair free methods are MS-friendly alternatives protecting the ionization sources from problematic contaminations. Additionally, the limited selectivity of IP-RPLC for certain analytical questions as well as applications of 2D-LC for oligonucleotide therapeutics analysis also demand for more alternative LC methods. For this purpose, various synthetic siRNA- and DNA oligonucleotides were used as test standards. Both 1D-LC and 2D-LC experiments have been developed to establish selectivity for these oligonucleotides without the usage of ion-pairing reagents or, at least, keeping them away from the ionization source of the MS.

The first publication in this study was to establish a 2D-LC system that permits ESI-MS incompatible extremely selective mixed-mode reversed-phase/weak anion exchange (RP/WAX) chromatography to be combined with non-selective but MS-compatible desalting RPLC for oligonucleotide ESI-MS characterisation. A multiple heartcutting configuration was used. In ^{1}D, structurally similar oligonucleotides are separated. The peaks of interest are then automatically transferred to ^{2}D, where MS-incompatible phosphate buffer may be eliminated using reversed-phase chromatography without the need of ion-pairing reagents. Now, the desalted species can be characterized by MS.

In Publication II, a sensitive ESI-MS identification and characterization of impurity peaks originating from a generic siRNA strand is enabled utilising a similar 2D-LC-MS

configuration as described in Publication I. Here, a classical ion-pairing RP chromatography using tripropylammonium acetate as ion-pairing reagent was considered as ^{1}D. Furthermore, the potential of WAX with a quinine-based selector ligand as ^{1}D and IPRP as ^{2}D in a multiple heart-cutting and selective comprehensive 2D-LC-UV approach, respectively, for the impurity profiling of the test strand was documented.

In Publication III and IV, the unique selectivity of a polybutylene-terephthalate-based stationary phase (PBT) has been tested. Without the presence of any ion-pairing reagents, unexpected selectivity of siRNA could be achieved by using ammonium formate or acetate as additives for the mobile phases. This unusual circumstance enabled direct MS detection avoiding ion suppression due to source contamination. Additionally, several systematic optimization series considering different parameters (e.g. flow rate, pH value, buffer type etc.) have been carried out for a better understanding of the column. In the next step, the chromatographic results of the novel column was compared to other LC modes such as HILIC, MMC, IPRP and more where the orthogonality between the LC modes was taken in account. For the quantification of orthogonality, both bins-counting method and Asterisk model were used. Due to the high orthogonality between PBT and HILIC, both methods were re-combined in another selective comprehensive 2D-LC-MS setup to gain enhanced resolution power for the main peak of the test siRNA strand.

The primary purpose of Publication V was to increase resolution by using cholesterol-based mixed-mode stationary phases under RP-mode to separate Patisiran analogue (as model siRNA) from its contaminants and identify them by MS. To determine their suitability for ON research, cholesterol and alkylamide columns were tested for selectivity under reversed phase conditions. Furthermore, the retention orthogonality

between cholesterol and amide stationary phases (in HILIC mode) was investigated to confirm the viability of using 2D-LC to boost separation power.

Finally, in Publication VI, 9 short phosphorothioated oligonucleotides (PSOs) with similar base sequences but variable numbers of PS linkages and a PSO RNA-based active pharmaceutical ingredient (API) were studied for their diastereoselective behaviour on an octadecylsilyl modified column under various IP-RP setting investigating key influencing factors like buffer concentration, buffer hydrophobicity, and column temperature. Because of the fact that a compromising separation of individual diastereomers is limited to PSOs that contain no more than four or five PS linkages, the one-dimensional LC results were not satisfying considering the number of distinguished diastereomers. Therefore, it is reasonable to believe that two-dimensional LC might be a powerful tool enabling efficient separation of phosphorothioates. In the follow-up experiments, RP-LC using C18-based stationary phase was combined with another RP-LC using poly-saccharide based column in a sequential selective comprehensive 2D-LC setup. Partially separated diastereomers from the ^{1}D were transferred into the second dimension to achieve higher diastereomer separation power.

X. Results and discussion

1. Publication I

Multiple Heart-Cutting Mixed-mode chromatography-reversed-phase 2D-liquid chromatography method for separation and mass spectrometric characterization of synthetic oligonucleotides

Feiyang Li, Xiaoli Su, Stefanie Bäurer, Michael Lämmerhofer*

Institute of Pharmaceutical Sciences, Pharmaceutical (Bio-)Analysis,

University of Tübingen, Auf der Morgenstelle 8, 72076 Tübingen, Germany

*Author for correspondence:

Prof. Dr. Michael Lämmerhofer

Pharmaceutical (Bio-)Analysis

Institute of Pharmaceutical Sciences

University of Tübingen

Auf der Morgenstelle 8

72076 Tübingen, Germany

T +49 7071 29 78793, F +49 7071 29 4565

E-mail: michael.laemmerhofer@uni-tuebingen.de

Journal of Chromatography A

Year 2020, 1625, 461338

DOI: 10.1016/j.chroma.2020.461338

Journal of Chromatography A 1625 (2020) 461338

Contents lists available at ScienceDirect

Journal of Chromatography A

journal homepage: www.elsevier.com/locate/chroma

Multiple heart-cutting mixed-mode chromatography-reversed-phase 2D-liquid chromatography method for separation and mass spectrometric characterization of synthetic oligonucleotides

Feiyang Li, Xiaoli Su, Stefanie Bäurer, Michael Lämmerhofer*

Institute of Pharmaceutical Sciences, Pharmaceutical (Bio-)Analysis, University of Tübingen, Auf der Morgenstelle 8, 72076 Tübingen, Germany

ARTICLE INFO

Article history:
Received 24 April 2020
Revised 8 June 2020
Accepted 11 June 2020
Available online 12 June 2020

Keywords:
Oligonucleotide
Multidimensional liquid chromatography
Mass spectrometry
Mixed-mode chromatography
Reversed-phase/weak anion-exchange

ABSTRACT

Until today, ion-pair reversed-phase chromatography is still the dominating method for analytical characterization of synthetic oligonucleotides. Its hyphenation with mass spectrometry, however, has some drawbacks such as ion-suppression in electrospray ionization. To overcome this problem, we present in this work a multiple heart-cutting (MHC) two-dimensional liquid chromatography (2D-LC) method with ultra-violet (UV) and electrospray ionization (ESI) mass spectrometry (MS) detection. A reversed-phase/weak anion-exchange (RP/WAX) stationary phase in the first dimension (^{1}D) provides the selectivity for separation of structurally closely related oligonucleotide sequences and deletions (shortmers), respectively, using a mixed pH/triethylammonium phosphate buffer gradient at constant organic modifier content. Heart cuts of the oligonucleotide peaks are transferred to the second dimension (^{2}D) via a multiple heart-cutting valve which is equipped with two loop decks. The ^{2}D RP column is used for desalting via a diverter valve. Active solvent modulation enables to refocus the oligonucleotide peak into a sharp zone by ^{2}D RP entirely free of non-volatile buffer components and ion-pair agents. Oligonucleotides can thus be sensitively detected by ESI-QTOF-MS under MS-compatible conditions.

1. Introduction

Synthetic oligonucleotide therapeutics are on the rise and have become a promising therapeutic concept for the regulation of gene expression. This class of synthetic nucleic acids comprises antisense oligonucleotides (ASOs), which are generally 12 to 30 nucleotides in length and chemically often phosphorothioates, aptamers, and oligonucleotides for RNA interference (RNAi). The latter can be distinguished into short interfering RNA (siRNA) and microRNA (miRNA) mimics with around 21 to 23 nucleotides.

Oligonucleotides are mostly synthesized using phosphoramidite chemistry [1]. For pharmaceutical applications in humans and clinical trials, the products must be of high purity. However, oligonucleotide impurities with deleted or extended base sequences (N±1, N±2) (shortmers and longmers, respectively), base modifications (deaminations), depurination, and incomplete cleavage of protection groups are commonly found in raw products of synthetic oligonucleotides [2]. The development and production of pharmaceutical grade oligonucleotide therapeutics require adequate purification methods and assays for their quality control [1,3–5]. For both, ion-pair reversed-phase liquid chromatography (IP-RPLC) with triethylammonium acetate as ion-pairing agent is the state-of-the-art technology because oligonucleotides are only poorly retained by common RPLC [6,7].

The type of ion-pairing agent utilized may significantly affect selectivities and is a prime variable for optimization; triethylamine (TEA), propylamine, tripropylamine, dibutylamine and hexylamine are some preferred choices [8–13]. The effect of stationary phases in IP-RPLC has been investigated as well [14–16]. While the ion-pairing agents in the mobile phase increase retention and improve selectivity, they are detrimental for ESI-MS detection leading to reduced sensitivity due to ion suppression [1,9,17,21,22]. 1,1,1,3,3,3-Hexafluoro-2-propanol (HFIP) has been suggested as mobile phase additive, combined with TEA, to enhance sensitivity in LC-ESI-MS detection of oligonucleotides [2,18–22]. It has been reported that the type of ion-pairing reagent can significantly influence the MS signal intensity [13,19,22,23], however, the problem of ion suppression cannot be completely overcome. Therefore, suitable alternative methods with sufficient selectivity and better compatibility for MS detection are still in high demand. Hydrophilic interaction liquid chromatography (HILIC) [25–30] and size-exclusion chromatography (SEC) [24] have been suggested as alternative separation technologies with better MS compatibility.

* Corresponding author.
E-mail address: michael.laemmerhofer@uni-tuebingen.de (M. Lämmerhofer).

https://doi.org/10.1016/j.chroma.2020.461338
0021-9673/

Table 1
Overview of the oligonucleotides used in this study.

Mixture Name	Oligonucleotide Sequence	Sample Name	Molecular Formula	Monoisotopic mass [m/z]	Molecular weight [gmol^{-1}]
N-x Mixture	5'-GAATCTTACGAAATACCTGAGAG-3'	N	$C_{226}H_{282}N_{92}O_{132}P_{22}$	7077.233	7080.70
	5'-GAATCTTACGAAATACCTGAGA_-3'	N-1	$C_{216}H_{270}N_{87}O_{126}P_{21}$	6748.181	6751.49
	5'-GAATCTTACGAAATACCTGAG__-3'	N-2	$C_{206}H_{258}N_{82}O_{121}P_{20}$	6435.123	6438.28
	5'-GAATCTTACGAAATACCTGA___-3'	N-3	$C_{196}H_{246}N_{77}O_{115}P_{19}$	6106.071	6109.07
Oligomix I (Oligo I+II+III)	5'-GAATCTTACGAA_TACCTGAGAA-3'	Oligo I	$C_{216}H_{270}N_{87}O_{126}P_{21}$	6748.181	6751.49
	5'-GAATCTTACGAAATACCTGAGAA-3'	Oligo II	$C_{226}H_{282}N_{92}O_{131}P_{22}$	7061.238	7064.70
Oligomix II (Oligo II+III+IV)	5'-GAATCTTAGGAATTACCTGAGAA-3'	Oligo III	$C_{227}H_{283}N_{91}O_{133}P_{22}$	7092.232	7095.71
	5'-GAATCTTACGAA_AACCTGAGAA-3'	Oligo IV	$C_{216}H_{269}N_{90}O_{124}P_{21}$	6757.192	6760.50

Anion-exchange chromatography [31,32] and mixed-mode stationary phases with both anion-exchange ligands combined with hydrophobic moieties demonstrated excellent separation potential for structurally related oligonucleotides [22,23,33–36]. Nevertheless, both plain and mixed-mode anion-exchange chromatography have also a major drawback: For efficient elution of multiply negatively charged oligonucleotides strong eluents containing sufficiently high concentrations of counterions are required in order to elute the analytes within reasonable run time. The use of phosphate buffer allows efficient elution, however, makes the effluent MS-incompatible.

For this reason, a desalting 2D-LC method was developed in this work which allows direct online coupling of MS-incompatible LC with ESI-MS. A few prior studies already documented the potential of two-dimensional LC (2D-LC) for oligonucleotide separations [26,38]. Di- to deca-oligonucleotides were separated by comprehensive HILIC × IP-RPLC by Li *et al.* [26]. Comprehensive RP × IP-RPLC was employed for MS characterization of modified oligonucleotide impurities while IP-RPLC ×IP-RPLC was not sufficiently orthogonal [32]. A heart-cut configuration using IP-RPLC in both the first (^{1}D) and second dimension (^{2}D) (IP-RPLC – IP-RPLC) was used to confirm the identity of an n-1 impurity from a dye-conjugated oligonucleotide by a single quadrupole MS detector [38]. Antisense oligonucleotide impurities were characterized by MHC IP-RPLC and anion exchange chromatography, respectively, in ^{1}D and HILIC in the ^{2}D by orbitrap MS [39]. ^{2}D-HILIC was performed under ESI-MS compatible conditions.

The aim of this work was to develop a 2D-LC setup which allows to combine an ESI-MS incompatible highly selective mixed-mode reversed-phase/weak anion exchange (RP/WAX) chromatography with non-selective but MS-compatible desalting RPLC for ESI-MS characterization of oligonucleotides. A multiple heart-cutting setup was selected., Structurally closely related oligonucleotides are separated in ^{1}D. After that, peaks of interests are automatically transferred into ^{2}D where MS-incompatible phosphate buffer can be removed by using reversed-phase chromatography without the presence of ion-pairing reagents. The desalted ^{2}D-effluent can finally be investigated by MS.

2. Experimental

2.1. Materials

The oligonucleotide test samples (see Table 1) were synthesized by Oligo Sigma (Merck, Munich, Germany) and purchased as desalted raw-products. Ortho-phosphoric acid (85% in H_2O), ammonium hydroxide (ACS reagent, 28-30%) and ammonium acetate (LC-MS grade) were purchased from Sigma-Aldrich (Merck, Munich, Germany). HPLC-grade acetonitrile was from Honeywell (Munich, Germany). HPLC-MS-grade methanol was purchased from Roth (Karlsruhe, Germany). Ultrapure water was obtained by purification of deionized water using Elga PurLab Ultra purification system (Celle, Germany).

2.2. Synthesis of polymeric RP/WAX mixed-mode stationary phase (Poly-RP/WAX)

The polymeric reversed-phase/weak anion exchanger mixed-mode stationary phase (Fig. 1) was synthesized as described elsewhere [35–37,40]. Briefly, a poly(3-mercaptopropyl)methylsiloxane film was coated onto vinyl-silica (100 Å, 5 µm) which was then simultaneously crosslinked to the surface and *in situ* functionalized with *N*-(10-undecenoyl)-3-aminoquinuclidine by solvent-less thiol-ene double click reaction [36]. The designated selector was prepared by reaction of *N*-10-undecenoic acid chloride with 3-aminoquinuclidine base [37].

2.3. Column packing

The Poly-RP/WAX-modified silica was slurry packed into stainless-steel columns of dimensions 50 × 3.0 mm i d. at 11603 psi (800 bar) and use of methanol as delivery solvent.

2.4. Sample preparation

Stock solutions of individual oligonucleotides with a concentration of 100 µM were prepared in purified water and stored at 4°C until use. The first oligonucleotide test mixture (*N-x Mixture, shortmer mixture*) contained 50 µM *Oligo N* as main product and *Oligo N-1, N-2, N-3* (see Table 1) with a concentration of 10 µM each as impurities. The second oligonucleotide test mixture (*Oligomix I*) contained 33 µM of *Oligo I, Oligo II* and *Oligo III* (see Table 1). The third oligonucleotide test mixture (*Oligomix II*) contained 33 µM of *Oligo IV, Oligo II* and *Oligo III* (see Table 1). All mixtures were prepared in ultrapure water.

2.5. Instrumentation

The instrumentation used in this work for the multiple heart-cutting 2D-LC-MS experiments is schematically shown in Fig. 2. The Agilent 1290 Infinity II 2D-LC Solution from Agilent Technologies (Waldbronn, Germany) consisted of a (quaternary gradient) Flexible Pump (G7104A), Multisampler (G7167B) and Variable Wavelength Detector (VWD) (G7114B) with 14 µL flow cell (G1314-60186) and a pressure relief device (pressure release kit, G4236-60010) between ^{1}D UV-detector and 2D-interface for the first dimension (^{1}D) of LC. The sampling frequency of VWD in ^{1}D was 5 Hz. The ^{2}D LC consisted of a (binary gradient) High-Speed Pump (G7120A) and a Diode Array Detector (DAD) (G7117B) with 1 µL flow cell (G4212-60008). The sampling frequency of DAD in ^{2}D was 80 Hz. Both ^{1}D and ^{2}D columns were accommodated in two separate Infinity column compartments (G7116B). The two dimensions were connected by a valve drive (G1170A) equipped with 5-position/10-port 2D-LC ASM valve (#5067-4266) connected to two 6-position/14-port valve heads (#5067-4142) (Multiple heart-cutting (MHC) valves) carrying six 40 µL loops each. Experiments utilizing active solvent modulation (ASM) were performed with the

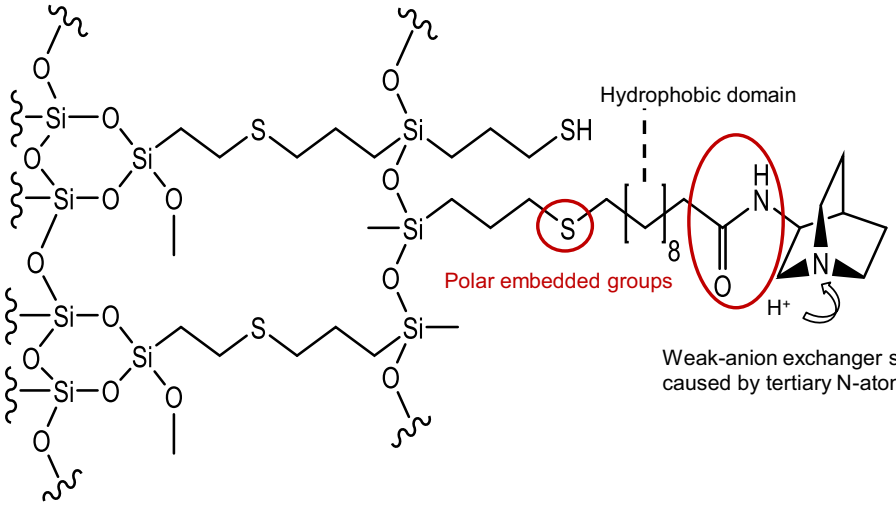

Fig. 1. Chemical structure and interaction sites of the stable-bond polymeric reversed-phase/weak anion-exchange mixed mode (Poly-RP/WAX) stationary phase which was used in this study.

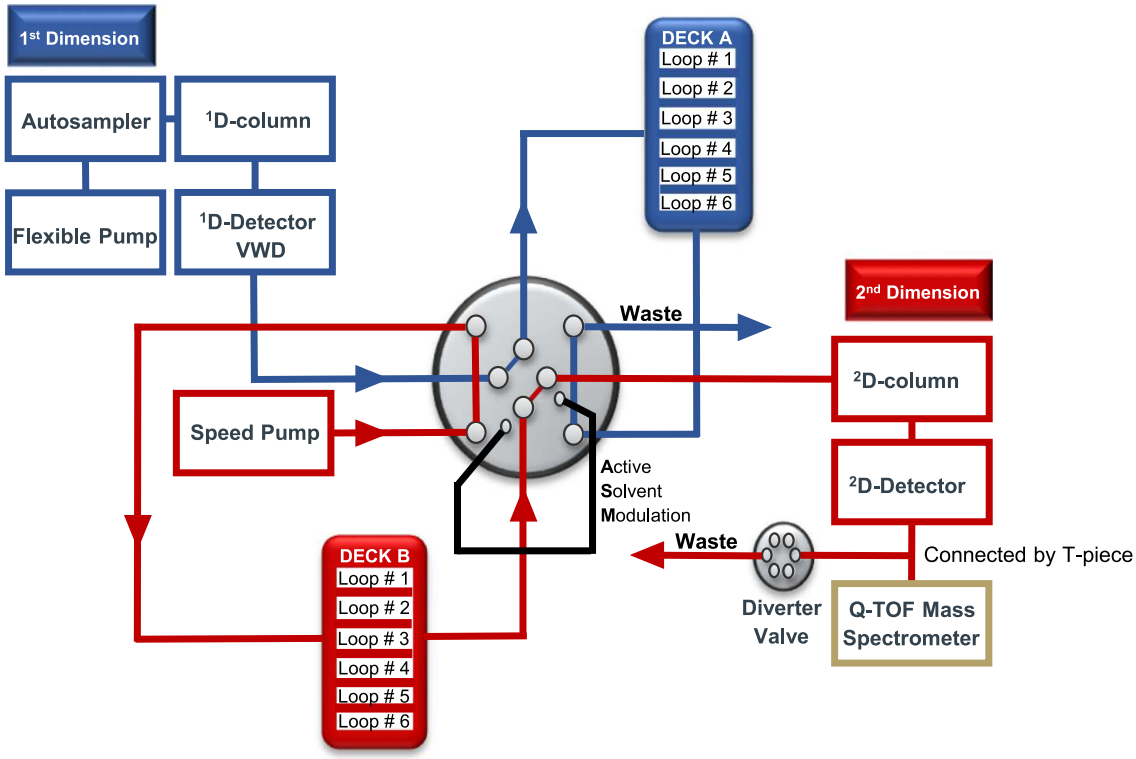

Fig. 2. Scheme of 2D-LC-ESI-QTOF-MS setup with an active solvent modulation (ASM) valve connected to two multiple heart-cutting (deck A and B) valves. Peaks of interest from the ^{1}D-separation can be stored in the loops of deck A and B (each one equipped with six 40 µL sampling loops) and transferred into ^{2}D for analysis under ESI-MS friendly conditions. The MS-incompatible components from ^{1}D can be removed by RPLC using a C18 column, transferring the first part of the ^{2}D chromatogram to waste with a diverter valve installed after the ^{2}D column. Finally, the diverter valve directs the effluent from ^{2}D RPLC with the desalted analytes of interest into the ion source for MS identification.

ASM factor 5 (split ratio of loop to ASM = 1:4) with a restriction capillary (85 × 0.12 mm, 0.96 µL, #5500-1300). The 2D-LC experiment was controlled by Agilent OpenLAB CDS ChemStation Rev. C.01.10 with 2D-LC add-on software.

In the MHC 2D-LC experiments with MS detection, an Agilent 2-position/6-port valve head (pressure limit: 800 bar, #5067-4282) driven by a valve drive (G1170A) was used as diverter valve to deliver the MS incompatible components of the early part of the ^{2}D chromatogram into the waste. After 0.81 minutes, the ^{2}D effluent was switched to a Sciex TripleTOF 5600+ QTOF mass spectrometer which was equipped with a Duospray ion source (operated in ESI mode). The TripleTOF MS instrument was connected to the 2D-LC system using the contact closure connection for peripheral devices from Sciex and was controlled with Analyst TF 1.7 software (AB Sciex, Darmstadt, Germany).

For ^{2}D method development, an Agilent 1290 Infinity UHPLC and an Agilent 1260 Infinity II HPLC system were additionally used. For the detection of phosphate buffers, the Agilent 1260 Infinity II HPLC system was coupled to a Corona Veo Charged Aerosol Detector (CAD) of Thermo Fisher Scientific (Germering, Germany).

2.6. LC-MS conditions and general working procedures

LC conditions for ^{1}D and ^{2}D are specified in detail in Table 2 and Figure captions, respectively. In general, TEAP and AP buffers for the ^{1}D separation were prepared from aqueous phosphoric acid solutions of specified molar concentration and the pH adjusted using triethylamine and ammonium hydroxide, respectively, prior to mixing with acetonitrile or methanol. The peaks of interest from the ^{1}D separation, containing MS-incompatible phosphate buffer, were parked in the 40 µL loops installed on the two loop decks A and B of the MHC valve until ^{2}D analysis by an MS-compatible RP separation system using ZORBAX Eclipse Plus C18 RRHD column (1.8 µm particle size, 100 Å pore size, 50 × 2.1 mm i.d.) of Agilent Technologies without ion-pair in ^{2}D eluent. ^{2}D eluents were prepared by dissolving 10 mM ammonium acetate in water (MP A) and methanol (MP B) without adjusting the pH value.

In the first part of the ^{2}D separation, the MS diverter valve directed ^{2}D effluent containing the MS incompatible components of the ^{1}D eluent to waste. After 0.81 min the position of the diverter valve was switched to direct the ^{2}D flow with the desalted oligonucleotide peak into the ESI-QTOF-MS system without contaminating the ion source. Mass spectrometric detection was performed in negative polarity mode with an ESI source. The data for the TOF full scan MS experiment were acquired in a scan range of m/z 300-2000. The MS parameters for nebulizer gas, heater gas, curtain gas, source temperature, ion spray voltage, declustering potential and collision energy were set as follows: 30 psi, 50 psi, 40 psi, 450°C, -4500 V, -50 V, -10 V. Accumulation time was 250 ms and period cycle time 275 ms.

3. Results and discussion

3.1. RP/WAX mixed-mode chromatography for ^{1}D-separation

In prior work, we have documented that mixed-mode RP/WAX chromatography provides improved selectivity for structurally closely related oligonucleotides over both IP-RPLC with triethylammonium acetate eluent and plain anion-exchange chromatography [35]. This peculiar chromatographic mode exhibited exceptional selectivity for oligonucleotides differing in length (shortmers N-1, N-2, N-3), single nucleotide exchanges at the 5' and 3' ends as well as in the middle of the sequence. Furthermore, the RP/WAX mixed-mode material offered unique flexibility to optimize separations using one parameter organic modifier, buffer concentration and pH gradients as well as two and three parameter mixed gradients for efficient elution. The specific selectivity profiles may be the result of chemoaffinity-type simultaneous multiple interactions arising from ionic interactions between negatively charged oligonucleotides and positively charged quinuclidinium moiety, hydrophobic interactions as well as hydrophilic (dipole-dipole, hydrogen bonding) interactions with embedded polar groups (Fig. 1). The Poly-RP/WAX mixed-mode phase utilized in the present study features improved stability [35,36]. Fig. 3A shows the separation of the test mixture with *Oligo I, II*, and *III* on a 50 mm long Poly-RP/WAX column. Triethylammonium phosphate (TEAP) was utilized in Fig. 3A and ammonium phosphate buffer (AP) in Fig. 3B, both with a constant acetonitrile content of 20% (v/v) as organic modifier. Retention in anion-exchange chromatography increases with increasing effective charge numbers i.e. oligonucleotide length. Strong retention is observed due to multiple negative charges. Thus, a two-parameter mixed buffer concentration/pH gradient was employed for efficient elution. Phosphate is a strong counterion (in contrast to volatile formate and acetate) and in accordance to an increasing elution strength in the anion-exchange process its concentration was increased from 50 mM to 100 mM during the gradient. Superimposed was a pH gradient from 6.8 to 7.8. Due to reduced ionization of the quinuclidine ring and increasing ionization of residual silanols at higher pH the net positive surface charge decreases in the course of the pH gradient [35]. Thereby, the anion-exchange process gets attenuated and the oligonucleotides elute. It can be seen that the three structurally closely related oligonucleotide sequences are baseline separated both with TEAP and AP. However, TEAP exhibited stronger elution strength while with AP the concentration needed to be increased significantly to elute the oligonucleotides in about the same time. Ion-pairing with TEA seems to reduce ionic interactions with the stationary phase. These separations confirm the practical utility of the poly-RP/WAX phase.

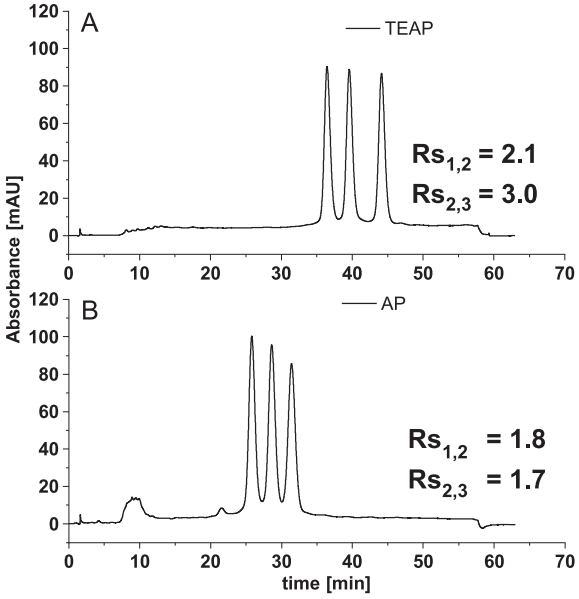

Fig. 3. ^{1}D chromatograms of the *Oligomix I* on Poly-RP/WAX. Experimental conditions (see Table 2): (A) Method A2. (B) Method A3. UV detection at 254 nm.

Although the separation is dominated by an anion-exchange process, the organic modifier plays a crucial role [35]. In this work, we also tested methanol as organic modifier besides acetonitrile (Fig. 4). It has lower elution strength in the ^{2}D-desalting RPLC and could therefore be of advantage. In general, it showed good selectivity as organic modifier, like acetonitrile. However, because of its lower elution strength, the peaks are broader and an elution in acceptable time range could only be achieved under isocratic condition with 100% of stronger elution solvent (100% B). Therefore, further separations were performed with acetonitrile to ensure higher analyte concentrations in the transferred cuts.

3.2. Development of the ^{2}D RPLC method

The developed ^{1}D separation system was deemed to be a good model to develop and document the utility of a desalting 2D-LC method because it contains both positively charged ion-pair agent and negatively charged involatile buffer anion. The use of phosphate buffer as counter ion and triethylamine as ion-pairing agent in the ^{1}D separation preclude a direct coupling to ESI-MS. Hence, the ^{2}D of the 2D-LC setup (Fig. 2) was devised as an on-line desalting tool to remove the MS-incompatible TEAP buffer from the ^{1}D fractions (cuts). Due to the low retention of oligonucleotides in RPLC, some optimization experiments had to be performed.

To mimic conditions as given by a real 2D-LC run, the oligonucleotide samples were prepared in ^{1}D eluent (i.e. 100 mM TEAP, 20% ACN, pH 8). A small column screen with a limited number of distinct RP phases was carried out to evaluate their retention

Table 2
Summary of the chromatographic methods (^{1}D and ^{2}D)

	First Dimension (^{1}D)						Second Dimension (^{2}D)											
Conditions	Method A1		Method A2		Method A3		Method B	Method C		Method D		Method E		Method F		Method G		Method H	
Column Dimension	Poly-RP/WAX 50x3 mm i.d.		Poly-RP/WAX 50x3 mm i.d.		Poly-RP/WAX 50x3 mm i.d.		Poly- RP/WAX 50x3 mm i.d.	Agilent ZORBAX Eclipse Plus C18 50x2.1 mm i.d.		Agilent ZORBAX Eclipse Plus C18 50x2.1 mm i.d.		Agilent ZORBAX Eclipse Plus C18 50x2.1 mm i.d.		Waters Acquity UPLC CSH C18 100x2.1 mm i.d.		Agilent ZORBAX Eclipse Plus C18 50x2.1 mm i.d.		Agilent ZORBAX Eclipse Plus C18 50x2.1 mm i.d.	
Mobile Phase A	ACN/50 mM TEAP, pH 6.8 (20:80; v/v)		ACN/50 mM TEAP, pH 6.8 (20:80; v/v)		ACN/100 mM AP, pH 6.8 (20:80; v/v)		MeOH/50 mM TEAP, pH 6.8 (20:80; v/v)	10 mM AA in water		10 mM AA in water		10 mM AA in water		10 mM AA in water		10 mM AA in water		10 mM AA in water	
Mobile Phase B	ACN/100 mM TEAP, pH 7.8 (20:80; v/v)		ACN/100 mM TEAP, pH 7.8 (20:80; v/v)		ACN/200 mM AP, pH 7.8 (20:80; v/v)		MeOH/100 mM TEAP, pH 7.8 (20:80; v/v)	MeOH, 10 mM AA		MeOH, 10 mM AA		MeOH, 10 mM AA		MeOH, 10 mM AA		ACN/10 mM AA (90:10; v/v)		MeOH, 10 mM AA	
Gradient	Min	%B	Min	%B	Min	%B	Isocratic run with 100% B	Min	%B	Min	%B	Min	%B	Min	%B	Min	%B	Min	%B
	0	80	0	0	0	0		0	5	0	5	0	5	0	5	0	5	0	5
	25	100	5	0	5	0		0.8	5	0.8	5	0.8	5	0.9	5	0.5	5	0.25	5
	25.5	80	6	60	6	60		0.9	80	0.9	80	0.9	80	3.9	100	1.5	100	2	60
	36	80	42.67	100	42.67	100		1.2	80	1.2	80	1.2	80	4	5	1.6	5	2.5	60
			50.67	100	50.67	100		1.3	5	1.3	5	1.3	5	5	5	2.6	5	2.6	5
			51.67	0	51.67	0		1.8	5	3.3	5	6.3	5					3.6	5
			61.67	0	61.67	0													
Injection	4 µL		3 µL		3 µL		10 µL	-		-		-		5 µL		5 µL		5 µL	
Flow rate	0.168 ml/min		0.168 ml/min		0.168 ml/min		0.5 ml/min	1 ml/min		1 ml/min		1 ml/min		0.4 ml/min		0.8 ml/min		0.4 ml/min	

TEAP: Triethylammonium phosphate; AA: ammonium acetate; AP: Ammonium phosphate.
Column temperature in ^{1}D and ^{2}D: always 40 °C.
ASM activated in Method C, D and E: 0.61 min, sample loop was flushed 3 times, factor 5.

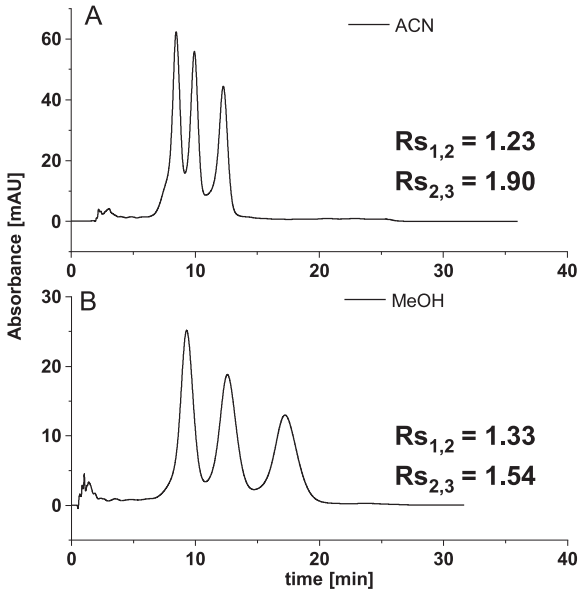

Fig. 4. Separation of the *Oligomix I* on Poly-RP/WAX with ACN (A) and MeOH (B) as organic modifiers. Experimental conditions (see Table 2): (A) Method A1. (B) Method B. UV detection at 254 nm.

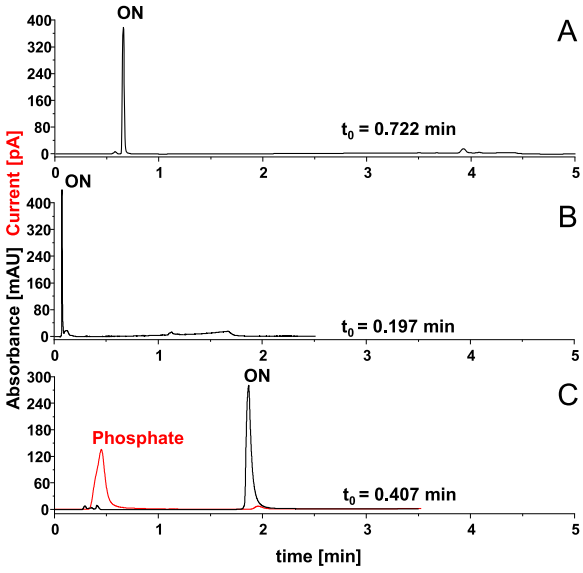

Fig. 5. Chromatograms of *Oligo I* using different types of C18 columns. Experimental conditions (see Table 2): (A) Method F. (B) Method G. (C) Method H.. UV detection at 254 nm (black trace) and CAD (red trace).

capability for oligonucleotides. For effective desalting the oligonucleotides must be sufficiently retained while the phosphate buffer should elute in the void volume. In general, it turned out to be challenging to separate the oligonucleotides from the phosphate buffer since both are inherently polar compounds. Fig. 5 shows selected results. An Acquity CSH C18 column was initially examined because it was expected that the underlying cationic charged polymer layer exerts some weak electrostatic forces to retain the oligonucleotides under low organic modifier conditions. However, both with 5% (v/v) ACN and MeOH as organic modifier in the eluent, the tested oligonucleotides eluted together with phosphate buffer with t_0 (Fig. 5A). An Agilent Zorbax Bonus-RP column was evaluated but no suitable conditions could be found. No retention, on the other hand, could be achieved with a hydrophobic YMC Triart C18 ExRS either. The same was observed with ZORBAX Eclipse Plus C18 RRHD when 5% (v/v) of acetonitrile was used as organic modifier; the oligonucleotide eluted with t_0 unresolved from phosphate (Fig. 5B). However, when acetonitrile was replaced by methanol as organic modifier, the ZORBAX Eclipse Plus C18 RRHD column provided sufficient retention for the oligonucleotide (see Fig. 5C, black trace). In order to document the selectivity between oligonucleotide and phosphate buffer, a charged aerosol detector was connected in series to UV in order to detect the nonvolatile phosphate. It can be seen in Fig. 5C, red trace that phosphate eluted with t_0 in the early part of the chromatogram with sufficient selectivity to avoid interference with oligonucleotide detection by ESI-MS. This peculiar retention behaviour enables Agilent Zorbax Eclipse Plus C18 RRHD to be used in ^{2}D as on-line desalting column.

3.3. Multiple heart-cutting RP/WAX-RP 2D-LC-UV

The two separately developed ^{1}D and ^{2}D methods were then combined in a MHC 2D-LC-UV method: The ^{1}D RP/WAX separation provides the selectivity between structurally closely related oligonucleotides and ^{2}D RPLC is used to remove the nonvolatile TEAP salt from the ^{1}D effluent prior to ESI-MS. For the online coupling of the two LC methods, some additional factors need to be considered and optimized. In a MHC 2D-LC experiment, the analysis time of the ^{2}D is less critical as it is decoupled from sampling in the ^{1}D (through the possibility of storing fractions in loops until the ^{2}D LC system is available), but adds to the total analysis time of the 2D-LC method. To keep it short, fast ^{2}D separations are preferable, in particular in the present case in which the ^{2}D is just used for desalting. The ^{2}D analysis of the ^{1}D fractions starts immediately after the first cut and the following cuts are analyzed subsequently in the ^{2}D. An important factor is the compatibility of the ^{1}D effluent with ^{2}D separation. The cuts are sampled from ^{1}D eluent which represents the sample matrix and injection solvent, respectively, in the ^{2}D LC system. Due to transfer of large volumes (cuts with 40 µL loops) peak broadening, peak splitting and breakthrough may easily occur if the elution strength of ^{1}D mobile phase in the ^{2}D phase system is significantly higher than that of the ^{2}D eluent. Since refocusing of oligonucleotides is not extremely efficient on RP due to their hydrophilicity, mobile phase compatibility is of utmost importance.

ACN leads to an immediate elution of oligonucleotides on the C18 column, even at very low concentrations (Fig. 5B). Thus, initially MeOH was tested as organic modifier in both dimensions. The ^{1}D eluent contained 20% MeOH and elution on the ^{1}D RP/WAX column was performed under isocratic condition with 100% B (20% MeOH, 100 mM TEAP, pH 7.8). In ^{2}D, desalting started with 5% (v/v) MeOH in the eluent on the Agilent Zorbax Eclipse Plus C18 RRHD column. The oligonucleotides were then eluted with a steep MeOH gradient (5-80% MeOH) (see Suppl. Fig. S1 and S2). Unfortunately, with MeOH as organic modifier poor peak shapes were observed in both ^{1}D and ^{2}D. Peaks were broad in ^{1}D resulting in partly worse resolution and stronger dilution of the transferred fractions which is disadvantageous in terms of sensitivity in MS detection. Further, peak shapes were suboptimal in the ^{2}D chromatogram and in some cuts a breakthrough of the oligonucleotides was observed (Suppl. Fig. S1 and S2). Hence, ACN was tested as modifier in the ^{1}D eluent at constant 20% with mixed pH/TEAP gradient and MeOH as organic modifier of ^{2}D. The considerable amount of ACN which was transferred into ^{2}D was counterbalanced by using Active Solvent Modulation (ASM) [41]. ASM dilutes the sample from ^{1}D with weak ^{2}D eluent. Indeed, the dilution of ^{1}D effluent with weak solvent prior to transfer into ^{2}D turned out to be crucial to suppress breakthrough effects. Additionally, the duration of re-equilibration must also be taken in account. As can be seen in Fig. 6, the ^{2}D column was perfectly equi-

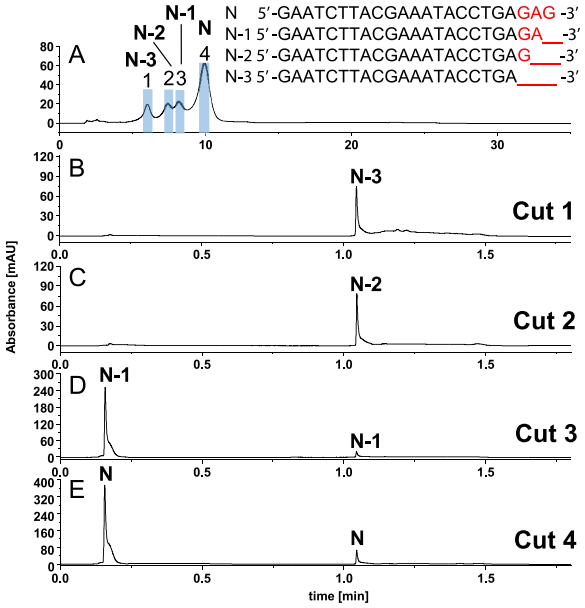

Fig. 6. Multiple Heart Cutting 2D-LC chromatograms of *N-x Mixture* demonstrating the relevance of ^{2}D equilibration time: (A) ^{1}D separation of the synthetic oligonucleotides on Poly-RP/WAX with indicated sampling times (always 14.4 sec) in light blue, (B-E) ^{2}D analysis of the heart cuts by RPLC. Experimental conditions (see Table 2): (A) Method A1. (B-E) Method C. UV detection at 254 nm. Sampling table: Cut #1: ^{1}D cut start at 5.86 min, ^{2}D run start at 6.11 min; Cut #2: ^{1}D cut start at 7.25 min, ^{2}D run start at 9.81 min; Cut #3: ^{1}D cut start at 8.03 min, ^{2}D run start at 15.36 min; Cut #4: ^{1}D cut start at 9.78 min, ^{2}D run start at 13.51 min.(For interpretation of the references to color in this figure legend, the reader is referred to the web version of this article.)

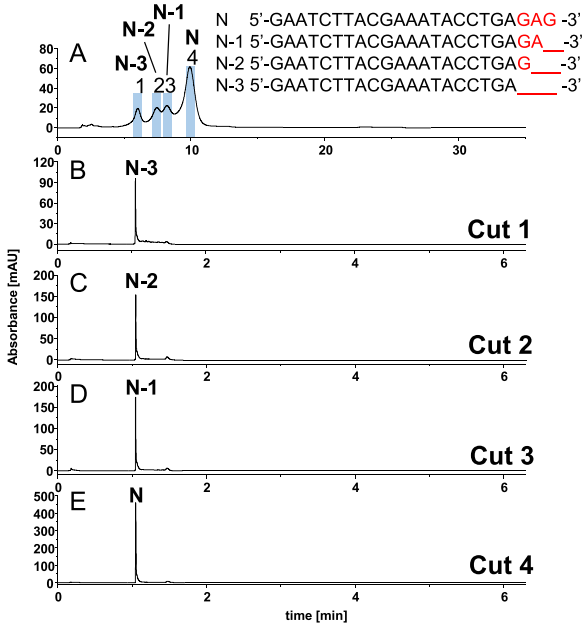

Fig. 7. Multiple Heart-Cutting 2D-LC chromatograms of *N-x Mixture* with ASM and optimized conditions concerning column equilibration time: (A) Mixed-mode separation of oligonucleotides on Poly-RP/WAX in ^{1}D, sampling time (always 14.4 sec) for ^{2}D analysis indicated in light blue; conditions as specified in Table 2, Method A1, (B-E) ^{2}D chromatograms of the sampled oligonucleotides; experimental conditions can be found in Table 2, Method E. UV detection at 254 nm. Sampling table: Cut #1: ^{1}D cut start at 5.83 min, ^{2}D run start at 6.08 min; Cut #2: ^{1}D cut start at 7.25 min, ^{2}D run start at 31.48 min; Cut #3: ^{1}D cut start at 8.03 min, ^{2}D run start at 25.13 min; Cut #4: ^{1}D cut start at 9.78 min, ^{2}D run start at 18.78 min. (For interpretation of the references to color in this figure legend, the reader is referred to the web version of this article.)

librated for *cut 1* and *cut 2* (Fig. 6B-C) without breakthrough. However, breakthrough of oligonucleotides was observed for *cut 3 and cut 4* (Fig. 6D-E), although also ASM was used. It clearly indicates that the duration of re-equilibration of the ^{2}D column was not sufficient. At this point, it should also be mentioned that the oligonucleotides show retention under the given RP conditions, but no selectivity between different oligonucleotides can be observed without ion-pairing reagent in the ^{2}D eluent. In order to preclude breakthroughs, the re-equilibration time of ^{2}D was extended from 0.5 min to 2.0 min. As can be seen from Suppl. Fig. 3, this extension of re-equilibration in combination with ASM was leading to some improvements of the results. However, *cut 4* still revealed a breakthrough of oligonucleotide. The problem of oligonucleotide breakthrough could be entirely solved with a further extension to 5 min re-equilibration (see Fig. 7). Under these conditions, all 4 cuts resulted in a sharp oligonucleotide peak (at 1.04 min) sufficiently retained and resolved from the phosphate buffer peak at t_0 in ^{2}D. This method was deemed to be suitable for hyphenation with ESI-MS.

3.4. Hyphenation of MHC 2D-LC-UV with ESI-MS

The optimized MHC RP/WAX-RP 2D-LC-UV method was then coupled to ESI-QTOF-MS. Via the diverter valve, the salt plug at the beginning of each ^{2}D run was directed to waste (see Fig. 2). After 0.81 min, the diverter was switched to MS and the desalted oligonucleotide samples could reach the ESI ion source preventing the contamination with phosphate buffer. In this study, the *Oligomix II* composed of *Oligo II, III* and *IV* was used to document the practical utility of the MHC 2D-LC-UV-ESI-MS workflow.

Fig. 8A shows the ^{1}D separation of the *Oligomix II* on RP/WAX with TEAP buffer using method A (Table 2). A heart cut with a sampling time of 14.4 seconds was taken on each oligonucleotide peak in ^{1}D. It is evident that only a fraction of the peak is transferred to the ^{2}D separation which is suboptimal in terms of overall sensitivity of the assay. However, the ^{2}D RPLC separation provided sharp peaks of each of the oligonucleotides (Figs. 8B, 8C, and 8D). Cut 1 was sampled into loop #1 of deck A and immediately analysed after its collection. While the analysis of *cut 1* was running in the ^{2}D, *cut 2* and *cut 3* were collected into loop #1 and #2 of deck B, respectively. They were then analysed subsequently in reversed order after the finished ^{2}D analysis of *cut 1* (^{2}D analysis start of cut #3 at 21.35 min and of cut #2 at 27.2 min). The entire MHC 2D-LC-UV-ESI-MS analysis was finished after around 35 min.

Oligonucleotides are negatively charged and hence they were analysed in negative ion mode. The negative ESI TOF-MS spectra of all three oligonucleotide samples feature two different preferential charge states, viz. 4- and 5- (see Fig. 8E, 8F, 8G). It is in agreement with literature reports [42]. Those charge states have the general formula $[M\text{-}nH]^{n-}$ with M being the monoisotopic mass calculated from the sequence. However, for the present oligonucleotides the most intensive ions are no longer the ions with m/z corresponding to the monoisotopic masses. In general, with the ESI-TOF-MS results of the current MHC 2D-LC assay, the oligonucleotide structures can be characterized in detail. However, the current ESI-MS spectra show a more complex pattern for each 4- and 5- charge state. When we zoom in, we see in each peak group of the MS spectra a substructure of NH_4 adducts of the general formula $[M\text{-}mH+mNH_4\text{-}nH]^{n-}$ [42] (see Suppl. Fig. S4-S9). These NH_4 adducts result from the ammonium acetate buffer used in the ^{2}D separation. It proves that the desalting was successful because otherwise triethylammonium adducts would have been expected. On the other hand, the splitting of the signal into distinct charge states and different adducts is clearly disadvantageous due to the lower MS detection sensitivity [43]. However, as can be seen from

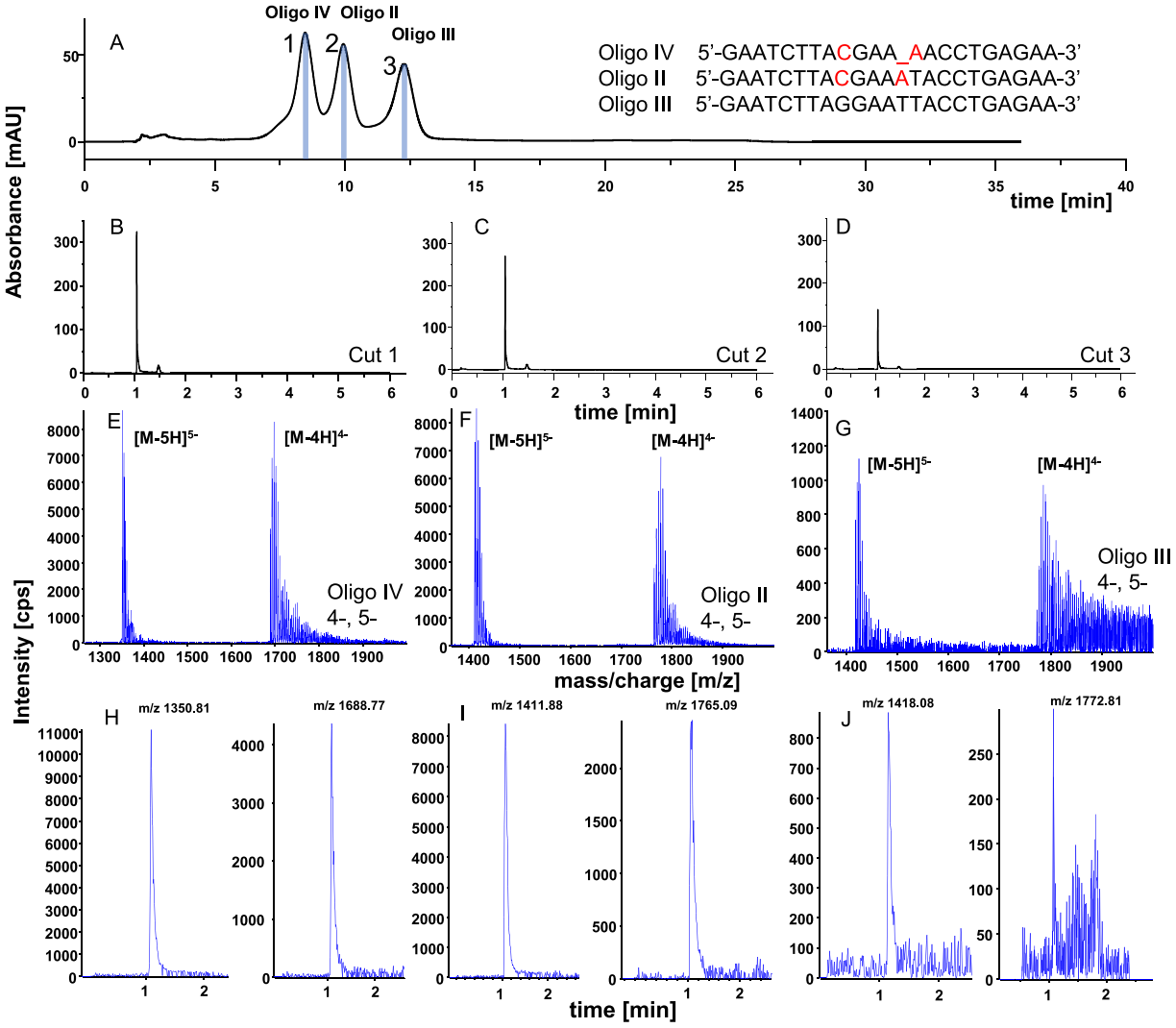

Fig. 8. Multiple Heart-Cutting 2D-LC with hyphenation to ESI-QTOF-MS in negative mode. (A) ^{1}D separation on Poly-RP/WAX. (B-D) ^{2}D RPLC-UV chromatograms of cuts #1-3. (E-G) TOF-MS spectra of oligonucleotide peaks from ^{2}D RPLC analysis. (H-J) EICs of most abundant m/z of each peak group (4- and 5-) from MS spectra. Chromatographic conditions: (A) see Table 2, Method A1. (B-G) see Table 2, Method E. Diverter valve switch time: always after 0.81 min. MHC sampling table (B-D): Sampling time always 14.4 sec; Cut #1: ^{1}D cut start at 8.4 min, ^{2}D run start at 8.65 min; Cut #2: ^{1}D cut start at 9.92 min, ^{2}D run start at 27.7 min; Cut #3: ^{1}D cut start at 12.24 min, ^{2}D run start at 21.35 min. (E-G) for detailed MS spectra see suppl. Figs. S4-S9. (H): EICs of m/z 1350.8148 (±10 mDa) (most abundant signal of $[M-5H]^{5-}$ peak group) and of m/z 1688.7715 (±10 mDa) (most abundant signal of $[M-4H]^{4-}$ peak group); (I): EICs of m/z 1411.8770 (±10 mDa) (most abundant signal of $[M-5H]^{5-}$ peak group) and m/z 1765.0850 (±10 mDa) (most abundant signal of $[M-4H]^{4-}$ peak group); (J): EICs of m/z 1418.0797 (±10 mDa) (most abundant signal of $[M-5H]^{5-}$ peak group) and m/z 1772.8049 (±10 mDa) (most abundant signal of $[M-4H]^{4-}$ peak group).

Fig. 8H, 8I and 8J extracted ion chromatograms (EICs) have a nice peak shape and are detected with good signal-to-noise which confirms the successful MHC 2D-LC-UV-ESI-MS analysis of the present oligonucleotide mixture. Interestingly, the EIC generated from the higher 5- charge state was always more sensitive than the EIC of the most abundant m/z of the 4- charge state. A dilution series of *Oligo IV* in the range of 100 to 1000 nM was analysed by the ^{2}D method with ESI-MS detection using the EIC of m/z 1350.8148 for generation of the chromatograms. The calibration function was highly linear ($R^2 = 0.9977$) (see Suppl. Fig. S10). The LOD (S/N=3) was determined to be 124 nM with the current method corresponding to 838.3 fg/µL. So, in general, the method has good potential although there are some factors to be optimized like ^{1}D efficiency and/or loop size of modulator, mobile phase conditions in the second dimension in view of enhanced detection sensitivities, amongst others.

4 Conclusion

A multiple heart-cutting 2D-LC system making use of selective RP/WAX mixed-mode chromatography in ^{1}D and MS compatible RPLC without ion-pairing agents in ^{2}D as well as UV detection after ^{1}D and ^{2}D separations and ESI-MS detection hyphenated in-line with ^{2}D UV detector via a diverter valve has been successfully established for the mass spectrometric characterization of oligonucleotides. Active solvent modulation is required to avoid breakthrough of oligonucleotide due to the organic modifier (acetonitrile) in the ^{1}D eluent. Also, the re-equilibration time of the ^{2}D column turned out to be a critical factor. With this MHC 2D-LC assay, the oligonucleotides can be sensitively detected by ESI-MS in absence of ion-pairing agent. Negative mode ESI-QTOF-MS revealed 4- and 5- charge species each split into signals of different NH_4 adducts. In spite of it, EICs from ^{2}D RP-ESI-MS allowed oligonu-

cleotide detection down to around 124 nM. Since only a heart cut (i.e. a fraction) and not the entire peak was transferred from the ^{1}D into the ^{2}D, in which efficient refocussing occurred, some sensitivity was still sacrificed in the current MHC-2D-LC setup. Hence, to achieve the full sensitivity of the ^{2}D RP-ESI-MS also in the MHC 2D-LC setup requires some further optimizations. ^{2}D eluent composition should be optimized in view of optimal ESI-MS sensitivity, a larger volume and/or entire ^{1}D peak should be transferred to the ^{2}D, and efficiency in the first dimension is worth to be optimized as well, in order to reduce the dilution of the oligonucleotide sample in the ^{1}D peak. Overall, the current MHC 2D-LC-ESI-MS shows great potential of sensitive mass spectrometric characterization of oligonucleotide samples. Its applicability to therapeutic oligonucleotides including those with phosphorothioated backbones will be evaluated next. For pharmaceutical analysis some other factors like availability of commercial (replacement) columns, precise control of complicated gradient conditions and method robustness, run-to-run repeatability and reproducibility of complicated separation conditions may be an issue. In this context, the potential of using IP-RPLC as ^{1}D separation principle is currently investigated with a real oligonucleotide therapeutics. The sharper peaks in ^{1}D should allow to transfer higher concentrations of oligonucleotides into the ^{2}D desalting RPLC separation and such a method is also less complicated. Orthogonality of RP/WAX mixed-mode chromatography and IP-RPLC, however, may be of particular interest and will be evaluated along with their coupling in a 2D-LC setup for achieving maximal selectivity to separate more complex oligonucleotide pharmaceuticals.

Declaration of Competing Interest

The authors declare no conflict of interests.

The authors declare that they have no known competing financial interests or personal relationships that could have appeared to influence the work reported in this paper.

Acknowledgements

We are grateful to Agilent Technologies for support of this research by an Agilent Research Award (#4068). The authors thank Dr. Stephan Buckenmaier from Agilent Technologies, Waldbronn, Germany, for technical advice and valuable discussions.

Supplementary materials

Supplementary material associated with this article can be found, in the online version, at doi:10.1016/j.chroma.2020.461338.

References

[1] N.M. El Zahar, N. Magdy, A.M. El-Kosasy, M.G. Bartlett, Chromatographic approaches for the characterization and quality control of therapeutic oligonucleotide impurities, Biomed. Chromatogr. (2018) 32, doi:10.1002/bmc.4088.
[2] A. Goyon, P. Yehl, K. Zhang, Characterization of therapeutic oligonucleotides by liquid chromatography, J. Pharm. Biomed. Anal. 182 (2020) 113105, doi:10.1016/j.jpba.2020.113105.
[3] M. Enmark, J. Bagge, J. Samuelsson, L. Thunberg, E. Örnskov, H. Leek, F. Limé, T. Fornstedt, Analytical and preparative separation of phosphorothioated oligonucleotides: columns and ion-pair reagents, Anal. Bioanal. Chem. 412 (2020) 299–309, doi:10.1007/s00216-019-02236-9.
[4] M. Enmark, M. Rova, J. Samuelsson, E. Örnskov, F. Schweikart, T. Fornstedt, Investigation of factors influencing the separation of diastereomers of phosphorothioated oligonucleotides, Anal. Bioanal. Chem. 411 (2019) 3383–3394, doi:10.1007/s00216-019-01813-2.
[5] D. Capaldi, K. Ackley, D. Brooks, J. Carmody, K. Draper, R. Kambhampati, M. Kretschmer, D. Levin, J. McArdle, B. Noll, R. Raghavachari, I. Roymoulik, B.P. Sharma, R. Thürmer, F. Wincott, Quality aspects of oligonucleotide drug development: specifications for active pharmaceutical ingredients, Drug Inf. J. 46 (2012) 611–626, doi:10.1177/0092861512445311.
[6] S.M. McCarthy, M. Gilar, J. Gebler, Reversed-phase ion-pair liquid chromatography analysis and purification of small interfering RNA, Anal. Biochem. 390 (2009) 181–188, doi:10.1016/j.ab.2009.03.042.
[7] M. Gilar, K.J. Fountain, Y. Budman, J.L. Holyoke, H. Davoudi, J.C. Gebler, Characterization of therapeutic oligonucleotides using liquid chromatography with on-line mass spectrometry detection, Oligonucleotides 13 (2003) 229–243, doi:10.1089/154545703322460612.
[8] C.G. Huber, P.J. Oefner, G.K. Bonn, High-resolution liquid chromatography of oligonucleotides on nonporous alkylated styrene-divinylbenzene copolymers, Anal. Biochem. 212 (1993) 351–358, doi:10.1006/abio.1993.1340.
[9] C.G. Huber, A. Krajete, Analysis of nucleic acids by capillary ion-pair reversed-phase HPLC coupled to negative-ion electrospray ionization mass spectrometry, Anal. Chem. 71 (1999) 3730–3739, doi:10.1021/ac990378j.
[10] S.G. Roussis, M. Pearce, C. Rentel, Small alkyl amines as ion-pair reagents for the separation of positional isomers of impurities in phosphate diester oligonucleotides, J. Chromatogr. A. 1594 (2019) 105–111, doi:10.1016/j.chroma.2019.02.026.
[11] N. Li, N.M. El Zahar, J.G. Saad, E.R.E. van der Hage, M.G. Bartlett, Alkylamine ion-pairing reagents and the chromatographic separation of oligonucleotides, J. Chromatogr. A. 1580 (2018) 110–119, doi:10.1016/j.chroma.2018.10.040.
[12] S. Studzińska, R. Rola, B. Buszewski, The impact of ion-pairing reagents on the selectivity and sensitivity in the analysis of modified oligonucleotides in serum samples by liquid chromatography coupled with tandem mass spectrometry, J. Pharm. Biomed. Anal. 138 (2017) 146–152, doi:10.1016/j.jpba.2017.02.014.
[13] L. Gong, J.S.O. McCullagh, Comparing ion-pairing reagents and sample dissolution solvents for ion-pairing reversed-phase liquid chromatography/electrospray ionization mass spectrometry analysis of oligonucleotides, Rapid Commun. Mass Spectrom. 28 (2014) 339–350, doi:10.1002/rcm.6773.
[14] S. Studzińska, L. Pietrzak, B. Buszewski, The effects of stationary phases on retention and selectivity of oligonucleotides in IP-RP-HPLC, Chromatographia 77 (2014) 1589–1596, doi:10.1007/s10337-014-2766-x.
[15] S. Studzińska, S. Bocian, L. Siecińska, B. Buszewski, Application of phenyl-based stationary phases for the study of retention and separation of oligonucleotides, J. Chromatogr. B. 1060 (2017) 36–43, doi:10.1016/j.jchromb.2017.05.033.
[16] S. Studzińska, B. Buszewski, Evaluation of ultrahigh-performance liquid chromatography columns for the analysis of unmodified and antisense oligonucleotides, Anal. Bioanal. Chem. 406 (2014) 7127–7136, doi:10.1007/s00216-014-7959-5.
[17] A. Kaczmarkiewicz, Ł. Nuckowski, S. Studzińska, B. Buszewski, Analysis of antisense oligonucleotides and their metabolites with the use of ion pair reversed-phase liquid chromatography coupled with mass spectrometry, Crit. Rev. Anal. Chem. 49 (2019) 256–270, doi:10.1080/10408347.2018.1517034.
[18] A. Apffel, J.A. Chakel, S. Fischer, K. Lichtenwalter, W.S. Hancock, Analysis of oligonucleotides by HPLC-electrospray ionization mass spectrometry, Anal. Chem. 69 (1997) 1320–1325, doi:10.1021/ac960916h.
[19] R. Liu, Y. Ruan, Z. Liu, L. Gong, The role of fluoroalcohols as counter anions for ion-pairing reversed-phase liquid chromatography/high-resolution electrospray ionization mass spectrometry analysis of oligonucleotides, Rapid Commun. Mass Spectrom. 33 (2019) 697–709, doi:10.1002/rcm.8386.
[20] A. Kanavarioti, HPLC methods for purity evaluation of man-made single-stranded RNAs, Sci. Rep. 9 (2019) 1–13, doi:10.1038/s41598-018-37642-z.
[21] M. Holčapek, K. Volná, P. Jandera, L. Kolářová, K. Lemr, M. Exner, A. Církva, Effects of ion-pairing reagents on the electrospray signal suppression of sulphonated dyes and intermediates, J. Mass Spectrom. 39 (2004) 43–50, doi:10.1002/jms.551.
[22] B. Chen, S.F. Mason, M.G. Bartlett, The effect of organic modifiers on electrospray ionization charge-state distribution and desorption efficiency for oligonucleotides, J. Am. Soc. Mass Spectrom. 24 (2013) 257–264, doi:10.1007/s13361-012-0509-5.
[23] B. Basiri, M.M. Murph, M.G. Bartlett, Assessing the interplay between the physicochemical parameters of ion-pairing reagents and the analyte sequence on the electrospray desorption process for oligonucleotides, J. Am. Soc. Mass Spectrom. 28 (2017) 1647–1656, doi:10.1007/s13361-017-1671-6.
[24] A. Shimoyama, A. Fujisaka, S. Obika, Evaluation of size-exclusion chromatography for the analysis of phosphorothioate oligonucleotides, J. Pharm. Biomed. Anal. 136 (2017) 55–65, doi:10.1016/j.jpba.2016.12.036.
[25] P.A. Lobue, M. Jora, B. Addepalli, P.A. Limbach, Oligonucleotide analysis by hydrophilic interaction liquid chromatography-mass spectrometry in the absence of ion-pair reagents, J. Chromatogr. A. 1595 (2019) 39–48, doi:10.1016/j.chroma.2019.02.016.
[26] Q. Li, F. Lynen, J. Wang, H. Li, G. Xu, P. Sandra, Comprehensive hydrophilic interaction and ion-pair reversed-phase liquid chromatography for analysis of di-to deca-oligonucleotides, J. Chromatogr. A. 1255 (2012) 237–243, doi:10.1016/j.chroma.2011.11.062.
[27] R. Easter, C. Barry, J. Caruso, P. Limbach, Separation and identification of phosphorothioate oligonucleotides by HILIC-ESIMS, Anal. Methods. 5 (2013) 2657–2659, doi:10.1039/c3ay26519f.
[28] A.J. Alpert, Hydrophilic-interaction chromatography for the separation of peptides, nucleic acids and other polar compounds, J. Chromatogr. A. 499 (1990) 177–196, doi:10.1016/S0021-9673(00)96972-3.
[29] A. Demelenne, M.-J. Gou, G. Nys, C. Parulski, J. Crommen, A.-C. Servais, M. Fillet, Evaluation of hydrophilic interaction liquid chromatography, capillary zone electrophoresis and drift tube ion-mobility quadrupole time of flight mass spectrometry for the characterization of phosphodiester and phosphorothioate oligonucleotides, J. Chromatogr. A. 1614 (2020) 460716, doi:10.1016/j.chroma.2019.460716.

[30] R.N. Easter, K.K. Kröning, J.A. Caruso, P.A. Limbach, Separation and identification of oligonucleotides by hydrophilic interaction liquid chromatography (HILIC) - Inductively coupled plasma mass spectrometry (ICPMS), Analyst 135 (2010) 2560–2565, doi:10.1039/c0an00399a.
[31] K. Cook, J. Thayer, Advantages of ion-exchange chromatography for oligonucleotide analysis, Bioanalysis 3 (2011) 1109–1120, doi:10.4155/bio.11.66.
[32] S.G. Roussis, I. Cedillo, C. Rentel, Two-dimensional liquid chromatography-mass spectrometry for the characterization of modified oligonucleotide impurities, Anal. Biochem. 556 (2018) 45–52, doi:10.1016/j.ab.2018.06.019.
[33] M. Biba, E. Jiang, B. Mao, D. Zewge, J.P. Foley, C.J. Welch, Factors influencing the separation of oligonucleotides using reversed-phase/ion-exchange mixed-mode high performance liquid chromatography columns, J. Chromatogr. A. 1304 (2013) 69–77, doi:10.1016/j.chroma.2013.06.050.
[34] L.W. Mclaughlin, Mixed-mode chromatography of nucleic acids, Chem. Rev. 89 (1989) 309–319, doi:10.1021/cr00092a003.
[35] A. Zimmermann, R. Greco, I. Walker, J. Horak, A. Cavazzini, M. Lämmerhofer, Synthetic oligonucleotide separations by mixed-mode reversed-phase/weak anion-exchange liquid chromatography, J. Chromatogr. A. 1354 (2014) 43–55, doi:10.1016/j.chroma.2014.05.048.
[36] S. Bäurer, A. Zimmermann, U. Woiwode, O.L. Sánchez-Muñoz, M. Kramer, J. Horak, W. Lindner, W. Bicker, M. Lämmerhofer, Stable-bond polymeric reversed-phase/weak anion-exchange mixed-mode stationary phases obtained by simultaneous functionalization and crosslinking of a poly(3-mercaptopropyl)methylsiloxane-film on vinyl silica via thiol-ene double click reaction, J. Chromatogr. A. 1593 (2019) 110–118, doi:10.1016/j.chroma.2019.01.078.
[37] R. Nogueira, M. Lämmerhofer, W. Lindner, Alternative high-performance liquid chromatographic peptide separation and purification concept using a new mixed-mode reversed-phase/weak anion-exchange type stationary phase, J. Chromatogr. A. 1089 (2005) 158–169, doi:10.1016/j.chroma.2005.06.093.
[38] B. Koshel, R. Birdsall, W. Chen, Two-dimensional liquid chromatography coupled to mass spectrometry for impurity analysis of dye-conjugated oligonucleotides, J. Chromatogr. B Anal. Technol. Biomed. Life Sci. 1137 (2020) 121906, doi:10.1016/j.jchromb.2019.121906.
[39] A. Goyon, K. Zhang, Characterization of antisense oligonucleotide impurities by ion-pairing reversed-phase and anion exchange chromatography coupled to HILIC/MS using a versatile 2D-LC setup, Anal. Chem. (2020), doi:10.1021/acs.analchem.0c00114.
[40] A. Zimmermann, J. Horak, A. Sievers-Engler, C. Sanwald, W. Lindner, M. Kramer, M. Lämmerhofer, Surface-crosslinked poly(3-mercaptopropyl)methylsiloxane-coatings on silica as new platform for low-bleed mass spectrometry-compatible functionalized stationary phases synthesized via thiol-ene click reaction, J. Chromatogr. A. 1436 (2016) 73–83, doi:10.1016/j.chroma.2016.01.058.
[41] D.R. Stoll, K. Shoykhet, P. Petersson, S Buckenmaier, Active solvent modulation: a valve-based approach to improve separation compatibility in two-dimensional liquid chromatography, Anal. Chem. 89 (2017) 9260–9267, doi:10.1021/acs.analchem.7b02046.
[42] W.D. Van Dongen, Bioanalytical LC-MS of therapeutic oligonucleotides, Chim. Oggi. 30 (2012) 65–67.
[43] E. Nordhoff, F. Kirpekar, P. Roepstorff, Mass spectrometry of nucleic acids, Mass Spectrom. Rev. 15 (1996) 67–138 10.1002/(SICI)1098-2787(1996)15:2<67::AID-MAS1>3.0.CO;2-8.

Supplementary Material

A Multiple Heart-Cutting Mixed-mode Chromatography-Reversed-phase 2D-Liquid Chromatography Method for Separation and Mass Spectrometric Characterization of Synthetic Oligonucleotides

Feiyang Li, Xiaoli Su, Stefanie Bäurer, Michael Lämmerhofer*

Institute of Pharmaceutical Sciences, Pharmaceutical (Bio-)Analysis, University of Tübingen, Auf der Morgenstelle 8, 72076 Tübingen, Germany

*Author for correspondence:

Prof. Dr. Michael Lämmerhofer

Pharmaceutical (Bio-)Analysis

Institute of Pharmaceutical Sciences

University of Tübingen

Auf der Morgenstelle 8

72076 Tübingen, Germany

T +49 7071 29 78793, F +49 7071 29 4565

E-mail: michael.laemmerhofer@uni-tuebingen.de

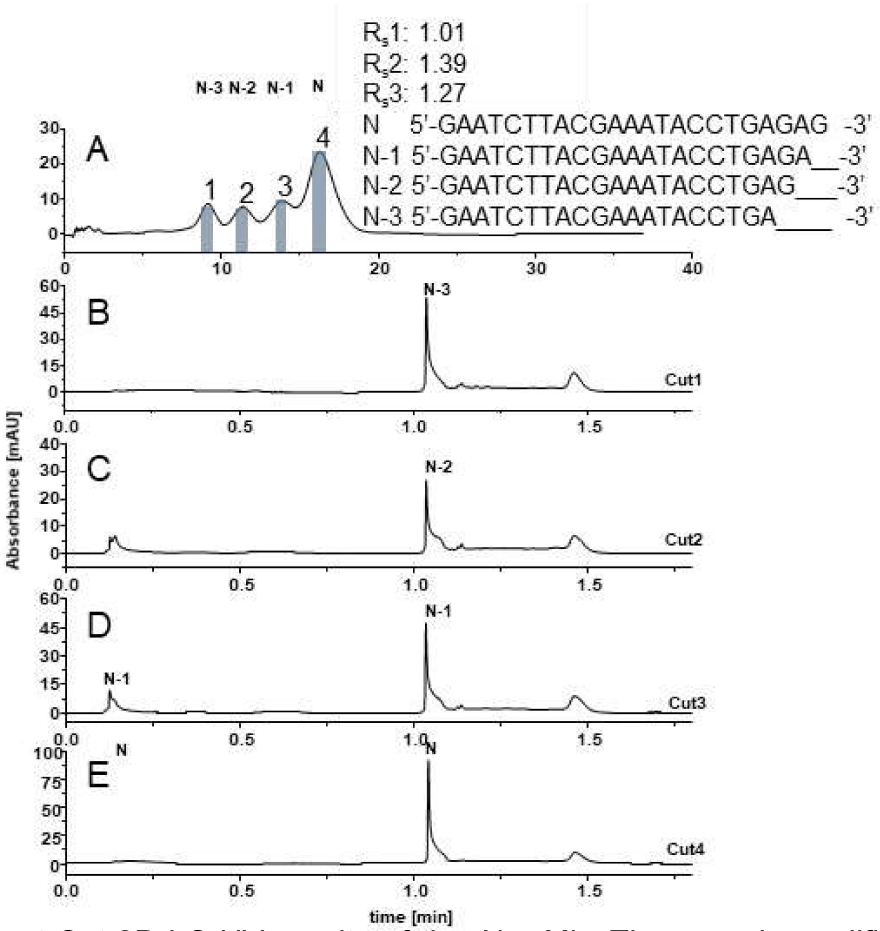

Figure S1. Heart-Cut-2D-LC-UV results of the *N-x Mix*. The organic modifier in the mobile phases from the first dimension (^{1}D) was MeOH. Experimental conditions in ^{1}D: column dimension: Poly-RP-WAX, 50x3 mm i.d., 100 Å, 5 µm. Mobile phase A: 20% MeOH, 50 mM phosphoric acid, pH 6.8 adjusted with triethylamine prior to the mixing with MeOH, B: 20% MeOH, 100 mM phosphoric acid, pH 7.8 adjusted with triethylamine prior to the mixing with MeOH. Isocratic run by 100% B. 40 °C. 10 µL. 254 nm. Flow rate: 0.5 ml/min. Experimental conditions in ^{2}D: column dimension: Agilent ZORBAX Eclipse Plus C18 RRHD, 50x3.1 mm i.d., 100 Å, 1.8 µm. Mobile phase A: water, 10 mM ammonium acetate, B: MeOH, 10 mM ammonium acetate. Gradient: hold 5% B for 0.8 min, 0.1 min 5-80% B, hold 80% B for 0.3 min, 0.1 min 80-5% B, hold 5% B for 0.5 min. 40 °C. 254 nm. Flow rate: 1 ml/min, active solvent modulation ASM: Factor 5, 0.61 min, sample loop was flushed 3 times.

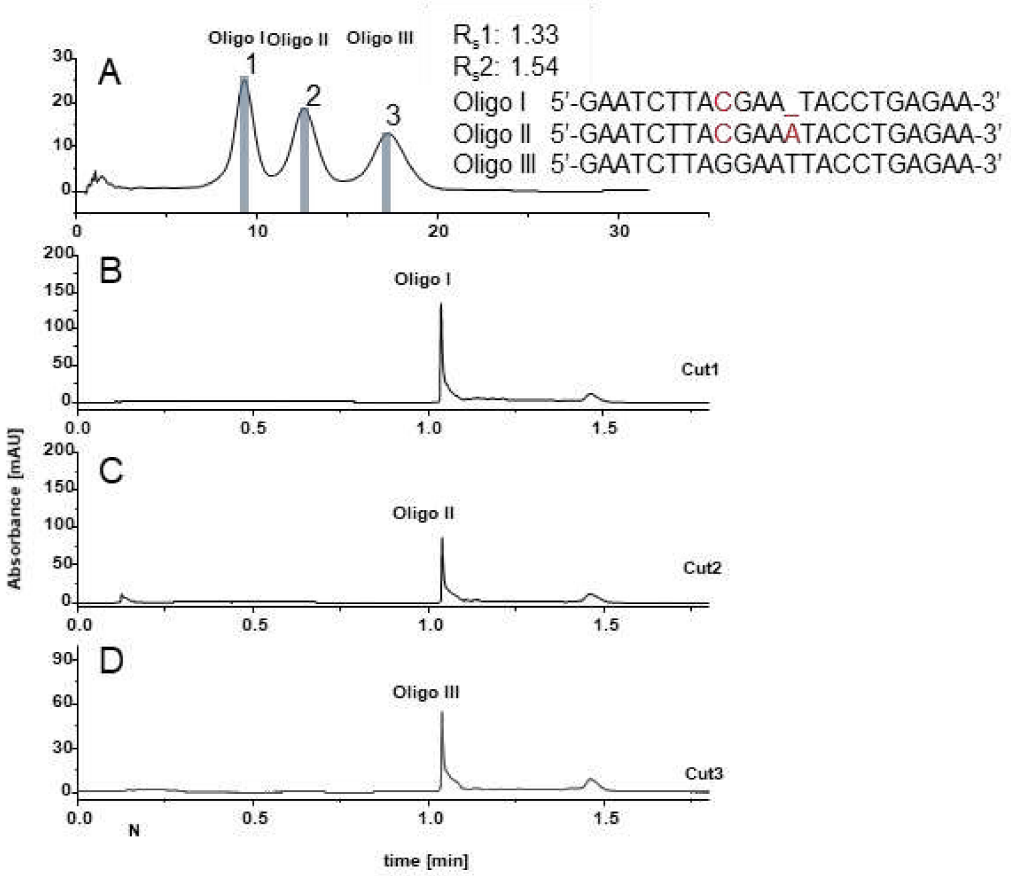

Figure S2. Heart-Cut-2D-LC-UV results of the *Oligomix*. The organic modifier in the ^{1}D mobile phases was MeOH. Experimental conditions in ^{1}D: column: Poly-RP-WAX, 50x3 mm i.d., 100 Å, 5 µm. Mobile phase A: 20% MeOH, 50 mM phosphoric acid, pH 6.8 adjusted with triethylamine prior to the mixing with MeOH, B: 20% MeOH, 100 mM phosphoric acid, pH 7.8 adjusted with triethylamine prior to the mixing with MeOH. Isocratic run by 100% B. 40 °C. 10 µL. 254 nm. Flow rate: 0.5 ml/min. Experimental conditions in ^{2}D: column: Agilent ZORBAX Eclipse Plus C18 RRHD, 50x3.1 mm i.d., 100 Å, 1.8 µm. Mobile phase A: water, 10 mM ammonium acetate, B: MeOH, 10 mM ammonium acetate. Gradient: hold 5% B for 0.8 min, 0.1 min 5-80% B, hold 80% B for 0.3 min, 0.1 min 80-5% B, hold 5% B for 0.5 min. 40 °C. 254 nm. Flow rate: 1 ml/min, active solvent modulation ASM: Factor 5, 0.61 min, sample loop was flushed 3 times.

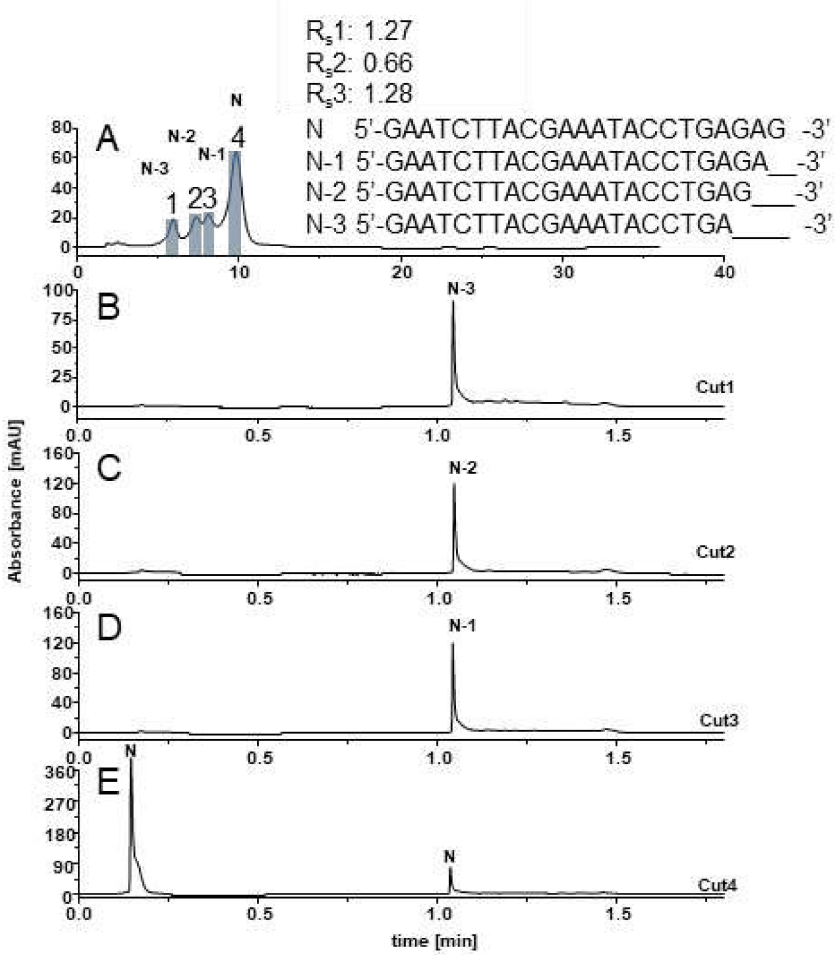

Figure S3. Heart-Cut-2D-LC-UV results of *N-Mixture*. The organic modifier in the ^{1}D mobile phase was ACN. Experimental conditions in ^{1}D: column dimension: Poly-RP-WAX, 50x3 mm i.d., 100 Å, 5 µm. Mobile phase A: 20% ACN, 50 mM phosphoric acid, pH 6.8 adjusted with triethylamine prior to the mixing with ACN, B: 20% ACN, 100 mM phosphoric acid, pH 7.8 adjusted with triethylamine prior to the mixing with ACN. Gradient: Start with 80% B, 25 min 80-100% B, 0.5 min 100-80% B, hold 80% B for 10.5 min. 40 °C. 4 µL. 254 nm. Flow rate: 0.168 ml/min. Experimental conditions in ^{2}D: column dimension: Agilent ZORBAX Eclipse Plus C18 RRHD, 50x3.1 mm i.d., 100 Å, 1.8 µm. Mobile phase A: water, 10 mM ammonium acetate, B: MeOH, 10 mM ammonium acetate. Gradient: hold 5% B for 0.8 min, 0.1 min 5-80% B, hold 80% B for 0.3 min, 0.1 min 80-5% B, hold 5% B for 2 min. 40 °C. 254 nm. Flow rate: 1 ml/min, active solvents modulation ASM: Factor 5, 0.61 min, sample loop was flushed 5 times.

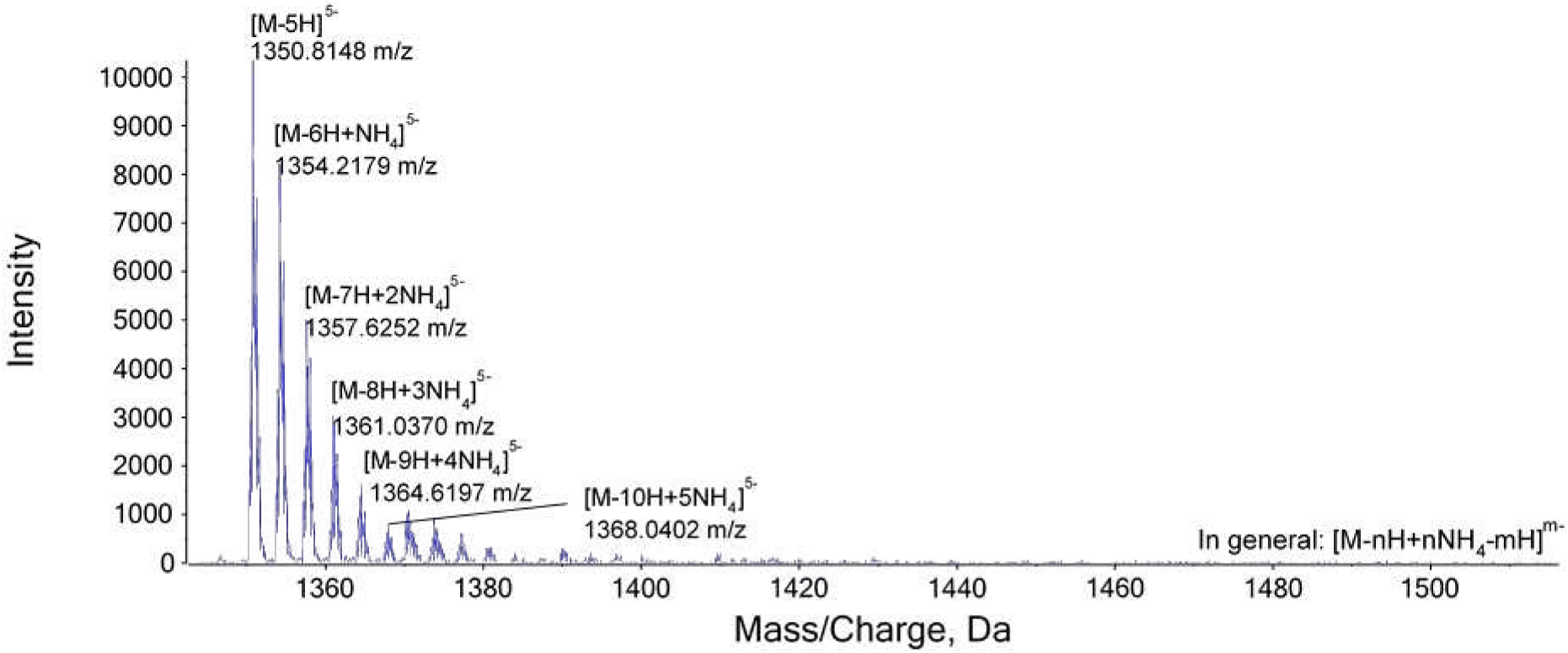

Figure S4. ESI-Negative-TOF spectrum of Oligo IV in its 5- charged state. Besides the envelop of $[M-5H]^{5-}$, further isotope patterns assigning to the ammonium adducts are visible.

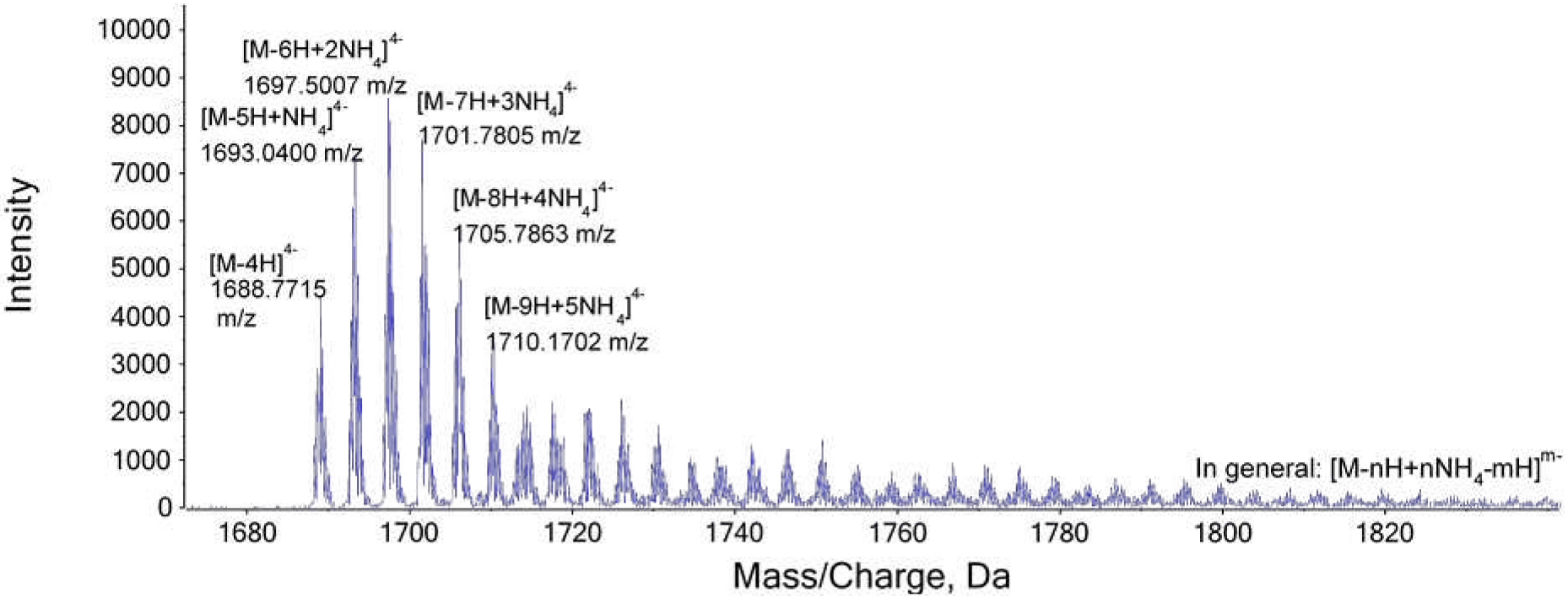

Figure S5. ESI-Negative-TOF spectrum of Oligo IV in its 4- charged state. Besides the envelop of $[M-4H]^{4-}$, further isotope patterns assigning to the ammonium adducts are visible.

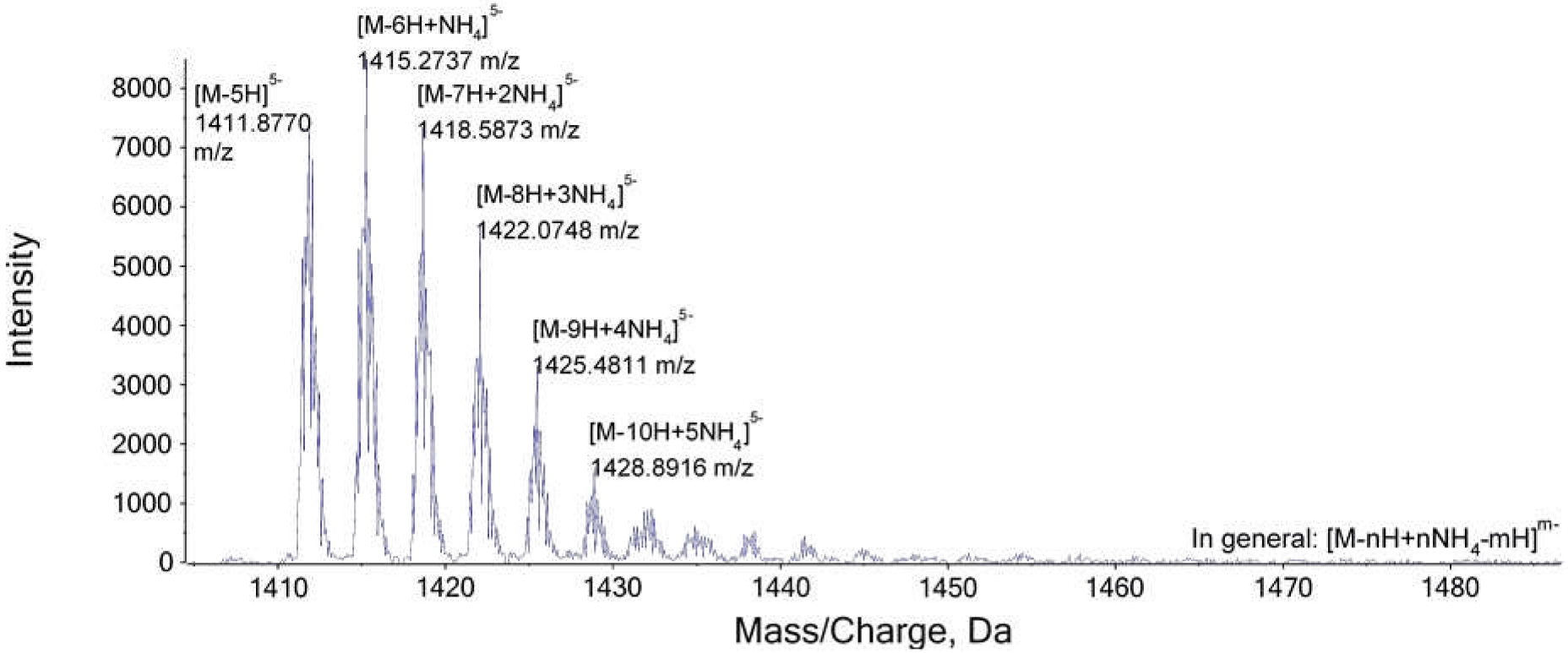

Figure S6. ESI-Negative-TOF-ESI spectrum of Oligo II in 5- charged state. The related ammonium adducts are illustrated as well.

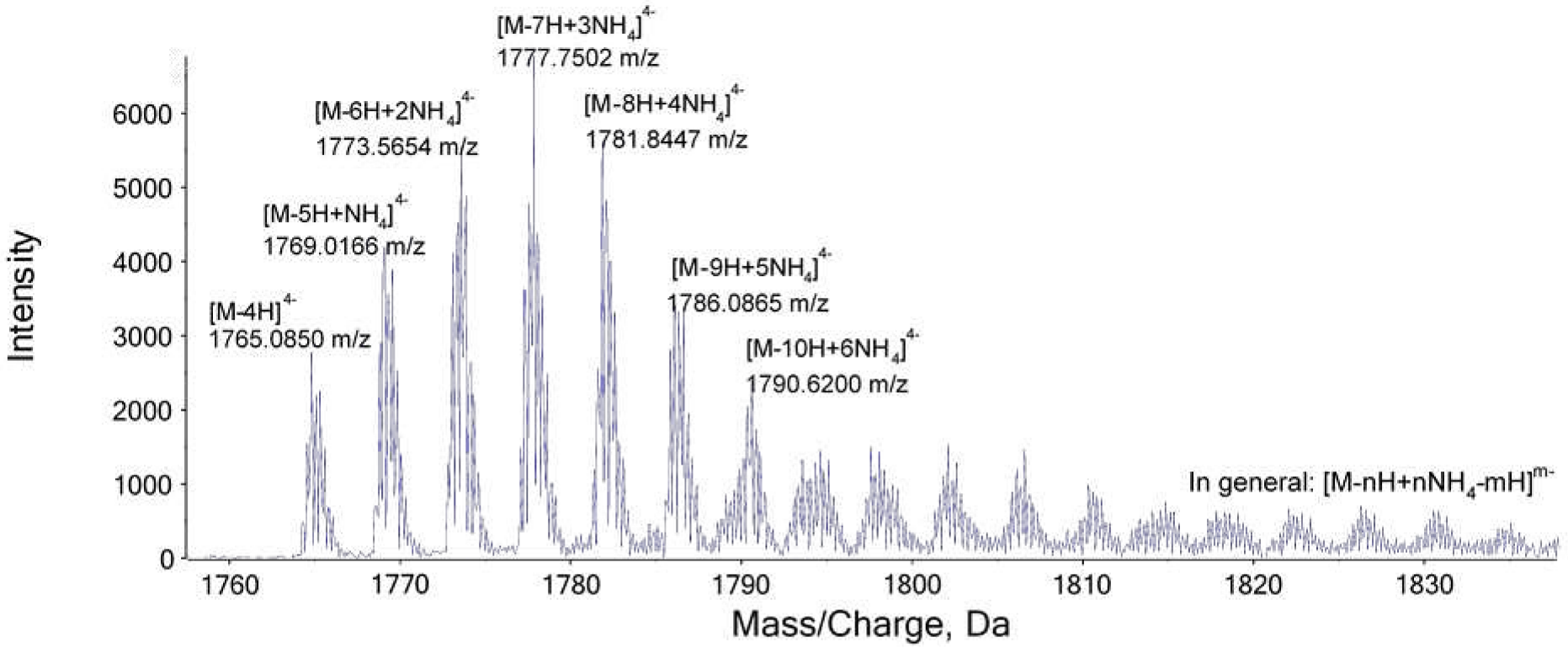

Figure S7. ESI-Negative-TOF spectrum of Oligo II in 4- charged state. Multiple ammonium adducts are illustrated.

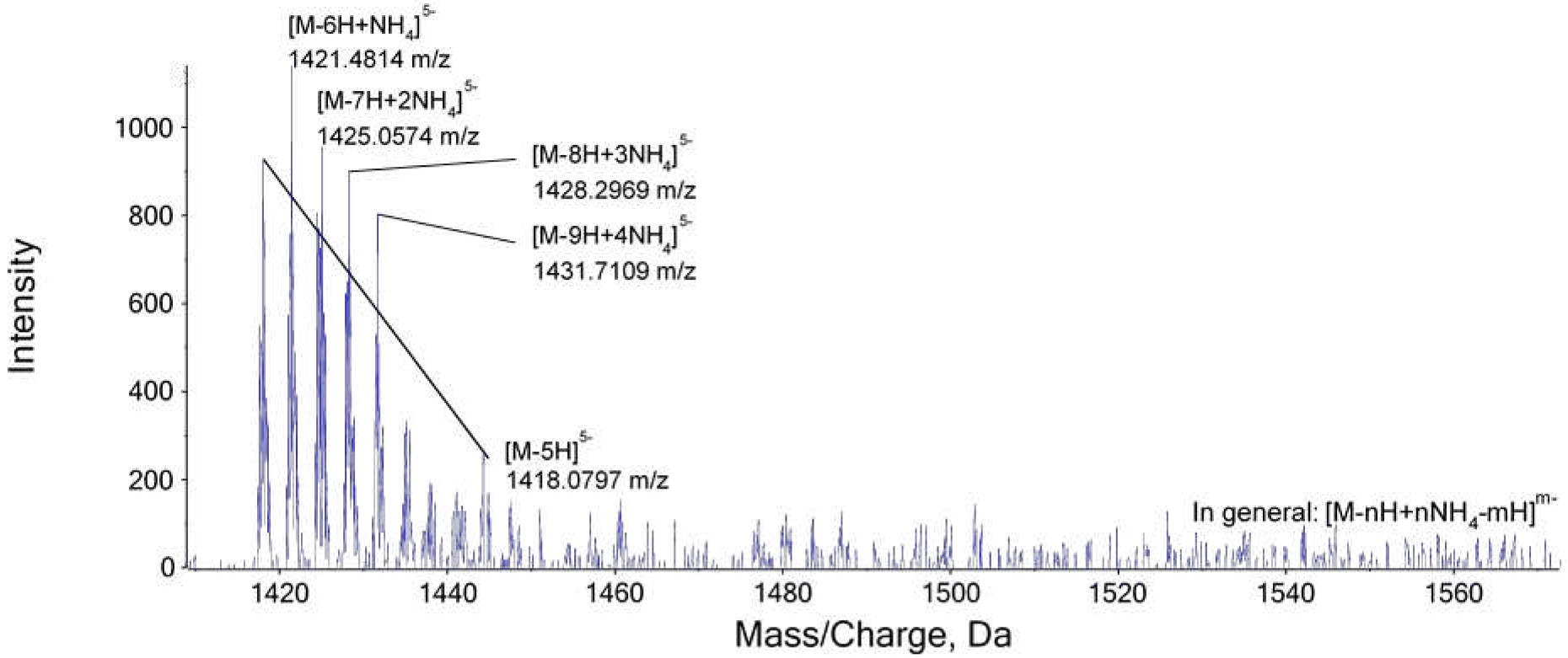

Figure S8. ESI-Negative-TOF spectrum of Oligo III in its 5- charged state. The ammonium adducts are also illustrated.

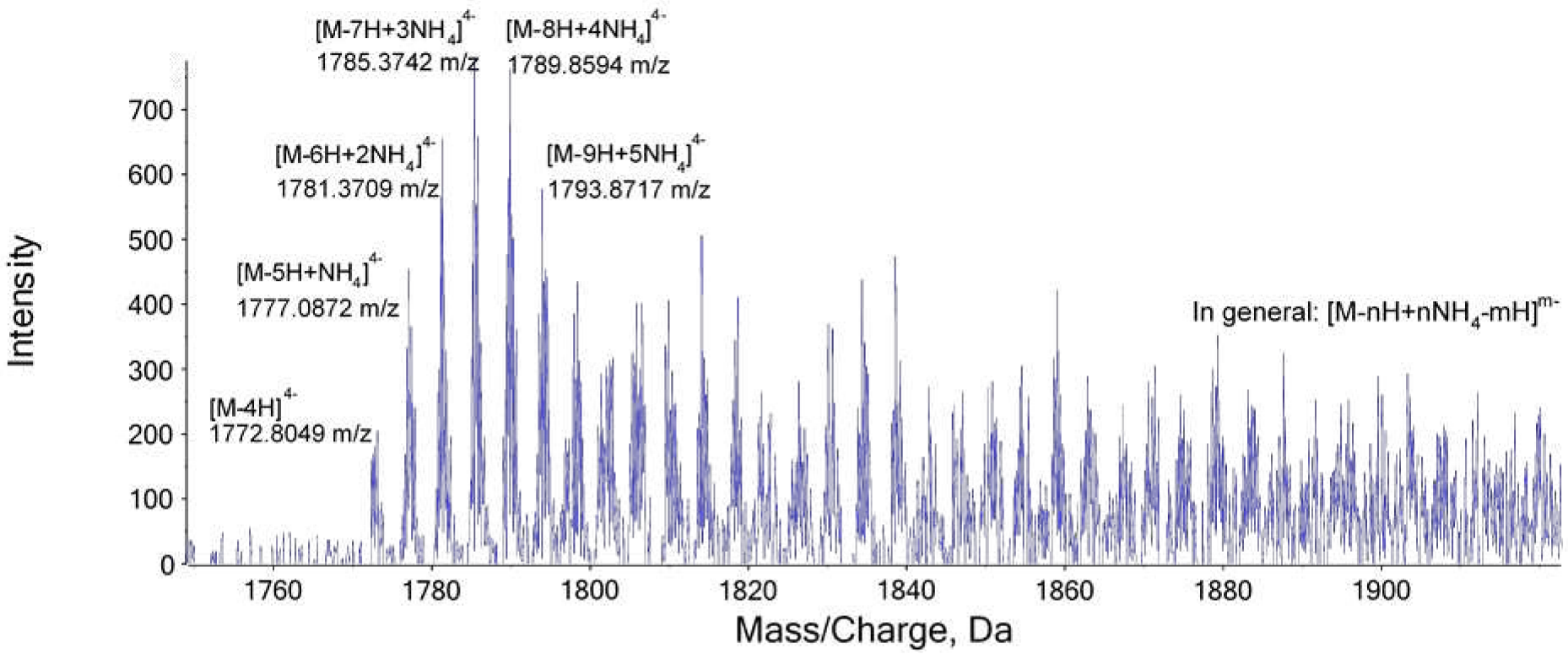

Figure S9. ESI-Negative-TOF spectrum of Oligo III in its 4- charged state. The ammonium adducts are visible and assigned.

Quantitative 1D-RPLC-ESI-MS Analysis

The dilution of sample is a problem that we have to take into consideration by 2D-LC-MS analysis. A solution of Oligo IV with different concentration is injected (10 µL) into the MS-system by coupling with the C18-column at first. With the resulting calibration we can determine the LOD and LOQ for our LC-MS method in a 1D-LC-MS setup.

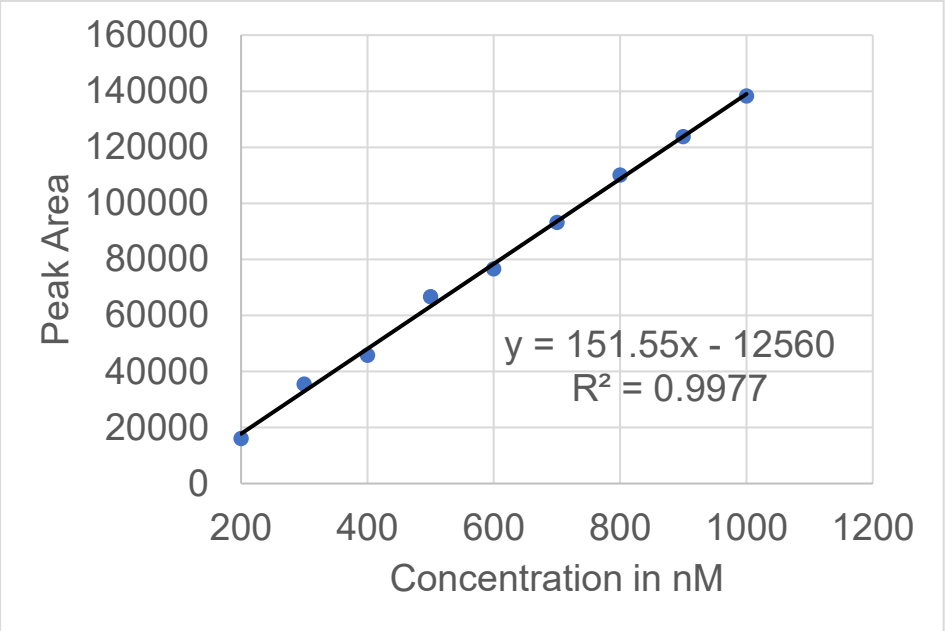

Fig. S10. Calibration of the LC-MS method for the second dimension (based on EIC m/z 1350.8148).

Concentration (nM)	On-column amount (pmol)	Peak area
200	2	16023
300	3	35374
400	4	45666
500	5	66584
600	6	76555
700	7	93100
800	8	110000
900	9	123762
1000	10	138260

LOD	124
LOQ	376

2. Publication II

Impurity profiling of siRNA by two-dimensional liquid chromatography-mass spectrometry with quinine carbamate anion-exchanger and ion-pair reversed-phase chromatography

Feiyang Li, Michael Lämmerhofer*

Institute of Pharmaceutical Sciences, Pharmaceutical (Bio-)Analysis,

University of Tübingen, Auf der Morgenstelle 8, 72076 Tübingen, Germany

*Author for correspondence:

Prof. Dr. Michael Lämmerhofer

Pharmaceutical (Bio-)Analysis

Institute of Pharmaceutical Sciences

University of Tübingen

Auf der Morgenstelle 8

72076 Tübingen, Germany

T +49 7071 29 78793, F +49 7071 29 4565

E-mail: michael.laemmerhofer@uni-tuebingen.de

Journal of Chromatography A

Year 2021, 1643, 462065

DOI: 10.1016/j.chroma.2021.462065

Journal of Chromatography A 1643 (2021) 462065

Contents lists available at ScienceDirect

Journal of Chromatography A

journal homepage: www.elsevier.com/locate/chroma

Impurity profiling of siRNA by two-dimensional liquid chromatography-mass spectrometry with quinine carbamate anion-exchanger and ion-pair reversed-phase chromatography

Feiyang Li, Michael Lämmerhofer*

Institute of Pharmaceutical Sciences, Pharmaceutical (Bio-)Analysis, University of Tübingen, Auf der Morgenstelle 8, 72076 Tübingen, Germany

ARTICLE INFO

Article history:
Received 12 January 2021
Revised 10 March 2021
Accepted 11 March 2021
Available online 15 March 2021

Keywords:
Two-dimensional liquid chromatography
Electrospray ionization mass spectrometry
Synthetic oligonucleotides
Pharmaceutical analysis
Impurity profiling
Anion-exchange chromatography
Ion-pairing reversed-phase chromatography

ABSTRACT

A short RNA with the sequence of the antisense strand of Patisiran has been selected as test material for the investigation of its common impurities using three different two-dimensional liquid chromatography (2D-LC) platforms. On the one hand, a quinine (QN) carbamate-based weak anion-exchange (AX) stationary phase (QN-AX) and a classical C18 reversed phase (RP) stationary phase in ion-pair (IP) mode with tripropylammonium acetate, respectively, have been used in the first dimension (^{1}D) to provide the selectivity for impurities formed during the synthesis of the RNA. In the next step, certain peaks of interest from ^{1}D have been transferred by multiple-heart-cutting (MHC) into a ^{2}D in which an ESI-MS-compatible non-ionpairing RP method has been used for desalting via a diverter valve to remove non-volatile phosphate buffer components and ion-pair agents, respectively. Thus, a sensitive electrospray-ionization quadrupole time of flight mass spectrometry (ESI-TOF-MS) analysis of resolved impurity peaks of the siRNA has become possible under MS-friendly conditions. With both 2D-LC setups, peak purity of the ON has been evaluated by selective comprehensive (high resolution) sampling of the main peak. In a third MHC 2D-LC approach, the QN-AX LC mode was online coupled with the IP-RPLC in the ^{2}D using UV detection. It allows the separation of additional impurities which coeluted in the first dimension. The potential of these methods for comprehensive impurity profiling of ON therapeutics is illustrated and discussed.

1. Introduction

In August 2018, the oligonucleotide therapeutics Patisiran (tradename: Onpattro, Alnylam Pharmaceuticals) was approved by the U.S. Food & Drug Administration (FDA) as the first small-interfering ribonucleic acid-based (siRNA) drug for the treatment of hereditary transthyretin-mediated amyloidosis [1]. Apart from siRNA, several other classes of nucleic acids are being investigated for therapeutic applications and a further growth of this class of next generation drugs can be expected [2–6]. For their characterization, sophisticated LC-MS methods for advanced investigation of oligonucleotides are on high demand. Especially the detection of impurities in therapeutic oligonucleotides is of great relevance. The common impurities in synthetic oligonucleotides are shortmers, such as n-1, n-2 nucleotides and so forth [7–9]. Other common impurities are oxidized compounds of guanine or deamination and depurination of nucleobases [10]. Furthermore, impurities originating from therapeutic ONs with incompletely cleaved protective groups also often represent a separation challenge for the LC analysis of oligonucleotides [11]. Over the years, many chromatographic strategies have been developed to investigate these impurities [10,12]. One of the most commonly used LC modes for oligonucleotide analysis is IP-RP liquid chromatography. In this LC mode, a wide range of ion-pairing agents can be applied depending on samples and analytical questions [13–15]. Particularly the use of 1,1,1,1,3,3,3-hexafluoro-2-propanol (HFIP) as additive in combination with triethylamine (TEA) has become the golden-standard method for many LC-MS experiments with oligonucleotides [16–19]. In one application double-stranded siRNA was successfully separated from phospholipids, cholesterol and another short-chain lipid in lipid nanoparticles (LNP) using IR-RP chromatography [20].

Besides IP-RP, there are several alternatives for the separation of oligonucleotides and similar samples. Since the 70 s, many distinct approaches employing anion exchange chromatography (AEX) based on the differences in local charge distribu-

* Corresponding author: Prof. Dr. Michael Lämmerhofer, Pharmaceutical (Bio-)Analysis, Institute of Pharmaceutical Sciences, University of Tübingen, Auf der Morgenstelle 8, 72076 Tübingen, Germany.
E-mail address: michael.laemmerhofer@uni-tuebingen.de (M. Lämmerhofer).

https://doi.org/10.1016/j.chroma.2021.462065
0021-9673/

tion of oligonucleotides and DNAs have been reported [21–25]. On the other hand, mixed-mode chromatography (MMC) using more than one principle of interaction between the stationary phase and analytes has demonstrated great potential for separations of oligonucleotides. Biba et al. were able to separate phosphodiester oligonucleotides (PO–ON) with a NaCl gradient using commercial Scherzo columns [26]. A mixed-mode reversed-phase/weak anion-exchange (WAX) stationary phase based on an *N*'-(10-undecenoyl)−3-aminoquinuclidine as chromatographic ligand immobilized on silica enabled successful separations of structurally closely related PO–ONs (n-1 shortmers, single nucleotide variants), with improved selectivity over IP-RP and plain WAX [27]. Hydrophilic interaction liquid chromatography (HILIC) was promoted for oligonucleotide separations because of its advantage of being more MS-friendly [28–30]. Besides the stationary phase chemistry, the pore size of the chromatographic material does have a significant impact on the separation performance of ON shortmers [31].

Since none of the chromatography techniques described above provides full separation of all impurities, they have been combined in 2D-LC to yield enhanced performance of oligonucleotide separations in acceptable analysis times. A first comprehensive online 2D-LC-MS method (HILIC × IP-RP) for PO–ONs was presented by Li et al. in 2012 [32]. Zhang and coworkers combined IR-RP and HILIC in a 2D-LC-MS setup to characterize impurities in antisense oligonucleotides [28]. Roussis et al. used ^{1}D AEX and ^{2}D IP-RP to develop a MHC-2D-LC/MS method to characterize PO- and PS-ON impurities [33]. In our recent work, we coupled ESI-MS-incompatible mixed-mode RP/WAX chromatography with RP-LC in a multiple heart cutting 2D-LC approach to allow sensitive detection of ONs by ESI-TOF-MS [34].

In this work, we investigate the potential of MHC and selective comprehensive 2D-LC for the impurity analysis of RNA-based therapeutics using the siRNA pharmaceutical Patisiran as test compound. To this end, RNA with the sequence of the antisense strand of Patisiran is investigated with a 2D-LC method consisting of ^{1}D AEX using a commercial Chiralpak QN-AX column based on a quinine carbamate selector with a mixed pH/triethylammonium phosphate (TEAP) buffer gradient. This column is commonly used for enantiomer separation of acidic chiral compounds and revealed also interesting selectivities for plasmid DNA isoforms and topoisomers, respectively [35,36]. Furthermore, a classical ion-pairing RP chromatography with tripropylammonium acetate (TPAA) as ion-pairing reagent using a C18 column is evaluated as ^{1}D in a MHC and selective comprehensive 2D-LC approach. With a similar 2D-LC-MS setup as described in our recent work i.e. using a C18 desalting step in the ^{2}D, a sensitive ESI-MS detection and characterization of impurity peaks is enabled [34]. Finally, the potential of WAX chromatography with QN-AX as ^{1}D and IP-RPLC with TPAA as ^{2}D in a MHC and high-resolution sampling (selective comprehensive) 2D-LC-UV approach, respectively, for the impurity profiling of the Patisiran antisense strand is documented.

2. Experimental

2.1. Materials

The antisense strand of Patisiran (see Fig. 1A) and the DNA oligonucleotide (GAA TCT TAC GAA ATA CCT GAG AG) used for the determination of LODs were synthesized by Oligo Sigma (Merck, Munich, Germany) and purchased as desalted raw product. Since this oligonucleotide was synthesized as analytical standard and not purified, its quality does not represent that of a typical Patisirin API. Thus, it is reasonable to assume that the impurity profile of the present ON standard does not match the one of Patisiran in real pharmaceutical products, however, serves as a useful model.

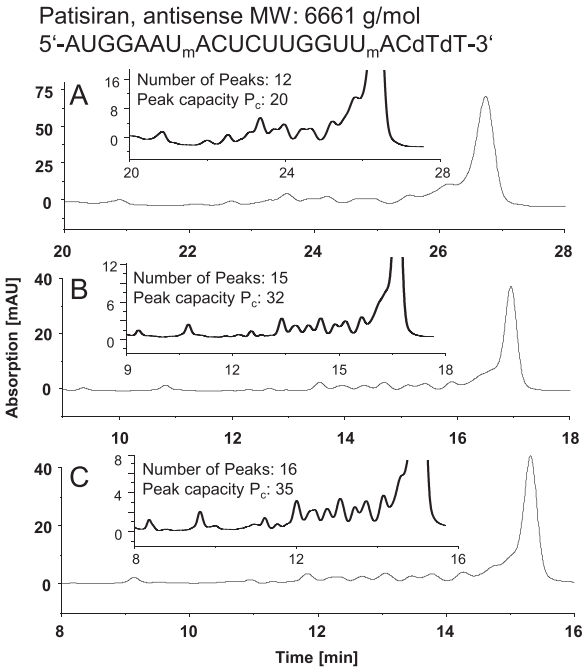

Fig. 1. ^{1}D Chiralpak QN-AX HPLC-UV chromatogram of Patisiran with various flow rates (A: 0.2 ml/min; B: 0.6 ml/min; C: 0.8 ml/min) and a pH gradient from 5.8 to 7.8. Inserts represent zoom-in from the same chromatogram . Gradient: 0–100% B in 20 min, 10 min at 100% B. Further LC-conditions see chapter 2.5 and supplementary material. dT, desoxythymidine (DNA nucleotide in RNA strand); mU, *O*-Methyl-Uridine.

Ortho phosphoric acid (85% in H_2O), acetic acid (ACS reagent, ≥ 99.8%), triethylamine (≥ 99%), tripropylamine (≥ 98%), ammonium hydroxide (ACS reagent, 28–30%) and ammonium acetate (LC-MS grade) were purchased from Sigma-Aldrich (Merck, Munich, Germany). HPLC-grade acetonitrile was delivered by Honeywell (Munich, Germany). HPLC-MS-grade methanol was purchased from Carl Roth (Karlsruhe, Germany). Ultrapure water was obtained by purification of deionized water using Elga PurLab Ultra purification system (Celle, Germany). For the ^{1}D-separation, two different columns have been used. The quinine carbamate-based Chiralpak QN-AX anion-exchange column (150 × 4 mm i.d., 5 µm particle size, 120 Å) is available from Chiral Technologies Europe (Illkirch, France). A wider pore size (e.g. 300 Å) might be preferable for ONs [31]. Unfortunately, a QN-AX column with this pore size is commercially not available yet. The IP-RP chromatography was performed using Acquity UPLC Oligonucleotide BEH C18 column by Waters (50 × 2.1 mm i.d., 1.7 µm particle size, 130 Å pore size). In the second dimension, a ZORBAX Eclipse Plus C18 RRHD column from Agilent Technologies (50 × 2.1 mm i.d., 1.8 µm particle size, 100 Å pore size) was applied to remove the MS-incompatible components of the ^{1}D-effluents.

2.2. Sample preparation

A stock solution of Patisiran antisense strand with a concentration of 100 µM was prepared in purified water and stored at 4 °C until use. For all the analyses, the final concentration of Patisiran was 50 µM by diluting the stock solution with ultrapure water.

2.4. Instrumentation

A scheme of the MHC 2D-LC-MS setup can be found in our last report, Fig. 2 [34]). In general, it is based on the Agilent 1290 Infinity II 2D-LC Solution from Agilent Technologies (Waldbronn, Germany) which consisted of a (quaternary gradient) Flexible pump

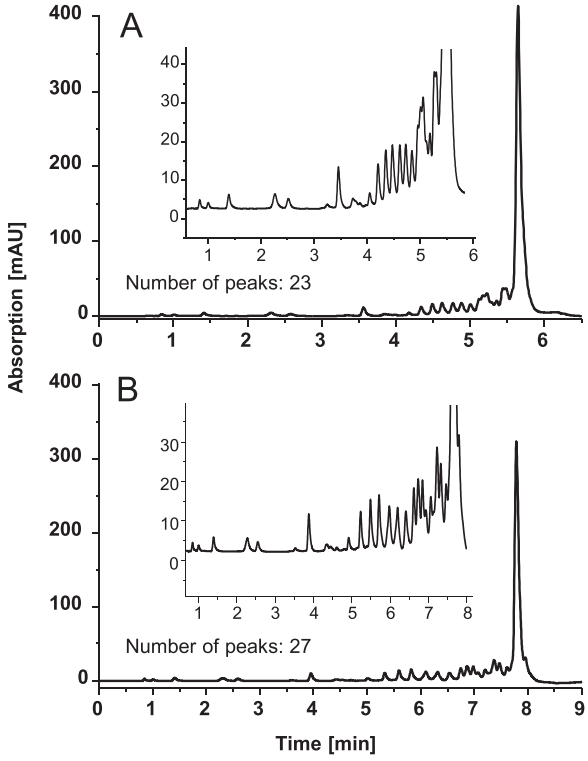

Fig. 2. ^{1}D IP-RP UV chromatogram of Patisiran using TPAA as ion pairing reagent with a linear gradient within 10 or 20 min. Inserts represent zoom-in from the same chromatogram. Gradient: 0–100% B in 10 or 20 min. Further LC-conditions see chapter 2.5 and supplementary materials.

(G7104A), Multisampler (G7167B) and Variable Wavelength Detector (VWD) (G7114B) with 14 µL flow cell (G1314–60,186) and a pressure relief device (pressure release kit, G4236–60,010) between the VWD of the ^{1}D and 2D-interface. The sampling frequency of the VWD in the ^{1}D was 5 Hz. For the ^{2}D-LC, a (binary gradient) High Speed Pump (G7120A) and a Diode Array Detector (DAD) (G7117B) with 1 µL flow cell (G4212–60,008) were employed. The sampling frequency of the DAD in the ^{2}D was 80 Hz. Both ^{1}D and ^{2}D columns were connected to two separate Infinity column compartments (G7116B). Both dimensions were attached by a valve drive (G1170A) equipped with 5-position/10-port 2D-LC active solvent modulation (ASM) valve (#5067–4266) coupled to two 6-position/14-port valve heads (#5067–4142, MHC valves) carrying six 40 µL loops each. The ASM valve was equipped with a restriction capillary (85 × 0.12 mm, 0.96 µL, #5500–1300). Experiments utilizing ASM were performed with an ASM factor of 5 (split ratio of loop to ASM = 1:4). The 2D-LC experiment was controlled by Agilent OpenLAB CDS ChemStation Rev. C.01.10 with 2D-LC add-on software. The contour plot (Fig. 9) was created using GC image LCxLC HRMS V2.7 Edition Software (GC Image, Lincoln, Nebraska, USA).

For the MS detection, the incompatible components of the ^{1}D eluting with t_0 in the ^{2}D chromatogram must be removed to avoid further contamination of the ion source. Thus, an Agilent 2-position/6-port valve head (#5067–4282) controlled by a valve drive (G1170A) was used as diverter valve. After 0.81 min, the buffer-free effluent was directed into a Sciex TripleTOF 5600+ QTOF mass spectrometer with a Duospray ion source (operated in negative ESI mode). 2D-LC and TripleTOF MS instruments were coupled using the contact closure connection for peripheral devices from Sciex and the MS instrument was controlled with Analyst TF 1.7 software (AB Sciex, Darmstadt, Germany).

2.5. LC-MS conditions

Anion-exchange chromatography in the ^{1}D was performed using the Chiralpak QN-AX column with a mixed pH/triethylammonium phosphate (TEAP) buffer gradient. Mobile phase A (MPA) consisted of 80/20 (v/v) water/acetonitrile (ACN) with 100 mM TEAP at pH 4.8. Mobile phase B (MPB) was composed of 80/20 (v/v) water/ACN with 200 mM TEAP at pH 7.8. Ion-pairing reversed-phase chromatography in ^{1}D was carried out using an Acquity UPLC Oligonucleotide BEH C18 with an ACN gradient. MPA consisted of 100 mM tripropylammonium acetate (TPAA) in water as ion-pairing reagent at pH 7. MPB was 100% acetonitrile. For further description, see supplementary materials.

For the online desalting in the ^{2}D, a ZORBAX Eclipse Plus C18 RRHD column was used with a methanol (MeOH) gradient. MPA consisted of an aqueous solution of 10 mM ammonium acetate (AA), pH value not adjusted. MPB was MeOH with 10 mM AA, pH value not adjusted. The used 2D-LC setup has been described in our recent report [34]. For all measurements, the injection volume was 5 µL. The wavelength of the UV-detection in all figures was by 254 nm. For detailed description regarding the LC conditions, please see supplementary materials.

Mass spectrometric detection was performed in negative polarity mode with an ESI source. The scan range for the TOF full scan MS experiment was 300–2000 *m/z*. The MS parameters for nebulizer gas, heater gas, curtain gas, source temperature, ion spray voltage, declustering potential and collision energy were set as follows: 70 psi, 70 psi, 40 psi, 500 °C, −4500 V, −250 V, −20 V. The data processing was accomplished by using PeakView (AB Sciex, Darmstadt, Germany). The deconvolution of the oligonucleotide spectra was performed with Bio Tool Kit add-on in PeakView. For further details of MS-data processing, see supplementary materials.

3. Results and discussion

3.1. LC-UV experiments for optimization of the separation in the first dimension

3.1.1. Anion exchange chromatography with Chiralpak QN-AX stationary phase

For effective ON impurity profiling, the ^{1}D should provide sufficient selectivity to separate the impurities from the main ON product into pure zones, in order to allow the interference-free characterization by ESI-MS analysis. IP-RP, anion-exchange and mixed-mode chromatography are common options. A chiral weak anion exchange material, Chiralpak QN-AX, has also great potential for achieving orthogonal selectivities to the former. This quinine carbamate-based ligand, commonly used in enantiomer separations of acidic chiral compounds [35,37–41], exhibits mixed-mode chromatography character (RP/WAX with capability of multiple affinity-type interactions involving hydrogen bond interactions) and has been successfully used for separation of structurally closely related nucleic acid-type analytes such as pDNA isoforms and topoisomers [36]. Its chromatographic potential for the separation of oligonucleotides has not been exploited yet. In a preliminary experiment, Chiralpak QN-AX was compared to a poly(RP/WAX) column and its oxidized version with sulfonic acid endcappings for ON impurity separation (see suppl. Material. Fig. 25). All exhibited resolving power for the siRNA impurities. Further experiments were then performed with the commcercially available Chiralpak QN-AX. Next, initial experiments focused on finding suitable elution conditions for the antisense strand of Patisiran and its impurities from the Chiralpak QN-AX column within an acceptable analysis time (about 30 min). Oligonucleotides are multiply negatively charged and hence may exert strong retention on anion-exchange materials as in ion-exchange chromatography *k* usually

increases exponentially with the effective charge number z_{eff} of the analyte [42]. For this reason, high concentrations of counterions may be necessary for efficient elution. On the other hand, it has been shown that the ζ-potential and anion-exchange capacity, respectively, of QN-AX is significantly reduced above pH 6 due to decreasing dissociation of the WAX site (i.e. of the tertiary amine of the quinuclidine ring) as well as increasing dissociation of residual silanols [43,44]. Above pH 8, the surface charge turns to negative ζ-potentials allowing efficient elution by repulsive charge-inducted desorption.

In the first screening attempt, two different mixed pH/TEAP buffer gradients have been tested. While in both cases the TEAP gradient was from 100 to 200 mM, the pH-range was different i.e. from 6.8 to 7.8 (see Fig. S1A) and from 5.8 to 7.8 (see Fig.S1B). From the chromatograms it is obvious that a lower start pH of 5.8 is beneficial for the resolution of impurity peaks as compared to an initial pH of 6.8.

In the next step, the flow rate of the gradient was adjusted to achieve a better peak capacity (PC) which was calculated in accordance to Eq. (1)

$$PC = \frac{t_\omega - t_\alpha}{w} \sim \frac{t_G - t_0}{\frac{4 \cdot w_{1/2}}{2.355}} \quad (1)$$

wherein t_α and t_ω are the retention times of the first and last peak, w and $w_{1/2}$ the peak width at the base and at half height, t_G and t_0 the gradient time and void time [45,46]. As expected, with increasing flow rate the average PC of all detected peaks has continuously increased (PC1, flow rate 0.2 ml/min: 26.8; PC2, flow rate 0.6 ml/min: 53.6; PC3, flow rate 0.8 ml/min: 63.5) and the chromatographic performance of QN-AX columns has become superior revealing an increasing number of impurity peaks resolved from the main peak of Patisiran antisense strand (see Fig. 1 and Supplementary Material, Fig. S2-S4 for more detailed data, a third optimization series with different initial pH values is shown in Fig. S5).

The final ^{1}D method for QN-AX in our 2D-LC experiment has been established as described in chapter 2.5 with a mixed pH (from 4.8 to 7.8)/TEAP (from 100 mM to 200 mM) gradient with constant organic modifier of 20% ACN employing a flow rate of 0.8 ml/min (linear flow velocity: 6.4 cm/min).

3.1.2. Ion-pairing reversed phase chromatography with Oligonucleotide BEH C18 stationary phase

The method development for the ion-paring RP chromatography in ^{1}D was straightforward and followed established procedures [15,47]. Here, tripropylammonium acetate (TPAA) was selected as ion-pairing reagent leading to a much stronger hydrophobic interaction between the stationary phase and the ion-paired analytes, thus stronger retention and better resolution. When TPAA was present in both mobile phase A and B leading to a final content of ACN at 20%, the retention was strong and analysis times rather long. Furthermore, with a 20 min gradient, the peak capacity of the main peak was around 22. The main peak could only be eluted with extended elution step at 100% MPB (consisting of 20% ACN, see Suppl. Fig. S6). For this reason, TPAA was only included in A, resulting in short analysis time at little expense of resolution. As illustrated in Fig. 2, both 10 min and 20 min gradients provided reasonable selectivity for the impurities. At the same time, the peak shape was significantly improved and the number of distinguishable impurities was greatly increased (Suppl. Fig. S7). Twenty seven (27) peaks were separated within a gradient time of 20 min. The main peak could be eluted after 7.8 min with about 35% of ACN. Furthermore, the peak capacity of the main peak could be increased to 126. In case of triethylammonium acetate, about the same number (30) of peaks could be detected, but with a factor 2 longer gradient time of 40 min and lower resolution (Suppl. Fig. S8).

3.2. MHC-2D-LC-ESI-MS analysis of the impurities

Both ^{1}D methods lead to separation of the majority of impurities from the main peak. Unfortunately, both use MS-incompatible components in their mobile phases which must be removed before entering the ESI ion source. Therefore, an RP column is used in the ^{2}D for desalting and removal of ion-pairing agent, respectively, via a diverter valve. ASM enables to refocus the oligonucleotide peaks into a sharp zone which is then upon its elution in the ^{2}D completely free of non-volatile buffer components and ion-pair agent, respectively, that are present in the ^{1}D mobile phase [34,48]. Without ion-pairing reagents in ^{2}D-RPLC eluent, no further selectivity between different ONs is achieved and hence all ONs from different cuts elute at the same retention time. While this may be seen as a disadvantage from viewpoint of selectivity, it assures identical ionization conditions in the ESI source which makes the ON signals better comparable. For detection, full scan TOF-MS experiments are selected for data acquisition (for further details on the employed MS conditions as well as for data processing see chapter 2.5 and supplementary materials). For this study, two types of experiments have been performed: MHC on impurities and high-resolution sampling on the main peak, using the two different ^{1}D methods described above. Table 1 gives a summarizing overview of all detected oligonucleotide species. In general, two series of shortmers from 3′ and 5′ end have been detected and identified. For both ^{1}D methods, the retention time depends directly on the length of the oligonucleotide species. With the described data processing for MS, the structures of the impurities were determined. On Fig. S26 in the supplementary materials, the structures of some detected species from this study are illustrated. At first sight, the molecular formula deriving from the presumed structures show a reasonable mass accuracy allowing structural annotation (Table 1). However, it is important to emphasize that TOF-MS does not provide a full characterization of the oligonucleotide impurities but MS/MS experiments are needed to provide sequence information of the impurities. The suggested impurity structures listed in Table 1 are therefore tentative.

3.2.1. Mixed-mode chromatography with Chiralpak QN-AX in ^{1}D

3.2.1.1. Impurities analysis by MHC. In Fig. 3, the exemplary 2D-chromatograms of three detected ON species with various lengths obtained by QN-AX in the ^{1}D and RPLC in the ^{2}D using ESI-TOF-MS for detection are shown. As mentioned, all ONs eluted in the ^{2}D-RPLC at the same retention time. Only a single re-focussed peak was visible in the UV-chromatogram followed by some weak UV-signals due to the re-equilibration (Fig. 3, B-D). High sensitivity can be achieved for impurity detection if the EICs of the most abundant m/z for the detected oligonucleotide species are employed to generate the respective impurity chromatograms, as exemplarily illustrated in Fig. 3E-G. The corresponding ESI-MS spectra are showing the expected trend: with increasing m/z, the charge state of the most abundant ion rises as well (Fig. 3H-J). Up to 11-mer, the charge state of $z = -2$ was dominating (only $z = -1$ and -2 are found), between 11-mer and 17-mer, ions with the charge state of $z = -3$ were most abundant (only $z = -2$ and -3 are detected). Above 18-mer, $z = -4$ was then dominating as the most abundant species (z = - 4 and -5 species detected).

By combination of the QN-AX separation in the ^{1}D and desalting RP (without ion-pairing agent) in the ^{2}D, 18 different impurities could be identified by ESI-TOF (see Table 1). Most of the detected impurities in Patisiran antisense sample were shortmers with a truncation of base sequences on either the 3′ or 5′ end,

Table 1
Overview of the Patisiran antisense strand impurities detected with MHC 2D-LC-MS analysis.

Name of impurity	Base sequence (5‘ – 3‘)	Molecular Formula	Deconvoluted monoisotopic mass [Da]	Most abundant ion of ESI-MS spectrum [*m/z*] $[M\text{-}nH]^{n-}$	Calculated exact mass of the most abundant ion [*m/z*], *error* [ppm]	^{1}D retention time [min] with QN-AXE (Cut #)	^{1}D retention time [min] with IP C18 (Cut #)
3′ ON-5 mer	5‘-AUGGA-3‘	$C_{49}H_{60}N_{22}O_{32}P_4$	1592.3	795.1314 $[M\text{-}2H]^{2-}$	795.1264, *6.4*	9.429 (1#)	2.264(1#)
5′ ON-6 mer-H_2O	5‘-UU$_m$ACdTdT-3‘	$C_{58}H_{74}N_{16}O_{43}P_6$	1868.3	933.1239 $[M\text{-}2H]^{2-}$	933.1177, *6.6*	–	3.773(3#)
5′ ON-6 mer	5‘-UU$_m$ACdTdT-3‘	$C_{58}H_{76}N_{16}O_{44}P_6$	1886.3	942.1285 $[M\text{-}2H]^{2-}$	942.1230, *5.9*	–	3.994(4#)
5‘ ON-7 mer	5‘-GUU$_m$ACdTdT-3‘	$C_{68}H_{88}N_{21}O_{51}P_7$	2231.3	1114.6544 $[M\text{-}2H]^{2-}$	1114.6467, *6.9*	–	4.271(5#)
3′ ON-7 mer	5‘-AUGGAAU$_m$ −3‘	$C_{69}H_{85}N_{29}O_{46}P_6$	2241.4	1119.6818 $[M\text{-}2H]^{2-}$	1119.6730, *7.8*	11.219(2#)	3.518(2#)
5‘ ON-8 mer-H_2O	5‘-GGUU$_m$ACdTdT-3‘	$C_{78}H_{98}N_{26}O_{57}P_8$	2558.4	1278.1731 $[M\text{-}2H]^{2-}$	1278.1651, *6.2*	–	4.271(5#)
3′ ON-8 mer	5‘-AUGGAAU$_m$A-3‘	$C_{79}H_{97}N_{34}O_{52}P_7$	2570.4	1284.7064 $[M\text{-}2H]^{2-}$	1284.7006, *4.5*	12.191(3#)	3.773(3#)
5′ ON-8 mer	5‘-GGUU$_m$ACdTdT-3‘	$C_{78}H_{100}N_{26}O_{58}P_8$	2576.4	1287.1751 $[M\text{-}2H]^{2-}$	1287.1704, *3.6*	12.191(3#)	4.490(6#)
3′ ON-9 mer	5‘-AUGGAAU$_m$AC-3‘	$C_{88}H_{109}N_{37}O_{59}P_8$	2875.5	1436.7253 $[M\text{-}2H]^{2-}$	1436.7200, *3.7*	12.191(3#)	3.994(4#)
3′ ON-10 mer	5‘-AUGGAAU$_m$ACU-3‘	$C_{97}H_{120}N_{39}O_{67}P_9$	3181.5	1589.7411 $[M\text{-}2H]^{2-}$	1589.7326, *5.3*	12.569(4#)	4.271(5#)
5′ ON-10 mer	5‘-AUGGUU$_m$ACdTdT-3‘	$C_{96}H_{122}N_{30}O_{74}P_{10}$	3188.4	1593.2072 $[M\text{-}2H]^{2-}$	1593.1957, *7.2*	–	4.912(8#)
5′ ON-9 mer	5‘-UGGUU$_m$ACdTdT-3‘	$C_{87}H_{111}N_{28}O_{66}P_9$	2882.4	1440.1874 $[M\text{-}2H]^{2-}$	1440.1830, *3.0*	12.746(5#)	4.707(7#)
3′ ON-11 mer	5‘-AUGGAAU$_m$ACUC-3‘	$C_{106}H_{132}N_{42}O_{74}P_{10}$	3486.5	1742.2663 $[M\text{-}2H]^{2-}$	1742.2532, *7.5*	12.746(5#)	4.490(6#)
5′ ON-11 mer	5‘-CUUGGUU$_m$ACdTdT-3‘	$C_{105}H_{134}N_{33}O_{81}P_{11}$	3493.5	1163.8138 $[M\text{-}3H]^{3-}$	1163.8090, *4.1*	13.066(6#)	5.025(9#)
3′ ON-12 mer	5‘-AUGGAAU$_m$ACUCU-3‘	$C_{115}H_{143}N_{44}O_{82}P_{11}$	3792.6	1263.5150 $[M\text{-}3H]^{3-}$	1263.5087, *5.0*	13.066(6#)	4.912(8#)
5′ ON-12 mer	5‘-UCUUGGUU$_m$ACdTdT-3‘	$C_{114}H_{145}N_{35}O_{89}P_{12}$	3799.5	1265.4712 $[M\text{-}3H]^{3-}$	1265.4832, *−9.5*	13.365(7#)	–
3′ ON-14 mer	5‘-AUGGAAU$_m$ACUCUUG-3‘	$C_{134}H_{166}N_{51}O_{97}P_{13}$	4443.7	1480.2054 $[M\text{-}3H]^{3-}$	1480.1987, *4.5*	13.865(8#)	5.025(9#)
3′ ON-15 mer	5‘-AUGGAAU$_m$ACUCUUGG-3‘	$C_{144}H_{178}N_{56}O_{104}P_{14}$	4788.7	1595.2023 $[M\text{-}3H]^{3-}$	1595.2145, *−7.7*	14.216(9#)	–
3′ ON-17 mer	5‘-AUGGAAU$_m$ACUCUUGGUU$_m$-3‘	$C_{163}H_{202}N_{60}O_{120}P_{16}$	5415.0	1804.5580 $[M\text{-}3H]^{3-}$	1804.5717, *−7.3*	14.658(10#)	–
3′ ON-18 mer	5‘-AUGGAAU$_m$ACUCUUGGUU$_m$A-3‘	$C_{173}H_{214}N_{65}O_{126}P_{17}$	5743.8	1435.4278 $[M\text{-}4H]^{4-}$	1435.4398, *−8.4*	15.116(11#)	–
5′ ON-18 mer	5‘-GAAU$_m$ACUCUUGGUU$_m$ACdTdT-3‘	$C_{173}H_{218}N_{60}O_{129}P_{18}$	5756.8	1438.9232 $[M\text{-}4H]^{4-}$	1438.9341, *−7.6*	15.116(11#)	–
5‘ ON-19 mer	5‘-GGAAU$_m$ACUCUUGGUU$_m$ACdTdT-3‘	$C_{183}H_{230}N_{65}O_{136}P_{19}$	6101.8	1524.9579 $[M\text{-}4H]^{4-}$	1524.9453, *8.3*	15.5 (5#, HR experiment)	–
5‘ ON-20 mer	5‘-UGGAAU$_m$ACUCUUGGUU$_m$ACdTdT-3‘	$C_{192}H_{241}N_{67}O_{144}P_{20}$	6407.9	1601.4507 $[M\text{-}4H]^{4-}$	1601.4516, *−0.6*	15.4 (4#, HR experiment)	–
Onpattro, antisense	5‘-AUGGAAU$_m$ACUCUUGGUU$_m$ACdTdT-3‘	$C_{202}H_{252}N_{72}O_{147}P_{20}$	6656.9	1663.7273 $[M\text{-}4H]^{4-}$	1663.7232, *2.5*	15.736	5.952
Longmer (+1)	5‘-CAUGGAAU$_m$ACUCUUGGUU$_m$ACdTdT-3‘	$C_{211}H_{264}N_{75}O_{154}P_{21}$	6962.0	1740.2442 $[M\text{-}4H]^{4-}$	1740.2341, *5.8*	–	6.105(4#, HR experiment)

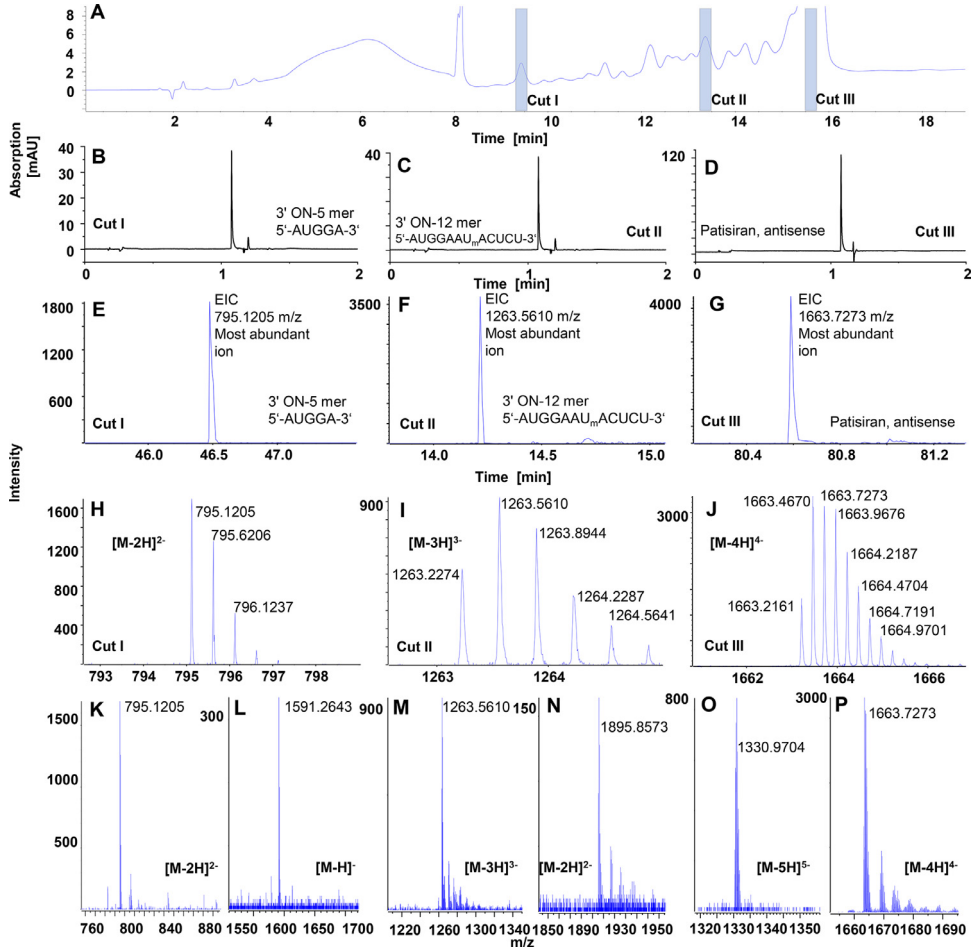

Fig. 3. Three representative MHC 2D-LC UV (QN-AX in ^{1}D) chromatograms of selected oligonucleotide species with various lengths (A, B-D). LC instrumental conditions see chapter 2.4. (E): EIC of 795.1205 *m/z* (± 10 mDa, most abundant signal of $[M-2H]^{-2}$ peak group); (F): EIC of 1263.5610 *m/z* (± 10 mDa, most abundant signal of $[M-3H]^{3-}$ peak group); (G): EIC of 1663.7273 *m/z* (± 10 mDa, most abundant signal of $[M-4H]^{4-}$ peak group); (H)-(J): ESI-MS spectra in negative mode of the most abundant signals from the corresponding $[M-nH]^{n-}$ peak group. (K)-(P): ESI-MS spectra in negative mode of different charge states, most abundant mass indicated. All MS conditions see chapter 2.5.

as expected [10,49]. The deconvoluted mass spectra of the impurity species are illustrated in Fig. 4 and Fig. S9-S11 in supplementary materials. Besides the isotopic distribution pattern of the respective oligonucleotide impurity, also the isotopic pattern of some alkali cation adducts of the shortmers are visible which is an inconvenient phenomenon by oligonucleotide MS as the distribution into distinct species reduces the detection sensitivity [29,49]. Birdsall et al. found out that the trace alkali metal salts in the mobile phases and reagents determined to be the main source of the metal salt adducts in LC/ESI-MS-based configuration. Non-specific adsorption of metal salts within the fluidic path lead to formation of adduct which must be considered to achieve acceptable signal intensity [50]. Ammonium adducts, on the other hand, have not been detected when the declustering potential DP and the collision energy CE were elevated from −50 to −250 V and −10 to −20 V, respectively. The elution order depends on the mass of the oligonucleotides; those with higher mass need longer to get eluted due to their higher content of phosphodiester bonds resulting in more negative charges [26,51].

3.2.1.2. Peak purity determination of the main peak by high-resolution sampling. In another experiment, the main peak of Patisiran antisense strand was subjected to high-resolution sampling with the established QNAX-RP 2D-LC-MS method; in order to cover the entire main peak with narrow slices of consecutive adjacent cuts, the procedure (selective comprehensive 2D-LC mode) was repeated in a second run sampling in total 21 fractions (cuts) across the main peak (see Fig. 5, Fig. S12 and Fig. S13). At the front end of the main peak (Cuts # 1–9), we were able to be detect n-1 and n-2 shortmers which are highly relevant but often challenging impurity species for the quality control of synthetic oligonucleotide (Fig. S12, B, Cut# 4: 5'-UGGAAU$_m$ACUCUUGGUU$_m$ACdTdT-3', n-1; Fig. S13, C, Cut# 5: 5'-GGAAU$_m$ACUCUUGGUU$_m$ACdTdT-3', n-2). Besides of the both shortmers, further impurity species were identified as well. From the middle part on (Fig. S13, G, Cut 10–21), the main peak does not contain further impurities indicating the great potential of the Chiralpak QN-AX column to be used for preparative purification of synthetic oligonucleotides.

3.2.2. Ion-pair RP-LC with C18 phase in the ^{1}D

3.2.2.1. Impurities analysis by MHC. Using the above described IP-RPLC method in the ^{1}D, 17 (of the 31) impurity species detected in the ^{1}D have been transferred by heart cutting into the ^{2}D for characterization by ESI-TOF (see Table 1). Exemplary ^{2}D-chromatograms of selected impurity species and the corresponding MS spectra with the EICs of the most abundant ions are shown in Suppl. Figure S14. The deconvoluted mass spectra are shown in Fig. 6, Figure S15 and Figure S16 in the supplementary materials. Again, different shortmers are the dominant impurities. However, also a condensation product of a shorter oligonucleotide could be

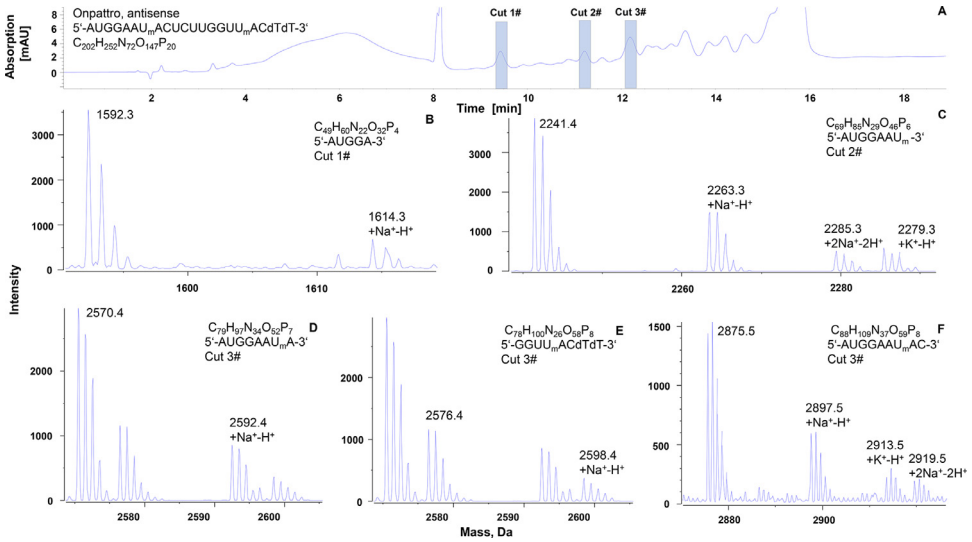

Fig. 4. MHC 2D-LC (QN-AX in ^{1}D) of the impurity peaks with hyphenation to ESI-TOF-MS in negative mode. All the instrumental and LC-MS conditions see chapter 2.4 and 2.5. All shown mass spectra are deconvoluted. Monoisotopic mass indicated only. For better overview, the detected impurity species are listed in table 1. Further MS results of Cut 4 – Cut 11 see supplementary materials Fig. S9-S11.

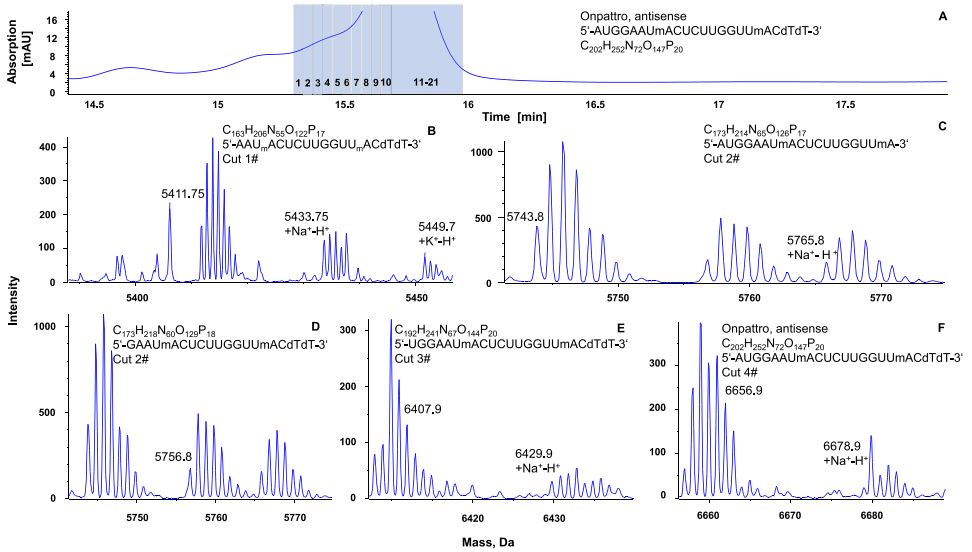

Fig. 5. High-resolution sampling 2D-LC (QN-AX in ^{1}D) of the main peak with hyphenation to ESI-TOF-MS in negative mode. Detailed instrumental and LC-MS conditions can be found in chapter 2.4 and 2.5. All shown mass spectra are deconvoluted. Monoisotopic mass indicated. Additional MS spectra of the further cuts see Fig. S12 and S13.

detected leading to a cyclic phosphodiester bond (Fig. 6, E). Here, the strand was truncated from the 5′ end. In consequence of that, the hydroxy group in the 2 position of the ribose sugar is free and probably has reacted to the phosphate backbone in the neighbourhood in a condensation reaction under the elimination of water (Suppl. Fig. S17, high-lighted in red). For unequivocal identification of the impurity and the location of the position of the condensation, tandem MS experiments need to be performed but was beyond the scope of the current work. Similar to the ^{1}D QN-AX method, the main trend of the elution order followed the same pattern: Oligonucleotides with higher mass have longer retention time. However, there is an exception between the elution order of 5′ ON-7 mer (Fig. S15C, Cut 5) and 3′ ON-7 mer (Fig. 6C, Cut 2). The 5′ ON-7 mer (Fig. S15C, Cut 5) is lighter than 3′ ON-7 mer (Fig. 6C, Cut 2), but still needs longer to get eluted. The same behaviour can also be observed between 5′ ON-8 mer (Fig. S15F, Cut 6) and 3′ ON-8 mer (Fig. 6E, Cut 3). A possible reason for this reversed elution order might be that the shortmers with the truncation at the 5′ end do have a phosphate-backbone more than the shortmers with the truncation at the 3′ end. Therefore, they can stronger interact with the stationary phase under ion-pairing conditions and have a longer retention time.

3.2.2.2. Peak purity determination of the main peak by high-resolution sampling. A high-resolution sampling experiment was performed for the main peak of Patisiran antisense strand with this IP-RPLC 2D-LC-ESI-MS method too (Fig. 7, Fig. S18). As the main peak is very narrow in IP-RPLC mode, only 4 cuts were transferred into the MS. With this attempt, even a longmer with an additional cytidine nucleotide in excess was identified which eluted right after the Patisiran antisense ON (cut #4) (Fig. S18E). Cut #2 (Fig. 7E) also contains the impurities species from cut #1 (Fig. 7A, 7B and 7C) but are not depicted again in Fig. 7E. Overall, none of the fractions from the high-resolution sampling contained pure Patisiran antisense ON when IP-RPLC was the ^{1}D separation.

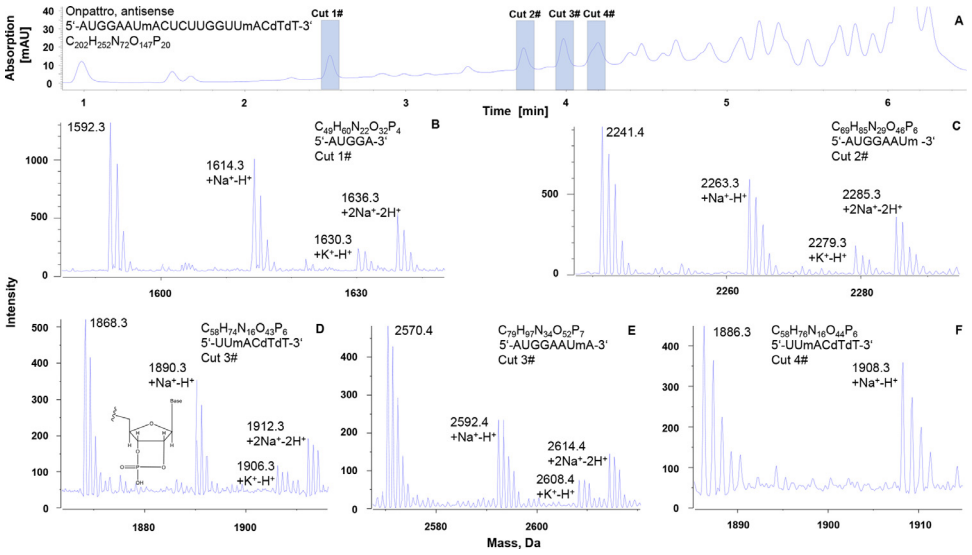

Fig. 6. MHC 2D-LC (IP-RP in ^{1}D) of the impurity peaks with hyphenation to ESI-TOF-MS in negative mode. For more instrumental and LC-MS conditions, see chapter 2.4 and 2.5. All shown mass spectra are deconvoluted. Monoisotopic mass indicated. All impurity species are listed in table 1. More MS spectra of the other cuts see Fig. S15 and S16.

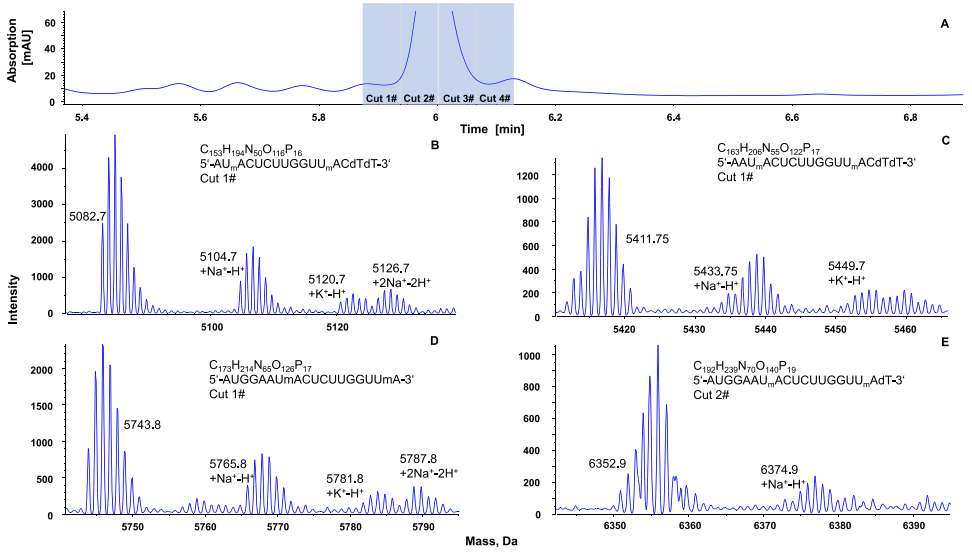

Fig. 7. High-resolution sampling 2D-LC (IP-RP in ^{1}D) of the main peak with hyphenation to ESI-TOF-MS in negative mode. Further instrumental and LC-MS conditions are described in chapter 2.4 and 2.5. All shown mass spectra are deconvoluted. Monoisotopic mass indicated. For Cut 3 and Cut 4, see Fig. S18 in the supplementary materials.

3.3.3. Comparison of the MHC-2D-LC-ESI-MS results

Both variants of the 2D-LC-ESI-MS experiments were able to detect the impurity by-products of Patisiran antisense strand at low concentrations (according to ^{1}UV detection peak areas of impurities are typically in the range between 0.6 and 8% related to the main peak; see Suppl. Table 1). In order to determine the limit of detection (LOD), a dilution series of a readily available DNA oligonucleotide standard (GAA TCT TAC GAA ATA CCT GAG AG, average mass: 7085 g/mol) in the range of 1 to 20 µM was analysed by both 2D-LC-ESI-MS methods using the EIC of *m/z* 1768.8126 ([M-4H]$^{4-}$, ± 30 mDa) for the generation of chromatograms. For each injection, one cut from the centre of the sample peak in the ^{1}D was transferred into ^{2}D. After desalting and MS detection, the peak area of the EIC was then used to create the calibration curve. Both calibration functions were highly linear (R^2= 0.9995 with C18 in ^{1}D, R^2= 0.9945 with QN-AX in ^{1}D) (Fig. S19 and S20) (for 2D-LC chromatograms and EICs see Fig. S21). The LOD (S/N = 3) was calculated to be 424 nM (3.07 pg/µL) with IP-RPLC using the C18 column in ^{1}D and 1999 nM (14.16 pg/µL) with Chiralpak QN-AX in ^{1}D. The LOD is higher in the case of QN-AX in the ^{1}D, since the local peak concentration is lower due to the broader peak and transfer of a heart cut (not the entire peak). Furthermore, two calibration curves using the ^{1}D UV traces were created (Fig. S22 and S23). The LOD of both methods is similar as now the entire peak and thus same quantity is used for the integration. The LOD with ^{1}D UV-detection is without further dilution in the ^{2}D lower than with the 2D-LC-ESI-MS methods. However, in a real sample the quantification by ^{1}UV detection would only be accurate if there is high peak purity. In contrast, the MHC 2D-HPLC-ESI-MS methods provide adequate assay specificity through additional MS selectivity from specific EICs.

3.3.4. QNAX-IPRP 2D-LC-UV method

For further advancement of the 2D-LC setup both QN-AX in ^{1}D and IP-RPLC on C18 column in ^{2}D can be combined. In this context, their orthogonality in terms of retention is of prime interest. As the effective peak capacity depends on the orthogonality of the separation modes in ^{1}D and ^{2}D, their complementarity was eval-

Table 2
Comparison of the normalized retention time $t_{norm.}$ of impurity species detected in both 2D-LC methods.

Name of impurity	Base sequence (5‘ – 3‘)	Molecular Formula	Deconvoluted monoisotopic mass [Da]	^{1}D retention time [min] with QN-AXE [a] (Cut #)	^{1}D retention time [min] with C18 [b] (Cut #)	Normalized retention time [min] with QN-AXE	Normalized retention time [min] with C18
3′ ON-5 mer	5‘-AUGGA-3‘	$C_{49}H_{60}N_{22}O_{32}P_4$	1592.3	9.429 (1#)	2.264(1#)	0.415	0.097
3′ ON-7 mer	5‘-AUGGAAU$_m$ −3‘	$C_{69}H_{85}N_{29}O_{46}P_6$	2241.4	11.219(2#)	3.518(2#)	0.514	0.161
3′ ON-8 mer	5‘-AUGGAAU$_m$A-3‘	$C_{79}H_{97}N_{34}O_{52}P_7$	2570.4	12.191(3#)	3.773(3#)	0.568	0.174
5′ ON-8 mer	5‘-GGUU$_m$ACdTdT-3‘	$C_{78}H_{100}N_{26}O_{58}P_8$	2576.4	12.191(3#)	4.490(6#)	0.568	0.210
3′ ON-9 mer	5‘-AUGGAAU$_m$AC-3‘	$C_{88}H_{109}N_{37}O_{59}P_8$	2875.5	12.191(3#)	3.994(4#)	0.568	0.185
5′ ON-8 mer	5‘-GGUU$_m$ACdTdT-3‘	$C_{78}H_{100}N_{26}O_{58}P_8$	2576.4	12.569(4#)	4.490(6#)	0.589	0.210
3′ ON-10 mer	5‘-AUGGAAU$_m$ACU-3‘	$C_{97}H_{120}N_{39}O_{67}P_9$	3181.5	12.569(4#)	4.271(5#)	0.589	0.199
5′ ON-10 mer	5‘-AUGGUU$_m$ACdTdT-3‘	$C_{87}H_{111}N_{28}O_{66}P_9$	2882.4	12.746(5#)	4.707(7#)	0.598	0.221
3′ ON-11 mer	5‘-AUGGAAU$_m$ACUC-3‘	$C_{106}H_{132}N_{42}O_{74}P_{10}$	3486.5	12.746(5#)	4.490(6#)	0.598	0.210
5′ ON-11 mer	5‘-CUUGGUU$_m$ACdTdT-3‘	$C_{105}H_{134}N_{33}O_{81}P_{11}$	3493.5	13.066(6#)	5.025(9#)	0.616	0.237
3′ ON-12 mer	5‘-AUGGAAU$_m$ACUCU-3‘	$C_{115}H_{143}N_{44}O_{82}P_{11}$	3792.6	13.066(6#)	4.912(8#)	0.616	0.232
3′ ON-14 mer	5‘-AUGGAAU$_m$ACUCUUG-3‘	$C_{134}H_{166}N_{51}O_{97}P_{13}$	4443.7	13.865(8#)	5.025(9#)	0.660	0.237
Onpattro, antisense	5‘-AUGGAAU$_m$ACUCUUGGUU$_m$ACdTdT-3‘	$C_{202}H_{252}N_{72}O_{147}P_{20}$	6656.9	15.736	5.952	0.764	0.285

[a] QN-AX column: Void time: 1.94 min, Gradient time: 20 min
[b] C18 column: Void time 0.365 min, Gradient time: 20 min

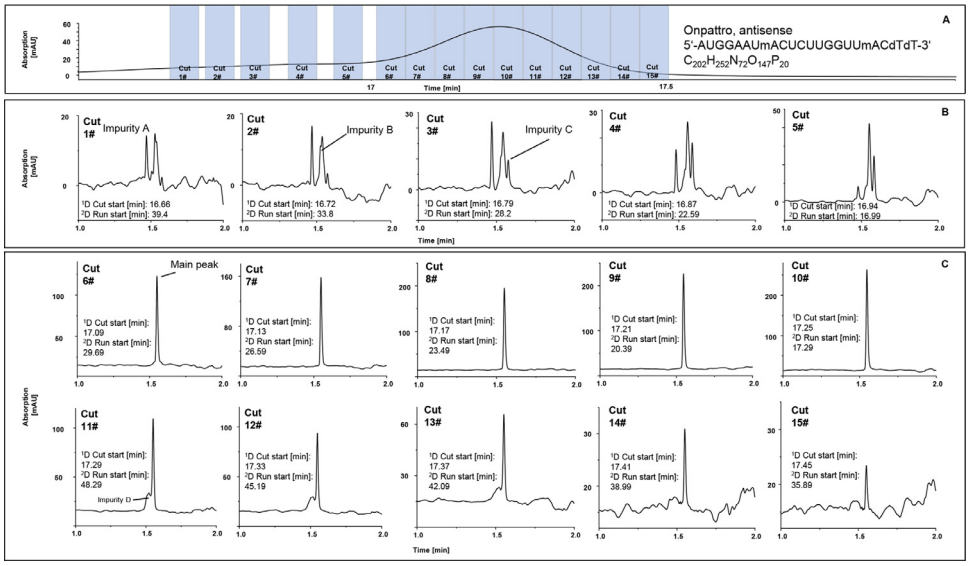

Fig. 8. High-resolution sampling 2D-LC-UV of the main peak with QN-AX in the ^{1}D and IP-RP in the ^{2}D. Additional UV-signals in the ^{2}D are high lighted as Impurity A, Impurity B, Impurity C and Impurity D. LC-conditions in the ^{1}D: MP A: 100 mM TEAP, 20% ACN, pH 4.8. MP B: 200 mM TEAP, 20% ACN, pH 7.8. Gradient: 0–100% MP B in 20 min. Flow rate: 0.8 ml/min. Temperature: 25 °C. Injection volume: 5 µL. Sample concentration: 50 µM. LC-conditions in the ^{2}D: MPA: 100 mM TPAA in water, pH 7. MPB: 100% ACN. Gradient: keep 10% for 0.5 min, ramping to 60% B within 2 min, re-equilibration for 3 min. Flow rate: 1.5 ml/min. Temperature: 60 °C. Active Solvent Modulation: activated, 0.41 min, sample loop was flushed 3 times, factor 5. 2D-LC mode: High-resolution sampling with a sampling time of 0.05 min. Sampling via time-based mode, countercurrent. Wavelength of UV detection was 254 nm in both dimensions.

uated by correlation of normalized retention times. To put this in numbers, 7 impurity species which could be found in both 2D-LC-ESI-MS experiments were correlated with regard to their normalized retention times (see Table 2), calculated according to eq (2)

$$t_{normalized} = \frac{t_R - t_0}{t_G - t_0} \quad (2)$$

with t_R as retention time in the respective mode. Although there is a high correlation of the normalized retention times in the two dimensions (r = 0.9239, Fig. S24), as can be expected because both are primarily ionic interaction-based separation mechanisms, the subtle selectivity differences should allow to resolve additional peaks in the 2DLC setup with QN-AX in the ^{1}D and IP-RPLC in the ^{2}D.

To this end, a combined MHC (for impurty peaks) and selective comprehensive (for main peak) 2D-LC-UV experiment with the QN-AX and IP-RP methods in ^{1}D and ^{2}D has been additionally conducted. The above described ^{1}D QN-AX method has not been further changed. The ^{2}D IP-RP method, on the other hand, has been adjusted considering the factors final composition of B (60%), gradient steepness (10–60% B in 2 min), temperature and flow rate (for further experimental details see figure caption of Fig. 8). The results of the fractionated samples across the main peak by the 2D-LC-UV setup to test for the peak purity is illustrated in Fig. 8.Since the number of the sample loops for ^{1}D fraction storage is limited and the ^{2}D chromatographic runs were not fast enough, two runs were needed to analyse all 15 cuts. In the first MHC-2D-LC run (Fig. 8, B), 5 cuts (#1–5) of the shoulder next to the main peak have been transferred into the ^{2}D. They could be further separated by ^{2}IP-RPLC resulting in several UV signals which indicated multiple impurity peaks in addition to the main peak (t_R= 1.54 min) in each cut. The ^{2}D UV signal after the main peak (impurity C), which is most likely corresponding to the longmer (of cut #4 in Fig. S18, E), was found in the first five ^{1}D cuts (Fig. 8, B). This might indicate a different elution order of the longmer using QN-AX column. Cuts #6–10 were sampled from the middle part of

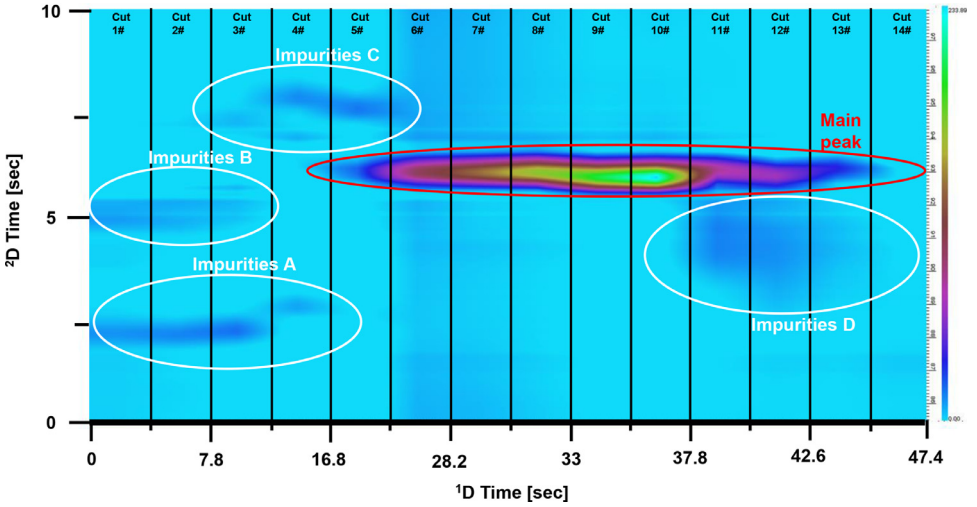

Fig. 9. Contour plot of the separation shown in Fig. 9 generated by merging all ^{2}D IP-RP UV cuts using GC Image in "column to column" mode. Besides the strong spot of the main peak, additional impurity spots are visible and indicated as A,B,C,D corresponding to Fig. 8. X-time axis is correlated to the ^{2}D start time on Fig. 8.

the main peak by high resolution sampling and did not show additional UV signals, hence seemed to be pure (Fig. 8, C). The final cuts #11–15 also contain some further compounds in addition to the Patisiran antisense strand (Fig 8,C). The additionally resolved peaks in the fractions of cuts 1–5 and 11–13 can be regarded as indication of at least some minor orthogonality between QN-AX and C18 stationary phase which is clearly emphasized by presenting these results in a contour plot (Fig. 9). Although this 2D-LC setup represents an improved impurity profiling method, more orthogonal separation modes with MS compatibility need to be developed for more effective 2D-LC ON separations which is the topic of ongoing work.

4. Conclusion

Two different chromatographic modes, viz. mixed-mode QN-AX and IP-RP, as ^{1}D separation were combined with desalting C18 RPLC, devoid of ion-pairing agent in the mobile phase, in the ^{2}D and ESI-TOF detection for the characterization of the impurity profile of the Patisiran antisense strand by MHC 2D-LC. In the ^{1}D UV trace, 16 impurity signals were detected with mixed mode QN-AX. With IP-RP, 26 distinguishable impurity peaks were detected in the UV trace. With both 2D-LC-ESI-MS experiments, a series of impurity by-products was detected and identified as shortmers with various lengths of nucleotide truncations. Besides those shortmers, one longmer and two further condensated oligonucleotide species were detected as by-products. Since the Patisiran standard in this work has been purchased as customized non-purified oligonucleotide standard by a non-pharmaceutical provider, the presented impurity profile might be not representative for a real active pharmaceutical ingredient and thus the current information limited. Nevertheless, both shortmers and longmers are the most common impurities by Patisiran and could be detected with the featured analytical methods [1]. Although the majority of impurities were identified in both chromatographic modes, i.e. QN-AX and IP-RP in the ^{1}D, a certain number of ON by-products could be detected only in one of these MHC 2D-LC modes. Hence, the combination of these two stationary phases in a 2D-LC-UV setup resulted in enhanced selectivity whereby the effluents from the ^{1}D QN-AX revealed several additional peaks in the ^{2}D with the IP-RP method. Hence, it can be concluded that the Chiralpak QN-AX column can be a useful complementary tool for oligonucleotide impurity profiling. Although synthetic oligonucleotides are not included in the scope of the International Council For Harmonisation of Technical Requirements For Pharmaceuticals for Human Use (ICH) for either synthetic drug substances (Q6A) or for products of biotechnology (Q6B), Capaldi et al. suggested to follow the ICH guideline Q3A for impurity profiling of oligonucleotides. Here, the identification threshold for the impurities should not exceed 0.1% [52]. In both MHC-2D-LC experiments, the lowest detected peak area of impurity in the ^{1}D UV trace was close to 0.1% related to the main peak (see Suppl.) but only larger peaks > 0.6% were selected for identification by ESI-MS. However, there is still room for further improvements in terms of sample loading (the QN-AX is expected to have higher loading capacity compared to classic IP-RPLC) and also optimization of ion source parameters providing further improvements in detection sensitivity. Overall, it can be concluded that the current MHC-2D-LC methods are suitable for oligonucleotide impurity profiling and at least to some extent orthogonal to the methods commonly established.

Declaration of Competing Interest

The authors declare no conflict of interests.

CRediT authorship contribution statement

Feiyang Li: Investigation, Methodology, Formal analysis, Data curation, Visualization, Writing – original draft, Writing – review & editing. **Michael Lämmerhofer:** Conceptualization, Methodology, Supervision, Writing – review & editing, Resources, Funding acquisition.

Acknowledgements

We are grateful to Agilent Technologies for support of this research by an Agilent Research Award (#4068).

Supplementary materials

Supplementary material associated with this article can be found, in the online version, at doi:10.1016/j.chroma.2021.462065.

References

[1] European Medicines Agency, European Public Assessment Report: onpattro (patisiran), 44 (2018). www.ema.europa.eu/contact.

[2] C.A. Stein, D. Castanotto, FDA-Approved Oligonucleotide Therapies in 2017, Mol. Ther. 25 (2017) 1069–1075, doi:10.1016/j.ymthe.2017.03.023.
[3] C. Rinaldi, M.J.A. Wood, Antisense oligonucleotides: the next frontier for treatment of neurological disorders, Nat. Rev. Neurol. 14 (2018) 9–22, doi:10.1038/nrneurol.2017.148.
[4] B. Hu, Y. Weng, X.H. Xia, X. jie Liang, Y. Huang, Clinical advances of siRNA therapeutics, J. Gene Med. 21 (2019) 1–14, doi:10.1002/jgm.3097.
[5] A. Bajaj, D.J. Rader, Antisense oligonucleotides for atherosclerotic disease, Nat. Med. 26 (2020) 471–472, doi:10.1038/s41591-020-0835-2.
[6] T.C. Roberts, R. Langer, M.J.A. Wood, Advances in oligonucleotide drug delivery, Nat. Rev. Drug Discov. 19 (2020) 673–694, doi:10.1038/s41573-020-0075-7.
[7] K.L. Fearon, J.T. Stults, B.J. Bergot, L.M. Christensen, A.M. Raible, Investigation of the 'n–1' impurity in phosphorothioate oligodeoxynucleotides synthesized by the solid-phase β-cyanoethyl phosphoramidite method using stepwise sulfurization, Nucleic Acids Res 23 (1995) 2754–2761, doi:10.1093/nar/23.14.2754.
[8] J. Temsamani, M. Kubert, S. Agrawal, Sequence identity of the n -1 product of a synthetic oligonucleotide, Nucleic Acids Res 23 (1995) 1841–1844, doi:10.1093/nar/23.11.1841.
[9] D. Chen, Z. Yan, D.L. Cole, G.S. Srivatsa, Analysis of internal (n-1)mer deletion sequences in synthetic oligodeoxyribonucleotides by hybridization to an immobilized probe array, Nucleic Acids Res 27 (1999) 389–395, doi:10.1093/nar/27.2.389.
[10] A. Goyon, P. Yehl, K. Zhang, Characterization of therapeutic oligonucleotides by liquid chromatography, J. Pharm. Biomed. Anal. 182 (2020) 113105, doi:10.1016/j.jpba.2020.113105.
[11] M. Enmark, M. Rova, J. Samuelsson, E. Örnskov, F. Schweikart, T. Fornstedt, Investigation of factors influencing the separation of diastereomers of phosphorothioated oligonucleotides, Anal. Bioanal. Chem. 411 (2019) 3383–3394, doi:10.1007/s00216-019-01813-2.
[12] A. Kanavarioti, HPLC methods for purity evaluation of man-made single-stranded RNAs, Sci. Rep. 9 (2019) 1–13, doi:10.1038/s41598-018-37642-z.
[13] A. Kaczmarkiewicz, Ł. Nuckowski, S. Studzińska, B. Buszewski, Analysis of Antisense Oligonucleotides and Their Metabolites with the Use of Ion Pair Reversed-Phase Liquid Chromatography Coupled with Mass Spectrometry, Crit. Rev. Anal. Chem. 49 (2019) 256–270, doi:10.1080/10408347.2018.1517034.
[14] N. Li, N.M. El Zahar, J.G. Saad, E.R.E. van der Hage, M.G. Bartlett, Alkylamine ion-pairing reagents and the chromatographic separation of oligonucleotides, J. Chromatogr. A. 1580 (2018) 110–119, doi:10.1016/j.chroma.2018.10.040.
[15] L. Gong, J.S.O. McCullagh, Comparing ion-pairing reagents and sample dissolution solvents for ion-pairing reversed-phase liquid chromatography/electrospray ionization mass spectrometry analysis of oligonucleotides, Rapid Commun. Mass Spectrom. 28 (2014) 339–350, doi:10.1002/rcm.6773.
[16] Waters, Application Solutions For OLIGONUCLEOTIDES, Waters Tech. Note, 2015.
[17] A. Apffel, J.A. Chakel, S. Fischer, K. Lichtenwalter, W.S. Hancock, Analysis of oligonucleotides by HPLC-electrospray ionization mass spectrometry, Anal. Chem. 69 (1997) 1320–1325, doi:10.1021/ac960916h.
[18] M. Gilar, K.J. Fountain, Y. Budman, U.D. Neue, K.R. Yardley, P.D. Rainville, R.J. Russell, J.C. Gebler, Ion-pair reversed-phase high-performance liquid chromatography analysis of oligonucleotides: retention prediction, J. Chromatogr. A. 958 (2002) 167–182, doi:10.1016/S0021-9673(02)00306-0.
[19] K.J. Fountain, M. Gilar, J.C. Gebler, Analysis of native and chemically modified oligonucleotides by tandem ion-pair reversed-phase high-performance liquid chromatography/electrospray ionization mass spectrometry, Rapid Commun. Mass Spectrom. 17 (2003) 646–653, doi:10.1002/rcm.959.
[20] L. Li, J.P. Foley, R. Helmy, Simultaneous separation of small interfering RNA and lipids using ion-pair reversed-phase liquid chromatography, J. Chromatogr. A. 1601 (2019) 145–154, doi:10.1016/j.chroma.2019.04.061.
[21] A.J. Alpert, F.E. Regnier, Preparation of a porous microparticulatee anion-exchange chromatography support for proteins, J. Chromatogr. A. 185 (1979) 375–392, doi:10.1016/S0021-9673(00)85615-0.
[22] J.R. Thayer, R.M. McCormick, N.B.T.-M. in E. Avdalovic, High-resolution nucleic acid separations by high-performance liquid chromatography, in: High Resolut. Sep. Anal. Biol. Macromol. Part B Appl., Academic Press, 1996, pp. 147–174, doi:10.1016/S0076-6879(96)71009-1.
[23] J.R. Thayer, Y. Wu, E. Hansen, M.D. Angelino, S. Rao, Separation of oligonucleotide phosphorothioate diastereoisomers by pellicular anion-exchange chromatography, J. Chromatogr. A. 1218 (2011) 802–808, doi:10.1016/j.chroma.2010.12.051.
[24] W. Haupt, A. Pingoud, Comparison of several high-performance liquid chromatography techniques for the separation of oligodeoxynucleotides according to their chain lengths, J. Chromatogr. A. 260 (1983) 419–427, doi:10.1016/0021-9673(83)80049-1.
[25] X. Yang, R.P. Hodge, B.A. Luxon, R. Shope, D.G. Gorenstein, Separation of Synthetic Oligonucleotide Dithioates from Monothiophosphate Impurities by Anion-Exchange Chromatography on a Mono-Q Column, Anal. Biochem. 306 (2002) 92–99, doi:10.1006/abio.2001.5694.
[26] M. Biba, E. Jiang, B. Mao, D. Zewge, J.P. Foley, C.J. Welch, Factors influencing the separation of oligonucleotides using reversed-phase/ion-exchange mixed-mode high performance liquid chromatography columns, J. Chromatogr. A. 1304 (2013) 69–77, doi:10.1016/j.chroma.2013.06.050.
[27] A. Zimmermann, R. Greco, I. Walker, J. Horak, A. Cavazzini, M. Lämmerhofer, Synthetic oligonucleotide separations by mixed-mode reversed-phase/weak anion-exchange liquid chromatography, J. Chromatogr. A. 1354 (2014) 43–55, doi:10.1016/j.chroma.2014.05.048.
[28] A. Goyon, K. Zhang, Characterization of antisense oligonucleotide impurities by ion-pairing reversed-phase and anion exchange chromatography coupled to HILIC/MS using a versatile 2D-LC setup, Anal. Chem. (2020), doi:10.1021/acs.analchem.0c00114.
[29] P.A. Lobue, M. Jora, B. Addepalli, P.A. Limbach, Oligonucleotide analysis by hydrophilic interaction liquid chromatography-mass spectrometry in the absence of ion-pair reagents, J. Chromatogr. A. 1595 (2019) 39–48, doi:10.1016/j.chroma.2019.02.016.
[30] R. MacNeill, T. Hutchinson, V. Acharya, R. Stromeyer, S. Ohorodnik, An oligonucleotide bioanalytical LC–SRM methodology entirely liberated from ion-pairing, Bioanalysis 11 (2019) 1155–1167, doi:10.4155/bio-2019-0031.
[31] M. Enmark, J. Bagge, J. Samuelsson, L. Thunberg, E. Örnskov, H. Leek, F. Limé, T. Fornstedt, Analytical and preparative separation of phosphorothioated oligonucleotides: columns and ion-pair reagents, Anal. Bioanal. Chem. 412 (2020) 299–309, doi:10.1007/s00216-019-02236-9.
[32] Q. Li, F. Lynen, J. Wang, H. Li, G. Xu, P. Sandra, Comprehensive hydrophilic interaction and ion-pair reversed-phase liquid chromatography for analysis of di- to deca-oligonucleotides, J. Chromatogr. A. 1255 (2012) 237–243, doi:10.1016/j.chroma.2011.11.062.
[33] S.G. Roussis, I. Cedillo, C. Rentel, Two-dimensional liquid chromatography-mass spectrometry for the characterization of modified oligonucleotide impurities, Anal. Biochem. 556 (2018) 45–52, doi:10.1016/j.ab.2018.06.019.
[34] F. Li, X. Su, S. Bäurer, M. Lämmerhofer, Multiple heart-cutting mixed-mode chromatography-reversed-phase 2D-liquid chromatography method for separation and mass spectrometric characterization of synthetic oligonucleotides, J. Chromatogr. A. 1625 (2020) 461338, doi:10.1016/j.chroma.2020.461338.
[35] M. Lämmerhofer, W. Lindner, Quinine and quinidine derivatives as chiral selectors. I. Brush type chiral stationary phases for high-performance liquid chromatography based on cinchonan carbamates and their application as chiral anion exchangers, J. Chromatogr. A. 741 (1996) 33–48, doi:10.1016/0021-9673(96)00137-9.
[36] M. Mahut, A. Gargano, H. Schuchnigg, W. Lindner, M. Lämmerhofer, Chemoaffinity Material for Plasmid DNA Analysis by High-Performance Liquid Chromatography with Condition-Dependent Switching between Isoform and Topoisomer Selectivity, Anal. Chem. 85 (2013) 2913–2920, doi:10.1021/ac3034823.
[37] A. Bajtai, I. Ilisz, D.H.O. Howan, G.K. Tóth, G.K.E. Scriba, W. Lindner, A. Péter, Enantioselective resolution of biologically active dipeptide analogs by high-performance liquid chromatography applying Cinchona alkaloid-based ion-exchanger chiral stationary phases, J. Chromatogr. A. 1611 (2020) 460574, doi:10.1016/j.chroma.2019.460574.
[38] R. Sardella, M. Lämmerhofer, B. Natalini, W. Lindner, Enantioselective HPLC of potentially CNS-active acidic amino acids with a cinchona carbamate based chiral stationary phase, Chirality 20 (2008) 571–576, doi:10.1002/chir.20529.
[39] C. Calderón, J. Horak, M. Lämmerhofer, Chiral separation of 2-hydroxyglutaric acid on cinchonan carbamate based weak chiral anion exchangers by high-performance liquid chromatography, J. Chromatogr. A. 1467 (2016) 239–245, doi:10.1016/j.chroma.2016.05.042.
[40] R. Pell, W. Lindner, Potential of chiral anion-exchangers operated in various subcritical fluid chromatography modes for resolution of chiral acids, J. Chromatogr. A. 1245 (2012) 175–182, doi:10.1016/j.chroma.2012.05.023.
[41] L. Zhao, F. Chen, F. Guo, W. Liu, K. Liu, Enantioseparation of chiral perfluorooctane sulfonate (PFOS) by supercritical fluid chromatography (SFC): effects of the chromatographic conditions and separation mechanism, Chirality 31 (2019) 870–878, doi:10.1002/chir.23120.
[42] W. Xu, F.E. Regnier, Protein-protein interactions on weak-cation-exchange sorbent surfaces during chromatographic separations, J. Chromatogr. A. 828 (1998) 357–364, doi:10.1016/S0021-9673(98)00641-4.
[43] O.L. Sánchez Muñoz, E.P. Hernández, M. Lämmerhofer, W. Lindner, E. Kenndler, Estimation and comparison of ζ-potentials of silica-based anion-exchange type porous particles for capillary electrochromatography from electrophoretic and electroosmotic mobility, Electrophoresis 24 (2003) 390–398, doi:10.1002/elps.200390049.
[44] S. Bäurer, M. Ferri, A. Carotti, S. Neubauer, R. Sardella, M. Lämmerhofer, Mixed-mode chromatography characteristics of chiralpak ZWIX(+) and ZWIX(−) and elucidation of their chromatographic orthogonality for LC × LC application, Anal. Chim. Acta. 1093 (2020) 168–179, doi:10.1016/j.aca.2019.09.068.
[45] M. Gilar, U.D. Neue, Peak capacity in gradient reversed-phase liquid chromatography of biopolymers. Theoretical and practical implications for the separation of oligonucleotides, J. Chromatogr. A. 1169 (2007) 139–150, doi:10.1016/j.chroma.2007.09.005.
[46] L.R. Snyder, J.J. Kirkland, J.W. Dolan, Gradient Elution, Introd. to Mod. Liq. Chromatogr. (2010) 403–473, doi:10.1002/9780470508183.ch9.
[47] A.C. McGinnis, E.C. Grubb, M.G. Bartlett, Systematic optimization of ion-pairing agents and hexafluoroisopropanol for enhanced electrospray ionization mass spectrometry of oligonucleotides, Rapid Commun. Mass Spectrom. 27 (2013) 2655–2664, doi:10.1002/rcm.6733.
[48] D.R. Stoll, K. Shoykhet, P. Petersson, S. Buckenmaier, Active Solvent Modulation: a Valve-Based Approach to Improve Separation Compatibility in Two-Dimensional Liquid Chromatography, Anal. Chem. 89 (2017) 9260–9267, doi:10.1021/acs.analchem.7b02046.
[49] W.D. Van Dongen, Bioanalytical LC-MS of therapeutic oligonucleotides, Chim. Oggi. 30 (2012) 65–67.

[50] R.E. Birdsall, M. Gilar, H. Shion, Y.Q. Yu, W. Chen, Reduction of metal adducts in oligonucleotide mass spectra in ion-pair reversed-phase chromatography/mass spectrometry analysis, Rapid Commun. Mass Spectrom. 30 (2016) 1667–1679, doi:10.1002/rcm.7596.
[51] K. Cook, J. Thayer, Advantages of ion-exchange chromatography for oligonucleotide analysis, Bioanalysis 3 (2011) 1109–1120, doi:10.4155/bio.11.66.
[52] D. Capaldi, K. Ackley, D. Brooks, J. Carmody, K. Draper, R. Kambhampati, M. Kretschmer, D. Levin, J. McArdle, B. Noll, R. Raghavachari, I. Roymoulik, B.P. Sharma, R. Thürmer, F. Wincott, Quality Aspects of Oligonucleotide Drug Development: specifications for Active Pharmaceutical Ingredients, Drug Inf. J. 46 (2012) 611–626, doi:10.1177/0092861512445311.

Supplementary Material

Impurity profiling of siRNA by two-dimensional liquid chromatography-mass spectrometry with quinine carbamate anion-exchanger and ion-pair reversed-phase chromatography

Feiyang Li, Michael Lämmerhofer*

Institute of Pharmaceutical Sciences, Pharmaceutical (Bio-)Analysis, University of Tübingen, Auf der Morgenstelle 8, 72076 Tübingen, Germany

*Author for correspondence:

Prof. Dr. Michael Lämmerhofer

Pharmaceutical (Bio-)Analysis

Institute of Pharmaceutical Sciences

University of Tübingen

Auf der Morgenstelle 8

72076 Tübingen, Germany

T +49 7071 29 78793, F +49 7071 29 4565

E-mail: michael.laemmerhofer@uni-tuebingen.de

Detailed LC conditions

Anion-exchange chromatography in the ^{1}D was performed using the Chiralpak QN-AX column with a mixed pH/triethylammonium phosphate (TEAP) buffer gradient. Mobile phase A (MPA) consisted of 80/20 (v/v) water/acetonitrile (ACN) with 100 mM TEAP at pH 4.8. Mobile phase B (MPB) was composed of 80/20 (v/v) water/ACN with 200 mM TEAP at pH 7.8. The TEAP buffer was prepared from aqueous phosphoric acid solutions of specified molar concentration and pH was adjusted with triethylamine, prior to mixing with acetonitrile. The linear gradient started at 0% MPB, was then ramped to 100% MPB within 20 min before 15 min re-equilibration. The column temperature was set at 25 °C. The flow rate during the gradient was adjusted to 0.8 ml/min and was increased to 1 ml/min for re-equilibration. Ion-pairing reversed-phase chromatography in ^{1}D was carried out using an Acquity UPLC Oligonucleotide BEH C18 with an ACN gradient. MPA consisted of 100 mM tripropylammonium acetate (TPAA) in water as ion-pairing reagent at pH 7. MPB was 100% acetonitrile. TPAA was created from aqueous tripropylamine solutions of specified molar concentration and pH adjusted with acetic acid. The gradient started at 10% MPB which was increased to 100% within 20 min before 10 min re-equilibration. The column temperature was kept constant at 20 °C. The flow rate was set to 0.4 ml/min during the gradient, 1 ml/min during the re-equilibration.

For the online desalting in the ^{2}D, a ZORBAX Eclipse Plus C18 RRHD column was used with a methanol (MeOH) gradient. MPA consisted of an aqueous solution of 10 mM ammonium acetate (AA), pH value not adjusted. MPB was MeOH with 10 mM AA, pH value not adjusted. The gradient started with a 0.8 min hold of 5% MPB, then ramped to 80% MPB in 0.1 min which was kept constant for 0.3 min before 5 min re-equilibration. The column temperature was 40 °C. The flow rate was adjusted to 1 ml/min. ASM was activated (capillary dimension: 0.12x85 mm, 0.96 µL) for 0.61 min with a factor of 5. The sample loop was flushed 3 times.

In general, multiple-heart cutting (MHC) was selected as the 2D-LC mode with time-based sampling and a sampling time of 0.1 min (with QN-AX in ^{1}D) and 0.05 min (with C18 in ^{1}D), respectively. The valve configuration of the 2D-LC was set as countercurrent regarding fill/analyse directions of loops. The void time of the C18 column was determined using uracil and of the QN-AX column with acetone.

Further MS-data processing

The characterization of the different oligonucleotide species has been conducted as follows: first, the structures of tentative impurity species were drawn with ChemDraw Professional 18 (Perkin Elmer) and their chemical formula as well as molecular mass calculated. In TOF full scan MS experiments, the mass spectra of oligonucleotides show a series of multiple deprotonated molecules $[M-nH]^{n-}$ resulting in a multiple charge state distribution. With these different charge states of a certain oligonucleotide species, its final mass was then determined via deconvolution. The deconvoluted masses of the oligonucleotides were then assigned to the tentative oligonucleotide structures. In the last step, the annotated oligonucleotide structures were verified using the mass calculator of PeakView. With the predicted chemical formula, the mass spectrum of a certain oligonucleotide species was simulated. The simulated mass spectrum could then be compared with the measured one enabling a direct control of the structural match and determination of mass errors.

Table S1. Peak area in relation to main peak in percentage according to [1]UV signals

Cut# (Ref. to Fig. 4, QN-AX)	Area	Peak Area in relation to main peak, in %
1	27.2	2.95
2	8.8	0.95
3	43.6	4.72
4	6.2	0.67
5	6.4	0.69
6	33.6	3.64
7	52.1	5.65
8	31.4	3.40
9	50.4	5.46
10	58.4	6.33
Main Peak	**921.8**	**-**
Cut# (Ref. to Fig. 6, IP-RPLC)	Area	Peak Area in relation to main peak, in %
1	70.14	3.62
2	91.78	4.73
3	117.27	6.05
4	164.51	8.49
5	99.92	5.16
6	104.54	5.39
7	155.11	8.01
8	140.93	7.27
9	140.5	7.25
Main Peak	**1936.39**	**-**

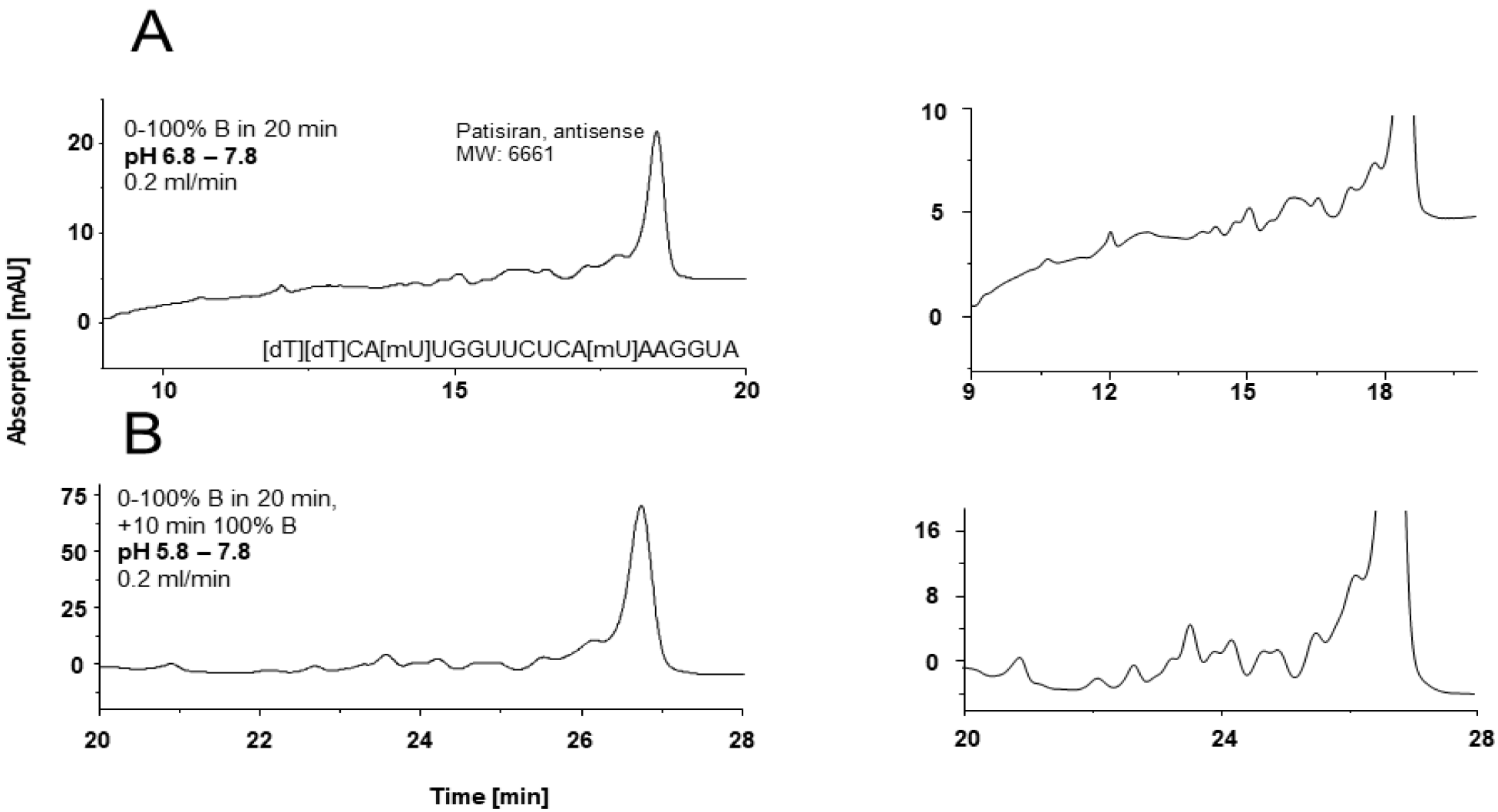

Figure S1. [1]D QN-AX UV chromatogram of Patisiran with different initial pH value in the mobile phase of A. (A): pH gradient from 6.8 to 7.8; (B): pH gradient from 5.8 to 7.8. Further LC-conditions see chapter 2.5. At the right side, zoom-ins of the elution are illustrated.

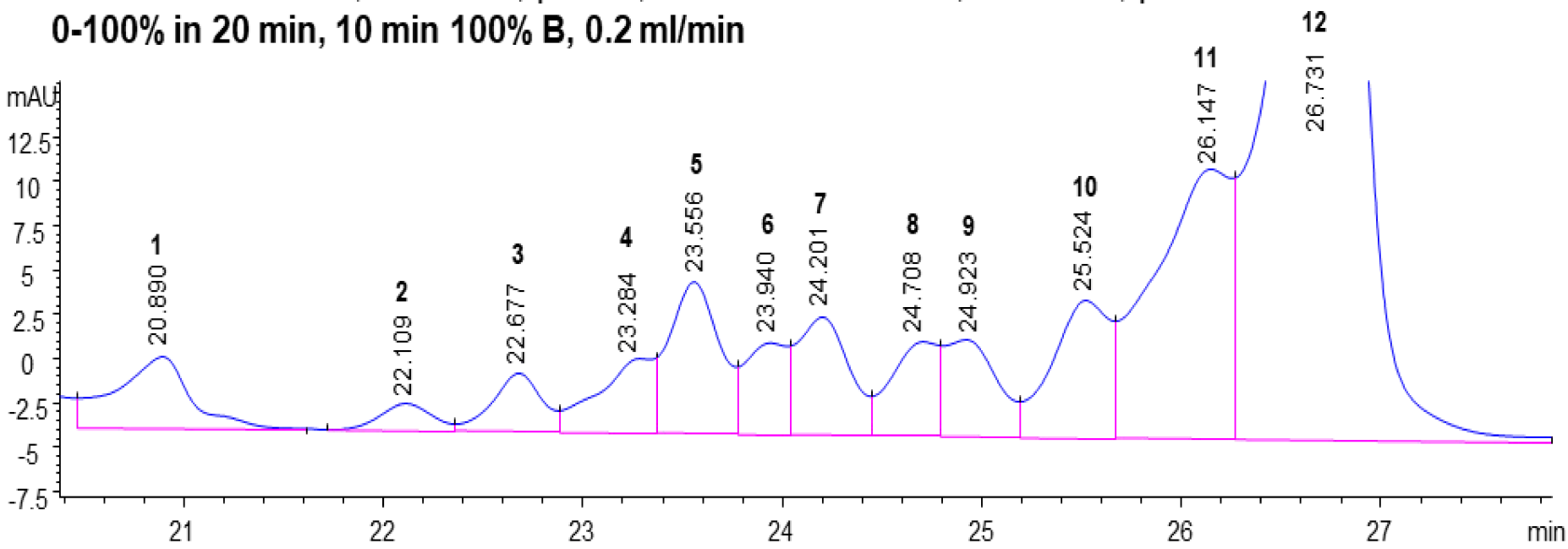

mobile phase	gradient	flow rate [mL/min]	impurity	t_0 [min]	t_R [min]	Area	Height [mAU]	$w_{1/2}$ [min]	Area [%]	Symmetry	t'_R [min]	k	α	R	N	PC	t_G [min]
A: 100 mM TEAP, 20% ACN, pH 5.8; B: 200 mM TEAP, 20% ACN, pH 7.8	0-100% B in 10 min, +10 min 100% B	0.2	1	7.850	20.890	53.7	3.1	0.2666	1.744	1.346	13.040	1.7	1.97	11.80	34 045	28	20
			2	7.850	22.109	24.8	1.4	0.2931	0.805	1.277	14.259	1.8	1.09	2.57	31 551	25	20
			3	7.850	22.677	54.4	3.2	0.2485	1.767	1.177	14.827	1.9	1.04	1.24	46 176	30	20
			4	7.850	23.284	72.0	4.1	0.2435	2.338	5.157	15.434	2.0	1.04	1.46	50 701	30	20
			5	7.850	23.556	155.1	8.5	0.2676	5.037	1.062	15.706	2.0	1.02	0.63	42 967	28	20
			6	7.850	23.940	71.3	5.1	0.2068	2.316	1.838	16.090	2.0	1.02	0.96	74 310	36	20
			7	7.850	24.201	121.8	6.6	0.2712	3.955	0.943	16.351	2.1	1.02	0.64	44 156	27	20
			8	7.850	24.708	88.3	5.2	0.2520	2.868	1.991	16.858	2.1	1.03	1.14	53 306	29	20
			9	7.850	24.923	93.3	5.3	0.2577	3.029	0.598	17.073	2.2	1.01	0.50	51 865	29	20
			10	7.850	25.524	149.7	7.6	0.2909	4.863	1.508	17.674	2.3	1.04	1.29	42 689	26	20
			11	7.850	26.147	389.5	15.0	0.3608	12.653	3.348	18.297	2.3	1.04	1.13	29 121	21	20
			12	7.850	26.731	1783.2	74.6	0.3519	57.925	1.364	18.881	2.4	1.03	0.97	31 996	21	20

Figure S2. [1]D QN-AX UV chromatogram of Patisiran sample with a flow rate at 0.2 ml/min during the gradient. In the table below, relevant parameters are calculated for the evaluation of the chromatographic performance. For further LC conditions, see chapter 2.5.

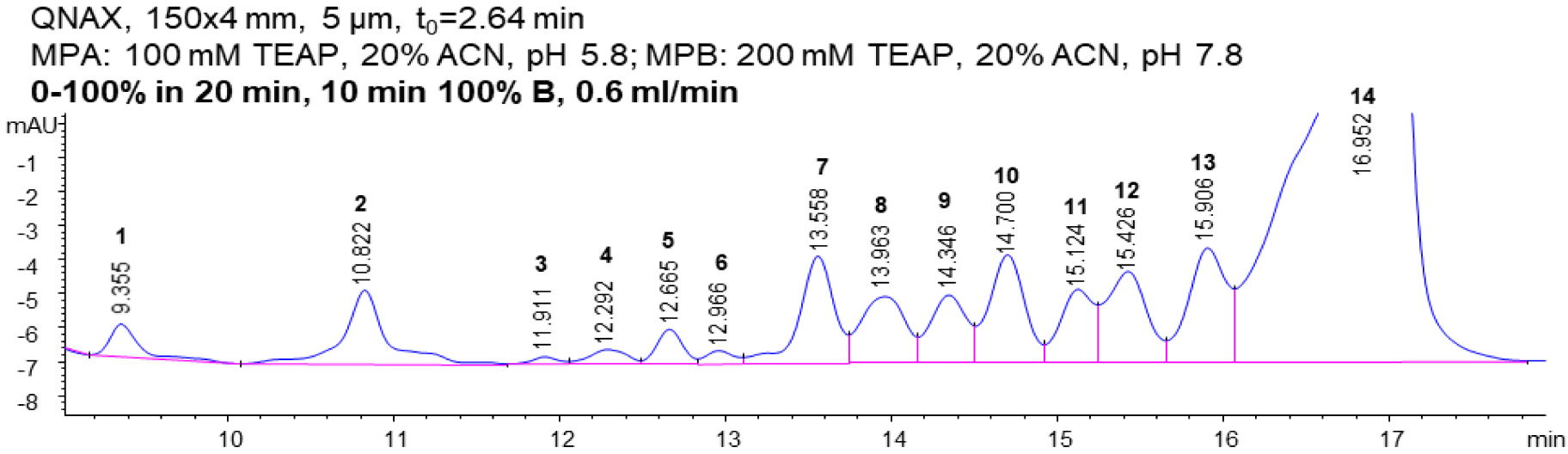

mobile phase	gradient	flow rate [mL/min]	impurity	t_0 [min]	t_R [min]	Area	Height [mAU]	$w_{1/2}$ [min]	Area [%]	Symmetry	t'_R [min]	k	α	R	N	PC	t_G [min]
A: 100 mM TEAP, 20% ACN, pH 5.8; B: 200 mM TEAP, 20% ACN, pH 7.8	0-100% B in 20 min, +10 min 100% B	0.6	1	2.640	9.355	9.2	0.9	0.1662	0.773	0.864	6.715	2.5	3.15	18.80	17 568	62	20
			2	2.640	10.822	32.9	2.1	0.2261	2.755	0.799	8.182	3.1	1.22	4.41	12 703	46	20
			3	2.640	11.911	2.7	0.2	0.2159	0.229	2.501	9.271	3.5	1.13	2.91	16 877	48	20
			4	2.640	12.292	3.8	0.3	0.2078	0.321	1.106	9.652	3.7	1.04	1.06	19 402	50	20
			5	2.640	12.665	8.7	0.9	0.1613	0.725	1.341	10.025	3.8	1.04	1.19	34 186	64	20
			6	2.640	12.966	2.9	0.3	0.1649	0.239	0.655	10.326	3.9	1.03	1.09	34 282	63	20
			7	2.640	13.558	45.6	3.1	0.2171	3.821	1.210	10.918	4.1	1.06	1.83	21 626	48	20
			8	2.640	13.963	36.0	1.9	0.2916	3.016	1.150	11.323	4.3	1.04	0.94	12 714	36	20
			9	2.640	14.346	30.1	2.0	0.2293	2.523	1.054	11.706	4.4	1.03	0.87	21 705	46	20
			10	2.640	14.700	46.7	3.2	0.2248	3.910	1.022	12.060	4.6	1.03	0.92	23 711	46	20
			11	2.640	15.124	29.8	2.1	0.2065	2.493	1.199	12.484	4.7	1.04	1.16	29 744	50	20
			12	2.640	15.426	44.6	2.7	0.2478	3.730	1.049	12.786	4.8	1.02	0.78	21 488	42	20
			13	2.640	15.906	53.8	3.3	0.2387	4.507	1.076	13.266	5.0	1.04	1.16	24 622	44	20
			14	2.640	16.952	839.1	37.9	0.3166	70.231	1.827	14.312	5.4	1.08	2.22	15 897	33	20

Figure S3. [1]D QN-AX UV chromatogram of Patisiran sample with a flow rate at 0.6 ml/min during the gradient. In the table below, relevant parameters are calculated for the evaluation of the chromatographic performance. For further LC conditions, see chapter 2.5.

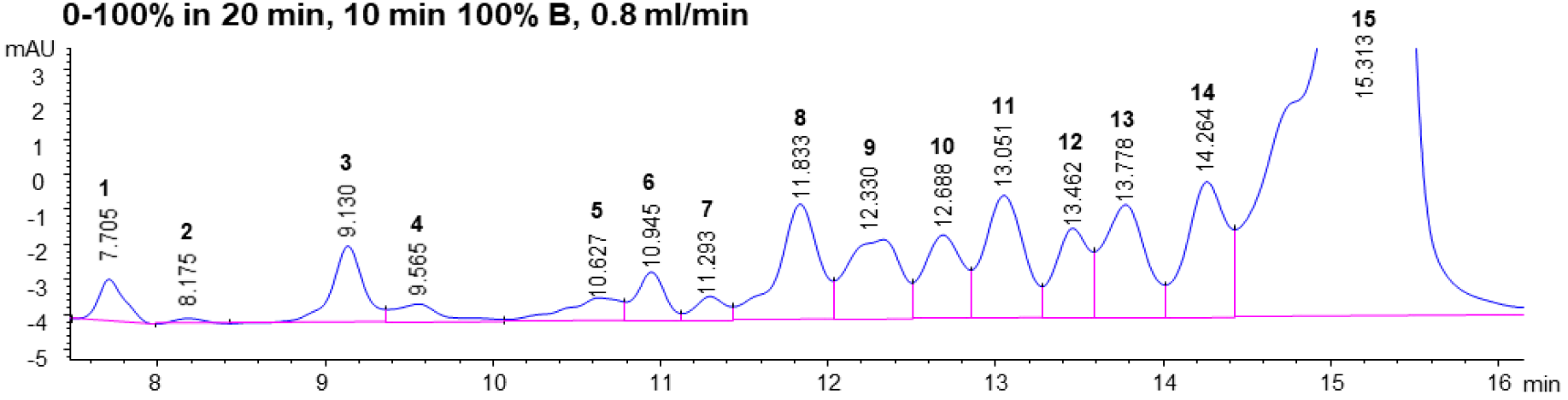

mobile phase	gradient	flow rate [mL/min]	impurity	t_0 [min]	t_R [min]	Area	Height [mAU]	$w_{1/2}$ [min]	Area [%]	Symmetry	t'_R [min]	k	α	R	N	PC	t_G [min]
A: 100 mM TEAP, 20% ACN, pH 5.8; B: 200 mM TEAP, 20% ACN, pH 7.8	0-100% B in 20 min, +10 min 100% B	0.8	1	1.975	7.705	13.6	1.2	0.1866	1.014	0.756	5.730	2.9	3.54	17.17	9 454	58	20
			2	1.975	8.175	2.0	0.2	0.2125	0.148	0.829	6.200	3.1	1.08	1.39	8 207	51	20
			3	1.975	9.130	27.0	2.1	0.1898	2.020	1.016	7.155	3.6	1.15	2.80	12 831	57	20
			4	1.975	9.565	3.4	0.3	0.1924	0.254	0.892	7.590	3.8	1.06	1.34	13 704	56	20
			5	1.975	10.627	2.0	0.2	0.1638	0.147	0.817	8.652	4.4	1.14	3.52	23 340	66	20
			6	1.975	10.945	9.1	1.0	0.1493	0.677	0.864	8.970	4.5	1.04	1.20	29 800	72	20
			7	1.975	11.293	3.0	0.4	0.1365	0.226	1.210	9.318	4.7	1.04	1.44	37 954	79	20
			8	1.975	11.833	52.0	3.2	0.2399	3.885	1.225	9.858	5.0	1.06	1.69	13 491	45	20
			9	1.975	12.330	46.8	2.1	0.2919	3.494	1.982	10.355	5.2	1.05	1.10	9 894	37	20
			10	1.975	12.688	35.1	2.3	0.2352	2.620	1.025	10.713	5.4	1.03	0.80	16 137	46	20
			11	1.975	13.051	54.3	3.4	0.2477	4.057	0.965	11.076	5.6	1.03	0.89	15 393	44	20
			12	1.975	13.462	32.5	2.4	0.1997	2.431	1.132	11.487	5.8	1.04	1.08	25 198	54	20
			13	1.975	13.778	52.5	3.1	0.2537	3.925	1.034	11.803	6.0	1.03	0.82	16 354	43	20
			14	1.975	14.264	60.0	3.7	0.2391	4.482	1.060	12.289	6.2	1.04	1.16	19 734	45	20
			15	1.975	15.313	936.0	43.5	0.3072	69.952	1.791	13.338	6.8	1.09	2.27	13 778	36	20

Figure S4. [1]D QN-AX UV chromatogram of Patisiran sample with a flow rate at 0.8 ml/min during the gradient. In the table below, relevant parameters are calculated for the evaluation of the chromatographic performance. For further LC conditions, see chapter 2.5.

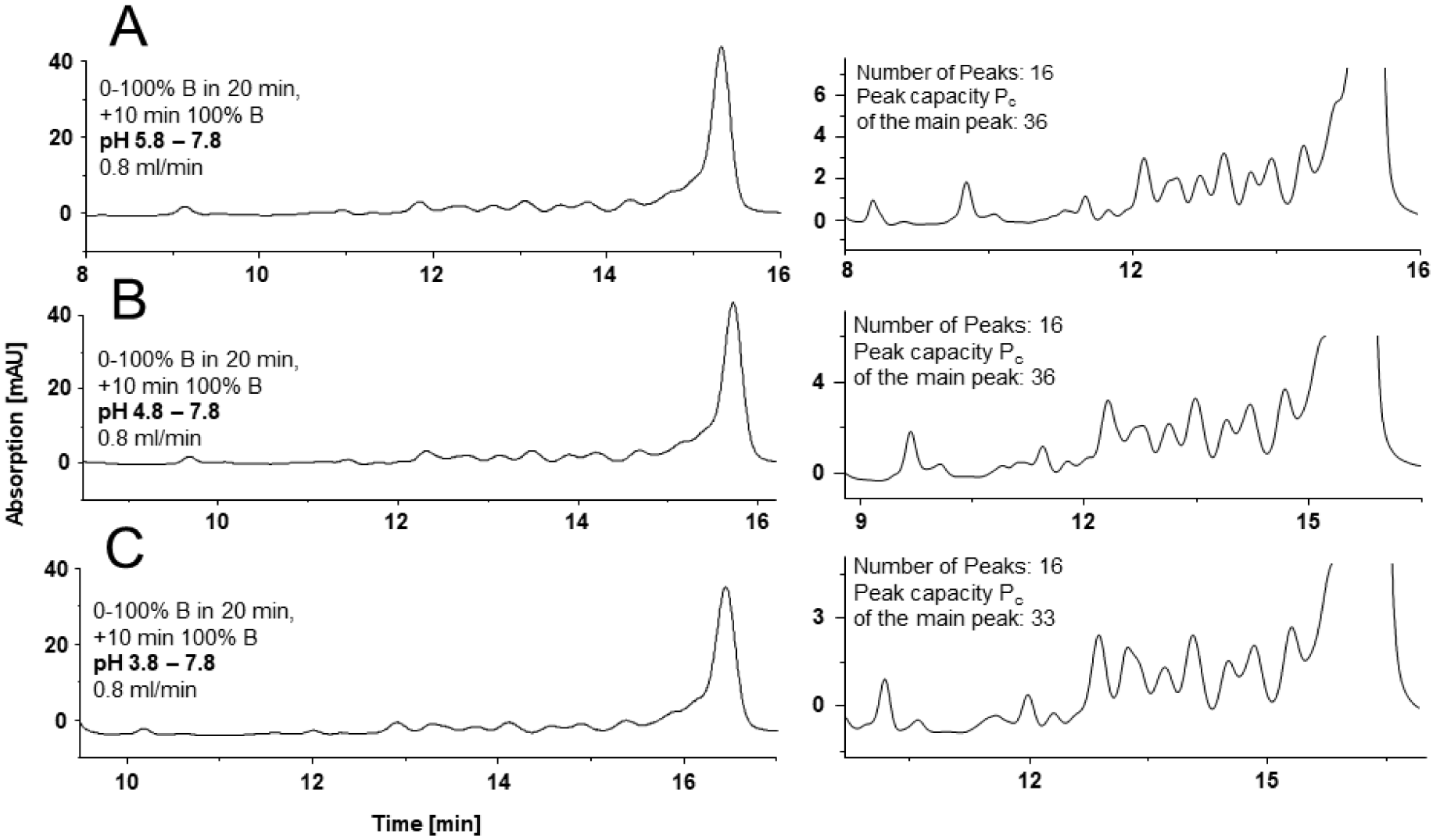

Figure S5. [1]D QN-AX UV chromatograms of Patisiran sample with further lower start pH-value in the mobile phase of A. Further LC conditions see chapter 2.5. In this optimization series (with the flow rate of 0.8 ml/min), the initial pH value of the mixed pH/TEAP gradient was further decreased. Unfortunately, a further decrease of the initial pH from 5.8 to 4.8 and 3.8, respectively, did not lead to a significant improvement of the separations

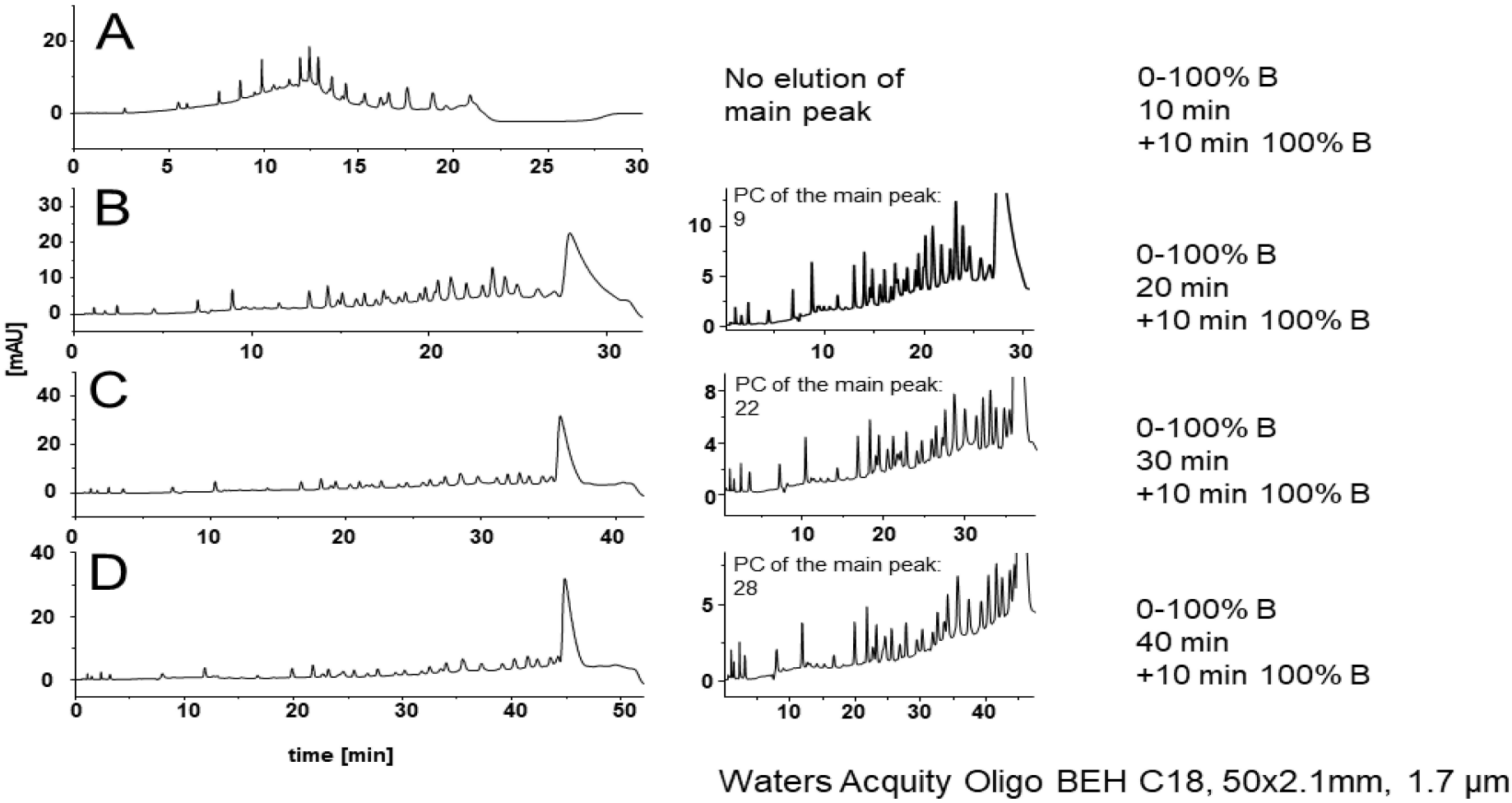

Figure S6. [1]D IP-RP UV chromatograms of Patisiran sample with TPAA as ion pairing reagents. LC-Conditions: MPA: 100 mM TPAA in water, pH 7. MPB: 20% ACN in MPA. Gradient: 0-100 % MPB in 10 (A), 20 (B), 30 (C), 40 (D) min, 10 min at 100% MPB. Flow rate: 0.2 ml/min. Temperature: 20 °C. Injection volume: 5 µL.

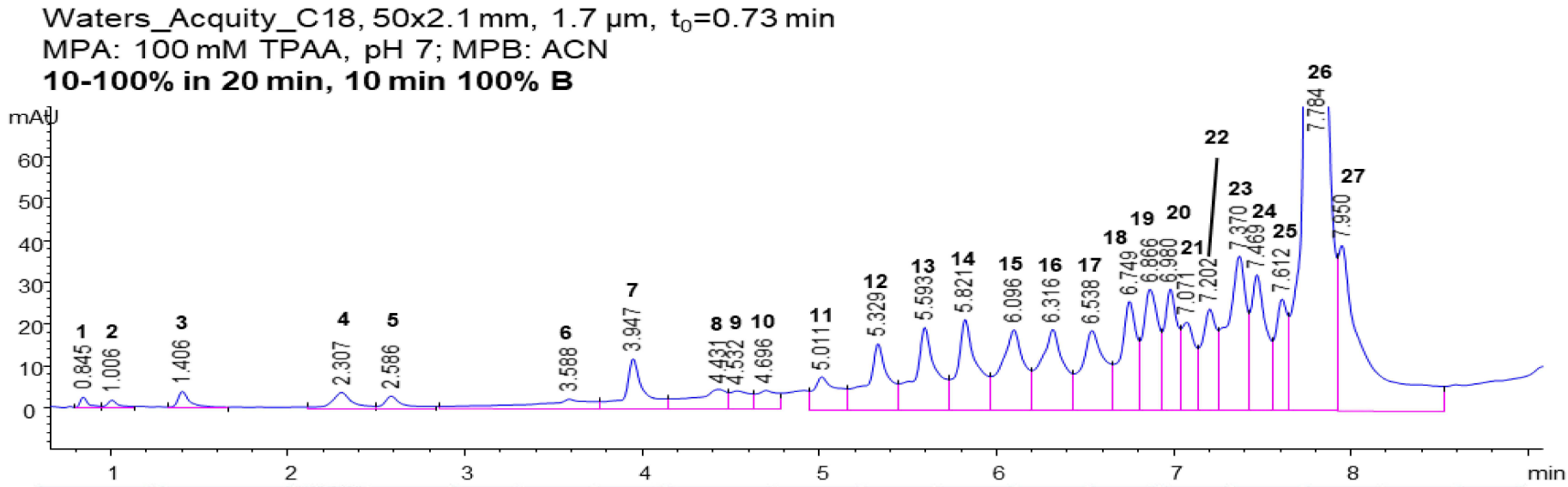

mobile phase	gradient	flow rate [mL/min]	Impurity	t_0 [min]	t_R [min]	Area	Height [mAU]	$w_{1/2}$ [min]	Area [%]	Symmetry	t'_R [min]	k	α	R	N	PC	t_G [min]
A: 100 mM TPAA, pH 7; B: ACN	10-100% B in 20 min, +10 min 100% B	0.2	1	0.730	0.845	8.9	2.5	0.0517	0.168	0.531	0.115	0.2			1 481	219	20
			2	0.730	1.006	8.8	1.8	0.0675	0.166	0.557	0.276	0.4	2.40	1.59	1 232	168	20
			3	0.730	1.406	21.3	4.0	0.0758	0.404	0.472	0.676	0.9	2.45	3.29	1 908	150	20
			4	0.730	2.307	31.3	3.9	0.1146	0.593	0.865	1.577	2.2	2.33	5.58	2 247	99	20
			5	0.730	2.586	21.7	2.9	0.1028	0.411	0.489	1.856	2.5	1.18	1.51	3 509	110	20
			6	0.730	3.588	60.9	2.3	0.3169	1.155	2.223	2.858	3.9	1.54	2.82	711	36	20
			7	0.730	3.947	90.9	12.1	0.1027	1.722	0.746	3.217	4.4	1.13	1.01	8 190	110	20
			8	0.730	4.431	67.4	4.8	0.1890	1.277	3.765	3.701	5.1	1.15	1.96	3 048	60	20
			9	0.730	4.532	34.3	4.4	0.1109	0.651	0.442	3.802	5.2	1.03	0.40	9 260	102	20
			10	0.730	4.696	36.3	4.6	0.1069	0.688	0.743	3.966	5.4	1.04	0.89	10 700	106	20
			11	0.730	5.011	74.1	7.8	0.1238	1.405	0.435	4.281	5.9	1.08	1.61	9 085	92	20
			12	0.730	5.329	136.4	15.7	0.1153	2.587	1.146	4.599	6.3	1.07	1.57	11 845	98	20
			13	0.730	5.593	169.5	19.6	0.1148	3.213	0.898	4.863	6.7	1.06	1.35	13 162	99	20
			14	0.730	5.821	167.0	21.6	0.1044	3.166	0.603	5.091	7.0	1.05	1.23	17 238	109	20
			15	0.730	6.096	176.0	19.1	0.1216	3.336	1.223	5.366	7.4	1.05	1.44	13 936	93	20
			16	0.730	6.316	181.1	19.2	0.1239	3.432	1.055	5.586	7.7	1.04	1.06	14 409	92	20
			17	0.730	6.538	176.3	19.0	0.1245	3.342	0.774	5.808	8.0	1.04	1.05	15 292	91	20
			18	0.730	6.749	159.2	26.0	0.0854	3.018	1.286	6.019	8.2	1.04	1.19	34 631	133	20
			19	0.730	6.866	173.8	28.9	0.0892	3.295	0.879	6.136	8.4	1.02	0.79	32 853	127	20
			20	0.730	6.980	150.9	29.0	0.0737	2.861	0.847	6.250	8.6	1.02	0.83	49 737	154	20
			21	0.730	7.071	110.6	21.1	0.0752	2.096	0.566	6.341	8.7	1.01	0.72	49 026	151	20
			22	0.730	7.202	136.2	24.2	0.0786	2.582	1.231	6.472	8.9	1.02	1.01	46 555	144	20
			23	0.730	7.370	275.3	36.9	0.1040	5.218	1.867	6.640	9.1	1.03	1.09	27 846	109	20
			24	0.730	7.469	193.5	32.4	0.0836	3.667	0.578	6.739	9.2	1.01	0.62	44 260	136	20
			25	0.730	7.612	130.8	26.7	0.0701	2.480	1.276	6.882	9.4	1.02	1.10	65 383	162	20
			26	0.730	7.784	2044.2	331.7	0.0899	38.751	0.685	7.054	9.7	1.02	1.27	41 571	126	20
			27	0.730	7.950	438.6	39.6	0.1422	8.315	0.133	7.220	9.9	1.02	0.84	17 332	80	20

Figure S7. [1]D IP-RP LC-UV chromatogram of Patisiran sample with TPPA as ion pairing reagent. In the table below, relevant parameters are calculated for the evaluation of the chromatographic performance. For further LC conditions, see chapter 2.5.

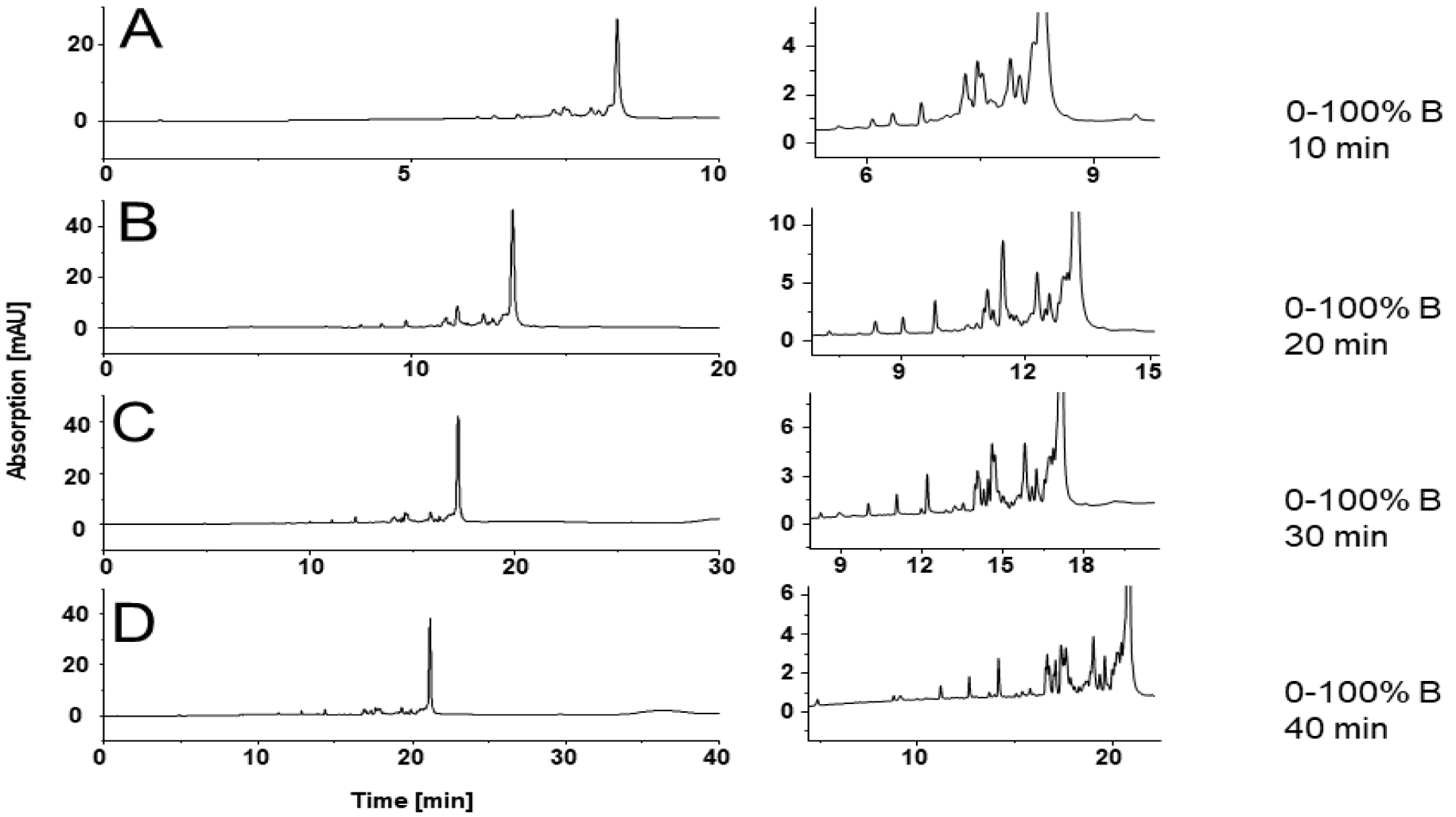

Figure S8. [1]D IP-RP UV chromatograms of Patisiran sample with TEAA as ion pairing reagents. Although many impurity peaks could be separated from the main peak, the resolution as well as the shape of many peaks was rather poor although a sub-2 µm column was employed. LC-Conditions: MPA: 100 mM TEAA in water, pH 7. MPB: 20% ACN in MPA. Gradient: 0-100 % in 10 (A), 20 (B), 30 (C), 40 (D) min. Flow rate: 0.2 ml/min. Temperature: 20 °C. Sample concentration: 10 µM. Injection volume: 5 µL.

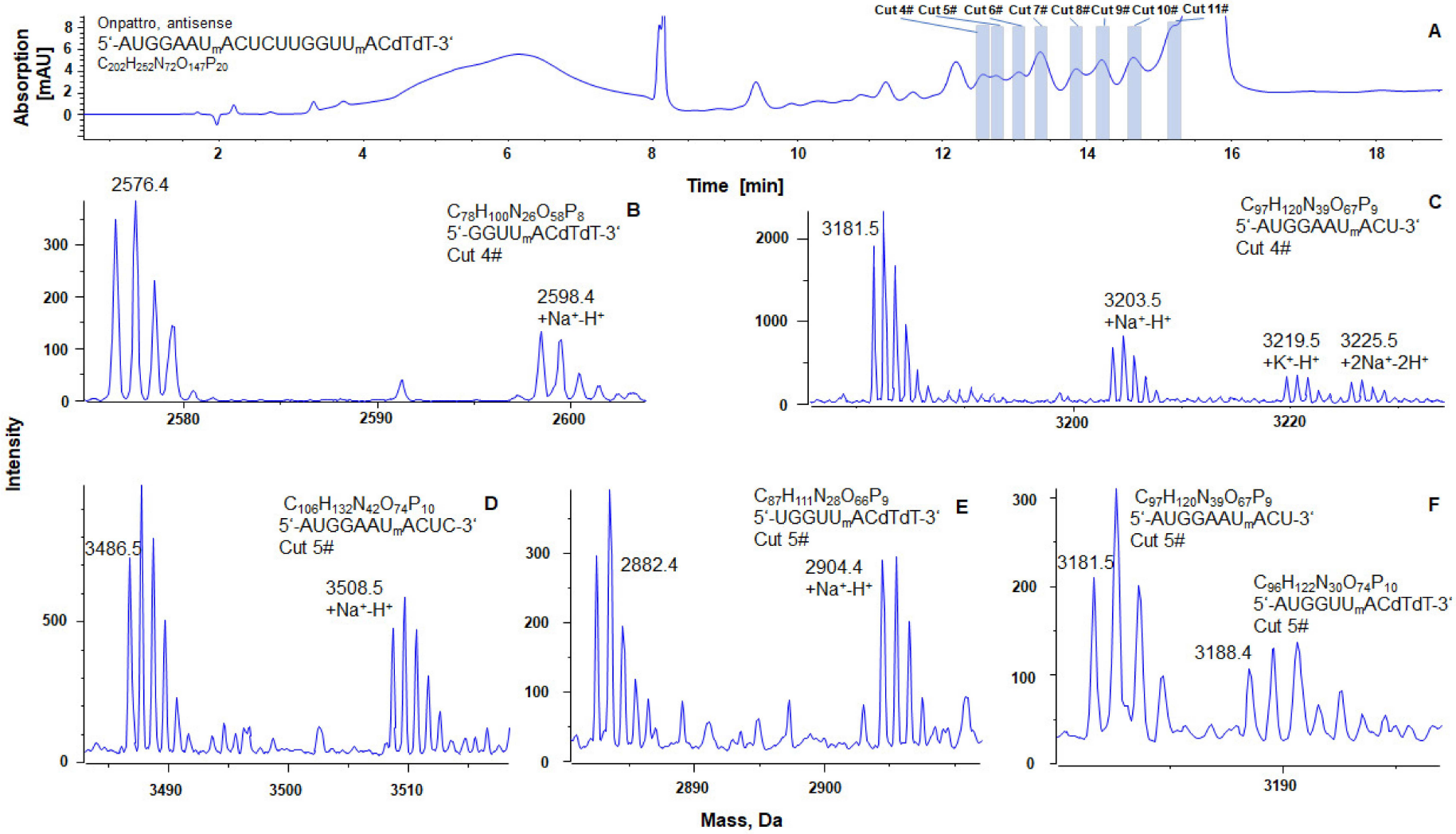

Figure S9. MHC 2D-LC (QN-AX in ^{1}D) of the impurity peaks with hyphenation to ESI-TOF-MS in negative mode. All the instrumental and LC-MS conditions see chapter 2.4 and 2.5. Extended contents from Fig. 4. All shown mass spectra are deconvoluted. Monoisotopic mass indicated only. For better overview, the detected impurity species are listed in table 1.

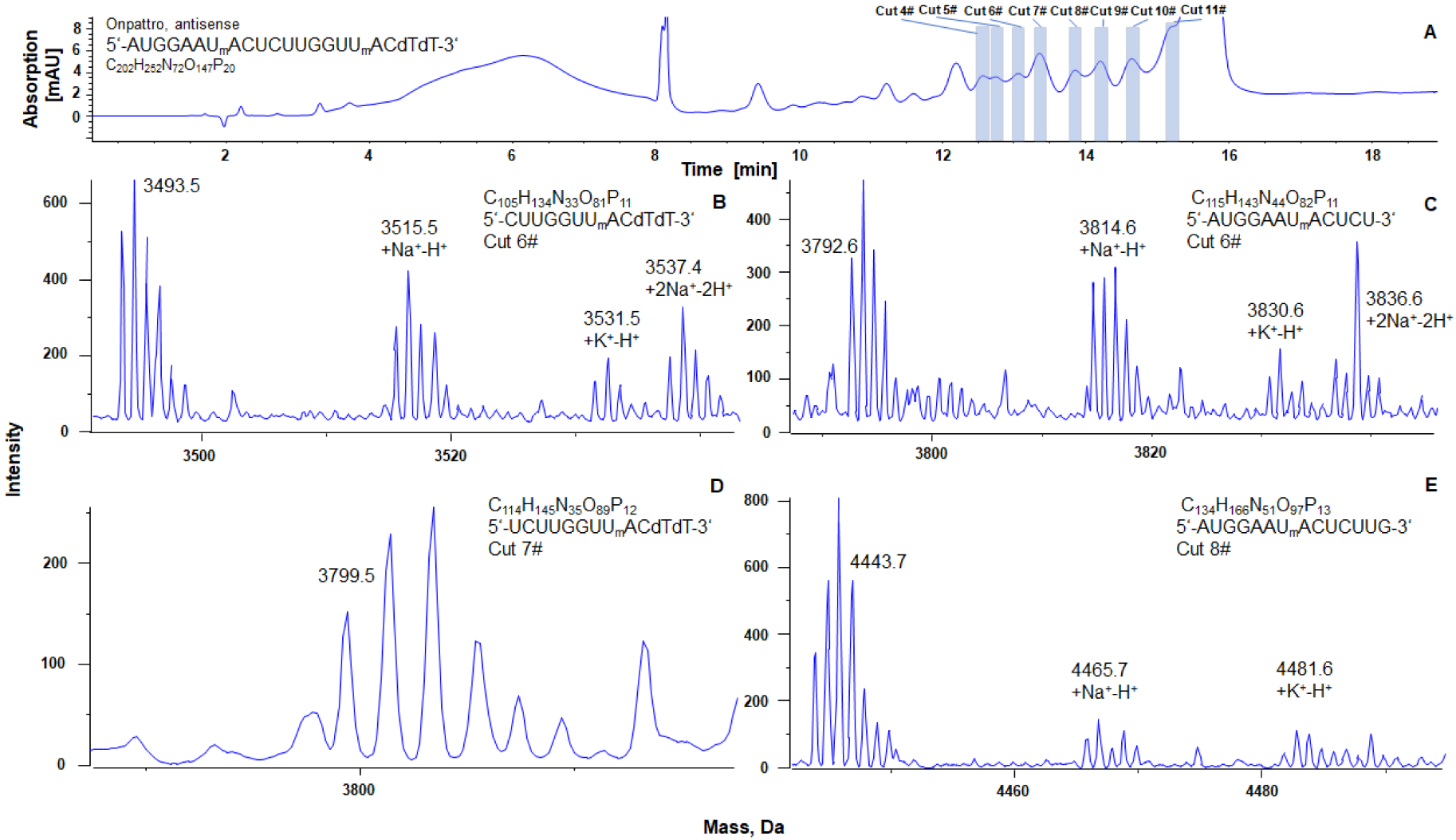

Figure S10. MHC 2D-LC (QN-AX in ^{1}D) of the impurity peaks with hyphenation to ESI-TOF-MS in negative mode. All the instrumental and LC-MS conditions see chapter 2.4 and 2.5. Extended contents from Fig. 4. All shown mass spectra are deconvoluted. Monoisotopic mass indicated only. For better overview, the detected impurity species are listed in table 1.

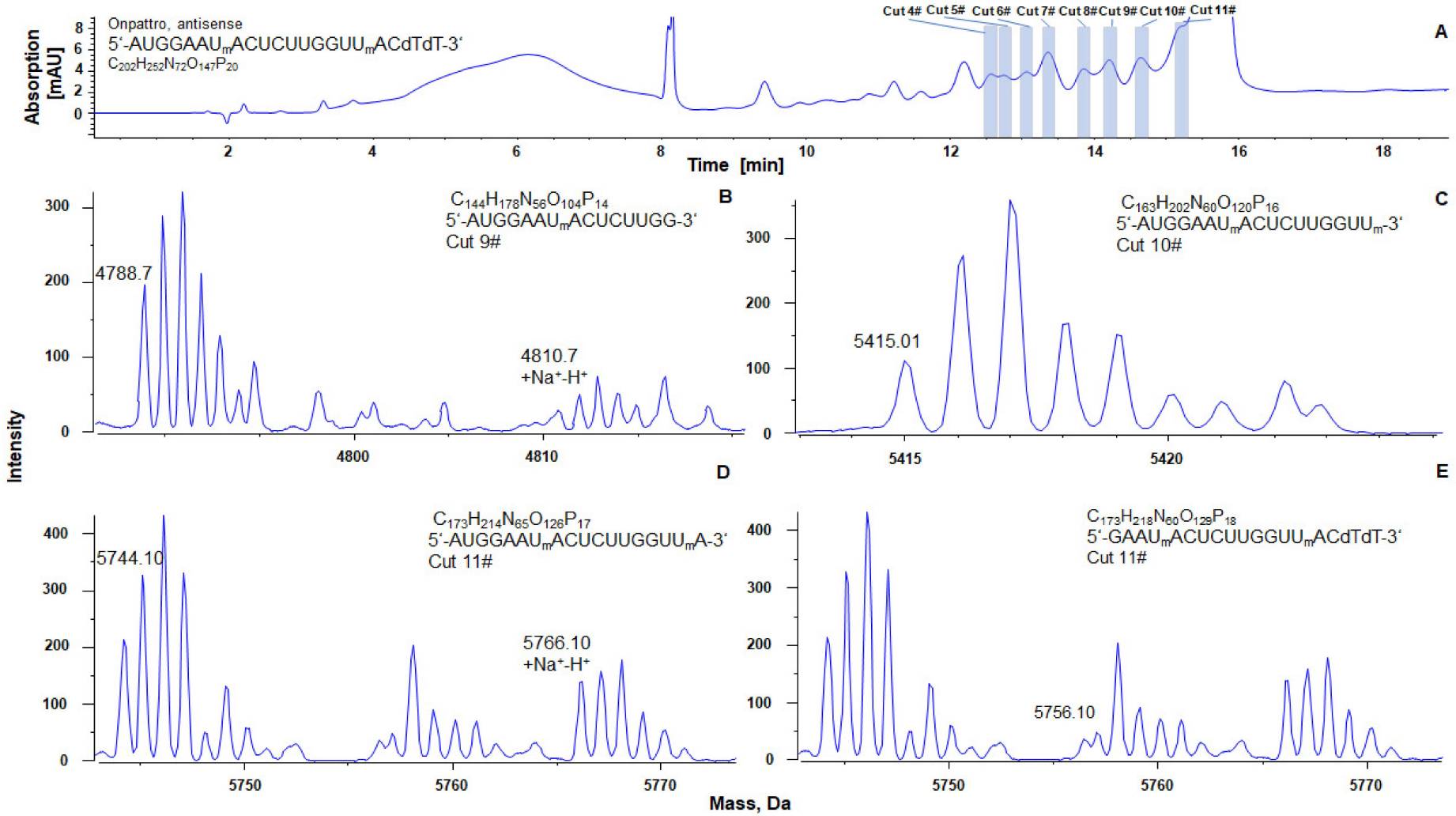

Figure S11. MHC 2D-LC (QN-AX in ^{1}D) of the impurity peaks with hyphenation to ESI-TOF-MS in negative mode. All the instrumental and LC-MS conditions see chapter 2.4 and 2.5. Extended contents from Fig. 4. All shown mass spectra are deconvoluted. Monoisotopic mass indicated only. For better overview, the detected impurity species are listed in table 1.

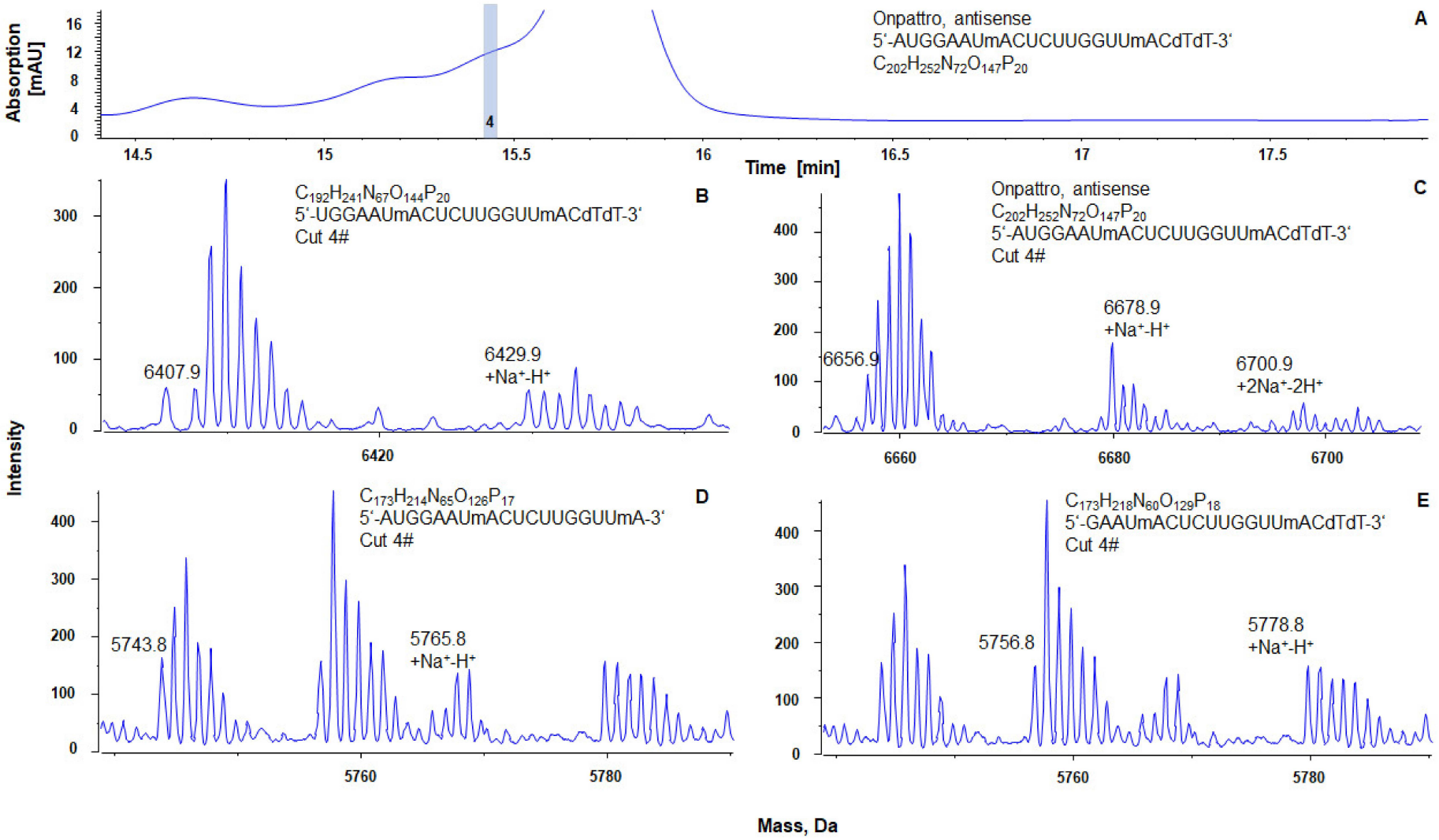

Figure S12. High-resolution sampling 2D-LC (QN-AX in [1]D) of the main peak with hyphenation to ESI-TOF-MS in negative mode. Detailed instrumental and LC-MS conditions can be found in chapter 2.4 and 2.5. All shown mass spectra are deconvoluted. Monoisotopic mass indicated.

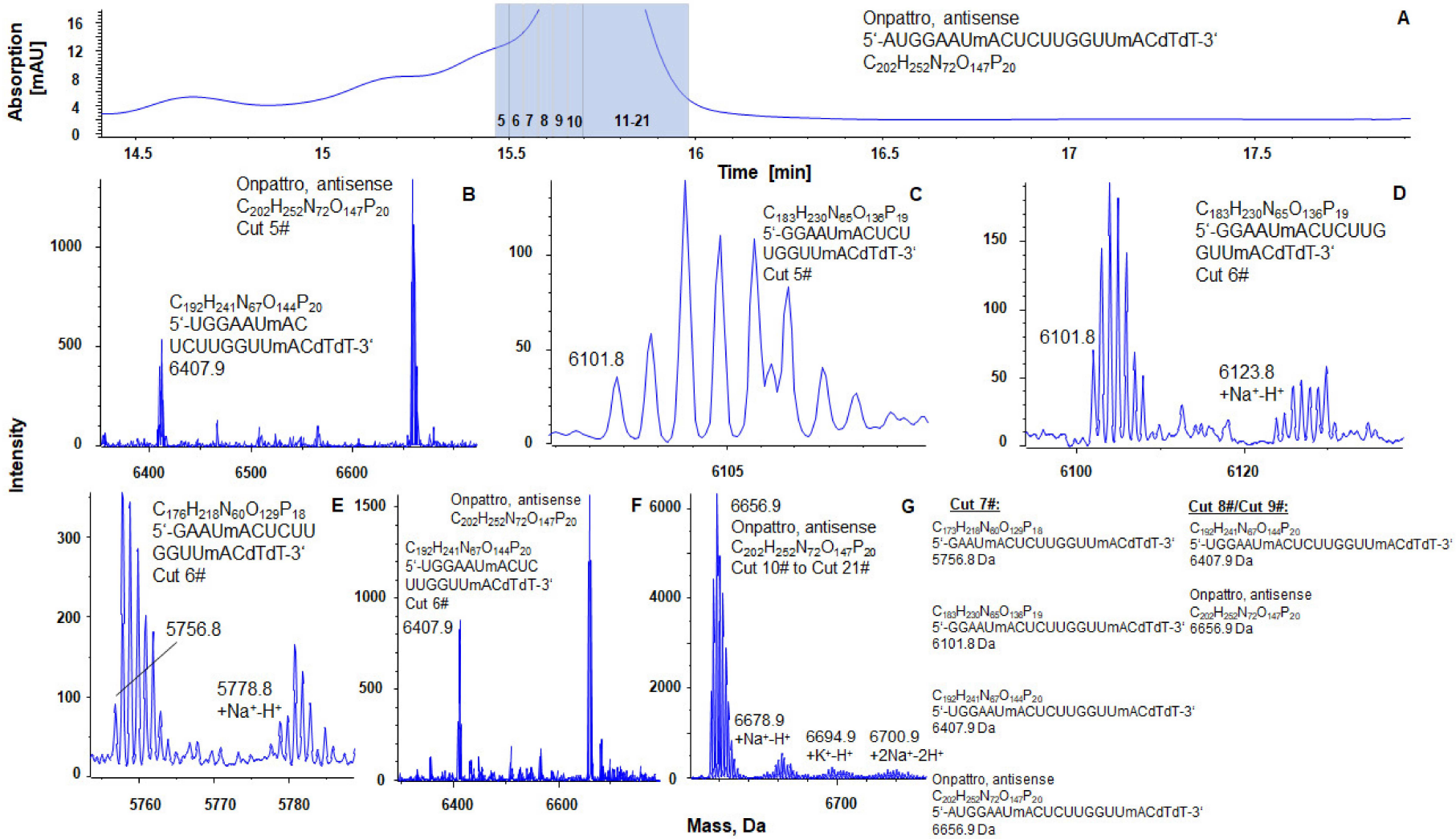

Figure S13. High-resolution sampling 2D-LC (QN-AX in ^{1}D) of the main peak with hyphenation to ESI-TOF-MS in negative mode. Detailed instrumental and LC-MS conditions can be found in chapter 2.4 and 2.5. All shown mass spectra are deconvoluted. Monoisotopic mass indicated. Due to lack of space, some mass spectra repetitively detected in the cuts 7-9 are not shown.

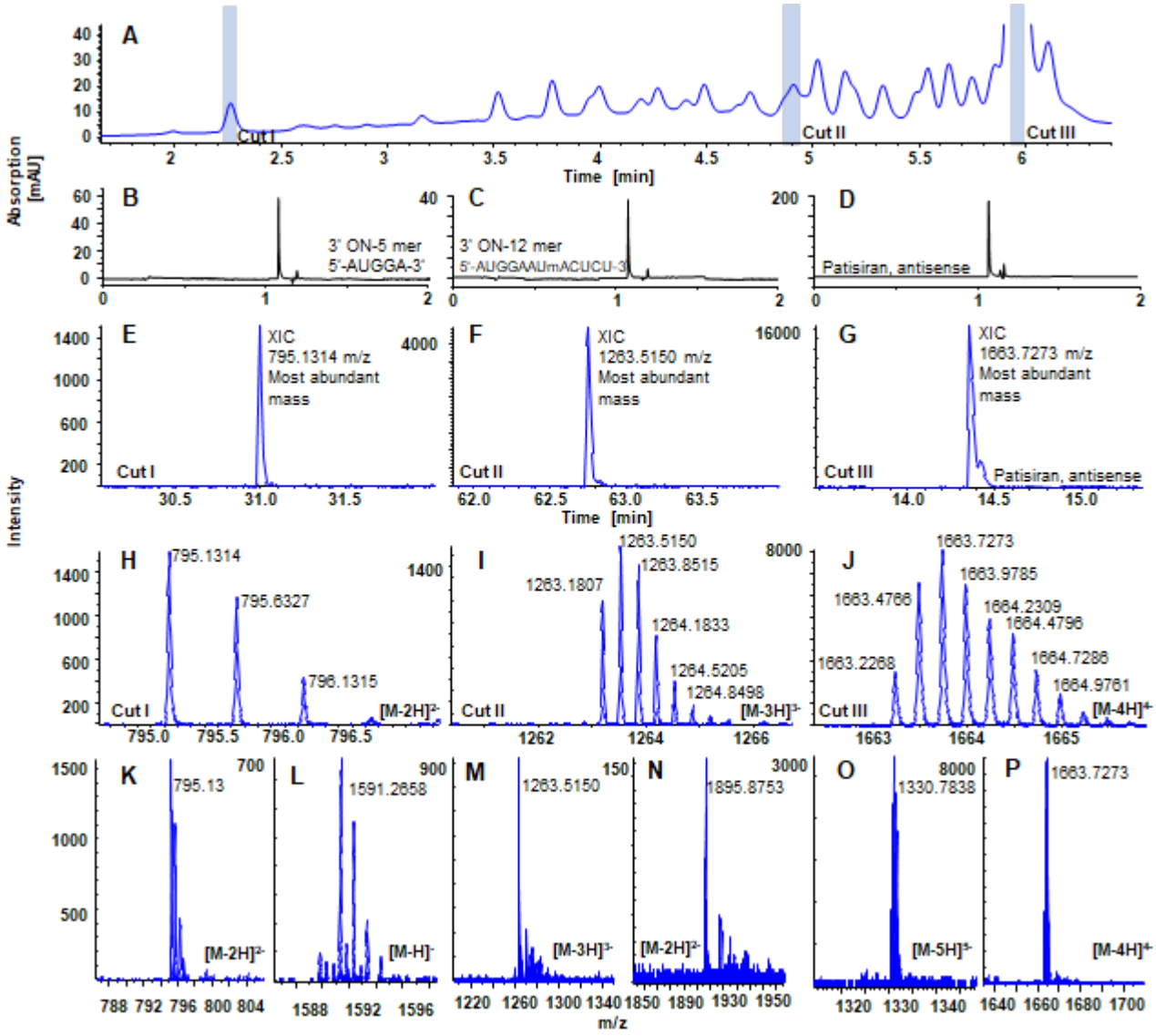

Figure. S14. Three representative MHC 2D-LC UV (C18 in ^{1}D) chromatograms of selected oligonucleotide species with various length (A, B-D). LC instrumental conditions see chapter 2.4. (E): EIC of 795.1314 m/z (± 10 mDa, most abundant signal of $[M-2H]^{-2}$ peak group); (F): EIC of 1263.5150 m/z (± 10 mDa, most abundant signal of $[M-3H]^{3-}$ peak group); (G): EIC of 1663.7273 m/z (± 10 mDa, most abundant signal of $[M-4H]^{4-}$ peak group); (H)-(J): ESI-MS spectra in negative mode of the most abundant signals from the corresponding $[M-nH]^{n-}$ peak group. (K)-(P): ESI-MS spectra in negative mode of a different charge states, most abundant mass indicated. All MS conditions see chapter 2.5.

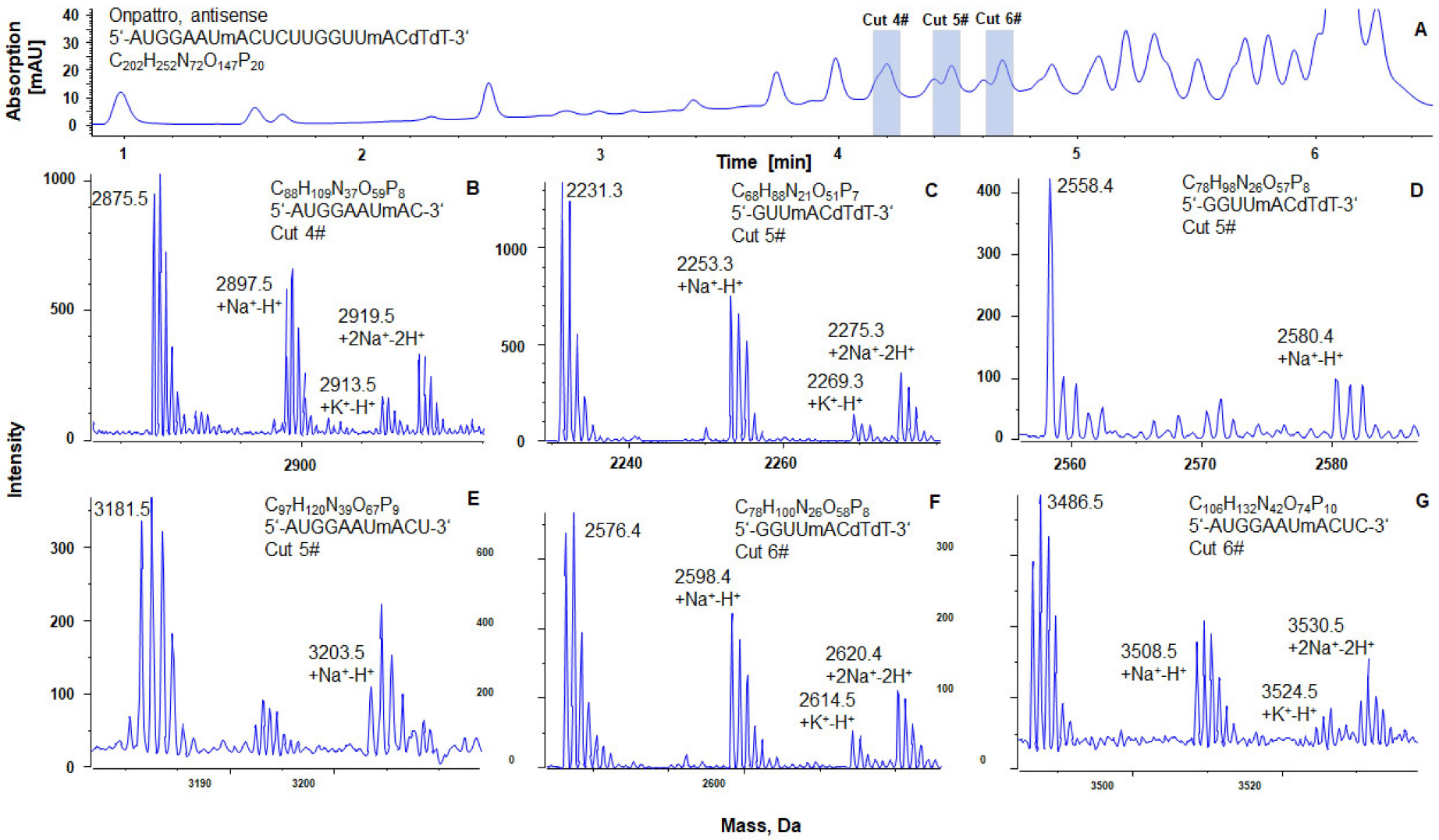

Figure S15. MHC 2D-LC (IP-RP in ^{1}D) of the impurity peaks with hyphenation to ESI-TOF-MS in negative mode. All the instrumental and LC-MS conditions see chapter 2.4 and 2.5. Extended contents from Fig. 6. All shown mass spectra are deconvoluted. Monoisotopic mass indicated only. For better overview, the detected impurity species are listed in table 1.

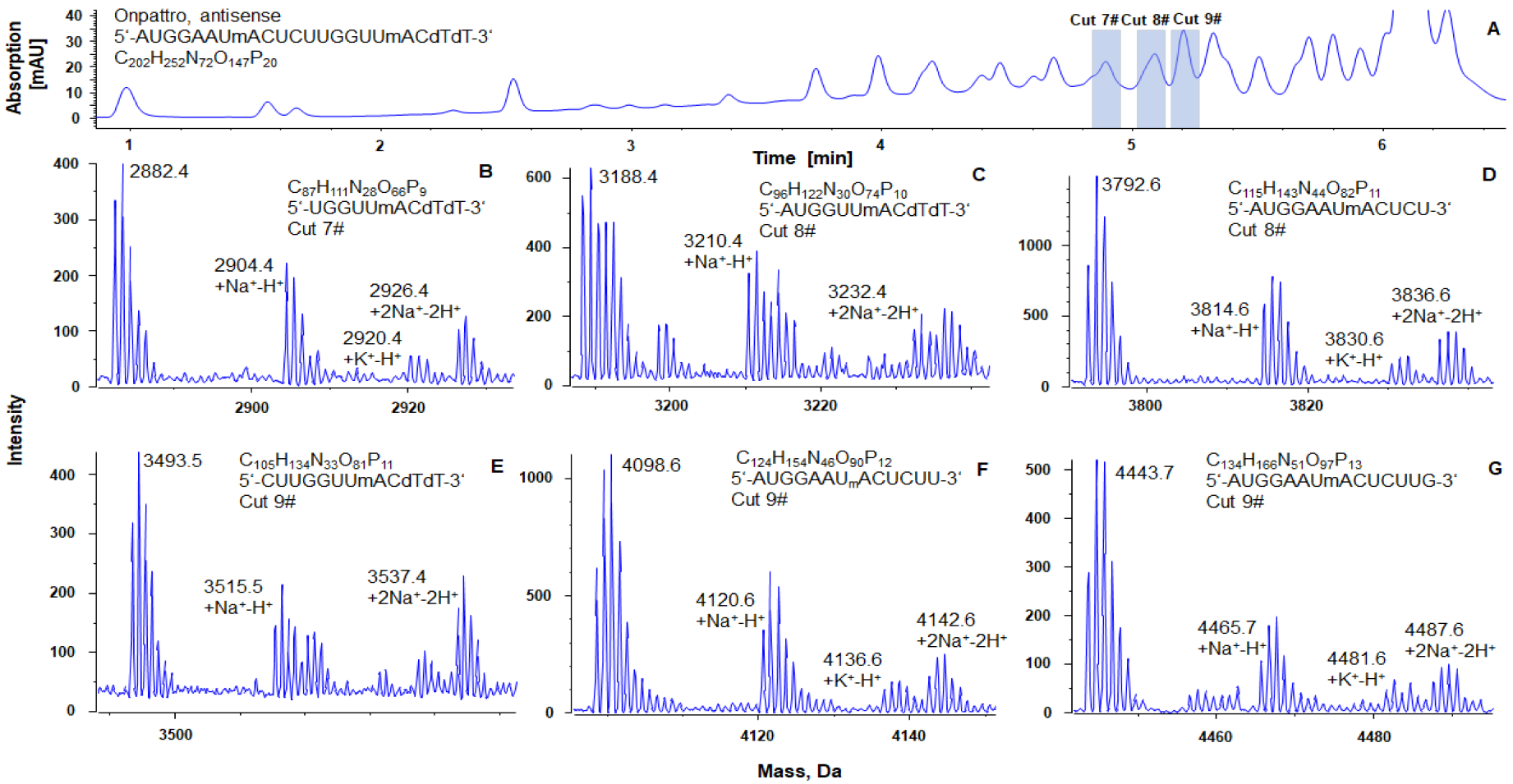

Figure S16. MHC 2D-LC (IP-RP in ^{1}D) of the impurity peaks with hyphenation to ESI-TOF-MS in negative mode. All the instrumental and LC-MS conditions see chapter 2.4 and 2.5. Extended contents from Fig. 6. All shown mass spectra are deconvoluted. Monoisotopic mass indicated only. For better overview, the detected impurity species are listed in table 1.

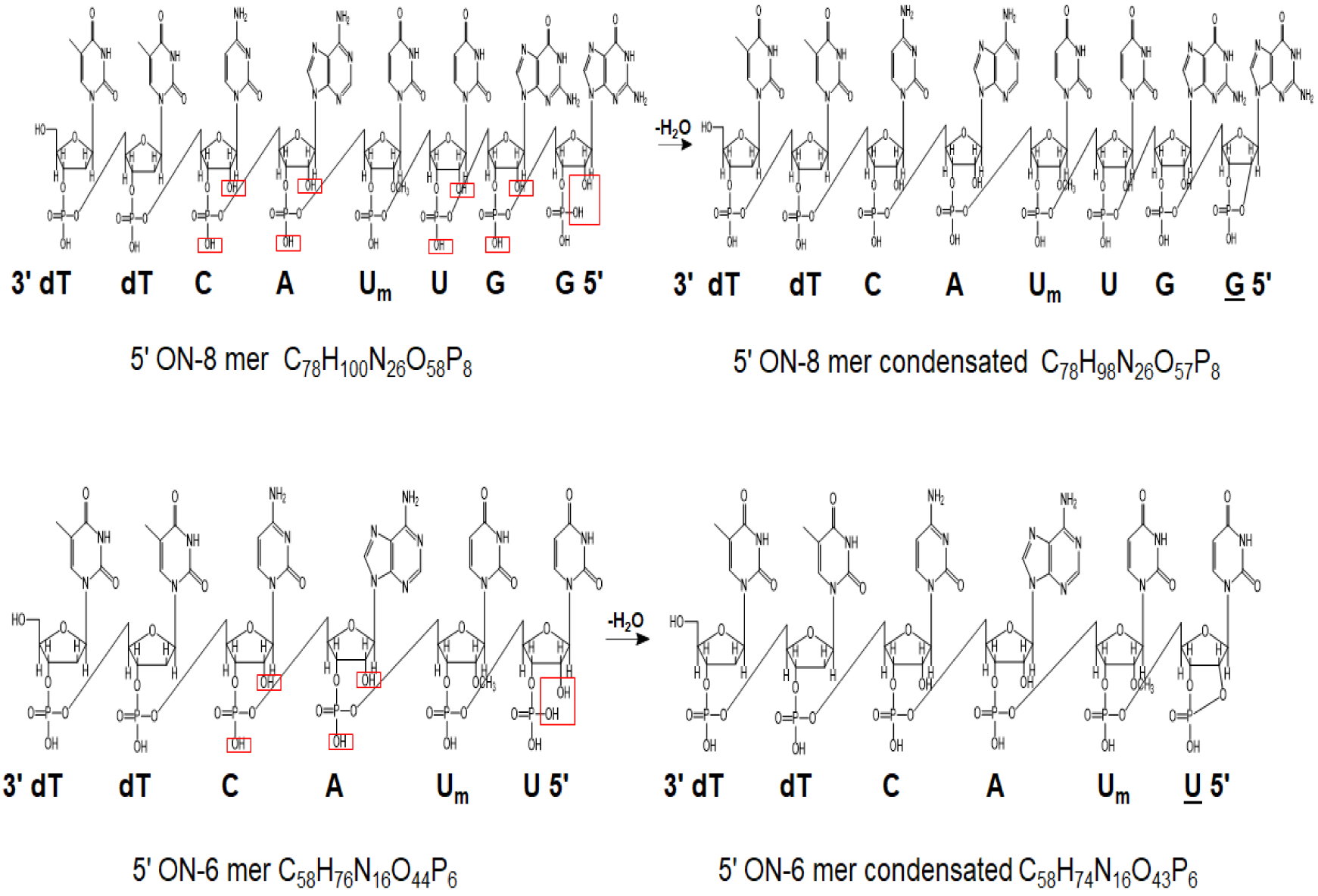

Figure S17. Assumed structure and reaction mechanism of the condensated species.

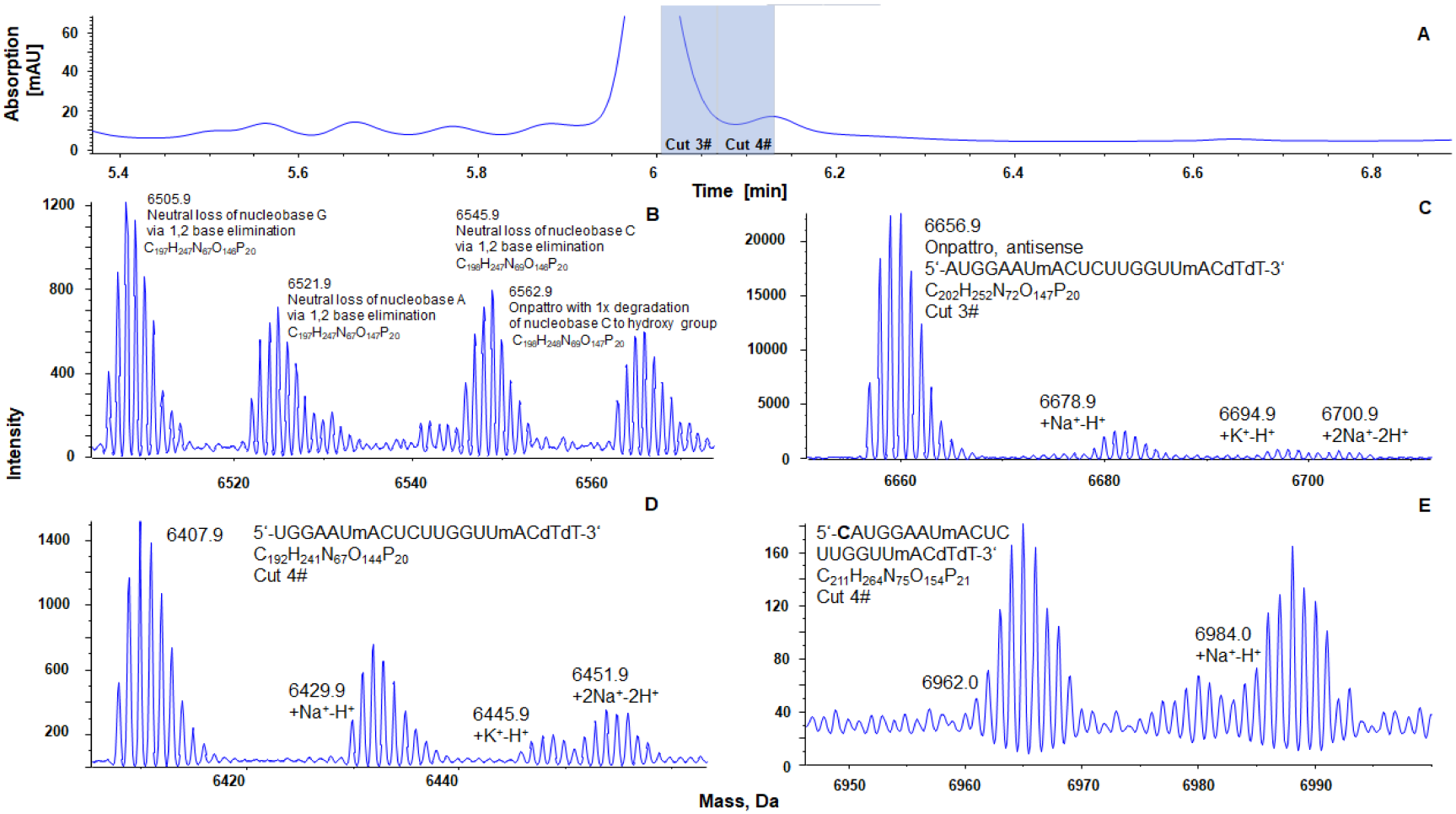

Figure S18. High-resolution sampling 2D-LC (IP-RP in ^{1}D) of the main peak with hyphenation to ESI-TOF-MS in negative mode. Further instrumental and LC-MS conditions are described in chapter 2.4 and 2.5. All shown mass spectra are deconvoluted. Monoisotopic mass indicated.

Concentration (µM)	Peak Area
20	87294
10	43941
5	24386
2	9908
1	6483

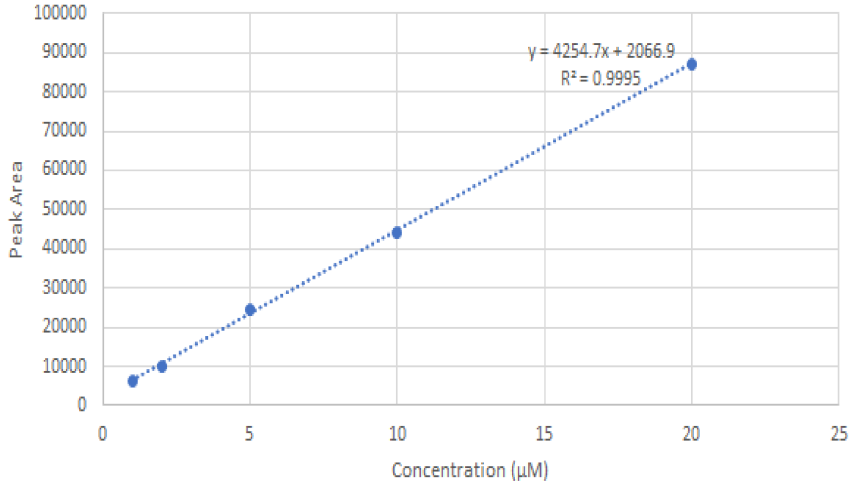

SUMMARY OUTPUT OF THE LINEAR REGRESSION

Regression Statistics	
Multiple R	0.99976688
R Square	0.99953381
Adjusted R Square	0.99937841
Standard Error	823.906112
Observations	5

ANOVA

	df	SS	MS	F	Significance F
Regression	1	4366266573	4366266573	6432.12976	4.2726E-06
Residual	3	2036463.85	678821.282		
Total	4	4368303037			

	Coefficients	Standard Error	t Stat	P-value	Lower 95%	Upper 95%	Lower 95.0%	Upper 95.0%
Intercept	2066.86401	546.187813	3.78416355	0.03235145	328.650625	3805.0774	328.650625	3805.0774
X Variable 1	4254.67579	53.0504501	80.2005596	4.2726E-06	4085.84558	4423.506	4085.84558	4423.506

Sample Concentration/On-Column Amount (Inj. Vol.: 5 µL):

20 µM	100 pmol
10 µM	50 pmol
5 µM	25 pmol
2 µM	10 pmol
1 µM	5 pmol

LOD = 3.3*(σ/S), σ=standard error intercept,
S=slope of the regression function

LOD of IP-RP/RP-2D-LC/MS method:
3.3*(546.187813/4254.67579)= 0.4236327
424 nM, 3.07 pg/µL

Figure S19. Calibration of the 2D-LC-MS method with C18 column in the ^{1}D.

Concentration (µM)	Peak Area
20	12958
10	5667
5	2211
2	1002

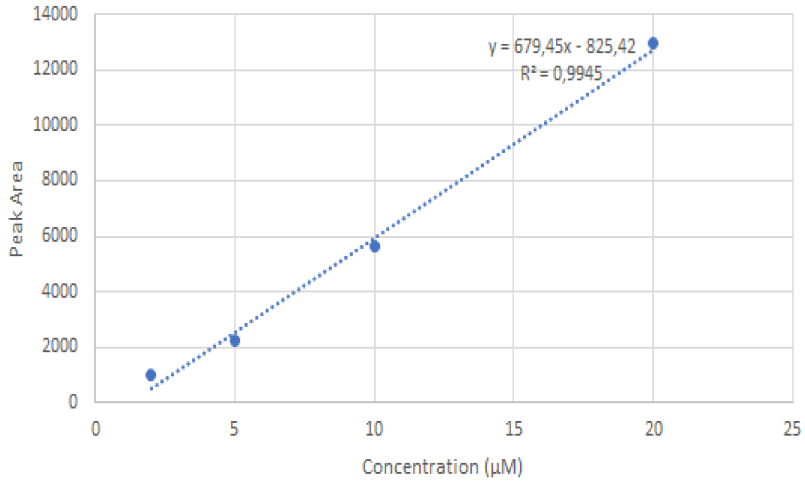

SUMMARY OUTPUT OF THE LINEAR REGRESSION

Regression Statistics	
Multiple R	0.99723492
R Square	0.99447749
Adjusted R Square	0.99171624
Standard Error	489.265133
Observations	4

ANOVA

	df	SS	MS	F	Significance F
Regression	1	86213856.3	86213856.3	360.154243	0.00276508
Residual	2	478760.742	239380.371		
Total	3	86692617			

	Coefficients	Standard Error	t Stat	P-value	Lower 95%	Upper 95%	Lower 95.0%	Upper 95.0%
Intercept	-825.423025	411.729327	-2.00477102	0.18285571	-2596.95134	946.105289	-2596.95134	946.105289
X Variable 1	679.451138	35.8025502	18.9777302	0.00276508	525.405197	833.497078	525.405197	833.497078

Sample Concentration/On-Column Amount (Inj. Vol.: 5 µL):

20 µM	100 pmol
10 µM	50 pmol
5 µM	25 pmol
2 µM	10 pmol

LOD = 3.3*(σ/S), σ=standard error intercept,
S=slope of the regression function

LOD of QN-AX/RP-2D-LC/MS method:
3.3*(411.729327/679.451138)= 1.99971227
1999 nM, 14.16 pg/µL

Figure S20. Calibration of the 2D-LC-MS method with QN-AX column in the ^{1}D.

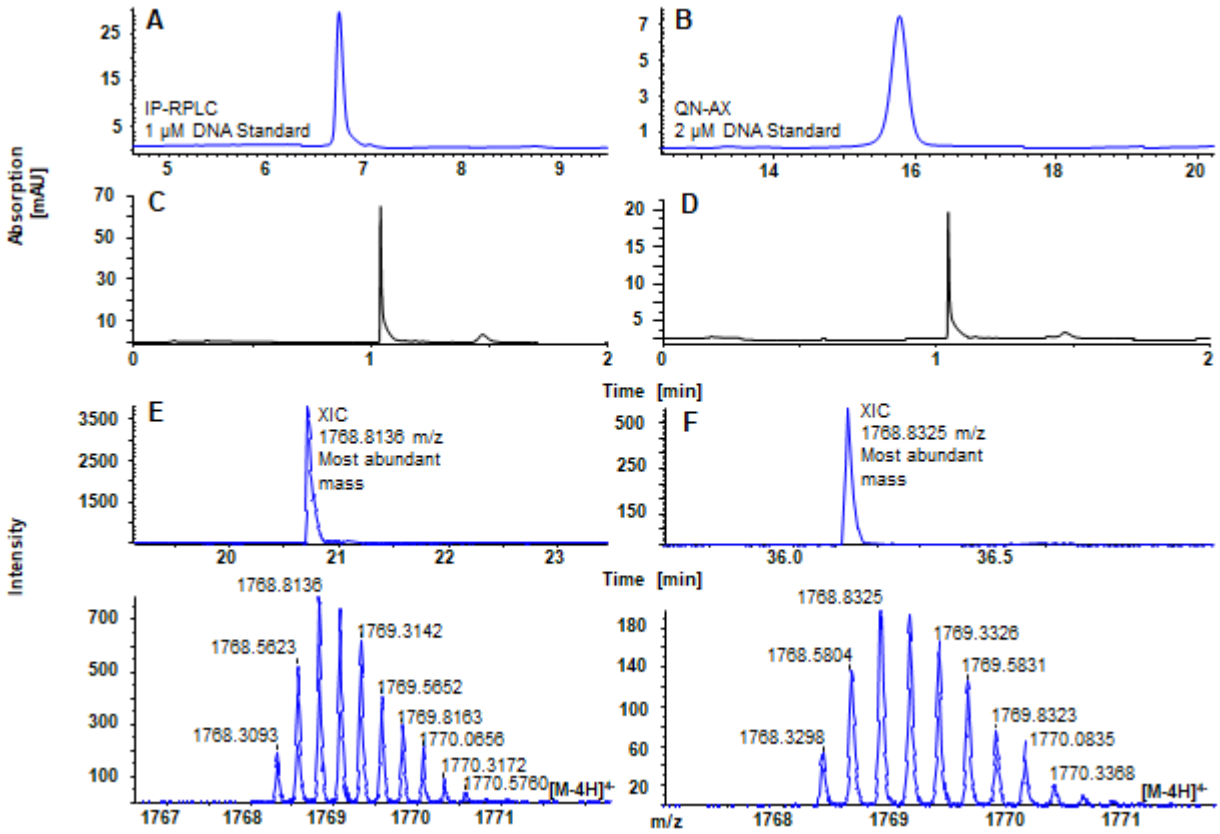

Figure S21. Representative 2D-LC UV chromatograms and results of ESI-MS hyphenation with both methods in ^{1}D for the dilution series of DNA standard. In both cases, only the results with the lowest concentration of injection are illustrated. S/N of (E): 3818; S/N of (F): 433. The injection of 1 µM by IP-RPLC is more than two times above the LOD (424 nM). The injection of 2 µM by QN-AX is almost at LOD (1999 nM).

Concentration (µM)	Peak Area
20	1591
10	757
5	374
2	127
1	64

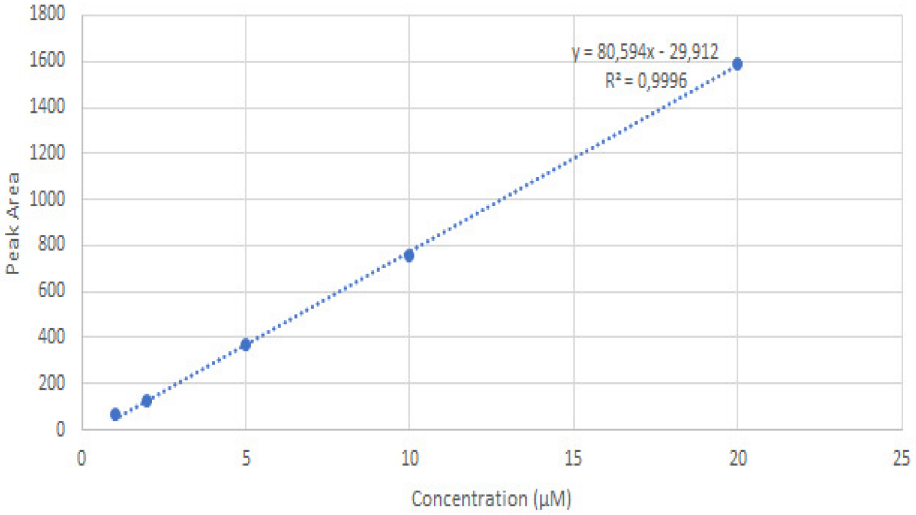

SUMMARY OUTPUT OF THE LINEAR REGRESSION

Regression Statistics	
Multiple R	0.999796
R Square	0.999592
Adjusted R Square	0.999455
Standard Error	14.60802
Observations	5

ANOVA

	df	SS	MS	F	Significance F
Regression	1	1566677	1566677	7341.706	3.5E-06
Residual	3	640.1824	213.3941		
Total	4	1567317			

	Coefficients	Standard Error	t Stat	P-value	Lower 95%	Upper 95%	Lower 95.0%	Upper 95.0%
Intercept	-29.9121	9.684017	-3.08881	0.053764	-60.731	0.906757	-60.731	0.906757
X Variable 1	80.5937	0.940595	85.68376	3.5E-06	77.60031	83.58709	77.60031	83.58709

Sample Concentration/On-Column Amount (Inj. Vol.: 5 µL):

20 µM	100 pmol
10 µM	50 pmol
5 µM	25 pmol
2 µM	10 pmol
1 µM	5 pmol

LOD = 3.3*(σ/S), σ=standard error intercept,
S=slope of the regression function

LOD of IP-RP UV method:
3.3*(9.684017/80.5937)= 0.396523

396 nM, 2.8 pg/µL

Figure S22. Calibration of the [1]D UV method with C18 column.

Concentration (µM)	Peak Area
20	502
10	246
5	113.4
2	44.3
1	22

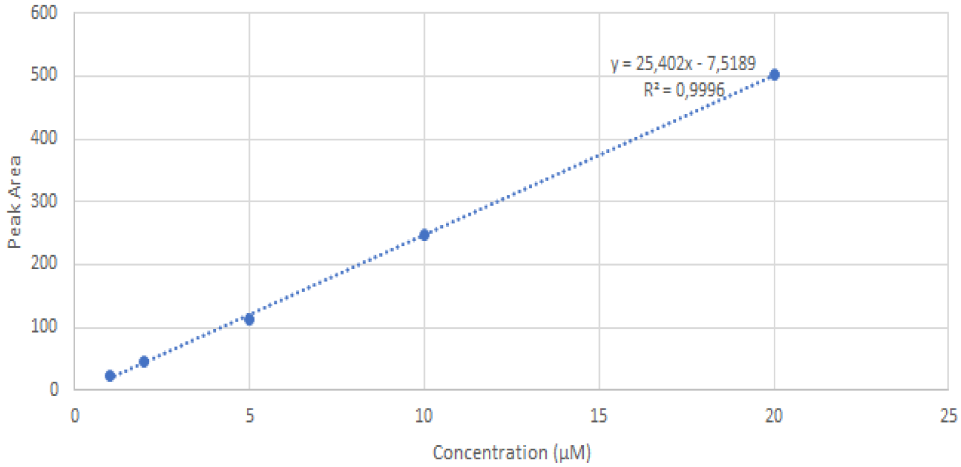

SUMMARY OUTPUT OF THE LINEAR REGRESSION								
Regression Statistics								
Multiple R	0.999815							
R Square	0.999631							
Adjusted R Square	0.999507							
Standard Error	4.37868							
Observations	5							
ANOVA								
	df	SS	MS	F	Significance F			
Regression	1	155643.1	155643.1	8117.895	3.01E-06			
Residual	3	57.51851	19.17284					
Total	4	155700.6						
	Coefficients	Standard Error	t Stat	P-value	Lower 95%	Upper 95%	Lower 95.0%	Upper 95.0%
Intercept	-7.51891	2.902735	-2.59028	0.081054	-16.7567	1.718894	-16.7567	1.718894
X Variable 1	25.40249	0.281939	90.09936	3.01E-06	24.50523	26.29974	24.50523	26.29974

Sample Concentration/On-Column Amount (Inj. Vol.: 5 µL):

20 µM	100 pmol
10 µM	50 pmol
5 µM	25 pmol
2 µM	10 pmol
1 µM	5 pmol

LOD = 3.3*(σ/S), σ=standard error intercept,
S=slope of the regression function

LOD of QN-AX UV method:
3.3*(2.902735/25.40249)= 0.37099
370 nM, 2.62 pg/µL

Figure S23. Calibration of the ^{1}D UV method with QN-AX column.

Name of impurity	Base sequence	Normalized retention time [min] with QN-AX	Normalized retention time [min] with C18
3' ON-5 mer	3' AGGUA 5'	0.415	0.097
3' ON-7 mer	3' U_mAAGGUA 5'	0.514	0.161
3' ON-8 mer	3' AU_mAAGGUA 5'	0.568	0.174
5' ON-8 mer	3' dTdTCAU_mUGG 5'	0.568	0.210
3' ON-9 mer	3' CAU_mAAGGUA 5'	0.568	0.185
5' ON-8 mer	3' dTdTCAU_mUGG 5'	0.589	0.210
3' ON-10 mer	3' UCAU_mAAGGUA 5'	0.589	0.199
5' ON-10 mer	3' dTdTCAU_mUGGU 5'	0.598	0.221
3' ON-11 mer	3' CUCAU_mAAGGUA 5'	0.598	0.210
5' ON-11 mer	3' dTdTCAU_mUGGUUC 5'	0.616	0.237
3' ON-12 mer	3' UCUCAU_mAAGGUA 5'	0.616	0.232
3' ON-14 mer	3' GUUCUCAU_mAAGGUA 5'	0.660	0.237
Onpattro, antisense	3' dTdTCAU_mUGGUUCUCAU_mAAGGUA 5'	0.764	0.285

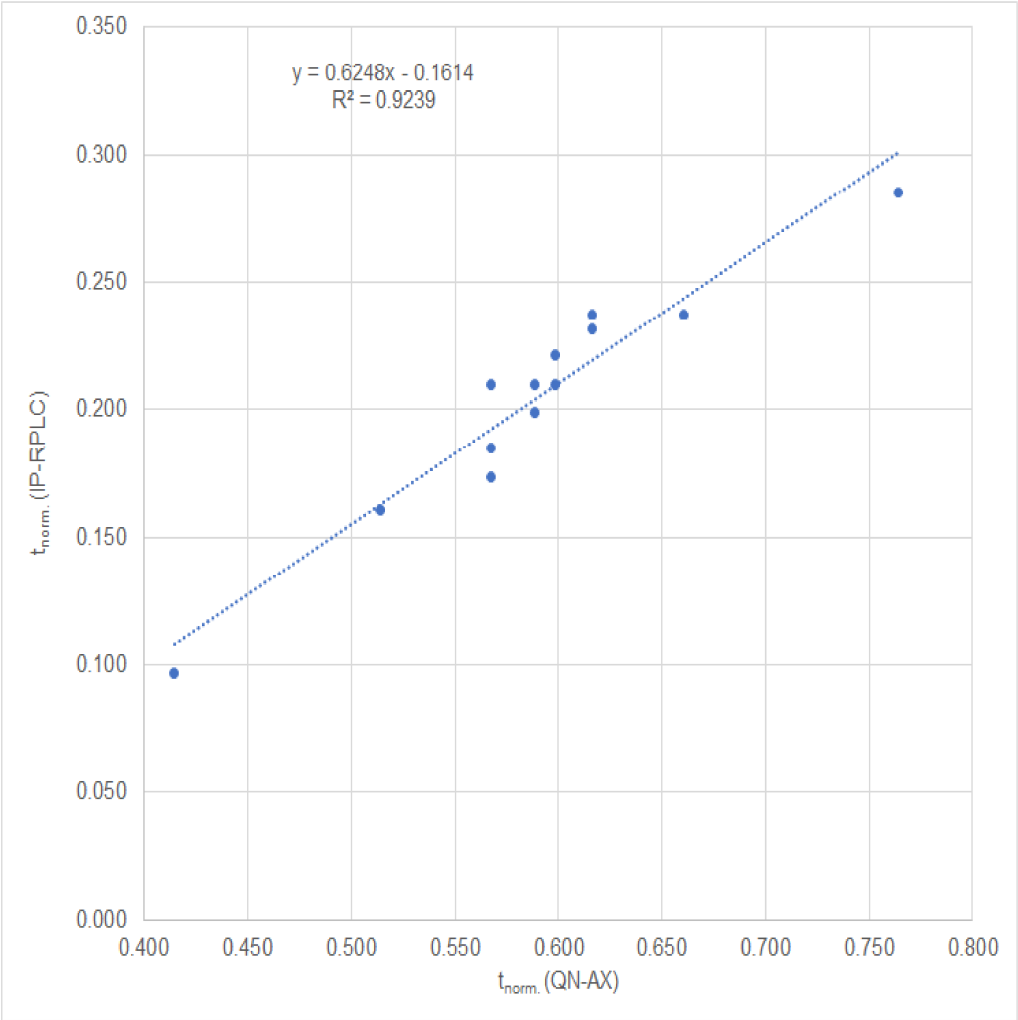

Figure S24. Correlation plot of the normalized time of detected impurity species with both methods.

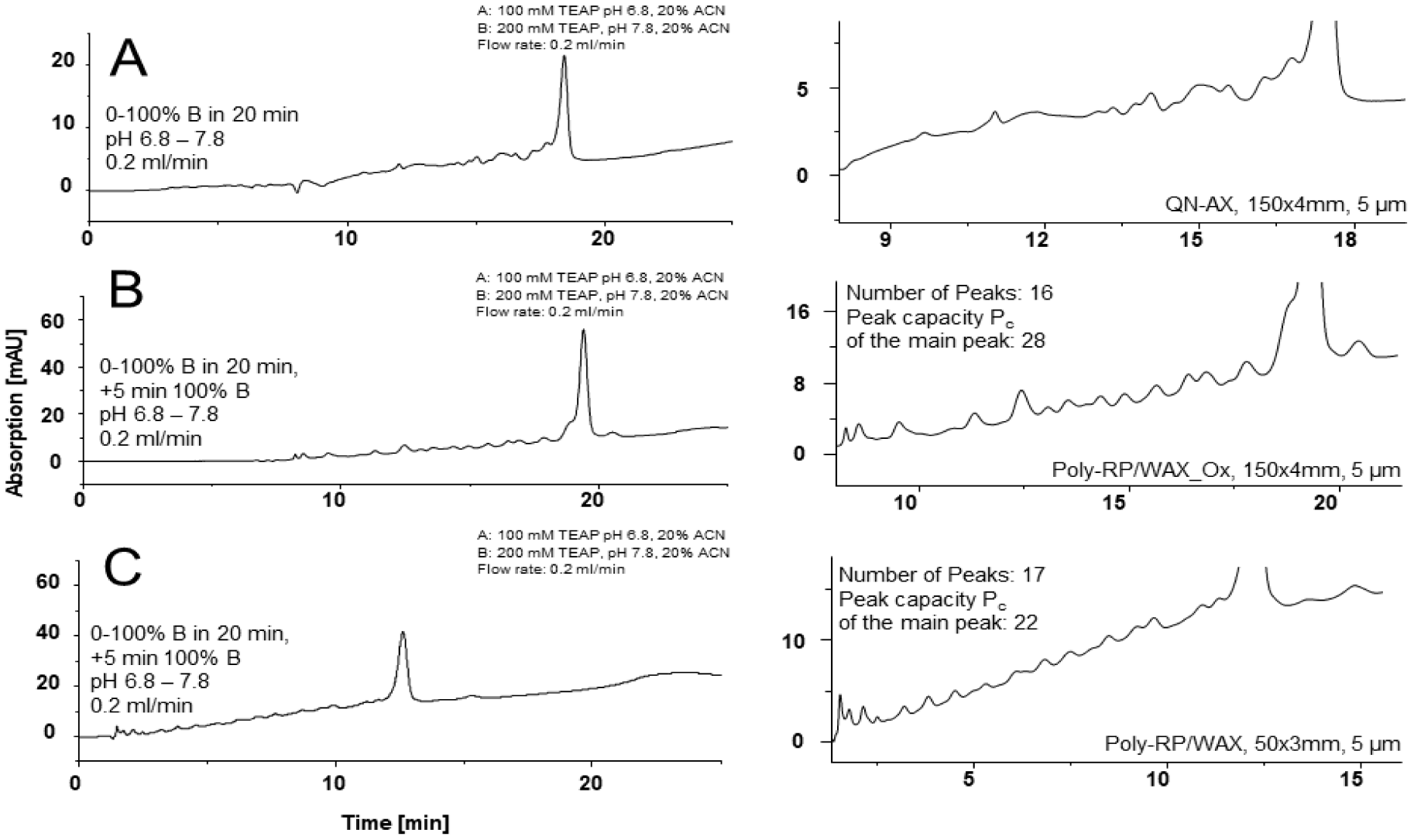

Figure S25. Preliminary experiments with Chiralpak QN-AX (A), Poly-RP/WAX (C) and its oxidized version with sulfonic acid endcappings for ON impurity separation of Patisiran. Identical LC-conditions have been carried out in all 3 experiments. Details see the annotations in the figures.

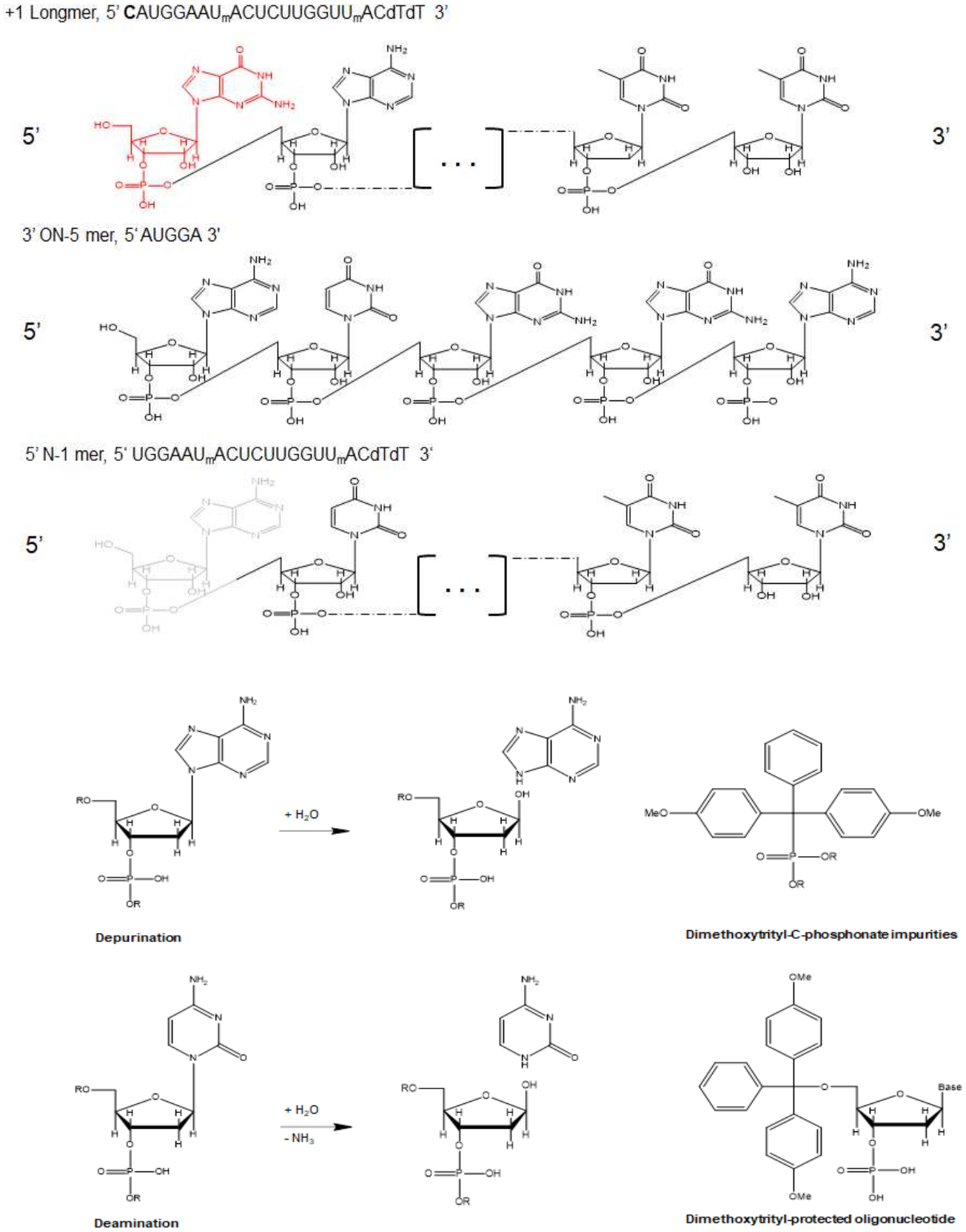

Figure S26. Structures of 3 detected oligo species (also see Table 1). Additionally, the structures of some most commonly impurities showing up in synthetic oligonucleotides are illustrated as below.

3. Publication III

Polybutylene terephthalate-based stationary phase for ion-pair-free reversed-phase liquid chromatography of small interfering RNA. Part 1: Direct coupling with mass spectrometry

Feiyang Li[a], Shenkai Chen[a], Sylwia Studzińska[a,b], Michael Lämmerhofer[a]*

[a] Institute of Pharmaceutical Sciences, Pharmaceutical (Bio-)Analysis, University of Tübingen, Auf der Morgenstelle 8, 72076 Tübingen, Germany

[b] Chair of Environmental Chemistry and Bioanalytics, Faculty of Chemistry, Nicolaus Copernicus University in Torun, 7 Gagarin Str., PL-87-100 Toruń, Poland

*Author for correspondence:

Prof. Dr. Michael Lämmerhofer

Pharmaceutical (Bio-)Analysis

Institute of Pharmaceutical Sciences

University of Tübingen

Auf der Morgenstelle 8

72076 Tübingen, Germany

T +49 7071 29 78793, F +49 7071 29 4565

E-mail: michael.laemmerhofer@uni-tuebingen.de

Journal of Chromatography A

Year 2023, 1694, 463898

DOI: 10.1016/j.chroma.2023.463898

Journal of Chromatography A 1694 (2023) 463898

Contents lists available at ScienceDirect

Journal of Chromatography A

journal homepage: www.elsevier.com/locate/chroma

Polybutylene terephthalate-based stationary phase for ion-pair-free reversed-phase liquid chromatography of small interfering RNA. Part 1: Direct coupling with mass spectrometry

Feiyang Li[a], Shenkai Chen[a], Sylwia Studzińska[a,b], Michael Lämmerhofer[a,*]

[a] Institute of Pharmaceutical Sciences, Pharmaceutical (Bio-)Analysis, University of Tübingen, Auf der Morgenstelle 8, Tübingen 72076, Germany
[b] Chair of Environmental Chemistry and Bioanalytics, Faculty of Chemistry, Nicolaus Copernicus University in Torun, 7 Gagarin Str., Toruń PL-87-100, Poland

ARTICLE INFO

Article history:
Received 22 October 2022
Revised 11 February 2023
Accepted 21 February 2023
Available online 24 February 2023

Keywords:
Oligonucleotide
Small interfering RNA (siRNA)
LC-MS
Patisiran
Impurity profiling

ABSTRACT

Nowadays, ion-pairing reversed-phase liquid chromatography (IP-RPLC) is the dominating generic method for the analysis of nucleic acid related compounds, such as antisense-oligonucleotides (ASO), small-interfering ribonucleic acid (siRNA) or other DNA or RNA type molecules and their conjugates. Despite of its effective performance, the usage of a high concentration of ion-pairing reagent in the eluent in IP-RPLC is unfavorable for the hyphenation with mass spectrometry (MS) which is required for a detailed structural characterization of the analytes and their structurally related impurities. In this work, we tested a polybutylene terephthalate (PBT)-bonded silica-based stationary phase for the separation of generically synthesized Patisiran as siRNA (antisense and sense single strands as well as their annealed double strand) giving some unexpected selectivity without any presence of ion-pairing reagents. Important chromatographic conditions affecting the separation have been investigated and evaluated. Furthermore, MS and tandem MS (MS/MS) characterization was possible without contamination of the MS system with ion-pair agent and related problems.

1. Introduction

Synthetic oligonucleotides, in particular antisense oligonucleotides and small interfering RNA (siRNA), have growing importance as new therapeutic modalities owing to their potential to treat a wide range of different diseases through gene expression regulation [1–3]. According to current regulatory agreements, impurities in drug substance must be controlled down to 0.2% (related to the main target oligonucleotide sequence) which was suggested as reporting threshold based on LOQs of current analytical methods for quality control [4,5]. Due to the high polarity resulting from the ribosyl phosphate backbones oligonucleotides often do not exhibit sufficient retention and selectivity on C18 stationary phases in common reversed-phase liquid chromatography (RPLC) [6], and hence require alkylamines as ion pairing reagent in the mobile phase [7]. To minimize ion-suppression effects in ESI-MS detection resulting from commonly employed triethylammonium acetate Apffel et al. proposed to combine hexafluoroisopropanol (HFIP) with triethylamine (TEA) as mobile phase additives instead to increase MS sensitivity [8] which is now the golden standard [4,5,9]. To further the understanding a variety of systematic studies on IP-RPLC of oligonucleotides and other nucleic acid-based molecules were reported, such as on the impact of pore size on chromatographic performance [10], factors influencing the separation of diastereomers of phosphorothioated oligonucleotides (PSO) [11], the effect of secondary structures on retention [12], variations of ion-pairing reagents and sample dissolution solvents [13,14], and influence of chromatographic conditions like initial organic solvent strength of the gradient, slope of the gradient or buffer concentration [15], influence of electrostatic and non-electrostatic interactions [16], amongst others. These works and the good performance of modern sub-2 µm particle columns paved the way for IP-RPLC as the number one technology in quality control to characterize degradation products of therapeutic oligonucleotides [17], as well as for the separation of siRNA duplexes [18], to separate siRNA from formulation excipients (phospholipids, cholesterol and a short-chain lipid) [19].

In spite of its popularity both in research and industry, drawbacks like ion suppression for some alkylamines, contamination of the ion-source and MS instruments with ion-pair agent, which is particularly detrimental when the instrument is not dedicated to oligonucleotide analysis alone, prompt researchers to develop alternatives [20,21]. Anion-exchange and mixed-mode chromatography have potential from viewpoint of selectivity, yet also rely on MS

* Corresponding author.
E-mail address: michael.laemmerhofer@uni-tuebingen.de (M. Lämmerhofer).

https://doi.org/10.1016/j.chroma.2023.463898
0021-9673/

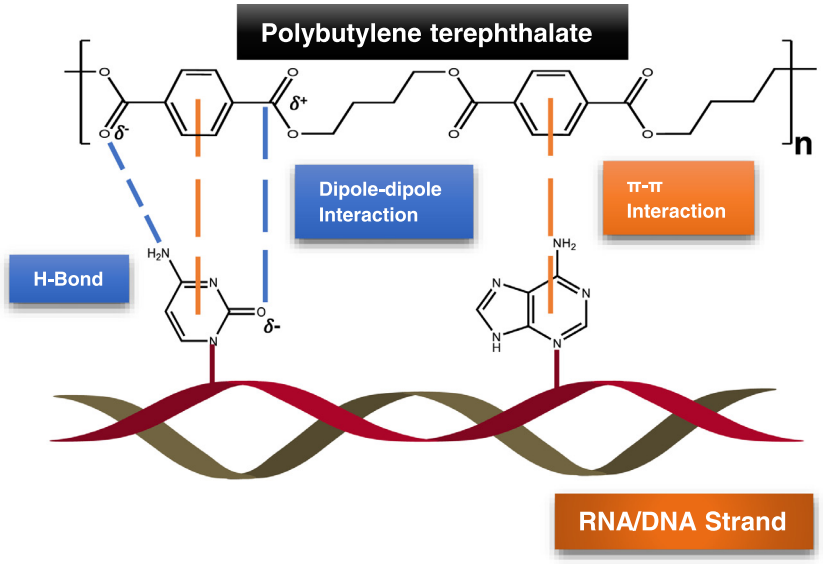

Fig. 1. The selector structure of DCpak PBT and the tentative mechanism for interaction with RNA/DNA.

incompatible eluents (high buffer or salt concentrations) [22–24]. The most promising strategy to avoid ion-pairs in the eluent, is the use of hydrophilic interaction liquid chromatography (HILIC), which showed similar performance in comparison to IP-RPLC by only using ammonium acetate as buffer [25–28]. Although HILIC does not fully reach the same efficiency as IP-RPLC, its ability to build up a water layer on the stationary phase surface that enables polar compounds to partition between this attached water layer and the bulk mobile phase, mixed with other interactions like hydrogen bonding, makes it a good alternative with remarkable selectivity for an ion-pairing free separation of oligonucleotides [5,29–31].

A different strategy to avoid ion-pairing reagents in the ion source while still taking benefit from IP-RPLC is to use two-dimensional liquid chromatography (2D-LC), viz. a second dimension LC (^{2}D) as a "desalting tool" to remove the MS-incompatible involatile buffers or salts from the effluent via a diverter valve [32,33]. In general, 2D-LC [34] has more and more shown its potential to be useful for oligonucleotides analysis, e.g. by combining size exclusion chromatography (SEC), RP and strong anion exchange chromatography (SAX) in ^{1}D with RP in ^{2}D [35], RP in ^{1}D and HILIC in ^{2}D or HILIC in ^{1}D and IP-RP in ^{2}D [36,37]. It allows to combine two selectivity principles overcoming limitations of a single chromatographic mode or column.

The goal of this study, was to evaluate for the first time a polybutylene terephthalate-based stationary phase (DCpak PBT) (see Fig. 1) for its suitability to separate structurally closely related oligonucleotides by RP-LC under typical MS-compatible elution conditions with ammonium formate or acetate buffers, yet completely without ion-pairing agent. This column was originally designed for supercritical fluid chromatography (SFC) and has previously been tested for aromatic compounds like plasticizers and bio-compounds like bee pollen [38,39]. It was, however, never tested for oligonucleotide separations. Owing to its multitude of functional groups, ranging from hydrophobic domains (butylene moiety) over π-π-interaction sites (aromatic phthalate group) to dipole and H-bond acceptor moieties (ester groups), this stationary phase can have a mixed-mode character enabling hydrophilic and aromatic binding increments besides hydrophobic interactions (Fig. 1). This allows to expect complementary selectivities for oligonucleotide impurity profiling. Chromatographic factors were evaluated to elucidate the retention mechanisms and effect of mobile phase conditions. To pursue this goal of retention and selectivity profiling on this PBT stationary phase, the oligonucleotide strands of the small interfering RNA (siRNA) therapeutics Patisiran (Fig. 2A) were used as model test compounds. Patisiran (Tradename: Onpattro, Alnylam Pharmaceuticals, US) which has been approved by the U.S. Food and Drug Administration (FDA) in 2018 is an siRNA therapeutics for the treatment of polyneuropathy in patients with hereditary transthyretin-mediated amyloidosis. In order to increase its stability against enzymatic degradation in human bodies to improve the bioavailability, several nucleotides of the RNA strands are modified by methylation in 2′-position of ribose residues (see Fig. 2A). This siRNA consists of two complementary RNA strands: Antisense (guide) and sense (passenger) strand. During RNA interference, the passenger strand is cleaved by the protein Argonaute 2 (Ago2). Simultaneously, the guide strand is incorporated into the RNA-induced silencing complex (RISC) which binds and degrades the target mRNA [40]. The employed oligonucleotides of this study were custom synthesized single stands of Patisiran which were just desalted after their synthesis, but not purified. The double-strand nucleic acid was obtained by annealing of the non-purified single strands using a published annealing protocol [41]. Hence, these oligonucleotides do not represent a pharmaceutical grade product, but are due to their multiple impurities with nucleotide deletions in their sequences highly suitable to characterize the retention behavior and selectivity of the PBT stationary phase between structurally closely related oligonucleotides. To obtain meaningful data for interpretation of the retention behavior, it was necessary to structurally annotate the oligonucleotide impurities in these single- and double strand oligonucleotides. Thus, the HPLC was directly coupled to electrospray ionization time-of-flight mass spectrometry (ESI-TOF-MS) for this purpose. The complementarity in the retention profiles of the PBT column to other common LC modes (IP-RPLC, HILIC, mixed-mode chromatography) along with their combination in a 2D-LC method will be outlined in a separate study.

2. Experimental

2.1. Chemicals and Patisiran as analyte

Acetic acid (ACS reagent, ≥ 99.8%), ammonium acetate (AA) (LC-MS grade), ammonium formate (AF) (LC-MS grade), ammonium hydroxide (ACS reagent, 28–30%), ethylenediaminetetraacetic

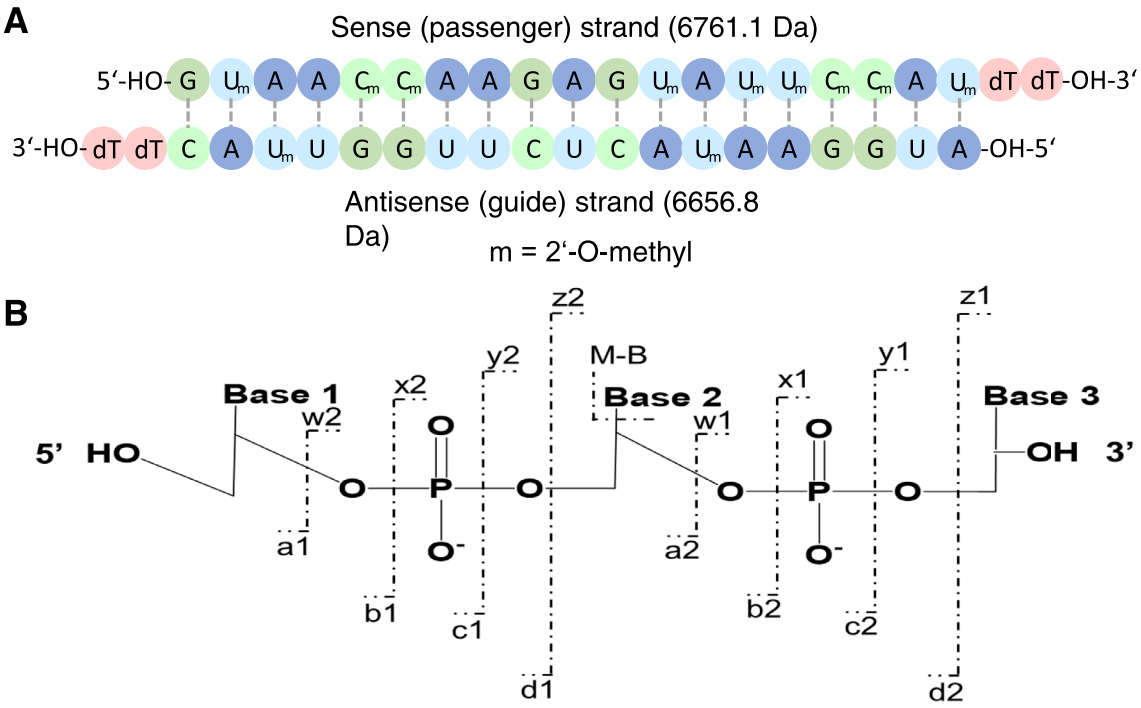

Fig. 2. Structure of the siRNA Patisiran consisting of antisense (guide) and sense (passenger) strand (A) and nomenclature of oligonucleotide fragmentation according to McLuckey (B).

acid (EDTA) (ACS reagent 99.4%, powder), Tris base (BioUltra grade, ≥99.8%) and sodium chloride (≥99%) were purchased from Sigma-Aldrich (Merck, Munich, Germany). HPLC-MS grade methanol (MeOH) and acetonitrile (ACN) were purchased from Carl Roth (Karlsruhe, Germany). Ultrapure water was obtained by treatment of deionized water with Elga PurLab Ultra purification system (Celle, Germany).

The structure of Patisiran is shown in Fig. 2. For this study, both passenger (sense, see Fig. 2) and guide strand (antisense, see Fig. 2) of Patisiran were custom synthesized by Oligo Sigma (Merck, Munich, Germany) and purchased as separate single strands. Both single RNA strands were obtained as desalted raw products without any further purification. The double stranded siRNA sample was obtained by annealing of equimolar amounts of the two single strands, non-purified RNA oligonucleotide raw products using a protocol described below. For this reason, these analytical standards can only be considered as model test substances for method development but do not represent pharmaceutical grade APIs of Patisiran as present in real pharmaceutical products. For better understanding, we will keep using the terminology sense/antisense for the upcoming discussions.

2.2. Stationary phase

The column tested in this work, the Daicel polybutylene terephthalate-bonded silica-based DCpak PBT column (150 × 3.0 mm, 3 µm particle size) for ion-pair-free RPLC was provided by Chiral Technologies (Illkirch, France) (other parameters like ligand density, pore size and carbon load are not disclosed by the manufacturer).

2.3. Sample preparation

An aqueous stock solution of antisense and sense strand with a concentration of 100 µM was prepared and stored under 4 °C until use. For all experiments, the final concentration was 50 µM. For the annealing of the complementary strands, a buffer consisting of 10 mM TRIS (pH 7.5–8.0), 50 mM NaCl and 1 mM EDTA was used. Equal volumes of equimolar antisense and sense strand were mixed in a microtube which was then incubated at 95 °C for 5 min. After that, the tube was allowed to slowly cool down to room temperature for 60 min.

2.4. Instrumentation

LC experiments were performed with an Agilent 1290 Infinity II UHPLC system from Agilent Technologies (Waldbronn, Germany) equipped with Multisampler (G4226A), binary Pump (G4220A), column compartment (G1316C) and Diode Array Detector (DAD) (G4212A). Additionally, both column compartment and multisampler were equipped with the Ultra-Low Dispersion Kit (5067–5963).

MS detection was performed on a SCIEX TripleTOF 5600+ QTOF mass spectrometer with a Duospray ion source operated in negative ESI mode. The MS instrument was controlled with Analyst TF 1.7 software (AB SCIEX, Darmstadt, Germany).

2.5. LC-MS conditions

In this subchapter, the final optimized LC conditions are described. For LC conditions during the optimization studies, please see the corresponding figure captions.

All pH values applied in this study were adjusted as follows: The electrode system was calibrated with standard aqueous buffers which were commercially available. The pH was measured and adjusted in the aqueous buffer ($^{w}_{w}$pH) before mixing it with the organic solvent (note, minor shifts in pH and pK_a scale result from the organic solvent) However, the mobile phase pH values reported herein always refer to $^{w}_{w}$pH [42]. As discussed by Schoenmaker et al., this pre-adjustment of pH before mixing with organic is more practical [43,44].

In case of ion-pair-free RP-LC with DCpak PBT (150 × 3 mm, 3 µm), a linear gradient of methanol (MeOH) as organic modifier was used. Mobile phase A (MPA) was composed of water with 20 mM ammonium formate (AF), $^{w}_{w}$pH 6.3. Mobile phase B (MPB) consisted of MeOH/water 9:1 (v/v), 20 mM AF, $^{w}_{w}$pH 6.3. For further pH studies, $^{w}_{w}$pH 3.7 and $^{w}_{w}$pH 4.7 were also adjusted for both MPA and MPB as described above. The following gradient profile was applied: 10–45% MPB in 28 min followed by 15 min re-equilibration. Temperature: 40 °C. Flow rate: 0.6 ml/min.

MS detection was carried out in negative polarity mode with an ESI source. The MS parameters for nebulizer gas, heater gas, curtain gas, source temperature, ion spray voltage, declustering potential and collision energy were set as follows: 90 psi, 90 psi, 35 psi, 550 °C, 4500 V in all experiments, 200 V, −10 V for TOF-MS and −35 V for MS/MS in all experiments. Mass (*m/z*) range of MS^1 experiments were from 100 to 2000. MS^2 data was generated by information dependent acquisition (IDA) mode (with one MS full scan experiment followed by four MS^2 experiments with an accumulation time of 200 ms each). The precursor isolation was set from 200 to 1250 *m/z*.

2.6. Software and data processing

The data processing was accomplished by using PeakView (AB Sciex, Darmstadt, Germany), basic data explorer in Sciex systems, and supported by RoboOligo [45]. Another software package called OPA/OMA developed for a semi-automated analysis of oligonucleotide fragmentation was used as well [46]. The identification of impurities was performed by assigning charge states of ions observed in the full scan spectra. Next, spectral deconvolution was executed (BioTool Kit, AB Sciex, Darmstadt, Germany) for the determination of molecular mass of various oligonucleotide species. For the deconvolution, BioTool Kit of Sciex collected all detected charge states within the MS spectra and calculated every possible molecular mass of the target species from the charge envelope. In a consecutive process, incorrect mass signals will become weaker and eventually, only the correctly deconvoluted mass remains. The input parameter for the deconvolution with BioTool Kit were set as follows: start *m/z*: 200, stop *m/z*: 2000, output mass range: 1000–7000 Da, input spectrum isotope resolution: 30,000 (maximal value). The sequence was identified with the use of free RoboOligo program. RoboOligo is able to execute automated sequencing using MS/MS data. For this purpose, the algorithm of RoboOligo is designed attempting to match expected product ions beginning with 5′-terminus. For detailed information see ref. [45]. After the sequence was firstly determined with the help of RoboOligo, the suggested sequence of the oligonucleotide was reanalyzed by OPA/OMA software package. OPA/OMA can create a databank containing all possible fragments of known sequences. With this supporting function, the tentative sequence suggested by RoboOligo was verified comparing the measured MS/MS data with the generated databank [46]. Additional confirmation was always performed by the extracted ion chromatograms (EIC). All masses and *m/z* values reported in this manuscript are experimental values. A comparison of theoretical and experimental *m/z* values along with mass errors are given in Suppl. Table S1 and S2.

3. Results and discussion

3.1. Ion-pair-free RP chromatography with polybutylene terephthalate-based column

To avoid problems originating from the use of ion-pairing agents the goal of this study was to find a stationary phase which gives sufficient retention and selectivity of structurally related oligonucleotides by RPLC without ion-pair reagents in the mobile phase. A recently developed dedicated SFC column DCpak PBT which is a silica-based stationary phase with polybutylene terephthalate coating (Fig. 1) was considered promising due to its expected stability and multitude of interaction modes. Due to its mixed-mode character with aromatic, hydrophobic and dipole interaction sites (see Fig. 1), stronger retentivity compared to C18 phases, in particular when operated with methanol as organic modifier, and altered selectivity was envisaged. Preliminary tests with the siRNA single strands confirmed the assumptions and therefore the chromatographic conditions were further optimized as discussed in this chapter.

3.1.1. Organic modifier

In the first gradient elution screening experiments, both acetonitrile and methanol were tested as organic modifiers (Fig. S1). With ACN, antisense and sense strands as well as ds-siRNA (annealed) eluted close to the void of the column or even slightly before (Fig. S1A). On contrary, both single strands were well retained with MeOH as organic modifier (Fig. S1B). Evidently, the elution strength of ACN is greater compared to MeOH, as expected. ACN efficiently disrupts both π-π interactions and hydrophobic interactions between oligonucleotides and the PBT-based stationary phase. As a consequence, the studied oligonucleotides and their impurities were not retained on the PBT-modified stationary phase surface under these RP conditions [47]. For this reason, MeOH is recommended for phenyl-type phases and was used as organic modifier in further screening experiments (Fig. S1B). Notably, symmetrical peaks were observed for antisense and sense strand, and some impurities were efficiently resolved from the main peak within 12 min run time. The annealed duplex was still eluted with t_0.

3.1.2. Salt type and concentration

Next, the impact of salt type and its concentration has been investigated in gradient elution with MeOH. For this purpose, ammonium acetate (AA) and ammonium formate (AF) with increasing concentrations (10/20/40 mM) were used and compared (pH unadjusted) (Fig. 3). It can be seen that AA has slightly higher elution strength compared to AF, as a consequence of the differences in the nature of acetate and formate ions [29]. In general, compared to AA (Fig. 3A), the mobile phase with AF provides an improved resolution power. Especially the shortmer species eluting next to the main peak are better separated by using AF as salt (Fig. 3B). It is further striking that with increasing salt concentration, the retention time of the siRNA strands increased leading to sharper peaks and better resolution. This observed trend might be explained by reduction of the solubility of oligonucleotides and strengthening of their hydrophobic interactions with the surface of the stationary phase (possibly due to a kind of salting out effect). At the same time, effective ionic shielding by formation of an ion cloud of ammonium ions around negatively charged silanol groups as well as phosphate groups (in oligonucleotide structure) may occur diminishing repulsive electrostatic interactions between oligonucleotides and silanols [29]. For both AA and AF, lower salt concentration (e.g. 10 mM) causes peak broadening and tailing leading to lower resolution. With 40 mM, both selectivity and efficiency are improved for both AF and AA. However, as a compromise considering the hyphenation with ESI-MS, 20 mM AF was the final salt concentration for further LC-MS experiments.

3.1.3. pH value

For more details about pH adjustment, please review chapter 2.5. The mobile phase pH plays an important role for the chro-

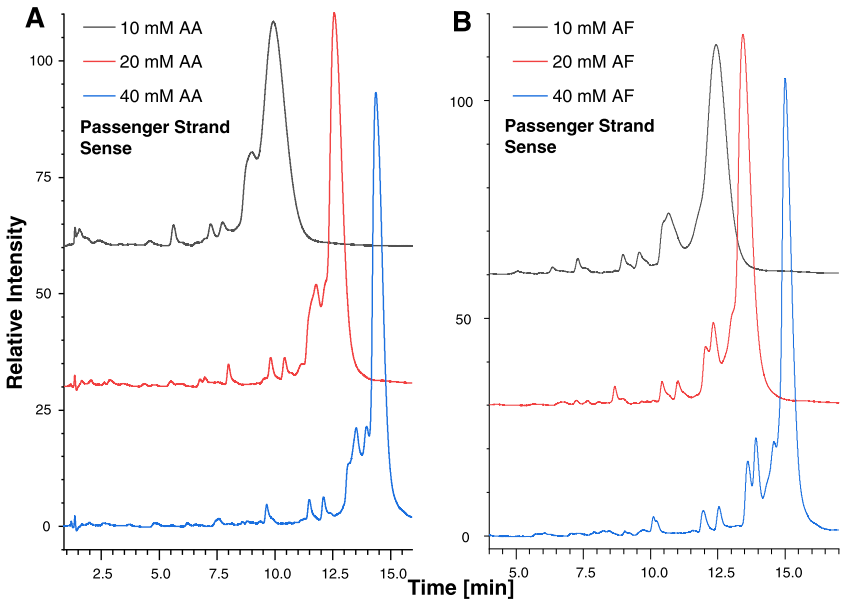

Fig. 3. RPLC-UV chromatograms of sense (passenger) strand with DCPak® PBT using (A) ammonium acetate (AA) and (B) ammonium formate (AF). The salt concentration was increased from 10 to 40 mM. LC–Conditions (A): MPA: water,10/20/40 mM AA, $^{w}_{w}$pH 6.8; MPB: MeOH/water 9:1 (v/v),10/20/40 mM AA ($^{w}_{w}$pH 6.8 of the aqueous fraction); Gradient: 10%–100% MPB in 30 min; Temperature: 40 °C; Flow rate: 0.6 ml/min. LC–Conditions (B): MPA: water, 10/20/40 mM AA, $^{w}_{w}$pH 6.8; MPB: MeOH/water 9:1 (v/v), 10/20/40 mM AA ($^{w}_{w}$pH 6.8 of the aqueous fraction); Gradient: 10%–45% MPB in 20 min; Temperature: 40 °C; Flow rate: 0.6 ml/min.

matographic performance of ionic substances. Hence, some experiments investigating its influence on the separation were carried out. In the test series with regard to AF as salt and its concentration, the $^{w}_{w}$pH was 6.3 without any further adjustment. As AF has a buffer range between 2.7–4.7, we also tested various pH values (3.7, 4.7). Besides, also a $^{w}_{w}$pH gradient from 4.7 (in channel A) to 6.3 (in channel B) superimposed over a modifier (MeOH) gradient was evaluated (see Fig. S2). At $^{w}_{w}$pH 4.7 and lower, oligonucleotides were not eluted within reasonable time. We suppose that this effect is due to the partial protonation of residual silanols at the stationary phase surface occurring under acidic pH and reducing electrostatic repulsion between tested compounds and support, typically occurring at higher $^{w}_{w}$pH. This effect may be also connected to the protonation of some of the nucleobases at pH below 4 (e.g. cytosine), leading possibly to stronger interaction with silanols. On the contrary, at $^{w}_{w}$pH 6.3 (non-adjusted 20 mM AF), silanol groups are more negatively charged causing repulsive electrostatic interactions with oligonucleotides resulting in their elution as reasonably well shaped peaks (Fig. S2, black trace). A $^{w}_{w}$pH gradient from 4.7 until 6.3 indeed significantly increased the retention of the oligonucleotides as compared to isocratic separation at $^{w}_{w}$pH 6.3 yet enabled their elution (Fig. S2, green trace). However, strong tailing of the main peak makes such elution conditions less attractive.

For 20 mM AA, the non-adjusted $^{w}_{w}$pH was 6.8 in channel A. The negatively charged silanols on the stationary phase surface are not efficiently shielded causing electrostatic repulsion between the oligonucleotides and the stationary phase surface. This repulsive interaction may partly compensate the contribution of hydrophobic and π-π interactions leading to efficient elution of the oligonucleotides under these conditions. When the $^{w}_{w}$pH was decreased to 5, the ionization of the silanol groups was reduced, and interaction of the oligonucleotide with the PBT bonding reinforced leading to stronger retention, at expense of chromatographic efficiencies (Fig. S3). Since impurities are present in oligonucleotide samples at low concentration levels, broad peaks deteriorate their detection limits for which reason unadjusted AF or AA based mobile phases were continued to be used.

3.2. Structural annotation of impurities of Patisiran single strand and annealed oligonucleotides with polybutylene terephthalate-based column under ion-pairing free RP mode

During oligonucleotide synthesis, a series of impurities may be formed [48]. Caused by coupling failures, impurity species which lack one or more nucleotides (e.g. N-1, N-2 shortmers, etc.) are obtained. In these shortmers, nucleotides can be missing on both 3′ and 5′ ends, depending on the mechanism of formation [48,49]. Besides, synthetic oligonucleotides may be contaminated by other structurally closely related synthesis by-products. Hence, a non-purified synthesis raw product as used herein was considered a suitable test sample for new stationary phases for evaluation of their retention increments and selectivity. However, the retention profiling to characterize the new PBT stationary phase would be relatively meaningless if the structure of the components is not known. This is particularly true for meaningful column comparisons and retention correlations between two stationary phases which relies on knowledge of the structures of the chromatographic probes, like herein the non-purified Patisiran single and double strand oligonucleotide impurities. Along this line, LC-ESI-QTOF-MS was employed to structurally annotate the separated impurity peaks.

In this study, the ion-pairing free RP chromatography with DC-pak PBT and optimized conditions was able to separate a remarkable series of different impurity species of Patisiran single strands and annealed product (see Fig. 4). Without the presence of ion-pairing agent, a direct coupling with ESI-TOF-MS was unproblematic enabling the straightforward characterization of the separated impurity species. Usually, the MS spectra of oligonucleotides show a series of multiple deprotonated molecular species $[M\text{-}nH]^{n-}$ resulting in a multiple charge state distribution [9]. Herein, with PBT column in RP mode, we observed only ions of two charge states in the full scan spectra and no wider charge envelope. Presumably, for these low abundant impurities only the most abundant charge states were above the LOD. Multiple charge states were only found for the main compound (antisense or sense) owing to their higher concentration. Nonetheless, identification of impurities was still

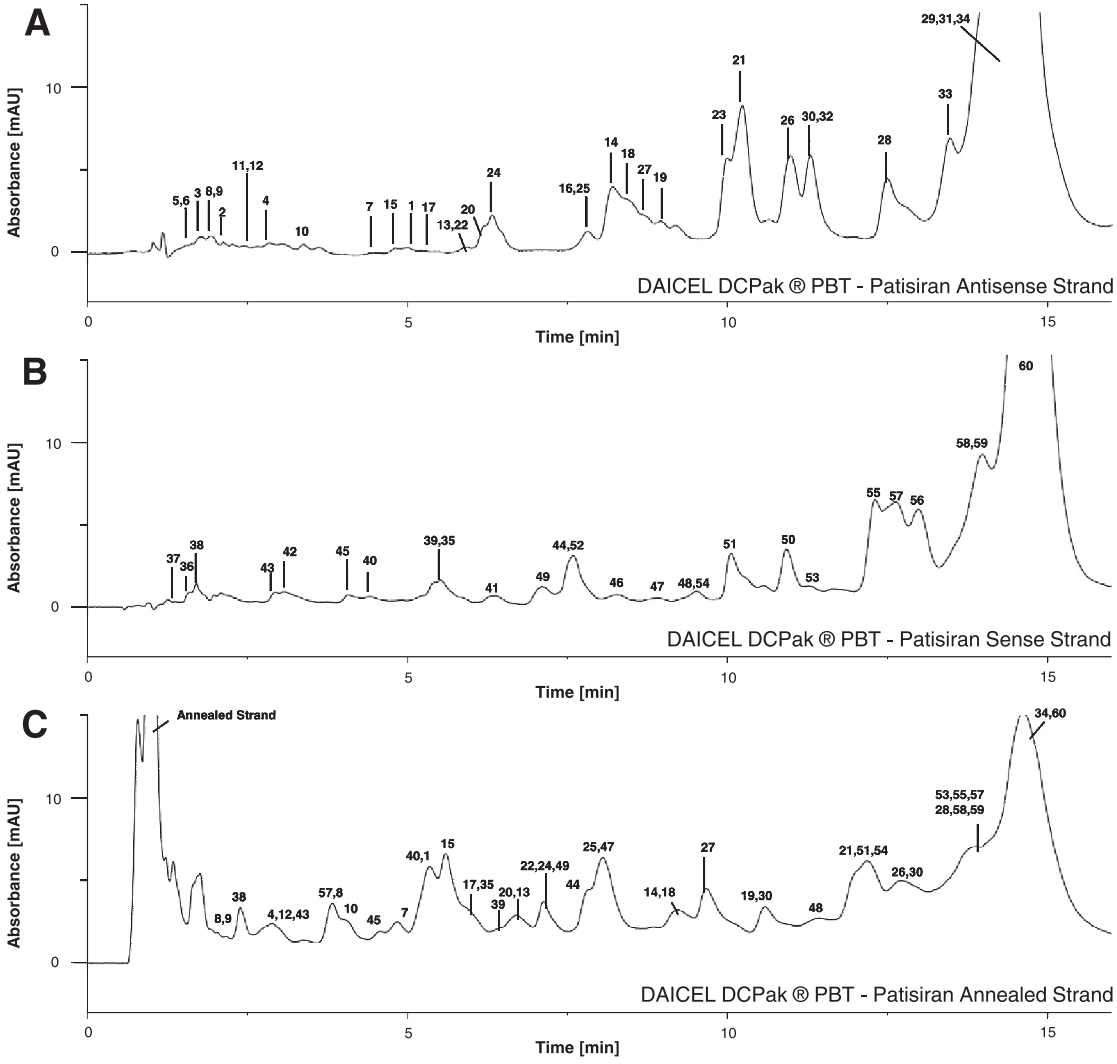

Fig. 4. RPLC-UV chromatograms of Patisiran antisense (guide) strand (A), sense (passenger) strand (B), and annealed siRNA duplex (C) on DCPak® PBT column. The detected peaks have been characterized by ESI-TOF-MS. For compound list see Table 1, 2 and S1. LC–Conditions (A-C): MPA: water, 20 mM AF, $^{w}_{w}$pH 6.3; MPB: MeOH/water 9:1 (v/v), 20 mM AF ($^{w}_{w}$pH 6.3 of the aqueous fraction); Gradient: 10%–45% MPB in 28 min; Temperature: 40 °C; Flow rate: 0.6 ml/min. For MS parameters see chapter 2.4.

possible due to charge state assignment and successful software-supported deconvolution. Additionally, the tentative determination of the oligonucleotide sequences was supported by different software packages [45,46].

3.2.1. Antisense (guide) strand

For rationalizing the retention mechanism on the PBT column, the oligonucleotide impurity peaks were first structurally annotated using MS^1 and MS^2 data (see Fig. 5 for exemplary results). All extracted ion chromatograms (EIC) of the monoisotopic mass of the most abundant charge state show reasonable peak shape (exemplified in Fig. 5A–C), yet early eluted peaks are a bit broader as they seem to be insufficiently refocused. It is also important to point out that those impurity species with an additional phosphate group (Np) at the 3′ end show broader peaks due to stronger polar interaction and/or metal surface interactions with column hardware. We observed previously that the charge state of the most abundant precursor ions of the impurity species of Patisiran (antisense) increases with higher molecular mass [33]. In this work, this trend can be confirmed (see Table S1). Small oligonucleotides like the 2-mer 5′-dTdT-OH-3′ exists in charge state 1- of the ion type $[M\text{-}H]^{1-}$ and no significant alkali cation adducts (Fig. 5D). For the longer oligonucleotides, besides the major adduct $[M\text{-}nH]^{n-}$ other alkali cation adducts were also detected (Fig. 5E and F) [9,50]. This follows the expected trends, since the degree of alkali cation adduction increases with the length of the oligonucleotides [9,51]. Information-dependent acquisition (IDA) based MS^2 experiments were also conducted to verify the suggested structure of the detected species. Different fragment ions were detected (Fig. 5G–I) and characterized using terminology as suggested by McLuckey et al. (see Fig. 2B) [52,53]. Fragmentation of the phosphodiester bond occurred from both 3′ - (w, x, y, z-fragments) and 5′ end (a, b, c, d-fragments). Partly, base cleavage also took place (e.g. Fig. 5G and I) as a result of collision induced dissociation. This way impurities could be confidently annotated using RoboOligo and OMA/OPA as described in the experimental section.

In total, 33 different impurity species could be detected by ESI-TOF-MS with PBT-RPLC (see Table 1). In general, 4 distinct structural variables can be distinguished in the oligonucleotides: (i) oligonucleotide length due to different number of deletions), (ii) base sequence (through 5′ and 3′ nucleotide deletions; coupling failure products with missing nucleotides on both 3′ and 5′ were present), (iii) 2′-modifications (hydroxyl, methoxy and hydrogen for 2nt-overhang), and (iv) 3′-end modifications. At the 3′ end, the oligonucleotides possess either a hydroxy end (OH), a phosphate end (Np) or a 2′,3′–cyclic phosphodiester end (cyc) [54]. Ba-

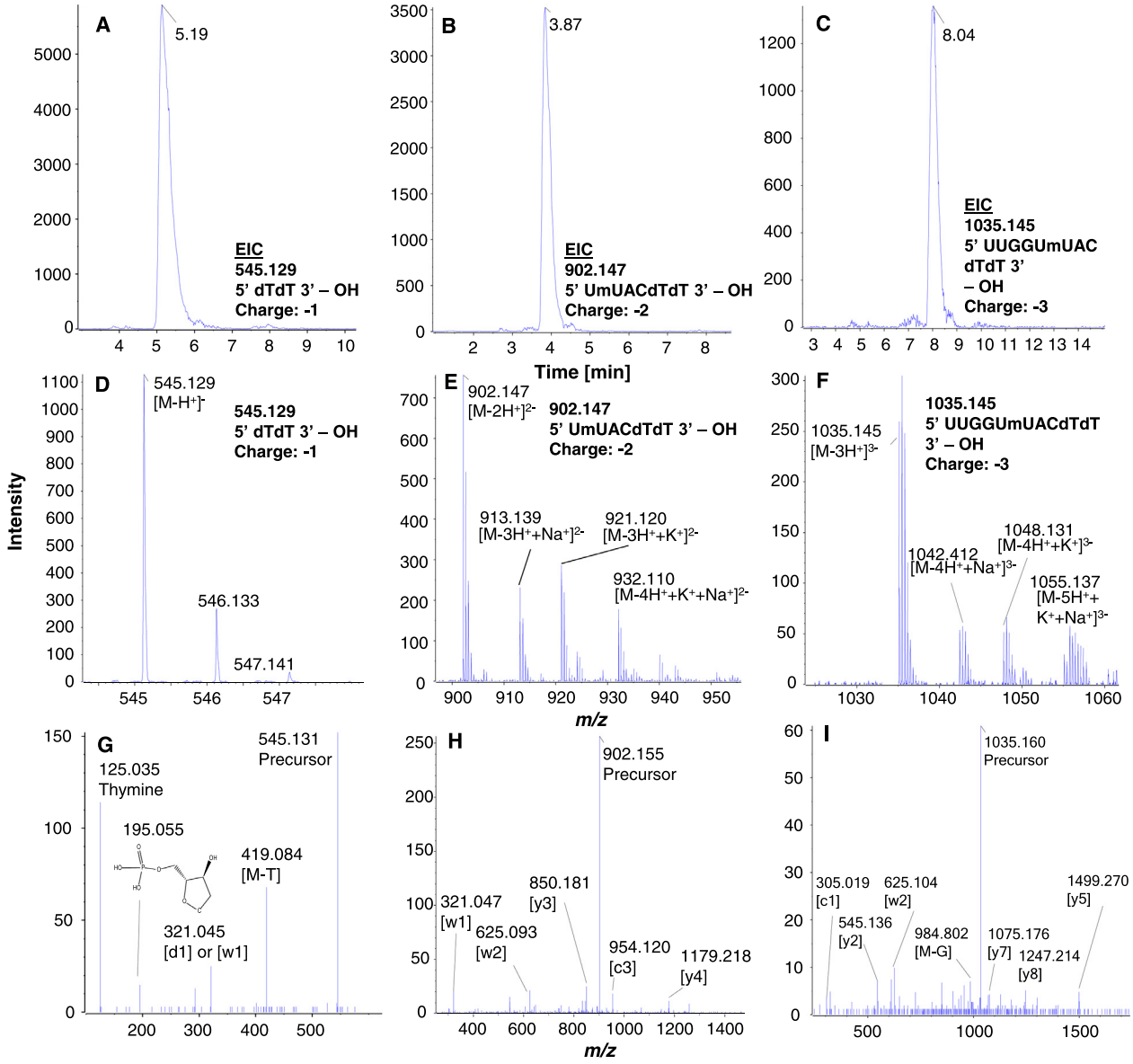

Fig. 5. RP-LC-derived MS^1 and MS^2 spectra and extracted ion chromatogram (EIC) of selected impurity species from antisense strand of Patisiran. (A-C): Extracted ion chromatograms of the monoisotopic mass of the most abundant charge states. (D-F): MS^1 spectra of impurity species with the most abundant charge states. (G-I): MS^2 spectra of the corresponding precursor ion. For MS-conditions see chapter 2.4.

sically, the detected impurity species can be divided into 3 subgroups according to these structural peculiarities: (i) a 3→5′ impurity series with nucleotide deletions at the 5′-end and a free 3′-OH (3′-OH end), (ii) a 5→3′ impurity series with nucleotide deletions at the 3′-end and a phosphorylated 3′-end (3′-Np end), and (iii) a corresponding 5′→3′ impurity series in which the 3′-Np end is converted to a 2′,3′-cyclic phosphodiester bond (3′-cyc end) (see Fig. 6A).Within each series retention increases with each additional nucleotide, yet not by equal retention increments for different nucleotides, as expected due to distinct base hydrophobicity (C<G<*A*<*T*/U according to [15]). There are a few negative retention shifts, though, with additional nucleotide e.g. from 2-mer to 3-mer of 3-OH-end series (switch from deoxynucleotide sequence to ribonucleotide series), from 3-mer to 4-mer (U after mU), from 6-mer to 7-mer (U after G), 10-mer to 11-mer (C after U), 15-mer to 16-mer (U after G). They cannot be explained by the hydrophobicity of the bases alone. The stronger retention for the 5′−2-mer-OH (5′-dTdT-OH-3′) compared to the 5′−3-mer-OH (5′-CdTdT-OH-3′) can be explained by its deoxy-ribonucleotides, in which a hydrogen atom instead of a hydroxyl group in 2′-position results in lower polarity and thus potentially stronger hydrophobic interactions with the surface of the stationary phase. It is interesting to mention that those negative shifts in retention mostly occur when the sequence is expanded by either U or C (vide infra).

3.2.2. Sense (passenger) strand

For the sense strand, the ESI-TOF-MS measurement was capable to distinguish 25 impurity species (see Table 2). The general pattern of impurities did not change in comparison to the antisense strand, as expected. Again, three subgroups of shortmer impurities considering their deletions from either the 5′ or 3′ end and different 3′ ends (Np and cyc), respectively, were detected (vide supra) (Fig. 6B). Exemplary chromatograms of impurities with different length are depicted in Fig. 7A–C along with their MS^1 (Fig. 7D–F) and MS^2 spectra (Fig. 7G–I). The retention behavior of the analysed species (Fig. 6B, Table S2) is following similar trends as described above.

Table 1
Overview of the Patisiran antisense (guide) strand impurities detected by RP-LC-MS (sorted in order of increasing mass [Da], t_R in minute).

Name	Sequence	Deconvoluted mass	Peak No. Fig. 4	t_R RP
5′ 2mer - OH	5′ dTdT 3′ - OH	546.129	1	5.19
3′ 2mer - cyc	5′ AU 3′ - cyc	635.071	2	2.03
3′ 2mer - Np	5′ AU 3′ - Np	653.082	3	1.79
5′ 3mer - OH	5′ CdTdT 3′ - OH	851.170	4	2.78
3′ 3mer - cyc	5′ AUG 3′ - cyc	980.118	5	1.61
3′ 3mer - Np	5′ AUG 3′ - Np	998.135	6	1.51
5′ 5mer - OH	5′ mUACdTdT 3′ - OH	1501.257	7	4.24
3′ 5mer - cyc	5′ AUGGA 3′ - cyc	1654.209	8	1.94
3′ 5mer - Np	5′ AUGGA 3′ - Np	1672.221	9	1.82
5′ 6mer - OH	5′ UmUACdTdT 3′ - OH	1806.282	10	3.87
3′ 6mer - cyc	5′ AUGGAA 3′ - cyc	1983.260	11	2.53
3′ 6mer - Np	5′ AUGGAA 3′ - Np	2001.264	12	2.53
5′ 7mer - OH	5′ GUmUACdTdT 3′ - OH	2151.330	13	5.58
5′ 8mer - OH	5′ GGUmUACdTdT 3′ - OH	2496.368	14	7.91
3′ 8mer - Np	5′ AUGGAAmUA 3′ - Np	2650.364	15	4.99
5′ 9mer - OH	5′ UGGUmUACdTdT 3′ - OH	2802.396	16	7.66
3′ 9mer - Np	5′ AUGGAAmUAC 3′ - Np	2955.407	17	5.28
5′ 10mer - OH	5′ UUGGUmUACdTdT 3′ - OH	3108.418	18	8.04
5′ 11mer - OH	5′ CUUGGUmUACdTdT 3′ - OH	3413.459	19	8.90
3′ 11mer - Np	5′ AUGGAAmUACUC 3′ - Np	3566.466	20	5.52
5′ 12mer - OH	5′ UCUUGGUmUACdTdT 3′-OH	3719.470	21	9.42
3′ 12mer - Np	5′ AUGGAAmUACUCU 3′ - Np	3873.496	22	5.85
5′ 13mer - OH	5′ CUCUUGGUmUACdTdT 3′ - OH	4024.528	23	9.08
3′ 13mer - Np	5′ AUGGAAmUACUCUU 3′ - Np	4178.519	24	6.46
3′ 14mer - Np	5′ AUGGAAmUACUCUUG 3′ - Np	4523.570	25	7.60
5′ 15mer - OH	5′ mUACUCUUGGUmUACdTdT 3′ - OH	4673.609	26	11.08
3′ 15mer - Np	5′ AUGGAAmUACUCUUGG 3′ - Np	4868.606	27	8.57
5′ 16mer - OH	5′ AmUACUCUUGGUmUACdTdT 3′ - OH	5002.661	28	12.45
5′ 18mer – OH	5′ GAAmUACUCUUGGUmUACdTdT 3′ - OH	5676.783	29	13.35
3′ 18mer - Np	5′ AUGGAAmUACUCUUGGUmUA 3′ - Np	5823.723	30	11.35
5′ 19mer - OH, N-2	5′ GGAAmUACUCUUGGUmUACdTdT 3′ - OH	6021.828	31	13.31
3′ 19mer - Np	5′ AUGGAAmUACUCUUGGUmUAC 3′ - Np	6128.748	32	11.58
5′ 20 mer - OH, N-1	5′ UGGAAmUACUCUUGGUmUACdTdT 3′ - OH	6327.814	33	12.95
Antisense	5′ AUGGAAmUACUCUUGGUmUACdTdT 3′ - OH	6656.866	34	13.73

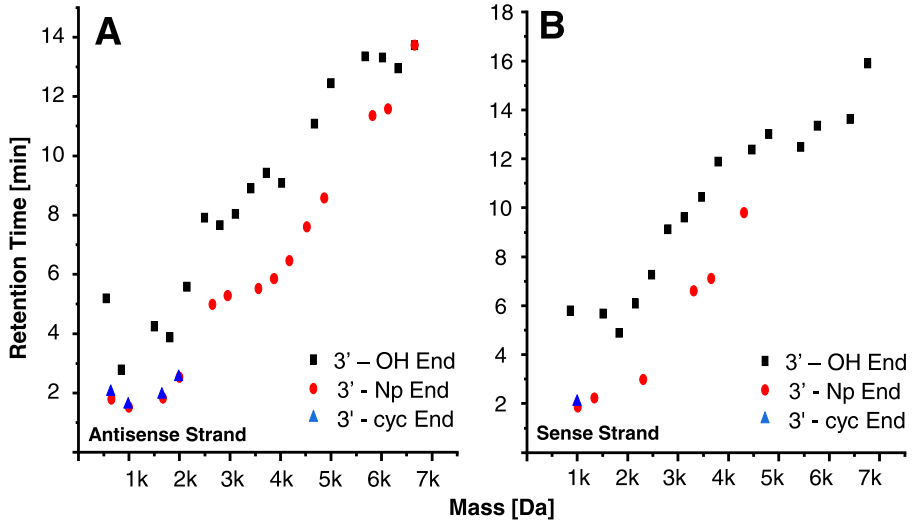

Fig. 6. A correlation between mass and retention time of detected impurities for Patisiran using DCPak PBT. Black trace, square: species with free hydroxy at 3′ end; red trace, circle: species with phosphate at 3′ end; blue trace, triangle: cyclic 2′,3′-phosphate (phosphodiester) end at 3′ end. **A**: Patisiran Antisense Strand; **B**: Patisiran Sense Strand.

3.2.3. Retention shifts due to nucleotide deletions and other structural increments

Above studies provided structural annotation of the detected oligonucleotide impurities of both antisense and sense single strands. Fig. 8A and B depict the EICs of the detected impurity series of antisense and sense strands, respectively. It becomes evident that response factors in ESI-MS are distinct for different oligonucleotide lengths, typically lower for larger oligonucleotides, probably due to splitting of the signals in a wider distribution of distinct molecular species. Aspects of quantitative analysis are out of scope here, but the question arises what is the retention shift with each nucleotide deletion on the PBT column. For this purpose, a retention difference matrix was prepared and the difference in retention times between different deletions including single nucleotide deletions calculated (see suppl. material for the complete data sets; suppl. Table S4-S6). Table 3 gives a summary of absolute retention shifts of single nucleotide deletions and of the retention time shifts occurring due to cyclic 2′,3′-phosphodiester bond for-

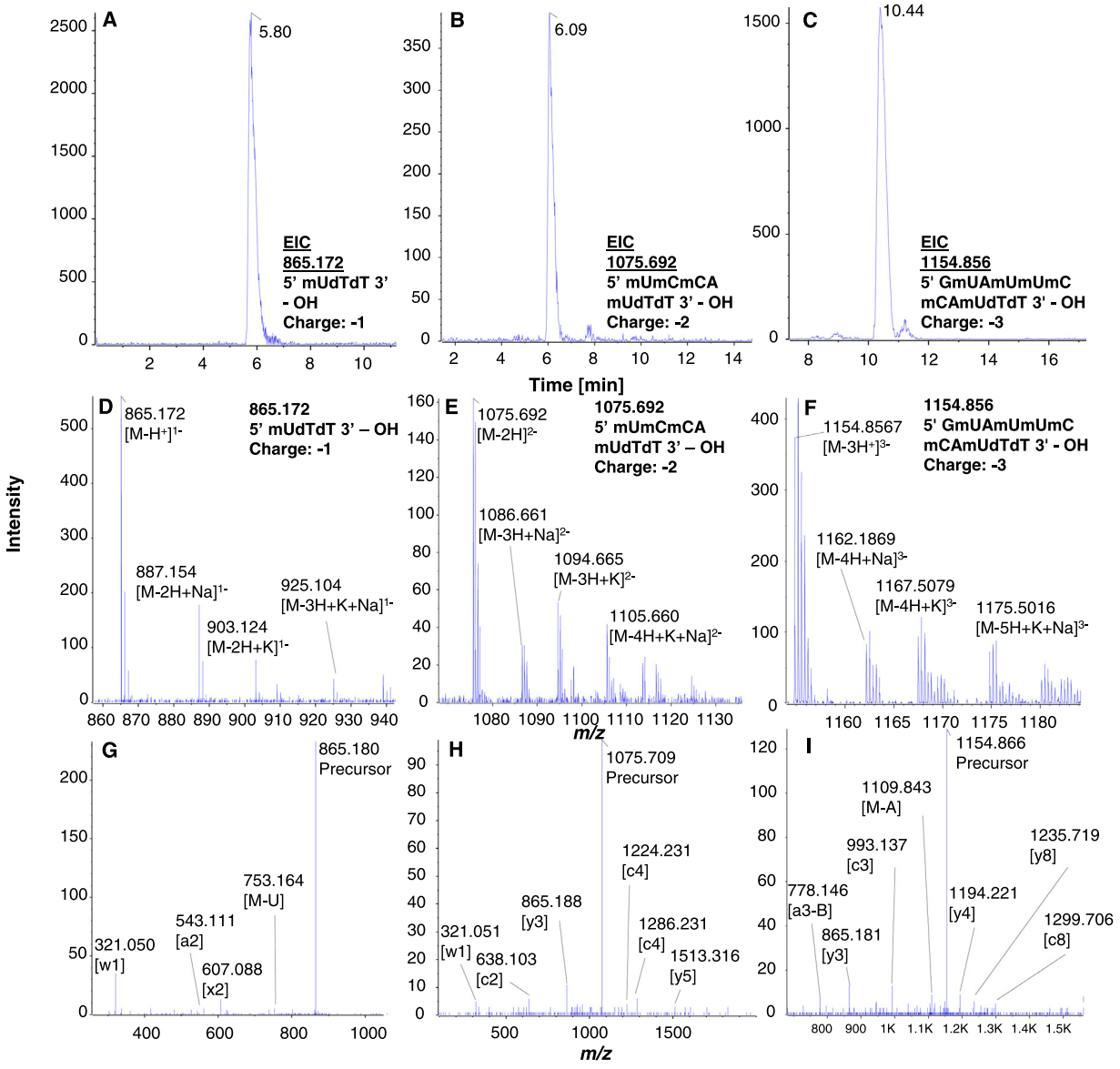

Fig. 7. RP-LC-derived MS^1 and MS^2 spectra and extracted ion chromatogram of selected impurity species from sense strand of Patisiran. (A-C): Extracted ion chromatograms of the monoisotopic mass. (D-F): MS^1 spectra of impurity species with the most abundant charge states. (G-I): MS^2 spectra of the corresponding precursor ion. For MS parameters see chapter 2.4.

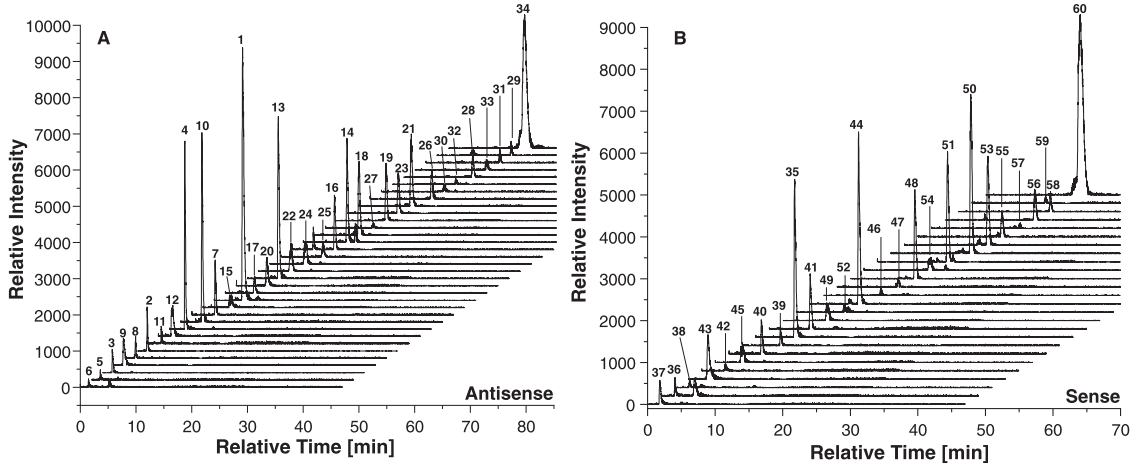

Fig. 8. Extracted ion chromatograms (EIC) of oligonucleotide impurity series of (A) antisense and (B) sense strands. Peak numbering as reported in Table 1 (A) and Table 2 (B), respectively. For conditions see caption of Fig. 4.

Table 2
Overview of the Patisiran sense (passenger) strand impurities detected by RP-LC-MS (sorted in order of increasing mass [Da], t_R in minute).

Name	Sequence	Deconvoluted mass	Peak No. Fig. 4	t_R RP
5′ 3mer-OH	5′ mUdTdT 3′ – OH	866.170	35	5.80
3′ 3mer - cyc	5′ GmUA 3′ - cyc	994.133	36	2.07
3′ 3mer -Np	5′ GmUA 3′ - Np	1012.130	37	1.85
3′ 4mer- Np	5′GmUAA 3′ - Np	1341.186	38	2.23
5′ 5mer- OH	5′ mCAmUdTdT 3′ - OH	1514.268	39	5.67
5′ 6mer - OH	5′ mCmCAmUdTdT 3′ - OH	1833.322	40	4.88
5′ 7mer - OH	5′ mUmCmCAmUdTdT 3′ - OH	2153.353	41	6.09
5′ 7mer - Np	5′ mUmCmCAmUdTdT 3′ - Np	2233.336	42	3.53
3′ 7mer – Np	5′ GmUAAmCmCA 3′ - Np	2308.347	43	2.98
5′ 8mer - OH	5′ mUmUmCmCAmUdTdT 3′ - OH	2473.396	44	7.26
3′ 8mer – Np	5′ GmUAAmCmCAA 3′ - Np	2637.394	45	4.02
5′ 9mer – OH (A->mU)	5′ mUmUmUmCmCAmUdTdT 3′ - OH	2793.442	46	8.50
5′ 9mer - OH	5′ AmUmUmCmCAmUdTdT 3′ - OH	2802.449	47	9.12
5′ 10mer - OH	5′ mUAmUmUmCmCAmUdTdT 3′ - OH	3122.492	48	9.60
3′ 10mer – Np	5′ GmUAAmCmCAAGA 3′ - Np	3311.495	49	6.61
5′ 11mer – OH (G->*A*)	5′ AmUAmUmUmCmCAmUdTdT 3′ - OH	3451.544	50	10.90
5′ 11mer – OH	5′ GmUAmUmUmCmCAmUdTdT 3′ - OH	3467.530	51	10.44
3′ 11mer – Np	5′ GmUAAmCmCAAGAG 3′ - Np	3656.547	52	7.10
5′ 12mer – OH	5′ AGmUAmUmUmCmCAmUdTdT 3′ - OH	3796.590	53	11.88
3′ 13mer - Np	5′ GmUAAmCmCAAGAGmUA 3′ - Np	4305.673	54	9.79
5′ 14mer – OH	5′ AGAGmUAmUmUmCmCAmUdTdT 3′ - OH	4470.688	55	12.37
5′ 15mer – OH	5′ AAGAGmUAmUmUmCmCAmUdTdT 3′ - OH	4799.718	56	13.01
5′ 17mer – OH	5′ mCmCAAGAGmUAmUmUmCmCAmUdTdT 3′ - OH	5437.841	57	12.48
5′ 18mer – OH	5′ AmCmCAAGAGmUAmUmUmCmCAmUdTdT 3′ - OH	5766.896	58	13.35
5′ 20mer - OH (N-1)	5′ mUAAmCmCAAGAGmUAmUmUmCmCAmUdTdT 3′ - OH	6416.030	59	13.63
Sense, Patisiran	5′ GmUAAmCmCAAGAGmUAmUmUmCmCAmUdTdT 3′ - OH	6761.087	60	15.90

Table 3
Summary of retention shifts due to nucleotide deletions and other structural increments considering deletion impurities in both antisense and sense strands.

	$\lvert\Delta t_R\rvert$ [min]								
								Mean	Standard deviation
G	1.71	2.33	0.28	0.97	0.84	2.27		1.40	0.76
A	1.37	0.78	0.71	1.86	1.44	0.64	0.87	1.10	0.43
U	0.37	0.25	0.38	0.52	0.36	0.33	0.61	0.40	0.11
mU	1.21	0.48						0.85	0.37
C	2.41	0.86	0.34	0.29	0.23			0.83	0.82
mC	0.79							0.79	-
cyc (Np-cyc)	0.24	0.22	0.10	0.12	0.00			0.14	0.09

mation from 3′-Np-end phosphorylated impurities. It can be seen that on average purine bases exhibit a larger retention shift upon their deletion than pyrimidine nucleotides and the mean absolute retention shifts are 1.4 (±0.76) and 1.10 (±0.43) min for G and A. 2′-Methylation of U appears to result also in a retention shift, however, the statistics is weak due to presence of only two 2′-O-methyl uridylates. On the other hand, C deletions appear to induce larger retention shifts (0.83±0.82 min) as compared to U (0.40±0.11 min). Cyclic phosphodiester formation brings a mean retention shift of 0.14±0.09 min on the PBT column whereby the retention increment clearly declines the longer the oligonucleotide becomes. The large variance in the specific nucleotide deletion retention shifts indicates there is some sequence specific effect or secondary structure effects. This becomes better visible from the presentation of the absolute retention shifts in dependence on their position in the oligonucleotide sequence (Fig. 9). Herein, 4 deletion series from antisense and sense each with 3′-OH-end and 3′-Np-end were considered. It becomes evident that the retention increments do not follow a simple strict trend but may depend on neighbouring nucleotides and length, or secondary structures.

3.2.4. Annealed strand

Antisense and sense single strands were hybridized to form the double-stranded siRNA shown in Fig 2A by use of an established annealing protocol as described in the experimental section. As mentioned before, the annealed strand with its molecular mass of 13,417 Da elutes close to t_0. This effect is observed probably due to a higher polarity (bases are mutually saturated in the ds oligonucleotide while both ribosyl phosphodiester backbones are exposed to the surface) (note, corresponding HILIC experiments confirm this assumption). At the same time, a high amount of annealing buffer consisting of EDTA, Tris and NaCl co-eluted with the annealed siRNA double-strand of Patisiran causing strong ion suppression. Thus, no MS signal was detected. But the strong UV signal (Fig. 4C) at the beginning of the chromatogram indicates the presence of annealed ds-siRNA, since the components of the annealing buffer are largely UV-inactive. Still, in the sample with annealed ds-siRNA, numerous impurities were also present, since the hybridization was performed for two single strands with impurity profiles as shown in Fig. 4A and B. The impurities in the sample of the annealed siRNA showed retention under RP conditions and could be identified with ESI-TOF-MS (similar to earlier results). Fourty nine impurity species, which have been already detected in antisense or sense strand, could be found also in the annealed sample (Table S3). Residual sense and antisense strand (Fig. S4) were also detected by MS due to incomplete hybridization process.

Overall, the PBT-based column shows interesting selectivities under ion-pair free mobile phase conditions, yet the chromatographic efficiency is lower than commonly seen in ion-pair RPLC with state-of-art sub-2 µm particle columns. This is partly due to the particle size (3 µm) of the PBT column which is currently not

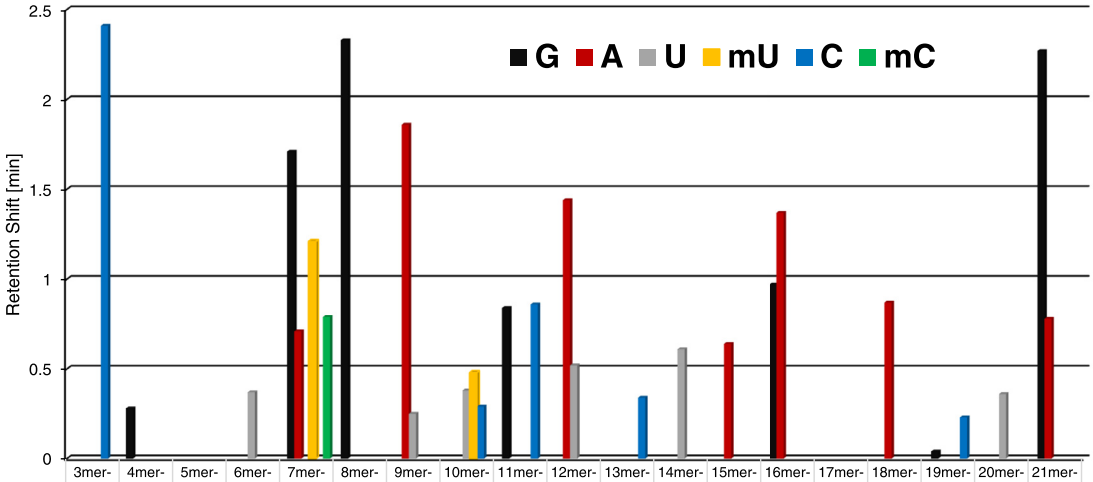

	3mer-2mer	4mer-3mer	5mer-4mer	6mer-5mer	7mer-6mer	8mer-7mer	9mer-8mer	10mer-9mer	11mer-10mer	12mer-11mer	13mer-12mer	14mer-13mer	15mer-14mer	16mer-15mer	17mer-16mer	18mer-17mer	19mer-18mer	20mer-19mer	21mer-20mer
G		0.28			1.71	2.33			0.84					0.97			0.04		2.27
A					0.71		1.86			1.44			0.64	1.37		0.87			0.78
U				0.37			0.25	0.38		0.52		0.61						0.36	
mU					1.21			0.48											
C	2.41							0.29	0.86		0.34						0.23		
mC					0.79														

Fig. 9. Absolute retention time shifts ($|\Delta t_R|$ in [min]) of various nucleotides in dependence of the position in the nucleotide sequence as calculated from 4 impurity series of antisense and sense strands for each with 3′-OH-end and 3′-Np-end impurities.

available as a sub-2 µm UHPLC column. However, it can be very useful if ion-pair agents should be avoided in LC-ESI-MS instruments which are not exclusively dedicated to oligonucleotide analysis. This PBT-RPLC method could also be of interest in preparative LC for the purification of Patisiran from single strand impurities by use of negative chromatography, i.e. retention of impurities and elution of the product with t_0.

4. Conclusion

In this study, we developed an ion-pair free reversed-liquid chromatography method using DCPak PBT which was originally designed for supercritical fluid chromatography. The ion-pair free RP provides sufficient retention and adequate selectivity for oligonucleotides (as documented for antisense and sense strand of Patisiran) to enable direct coupling to ESI-MS. The polybutylene terephthalate selector coated onto silica with its plethora of distinct interaction sites (hydrophobic moieties, aromatic systems and dipole interaction sites) interact with the oligonucleotides without requiring an ion-pairing reagent. Our results showed that retention and separation of impurities and main compound at the PBT stationary phase strongly depend on the type, concentration and pH of salt in the mobile, as well as on the type of organic solvent and flow rate. In general, a high number of impurities were resolved and characterized by ESI-TOF-MS with the use of the finally optimized method. The PBT-based ion-pairing free RPLC seems to be a suitable method for oligonucleotide analysis without contaminating the MS ion-sources and therefore useful for LC-ESI-MS instruments which are not dedicated for oligonucleotide analysis by ion-pairing reversed phase chromatography.

Declaration of Competing Interest

The authors declare that they have no known competing financial interests or personal relationships that could have appeared to influence the work reported in this paper.

CRediT authorship contribution statement

Feiyang Li: Investigation, Methodology, Formal analysis, Data curation, Visualization, Writing – original draft, Writing – review & editing. **Shenkai Chen:** Investigation. **Sylwia Studzińska:** Supervision, Writing – review & editing. **Michael Lämmerhofer:** Conceptualization, Methodology, Supervision, Writing – review & editing, Resources, Funding acquisition.

Data availability

Data will be made available on request.

Acknowledgments

We are grateful to Chiral Technologies Europe and Dr. Pilar Franco for providing DCpak PBT as test column. This work was financially supported by Torun Center of Excellence “Towards Personalized Medicine” operating under Excellence Initiative-Research University (Sylwia Studzińska).

Supplementary materials

Supplementary material associated with this article can be found, in the online version, at doi:10.1016/j.chroma.2023.463898.

References

[1] T.C. Roberts, R. Langer, M.J.A. Wood, Advances in oligonucleotide drug delivery, Nat. Rev. Drug Discov. 19 (2020) 673–694, doi:10.1038/s41573-020-0075-7.
[2] J.P. Bost, H. Barriga, M.N. Holme, A. Gallud, M. Maugeri, D. Gupta, T. Lehto, H. Valadi, E.K. Esbjörner, M.M. Stevens, S. El-Andaloussi, Delivery of oligonucleotide therapeutics: chemical modifications, lipid nanoparticles, and extracellular vesicles, ACS Nano 15 (2021) 13993–14021, doi:10.1021/acsnano.1c05099.
[3] G. Walsh, Biopharmaceutical benchmarks 2018, Nat. Biotechnol. 36 (2018) 1136–1145, doi:10.1038/nbt.4305.
[4] A. Goyon, P. Yehl, K. Zhang, Characterization of therapeutic oligonucleotides by liquid chromatography, J. Pharm. Biomed. Anal. 182 (2020) 113105, doi:10.1016/j.jpba.2020.113105.

[5] J.M. Sutton, G.J. Guimaraes, V. Annavarapu, W.D. Van Dongen, M.G. Bartlett, Current state of oligonucleotide characterization using liquid chromatography-mass spectrometry: insight into critical issues, J. Am. Soc. Mass Spectrom. 31 (2020) 1775–1782, doi:10.1021/jasms.0c00179.

[6] A. Zimmermann, J. Horak, O.L. Sánchez-Muñoz, M. Lämmerhofer, Surface charge fine tuning of reversed-phase/weak anion-exchange type mixed-mode stationary phases for milder elution conditions, J. Chromatogr. A 1409 (2015) 189–200, doi:10.1016/j.chroma.2015.07.036.

[7] H.J. Fritz, R. Belagaje, E.L. Brown, R.H. Fritz, R.A. Jones, R.G. Lees, H.G. Khorana, H.J. Fritz, R. Belagaje, E.L. Brown, R.H. Fritz, R.A. Jones, R.G. Lees, Studies on polynucleotides. 146. high-pressure liquid chromatography in polynucleotide synthesis, Biochemistry 17 (1978) 1257–1267, doi:10.1021/bi00600a020.

[8] A. Apffel, J.A. Chakel, S. Fischer, K. Lichtenwalter, W.S. Hancock, Analysis of oligonucleotides by HPLC-electrospray ionization mass spectrometry, Anal. Chem. 69 (1997) 1320–1325, doi:10.1021/ac960916h.

[9] W.D. Van Dongen, Bioanalytical LC-MS of therapeutic oligonucleotides, Chim. Oggi 30 (2012) 65–67.

[10] J. Bagge, M. Enmark, M. Leśko, F. Limé, T. Fornstedt, J. Samuelsson, Impact of stationary-phase pore size on chromatographic performance using oligonucleotide separation as a model, J. Chromatogr. A (2020) 461653, doi:10.1016/j.chroma.2020.461653.

[11] M. Enmark, M. Rova, J. Samuelsson, E. Örnskov, F. Schweikart, T. Fornstedt, Investigation of factors influencing the separation of diastereomers of phosphorothioated oligonucleotides, Anal. Bioanal. Chem. 411 (2019) 3383–3394, doi:10.1007/s00216-019-01813-2.

[12] O. Kohlbacher, S. Quinten, M. Sturm, B.M. Mayr, C.G. Huber, Structure-activity relationships in chromatography: retention prediction of oligonucleotides with support vector regression, Angew. Chem. Int. Ed. 45 (2006) 7009–7012, doi:10.1002/anie.200602561.

[13] L. Gong, J.S.O. McCullagh, Comparing ion-pairing reagents and sample dissolution solvents for ion-pairing reversed-phase liquid chromatography/electrospray ionization mass spectrometry analysis of oligonucleotides, Rapid Commun. Mass Spectrom. 28 (2014) 339–350, doi:10.1002/rcm.6773.

[14] S. Studzińska, R. Rola, B. Buszewski, The impact of ion-pairing reagents on the selectivity and sensitivity in the analysis of modified oligonucleotides in serum samples by liquid chromatography coupled with tandem mass spectrometry, J. Pharm. Biomed. Anal. 138 (2017) 146–152, doi:10.1016/j.jpba.2017.02.014.

[15] M. Gilar, K.J. Fountain, Y. Budman, U.D. Neue, K.R. Yardley, P.D. Rainville, R.J. Russell, J.C. Gebler, Ion-pair reversed-phase high-performance liquid chromatography analysis of oligonucleotides: retention prediction, J. Chromatogr. A 958 (2002) 167–182, doi:10.1016/S0021-9673(02)00306-0.

[16] M. Enmark, S. Harun, J. Samuelsson, E. Örnskov, L. Thunberg, A. Dahlén, T. Fornstedt, Selectivity limits of and opportunities for ion pair chromatographic separation of oligonucleotides, J. Chromatogr. A 1651 (2021) 462269, doi:10.1016/j.chroma.2021.462269.

[17] N.M. Elzahar, N. Magdy, A.M. El-Kosasy, M.G. Bartlett, Degradation product characterization of therapeutic oligonucleotides using liquid chromatography mass spectrometry, Anal. Bioanal. Chem. 410 (2018) 3375–3384, doi:10.1007/s00216-018-1032-8.

[18] V. Murugaiah, W. Zedalis, G. Lavine, K. Charisse, M. Manoharan, Reversed-phase high-performance liquid chromatography method for simultaneous analysis of two liposome-formulated short interfering RNA duplexes, Anal. Biochem. 401 (2010) 61–67, doi:10.1016/j.ab.2010.02.012.

[19] L. Li, J.P. Foley, R. Helmy, Simultaneous separation of small interfering RNA and lipids using ion-pair reversed-phase liquid chromatography, J. Chromatogr. A 1601 (2019) 145–154, doi:10.1016/j.chroma.2019.04.061.

[20] M. Holčapek, K. Volná, P. Jandera, L. Kolářová, K. Lemr, M. Exner, A. Církva, Effects of ion-pairing reagents on the electrospray signal suppression of sulphonated dyes and intermediates, J. Mass Spectrom. 39 (2004) 43–50, doi:10.1002/jms.551.

[21] B. Basiri, M.M. Murph, M.G. Bartlett, Assessing the interplay between the physicochemical parameters of ion-pairing reagents and the analyte sequence on the electrospray desorption process for oligonucleotides, J. Am. Soc. Mass Spectrom. 28 (2017) 1647–1656, doi:10.1007/s13361-017-1671-6.

[22] A. Zimmermann, R. Greco, I. Walker, J. Horak, A. Cavazzini, M. Lämmerhofer, Synthetic oligonucleotide separations by mixed-mode reversed-phase/weak anion-exchange liquid chromatography, J. Chromatogr. A 1354 (2014) 43–55, doi:10.1016/j.chroma.2014.05.048.

[23] M. Biba, C.J. Welch, J.P. Foley, Investigation of a new core-shell particle column for ion-pair reversed-phase liquid chromatography analysis of oligonucleotides, J. Pharm. Biomed. Anal. 96 (2014) 54–57, doi:10.1016/j.jpba.2014.03.029.

[24] M. Biba, C.J. Welch, J.P. Foley, B. Mao, E. Vazquez, R.A. Arvary, Evaluation of core-shell particle columns for ion-pair reversed-phase liquid chromatography analysis of oligonucleotides, J. Pharm. Biomed. Anal. 72 (2013) 25–32, doi:10.1016/j.jpba.2012.09.007.

[25] P.A. Lobue, M. Jora, B. Addepalli, P.A. Limbach, Oligonucleotide analysis by hydrophilic interaction liquid chromatography-mass spectrometry in the absence of ion-pair reagents, J. Chromatogr. A 1595 (2019) 39–48, doi:10.1016/j.chroma.2019.02.016.

[26] A. Goyon, B. Scott, K. Kurita, C.M. Crittenden, D. Shaw, A. Lin, P. Yehl, K. Zhang, Full sequencing of CRISPR/Cas9 single guide RNA (sgRNA) via parallel ribonuclease digestions and hydrophilic interaction liquid chromatography–high-resolution mass spectrometry analysis, Anal. Chem. (2021), doi:10.1021/acs.analchem.1c03533.

[27] M. Huang, X. Xu, H. Qiu, N. Li, Analytical characterization of DNA and RNA oligonucleotides by hydrophilic interaction liquid chromatography-tandem mass spectrometry, J. Chromatogr. A 1648 (2021) 462184, doi:10.1016/j.chroma.2021.462184.

[28] A. Demelenne, G. Nys, C. Nix, J.C. Fjeldsted, J. Crommen, M. Fillet, Separation of phosphorothioated oligonucleotide diastereomers using multiplexed drift tube ion mobility mass spectrometry, Anal. Chim. Acta. 1191 (2022) 339297, doi:10.1016/j.aca.2021.339297.

[29] S. Studzińska, F. Łobodziński, B. Buszewski, Application of hydrophilic interaction liquid chromatography coupled with mass spectrometry in the analysis of phosphorothioate oligonucleotides in serum, J. Chromatogr. B Anal. Technol. Biomed. Life Sci. 1040 (2017) 282–288, doi:10.1016/j.jchromb.2016.11.001.

[30] L. Gong, J.S.O. McCullagh, Analysis of oligonucleotides by hydrophilic interaction liquid chromatography coupled to negative ion electrospray ionization mass spectrometry, J. Chromatogr. A 1218 (2011) 5480–5486, doi:10.1016/j.chroma.2011.06.044.

[31] R. Easter, C. Barry, J. Caruso, P. Limbach, Separation and identification of phosphorothioate oligonucleotides by HILIC-ESIMS, Anal. Methods 5 (2013) 2657–2659, doi:10.1039/c3ay26519f.

[32] F. Li, X. Su, S. Bäurer, M. Lämmerhofer, Multiple heart-cutting mixed-mode chromatography-reversed-phase 2D-liquid chromatography method for separation and mass spectrometric characterization of synthetic oligonucleotides, J. Chromatogr. A 1625 (2020) 461338, doi:10.1016/j.chroma.2020.461338.

[33] F. Li, M. Lämmerhofer, Impurity profiling of siRNA by two-dimensional liquid chromatography-mass spectrometry with quinine carbamate anion-exchanger and ion-pair reversed-phase chromatography, J. Chromatogr. A 1643 (2021) 462065, doi:10.1016/j.chroma.2021.462065.

[34] B.W.J. Pirok, D.R. Stoll, P.J. Schoenmakers, Recent developments in two-dimensional liquid chromatography: fundamental improvements for practical applications, Anal. Chem. 91 (2019) 240–263, doi:10.1021/acs.analchem.8b04841.

[35] S.G. Roussis, I. Cedillo, C. Rentel, Two-dimensional liquid chromatography-mass spectrometry for the characterization of modified oligonucleotide impurities, Anal. Biochem. 556 (2018) 45–52, doi:10.1016/j.ab.2018.06.019.

[36] Q. Li, F. Lynen, J. Wang, H. Li, G. Xu, P. Sandra, Comprehensive hydrophilic interaction and ion-pair reversed-phase liquid chromatography for analysis of di- to deca-oligonucleotides, J. Chromatogr. A 1255 (2012) 237–243, doi:10.1016/j.chroma.2011.11.062.

[37] S. Studzińska, F. Li, M. Szumski, B. Buszewski, M. Lämmerhofer, Cholesterol stationary phase in the separation and identification of siRNA impurities by two-dimensional liquid chromatography-mass spectrometry, Int. J. Mol. Sci. 23 (2022), doi:10.3390/ijms232314960.

[38] K. Nagai, T. Shibata, S. Shinkura, A. Ohnishi, Poly(butylene terephthalate) based novel achiral stationary phase investigated under supercritical fluid chromatography conditions, J. Chromatogr. A 1549 (2018) 85–92, doi:10.1016/j.chroma.2018.03.032.

[39] L. Toribio, S. Arranz, A.M. Ares, J. Bernal, Polymeric stationary phases based on poly(butylene terephthalate) and poly(4-vinylpirydine) in the analysis of polyphenols using supercritical fluid chromatography. application to bee pollen, J. Chromatogr. A 1572 (2018) 128–136, doi:10.1016/j.chroma.2018.08.042.

[40] C. Matranga, Y. Tomari, C. Shin, D.P. Bartel, P.D. Zamore, Passenger-strand cleavage facilitates assembly of siRNA into Ago2-containing RNAi enzyme complexes, Cell 123 (2005) 607–620, doi:10.1016/j.cell.2005.08.044.

[41] Online protocol provided by *Sigma Adrich, Germany*: https://www.sigmaaldrich.com/DE/de/technical-documents/protocol/genomics/pcr/annealing-oligos.

[42] M. Rosés, X. Subirats, E. Bosch, Retention models for ionizable compounds in reversed-phase liquid chromatography. effect of variation of mobile phase composition and temperature, J. Chromatogr. A 1216 (2009) 1756–1775, doi:10.1016/j.chroma.2008.12.042.

[43] P.J. Schoenmakers, R. Tijssen, Modelling retention of ionogenic solutes in liquid chromatography as a function of pH for optimization purposes, J. Chromatogr. A 656 (1993) 577–590, doi:10.1016/0021-9673(93)80820-X.

[44] R.M. Lopez Marques, P.J. Schoenmakers, Modelling retention in reversed-phase liquid chromatography as a function of pH and solvent composition, J. Chromatogr. A 592 (1992) 157–182, doi:10.1016/0021-9673(92)85084-7.

[45] P.J. Sample, K.W. Gaston, J.D. Alfonzo, P.A. Limbach, RoboOligo: software for mass spectrometry data to support manual and de novo sequencing of post-transcriptionally modified ribonucleic acids, Nucleic Acids Res. 43 (2015) 1–13, doi:10.1093/nar/gkv145.

[46] A. Nyakas, L.C. Blum, S.R. Stucki, J.L. Reymond, S. Schürch, OMA and OPA - software-supported mass spectra analysis of native and modified nucleic acids, J. Am. Soc. Mass Spectrom. 24 (2013) 249–256, doi:10.1007/s13361-012-0529-1.

[47] M. Yang, S. Fazio, D. Munch, P. Drumm, Impact of methanol and acetonitrile on separations based on π-π interactions with a reversed-phase phenyl column, J. Chromatogr. A 1097 (2005) 124–129, doi:10.1016/j.chroma.2005.08.028.

[48] S.G. Roussis, I. Cedillo, C. Rentel, Automated determination of early eluting oligonucleotide impurities using ion-pair reversed-phase liquid chromatography high resolution-mass spectrometry, Anal. Biochem. 595 (2020) 113623, doi:10.1016/j.ab.2020.113623.

[49] T. Suzuki, S. Ohsumi, K. Makino, Mechanistic studies on depurination and apurinic site chain breakage in oligodeoxyribonucleotides, Nucleic Acids Res. 22 (1994) 4997–5003, doi:10.1093/nar/22.23.4997.

[50] R.E. Birdsall, M. Gilar, H. Shion, Y.Q. Yu, W. Chen, Reduction of metal adducts in oligonucleotide mass spectra in ion-pair reversed-phase chromatography/mass spectrometry analysis, Rapid Commun. Mass Spectrom. 30 (2016) 1667–1679, doi:10.1002/rcm.7596.

[51] M. Greig, R.H. Griffey, Utility of organic bases for improved electrospray mass spectrometry of oligonucleotides, Rapid Commun. Mass Spectrom. 9 (1995) 97–102, doi:10.1002/rcm.1290090121.
[52] S.A. Mcluckey, G.J. Van Berkel, G.L. Glish, Tandem mass spectrometry of small, multiply charged oligonucleotides, J. Am. Soc. Mass Spectrom. 3 (1992) 60–70, doi:10.1016/1044-0305(92)85019-G.
[53] S.A. McLuckey, G. Vaidyanathan, S. Habibi-Goudarzi, Charged vs. neutral nucleobase loss from multiply charged oligonucleotide anions, J. Mass Spectrom. 30 (1995) 1222–1229, doi:10.1002/jms.1190300903.
[54] M. Shigematsu, T. Kawamura, Y. Kirino, Generation of 2′,3′-cyclic phosphate-containing RNAs as a hidden layer of the transcriptome, Front. Genet. 9 (2018) 1–13, doi:10.3389/fgene.2018.00562.

Supplementary Material

Polybutylene terephthalate-based column for an ion-pair-free reversed-phase/ion-pairing reversed-phase liquid chromatography of small interfering RNA

Feiyang Li[a], Shenkai Chen[a], Sylwia Studzińska[a,b], Michael Lämmerhofer[a]*

[a] Institute of Pharmaceutical Sciences, Pharmaceutical (Bio-)Analysis, University of Tübingen, Auf der Morgenstelle 8, 72076 Tübingen, Germany

[b] Chair of Environmental Chemistry and Bioanalytics, Faculty of Chemistry, Nicolaus Copernicus University in Torun, 7 Gagarin Str., PL-87-100 Toruń, Poland

*Author for correspondence:

Prof. Dr. Michael Lämmerhofer

Pharmaceutical (Bio-)Analysis

Institute of Pharmaceutical Sciences

University of Tübingen

Auf der Morgenstelle 8

72076 Tübingen, Germany

T +49 7071 29 78793, F +49 7071 29 4565

E-mail: michael.laemmerhofer@uni-tuebingen.de

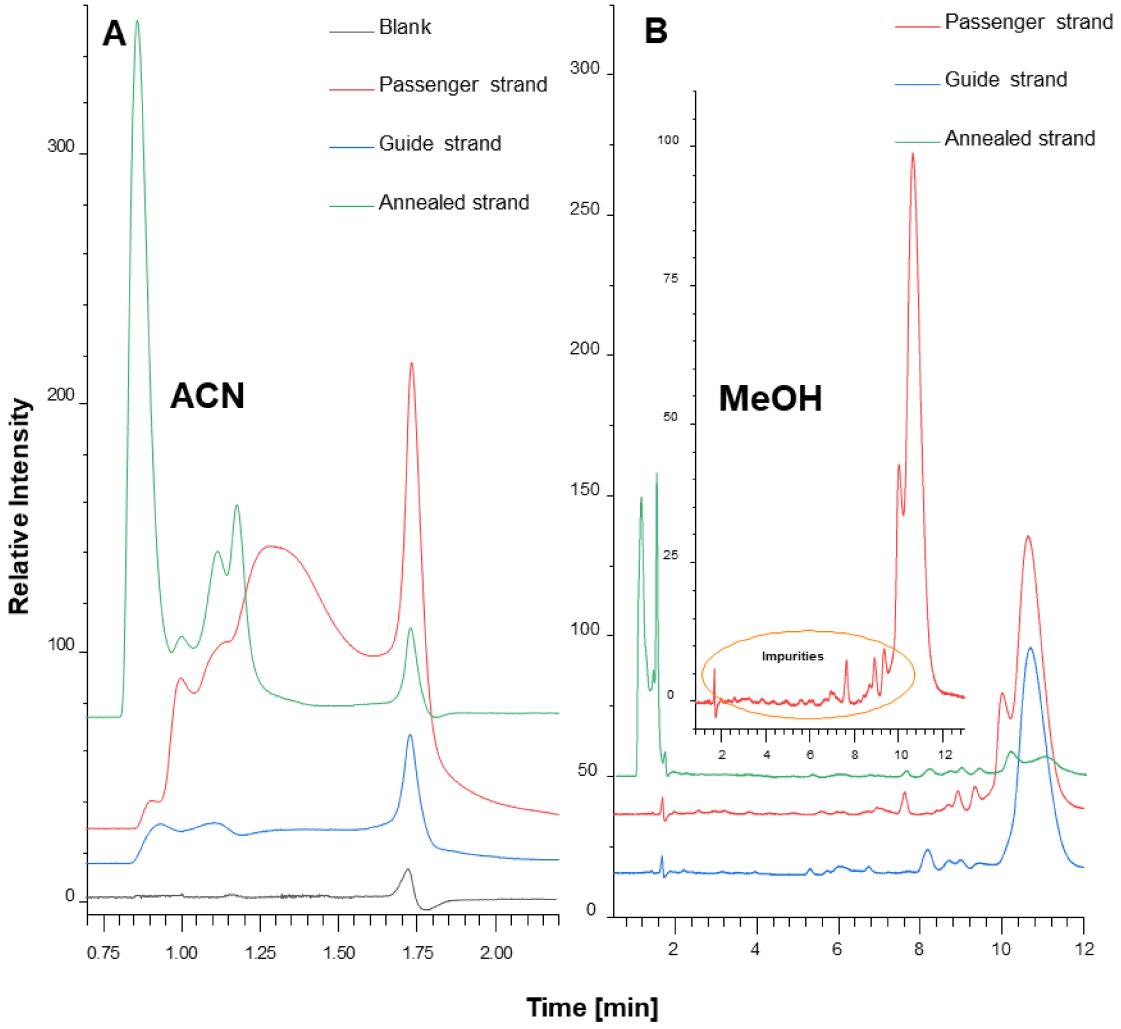

Fig. S1. Ion-pair-free RP-LC-UV chromatograms of antisense and sense single strands as well as annealed double strand of Patisiran raw products with DCpak® PBT. By using MeOH instead of ACN as organic modifier, sufficient retention and some selectivity was observed for the single strands while the annealed double strand still eluted with t_0. LC-Conditions (A): MPA: water,10 mM AA, ${}^{w}_{w}\mathrm{pH}$ 6.8; MPB: ACN/water 9:1 (v/v),10 mM AA (${}^{w}_{w}\mathrm{pH}$ 6.8 in the aqueous fraction); Gradient: 10%-100% MPB in 30 min; Temperature: 40 °C; Flow rate: 0.6 ml/min. LC-Conditions (B): MPA: water, 10 mM AA, ${}^{w}_{w}\mathrm{pH}$ 6.8; MPB: MeOH/water 9:1 (v/v), 10 mM AA (${}^{w}_{w}\mathrm{pH}$ 6.8 in the aqueous fraction); Gradient: 10%-100% MPB in 30 min; Temperature: 40 °C; Flow rate: 0.6 ml/min. Void time: 1.75 min

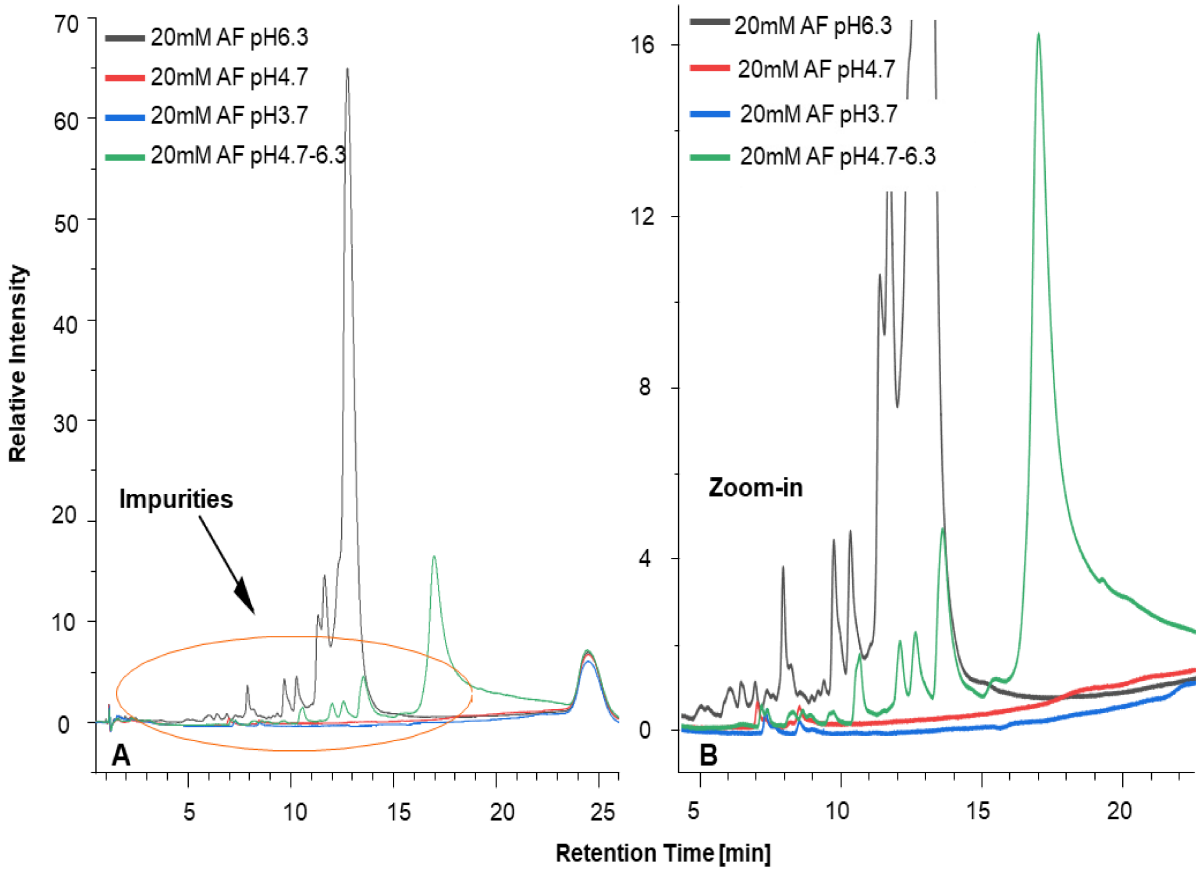

Fig. S2. The impact of the pH value for the separation of sense strand on DAICEL DCPak® using 20 mM ammonium formate. LC-Conditions (A): MPA: water, 20 mM AF, ${}^{w}_{w}pH$ 3.7/4.7/6.3; MPB: MeOH/water 9:1 (v/v), 20 mM AF (${}^{w}_{w}pH$ 6.3 in the aqueous fraction); Gradient: 10%-45% MPB in 20 min; Temperature: 40 °C; Flow rate: 0.6 ml/min.

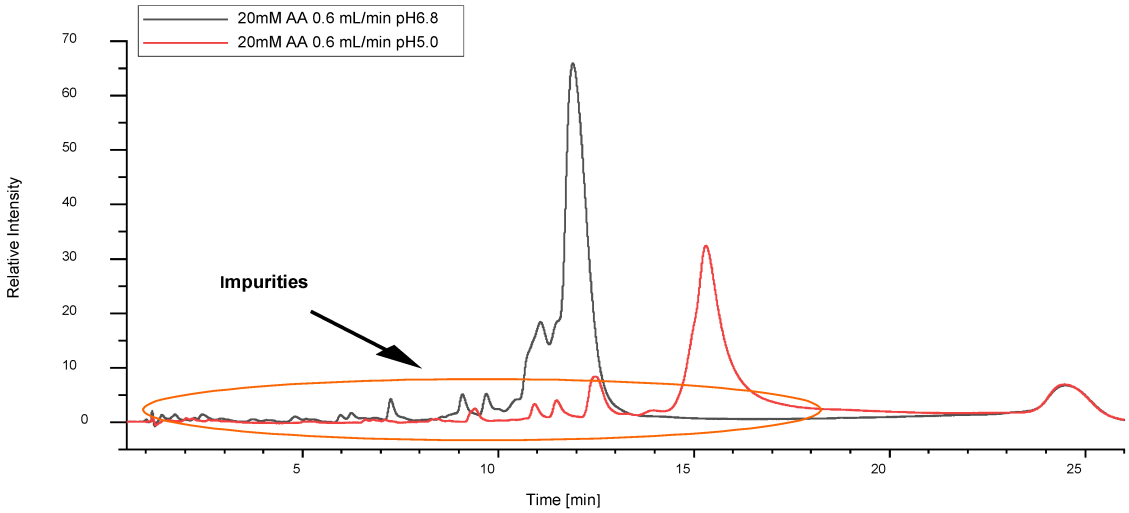

Fig. S3. The impact of the pH value for the separation of sense strand on DAICEL DCPak® using 20 mM ammonium acetate. LC-Conditions (A): MPA: water, 20 mM AA, $^{w}_{w}pH$ 6.8/5.0; MPB: MeOH/water 9:1 (v/v), 20 mM AA ($^{w}_{w}pH$ 6.3 in the aqueous fraction); Gradient: 10%-45% MPB in 20 min; Temperature: 40 °C; Flow rate: 0.1-0.7 ml/min. LC-Conditions (B): MPA: water, 40 mM AA, $^{w}_{w}pH$ 6.8; MPB: MeOH/water 9:1 (v/v), 40 mM AA ($^{w}_{w}pH$ 6.8 in the aqueous fraction); Gradient: 10%-45% MPB in 20 min; Temperature: 40 °C; Flow rate: 0.6 ml/min.

Table S1. All detected species of the guide strand of Patisiran from DCpak® PBT RPLC-MS analysis, sorted in order of increasing molecular mass. For more information see Table 1 (*m/z* refers to the monoisotopic mass, charge state to the most abundant one).

Peak No.	Chemical Formula	Charge state	Ion Type	Calculated *m/z*	Measured *m/z*	Error (ppm)	Deconvoluted mass
1	$C_{20}H_{27}N_4O_{12}P$	-1	$[M-H]^{-1}$	545.128	545.129	1.8	546.13
2	$C_{19}H_{23}N_7O_{14}P_2$	-1	$[M-H]^{-1}$	634.070	634.071	1.6	635.071
3	$C_{19}H_{25}N_7O_{15}P_{22}$	-1	$[M-H]^{-1}$	652.082	652.083	1.5	653.086
4	$C_{29}H_{39}N_7O_{19}P_2$	-1	$[M-H]^{-1}$	850.169	850.174	5.9	851.174
5	$C_{29}H_{35}N_{12}O_{21}P_3$	-1	$[M-H]^{-1}$	979.117	979.119	2.0	980.119
6	$C_{29}H_{37}N_{12}O_{22}P_3$	-1	$[M-H]^{-1}$	997.128	997.134	6.0	998.135
7	$C_{49}H_{64}N_{14}O_{33}P_4$	-2	$[M-2H]^{-2}$	749.128	749.131	4.7	1501.257
8	$C_{49}H_{59}N_{22}O_{34}P_5$	-2	$[M-2H]^{-2}$	826.105	826.109	5.4	1654.209
9	$C_{49}H_{61}N_{22}O_{35}P_5$	-2	$[M-2H]^{-2}$	835.110	835.115	6.0	1672.221
10	$C_{58}H_{75}N_{16}O_{41}P_5$	-2	$[M-2H]^{-2}$	902.140	902.146	6.3	1806.294
11	$C_{59}H_{71}N_{27}O_{40}P_6$	-2	$[M-2H]^{-2}$	990.631	990.637	6.1	1983.28
12	$C_{59}H_{73}N_{27}O_{41}P_6$	-2	$[M-2H]^{-2}$	999.636	999.642	6.0	2001.264
13	$C_{68}H_{87}N_{21}O_{48}P_6$	-2	$[M-2H]^{-2}$	1074.664	1074.671	6.5	2151.345
14	$C_{78}H_{99}N_{26}O_{55}P_7$	-2	$[M-2H]^{-2}$	1247.188	1247.196	6.4	2496.397
15	$C_{79}H_{98}N_{34}O_{55}P_8$	-2	$[M-2H]^{-2}$	1324.183	1324.192	6.8	2650.383
16	$C_{87}H_{110}N_{28}O_{63}P_8$	-3	$[M-3H]^{-3}$	933.131	933.135	4.3	2802.405
17	$C_{88}H_{110}N_{37}O_{62}P_9$	-3	$[M-3H]^{-3}$	984.133	984.137	3.7	2955.422
18	$C_{96}H_{121}N_{30}O_{71}P_9$	-3	$[M-3H]^{-3}$	1035.139	1035.145	5.5	3108.435
19	$C_{105}H_{133}N_{33}O_{78}P_{10}$	-3	$[M-3H]^{-3}$	1136.820	1136.826	5.6	3413.483
20	$C_{106}H_{133}N_{42}O_{77}P_{11}$	-3	$[M-3H]^{-3}$	1187.822	1187.829	5.9	3566.488
21	$C_{114}H_{144}N_{35}O_{86}P_{11}$	-3	$[M-3H]^{-3}$	1238.828	1238.831	2.2	3719.513
22	$C_{115}H_{144}N_{44}O_{85}P_{12}$	-3	$[M-3H]^{-3}$	1289.830	1289.837	5.2	3872.523
23	$C_{123}H_{156}N_{38}O_{93}P_{12}$	-3	$[M-3H]^{-3}$	1340.509	1340.515	4.7	4024.557
24	$C_{124}H_{155}N_{46}O_{93}P_{13}$	-3	$[M-3H]^{-3}$	1391.839	1391.841	1.4	4178.524
25	$C_{134}H_{167}N_{51}O_{100}P_{14}$	-3	$[M-3H]^{-3}$	1506.855	1506.858	2.2	4523.595
26	$C_{143}H_{181}N_{45}O_{107}P_{14}$	-3	$[M-3H]^{-3}$	1556.873	1556.877	2.4	4673.671
27	$C_{144}H_{179}N_{56}O_{107}P_{15}$	-4	$[M-4H]^{-4}$	1216.151	1216.160	7.4	4868.646
28	$C_{153}H_{193}N_{50}O_{113}P_{15}$	-3	$[M-3H]^{-3}$	1666.557	1666.561	2.2	5002.728
29	$C_{173}H_{217}N_{60}O_{126}P_{17}$	-4	$[M-4H]^{-4}$	1418.191	1418.193	1.4	5676.772
30	$C_{173}H_{215}N_{65}O_{129}P_{18}$	-4	$[M-4H]^{-4}$	1454.931	1454.938	5.2	5823.767
31	$C_{183}H_{229}N_{65}O_{133}P_{18}$	-4	$[M-4H]^{-4}$	1504.453	1504.457	2.7	6021.826
32	$C_{182}H_{227}N_{68}O_{136}P_{19}$	-4	$[M-4H]^{-4}$	1531.191	1531.200	5.9	6128.798
33	$C_{192}H_{240}N_{67}O_{141}P_{19}$	-4	$[M-4H]^{-4}$	1580.959	1580.966	4.3	6327.866
34	$C_{202}H_{252}N_{72}O_{147}P_{20}$	-4	$[M-4H]^{-4}$	1663.222	1663.233	6.5	6656.933

Table S2. All detected species of passenger strand of Patisiran from DCpak® PBT RPLC-MS analysis, sorted in order of increasing molecular mass. For more information see Table 2 (*m/z* refers to the monoisotopic mass, charge state to the most abundant one).

Peak No.	Chemical Formula	Chare state	Ion Type	Calculated *m/z*	Measured *m/z*	Error (ppm)	Deconvoluted mass
35	$C_{30}H_{40}N_6O_{20}P_2$	-1	$[M-H]^{-1}$	865.169	865.173	4.6	886.170
36	$C_{30}H_{37}N_{12}O_{21}P_3$	-1	$[M-H]^{-1}$	993.133	993.133	0.0	994.133
37	$C_{30}H_{39}N_{12}O_{22}P_3$	-1	$[M-H]^{-1}$	1011.144	1011.145	1.0	1012.130
38	$C_{40}H_{51}N_{17}O_{28}P_4$	-1	$[M-H]^{-1}$	1340.196	1340.206	7.5	1341.212
39	$C_{50}H_{66}N_{14}O_{33}P_4$	-2	$[M-2H]^{-2}$	756.136	756.134	-2.0	1514.268
40	$C_{60}H_{80}N_{17}O_{40}P_5$	-2	$[M-2H]^{-2}$	915.664	915.667	3.3	1833.337
41	$C_{70}H_{93}N_{19}O_{48}P_6$	-2	$[M-2H]^{-2}$	1075.685	1075.687	2.3	2153.353
42	$C_{70}H_{94}N_{19}O_{51}P_7$	-2	$[M-2H]^{-2}$	1115.668	1115.673	4.9	2233.352
43	$C_{70}H_{91}N_{28}O_{48}P_7$	-2	$[M-2H]^{-2}$	1153.178	1153.181	3.0	2308.362
44	$C_{80}H_{106}N_{21}O_{56}P_7$	-2	$[M-2H]^{-2}$	1235.705	1235.713	6.5	2473.396
45	$C_{80}H_{103}N_{33}O_{54}P_8$	-2	$[M-2H]^{-2}$	1317.704	1317.703	-0.4	2637.407
46	$C_{90}H_{119}N_{23}O_{64}P_8$	-2	$[M-2H]^{-2}$	1395.726	1395.721	-3.2	2793.442
47	$C_{90}H_{118}N_{26}O_{62}P_8$	-3	$[M-3H]^{-3}$	933.152	933.15	-1.8	2802.449
48	$C_{100}H_{131}N_{28}O_{70}P_9$	-3	$[M-3H]^{-3}$	1039.832	1039.831	-1.0	3122.492
49	$C_{100}H_{127}N_{43}O_{67}P_{10}$	-3	$[M-3H]^{-3}$	1102.833	1102.832	-0.9	3311.495
50	$C_{110}H_{143}N_{33}O_{76}P_{10}$	-3	$[M-3H]^{-3}$	1149.516	1149.515	-0.9	3451.544
51	$C_{110}H_{143}N_{33}O_{77}P_{10}$	-3	$[M-3H]^{-3}$	1154.848	1154.856	7.2	3467.530
52	$C_{110}H_{139}N_{48}O_{74}P_{11}$	-3	$[M-3H]^{-3}$	1217.849	1217.849	0.0	3656.547
53	$C_{120}H_{155}N_{38}O_{83}P_{11}$	-3	$[M-3H]^{-3}$	1264.532	1264.538	4.7	3796.590
54	$C_{130}H_{164}N_{55}O_{88}P_{13}$	-3	$[M-3H]^{-3}$	1434.213	1434.216	1.9	4305.673
55	$C_{140}H_{179}N_{48}O_{96}P_{13}$	-3	$[M-3H]^{-3}$	1489.232	1489.237	3.6	4470.688
56	$C_{150}H_{191}N_{53}O_{102}P_{14}$	-3	$[M-3H]^{-3}$	1598.916	1598.927	6.9	4799.718
57	$C_{170}H_{219}N_{59}O_{116}P_{16}$	-4	$[M-4H]^{-4}$	1358.464	1358.46	-2.6	5437.841
58	$C_{180}H_{231}N_{64}O_{122}P_{17}$	-4	$[M-4H]^{-4}$	1440.727	1440.724	-1.9	5766.896
59	$C_{200}H_{256}N_{71}O_{136}P_{19}$	-4	$[M-4H]^{-4}$	1603	1603.01	6.2	6416.030
60	$C_{210}H_{268}N_{76}O_{143}P_{20}$	-4	$[M-4H]^{-4}$	1689.262	1689.273	6.7	6761.087

Table S3. Overview of the impurities in duplex siRNA Patisiran (annealed strand) detected by RP-LC-MS analysis. Peak numbers are assigned as in Table 1 and 2.

Peak No.	Retention Time	Name	Sequence	Deconvoluted mass
9	2.24	3' 5mer - Np, AS	5' AUGGA 3' - Np	1672.221
8	2.31	3' 5mer - cyc, AS	5' AUGGA 3' - cyc	1654.209
38	2.54	3' 4mer- Np, S	5'GmUAA 3' - Np	1341.186
4	3.03	5' 3mer - OH, AS	5' CdTdT 3' - OH	851.17
12	3.2	3' 6mer - Np, AS	5' AUGGAA 3' - Np	2001.264
43	3.5	3' 7mer - Np, S	5' GmUAAmCmCA 3' - Np	2308.347
10	4.58	5' 6mer - OH, AS	5' UmUACdTdT 3' - OH	1806.282
45	4.84	3' 8mer - Np, S	5' GmUAAmCmCAA 3' - Np	2637.394
7	4.88	5' 5mer - OH, AS	5' mUACdTdT 3' - OH	1500.257
40	5.58	5' 6mer - OH, S	5' mCmCAmUdTdT 3' - OH	1833.322
1	5.58	5' 2mer - OH, AS	5' dTdT 3' - OH	546.129
15	5.98	3' 8mer - Np, AS	5' AUGGAAmUA 3' - Np	2650.364
17	6.36	3' 9mer - Np, AS	5' AUGGAAmUAC 3' - Np	2955.407
35	6.37	5' 3mer - OH, S	5' mUdTdT 3' - OH	866.177
39	6.53	5' 5mer- OH, S	5' mCAmUdTdT 3' - OH	1514.268
20	6.63	3' 11mer - Np, AS	5' AUGGAAmUACUC 3' - Np	3566.466
13	6.65	5' 7mer - OH, AS	5’ GUmUACdTdT 3' - OH	2151.33
22	7.03	3' 12mer - Np (isomer), AS	5' AUGGAAmUAUUUU 3' - Np	3873.496
24	7.71	3' 13mer - Np, AS	5' AUGGAAmUACUCUU 3' - Np	4178.519
49	7.75	3' 10mer - Np, S	5' GmUAAmCmCAAGA 3' - Np	3311.495
44	8.28	5' 8mer - OH, S	5' mUmUmCmCAmUdTdT 3' - OH	2473.396
25	8.95	3' 14mer - Np, AS	5' AUGGAAmUACUCUUG 3' - Np	4523.57
47	9.11	5' 9mer - OH, S	5' AmUmUmCmCAmUdTdT 3' - OH	2802.449
14	9.34	5' 8mer - OH, AS	5' GGUmUACdTdT 3' - OH	2496.368
18	9.55	5' 10mer - OH, AS	5' UUGGUmUACdTdT 3' - OH	3108.418
27	9.99	3' 15mer - Np, AS	5' AUGGAAmUACUCUUGG 3' - Np	4868.606
19	10.51	5' 11mer - OH, AS	5' CUUGGUmUACdTdT 3' - OH	3413.459
30	10.67	5' 13mer - OH, AS	5' CUCUUGGUmUACdTdT 3' - OH	4024.528
48	10.92	5' 10mer - OH, S	5' mUAmUmUmCmCAmUdTdT 3' - OH	3122.492
21	11.1	5' 12mer - OH, AS	5' UCUUGGUmUACdTdT 3'-OH	3719.47
54	11.23	3' 13mer - Np, S	5' GmUAAmCmCAAGAGmUA 3' - Np	4305.673
51	11.88	5' 11mer - OH, S	5' GmUAmUmUmCmCAmUdTdT 3' - OH	3467.53
26	12.71	5' 15mer - OH, AS	5' mUACUCUUGGUmUACdTdT 3' - OH	4673.609
30	12.91	3' 18mer - Np, AS	5' AUGGAAmUACUCUUGGUmUA 3' - Np	5823.723
53	13.41	5' 12mer - OH, S	5' AGmUAmUmUmCmCAmUdTdT 3' - OH	3796.59
55	13.89	5' 14mer - OH, S	5' AGAGmUAmUmUmCmCAmUdTdT 3' - OH	4470.688
57	14.07	5' 17mer - OH, S	5' mCmCAAGAGmUAmUmUmCmCAmUdTdT 3' - OH	5437.841
28	14.12	5' 16mer - OH (isomer), AS	5' AmUACUCUUGGCmUACdTdT 3' - OH	5002.661
58	14.96	5' 18mer - OH, S	5' AmCmCAAGAGmUAmUmUmCmCAmUdTdT 3' - OH	5766.896
59	15.38	5' 20mer - OH (N-1), S	5' mUAAmCmCAAGAGmUAmUmUmCmCAmUdTdT 3' - OH	6416.03
34	15.58	Antisense	5' AUGGAAmUACUCUUGGUmUACdTdT 3' - OH	6656.866

60	15.84	Sense, Patisiran	5' GmUAAmCmCAAGAGmUAmUmUmCmCAmUdTdT 3' - OH	6761.087

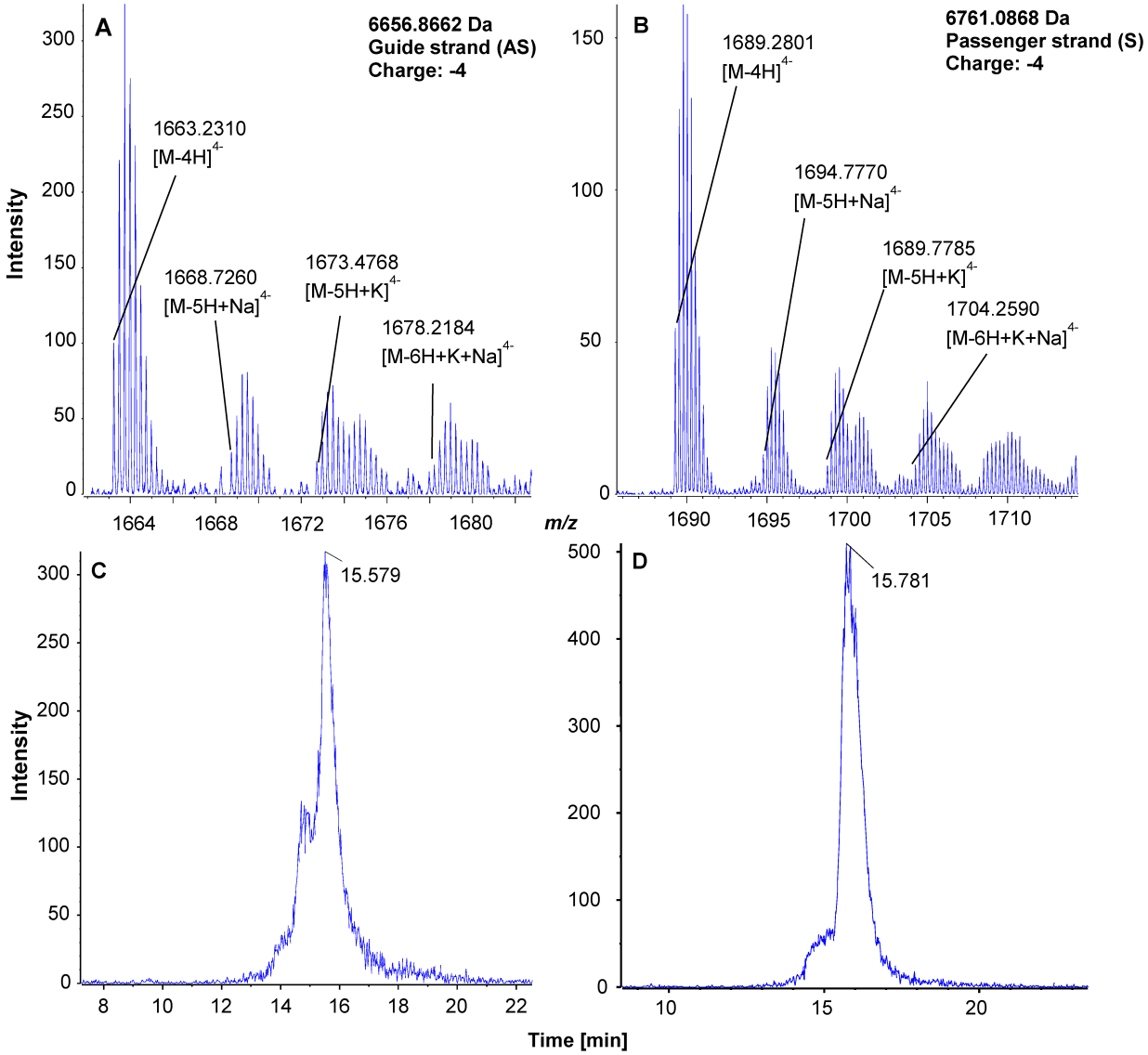

Fig. S4. LC-MS results of annealed guide (antisense) and passenger (sense) strand of Patisiran (duplex siRNA) with DCpak PBT. **A, B:** MS spectra of residual sense (passenger) and antisense (guide) strand. **C, D:** corresponding EIC.

4. Publication IV

Polybutylene terephthalate-based stationary phase for ion-pair-free reversed-phase liquid chromatography of small interfering RNA. Part 2: Use for selective comprehensive two-dimensional liquid chromatography

Feiyang Li[a], Shenkai Chen[a], Sylwia Studzińska[a,b], Michael Lämmerhofer[a]*

[a] Institute of Pharmaceutical Sciences, Pharmaceutical (Bio-)Analysis, University of Tübingen, Auf der Morgenstelle 8, 72076 Tübingen, Germany

[b] Chair of Environmental Chemistry and Bioanalytics, Faculty of Chemistry, Nicolaus Copernicus University in Torun, 7 Gagarin Str., PL-87-100 Toruń, Poland

*Author for correspondence:

Prof. Dr. Michael Lämmerhofer

Pharmaceutical (Bio-)Analysis

Institute of Pharmaceutical Sciences

University of Tübingen

Auf der Morgenstelle 8

72076 Tübingen, Germany

T +49 7071 29 78793, F +49 7071 29 4565

E-mail: michael.laemmerhofer@uni-tuebingen.de

Journal of Chromatography A

Year 2023, 1701, 464069

DOI: 10.1016/j.chroma.2023.464069

Journal of Chromatography A 1701 (2023) 464069

Contents lists available at ScienceDirect

Journal of Chromatography A

journal homepage: www.elsevier.com/locate/chroma

Polybutylene terephthalate-based stationary phase for ion-pair-free reversed-phase liquid chromatography of small interfering RNA. Part 2: Use for selective comprehensive two-dimensional liquid chromatography

Feiyang Li[a], Shenkai Chen[a], Sylwia Studzińska[a,b], Michael Lämmerhofer[a,*]

[a] Institute of Pharmaceutical Sciences, Pharmaceutical (Bio-)Analysis, University of Tübingen, Auf der Morgenstelle 8, 72076 Tübingen, Germany
[b] Chair of Environmental Chemistry and Bioanalytics, Faculty of Chemistry, Nicolaus Copernicus University in Torun, 7 Gagarin Str., PL-87-100 Toruń, Poland

ARTICLE INFO

Article history:
Received 6 March 2023
Revised 6 May 2023
Accepted 13 May 2023
Available online 14 May 2023

Keywords:
Oligonucleotides
Two-dimensional chromatography
Ion-pair RPLC
HILIC
Mixed-mode chromatography

ABSTRACT

With the increasing numbers of nucleic acid-based pharmaceuticals like antisense oligonucleotides (ASO), small interfering ribonucleic acid (siRNA) entering the market, research facilities, pharmaceutical industries and also regulatory authorities have been looking for efficient analytical methods for these synthetic oligonucleotides (ON). Besides of conventional one-dimensional (1D) reversed-phase liquid chromatography with or without ion-pairing (IP-RP-LC, RP-LC), hydrophilic liquid chromatography (HILIC) and mixed-mode chromatography (MMC), two-dimensional (2D) approaches combining two orthogonal chromatographic techniques also become more relevant due to the high structural complexity of oligonucleotides. Recently, we tested a polybutylene terephthalate(PBT)-based stationary phase under ion-pairing free RP mode for the liquid chromatography electrospray ionization mass spectrometry (LC-ESI-MS) analysis of siRNA (Patisiran). In this study, retention profile and chromatographic orthogonality, respectively, were compared to other LC-modes like HILIC, IP-RPLC, another ion-pair free cholesterol-bonded RPLC and MMC considering their normalized retention times. Finally, because of higher orthogonality, the ion-pairing free PBT-bonded RPLC as first dimension (^{1}D) was hyphenated with HILIC in the second dimension (^{2}D) in a selective comprehensive 2D-LC setup leading to an enhanced resolution for peak purity evaluation of the main ON entities.

1. Introduction

Since the official FDA-approval of Fomivirsene for medication of cytomegalovirus retinitis in 1998, oligonucleotide (ON) therapeutics like ASOs and siRNAs have been coming of age in the 2020s [1,2]. Meanwhile, 15 ONs therapeutics are on the market. A high number (more than 400) of further candidates is in phase 2 or phase 3 clinical studies. From 2015 to 2020, the market capitalization of oligonucleotide companies increased 94.2%, and continuing growth can be certainly expected [3,4]. Owing to the quickly increasing relevance, FDA published a new draft guideline for the development of oligonucleotide therapeutics in 2022 [5]. In this document, various structural parameters e.g. base sequence, chemical modifications of ONs, strandedness, purity, as well as secondary and tertiary structure are mentioned as critical quality attributes which need to be strictly controlled in ON drug products. To fulfil this demand, efficient and highly selective analytical methods are necessary. Because of its structural complexity caused by diverse modifications and nucleotide deletions, liquid chromatography has been the method of choice for this analytical purpose, typically with ion-pairing agents in the mobile phase and RPLC as separation technique [6–9]. For an effective characterization of impurities by LC-MS hyphenation, Apffel et al. suggested ion-pairing reversed-phase liquid chromatography using triethylamine and hexafluoroisopropanol (HFIP) in the eluent: it allows the use of lower triethylamine concentrations and thus is less prone to ion-suppression, and has therefore become the golden standard method for ON separations [10–13]. Over the years, various researchers systematically investigated different factors of IP-RPLC like the type of ion-pair reagents, column temperature, pH-value and more which do have significant influence on the achieved separations [11,14–18]. Thus, IP-RPLC has been used in various applications of oligonucleotide analysis and is well established now.

* Correspondence author at: Pharmaceutical (Bio-)Analysis, Institute of Pharmaceutical Sciences, University of Tübingen, Auf der Morgenstelle 8, 72076 Tübingen, Germany.
E-mail address: michael.laemmerhofer@uni-tuebingen.de (M. Lämmerhofer).

https://doi.org/10.1016/j.chroma.2023.464069
0021-9673/

Unfortunately, ion-pairing agents may contaminate mass spectrometry (MS) instruments. To avoid the presence of ion-pairing reagents in the ion source and the MS instrument, respectively, HILIC with volatile buffer has frequently been employed as alternative to IP-RPLC-MS analysis of various DNA/RNA- and phosphorothioated oligonucleotides [19–22]. The retention mechanism in HILIC is often discussed as partitioning of the ON analytes between acetonitrile-rich mobile phase and adsorbed water-layer on the polar stationary phase, such as silica, amide-bonded or zwitterionic sulfobetaine-bonded silica, however, depending on the surface chemistry may be superimposed by adsorptive interactions (e.g. through hydrogen bonding) and attractive/repulsive ionic interactions [23,24].

As mentioned above, oligonucleotides are complex biomolecules containing different functional groups which represent suitable interaction sites that can be conveniently targeted by various chromatographic modes. MMC combining multiple retention mechanisms turned out to be a powerful tool for highly selective ON separations. For instance, a RP/WAX mixed-mode stationary phase based on *N*-undecenyl-3-aminoquinuclidine better resolved structurally closely related ONs than ion-pair RPLC and pristine WAX [25,26]. Pyridylurea-based MMC phase also exhibited interesting selectivities for ONs [25,26]. Further, a quinine-based chiral selector which can be also classified as MMC phase constituted of a weak anion-exchanger site combined with hydrophobic, aromatic (quinoline) and hydrogen-donor-acceptor (carbamate) moieties was applied for the separation of DNA oligonucleotides and impurities, respectively [13]. Biba et al. tested successfully commercial MMC columns, composed of RP18/SAX and RP18/SCX blended column packing as well as corresponding weak ion-exchangers counterparts, for short RNA oligonucleotides and investigated factors influencing the chromatography [27].

Recently, we reported about the usage of polybutylene terephthalate- and a cholesterol-based stationary phase for ion-pair free reversed-phase liquid chromatography [28,29]. In both studies, RNA oligonucleotides could be retained and impurities resolved under RP conditions using ammonium formate as additive. Nevertheless, due to the complexity of impurity profiles and challenging character of oligonucleotides, standalone one-dimensional LC – including all the chromatography modes discussed above – usually does not deliver enough resolution power to separate all sample components resulting in problematic co-elutions especially of N-1 and N-2 shortmers as well as N+1 longmer impurities. For such coelutions especially with the main ON entity, a selective comprehensive 2D-LC for peak purity testing can provide improved selectivity [28]. Indeed, more and more 2D-LC methods addressing the separation of ONs have been published [30,31]. Goyon and Zhang combined IP-RP (^{1}D) with HILIC (^{2}D) in a multiple heart cutting setup to analyse ASO samples [32]. HILIC in the second dimension prevented contamination of the ion source of the MS with ion-pairing reagents leading to enhanced signal sensitivities [32]. Sandra and coworkers developed a full comprehensive (LC × LC) 2D-LC method with HILIC in the ^{1}D dimension and IP-RP in the ^{2}D, incorporating also C18 trap columns after the ^{1}D to enrich the di- to deca-oligonucleotide sample components before their transfer into the ^{2}D [33]. Under LC × LC, the ^{1}D eluate is completely transferred into the ^{2}D to achieve maximal peak capacity. Furthermore, our workgroup developed a multiple heart-cutting 2D-LC method with RP in ^{2}D providing on-line desalting which enables the removal of problematic effluents from ^{1}D to protect the ion source [34]. With this platform method, MS incompatible LC methods can be chosen in the first dimension which guarantees efficient separation of oligonucleotides [13,34].

Herein, we investigate the retention profiles of two complementary siRNA strands and their impurities on a polybutylene terephthalate phase under RPLC elution conditions without ion-pairing reagents in the mobile phase and compare them with those obtained by HILIC, MMC, ion-pair free RP (using a cholesterol-based stationary phase) and IP-RP. For any 2D-LC method to be successful, chromatographic systems in the ^{1}D and ^{2}D need to be orthogonal i.e. they must exhibit distinct retention mechanisms and selectivities. Hence, a major goal herein was to evaluate the orthogonality in the retention pattern of the mentioned LC modes using antisense and sense strand of the siRNA Patisiran as well as their deletion impurities as probe molecules (Fig. 1). Since the detected ON impurity peaks were previously structurally annotated, correlations of the normalized retention times between the different LC methods can be used to assess orthogonality. We used bin counting and Asterisk calculations to score the complementarity in retention profiles [35,36]. Two LC modes with high orthogonality were finally selected for establishing a selective comprehensive 2D-LC method for peak purity profiling of the main component peaks for above siRNA single strands. Considering that robust modern 2D-LC equipment is now offered by several HPLC vendors, such a selective comprehensive 2D-LC approach can be considered an adequate option for detecting impurity peaks hidden beneath the main peak in 1D-LC fully resolved in the ^{2}D allowing their quantification by UV. Since in 1D-LC-ESI-MS ion-suppression can hamper quantitative results of such coeluted impurity species, selective comprehensive 2D-LC-UV can be a valuable complementary option in ON impurity profiling [37,38].

2. Experimental

2.1. Chemicals

Acetic acid (ACS reagent, ≥ 99.8%), ammonium acetate (AA) (LC-MS grade), ammonium formate (AF) (LC-MS grade), ammonium hydroxide (ACS reagent, 28–30%), ortho-phosphoric acid (85% in H_2O), triethylamine (≥98%) and tripropylamine (≥ 98%) were purchased from Sigma-Aldrich (Merck, Munich, Germany). HPLC-MS grade methanol (MeOH) and acetonitrile (ACN) were purchased from Carl Roth (Karlsruhe, Germany). Ultrapure water was obtained by treatment of deionized water with Elga PurLab Ultra purification system (Celle, Germany).

2.2. Oligonucleotide samples

In this work, the two complementary single strands, antisense (guide) and sense (passenger) strand, of the siRNA oligonucleotide Patisiran (Fig. 1) and impurities contained in the purchased raw products were used as chromatographic probes. Patisiran (Tradename: Onpattro, Alnylam Pharmaceuticals, US) was approved by FDA in the year 2018 and is used for the medication of hereditary transthyretin-mediated amyloidosis [39,40]. The individual antisense and sense single strands of Patisiran were purchased from Oligo Sigma (Merck, Munich, Germany) as raw products, i.e. both single strands were delivered as desalted raw products without further purifications. Hence, they contain a full series of impurities which were structurally annotated as outlined in detail in our last report [41].These purchased ON standards do not have pharmaceutical quality and can only be considered as test samples for method development purposes. They do not represent pharmaceutical grade APIs of Patisiran. Both siRNA strands were stored as 100 μM aqueous stock solution under −20 °C. For LC-MS analysis, the stock solution was 1:1 diluted.

2.3. Instrumentation

One dimensional LC experiments were performed with an Agilent 1290 Infinity II UHPLC system from Agilent Technologies

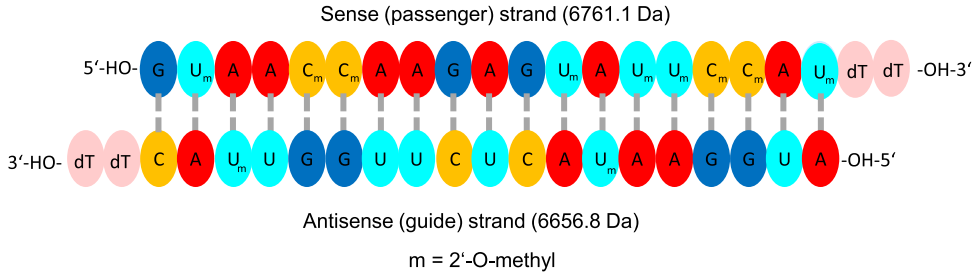

Fig. 1. Nucleotide sequence of the duplex siRNA Patisiran consisting of antisense and sense single strand.

(Waldbronn, Germany) equipped with Multisampler (G4226A), binary Pump (G4220A), column compartment (G1316C) and Diode Array Detector (DAD) (G4212A) with 1 µL flow cell (G4212-60008). Additionally, both column compartment and multisampler were equipped with the Ultra-Low Dispersion Kit (5067-5963).

The 2D-LC experiments were carried out on the Agilent 1290 Infinity II 2D-LC Solution from Agilent Technologies including a quaternary Flexible pump (G7104A), Multisampler (G7167B) and Variable Wavelength Detector (VWD) (G7114B) with 14 µL flow cell (G1314-60186) and a pressure relief valve (pressure release kit, G4236-600010) between the VWD and 2D-interface. The sampling frequency of the VWD was 5 Hz. In the second dimension, a binary High-Speed Pump (G7120A) and a Diode Array Detector (DAD) (G7117B) with 1 µL flow cell (G4212-60008) were employed. The sampling frequency of the DAD was 80 Hz. Two separate Infinity column compartments (G7116B) were used. Both dimensions were connected by a valve drive (G1170A) equipped with 5-position/10-port 2D-LC active solvent modulation (ASM) valve (#5067-4266) coupled to two 6-position/14-port valve heads (#5067-4142, multiple heart-cutting valves) equipped with six 40 µL loops each. The ASM valve contained the ASM capillary of dimension 85×0.12 mm (0.96 µL, #5500-1300) (ASM factor 5, split ratio loop:ASM).

In the MHC 2D-LC experiments with MS detection, an Agilent 2-position/6-port valve head (pressure limit: 800 bar, #5067–4282) driven by a valve drive (G1170A) was used as diverter valve to deliver the MS incompatible components of the early part of the ^{2}D chromatogram into the waste. The 2D-LC system was controlled by Agilent OpenLab CDS ChemStation Rev. C.01.10 with 2D-LC add-on software. The contour plot resulting from the High Resolution-Sampling-2D-LC experiment was created using GC image LC×LC HRMS V2.7 Edition Software (GC Image, Lincoln, Nebraska, USA).

MS detection was performed on a SCIEX TripleTOF 5600+ QTOF mass spectrometer with a Duospray ion source operated in negative ESI mode. 2D-LC and MS instruments were coupled with a contact closure connection for peripheral devices from SCIEX and the MS instrument was controlled with Analyst TF 1.7 software (AB SCIEX, Darmstadt, Germany).

2.4. Stationary phases

Polybutylene terephthalate-bonded silica-based DCpak PBT column (150×3.0 mm, 3 µm particle size; other parameters like ligand density, pore size and carbon load are not published by the manufacturer) for ion-pair free RPLC was provided by Chiral Technologies (Illkirch, France). Acquity UPLC BEH Amide (150×2.1 mm, 1.7 µm particle size, 130 Å, carbon load: 12%) column for HILIC was purchased from Waters (Eschborn, Germany). A cholesterol-based (CHOL) column (125×2.1 mm, 100 Å, 5 µm) previously reported by Buszewski and coworkers was used for ion-pair free RPLC as well [42]. For IP-RP, Acquity UPLC Oligonucleotide BEH C18 column (50×2.1 mm, 130 Å, 1.7 µm particle size, carbon load 18%) was purchased from Waters. For MMC, an *N*-(10-undecenoyl)−3-aminoquinuclidine ligand immobilized on thiol-modified silica and slurry packed into stainless steel column (150×4.0 mm, 100 Å, 5 µm) was used [34,43]. For the selective comprehensive 2D-LC, a shorter version of Acquity UPLC BEH Amide (50×2.1 mm) was used for the second dimension. For the assignment of the ON peaks in HILIC and CHOL-RPLC, the ESI-QTOF-MS was directly coupled to the column outlet in a 1D-LC approach. For the structural annotation of ON species in the MMC and IP-RPLC runs with ESI-MS incompatible mobile phases, a ZORBAX Eclipse Plus C18 (50×3.0 mm, 1.8 µm) from Agilent (Waldbronn, Germany) was applied in the ^{2}D as on-line desalting tool and was hyphenated to ESI-QTOF-MS for detection. Except for the C18 columns, the structures of the chromatographic ligands are illustrated in Fig. 2.

2.5. LC-MS method

In general, six different LC-MS methods are presented in this study. For a better overview, all relevant parameters can be found in Table 1 [44,45].

2.6. Data processing

A detailed description about the software supported characterization and structural assignment of oligonucleotide species can be found in our recent work [41]. For this study, 49 (36 for comparison with MMC) oligonucleotide species from both siRNA strands which were detected in all LC-methods were considered (Table 2). In order to evaluate the orthogonality of the LC-methods, the coefficient of determination R^2 of a linear regression was often used to evaluate the orthogonality between two LC methods [36]. However, it is not well describing orthogonality and therefore two other well established approaches were applied herein, the bin counting method originally suggested by Gilar et al. [35,36] and the Asterisk method proposed by Camenzuli and Schoenmakers [46]. Normalized retention times ($t_{\mathrm{normalized,i}}$) of the oligonucleotides between two distinct LC methods were used for the determination of the quantitative orthogonality parameters. For this purpose, $t_{\mathrm{normalized,i}}$ is defined in accordance to Eq. (1) as

$$t_{\mathrm{normalized,\ i}} = \frac{t_{\mathrm{R,i}} - t_{\mathrm{min}}}{t_{\mathrm{max}} - t_{\mathrm{min}}} \quad (1)$$

wherein $t_{R,i}$ is the retention time of the respective species, t_{max} and t_{min} represent the retention times of the most and least retained species.

For the bin counting method by Gilar et al. [35,36], the normalized retention times (according to eq. (1)) of two considered dimensions are plotted in the two-dimensional space. The 2D-space is then divided into a geometric distribution of equally spaced "bins". A hypothetical separation of 100 analytes can be divided into 10×10 = 100 bins. Depending on the coverage rate of the bins with the data points of $t_{\mathrm{normalized,\ i}}$, it is possible to quantify the orthogonality between two dimensions with the formula of Eq. (2)

$$O = \frac{\sum bins - \sqrt{P_{max}}}{0.63 P_{max}} \quad (2)$$

Table 1
Overview of all considered LC-MS methods.

	Method A		Method B		Method C	
Column	DCpak PBT		CHOL		BEH Amide	
Dimension[1]	150×3.0 mm, 3 µm		125×2.1 mm, 100 Å, 5 µm		150×2.1 mm, 130 Å, 1.7 µm	
Mobile Phase A[2]	20 mM AF, $^{w}_{w}$pH 6.3		20 mM AF, $^{w}_{w}$pH 6.3		15 mM AA in 70% ACN, $^{w}_{w}$pH 9	
Mobile Phase B[2]	20 mM AF in 90% MeOH, $^{w}_{w}$pH 6.3		20 mM AF in 90% MeOH, $^{w}_{w}$pH 6.3		15 mM AA, $^{w}_{w}$pH 9	
Gradient	10–45% B in 28 min; 10% B for 15 min		10–45% B in 28 min; 10% B for 15 min		0–60% B in 30 min; 0% B for 15 min	
Column Temperature	40 °C		40 °C		30 °C	
Flow rate	0.6 mL/min		0.6 mL/min		0.25 mL/min	
MS mode	ESI-TOF negative		ESI-TOF negative		ESI-TOF negative	
Nebulizer gas	90 psi		90 psi		80 psi	
Heater gas	90 psi		90 psi		80 psi	
Curtain gas	35 psi		35 psi		40 psi	
Source temperature	550 °C		550 °C		450 °C	
Ion spray voltage	−4500 V		−4500 V		−4500 V	
Declustering potential	−200 V		−200 V		−150 V	
Collision energy	−10 V, −35 V for MS[2]		10 V, −35 V for MS[2]		10 V, −35 V for MS[2]	
m/z range[3]	100–2000		100–2000		100–2000	
	Method D		**Method E**		**Method F**	
Column	BEH C18	ZORBAX Eclipse Plus C18	Poly-RP/WAX	ZORBAX Eclipse Plus C18	DCpak PBT	BEH Amide
Dimension[1] (^{1}D/^{2}D)	50×2.1 mm, 130 Å, 1.7 µm	50×3.0 mm, 1.8 µm	150×4.0 mm, 100 Å, 5 µm	50×3.0 mm, 1.8 µm	150×3.0 mm, 3 µm	50×2.1 mm, 130 Å, 1.7 µm
Mobile Phase A[2] (^{1}D/^{2}D)	100 mM TPAA, $^{w}_{w}$pH 7	10 mM AA, pH not adjusted	50 mM TEAP[4] in 20% ACN, $^{w}_{w}$pH 7	10 mM AA, pH not adjusted	20 mM AF, $^{w}_{w}$pH 6.3	15 mM AA in 70% ACN, $^{w}_{w}$pH 9
Mobile Phase B[2] (^{1}D/^{2}D)	100 mM TPAA in 90% ACN, $^{w}_{w}$pH 7	10 mM AA in 90% MeOH, pH not adjusted	100 mM TEAP[4] in 20% ACN, $^{w}_{w}$pH 8	10 mM AA in 90% MeOH, pH not adjusted	20 mM AF in 90% MeOH, $^{w}_{w}$pH 6.3	15 mM AA, $^{w}_{w}$pH 9
Gradient (^{1}D/^{2}D)	10–55% B in 32.5 min;10% B for 20 min	Hold 5% B for 0.22 min; 5–60% B in 0.5 min; 5% B for 1.5 min	10–80% B in 30 min; 10% B for 20 min	Hold 5% B for 0.22 min; 5–60% in 0.5 min; 5% B for 1.5 min	10–60% B in 100 min	Hold 0% B for 0.39 min; 0–60% B in 1.46 min, 0% B for 1.14 min
Column Temperature (^{1}D/^{2}D)	30 °C	60 °C	25 °C	60 °C	40 °C	80 °C
Flow rate (^{1}D/^{2}D)	0.3 mL/min	1 mL/min	1 mL/min	1 mL/min	50 µL/min	1.7 mL/min
2D-LC Mode	Multiple-Heart-Cutting		Multiple-Heart-Cutting		Selective-Comprehensive	
ASM[5]	Activated, 0.22 min		Activated, 0.22 min		Activated, 0.39 min	
MS mode	ESI-TOF negative		ESI-TOF negative		ESI-TOF negative	
Nebulizer gas	90 psi		90 psi		80 psi	
Heater gas	90 psi		90 psi		80 psi	
Curtain gas	35 psi		35 psi		40 psi	
Source temperature	600 °C		600 °C		450 °C	
Ion spray voltage	−4500 V		−4500 V		−4500 V	
Declustering potential	−200 V		−200 V		−150 V	
Collision energy	10 V, −35 V for MS[2]		10 V, −35 V for MS[2]		10 V, −35 V for MS[2]	
m/z range[3]	100–2000		100–2000		100–2000	

[1] for more information towards the used columns, see chapter 2.4.
[2] all pH values are depicted with the descriptor of *Rosés* [43].
[3] MS^2 data was generated by information dependent acquisition (IDA) mode (within one MS period cycle, four MS^2 experiments were carried out with an accumulation time of 200 ms each, MS^1 accumulation time was 400 ms). The precursor isolation was set from 200 to 1250 *m/z*.
[4] Triethylammonium phosphate.
[5] factor 5, loop flushing: 3 times, for more information about ASM see reference [44].

wherein *O* is defined as orthogonality. Σ *bins* stands for the total number of bins containing data points. P_{max} is the sum of all bins. In our case, we investigated 49 oligonucleotide species resulting in 7 × 7 = 49 bins (except for combination with MMC: 6 × 6 = 36 bins; less impurities detected due to broader peaks). The *O* values vary between 0 and 1. Expressed as percent, 100% would stand for a theoretical, full orthogonality i.e. each bin is occupied by 1 data point [36].

Secondly, the so-called asterisk calculation was applied to quantify the orthogonality rate between two different LC-methods [46]. Here, a series of equations describing the standard deviation of the peaks around four lines which cross the separation space (two orthogonal ones Z_1, and Z_2 corresponding to ^{1}D and ^{2}D, respectively, as well as two diagonal ones Z_- and Z_+ from left bottom to right top corners and left top to right bottom corners, respectively) were used to calculate the Z-parameters as described in detail in Eqs (1)-(9) in ref. [46]. These Z-parameters were then used in a combined equation (Eq. (3)) defining the orthogonality, known as the A_0 [46].

$$A_0 = \sqrt{Z_- Z_+ Z_1 Z_2} \tag{3}$$

The most important advantage of the asterisk calculation over bin counting is its independency of numbers of components. In our

Table 2
Overview of detected oligonucleotide species in antisense (AS) and sense (S) strand by different LC modes (t_R in min).

No.	Strand	Name	Sequence	Mass	t_R PBT	t_R HILIC	t_R CHOL	t_R MMC	t_R IPRP
1	AS	5′ 2mer - OH	5′ dTdT 3′ - OH	546.130	5.19	2.70	9.94	1.67	4.47
2	AS	3′ 2mer - Np	5′ AU 3′ - Np	653.086	1.79	6.27	4.39	2.17	8.31
3	AS	5′ 3mer - OH	5′ CdTdT 3′ - OH	851.174	2.78	4.42	9.06	1.70	5.44
4	AS	3′ 3mer - cyc	5′ AUG 3′ - cyc	980.119	1.61	6.37	13.76	–	7.40
5	AS	5′ 5mer - OH	5′ mUACdTdT 3′ - OH	1500.257	4.24	6.89	11.64	2.05	12.51
6	AS	3′ 5mer - Np	5′ AUGGA 3′ - Np	1672.221	1.82	11.24	9.33	3.86	14.02
7	AS	5′ 6mer - OH	5′ UmUACdTdT 3′ - OH	1806.294	3.87	8.41	11.56	2.20	14.02
8	AS	3′ 6mer - Np	5′ AUGGAA 3′ - Np	2001.264	2.53	11.99	10.73	4.86	15.55
9	AS	5′ 7mer - OH (U-C)	5′ GCmUACdTdT 3′ - OH	2151.345	5.58	10.34	13.01	2.52	14.59
10	AS	5′ 8mer - OH	5′ GGUmUACdTdT 3′ - OH	2496.397	7.91	11.80	14.23	3.08	15.55
11	AS	3′ 8mer - Np	5′ AUGGAAmUA 3′ - Np	2650.383	4.99	12.96	12.56	7.30	17.87
12	AS	3′ 9mer - Np	5′ AUGGAAmUAC 3′ - Np	2955.422	5.28	13.87	12.83	8.19	18.62
13	AS	5′ 10mer - OH	5′ UUGGUmUACdTdT 3′ - OH	3108.435	8.04	13.48	13.60	–	17.87
14	AS	5′ 11mer - OH	5′ CUUGGUmUACdTdT 3′ - OH	3413.483	8.90	14.35	14.00	5.35	18.62
15	AS	3′ 11mer - Np	5′ AUGGAAmUACUC 3′ - Np	3566.488	5.52	15.33	12.66	10.37	19.98
16	AS	5′ 12mer - OH	5′ UCUUGGUmUACdTdT 3′-OH	3719.513	9.42	14.96	14.12	6.36	19.39
17	AS	3′ 12mer - Np (C-U x2)	5′ AUGGAAmUAUUUU 3′ - Np	3872.523	5.85	15.94	12.51	11.64	20.58
18	AS	5′ 13mer - OH	5′ CUCUUGGUmUACdTdT 3′ - OH	4024.557	9.08	15.66	13.78	7.20	19.98
19	AS	3′ 13mer - Np	5′ AUGGAAmUACUCUU 3′ - Np	4178.524	6.46	16.54	12.52	12.52	21.07
20	AS	3′ 14mer - Np	5′ AUGGAAmUACUCUUG 3′ - Np	4523.595	7.60	17.12	13.13	–	21.49
21	AS	5′ 15mer - OH	5′ mUACUCUUGGUmUACdTdT 3′ - OH	4673.671	11.08	16.04	14.16	–	21.49
22	AS	3′ 15mer - Np	5′ AUGGAAmUACUCUUGG 3′ - Np	4868.646	8.57	17.63	13.55	16.66	21.92
23	AS	5′ 16mer - OH (U-C)	5′ AmUACUCUUGGCmUACdTdT 3′ - OH	5002.728	12.45	16.30	14.23	12.53	21.49
24	AS	5′ 18mer – OH (N-3)	5′ GAAmUACUCUUGGUmUACdTdT 3′ - OH	5676.772	13.35	17.12	15.46	14.64	22.39
25	AS	3′ 18mer - Np	5′ AUGGAAmUACUCUUGGUmUA 3′ - Np	5824.791	11.35	18.20	14.92	–	23.31
26	AS	5′ 19mer – OH (N-2)	5′ GGAAmUACUCUUGGUmUACdTdT 3′ - OH	6021.826	13.31	17.73	15.47	15.77	22.39
27	AS	3′ 19mer - Np	5′ AUGGAAmUACUCUUGGUmUAC 3′ - Np	6128.798	11.58	18.61	15.14	–	23.31
28	AS	5′ 20 mer - OH (N-1)	5′ UGGAAmUACUCUUGGUmUACdTdT 3′ - OH	6327.866	12.95	17.94	15.28	16.17	22.81
29	AS	Antisense (passenger strand)	5′ AUGGAAmUACUCUUGGUmUACdTdT 3′ - OH	6656.933	13.73	18.01	15.68	18.20	23.31
30	S	5′ 3mer - OH	5′ mUdTdT 3′ - OH	866.170	5.80	3.08	13.58	1.73	9.48
31	S	3′ 3mer - cyc	5′ GmUA 3′ - cyc	994.133	2.07	5.82	19.78	–	8.02
32	S	3′ 3mer -Np	5′ GmUA 3′ - Np	1012.130	1.85	8.05	11.77	2.49	10.40
33	S	3′ 4mer- Np	5′GmUAA 3′ - Np	1341.186	2.23	9.19	14.49	–	12.47
34	S	5′ 5mer- OH	5′ mCAmUdTdT 3′ - OH	1514.268	5.67	6.73	15.18	2.07	12.71
35	S	5′ 6mer - OH	5′ mCmCAmUdTdT 3′ - OH	1833.322	4.88	7.97	15.12	2.31	13.81
36	S	5′ 7mer - OH	5′ mUmCmCAmUdTdT 3′ - OH	2153.353	6.09	8.52	16.18	2.80	16.65
37	S	5′ 7mer - Np	5′ mUmCmCAmUdTdT 3′ - Np	2233.336	3.53	10.84	16.67	4.12	17.59
38	S	3′ 7mer - Np	5′ GmUAAmCmCA 3′ - Np	2308.347	2.98	11.62	17.92	4.98	16.65
39	S	5′ 8mer - OH	5′ mUmUmCmCAmUdTdT 3′ - OH	2473.396	7.26	9.13	17.21	3.40	18.21
40	S	3′ 8mer - Np	5′ GmUAAmCmCAA 3′ - Np	2637.394	4.02	12.20	18.87	6.41	18.21
41	S	5′ 9mer isomer - OH, A -> mU	5′ **mU**mUmUmCmCAmUdTdT 3′ - OH	2793.442	8.50	9.87	18.26	4.14	18.95
42	S	5′ 9mer - OH	5′ AmUmUmCmCAmUdTdT 3′ - OH	2802.449	5.00	10.04	18.65	–	17.83
43	S	5′ 10mer - OH	5′ mUAmUmUmCmCAmUdTdT 3′ - OH	3122.492	9.60	10.68	18.79	4.98	19.09
44	S	3′ 10mer - Np	5′ GmUAAmCmCAAGA 3′ - Np	3311.495	6.61	13.67	20.62	9.42	19.49
45	S	5′ 11mer - OH, isomer, G -> A	5′ **A**mUAmUmUmCmCAmUdTdT 3′ - OH	3451.544	10.90	11.42	19.51	–	19.49
46	S	5′ 11mer - OH	5′ GmUAmUmUmCmCAmUdTdT 3′ - OH	3467.530	10.44	12.01	19.14	5.79	19.49
47	S	3′ 11mer - Np	5′ GmUAAmCmCAAGAG 3′ - Np	3656.547	7.10	14.53	20.69	–	19.79
48	S	5′ 12mer - OH	5′ AGmUAmUmUmCmCAmUdTdT 3′ - OH	3796.590	11.88	12.47	20.31	7.45	20.21
49	S	5′ 14mer - OH	5′ AGAGmUAmUmUmCmCAmUdTdT 3′ - OH	4470.688	12.37	13.80	20.40	10.24	20.81
50[a]	S	5′ 15mer - OH	5′ AAGAGmUAmUmUmCmCAmUdTdT 3′ - OH	4799.718	13.01	14.12	20.58	–	21.36
51[a]	S	5′ 17mer - OH	5′ mCmCAAGAGmUAmUmUmCmCAmUdTdT 3′ - OH	5437.841	12.48	14.74	20.68	14.15	22.25
52[a]	S	5′ 18mer – OH (N-3)	5′ AmCmCAAGAGmUAmUmUmCmCAmUdTdT 3′ - OH	5766.896	13.35	14.95	22.71	16.27	23.18
53[a]	S	5′ 20mer - OH (N-1)	5′ mUAAmCmCAAGAGmUAmUmUmCmCAmUdTdT 3′ - OH	6416.030	13.63	15.38	21.08	–	23.44
54[a]	S	Sense (guide strand)	5′ GmUAAmCmCAAGAGmUAmUmUmCmCAmUdTdT 3′ - OH	6761.087	15.90	15.90	21.80	18.83	23.44

[a] Not included into the calculation of orthogonality.

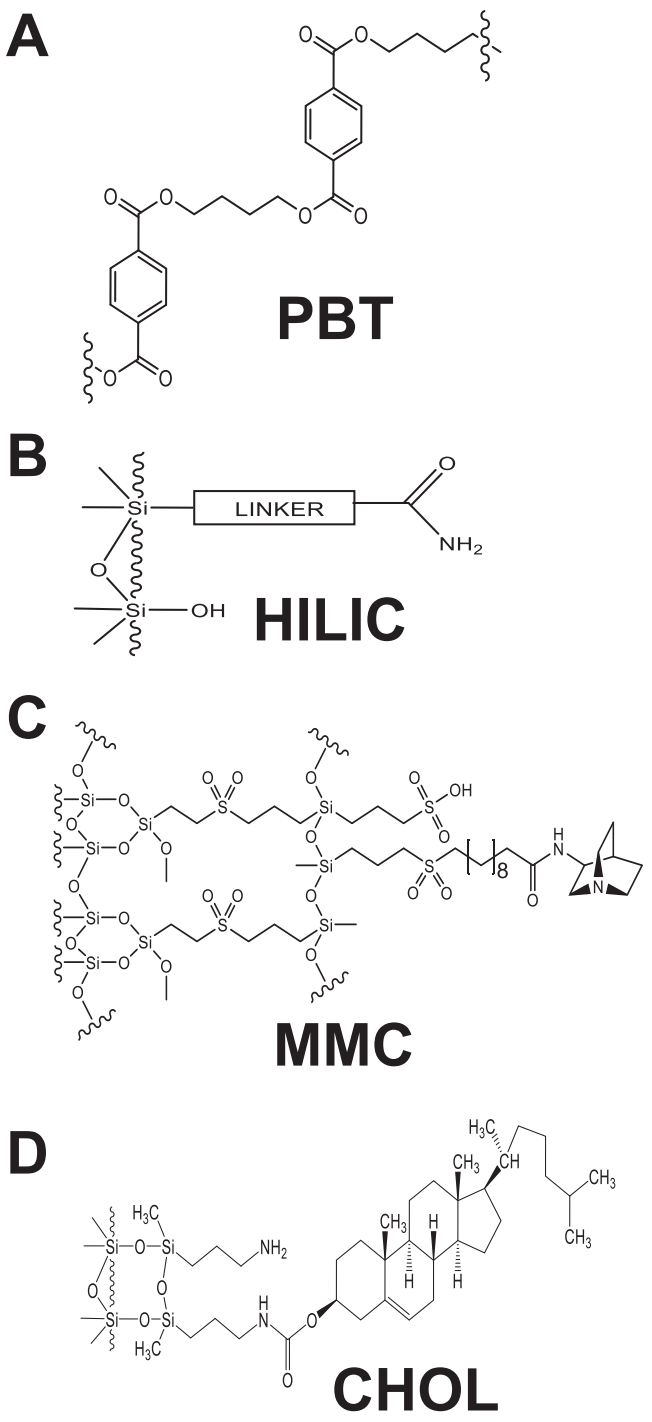

Fig. 2. Chromatographic ligand structures of employed stationary phases.

case, this is a relevant point when it comes to the results of MMC. Instead of 49, only 36 components were detected which makes a direct comparison by the bin counting method somewhat vague. This will be discussed in chapter 3.3.

Besides of those possibilities, there are other useful methods to calculate orthogonality like the capacity dimension algorithm by Schure or nearest neighbours metric by Nowik [47,48]. Furthermore, Jacova et al. and Mommers and van der Wal introduced a critical discussion and some improvements related to surface coverage methods which can be considered as advanced measure of complementary retention behaviour [49,50].

3. Results and discussion

3.1. Evaluated stationary phases and LC modes

As 1D-LC reaches its limitations for complex samples and structurally similar compounds such as oligomeric species with minor structural modification, 2D-LC is a promising tool to solve this shortcoming. The primary requirement for any successful 2D-LC mode, (multiple) heart-cutting, selective and full comprehensive, is orthogonality in retention mechanisms and complementary chromatographic retention profiles, respectively. To achieve orthogonality in retention for oligonucleotides is not a trivial task, not even when distinct LC modes are employed. Herein, we evaluated a number of distinct LC-modes ranging from common IP-RPLC and HILIC over MMC to ion-pair free RPLC. It is generally expected that the more distinct the LC mode the more orthogonal, yet potentially less compatible two coupled chromatographic modes will be. For oligonucleotides, some surprises may be observed (*vide infra*).

To keep the mobile phase simple and MS compatible without contamination from ion-pairs and other unpleasant additives, PBT-RPLC with ammonium formate-methanol based eluents was evaluated as one tentative separation dimension in a 2D-LC method. The structure of the PBT stationary phase is shown in Fig. 2A. It is a silica-based stationary phase with a polybutylene terephthalate surface coating developed for SFC applications. The PBT bonding harbours several distinct interaction sites: i) short alkyl strands similar to C4 ligands for hydrophobic interactions, ii) phenyl rings for aromatic π-π-interactions, and iii) dipoles from ester bond for hydrogen bonding (H-acceptor moieties) and dipole-dipole interactions. It is bare of ionic groups and hence ionic interactions except for some weak repulsive electrostatic interactions when residual silanols get dissociated (pH > 4). This plurality of heterogenous binding site appears attractive for noncovalent interactions with complementary binding sites of oligonucleotides via base side chains of the oligomeric phosphodiester-carbohydrate nucleic acid backbone.

Standard RP18 LC lacks this multiplicity of interactions and hydrophobic interactions with nucleobases are weak. For this reason, ion-pair reagents are added to the eluent inducing secondary equilibria (ion-pairing with phosphate groups) and dynamic anion-exchange process, respectively [17]. Retention increases with the hydrophobicity of the ion-pair and length of ON. For hydrophobic ion-pairs, which adsorb to the surface of C18 phase and create a dynamic anion-exchange, low concentrations are usually enough, which is favourable for ESI-MS detection, while for less hydrophobic ion-pairs higher concentrations are required with detrimental effect on ESI-MS detection sensitivity due to ion-suppression. With hydrophobic ion-pairs, high organic modifier contents are required and hydrophobic selectivity contributions to separation are effectively disrupted and therefore minor. Less hydrophobic ion-pairs are less adsorbed and elution can take place with less organic modifier which leads to a mixed hydrophobic interaction/dynamic ion-exchange retention mechanism. A systematic discussion of ion-pair effects can be found elsewhere [17]. Herein, we selected the hydrophobic tripropylammonium acetate (100 mM) in the IP-RPLC mode for orthogonality evaluation on sub 2 µm hybrid BEH C18 bonded stationary phase. The retention pattern follows increasing charges of the ONs.

HILIC has become an attractive alternative choice for ON LC separations and herein we employ BEH Amide (sub-2 µm particle) column (Fig. 2B) for orthogonality evaluation [19–21]. It offers amide hydrogen-donor acceptor sites for H-bonding and dipole interaction superimposed over the eluent-water layer partitioning mechanism. Except for residual silanols no ionic interaction sites are present (increasing repulsive electrostatic interaction with increasing pH at pH > 4).

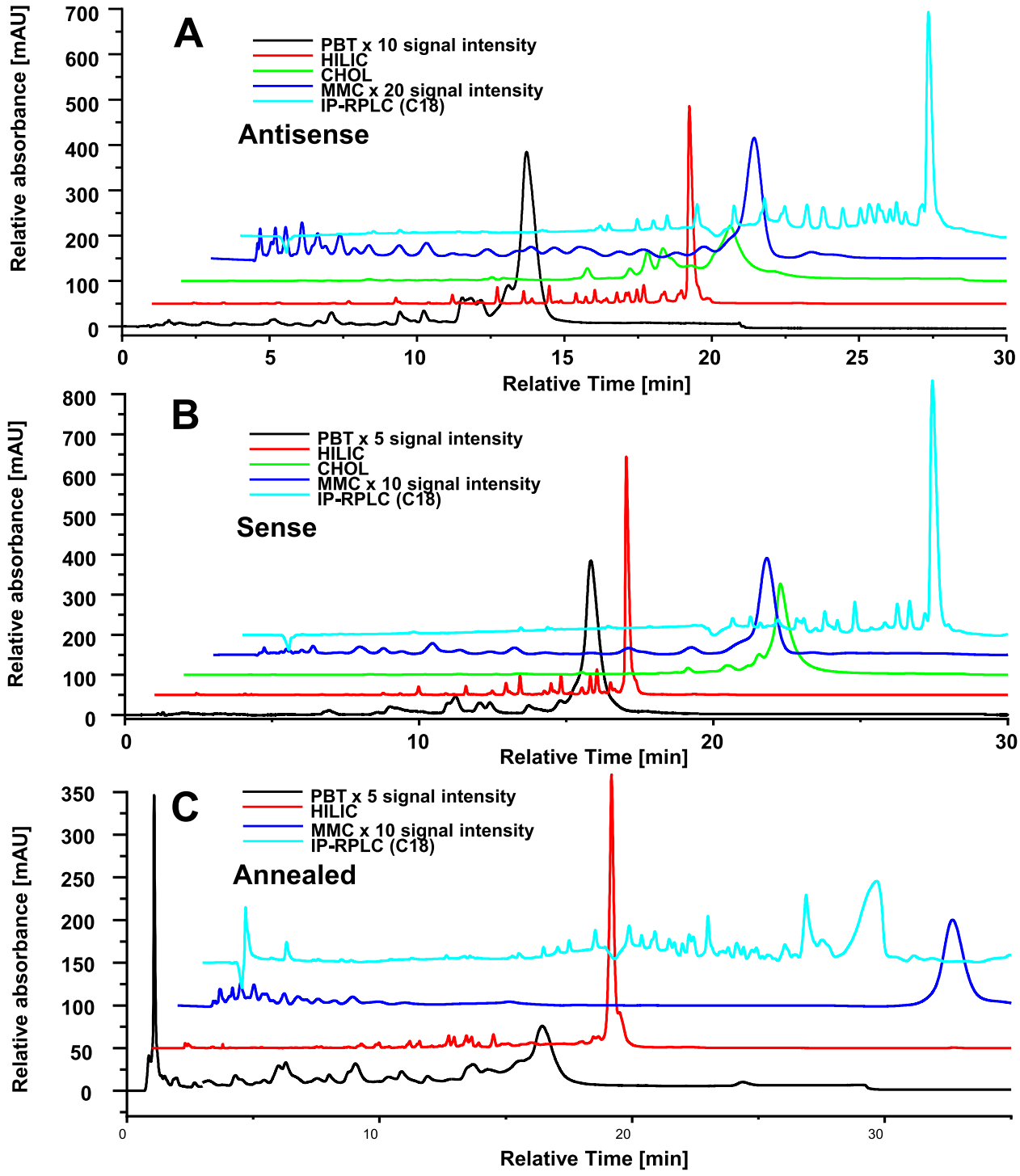

Fig. 3. 1D-LC UV-chromatograms of all investigated stationary phases for Patisiran. A: antisense strand; B: sense strand; C: annealed strand. For LC-conditions see chapter 2.5.

As outlined in the introduction, MMC established itself as attractive LC mode for ON separations. Both RP/WAX and zwitterionic MMC have shown potential [25,27]. The column we evaluate herein for MMC separation of ONs is an in-house synthesized RP/WAX material (5 µm, 100 Å), bonded via a polysiloxane film, with sulfonate endcapping (Fig 2C) [43,51]. This MMC stationary phase carries around 0.4 mmol *N*-(10-undecenoyl)-3-aminoquinuclidine ligand per g stationary phase (1.22 µmol/m^2) immobilized on a polysiloxane coated layer through thiol-ene click chemistry and subsequently oxidized to obtain sulfonate endcapping groups (total sulfur 0.7 mmol/g). The MMC phase exhibits positive ζ-potential of around 15–20 mV over a wide pH range between pH 3.5 and 7.5 in 10 mM KCl solution then slightly drops at pH 8.5 to 10 mV and becomes negative above pH 9 [43]. The sulfonate endcappings bring a shift of around −10 mV compared to the corresponding phase before oxidation. Hence, it was anticipated that this RP/WAX MMC material act primarily by a weak anion-exchange process while introducing additional interactions through hydrophobic (C11-alkyl strands) and polar non-covalent interactions (amide, sulfonyl groups). For efficient elution of multi-

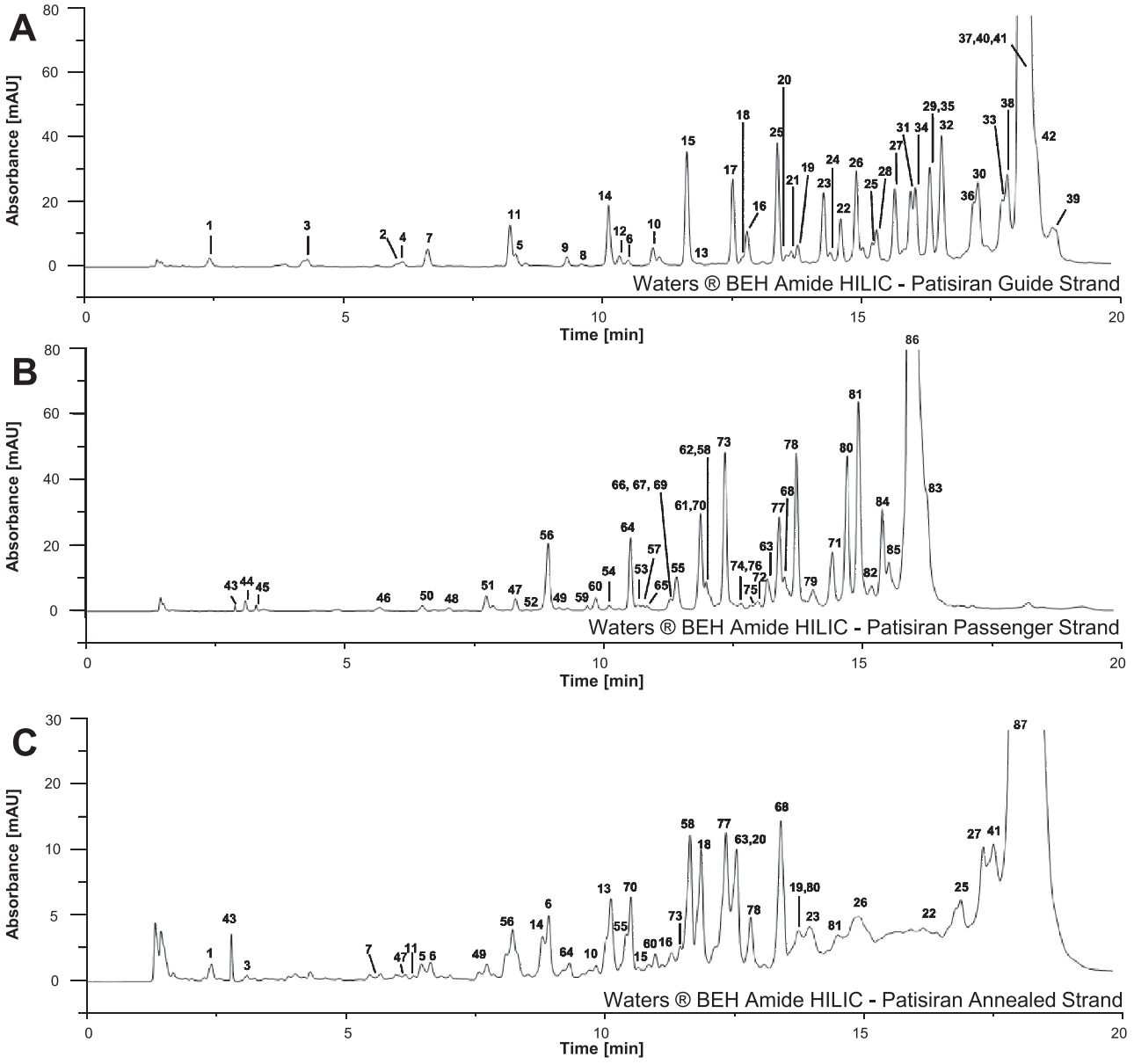

Fig. 4. 1D-LC UV-chromatograms of Patisiran under HILIC conditions with BEH Amide. All detected species are annotated. The annotations can be found in Table S1, Table S2 and Table S5. A: antisense strand; B: sense strand; C: annealed strand. For LC-condition see chapter 2.5.2.

ply negatively charged ONs, effective counterions are required and therefore, triethylammonium phosphate buffer was employed for elution.

The last tested stationary phase was a cholesterol-modified aminopropylsilica stationary phase (5 µm, 300 Å) (CHOL) (Fig. 2D) [28,37,38]. Cholesterol was bonded via carbamate linkage to 3-aminopropylsilica. The carbon content on the CHOL stationary phase was 9.97% with around 0.29 mmol of cholesterol ligand per g of stationary phase (2.61 µmol/m^2). Due to residual amino and silanol groups, attractive and repulsive ionic interactions may exist for ONs modulating the RP-type separation from the CHOL residue.

The chromatographic results for antisense and sense strands of Patisiran siRNA and deletion impurities are summarized in Table 2. Chromatograms are shown in Fig. 3A for antisense strand, in Fig. 3B for sense strand and in Fig. 3C for the annealed strand (duplex siRNA) of Patisiran. In general, retention increases with increasing number of nucleotides: i) in RP (PBT, CHOL) longer ONs have more nucleobases for hydrophobic and π-π-interactions, ii) in HILIC longer ON have more hydrophilic groups for polar interactions, iii) in MMC longer ONs have more negative charges leading to stronger anion-exchange interactions, and iv) in IP-RPLC longer ONs bind more IP agents leading to stronger hydrophobic interactions on C18 phases. Hence, there is always to some degree a correlation between different LC modes. However, it is already evident from these chromatograms that there are selectivity differences and the question emerged which is the most favourable column combination in ^{1}D and ^{2}D in view of orthogonality in their retention profiles.

3.2. Hydrophilic interaction chromatography with acquity UPLC BEH amide column

The retention behaviour of BPT-RPLC for Patisiran siRNA single strands and annealed strands (duplex siRNA as shown in Fig. 1) has been discussed in detail previously and corresponding separations by CHOL-RPLC in our recent reports [28,41]. Due to the promis-

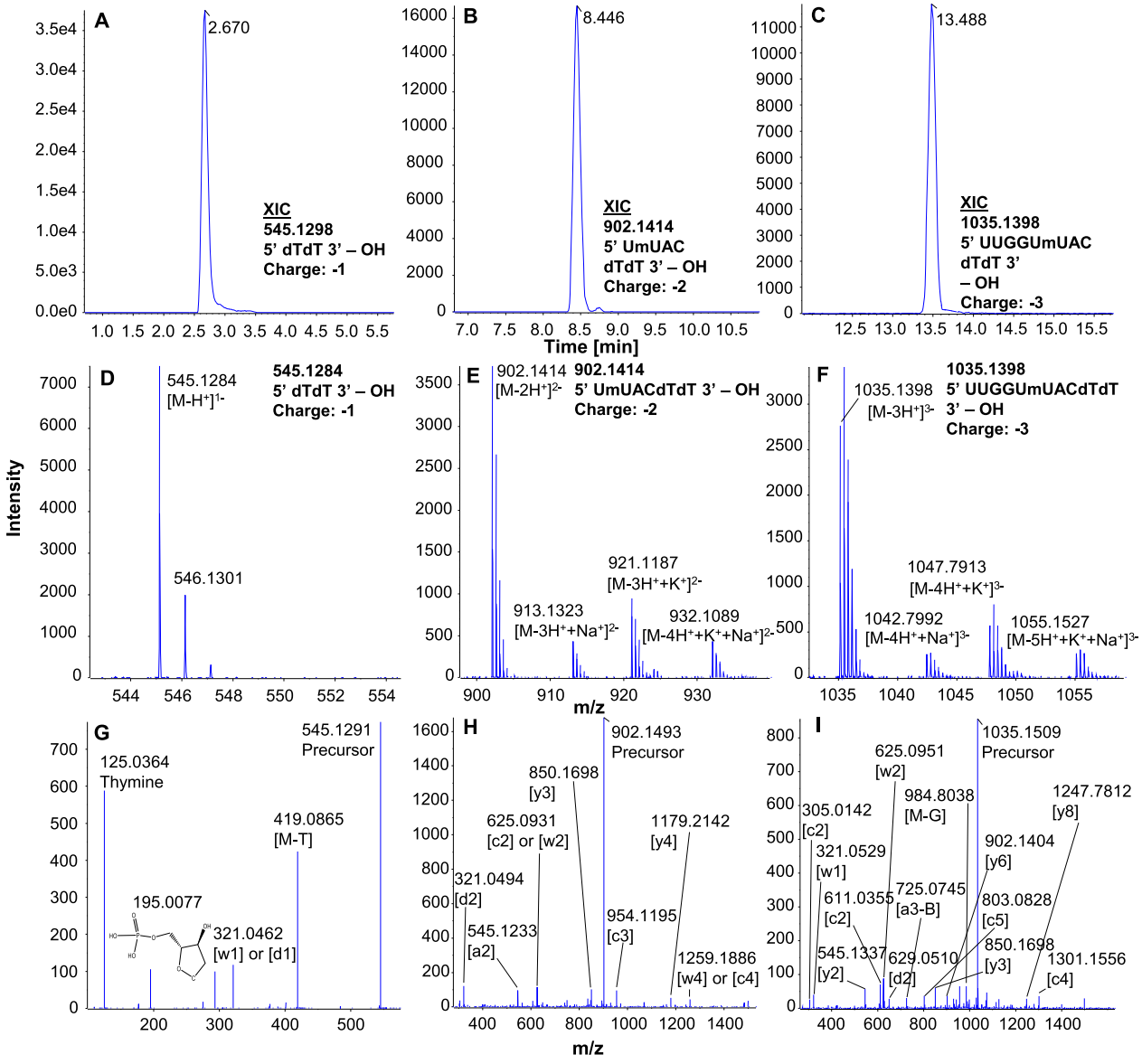

Fig. 5. HILIC-LC-MS and -MS^2 spectra and extracted ion chromatograms (EIC) of selected impurity species from antisense strand of Patisiran (for corresponding data of sense strand see suppl. Fig. S1). (A–C): EICs of the monoisotopic mass. (D–F): MS spectra of impurity species with the most abundant charge states. (G–I): MS^2 spectra of the corresponding precursor ion. For MS parameters see chapter 2.6.

ing results and high orthogonality towards PBT, the 1D-LC results with HILIC will be discussed in the upcoming chapter in more detail. Several groups recently reported successful HILIC separations of siRNAs and RNAs and outlined the great potential [19–21,52,53]. In this study, a series of HILIC separations with Patisiran siRNA (singe strands and duplex) was carried out on BEH Amide 1.7 µm (130 Å pore size) with mobile phases consisting of AA (15 mM) as buffer system and ACN. It was also used to verify the structural annotations of the impurities obtained by PBT-RPLC, described elsewhere [41]. As illustrated in Fig. 4, a significant number of impurity species could be well resolved from the main compound for both single strands and duplex of Patisiran within 20 min. However, it is also quite evident that several coelutions existed as well, in particular for the main component peaks. This makes robust HILIC-UV analysis of these impurities impossible. For this reason, ESI-MS detection is used for quantitative analysis of ON impurities coeluted with the main constituent, yet ion-suppression due to huge excess of main ON is compromising the quality and accuracy, respectively, for coeluted impurities.

One great benefit HILIC shares with PBT-RPLC and CHOL-RPLC is its preclusion of ion-pairing agents from the mobile phase, which in the direct ESI-coupling to MS avoids contamination of the MS instrument with ion-pair. For the other LC modes (MMC, IP-RPLC) an online desalting ^{2}D RPLC was coupled to remove ion-pair agent and non-volatile buffers via a diverter valve before introducing ONs into the ESI-MS, as described in detail previously [34]. For HILIC, ESI-MS was directly coupled and gave access to good quality spectra. This is exemplarily documented for ON impurities of different length in Fig 5. The EICs in Fig. 5A-C clearly demonstrate the increase in retention with length. MS (Fig. 5D-F) and MS^2 spectra (Fig. 5G-I) enabled the software-supported structural assignment of the ON impurities (BioToolkit for deconvolution of the charge envelopes, RoboOligo and OPA/OMA for sequence assignment as described in detail previously) [41,54,55]. More details about the structural annotation of the ON impurities are given in the suppl. material and in our last work [41]. Fourty one different impurity species besides the main compound were separated and characterized by ESI-TOF-MS in the antisense strand (see Fig. 4A and suppl.

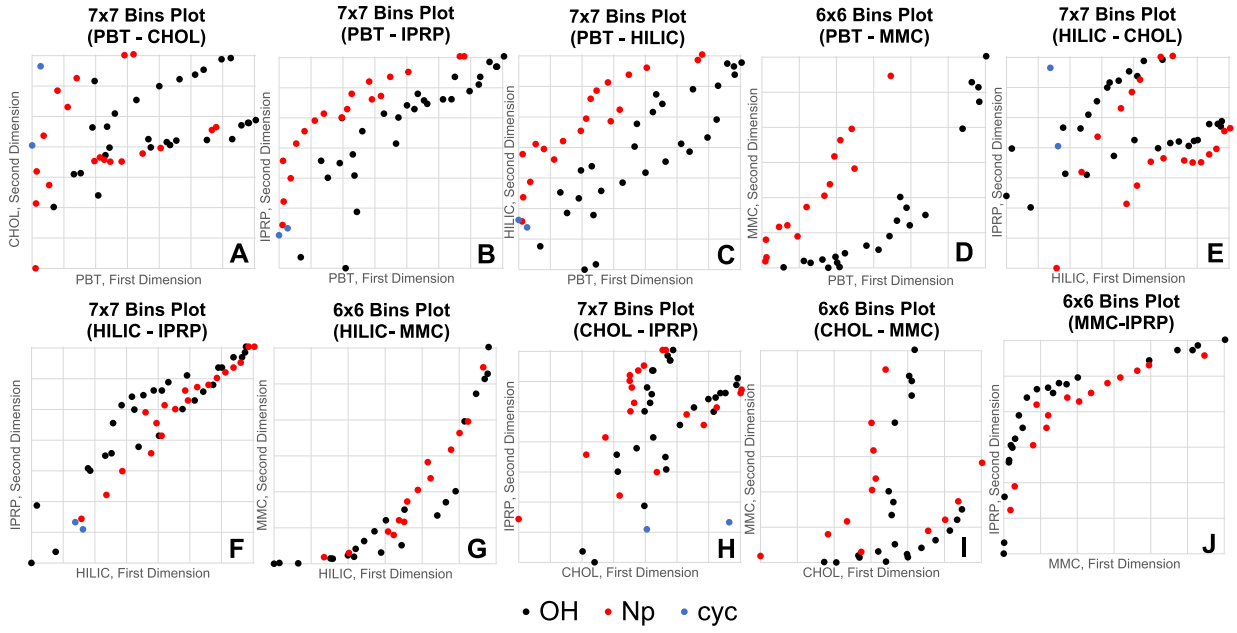

Fig. 6. Orthogonality evaluation of all column combinations by 2D bin plots. 2D Data sets are based on calculated normalized retention time in accordance to Eq. (1). A: PBT – CHOL, B: PBT – IPRP, C. PBT – HILIC, D: PBT – MMC, E: HILIC – CHOL, F: HILIC – IPRP, G: HILIC – MMC, H: CHOL – IPRP, I: CHOL – MMC, J: MMC – IPRP (note, all x- and y-scales from 0 to 1). ON impurity series with distinct substructures are in distinct colour; black, ON species with free hydroxy at 3′-end (OH); red, ON species with phosphate at 3′-end (Np); blue, cyclic 2′,3′-phosphate (phosphodiester) at 3′-end (cyc) (for more detailed description see ref. [29]).

Table S1). Due to the better chromatographic efficiency of the sub-2 µm HILIC column, 10 additional impurity species (Peak No.5, 6, 8, 18, 21, 22, 24, 32, 35, 42 in suppl. Table S1) were found. In the sense strand, 43 impurity species were resolved and detected by ESI-TOF-MS (see Fig. 4B, suppl. Fig. S1 and suppl. Table S2). Contrary to PBT-RPLC (where it eluted in the void volume), the duplex siRNA was retained under HILIC conditions (Fig. 4C). Although the duplex siRNA is bound by non-covalent bonds, it can withstand the ESI process in the gas phase without dissociation in the ion source or curtain plate (see Fig. S3 and S4 of suppl. material). Thus, RNA/DNA duplex can be detected intact by using this electrospray ionization technique for MS applications [56,57]. Hence, HILIC was deemed to be a powerful LC-mode for 2D-LC, yet a major criteria for its suitability is its orthogonality to other LC-modes.

3.3. Orthogonality

To quantify the orthogonality between the LC modes, we implemented both bin counting [35,36] and asterisk calculation [46] by plotting the normalized retention times of two columns to be compared in a 2D space. The results are graphically illustrated in Fig. 6 and the quantitative estimates of orthogonality are summarized in Table 3. From Table 3 it becomes evident that based on the bin counting method orthogonality declines in the order of the LC-pairs BPT-HILIC > PBT-CHOL > PBT-IPRP >CHOL-HILIC > CHOL-IPRP > IPRP-HILIC > PBT-MMC ~ CHOL-MMC > HILIC-MMC > IPRP-MMC. These orthogonality scores and the ranking, respectively, are related to the specific phase systems, i.e. stationary-mobile phase combination, and other employed experimental conditions like column temperature. With an overall orthogonality rate of 68%, the combination of RP-PBT and HILIC seems to be most promising for a 2D-LC setup. The interaction mechanism of PBT with ONs is based on hydrophobic and π-π-interactions while in HILIC it is a partitioning mechanism between adsorbed water-layer and bulk mobile phase, possibly with superimposed hydrogen-bonding and dipole-dipole interactions, which cause some spread in the 2D-retention space in spite of a general correlation as discussed above. Surprisingly, orthogonality is also significant between PBT- and CHOL-RPLC (O = 64%) although both are based primarily on hydrophobic interactions. Different secondary interactions of the CHOL phase (weak anion exchange resulting from the aminopropyl-backbone and steric interactions) and PBT (superimposed aromatic interactions) may be the origin of their complementary retention profiles. The O rate of PBT-RPLC with IP-RPLC and MMC is significantly lower (48% and 31%, respectively). Somewhat surprisingly, it was the lowest for the combination of IP-RPLC and MMC (O = 22%) which tentatively work by distinct retention mechanisms, hydrophobic interactions and anion-exchange. However, the former also relies on strong ionic interaction between the negatively charged analytes and positively charged quasi-stationary phase and with the IP agent, respectively, hence the modest orthogonality can be readily rationalized.

In the case of MMC, only 36 ONs could be detected and structurally annotated by MS which can be divided into 6 × 6 2D-separation space with 36 bins. A direct comparability of orthogonality values from different bin numbers (e.g. 6 × 6 vs. 7 × 7) seems to be questionable. To avoid this problem, the asterisk calculation has been applied as alternative, since this method does not depend on the numbers of components. The outcome of the orthogonality rate (A_0) was significantly different from the bin counting method (O). Overall, the A_0 values for MMC in combination with other LC modes were all increased (Table 3). Especially for MMC-CHOL and MMC-IPRP, the orthogonality rates increased by around 30%. Considering the other column combinations, the orthogonality rates mostly increased. Only for PBT-HILIC, the A_0 was reduced down to 60%. For CHOL, all A_0 values also become much higher. Recently, we also presented a 2D-LC method with HILIC-

Table 3
Orthogonality rate *O* (%) and asterisk value A_o (%) in accordance to Eqs. (2) and (3), respectively, between different LC modes. Numbers of bins and occupied bins are shown. The colorized cells in the right-hand triangle indicate the 2D-compatibility of the investigated stationary phases considering their mobile phases. Green: good compatibility, direct coupling possible; Yellow: limited, diverter valve required; Orange: ASM mandatory; Red: critical, diverter valve and ASM recommended (red).

A_O in % [a] / *O* in % [b] / Bin number / Number of occupied bins	RP-PBT	RP-CHOL		IP-RP		HILIC		MMC	
RP-PBT (27% MeOH)[c]	-	^{1}D	^{2}D	^{1}D	^{2}D	^{1}D	^{2}D	^{1}D	^{2}D
RP-CHOL (32% MeOH)[c]	68 64 49 27	-		^{1}D	^{2}D	^{1}D	^{2}D	^{1}D	^{2}D
IP-RP (38% ACN)[c]	55 48 49 22	64 39 49 19		-		^{1}D	^{2}D	^{1}D	^{2}D
HILIC (45% ACN)[c]	60 68 49 28	69 45 49 21		40 35 49 18		-		^{1}D	^{2}D
MMC (20% ACN)[c]	59 49 36	72 40 36		51 26 36		44 22 36		-	
	13	13		9		19			

[a] Defined according to Camenzuli and Schoenmakers [45]

[b] Defined according to Gilar et al. [36]

[c] Percentage of organic solvent at which the main peak (AS) eluted

: 60%-75% : 40-59% : 30-40% : below 30%

CHOL due to the high orthogonality (A_0=69%) [28]. The combination of hydrophobic and electrostatic interactions (resulting from residual amino groups) presumably strongly influence the retention of oligonucleotides on the surface of the CHOL. Thus, a mixed-mode mechanism can be assumed. This may be also one of the reasons for the satisfactory orthogonality of this stationary phase with many other LC modes [28].

From a more practical point of view, orthogonality may be estimated as sufficient if the ON impurities coeluted in the ^{1}D with the main peak can be resolved by the complementary ^{2}D method. To get a better idea how the distinct evaluated methods behave in this regard, Suppl. Table S6 provides specific information on this issue. As discussed, structurally similar shortmers like N-1 and N-2 are typically eluted beneath the main peak [41]. N-1, N-2, N-3 ON impurities and corresponding 3′-phosphorylated ON impurities were specifically evaluated in terms of their retention behaviour on the distinct columns and LC modes, and their separation from the main peak. With the PBT column, the ON peaks no 24 (5′ 18mer-OH; N-3) and 26 (5′ 19mer-OH; N-2) coeluted with the main ON peak of the antisense strand (peak no 29). On the HILIC column, peaks no 25 (3′ 18mer-Np) and 28 (3′ 19mer-Np) coeluted with the main ON peak 29 (AS), but ONs no 24 and 26 were separated.

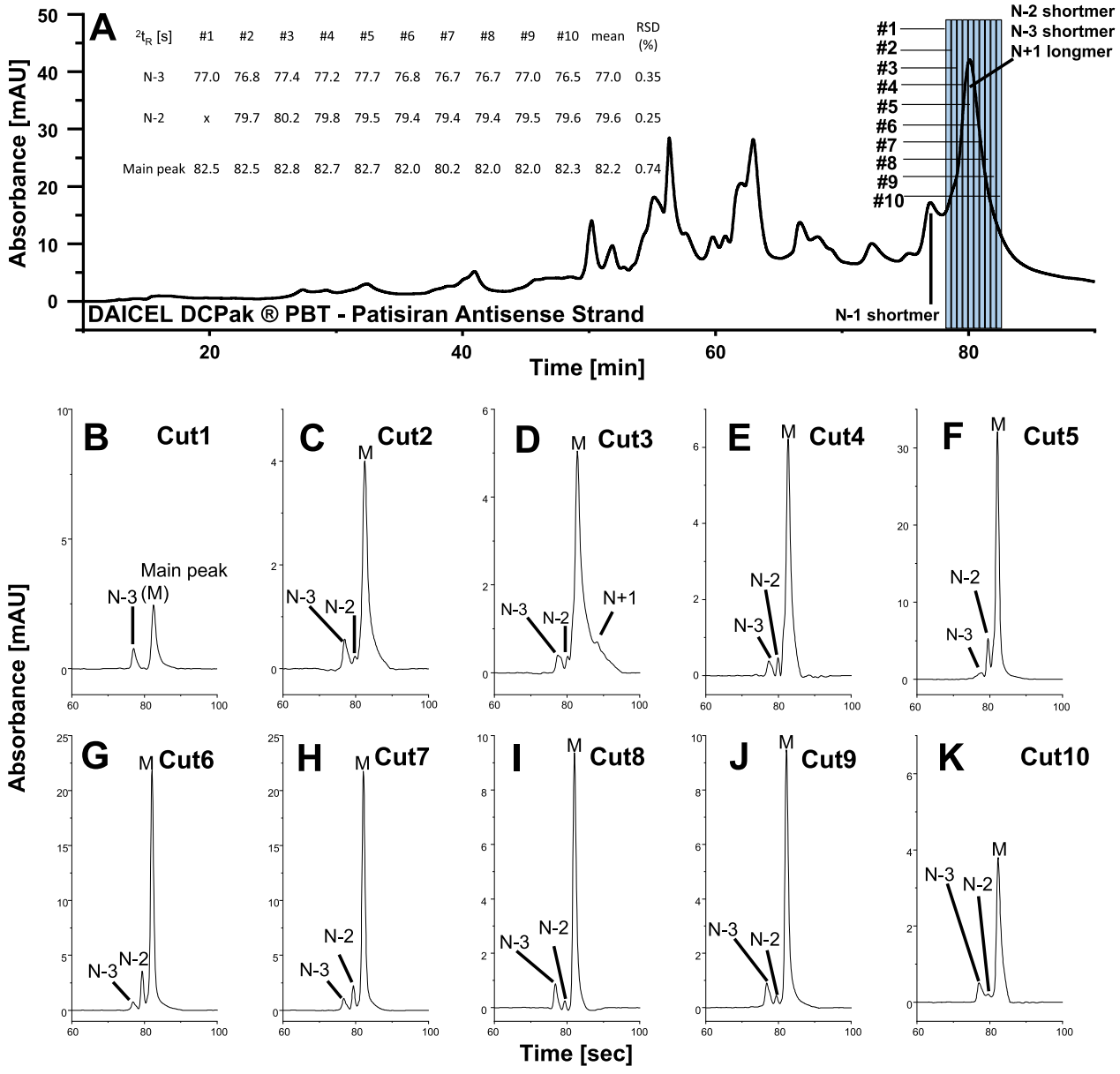

Fig. 7. Selective comprehensive sRP-HILIC-UV of the antisense strand of Patisiran (raw product without purification). A: The ^{1}D UV chromatogram with PBT. B-K: ^{2}D HILIC chromatograms of the 10 cuts. For LC conditions see chapter 2.5.5.

On the CHOL column, peaks no 24, 25, 26, 27, and 28 coeluted. On the MMC column, none of the impurities no 24, 26 and 28 coeluted with the main peak, but peaks no 25 and 27 were not detected which does not unequivocally allow to decide on their separation or coelution. In IP-RPLC, peaks no 25 and 27 coeluted with the main ON peak. From the selectivity stand point, PBT could be successfully coupled in a selective comprehensive 2D-LC method with the proposed HILIC, MMC and IP-RPLC methods. However, MMC and IP-RPLC are either not well ESI-MS compatible or lead to contamination of our MS instrument with ion-pair, respectively, for which reason the combination PBT-HILIC was selected for selective comprehensive 2D-LC of the antisense and sense ON strands of Patisiran.

3.4. Selective comprehensive (High resolution sampling) sRP×HILIC-2D-LC

Both PBT-RPLC and HILIC provided reasonable selectivity delivering impurity separations for antisense and sense strands, yet in both methods the main peaks were contaminated with coeluting impurities representing a problem for purity determination of pharmaceutical grade oligonucleotides by the preferred LC-UV method. In particular, N-1 and N-2 shortmers tend to coelute with the main peak [58]. PBT is capable to separate the N-1 impurities for both guide and passenger strand. However, for the N-2 impurities the PBT-RP method was not able to deliver enough selectivity leading to co-elution with the main peak. The situation is similar for HILIC in which co-elution existed in both guide and passenger strands. Thus, for peak purity testing of a pharmaceutical grade oligonucleotide a selective comprehensive (High-Resolution Sampling) sRP×HILIC-2D-LC method might be an appealing solution of the coelution problem [41].

Suppl. Fig. S6 and Table 3 can be used as guide for the selection of ^{1}D and ^{2}D LC-mode. Orthogonality and mobile phase compatibility are prime criteria for this purpose. Undersampling considerations may also be relevant in selective comprehensive if the ^{2}D does not show selectivity for the remixed compounds. If

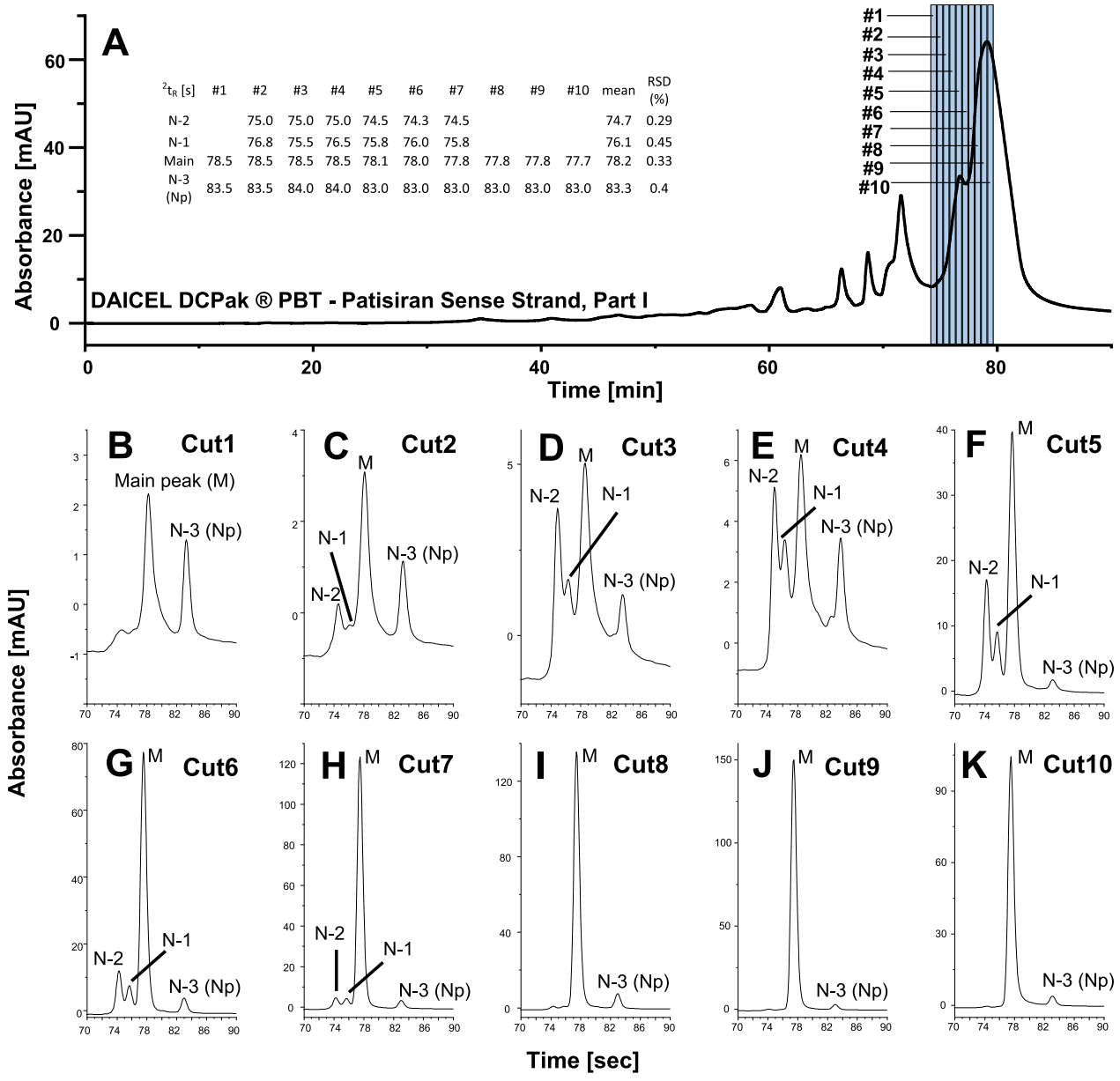

^2t_R [s]	#1	#2	#3	#4	#5	#6	#7	#8	#9	#10	mean	RSD (%)
N-2		75.0	75.0	75.0	74.5	74.3	74.5				74.7	0.29
N-1		76.8	75.5	76.5	75.8	76.0	75.8				76.1	0.45
Main	78.5	78.5	78.5	78.5	78.1	78.0	77.8	77.8	77.8	77.7	78.2	0.33
N-3 (Np)	83.5	83.5	84.0	84.0	83.0	83.0	83.0	83.0	83.0	83.0	83.3	0.4

Fig. 8. Selective comprehensive sRP-HILIC-UV of the sense strand of Patisiran (raw product without purification) (front end of the peak; for rear end of the back see suppl. Fig. S6). A: The ^{1}D UV chromatogram with PBT. B-K: ^{2}D HILIC chromatograms of the 10 cuts. For LC conditions see chapter 2.5.5.

we look at the chromatograms in Fig. 3, IP-RPLC and HILIC might appear as preferential choice due to their highest peak capacities. However, in Table 3 we can see that the orthogonality is only 35% which bears a high risk that coeluted compounds of the ^{1}D also coelute in the ^{2}D. Furthermore, if stable ion-pairs are injected into the ^{2}D with HILIC as separation mode, slow dissociation may easily cause peak broadening or even break through. The reversed order with HILIC in ^{1}D and IP-RPLC in the ^{2}D requires ASM. Due to the low O-value it was discarded. A high orthogonality (O = 68%, A_0=60%) was observed for the PBT-HILIC combination as outlined above which was finally selected, although there is no perfect match in mobile phase compatibility. The latter problem can be readily solved by ASM. To this end, the PBT method was selected as a ^{1}D and a short HILIC BEH Amide column (50 mm) as the ^{2}D due to its higher peak capacity while PBT and CHOL are more convenient form compatibility considerations. Since a MeOH gradient (negative water gradient from 91% to 46%) was used for the ^{1}D which is still a very strong eluent for the HILIC in the ^{2}D, some adjustments were implemented to avoid chromatographic problems due to incompatibility issues. The loop filling (loop volume: 40 µL) was kept at 50%. Thus, the transferred volume into the ^{2}D was 20 µL which is equivalent to ca. 11% of the void volume of the column of the ^{2}D. In order to enable a dilution of ^{1}D effluent containing MeOH with weak solvent prior to transfer to the ^{2}D, the ASM option was activated (ASM loop was flushed 3 times for 0.39 min) [45]. With these adjustments, no break-through or other incompatibility phenomena were observed. The results of the peak purity testing by sRP×HILIC-UV are presented for the antisense strand in Fig. 7 and for the sense strand in Fig. 8 and Fig. S5 of supplementary materials.

In Fig 7A, the chromatogram of the PBT-RPLC separation of the ^{1}D is depicted. Ten consecutive cuts across the main peak were taken and injected into the ^{2}D with HILIC-LC-UV; the individual chromatograms of each cut are shown in Fig. 7B-7K. The most critical impurity from LC separation point of view is the N-1 shortmer which in the majority of LC modes coelutes with the main

entity. In Fig. 7A, it becomes readily evident that this N-1 impurity is already separated in the ^{1}D PBT-RPLC while it is coeluted in the HILIC method of the ^{2}D (Table 2, no. 28 or Table S1, no. 40). On the other hand, two additional peaks (N-3 and N-2 shortmers) are separated from the main peak (M) of the antisense strand in the ^{2}D-HILIC (Fig. 7B-K) and further an additional shoulder of the $N + 1$ longmer becomes visible on the tailing edge of the main peak in cut #3 (Fig. 7D). Impurity N-2 shortmer and N-3 shortmer were not detected in the ^{1}D-RPLC method and now clearly separated in the sRPLC×HILIC 2D-LC method enabling quantitative estimation by UV, without interferences, instead of ESI-MS which may be influenced more strongly by the detector response and ion-suppression, respectively [59]. In the case of shortmers, N-3 and N-2 are present in relatively high amounts in the present non-purified test sample exceeding common thresholds [60]. In the case of the sense strand shown in Fig. 8 and Fig. S5, 20 cuts (divided into two consecutive experiments) across the main peak in the ^{1}D PBT-RPLC separation were sampled into the 2 loop decks (Fig. 7A, Fig. S5A) and injected into the ^{2}D-HILIC phase system. Co-eluting N-1, N-2, N-3 and N-3(Np) impurities underneath the main peak of the sense strand (Fig 8, A) with PBT-RPLC were well separated in the ^{2}D HILIC separation (Fig. 8B-8K). Here, it becomes evident that the N-1 shortmer can also be well resolved by HILIC because the retention shift of the ON with G less is significantly more pronounced than in case of the antisense strand where the N-1 impurity had an A less. N-2 and 3′-phosphorylated N-3 (Np) were further resolved. Again, the sRPLC×HILIC 2D-LC method provides a good overview of the peak purity of the sense strand in the PBT-RPLC separation and can be a useful tool for method optimization and quality control of pharmaceutical grade siRNA and ONs, respectively. Since the main component peak of the PBT-RPLC separation of the sense strand could not be completely transferred into the second dimension with the 10 cuts, the remaining second part of the peak was sampled into the ^{2}D by a second run. No additional impurities could be detected in the tailing edge of the peak (see suppl. Fig. S5). A critical issue when HILIC is employed as ^{2}D is its reproducibility. It has been discussed that column reequilibration is slow in HILIC [61]. It might be a problem with fast second dimensions as used herein (^{2}D run time 90 s). With a re-equilibration time of 1.14 min, we determined retention time repeatabilities of typically 0.2 and 0.4% RSD. It is considered adequate for allowing to assign the corresponding peaks between the different cuts.

It is thus concluded that the combination of two different LC-modes resulted in higher selectivity that is not achievable in a one-dimensional analysis of oligonucleotide impurities. If only 1D PBT-RPLC-UV or only 1D HILIC-UV were considered for comparison, new impurity peaks would have been detected by sRP×HILIC-UV. In the same time no ion-pairing agent was needed in this separation (precluding contamination of the MS system, also extending column lifetime) and satisfactory sensitivity was achieved because of the efficient HILIC application in the ^{2}D. The negative effect on sensitivity arising from unavoidable dilution is less critical for quality control of pharmaceuticals because there is no sample shortage and hence the dilution effect can be compensated by injecting higher sample loads. From this perspective it makes sense to have a high capacity stationary phase in the first dimension.

4. Conclusion

In this work, we compared the retention profiles of five different stationary phases and LC modes, respectively, to investigate the orthogonality between them. As result, a very high orthogonality rate of 68% (calculated with bin counting method) was revealed by the combination of PBT with BEH Amide (RP – HILIC). Both are used with MS-friendly mobile phases (ion-pair free, volatile buffers) and avoid contamination of the MS instrument which is of importance in non-dedicated MS systems. The high orthogonality is favourable for the combination of the two LC modalities in a 2D-LC setup. Herein we evaluated sRPLC×HILIC 2D-LC to resolve critical shortmer impurities co-eluting with the main peak in 1D-LC. Due to the lack of separation power to distinguish structurally closely related ON species like N-1, N-2 and N-3 for both RP and HILIC in 1D-LC methods, a peak purity determination by selective comprehensive 2D-LC can be a powerful tool for quality control of pharmaceutical grade ONs, also in other combination of phase systems and LC modes. Currently, it is believed that 2D-LC is too complicated and not robust enough to be used on a routine basis in QC of pharmaceuticals. However, with modern instruments and dedicated software this situation seems to gradually change. Especially for very complex pharmaceuticals, 2D-LC in multiple heart-cutting and selective comprehensive mode can be easily implemented by experienced chromatographers with significant gain in information and reliability about product quality. For the majority of disadvantages, some solutions have been presented, e.g. active solvent modulation for the compatibility problem, dilution effects by trapping columns, and so forth. Higher investments costs (as instrumentation and columns are duplicated) must be seen in relation to the faster acquisition of information by 2D-LC as compared to 1D-LC if a set of generic 2D-LC methods with broader applicability are established in the lab.

Declaration of Competing Interest

The authors declare that they have no known competing financial interests or personal relationships that could have appeared to influence the work reported in this paper.

CRediT authorship contribution statement

Feiyang Li: Investigation, Methodology, Formal analysis, Data curation, Visualization, Writing – original draft, Writing – review & editing. **Shenkai Chen:** Investigation. **Sylwia Studzińska:** Methodology, Investigation, Supervision, Writing – review & editing. **Michael Lämmerhofer:** Conceptualization, Methodology, Supervision, Writing – review & editing, Resources, Funding acquisition.

Data availability

The raw data reported in this work (wiff files) are available at Mendeley Data. DOI:10.17632/3zk8cvxc7m.1.

Acknowledgments

We are grateful to Agilent Technologies for support of this research by an Agilent Research Award (#4068). The authors thank Dr. Stephan Buckenmaier from Agilent Technologies, Waldbronn, Germany, for technical advice and valuable discussions. This work was financially supported by Torun center of Excellence “Towards Personalized Medicine” operating under Excellence Initiative-Research University (Sylwia Studzińska). We are grateful to Chiral Technologies Europe and Dr. Pilar Franco for providing DCpak PBT as test column.

Supplementary materials

Supplementary material associated with this article can be found, in the online version, at doi:10.1016/j.chroma.2023.464069.

References

[1] C.F. Bennett, Therapeutic antisense oligonucleotides are coming of age, Annu. Rev. Med. 70 (2019) 307–321, doi:10.1146/annurev-med-041217-010829.

[2] A. Khvorova, J.K. Watts, The chemical evolution of oligonucleotide therapies of clinical utility, Nat. Biotechnol. 35 (2017) 238–248, doi:10.1038/nbt.3765.
[3] F. Wang, T. Zuroske, J.K. Watts, RNA therapeutics on the rise, Nat. Rev. Drug Discov. (2020), doi:10.1038/d41573-020-00078-0.
[4] S. Thakur, A. Sinhari, P. Jain, H.R. Jadhav, A perspective on oligonucleotide therapy: approaches to patient customization, Front. Pharmacol. 13 (2022) 1–22, doi:10.3389/fphar.2022.1006304.
[5] FDA, Clinical pharmacology considerations for the development of oligonucleotide therapeutics guidance for industry DRAFT GUIDANCE, FDA Guid. 1 (2022) 1–10 https://www.fda.gov/drugs/guidance-compliance-regulatory-information/guidances-drugs.
[6] F. Hannauer, R. Black, A.D. Ray, E. Stulz, G.J. Langley, S.W. Holman, Advancements in the characterisation of oligonucleotides by high performance liquid chromatography-mass spectrometry in 2021: a short review, Anal. Sci. Adv. 3 (2022) 90–102, doi:10.1002/ansa.202100066.
[7] A. Goyon, P. Yehl, K. Zhang, Characterization of therapeutic oligonucleotides by liquid chromatography, J. Pharm. Biomed. Anal. 182 (2020) 113105, doi:10.1016/j.jpba.2020.113105.
[8] E. Urban, C.R. Noe, Structural modifications of antisense oligonucleotides, Farmaco 58 (2003) 243–258, doi:10.1016/S0014-827X(03)00022-3.
[9] A. Kanavarioti, HPLC methods for purity evaluation of man-made single-stranded RNAs, Sci. Rep. 9 (2019) 1–13, doi:10.1038/s41598-018-37642-z.
[10] A. Apffel, J.A. Chakel, S. Fischer, K. Lichtenwalter, W.S. Hancock, Analysis of oligonucleotides by HPLC-electrospray ionization mass spectrometry, Anal. Chem. 69 (1997) 1320–1325, doi:10.1021/ac960916h.
[11] M. Gilar, K.J. Fountain, Y. Budman, J.L. Holyoke, H. Davoudi, J.C. Gebler, Characterization of therapeutic oligonucleotides using liquid chromatography with on-line mass spectrometry detection, Oligonucleotides 13 (2003) 229–243, doi:10.1089/154545703322460612.
[12] M. Gilar, K.J. Fountain, Y. Budman, U.D. Neue, K.R. Yardley, P.D. Rainville, R.J. Russell, J.C. Gebler, Ion-pair reversed-phase high-performance liquid chromatography analysis of oligonucleotides: retention prediction, J. Chromatogr. A 958 (2002) 167–182, doi:10.1016/S0021-9673(02)00306-0.
[13] F. Li, M. Lämmerhofer, Impurity profiling of siRNA by two-dimensional liquid chromatography-mass spectrometry with quinine carbamate anion-exchanger and ion-pair reversed-phase chromatography, J. Chromatogr. A 1643 (2021) 462065, doi:10.1016/j.chroma.2021.462065.
[14] S. Studzińska, R. Rola, B. Buszewski, The impact of ion-pairing reagents on the selectivity and sensitivity in the analysis of modified oligonucleotides in serum samples by liquid chromatography coupled with tandem mass spectrometry, J. Pharm. Biomed. Anal. 138 (2017) 146–152, doi:10.1016/j.jpba.2017.02.014.
[15] M. Enmark, S. Harun, J. Samuelsson, E. Örnskov, L. Thunberg, A. Dahlén, T. Fornstedt, Selectivity limits of and opportunities for ion pair chromatographic separation of oligonucleotides, J. Chromatogr. A 1651 (2021) 462269, doi:10.1016/j.chroma.2021.462269.
[16] M. Enmark, M. Rova, J. Samuelsson, E. Örnskov, F. Schweikart, T. Fornstedt, Investigation of factors influencing the separation of diastereomers of phosphorothioated oligonucleotides, Anal. Bioanal. Chem. 411 (2019) 3383–3394, doi:10.1007/s00216-019-01813-2.
[17] M. Donegan, J.M. Nguyen, M. Gilar, Effect of ion-pairing reagent hydrophobicity on liquid chromatography and mass spectrometry analysis of oligonucleotides, J. Chromatogr. A 1666 (2022) 462860, doi:10.1016/j.chroma.2022.462860.
[18] Z. Kadlecová, K. Kalíková, E. Tesařová, M. Gilar, Phosphorothioate oligonucleotides separation in ion-pairing reversed-phase liquid chromatography: effect of ion-pairing system, J. Chromatogr. A 1676 (2022) 463473, doi:10.1016/j.chroma.2022.463201.
[19] M. Huang, X. Xu, H. Qiu, N. Li, Analytical characterization of DNA and RNA oligonucleotides by hydrophilic interaction liquid chromatography-tandem mass spectrometry, J. Chromatogr. A 1648 (2021) 462184, doi:10.1016/j.chroma.2021.462184.
[20] A. Demelenne, G. Nys, C. Nix, J.C. Fjeldsted, J. Crommen, M. Fillet, Separation of phosphorothioated oligonucleotide diastereomers using multiplexed drift tube ion mobility mass spectrometry, Anal. Chim. Acta 1191 (2022) 339297, doi:10.1016/j.aca.2021.339297.
[21] P.A. Lobue, M. Jora, B. Addepalli, P.A. Limbach, Oligonucleotide analysis by hydrophilic interaction liquid chromatography-mass spectrometry in the absence of ion-pair reagents, J. Chromatogr. A. 1595 (2019) 39–48, doi:10.1016/j.chroma.2019.02.016.
[22] A.M. Abdullah, C. Sommers, J. Hawes, J.D. Rodriguez, K. Yang, Tandem mass spectrometric sequence characterization of synthetic thymidine-rich oligonucleotides, J. Mass Spectrom. 57 (2022), doi:10.1002/jms.4819.
[23] Q. Li, F. Lynen, J. Wang, H. Li, G. Xu, P. Sandra, Comprehensive hydrophilic interaction and ion-pair reversed-phase liquid chromatography for analysis of dito deca-oligonucleotides, J. Chromatogr. A 1255 (2012) 237–243, doi:10.1016/j.chroma.2011.11.062.
[24] H. Lardeux, D. Guillarme, V. D'Atri, Comprehensive evaluation of zwitterionic hydrophilic liquid chromatography stationary phases for oligonucleotide characterization, J. Chromatogr. A (2023) 1690, doi:10.1016/j.chroma.2023.463785.
[25] A. Zimmermann, R. Greco, I. Walker, J. Horak, A. Cavazzini, M. Lämmerhofer, Synthetic oligonucleotide separations by mixed-mode reversed-phase/weak anion-exchange liquid chromatography, J. Chromatogr. A 1354 (2014) 43–55, doi:10.1016/j.chroma.2014.05.048.
[26] S. Bäurer, S. Polnick, O.L. Sánchez-Muñoz, M. Kramer, M. Lämmerhofer, N-Propyl-N′-2-pyridylurea-modified silica as mixed-mode stationary phase with moderate weak anion exchange capacity and pH-dependent surface charge reversal, J. Chromatogr. A 1560 (2018) 45–54, doi:10.1016/j.chroma.2018.05.012.
[27] M. Biba, E. Jiang, B. Mao, D. Zewge, J.P. Foley, C.J. Welch, Factors influencing the separation of oligonucleotides using reversed-phase/ion-exchange mixed-mode high performance liquid chromatography columns, J. Chromatogr. A 1304 (2013) 69–77, doi:10.1016/j.chroma.2013.06.050.
[28] S. Studzińska, F. Li, M. Szumski, B. Buszewski, M. Lämmerhofer, Cholesterol stationary phase in the separation and identification of siRNA impurities by two-dimensional liquid chromatography-mass spectrometry, Int. J. Mol. Sci. 23 (2022), doi:10.3390/ijms232314960.
[29] F. Li, S. Chen, S. Studzińska, M. Lämmerhofer, Polybutylene terephthalate-based stationary phase for ion-pair-free reversed-phase liquid chromatography of small interfering RNA. Part 1: direct coupling with mass spectrometry, J. Chromatogr. A 1694 (2023) 463898, doi:10.1016/j.chroma.2023.463898.
[30] B.W.J. Pirok, D.R. Stoll, P.J. Schoenmakers, Recent developments in two-dimensional liquid chromatography: fundamental improvements for practical applications, Anal. Chem. 91 (2019) 240–263, doi:10.1021/acs.analchem.8b04841.
[31] S. Studzińska, Ł. Nuckowski, B. Buszewski, Oligonucleotides isolation and separation—a review on adsorbent selection, Int. J. Mol. Sci. 23 (2022), doi:10.3390/ijms23179546.
[32] A. Goyon, K. Zhang, Characterization of antisense oligonucleotide impurities by ion-pairing reversed-phase and anion exchange chromatography coupled to HILIC/MS using a versatile 2D-LC setup, Anal. Chem. (2020), doi:10.1021/acs.analchem.0c00114.
[33] Q. Li, F. Lynen, J. Wang, H. Li, G. Xu, P. Sandra, Comprehensive hydrophilic interaction and ion-pair reversed-phase liquid chromatography for analysis of dito deca-oligonucleotides, J. Chromatogr. A 1255 (2012) 237–243, doi:10.1016/j.chroma.2011.11.062.
[34] F. Li, X. Su, S. Bäurer, M. Lämmerhofer, Multiple heart-cutting mixed-mode chromatography-reversed-phase 2D-liquid chromatography method for separation and mass spectrometric characterization of synthetic oligonucleotides, J. Chromatogr. A 1625 (2020) 461338, doi:10.1016/j.chroma.2020.461338.
[35] M. Gilar, J. Fridrich, M.R. Schure, A. Jaworski, Comparison of orthogonality estimation methods for the two-dimensional separations of peptides, Anal. Chem. 84 (2012) 8722–8732, doi:10.1021/ac3020214.
[36] M. Gilar, P. Olivova, A.E. Daly, J.C. Gebler, Orthogonality of separation in two-dimensional liquid chromatography, Anal. Chem. 77 (2005) 6426–6434, doi:10.1021/ac050923i.
[37] S. Studzińska, K. Krzemińska, M. Szumski, B. Buszewski, Application of a cholesterol stationary phase in the analysis of phosphorothioate oligonucleotides by means of ion pair chromatography coupled with tandem mass spectrometry, Talanta 154 (2016) 270–277, doi:10.1016/j.talanta.2016.03.082.
[38] S. Studzińska, L. Pietrzak, B. Buszewski, The effects of stationary phases on retention and selectivity of oligonucleotides in IP-RP-HPLC, Chromatographia 77 (2014) 1589–1596, doi:10.1007/s10337-014-2766-x.
[39] European Medicines Agency, European Public Assessment Report: Onpattro (Patisiran), 44 (2018). www.ema.europa.eu/contact.
[40] Food and, Approval Package for: Onpattro, Dep. Heal. Hum. Serv., 2018.
[41] F. Li, M. Laemmerhofer, S. Studzińska, S. Chen, Polybutylene terephthalate-based stationary phase for ion-pair-free reversed- phase liquid chromatography-mass spectrometry of small interfering RNA Feiyang Li, J. Chromatogr. A (2023) In Press.
[42] B. Buszewski, M. Jezierska-Switala, R. Kaliszan, A. Wojtczak, K. Albert, S. Bachmann, M.T. Matyska, J.J. Pesek, Selectivity tuning and molecular modeling of new generation packings for RP HPLC, Chromatographia 53 (2001), doi:10.1007/bf02490329.
[43] S. Bäurer, A. Zimmermann, U. Woiwode, O.L. Sánchez-Muñoz, M. Kramer, J. Horak, W. Lindner, W. Bicker, M. Lämmerhofer, Stable-bond polymeric reversed-phase/weak anion-exchange mixed-mode stationary phases obtained by simultaneous functionalization and crosslinking of a poly(3-mercaptopropyl)methylsiloxane-film on vinyl silica via thiol-ene double click reaction, J. Chromatogr. A 1593 (2019) 110–118, doi:10.1016/j.chroma.2019.01.078.
[44] M. Rosés, X. Subirats, E. Bosch, Retention models for ionizable compounds in reversed-phase liquid chromatography. Effect of variation of mobile phase composition and temperature, J. Chromatogr. A 1216 (2009) 1756–1775, doi:10.1016/j.chroma.2008.12.042.
[45] D.R. Stoll, K. Shoykhet, P. Petersson, S. Buckenmaier, Active solvent modulation: a valve-based approach to improve separation compatibility in two-dimensional liquid chromatography, Anal. Chem. 89 (2017) 9260–9267, doi:10.1021/acs.analchem.7b02046.
[46] M. Camenzuli, P.J. Schoenmakers, A new measure of orthogonality for multi-dimensional chromatography, Anal. Chim. Acta. 838 (2014) 93–101, doi:10.1016/j.aca.2014.05.048.
[47] M.R. Schure, The dimensionality of chromatographic separations, J. Chromatogr. A 1218 (2011) 293–302, doi:10.1016/j.chroma.2010.11.016.
[48] W. Nowik, S. Héron, M. Bonose, M. Nowik, A. Tchapla, Assessment of two-dimensional separative systems using nearest-neighbor distances approach. Part 1: orthogonality aspects, Anal. Chem. 85 (2013) 9449–9458, doi:10.1021/ac4012705.
[49] J. Jáčová, A. Gardlo, J.M.D. Dimandja, T. Adam, D. Friedecký, Impact of sample dimensionality on orthogonality metrics in comprehensive two-dimensional separations, Anal. Chim. Acta 1064 (2019) 138–149, doi:10.1016/j.aca.2019.03.018.
[50] J. Mommers, S. van der Wal, Two metrics for measuring orthogonality for two-dimensional chromatography, J. Chromatogr. A 1586 (2019) 101–105, doi:10.1016/j.chroma.2018.11.081.

[51] A. Zimmermann, J. Horak, A. Sievers-Engler, C. Sanwald, W. Lindner, M. Kramer, M. Lämmerhofer, Surface-crosslinked poly(3-mercaptopropyl)methylsiloxane-coatings on silica as new platform for low-bleed mass spectrometry-compatible functionalized stationary phases synthesized via thiol-ene click reaction, J. Chromatogr. A 1436 (2016) 73–83, doi:10.1016/j.chroma.2016.01.058.
[52] R. MacNeill, T. Hutchinson, V. Acharya, R. Stromeyer, S. Ohorodnik, An oligonucleotide bioanalytical LC–SRM methodology entirely liberated from ion-pairing, Bioanalysis 11 (2019) 1155–1167, doi:10.4155/bio-2019-0031.
[53] A. Demelenne, M.-J. Gou, G. Nys, C. Parulski, J. Crommen, A.-C. Servais, M. Fillet, Evaluation of hydrophilic interaction liquid chromatography, capillary zone electrophoresis and drift tube ion-mobility quadrupole time of flight mass spectrometry for the characterization of phosphodiester and phosphorothioate oligonucleotides, J. Chromatogr. A 1614 (2020) 460716, doi:10.1016/j.chroma.2019.460716.
[54] P.J. Sample, K.W. Gaston, J.D. Alfonzo, P.A. Limbach, RoboOligo: software for mass spectrometry data to support manual and de novo sequencing of post-transcriptionally modified ribonucleic acids, Nucleic Acids Res. 43 (2015) 1–13, doi:10.1093/nar/gkv145.
[55] A. Nyakas, L.C. Blum, S.R. Stucki, J.L. Reymond, S. Schürch, OMA and OPA - software-supported mass spectra analysis of native and modified nucleic acids, J. Am. Soc. Mass Spectrom. 24 (2013) 249–256, doi:10.1007/s13361-012-0529-1.
[56] D.C. Gale, R.D. Smith, Characterization of noncovalent complexes formed between minor groove binding molecules and duplex DNA by electrospray ionization-mass spectrometry, J. Am. Soc. Mass Spectrom. 6 (1995) 1154–1164, doi:10.1016/1044-0305(95)00530-7.
[57] E. Bayer, T. Bauer, K. Schmeer, K. Bleicher, M. Maier, H.J. Gaus, Analysis of double-stranded oligonucleotides by electrospray mass spectrometry, Anal. Chem. 66 (1994) 3858–3863, doi:10.1021/ac00094a004.
[58] J. Abi-Ghanem, V. Gabelica, Nucleic acid ion structures in the gas phase, Phys. Chem. Chem. Phys. 16 (2014) 21204–21218, doi:10.1039/c4cp02362e.
[59] B. Basiri, M.M. Murph, M.G. Bartlett, Assessing the interplay between the physicochemical parameters of ion-pairing reagents and the analyte sequence on the electrospray desorption process for oligonucleotides, J. Am. Soc. Mass Spectrom. 28 (2017) 1647–1656, doi:10.1007/s13361-017-1671-6.
[60] D. Capaldi, K. Ackley, D. Brooks, J. Carmody, K. Draper, R. Kambhampati, M. Kretschmer, D. Levin, J. McArdle, B. Noll, R. Raghavachari, I. Roymoulik, B.P. Sharma, R. Thürmer, F. Wincott, Quality aspects of oligonucleotide drug development: specifications for active pharmaceutical ingredients, Drug Inf. J. 46 (2012) 611–626, doi:10.1177/0092861512445311.
[61] D.V. McCalley, Managing the column equilibration time in hydrophilic interaction chromatography, J. Chromatogr. A. 1612 (2020) 460655, doi:10.1016/j.chroma.2019.460655.

Supplementary Material

Polybutylene terephthalate-based stationary phase for ion-pair-free reversed-phase liquid chromatography of small interfering RNA. Part 2: Use for selective comprehensive two-dimensional liquid chromatography

Feiyang Li[a], Shenkai Chen[a], Sylwia Studzińska[a,b], Michael Lämmerhofer[a]*

[a] Institute of Pharmaceutical Sciences, Pharmaceutical (Bio-)Analysis, University of Tübingen, Auf der Morgenstelle 8, 72076 Tübingen, Germany

[b] Chair of Environmental Chemistry and Bioanalytics, Faculty of Chemistry, Nicolaus Copernicus University in Torun, 7 Gagarin Str., PL-87-100 Toruń, Poland

*Author for correspondence:

Prof. Dr. Michael Lämmerhofer

Pharmaceutical (Bio-)Analysis

Institute of Pharmaceutical Sciences

University of Tübingen

Auf der Morgenstelle 8

72076 Tübingen, Germany

T +49 7071 29 78793, F +49 7071 29 4565

E-mail: michael.laemmerhofer@uni-tuebingen.de

Characterization and structural annotation of ON impurities by HILIC-ESI-MS

1. Antisense strand

Fourty one different impurity species besides the main compound were separated and characterized by ESI-TOF-MS (Suppl. Table S1, Fig. 4A of the main document). Contrary to RP-LC with DCpak PBT, 10 additional species (Peak No.5, 6, 8, 18, 21, 22, 24, 32, 35, 42; Table S1) were found which could be separated from the main product and identified by MS^1 and MS^2 spectra. Since the partition of the analytes between the water- and organic layer is the predominating interaction mechanism of BEH Amide, the increasing polarity of heavier/longer RNA strands leads to stronger retention. Also, more impurities with a cyclic phosphate at 3' end could be distinguished due to the higher chromatographic efficiency by HILIC using sub-2µm particle. Furthermore, an N+1 longmer impurity with an additional nucleotide at 5' end was detected as well (Peak No.42, Table S1). These effects can probably be attributed also to a better ionization efficiency and consequently improved sensitivity due to highly organic mobile phases used in HILIC (Fig. 5, A, B, C of the main document). Furthermore, both MS^1 and MS^2 spectra of three representative impurity species with different most abundant charge states are illustrated (Fig. 5 D-I of the main document; MS^2 annotations based on the McLuckey nomenclature) [1]. In Table S3, chemical formulae of the detected species are listed. Simultaneously, the mass variance as error in ppm is indicated as well (always < 5 ppm).

Table S1. Overview of the Patisiran (antisense strand) impurities detected by HILIC ESI-MS analysis (deconvoluted mass in Da; t_R in min).

Name	Sequence	Deconvoluted mass	Peak No. Fig. 4A	t_R HILIC
5' 2mer - OH	5' dTdT 3' - OH	546.129	1	2.70
3' 2mer - Np	5' AU 3' - Np	653.082	2	6.27
5' 3mer - OH	5' CdTdT 3' - OH	851.170	3	4.42
3' 3mer - cyc	5' AUG 3' - cyc	980.118	4	6.37
3' 4mer - cyc	5' AUGG 3' - cyc	1325.157	5	8.55
3' 4mer - Np	5' AUGG 3' - Np	1343.165	6	10.56
5' 5mer - OH	5' mUACdTdT 3' - OH	1501.257	7	6.89
5' 5mer - Np	5' mUACdTdT 3' - Np	1580.226	8	9.82
3' 5mer - cyc	5' AUGGA 3' - cyc	1654.209	9	9.53
3' 5mer - Np	5' AUGGA 3' - Np	1672.221	10	11.24
5' 6mer - OH	5' UmUACdTdT 3' - OH	1806.282	11	8.41
3' 6mer - cyc	5' AUGGAA 3' - cyc	1983.260	12	10.37
3' 6mer - Np	5' AUGGAA 3' - Np	2001.264	13	11.99
5' 7mer - OH	5' GUmUACdTdT 3' - OH	2151.330	14	10.34
5' 8mer - OH	5' GGUmUACdTdT 3' - OH	2496.368	15	11.80
3' 8mer - Np	5' AUGGAAmUA 3' - Np	2650.364	16	12.96
5' 9mer - OH	5' UGGUmUACdTdT 3' - OH	2802.396	17	12.63
3' 9mer - cyc	5' AUGGAAmUAC 3' - cyc	2937.378	18	12.80
3' 9mer - Np	5' AUGGAAmUAC 3' - Np	2955.407	19	13.87
5' 10mer - OH	5' UUGGUmUACdTdT 3' - OH	3108.418	20	13.48
3' 10mer - cyc	5' AUGGAAmUACU 3' - cyc	3243.417	21	13.63
3' 10mer - Np	5' AUGGAAmUACU 3' - Np	3261.427	22	14.70
5' 11mer - OH	5' CUUGGUmUACdTdT 3' - OH	3413.459	23	14.35
3' 11mer - cyc	5' AUGGAAmUACUC 3' - cyc	3548.464	24	14.46
3' 11mer - Np	5' AUGGAAmUACUC 3' - Np	3566.466	25	15.33
5' 12mer - OH	5' UCUUGGUmUACdTdT 3'-OH	3719.470	26	14.96
3' 12mer - Np	5' AUGGAAmUACUCU 3' - Np	3873.496	27	15.94
5' 13mer - OH	5' CUCUUGGUmUACdTdT 3' - OH	4024.528	28	15.66
3' 13mer - Np	5' AUGGAAmUACUCUU 3' - Np	4178.519	29	16.54
3' 14mer - Np	5' AUGGAAmUACUCUUG 3' - Np	4523.570	30	17.12
5' 15mer - OH	5' mUACUCUUGGUmUACdTdT 3' - OH	4673.609	31	16.04
3' 15mer - cyc	5' AUGGAAmUACUCUUGG 3' - cyc	4850.595	32	16.91
3' 15mer - Np	5' AUGGAAmUACUCUUGG 3' - Np	4868.606	33	17.63
5' 16mer - OH	5' AmUACUCUUGGUmUACdTdT 3' - OH	5002.661	34	16.30
5' 17mer - OH	5' AAmUACUCUUGGUmUACdTdT 3' - OH	5331.708	35	16.54
5' 18mer – OH	5' GAAmUACUCUUGGUmUACdTdT 3' - OH	5676.783	36	17.12
3' 18mer - Np	5' AUGGAAmUACUCUUGGUmUA 3' - Np	5823.723	37	18.20
5' 19mer - OH, N-2	5' GGAAmUACUCUUGGUmUACdTdT 3' - OH	6021.828	38	17.73
3' 19mer - Np	5' AUGGAAmUACUCUUGGUmUAC 3' - Np	6128.748	39	18.61
5' 20mer - OH, N-1	5' UGGAAmUACUCUUGGUmUACdTdT 3' - OH	6327.814	40	17.94
Antisense	5' AUGGAAmUACUCUUGGUmUACdTdT 3' - OH	6656.866	41	18.01
5' 21mer - OH, N+1	5' CAUGGAAmUACUCUUGGUmUACdTdT 3' - OH	6962.000	42	18.46

2. Sense strand

As far as the sense strand concerns, 43 impurity species were resolved and detected by ESI-TOF-MS. To large extent, the impurity profiles of the HILIC separation matches the one from PBT-RPLC. There is, however, a difference in the assay specificity for the 3' 3mer – OH (Fig.S1A, Peak No. 43-45, see Table S2) in HILIC mode compared to pBT-RPLC. In case of HILIC, three isobaric forms of this impurity were detected, contrary to PBT-RPLC where only one peak was observed for these compounds. The EIC of *m/z* 865 clearly indicated the presence of 3 isomers with different retention times which are also visible in the UV-chromatogram (Fig. S1A). Since they consist of only three nucleotides, these isobaric oligonucleotide impurities are considered to be isomers which only differ in their nucleotide sequence. Although these isobaric species share the same most abundant fragment ion (*m/z*: 321.05, dT-Fragment, Fig. S2, A-C), the positions of the fragmentation are probably different. Unfortunately, the MS spectra lack other specific fragment ions which would allow their distinction. Hence further studies by standards or advanced fragmentation experiments are required to assign the three isomeric peaks. Besides of 3' 3mer – OH, two further isobaric impurity species were detected (Peaks No. 65 and 74, Table S2). Comparable to the antisense strand, the HILIC-ESI-MS method was capable to detect a small series of impurity species with a cyclic phosphate at the 3' termini for the sense strand as well (Peaks No. 46, 48, 54, 57, 62, 82; Table S2). Chemical formulae and mass error of the detected species for the passenger strand are listed in Table S4.

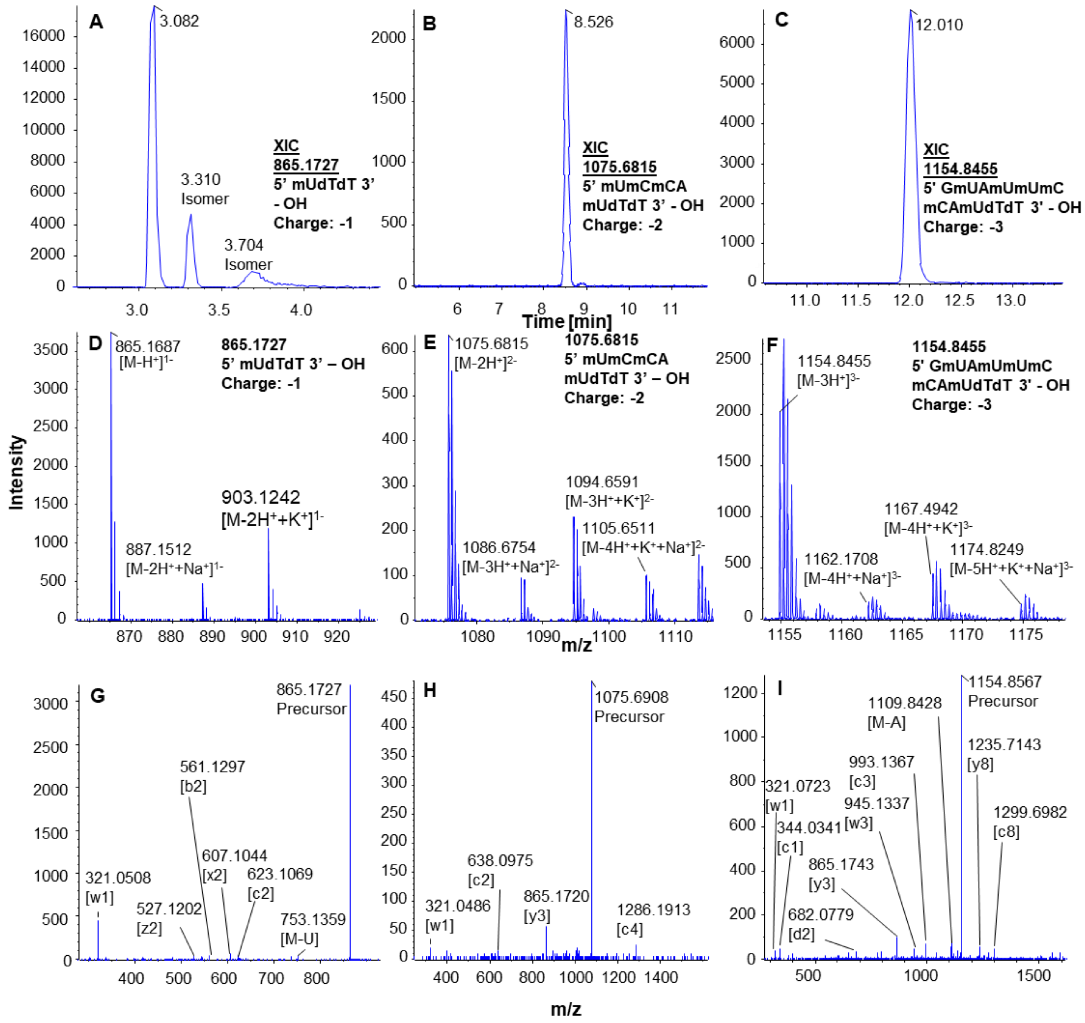

Fig. S1. HILIC-LC-MS^1 and -MS^2 spectra and extracted ion chromatogram of selected impurity species from sense strand of Patisiran. (A-C): Extracted ion chromatograms of the monoisotopic mass. (D-F): MS spectra of impurity species with the most abundant charge states. (G-I): MS^2 spectra of the corresponding precursor ion. For details towards MS measurement see chapter 2.6

Table S2. Overview of the Patisiran (sense strand) impurities detected by HILIC-ESI-MS analysis (deconvoluted mass in Da; t_R in min).

Name	Sequence	Deconvoluted mass	Peak No. Fig. 4B	t_R HILIC
5' 3mer_A-OH	5' mUdTdT 3' – OH	866.170	43	3.08
5' 3mer_B-OH	5' dTdTmU 3' - OH	866.170	44	3.31
5' 3mer_C-OH	5' dTmUdT 3' - OH	866.170	45	3.70
3' 3mer - cyc	5' GmUA 3' - cyc	994.133	46	5.82
3' 3mer -Np	5' GmUA 3' - Np	1012.130	47	8.05
3' 4mer - cyc	5' GmUAA 3' - cyc	1323.176	48	7.24
3' 4mer- Np	5'GmUAA 3' - Np	1341.186	49	9.19
5' 5mer- OH	5' mCAmUdTdT 3' - OH	1514.268	50	6.73
5' 6mer - OH	5' mCmCAmUdTdT 3' - OH	1833.322	51	7.97
5' 7mer - OH	5' mUmCmCAmUdTdT 3' - OH	2153.353	52	8.52
5' 7mer - Np	5' mUmCmCAmUdTdT 3' - Np	2233.336	53	10.84
3' 7mer - cyc	5' GmUAAmCmCA 3' - cyc	2290.335	54	10.29
3' 7mer – Np	5' GmUAAmCmCA 3' - Np	2308.347	55	11.62
5' 8mer - OH	5' mUmUmCmCAmUdTdT 3' - OH	2473.396	56	9.13
3' 8mer - cyc	5' GmUAAmCmCAA 3' - cyc	2619.391	57	10.93
3' 8mer – Np	5' GmUAAmCmCAA 3' - Np	2637.394	58	12.20
5' 9mer – OH (A->mU)	5' mUmUmUmCmCAmUdTdT 3' - OH	2793.442	59	9.87
5' 9mer - OH	5' AmUmUmCmCAmUdTdT 3' - OH	2802.449	60	10.04
5' 9mer – Np	5' AmUmUmCmCAmUdTdT 3' - Np	2882.405	61	11.97
3' 9mer – cyc	5' GmUAAmCmCAAG 3' - cyc	2964.428	62	12.12
3' 9mer – Np	5' GmUAAmCmCAAG 3' - Np	2982.445	63	13.34
5' 10mer - OH	5' mUAmUmUmCmCAmUdTdT 3' - OH	3122.492	64	10.68
5' 10mer - OH (isomer)	Unknown	3122.492	65	11.00
5' 10mer - OH (Ox-A)	5' mUAmUmUmCmCA(ox)mUdTdT 3' -OH	3138.480	66	11.43
5' 10mer - OH (mC->mU, mC->mA)	5' mUAmUmUmUmAAmUdTdT 3' - OH	3147.483	67	11.48
3' 10mer – Np	5' GmUAAmCmCAAGA 3' - Np	3311.495	68	13.67
5' 11mer – OH (G->A)	5' AmUAmUmUmCmCAmUdTdT 3' - OH	3451.544	69	11.42
5' 11mer – OH	5' GmUAmUmUmCmCAmUdTdT 3' - OH	3467.530	70	12.01
3' 11mer – Np	5' GmUAAmCmCAAGAG 3' - Np	3656.547	71	14.53
5' 12mer - OH (mC-mU, mC-U)	5' AGmUAmUmUmUUAmUdTdT 3' - OH	3784.590	72	13.11
5' 12mer – OH	5' AGmUAmUmUmCmCAmUdTdT 3' - OH	3796.590	73	12.47
5' 12mer - OH (isomer)	Unknown	3796.590	74	12.80
5' 12mer - OH (Ox-A)	5' A(ox)GmUAmUmUmCmCAmUdTdT 3' - OH	3812.590	75	13.07
5' 13mer - OH (G->A)	5' AAGmUAmUmUmCmCAmUdTdT 3' - OH	4125.643	76	12.97
5' 13mer – OH	5' GAGmUAmUmUmCmCAmUdTdT 3' - OH	4141.629	77	13.48
5' 14mer – OH	5' AGAGmUAmUmUmCmCAmUdTdT 3' - OH	4470.688	78	13.80
5' 15mer – OH	5' AAGAGmUAmUmUmCmCAmUdTdT 3' - OH	4799.718	79	14.12
5' 17mer – OH	5' mCmCAAGAGmUAmUmUmCmCAmUdTdT 3' - OH	5437.841	80	14.74
5' 18mer – OH	5' AmCmCAAGAGmUAmUmUmCmCAmUdTdT 3' - OH	5766.896	81	14.95
3' 18mer – cyc	5' GmUAAmCmCAAGAGmUAmUmUmCmCA 3' - cyc	5894.882	82	14.94
3' 18mer – Np	5' GmUAAmCmCAAGAGmUAmUmUmCmCA 3' - Np	5912.886	83	16.15
5' 19mer - OH (N-2)	5' AAmCmCAAGAGmUAmUmUmCmCAmUdTdT 3' - OH	6095.956	84	15.19
5' 20mer - OH (N-1)	5' mUAAmCmCAAGAGmUAmUmUmCmCAmUdTdT 3' - OH	6416.030	85	15.38
Sense, Patisiran	5' GmUAAmCmCAAGAGmUAmUmUmCmCAmUdTdT 3' - OH	6761.087	86	15.90

3. Annealed strands (duplex siRNA)

On contrary to PBT-RPLC, the duplex siRNA was retained under HILIC conditions and hence a size exclusion effect can be ruled out for the elution with t_0 on PBT [2]. The higher polarity of the annealed siRNA single strands may result from the duplicated phosphodiester-sugar backbone partially shielding the pendant bases.

Duplex siRNA can be detected in the MS spectra. It has been stated that the total charge is equally contributed form the two annealed singe strands: if the charge state of the duplex is 8-, then both single strands have charge state of 4- [3,4]. Due to the high molecular weight of the annealed siRNA, the most abundant charge state was 7- (Fig. S3). In Fig. S3, the MS^1 spectrum of the annealed siRNA is shown. As mentioned above, both complementary single strands with the charge states 4- (sense strand: *m/z* 1690.02; antisense strand: *m/z* 1663.68 m/z) are visible next to the duplex with the charge state 8- (duplex 8-: *m/z* 1676.99). It is obvious that some other duplex species are also detected. Since no single strands of these miscellaneous duplex species are present, it can be assumed that these unknown duplex species are not further annealed impurity products, but the results of in-source fragmentation. Furthermore, a complex pattern consisting of numerous impurity species from both antisense and sense strand was separated (Fig. 4C of the main document, Table S5). Fig. S4A shows the zoom of the most abundant charge state (7-) of the duplex siRNA and some of its adduct types. The corresponding EIC (Fig. S4B) reveals a well-shaped quite efficient peak.

Table S3. All detected species of the antisense (guide) strand of Patisiran from HILIC-MS analysis, sorted in order of increasing molecular mass (*m/z* refers to the monoisotopic mass, charge state to the most abundant one; peak no as in Fig. 4A).

Peak No.	Chemical Formula	Charge state	Ion Type	Calculated m/z	Measured m/z	Error (ppm)	Deconvoluted mass
1	$C_{20}H_{27}N_4O_{12}P$	-1	$[M-H]^{-1}$	545.128	545.128	0.0	546.13
2	$C_{19}H_{25}N_7O_{15}P_{22}$	-1	$[M-H]^{-1}$	652.082	652.079	-4.6	653.086
3	$C_{29}H_{39}N_7O_{19}P_2$	-1	$[M-H]^{-1}$	850.169	850.17	1.2	851.174
4	$C_{29}H_{35}N_{12}O_{21}P_3$	-1	$[M-H]^{-1}$	979.117	979.118	1.0	980.119
5	$C_{39}H_{47}N_{17}O_{28}P_4$	-2	$[M-2H]^{-2}$	661.579	661.578	-0.8	1325.157
6	$C_{39}H_{49}N_{17}O_{29}P_4$	-2	$[M-2H]^{-2}$	670.584	670.583	-1.5	1343.165
7	$C_{49}H_{64}N_{14}O_{33}P_4$	-2	$[M-2H]^{-2}$	749.128	749.128	0.7	1501.257
8	$C_{49}H_{59}N_{22}O_{34}P_5$	-2	$[M-2H]^{-2}$	826.105	826.104	-0.6	1654.209
9	$C_{49}H_{61}N_{22}O_{35}P_5$	-2	$[M-2H]^{-2}$	835.110	835.110	0.0	1672.221
10	$C_{58}H_{75}N_{16}O_{41}P_5$	-2	$[M-2H]^{-2}$	902.140	902.142	1.8	1806.294
11	$C_{59}H_{71}N_{27}O_{40}P_6$	-2	$[M-2H]^{-2}$	990.631	990.629	-2.0	1983.28
12	$C_{59}H_{73}N_{27}O_{41}P_6$	-2	$[M-2H]^{-2}$	999.636	999.636	0.0	2001.264
13	$C_{68}H_{87}N_{21}O_{48}P_6$	-2	$[M-2H]^{-2}$	1074.664	1074.664	0.0	2151.345
14	$C_{78}H_{99}N_{26}O_{55}P_7$	-2	$[M-2H]^{-2}$	1247.188	1247.185	-2.4	2496.397
15	$C_{79}H_{98}N_{34}O_{55}P_8$	-2	$[M-2H]^{-2}$	1324.183	1324.181	-1.5	2650.383
16	$C_{87}H_{110}N_{28}O_{63}P_8$	-3	$[M-3H]^{-3}$	933.131	933.132	1.1	2802.405
17	$C_{88}H_{108}N_{37}O_{61}P_9$	-3	$[M-3H]^{-3}$	978.130	978.128	-1.7	2937.378
18	$C_{88}H_{110}N_{37}O_{62}P_9$	-3	$[M-3H]^{-3}$	984.133	984.133	-0.3	2955.422
19	$C_{96}H_{121}N_{30}O_{71}P_9$	-3	$[M-3H]^{-3}$	1035.139	1035.140	0.6	3108.435
20	$C_{97}H_{119}N_{39}O_{69}P_{10}$	-3	$[M-3H]^{-3}$	1080.138	1080.138	0.0	3243.417
21	$C_{97}H_{121}N_{39}O_{70}P_{10}$	-3	$[M-3H]^{-3}$	1086.142	1086.142	0.3	3261.427
22	$C_{105}H_{133}N_{33}O_{78}P_{10}$	-3	$[M-3H]^{-3}$	1136.820	1136.819	-0.6	3413.483
23	$C_{106}H_{131}N_{42}O_{76}P_{11}$	-3	$[M-3H]^{-3}$	1181.819	1181.818	-0.6	3548.464
24	$C_{106}H_{133}N_{42}O_{77}P_{11}$	-3	$[M-3H]^{-3}$	1187.822	1187.823	0.8	3566.488
25	$C_{114}H_{144}N_{35}O_{86}P_{11}$	-3	$[M-3H]^{-3}$	1238.828	1238.828	-0.3	3719.513
26	$C_{115}H_{144}N_{44}O_{85}P_{12}$	-3	$[M-3H]^{-3}$	1289.830	1289.831	0.5	3872.523
27	$C_{123}H_{156}N_{38}O_{93}P_{12}$	-3	$[M-3H]^{-3}$	1340.509	1340.510	1.0	4024.557
28	$C_{124}H_{155}N_{46}O_{93}P_{13}$	-3	$[M-3H]^{-3}$	1391.839	1391.840	0.7	4178.524
29	$C_{134}H_{167}N_{51}O_{100}P_{14}$	-3	$[M-3H]^{-3}$	1506.855	1506.855	0.2	4523.595
30	$C_{143}H_{181}N_{45}O_{107}P_{14}$	-3	$[M-3H]^{-3}$	1556.873	1556.873	-0.2	4673.671
31	$C_{144}H_{177}N_{56}O_{106}P_{15}$	-4	$[M-4H]^{-4}$	1211.648	1211.648	-0.2	4850.595
32	$C_{144}H_{179}N_{56}O_{107}P_{15}$	-4	$[M-4H]^{-4}$	1216.151	1216.151	0.0	4868.646
33	$C_{153}H_{193}N_{50}O_{113}P_{15}$	-3	$[M-3H]^{-3}$	1666.557	1666.560	1.6	5002.728
34	$C_{163}H_{205}N_{55}O_{119}P_{16}$	-4	$[M-4H]^{-4}$	1331.929	1331.931	1.3	5331.708
35	$C_{173}H_{217}N_{60}O_{126}P_{17}$	-4	$[M-4H]^{-4}$	1418.191	1418.191	0.0	5676.772
36	$C_{173}H_{215}N_{65}O_{129}P_{18}$	-4	$[M-4H]^{-4}$	1454.931	1454.932	1.0	5823.767
37	$C_{183}H_{229}N_{65}O_{133}P_{18}$	-4	$[M-4H]^{-4}$	1504.453	1504.453	0.0	6021.826
38	$C_{182}H_{227}N_{68}O_{136}P_{19}$	-4	$[M-4H]^{-4}$	1531.191	1531.194	2.0	6128.798
39	$C_{192}H_{240}N_{67}O_{141}P_{19}$	-4	$[M-4H]^{-4}$	1580.959	1580.962	1.7	6327.866

40	$C_{202}H_{252}N_{72}O_{147}P_{20}$	**-4**	$[M-4H]^{-4}$	1663.222	1663.223	0.5	6656.933
41	$C_{211}H_{264}N_{75}O_{154}P_{21}$	**-5**	$[M-5H]^{-5}$	1391.3846	1391.391	4.6	6962

Table S4. All detected species of sense (passenger) strand of Patisiran from HILIC-MS, sorted in order of increasing molecular mass (*m/z* refers to the monoisotopic mass, charge state to the most abundant one; peak no as in Fig. 4B).

Peak No.	Chemical Formula	Charge state	Ion Type	Calculated m/z	Measured m/z	Error (ppm)	Deconvoluted mass
43	$C_{30}H_{40}N_6O_{20}P_2$	-1	$[M-H]^{-1}$	865.169	865.169	0.0	866.17
44	$C_{30}H_{40}N_6O_{20}P_2$	-1	$[M-H]^{-1}$	865.169	865.169	0.0	866.17
45	$C_{30}H_{40}N_6O_{20}P_2$	-1	$[M-H]^{-1}$	865.169	865.169	0.0	866.17
46	$C_{30}H_{37}N_{12}O_{21}P_3$	-1	$[M-H]^{-1}$	993.133	993.133	0.0	994.133
47	$C_{30}H_{39}N_{12}O_{22}P_3$	-2	$[M-2H]^{-2}$	505.068	505.066	-4.0	1012.13
48	$C_{40}H_{49}N_{17}O_{27}P_4$	-2	$[M-2H]^{-2}$	660.589	660.588	-1.5	1323.176
49	$C_{40}H_{51}N_{17}O_{28}P_4$	-2	$[M-2H]^{-2}$	669.594	669.593	-1.5	1341.186
50	$C_{50}H_{66}N_{14}O_{33}P_4$	-2	$[M-2H]^{-2}$	756.136	756.134	-2.0	1514.268
51	$C_{60}H_{80}N_{17}O_{40}P_5$	-2	$[M-2H]^{-2}$	915.664	915.669	5.5	1833.322
52	$C_{70}H_{93}N_{19}O_{48}P_6$	-3	$[M-3H]^{-3}$	716.787	716.784	-4.2	2153.353
53	$C_{70}H_{94}N_{19}O_{51}P_7$	-2	$[M-2H]^{-2}$	1115.668	1115.666	-1.3	2233.336
54	$C_{70}H_{89}N_{28}O_{47}P_7$	-2	$[M-2H]^{-2}$	1144.172	1144.17	-1.7	2290.335
55	$C_{70}H_{91}N_{28}O_{48}P_7$	-2	$[M-2H]^{-2}$	1153.178	1153.174	-3.0	2308.347
56	$C_{80}H_{106}N_{21}O_{56}P_7$	-3	$[M-3H]^{-3}$	823.467	823.465	-2.8	2473.396
57	$C_{80}H_{101}N_{33}O_{53}P_8$	-3	$[M-3H]^{-3}$	872.130	872.13	0.4	2619.391
58	$C_{80}H_{103}N_{33}O_{54}P_8$	-3	$[M-3H]^{-3}$	878.133	878.131	-2.3	2637.394
59	$C_{90}H_{119}N_{23}O_{64}P_8$	-3	$[M-3H]^{-3}$	930.148	930.147	-0.7	2793.442
60	$C_{90}H_{118}N_{26}O_{62}P_8$	-3	$[M-3H]^{-3}$	933.152	933.15	-1.8	2802.449
61	$C_{90}H_{119}N_{26}O_{65}P_9$	-3	$[M-3H]^{-3}$	959.807	959.802	-5.2	2882.405
62	$C_{90}H_{113}N_{38}O_{60}P_9$	-3	$[M-3H]^{-3}$	987.145	987.143	-2.4	2964.428
63	$C_{90}H_{115}N_{38}O_{61}P_9$	-3	$[M-3H]^{-3}$	993.149	993.148	-1.0	2982.445
64	$C_{100}H_{131}N_{28}O_{70}P_9$	-3	$[M-3H]^{-3}$	1039.832	1039.831	-1.0	3122.492
66	$C_{100}H_{131}N_{28}O_{71}P_9$	-3	$[M-3H]^{-3}$	1045.163	1045.16	-3.2	3138.48
67	$C_{101}H_{130}N_{29}O_{70}P_9$	-3	$[M-3H]^{-3}$	1048.163	1048.161	-2.2	3147.483
68	$C_{100}H_{127}N_{43}O_{67}P_{10}$	-3	$[M-3H]^{-3}$	1102.833	1102.832	-0.9	3311.495
69	$C_{110}H_{143}N_{33}O_{76}P_{10}$	-3	$[M-3H]^{-3}$	1149.516	1149.518	1.7	3451.544
70	$C_{110}H_{143}N_{33}O_{77}P_{10}$	-4	$[M-4H]^{-4}$	865.884	865.882	-2.0	3467.53
71	$C_{110}H_{139}N_{48}O_{74}P_{11}$	-3	$[M-3H]^{-3}$	1217.849	1217.849	0.0	3656.547
72	$C_{119}H_{151}N_{36}O_{85}P_{11}$	-3	$[M-3H]^{-3}$	1260.516	1260.524	6.3	3784.59
73	$C_{120}H_{155}N_{38}O_{83}P_{11}$	-3	$[M-3H]^{-3}$	1264.532	1264.53	-1.6	3796.59
75	$C_{120}H_{155}N_{38}O_{84}P_{11}$	-3	$[M-3H]^{-3}$	1269.863	1269.863	-0.3	3812.59
76	$C_{130}H_{167}N_{43}O_{89}P_{12}$	-3	$[M-3H]^{-3}$	1374.216	1374.217	0.7	4125.643
77	$C_{130}H_{167}N_{43}O_{90}P_{12}$	-4	$[M-4H]^{-4}$	1034.40875	1034.407	-1.7	4141.629

78	$C_{140}H_{179}N_{48}O_{96}P_{13}$	-4	$[M-4H]^{-4}$	1116.672	1116.672	0.0	4470.688
79	$C_{150}H_{191}N_{53}O_{102}P_{14}$	-4	$[M-4H]^{-4}$	1198.935	1198.93	-4.2	4799.718
80	$C_{170}H_{219}N_{59}O_{116}P_{16}$	-4	$[M-4H]^{-4}$	1358.4635	1358.46	-2.6	5437.841
81	$C_{180}H_{231}N_{64}O_{122}P_{17}$	-4	$[M-4H]^{-4}$	1440.72675	1440.724	-1.9	5766.896
82	$C_{180}H_{228}N_{70}O_{123}P_{18}$	-4	$[M-4H]^{-4}$	1472.7175	1472.72	1.7	5894.882
83	$C_{180}H_{230}N_{70}O_{124}P_{18}$	-4	$[M-4H]^{-4}$	1477.22	1477.223	2.0	5912.886
84	$C_{190}H_{243}N_{69}O_{128}P_{18}$	-4	$[M-4H]^{-4}$	1522.98975	1522.989	-0.5	6095.956
85	$C_{200}H_{256}N_{71}O_{136}P_{19}$	-4	$[M-4H]^{-4}$	1603	1602.995	-3.1	6416.030
86	$C_{210}H_{268}N_{76}O_{143}P_{20}$	-5	$[M-5H]^{-5}$	1351.208	1351.205	-2.2	6761.086

Table S5. Summary of the impurities in duplex siRNA Patisiran (annealed strand) detected by HILIC-ESI-MS (deconvoluted mass in Da; t_R in min; peak no. as Fig. 4C).

Peak No.	t_R [min]	Name	Sequence	Deconvoluted mass
1	2.43	5' 2mer - OH	5' dTdT 3' - OH, AS	546.129
43	2.65	5' 3mer_A-OH	5' mUdTdT 3' - OH, S	866.169
3	2.9	5' 3mer - OH	5' CdTdT 3' - OH, AS	851.17
7	5.43	5' 5mer - OH	5' mUACdTdT 3' - OH, AS	1500.257
47	6.64	3' 3mer -Np	5' GmUA 3' - Np, S	1012.13
11	7.03	5' 6mer - OH	5' UmUACdTdT 3' - OH, AS	1806.282
5	7.19	3' 4mer - cyc	5' AUGG 3' - cyc, AS	1325.157
49	7.57	3' 4mer- Np	5'GmUAA 3' - Np,S	1341.186
56	7.66	5' 8mer - OH	5' mUmUmCmCAmUdTdT 3' - OH, S	2473.396
14	9.01	5' 7mer - OH	5' GUmUACdTdT 3' - OH, AS	2151.33
6	9.2	3' 4mer - Np	5' AUGG 3' - Np, AS	1343.165
64	9.33	5' 10mer - OH	5' mUAmUmUmCmCAmUdTdT 3' - OH, S	3122.492
10	9.79	3' 5mer - Np	5' AUGGA 3' - Np, AS	1672.221
13	10.34	3' 6mer - Np	5' AUGGAA 3' - Np, AS	2001.264
55	10.51	3' 7mer - Np	5' GmUAAmCmCA 3' - Np, S	2308.347
70	10.53	5' 11mer - OH	5' GmUAmUmUmCmCAmUdTdT 3' - OH, S	3467.53
15	10.6	5' 8mer - OH	5' GGUmUACdTdT 3' - OH, AS	2496.368
73	11.11	5' 12mer - OH	5' AGmUAmUmUmCmCAmUdTdT 3' - OH, S	3796.59
58	11.19	3' 8mer - Np	5' GmUAAmCmCAA 3' - Np, S	2637.394
60	11.45	5' 9mer - OH	5' AmUmUmCmCAmUdTdT 3' - OH, S	2802.449
16	11.51	3' 8mer - Np	5' AUGGAAmUA 3' - Np, AS	2650.364
18	11.8	3' 9mer - cyc	5' AUGGAAmUAC 3' - cyc	2937.378
77	12.17	5' 13mer - OH	5' GAGmUAmUmUmCmCAmUdTdT 3' - OH, S	4141.629
63	12.33	3' 9mer - Np	5' GmUAAmCmCAAG 3' - Np, S	2982.445
20	12.37	5' 10mer - OH	5' UUGGUmUACdTdT 3' - OH, AS	3108.418
78	12.42	5' 14mer - OH	5' AGAGmUAmUmUmCmCAmUdTdT 3' - OH, S	4470.688
68	12.61	3' 10mer - Np	5' GmUAAmCmCAAGA 3' - Np, S	3311.495
19	13	3' 9mer - Np	5' AUGGAAmUAC 3' - Np, AS	2955.407
80	13.31	5' 17mer - OH	5' mCmCAAGAGmUAmUmUmCmCAmUdTdT 3' - OH, S	5437.841
23	13.32	5' 11mer - OH	5' CUUGGUmUACdTdT 3' - OH, AS	3413.459
81	14.72	5' 18mer - OH	5' AmCmCAAGAGmUAmUmUmCmCAmUdTdT 3' - OH, S	5766.896
26	14.87	5' 12mer - OH	5' UCUUGGUmUACdTdT 3'-OH, AS	3719.47
22	16.13	3' 10mer - Np	5' AUGGAAmUACU 3' - Np, AS	3261.427
25	17.1	3' 11mer - Np	5' AUGGAAmUACUC 3' - Np, AS	3566.465
27	17.5	3' 12mer - Np	5' AUGGAAmUACUCU 3' - Np, AS	3873.495
41	17.6	Sense, Patisiran	5' GmUAAmCmCAAGAGmUAmUmUmCmCAmUdTdT 3' - OH	6761.086
87	18.14	Annealed, Patisiran	Duplex	13419.884

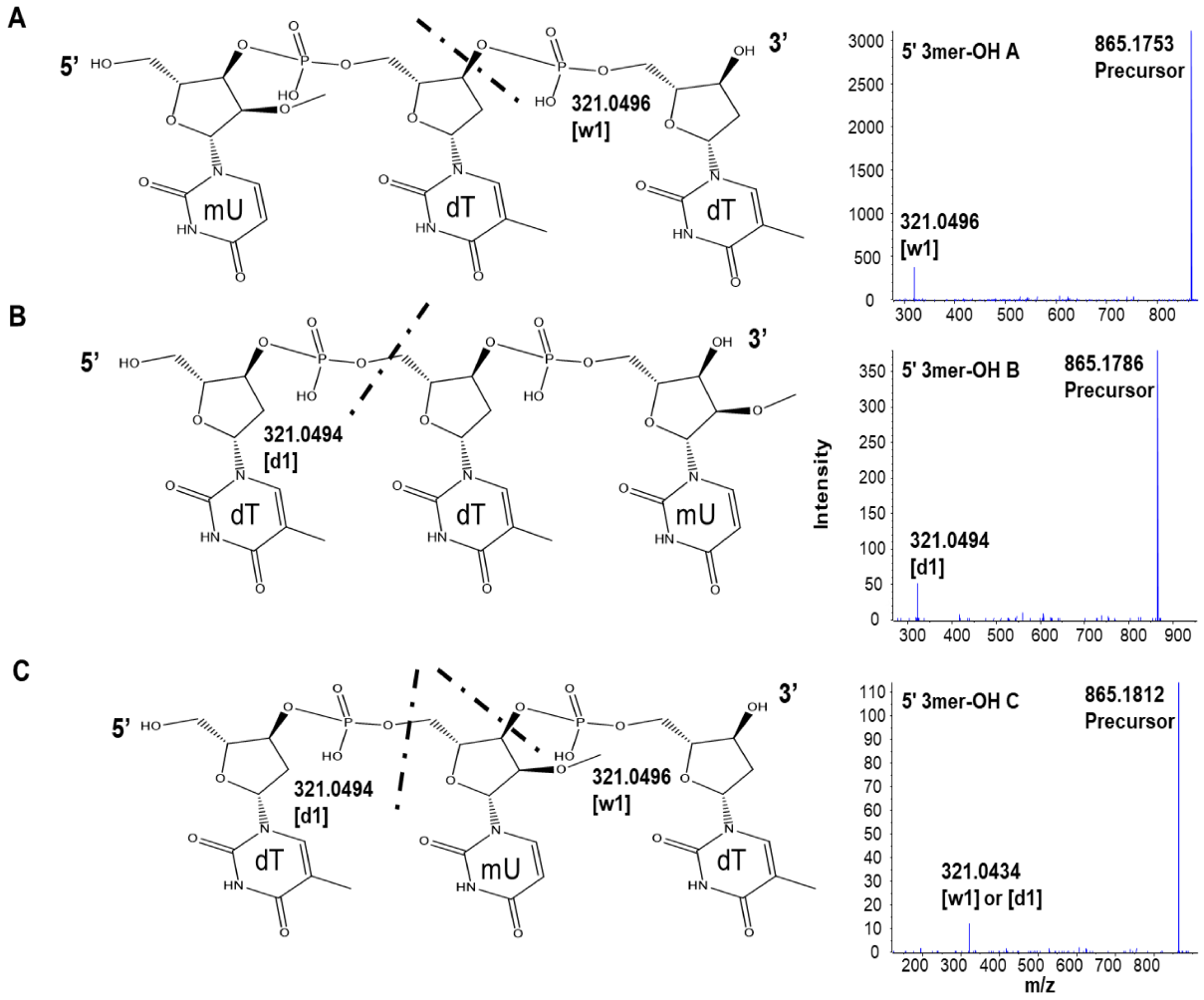

Fig. S2. MS^2 spectra, chemical structures and fragmentation patterns of 3 isobaric impurity species (*m/z*: 865.1812). Hypothetically, for 5' 3mer_A-OH (Table 4, HILIC mode impurity No. 43), the molecule was fragmented at w1 (A). In contrast, 5' 3mer_B-OH (Table 4, HILIC mode impurity No. 44) was fragmented at d1 (B). 5' 3mer_C-OH (Table 4, HILIC mode impurity No. 45) consists of two dT nucleotides at both 3'- and 5' end. Consequently, the fragment ion can be assigned to either w1 or d1 (C). Due to lack of other sequence-specific fragments, this hypothesis cannot be verified experimentally at this point.

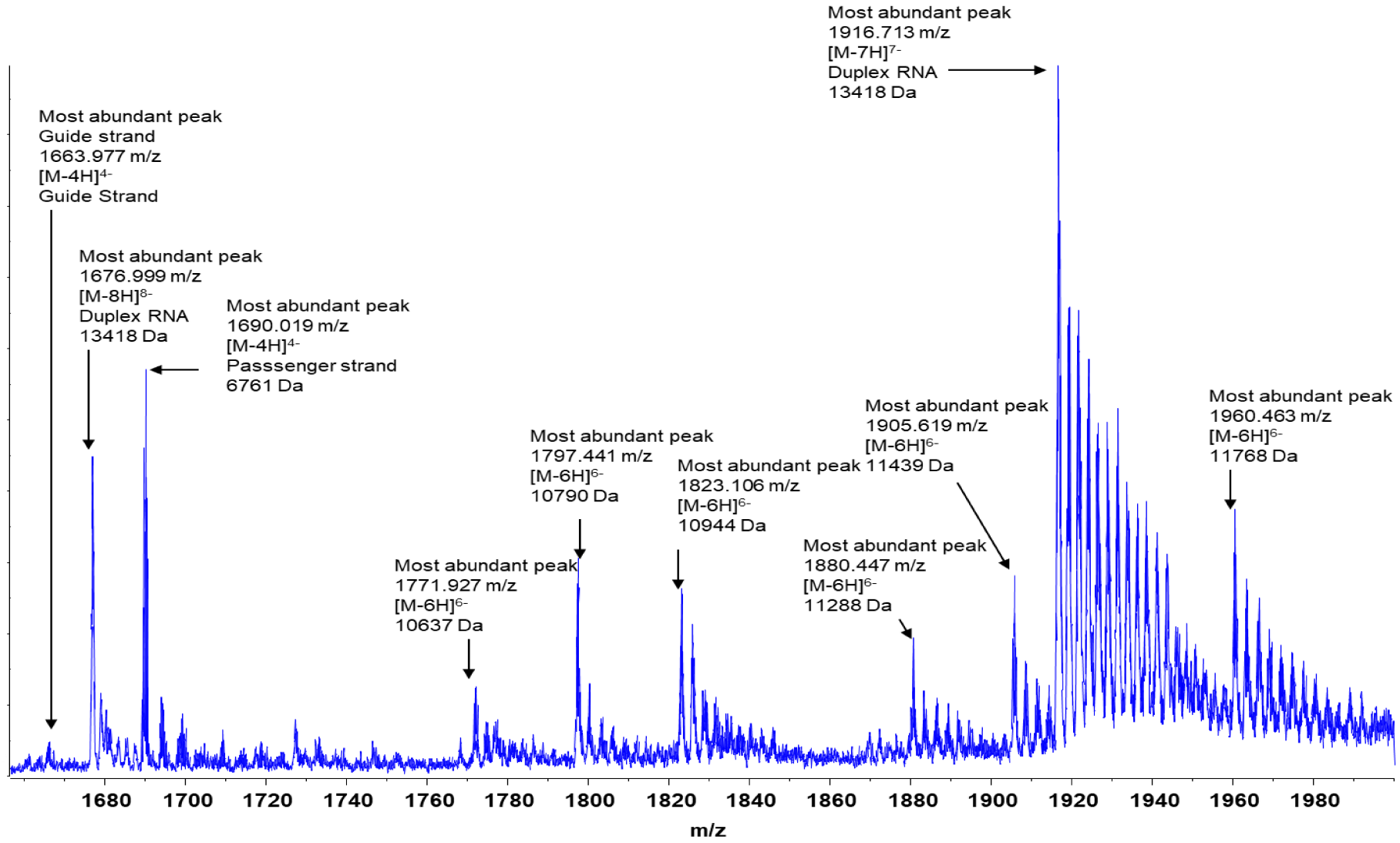

Fig. S3. Extended HILIC-ESI-MS spectra of annealed duplex. Besides of duplex, further mass signals are visible

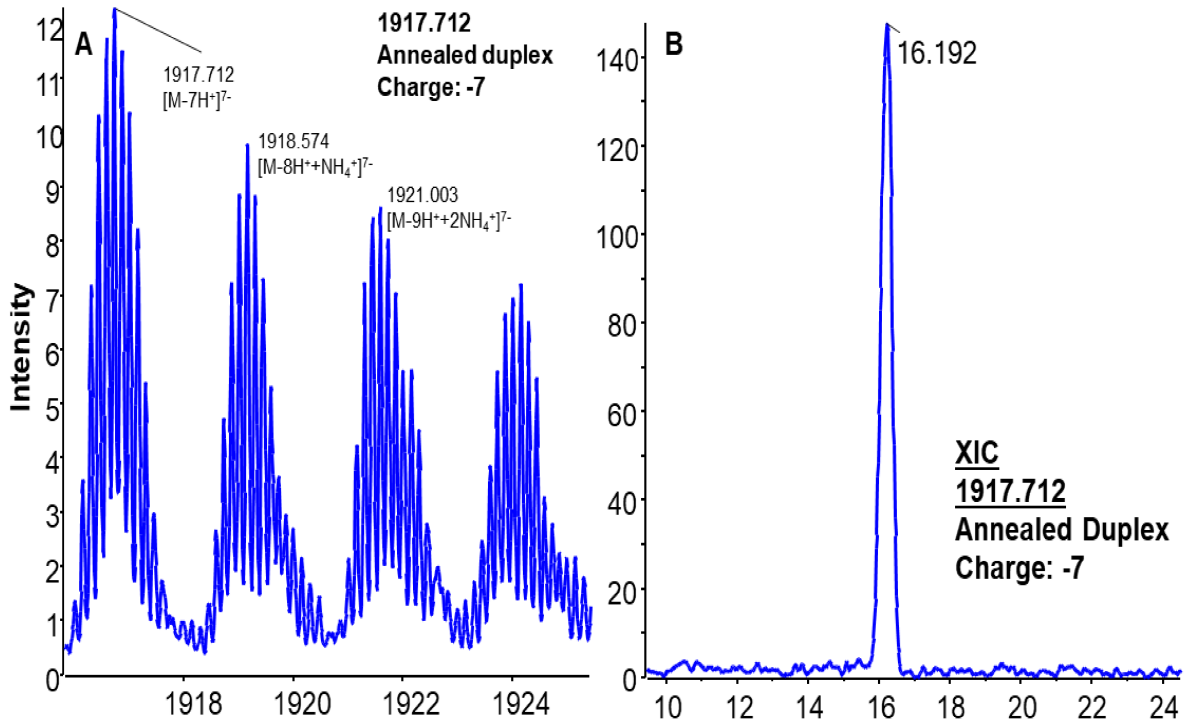

Fig. S4. HILIC-ESI-MS spectra and extracted ion chromatogram of annealed duplex of Patisiran siRNA.

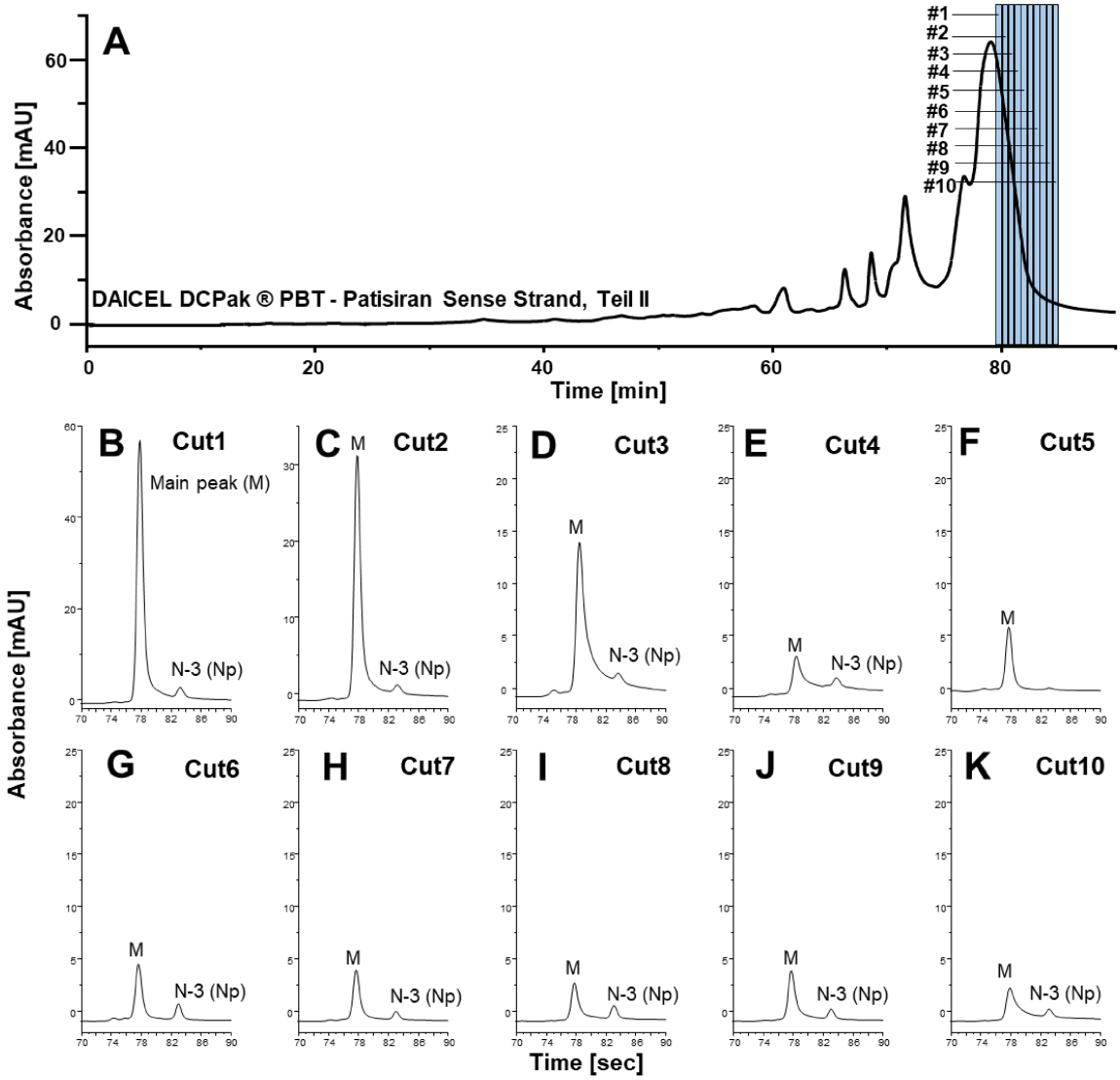

Fig. S5. Selective comprehensive sRP×HILIC-UV of the sense strand of Patisiran (raw product without purification) (rear end of the peak; for front end of the back see Fig. 8 of main document). A: The ^{1}D UV chromatogram with PBT. B-K: ^{2}D HILIC chromatograms of the 10 cuts. For LC conditions see chapter 2.5.5. of the main document.

Table S6. Compatibility chart of separation dimensions.

2DLC-UV	OSC	BV	IPC	Total Score	Technical Requirements
^{1}PBT-^{2}CHOL	+++	+++	+++	9	
^{1}CHOL-^{2}PBT	+++	+++	+++	9	
^{1}PBT-^{2}IPRP	+++	+++	+	7	
^{1}IPRP-^{2}PBT	+	+++	+	5	
^{1}PBT-^{2}HILIC	+	+++	+++	7	
^{1}HILIC-^{2}PBT	+	+++	+++	7	
^{1}PBT-^{2}MMC	+++	+	+	5	
^{1}MMC-^{2}PBT	++	+	+	4	
^{1}CHOL-^{2}IPRP	+++	+++	+	7	
^{1}IPRP-^{2}CHOL	+	+++	+	5	
^{1}CHOL-^{2}HILIC	+	+++	+++	7	
^{1}HILIC-^{2}CHOL	+	+++	+++	7	
^{1}CHOL-^{2}MMC	+++	+	+	5	
^{1}MMC-^{2}CHOL	++	+	+	4	
^{1}IPRP-^{2}HILIC	++	+++	+	6	
^{1}HILIC-^{2}IPRP	++	+++	++	7	
^{1}IPRP-^{2}MMC	+	++	+	4	
^{1}MMC-^{2}IPRP	+++	+	++	6	
^{1}HILIC-^{2}MMC	+++	+	++	6	
^{1}MMC-^{2}HILIC	+	+	+	3	

Criteria: Organic solvent compatibility (OSC); Buffer volatility (BV); Ion-pair contamination avoided (IPC)
Technical Requirements: Direct coupling possible (green); diverter valve required (yellow); ASM mandatory (orange); Diverter valve and ASM recommended (red)

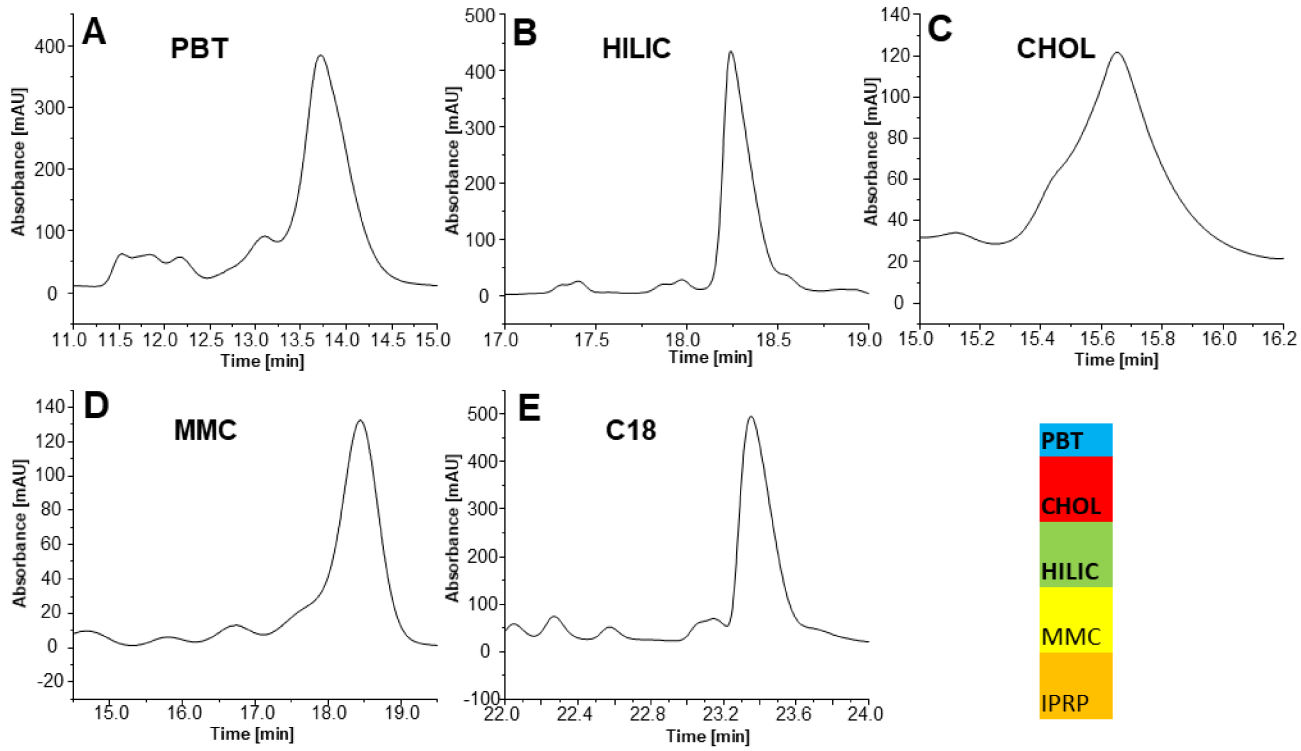

Peak No. Table 2	Name	Mass (Da)	t_R PBT	$t_{norm.}$ PBT	t_R HILIC	$t_{norm.}$ HILIC	t_R CHOL	$t_{norm.}$ CHOL	t_R MMC	$t_{norm.}$ MMC	t_R IPRP	$t_{norm.}$ IPRP
24	5' 18mer – OH (N-3)	5676.77	13.35	0.97	17.12	0.91	15.46	0.68	14.64	0.78	22.39	0.95
25	3' 18mer - Np	5824.79	11.35	0.80	18.2	0.97	14.92	0.65	-	-	23.31	1.00
26	5' 19mer – OH (N-2)	6021.82	13.31	0.97	17.73	0.94	15.47	0.68	15.77	0.85	22.39	0.95
27	3' 19mer - Np	6128.79	11.58	0.82	18.61	1.00	15.14	0.66	-	-	23.31	1.00
28	5' 20 mer - OH (N-1)	6327.86	12.95	0.94	17.94	0.96	15.28	0.67	16.17	0.88	22.81	0.97
29	Antisense	6656.93	13.73	1.00	18.01	0.96	15.68	0.69	18.2	1.00	23.31	1.00

Fig. S6. LC mode and column selection guidance for selective comprehensive 2DLC. Coelutions of ON impurities with the main peak occurring on different columns and LC modes, respectively. Colour code see insert. With PBT column, the ON peaks no 24 and 26 coeluted with the main ON peak (peak no 29). On the HILIC column, peaks no 25 and 28 coeluted with the main ON peak 29, but ONs no 24 and 26 were separated. On the CHOL column, peaks no 24, 25, 26, 27, and 28 coeluted. On the MMC column, none of the impurities no 24, 26 and 28 coeluted with the main peak, but peaks no 25 and 27 were not detected which does not allow to decide on their separation or coelution. In IPRP, peaks no 25 and 27 coeluted with the main ON peak.

References

[1] S.A. Mcluckey, G.J. Van Berkel, G.L. Glish, Tandem Mass Spectrometry of Small, Multiply Charged Oligonucleotides, J. Am. Soc. Mass Spectrom. 3 (1992) 60–70. https://doi.org/10.1016/1044-0305(92)85019-G.

[2] F. Li, M. Laemmerhofer, S. Studzińska, S. Chen, Polybutylene terephthalate-based stationary phase for ion-pair-free reversed- phase liquid chromatography-mass spectrometry of small interfering RNA Feiyang Li, J. Chromatogr. A. In Press. (2023).

[3] J. Abi-Ghanem, V. Gabelica, Nucleic acid ion structures in the gas phase, Phys. Chem. Chem. Phys. 16 (2014) 21204–21218. https://doi.org/10.1039/c4cp02362e.

[4] E. Bayer, T. Bauer, K. Schmeer, K. Bleicher, M. Maier, H.J. Gaus, Analysis of Double-Stranded Oligonucleotides by Electrospray Mass Spectrometry, Anal. Chem. 66 (1994) 3858–3863. https://doi.org/10.1021/ac00094a004.

5. Publication V

Cholesterol stationary phase in the separation and identification of siRNA impurities by two-dimensional liquid chromatography-mass spectrometry

Sylwia Studzińska[a,b*], Feiyang Li[b], Michał Szumski[c], Michael Lämmerhofer[b] and Bogusław Buszewski[a]

[a] Chair of Environmental Chemistry and Bioanalytics, Faculty of Chemistry, Nicolaus Copernicus University in Toruń, 7 Gagarin Str., PL-87-100 Toruń (Poland)

[b] Institute of Pharmaceutical Sciences, Pharmaceutical (Bio-)Analysis, University of Tübingen, Auf der Morgenstelle 8, 72076 Tübingen, Germany

[c] Centre for Modern Interdisciplinary Technologies, Nicolaus Copernicus University in Toruń, 4 Wilenska St., 87-100 Toruń, Poland

*Author for correspondence:
Prof. Dr. Sylwia Studzińska

Chair of Environmental Chemistry and Bioanalytics,

Faculty of Chemistry,

Nicolaus Copernicus University in Toruń,

7 Gagarin Str., PL-87-100 Toruń (Poland)

T: +48 56 6114753

E-mail: kowalska@chem.umk.pl

International Journal of Molecular Sciences

Year 2022, 23, 14960

DOI: 10.3390/ijms232314960

International Journal of
Molecular Sciences

MDPI

Article

Cholesterol Stationary Phase in the Separation and Identification of siRNA Impurities by Two-Dimensional Liquid Chromatography-Mass Spectrometry

Sylwia Studzińska [1,2,*], Feiyang Li [2], Michał Szumski [3], Bogusław Buszewski [1] and Michael Lämmerhofer [2]

[1] Chair of Environmental Chemistry and Bioanalytics, Faculty of Chemistry, Nicolaus Copernicus University in Toruń, 7 Gagarin Str., 87-100 Toruń, Poland
[2] Institute of Pharmaceutical Sciences, Pharmaceutical (Bio-)Analysis, University of Tübingen, Auf der Morgenstelle 8, 72076 Tübingen, Germany
[3] Centre for Modern Interdisciplinary Technologies, Nicolaus Copernicus University in Toruń, 4 Wilenska St., 87-100 Toruń, Poland
* Correspondence: kowalska@chem.umk.pl; Tel.: +48-56-6114753

Abstract: The aim of this research was to develop a simple and efficient ion-pair reagent-free chromatographic method for the separation and qualitative determination of oligonucleotide impurities, exemplified by synthesis of raw products of the two single strands of patisiran siRNA. The stationary phases with mixed hydrophobic/hydrophilic properties (cholesterol and alkylamide) were firstly used for this purpose with reversed-phased high-performance liquid chromatography. Several different chromatographic parameters were tested for their impact on impurities separation: type, concentration, pH of salt, as well as organic solvent type in the mobile phase. The pH was the most influential factor on the separation and signal intensities in mass spectrometry detection. Finally, the optimized method included the application of cholesterol stationary phase, with mobile phase containing 20 mM ammonium formate (pH 6.5) and methanol. It allowed good separation and the identification of most impurities within 25 min. Since not all closely related impurities could be fully resolved from the main peak in this oligonucleotide impurity profiling, two-dimensional liquid chromatography was used for peak purity determination of the target oligonucleotides. The Ethylene Bridged Hybrid (BEH) Amide column in hydrophilic interaction liquid chromatography was applied in the second dimension, allowing additional separation of three closely related impurities.

Keywords: oligonucleotide; impurities; stationary phase; separation; two-dimensional liquid chromatography; mass spectrometry

Citation: Studzińska, S.; Li, F.; Szumski, M.; Buszewski, B.; Lämmerhofer, M. Cholesterol Stationary Phase in the Separation and Identification of siRNA Impurities by Two-Dimensional Liquid Chromatography-Mass Spectrometry. *Int. J. Mol. Sci.* **2022**, *23*, 14960. https://doi.org/10.3390/ijms232314960

Academic Editor: Elena V. Bichenkova

Received: 28 October 2022
Accepted: 25 November 2022
Published: 29 November 2022

1. Introduction

In manufacturing a drug and ensuring its proper therapeutic activity, one of the most important factors is the purity of the active substance. Impurities must be firstly qualitatively determined so that a purification method could be successfully developed. This stage of drug development is often difficult, particularly for oligonucleotides (OGNs), which are increasingly used to treat a wide range of diseases [1–3]. Therapies involve the introduction of synthetic, usually chemically modified OGNs into the cell [1,2]. Various OGNs with different mechanisms of action are currently being used: antisense OGNs, micro-RNAs, aptamers, and small interfering RNAs [4–6]. Their impurities can be classified into several groups: products of modification at a single phosphodiester linkage, sugar or base residue, products of deletion of a single nucleotide (N − 1, N − 2), or incorporation of a single nucleotide repeat (N + 1) and other longmers [7,8]. The difficulties associated with characterizing these impurities are their large molecular weights and closely related structure [3,8]. For this reason, their complete structural elucidation is challenging, and the

development of improved analytical methods should be pursued to enable their separation from the parent OGN and from each other [3,7,8].

Historically, the first separation technique used for this purpose was anion exchange chromatography (AEC). However, it has been used less frequently recently, due to its incompatibility with mass spectrometry (MS) [3,9]. In some cases, capillary gel electrophoresis was also applied [10]. The most popular technique for achieving length-based separations is high-performance liquid chromatography, especially in ion-pair mode (IP RP HPLC) [3,11–16]. Its combination with electrospray ionization mass spectrometry (ESI-MS) makes it generally suitable for the analysis of impurities, due to, e.g., the high mass spectral response [11–13]. Consequently, IP RP HPLC ESI-MS has become a method of first choice for the analysis of impurities, although it often fails to separate impurities such as N − 1 or N + 1 that co-elute with the parent OGN [13]. Moreover, even though ion pair reagents are used in the mobile phase, the separation efficiency of IP RP HPLC for a complex mixture of impurities that elute before and after the main OGN is often limited, tedious, and time-consuming [13,14]. The application of methods for automated impurities determination or mobile phases containing small alkylamines may be useful, as shown by Roussis et al. [13–16]. However, even for an optimized IP RP HPLC method, the complete separation of positional isomers and isobaric species for example still remains very challenging [15,16]. Moreover, the utilization of alkylamines in the mobile phase causes ionization suppression, ion source contamination, and MS memory effect [17]. For these reasons, additional methods are continuously developed, such as new methods based on the application of various stationary and mobile phases (e.g., hydrophilic interaction liquid chromatography—HILIC, reversed-phase liquid chromatography—RP HPLC, or mixed mode liquid chromatography) or combining of two different liquid chromatography modes in two-dimensional liquid chromatography (2D-LC) [18–26]. Each of these attempts usually improves separation, MS sensitivity, or simplifies the method compared to IP RP HPLC. Comprehensive RP HPLC × IP RP HPLC, AEC × IP RP HPLC provides orthogonal separation of some isobaric impurities [24]. Moreover, a multiple heart-cutting AEC—HILIC, IP RP HPLC—HILIC, AEC RP HPLC, or mixed mode RP/AEC—RP HPLC allow online desalting, the separation of additional impurities, and the identification of impurities by MS in the absence of ion-pairing reagents, respectively [22,23,26]. On the other hand, 2D-LC has its limitations, namely dilution problems, as well as the necessity of high peak capacity in the first dimension (^{1}D) so that the majority of components can be separated in the ^{1}D [24,26]. Interestingly, mixed-mode stationary phases with anion-exchange and hydrophobic moieties at the surface exhibited good separation potential for structurally related OGNs [18,27]. Nevertheless, eluents containing sufficiently high concentrations of counterions (usually MS-incompatible) are required in order to elute OGNs [18,24]. Based on this short literature review, in our opinion, there is still a gap to fill with new methods allowing OGN impurities separation and identification.

The main goal of the present study was to improve the resolution via the application of mixed-mode stationary phases in RP HPLC for the separation of patisiran analogue (as model siRNA OGN) from its impurities and their identification by quadrupole time-of-flight mass spectrometry (Q-TOF-MS). This made it possible to test whether the use of such a simple chromatographic system (stationary phases of mixed properties and MS-compatible mobile phases) could be useful in the analysis of OGN impurities. Cholesterol and alkylamide columns were evaluated for their selectivity under reversed phase conditions to elucidate their potential for OGN studies. Moreover, the retention orthogonality between cholesterol and amide stationary phases (in HILIC mode) was also tested in order to verify the possibility of 2D-LC application to improve separation power.

2. Results and Discussion

2.1. Retention and Separation Studies for CHOL and AP Columns

Two different stationary phases were chosen for the preliminary study. Our previous work has shown that the use of a reversed-phase system for the determination of OGN

impurities is successful if stationary phases with mixed hydrophobic/hydrophilic properties are used. For these reasons, CHOL and AP columns were tested in the present study. Both stationary phases have previously been used for the separation of OGN mixtures, but only in ion pair mode [27,28]. The aim herein was to test their suitability in the much simpler reversed-phase mode, since both polar (residual silanols, amino, amide groups) and non-polar groups (cholesterol molecule or alkyl chain) are localized in their structure, so they appear to be good candidates for the separation and analysis of OGN impurities (Figure 1).

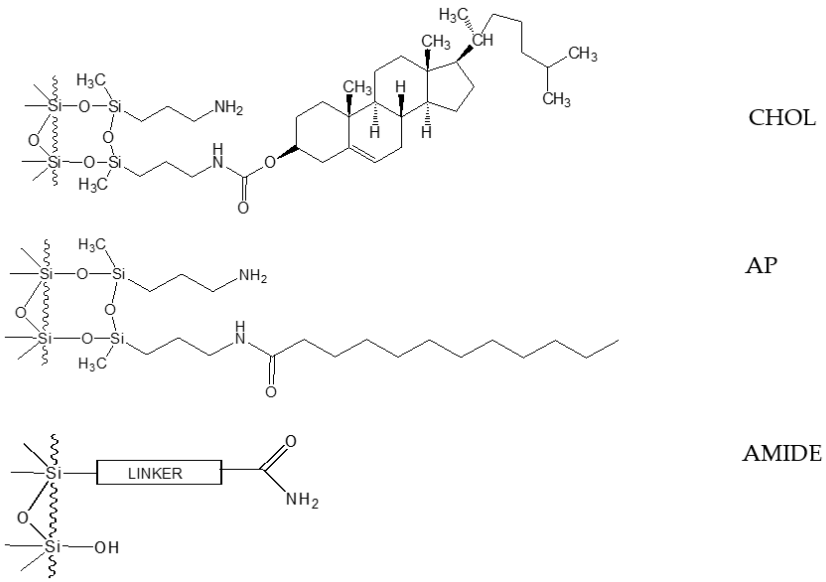

Figure 1. Schematic structure of stationary phases used in the present study.

Retention studies were conducted under gradient elution conditions, with the elution program remaining constant regardless of the column or chromatographic parameter being tested. During the preliminary experiments, we tested the influence of various parameters on impurity separation and retention: pH, salt concentration, type of salt, and type of organic solvent. Table 1 summarizes the retention factor values (k) for the main compound of sense and antisense strands for different parameters, whereas Figure 2 shows selected chromatograms for CHOL stationary phase. The other most important chromatograms are collected in the Supplementary Materials (Figures 2 and S1–S3).

Irrespective of the chromatographic column used, the trends were analogous. With higher pH, the retention of the main compounds decreases (Figures 2A, S1A and S2A, Table 1). It is the effect of protonation of the residual aminopropyl groups that leads to enhanced retention of tested compounds due to electrostatic interactions with negatively charged OGNs. The use of ammonium formate with a pH 4.5 resulted in a lack of elution of the OGNs under the conditions of the gradient used (they were eluted from the column during the washing step). As pH decreased, not only the retention of the main compounds (sense or antisense strands) increased, but also the retention of impurities (Figures 2A, S1A and S2A). This should have resulted in a better separation of the structurally related impurities for pH 5.5, but the width of the peaks also increased with decreasing pH (due to an increased contribution of hydrogen bonding and electrostatic interactions in the retention mechanism). As a result, peak intensities decreased with pH 5.5, which had a negative impact on detection. Consequently, pH 6.3 and 7.5 were selected for further testing.

Table 1. Exemplary results of retention factor (*k*) values determined for sense strand of patisiran analogue with regard to different chromatographic conditions applied during the study (under gradient elution: MPA: salt solution; MPB: MeOH/salt solution 9:1 (*v*/*v*); gradient elution: 10–45% MPB in 20 min).

Stationary Phase	***k***			
	pH of 20 mM ammonium formate			
	4.5	5.5	6.3	7.5
CHOL	-	16.62 ± 0.21	15.23 ± 0.16	13.09 ± 0.09
AP	-	13.22 ± 0.30	9.93 ± 0.02	7.15 ± 0.02
	Concentration of ammonium formate			
	10 mM	20 mM	40 mM	
CHOL	10.44 ± 0.11	15.23 ± 0.27	13.96 ± 0.20	
AP	8.08 ± 0.18	9.93 ± 0.13	9.12 ± 0.08	
	Type of salt			
	20 mM ammonium formate		20 mM ammonium acetate	
CHOL	15.23 ± 0.14		10.98 ± 0.25	
AP	9.93 ± 0.09		7.72 ± 0.13	
	Type of organic solvent			
	MeOH		ACN	
CHOL	15.23 ± 0.29		14.17 ± 0.22	
AP	9.93 ± 0.018		8.18 ± 0.21	

With regard to the influence of the salt concentration (for ammonium formate, pH 6.3), the observed effects were the same for CHOL and AP columns (Figures 2B, S1B and S2B). When raising the concentration from 10 to 20 mM, the *k* values increased, but a further increase in concentration to 40 mM resulted in a reduction of retention (Table 1). These effects can be explained by a superposition of two retention principles, viz. reversed-phase LC (an increase of OGN retention with increasing salt concentration) and ion chromatography (reduction of retention with increasing concentration). It can be assumed that in the case of tested stationary phases, the dominating retention mechanism may change depending on the chromatographic conditions used, e.g., for low pH of salt or high salt concentration, ion exchange becomes predominant. The best separation of impurities was achieved with 20 and 40 mM ammonium formate (Figures 2B, S1B and S2B), due to the greater retention. For further studies, 20 mM was selected due to the intended identification of impurities by Q-TOF-MS, for which a high concentration of 40 mM would lead to ion suppression and contamination of the ion source.

Ammonium acetate has a higher elution strength of OGNs compared to ammonium formate (for the same concentration of both salts) for CHOL and AP. This effect is greater for the CHOL, for which an almost twofold reduction of *k* values was observed (Table 1). In both cases, better separation of impurities was obtained for ammonium formate (Figures 2C and S1C).

The final parameter tested in this research was the type of organic solvent. As expected, OGNs and their impurities were eluted from the column more rapidly with acetonitrile (Figures 2D and S1D). However, this resulted in a lower resolution due to insufficient retention, which is why methanol was finally chosen.

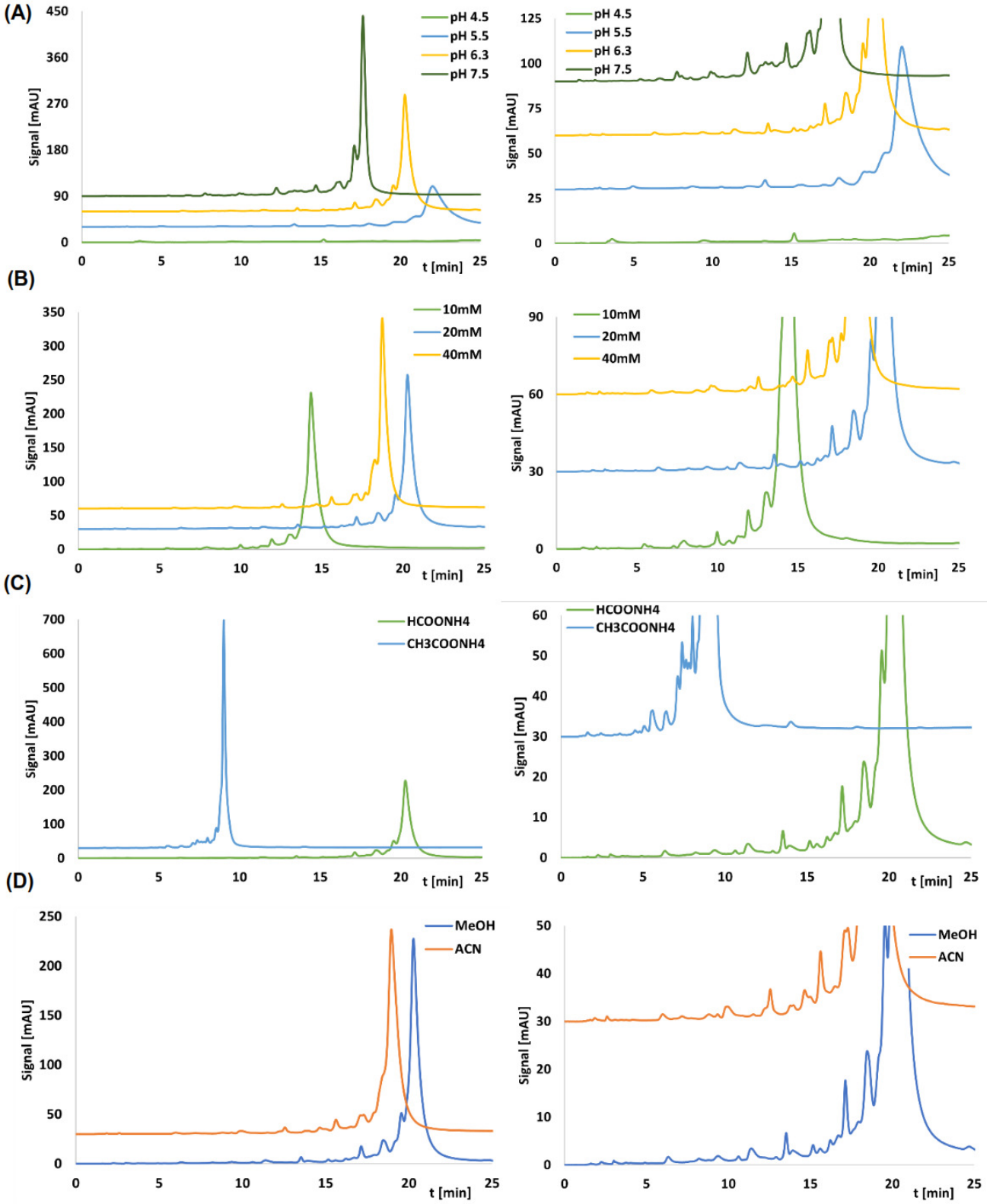

Figure 2. Exemplary chromatograms (left side) with the enlarged view (right side) for sense strand of patisiran analogue for CHOL stationary phase obtained for: (**A**) different pH values (for 20 mM ammonium formate); (**B**) different salt concentration (for ammonium formate); (**C**) two different salts (both of them were 20 mM solutions); (**D**) two different organic solvents. Experimental conditions: MPA: salt solution; MPB: MeOH/salt solution 9:1 (*v*/*v*); gradient elution: 10–45% MPB in 20 min (20 min re-equilibration); column temperature, 40 °C; autosampler temperature, 10 °C; flow rate, 0.3 mL/min; injection volume, 8 µL.

Comparing the results obtained for CHOL and AP (Figure S3), it should be noted that in the case of AP, the retention of the studied OGNs and their impurities was always lower. This is most probably the result of the differences in the structure of both stationary phases, as according to the results obtained previously in our group, their hydrophobicity is almost the same [29] (Figure 1). The CHOL phase has a higher carbon content (9.97%) than AP (6.52%) because the ligand molecule is larger (more bulky) than C12 of the AP ligand (which is straight, but can collapse at high water content). However, the surface density of the CHOL ligands is lower (2.61 μmol/m^2). With a lower surface density of CHOL, the separated molecules have a chance to enter between CHOL ligands, whereas on more densely distributed C12 (3.49 μmol/m^2), they may slide on their top instead [29]. So, together with good interaction with the CHOL molecules, some interaction with aminopropyl groups or so called "hydrolytic pillow" is possible [30]. Taking this into account, it is very likely that better separation on the CHOL phase is possible due to the steric effect and electrostatic interactions with residual amino groups.

2.2. Impurities Analysis with the Use of Q-TOF-MS

In the next stage of the study, Q-TOF-MS was used to identify impurities in both OGNs. In line with previous results, we tested two different pH values of ammonium formate. These were chosen because of the satisfactory separation of the impurities, but it was necessary to additionally check how the pH of the salt in the mobile phase affects the sensitivity, which is an equally important parameter in the determination of impurities. For this reason, we compared peak areas at extracted ion chromatograms (EIC) for several selected ions (assuming that tendencies for other ions were the same). The results are summarized in Table 2. Surprisingly, larger peak areas were obtained for the mobile phase, which included a salt with a lower pH. The OGNs are negatively charged in the whole range of pH used during the present study (due to the pK_a values of phosphate groups). Despite the fact that nucleobases can also contribute to the overall charge of OGN (protonation), the phosphate backbone will contribute to the greatest extent. Consequently, it will be also the most influential factor during the electrospray ionization of OGNs. It has been shown that usually for high pH values of the mobile phase, their ionisation is more efficient; hence, higher peak areas and sensitivity in mass spectrometry, especially in ion pair chromatography, are observed [31,32]. However, our results for the two tested OGNs do not entirely confirm these effects, as we have obtained higher sensitivity for lower pH.

Despite the differences in intensity, exactly the same impurities were identified for both mobile phases. Thus, in this case, the higher peak areas for pH 6.3 did not lead to the identification of more impurities (due to the higher sensitivity). With regard to relative abundance of the different charge states, no differences were observed here either. For both pH 6.3 and 7.5, the same charge states (either −2 or −3) were the most abundant ones (Figure S4).

The low concentrations of most of the impurities present in the sample caused the presence of only one charge state at the full scan spectra (e.g., −1 for *m/z* 1011.149, 865.173 ions, and −2 for *m/z* 915.668, 1075.689 ions) (Figure S5). In the case of the main compound (sense and antisense strands of patisiran analogue), for which the concentration was the highest, three different charge states were observed, whereas for compounds with intermediate concentrations, there were two charge states, typically −2 and −3 or −3 and −4 (e.g., *m/z* 823.469 (−3) and 1235.711 (−2) for 5′ N-13s; *m/z* 1153.181 (−3) and 1733.289 (−2) for 5′N-14s; *m/z* 1489.237 (−3) and 1116.928 (−4) for 5′ N-7s) (Table 3, Figures S5 and S6). For some impurities, the ion with the lower charge state was more abundant, whereas for others, it was the one with the higher charge state (Table 3, Figures S4–S6).

Table 2. Peak areas for selected ions of extracted ion chromatograms (EIC).

Ion (*m*/*z*)	EIC Peak Area	
	pH 6.3	**pH 7.5**
	Sense strand	
865.173	236,618 ± 1302	81,850 ± 591
1235.711	151,654 ± 973	68,514 ± 462
1155.188	66,958 ± 664	51,524 ± 349
1489.9089	87,257 ± 471	32,500 ± 588
1690.023	501,090 ± 1364	259,873 ± 1147
	Antisense strand	
	pH 6.3	pH 7.5
850.172	198,963 ± 1197	71,599 ± 759
902.147	201,337 ± 1372	98,004 ± 1024
1074.673	73,951± 1005	33,820 ± 1153
1247.197	89,620 ± 826	38,391 ± 944
1663.732	296,281 ± 1277	139,009 ± 1039

Deconvolution was used during the study to provide zero-charge state mass spectra and accurate masses of OGN impurities. The PeakView software equipped with Bio Tool Kit Plug-in was used, and deconvolution was performed according to the scheme presented in Figure S7. The neutral monoisotopic masses of OGN impurity series in which each OGN had one nucleotide less were calculated. Primarily, the structural assignment of the nucleotide sequence was based on MS1 accuracy between experimental and calculated masses. Secondly, the structural assignment of the nucleotide sequence was confirmed by MS2 spectra. RoboOligo and OPA/OMA developed by Limbach et al. [33] and Schürch et al. [34] were also used for this purpose. Moreover, the annotated sequences were confirmed by the MS/MS spectra which feature characteristic fragment ions of the oligonucleotide impurities. Exemplary fragmentation spectra for several impurities of sense and antisense patisiran were presented in Figures S8 and S9. The most common fragmentation pathway corresponds to the loss of a nucleobase followed by inter-nucleotide backbone cleavage. The ions were assigned to the sequence fragments based on the oligonucleotide MS/MS fragmentation scheme proposed by McCloskey (Figure S10). Oligonucleotides are fragmentated along the phosphate backbone and produce a set of ions containing the 5′ terminus (a, a-B, b, c, d) and 3′ end group (w, x, y) (Figures S8G–I and S9G–I). The number of nucleotides from the end group is presented as the subscript to the letter. The a-B ions orginate from base loss (cleavage of *N*-glycoside bond) in addition to cleavage at the phosphodiester bonds at the 3′ or 5′ end. Representative examples are shown for the sense strand of patisiran (Figure S8G–I). In the case of our study with CID, signals from b, c, y, and w ions were mainly observed in the MS/MS spectra (Figures S8 and S9).

Table 3. Impurities identified in antisense and sense patisiran strands during their RP HPLC analysis with the use of CHOL stationary phase.

m/*z* Values for the Most Abundant Ion	Charge	Impurity	Impurity Sequence	Deconvoluted Mass (Da)	Retention Time CHOL pH 6.3 (min)	Retention Time CHOL pH 7.5 (min)
			ANTISENSE STRAND			
652.082	−1	3′ N-19as	5′ AU 3′—PO	653.082	8.46	5.06
979.118	−1	3′ N-18as	5′ AUG 3′—cyc	980.118	10.76	8.68
850.170	−1	5′ N-18as	5′ CdTdT 3′—OH	851.170	10.73	9.06
545.129	−1	5′ N-19as	5′ dTdT 3′—OH	546.129	11.15	9.94
749.128	−2	5′ N-16as	5′ mUACdTdT 3′—OH	1500.257	13.95	11.64
835.110	−2	3′ N-16as	5′ AUGGA 3′—PO	1672.221	14.03	9.33
902.141	−2	5′ N-15as	5′ UmUACdTdT 3′—OH	1806.282	14.06	11.56
1074.665	−2	5′ N-14as	5′ GCmUACdTdT 3′—OH	2151.330	15.62	13.01
999.632	−2	3′ N-15as	5′ AUGGAA 3′—PO	2001.264	16.11	10.73
1035.139	−3	5′ N-11as	5′ UUGGUmUACdTdT 3′—OH	3108.418	16.35	13.6
831.122	−3	5′ N-13as	5′ GGUmUACdTdT 3′—OH	2496.367	16.8	14.23
1136.820	−3	5′ N-10as	5′ CUUGGUmUACdTdT 3′—OH	3413.459	17.04	14
1043.630	−4	3′ N-8as	5′ AUGGAAmUACUCUU 3′—PO	4178.519	17.28	12.52
967.3734	−4	3′ N-9as	5′ AUGGAAmUAUUUU 3′—PO	3873.496	17.28	12.51
928.867	−4	5′ N-9as	5′ UCUUGGUmUACdTdT 3′-OH	3719.470	17.46	14.12
1005.132	−4	5′ N-8as	5′ CUCUUGGUmUACdTdT 3′—OH	4024.528	17.46	13.78
882.455	−3	3′ N-13as	5′ AUGGAAmUA 3′—PO	2650.364	17.66	12.56
1187.822	−3	3′ N-10as	5′ AUGGAAmUACUC 3′—PO	3566.466	17.94	12.66
1167.402	−4	5′ N-6as	5′ mUACUCUUGGUmUACdTdT 3′—OH	4673.609	18.21	14.16
984.135	−3	3′ N-12as	5′ AUGGAAmUAC 3′—PO	2955.406	18.41	12.83

Table 3. *Cont.*

m/z Values for the Most Abundant Ion	Charge	Impurity	Impurity Sequence	Deconvoluted Mass (Da)	Retention Time CHOL pH 6.3 (min)	Retention Time CHOL pH 7.5 (min)
1129.892	−4	3′ N-7as	5′ AUGGAAmUACUCUUG 3′—PO	4523.570	18.7	13.13
1249.665	−4	5′ N-5as	5′ AmUACUCUUGGCmUACdTdT 3′—OH	5002.661	18.95	14.23
1216.152	−4	3′ N-6as	5′ AUGGAAmUACUCUUGG 3′—PO	4868.606	19.04	13.55
1580.954	−4	5′ N-1as	5′ UGGAAmUACUCUUGGUmUACdTdT 3′—OH	6327.814	19.16	15.28
1418.703	−4	5′ N-3as	5′ GAAmUACUCUUGGUmUACdTdT 3′—OH	5676.783	19.29	15.46
1504.957	−4	5′ N-2as	5′ GGAAmUACUCUUGGUmUACdTdT 3′—OH	6021.828	19.33	15.47
1531.187	−4	3′ N-2as	5′ AUGGAAmUACUCUUGGUmUAC 3′—PO	6128.748	19.54	15.14
1454.931	−4	3′ N-3as	5′ AUGGAAmUACUCUUGGUmUA 3′—PO	5823.723	19.74	14.92
1663.732	**−4**	**Antisense**	**5′ AUGGAAmUACUCUUGGUmUACdTdT 3′—OH**	**6656.866**	**20.03**	**15.68**
			SENSE STRAND			
1011.145	−1	3′ N-18s	5′ GmUA 3′—PO	1012.130	11.77	7.49
865.169	−1	5′ N-18s	5′ mUdTdT 3′—OH	866.169	13.58	11.94
1340.212	−1	3′ N-17s	5′GmUAA 3′—PO	1341.212	14.49	9.42
915.667	−2	5′ N-15s	5′ mCmCAmUdTdT 3′—OH	1833.337	15.12	12.44
756.134	−2	5′ N-16s	5′ mCAmUdTdT 3′—OH	1514.268	15.18	12.94
1075.689	−2	5′ N-14 OHs	5′ mUmCmCAmUdTdT 3′—OH	2153.353	16.18	13.22
1115.676	−2	5′ N-14 POs	5′ mUmCmCAmUdTdT 3′—PO	2233.352	16.67	16.62
1235.714	−2	5′ N-13s	5′ mUmUmCmCAmUdTdT 3′—OH	2473.396	17.21	14.12
1153.181	−2	3′ N-14s	5′ GmUAAmCmCA 3′—PO	2308.362	17.92	15.7
1395.741	−2	5′ N-12 (A-mU)s	5′ mUmUmUmCmCAmUdTdT 3′—OH	2793.442	18.26	14.9
933.150	−3	5′ N-12s	5′ AmUmUmCmCAmUdTdT 3′—OH	2802.450	18.65	15.33

Table 3. *Cont.*

m/*z* Values for the Most Abundant Ion	Charge	Impurity	Impurity Sequence	Deconvoluted Mass (Da)	Retention Time CHOL pH 6.3 (min)	Retention Time CHOL pH 7.5 (min)
1039.831	−3	5′ N-11s	5′ mUAmUmUmCmCAmUdTdT 3′—OH	3122.492	18.79	15.48
1317.703	−2	3′ N-13s	5′ GmUAAmCmCAA 3′—Np	2637.407	18.87	12.17
1154.857	−3	5′ N-10s	5′ GmUAmUmUmCmCAmUdTdT 3′—OH	3467.530	19.14	15.7
1264.544	−3	5′ N-9s	5′ AGmUAmUmUmCmCAmUdTdT 3′—OH	3796.590	20.31	16.95
1489.237	−3	5′ N-7s	5′ AGAGmUAmUmUmCmCAmUdTdT 3′—OH	4470.688	20.4	16.63
1598.928	−3	5′ N-6s	5′ AAGAGmUAmUmUmCmCAmUdTdT 3′—OH	4799.718	20.58	16.96
1103.173	−3	3′ N-11s	5′ GmUAAmCmCAAGA 3′—PO	3311.495	20.62	13.39
1217.849	−3	3′ N-10s	5′ GmUAAmCmCAAGAG 3′—PO	3656.547	20.69	13.59
1358.973	−4	5′ N-4s	5′ mCmCAAGAGmUAmUmUmCmCAmUdTdT 3′—OH	5437.841	20.68	16.58
1603.513	−4	5′ N-1s	5′ mUAAmCmCAAGAGmUAmUmUmCmCAmUdTdT 3′—OH	6416.030	21.08	17.07
1690.023	**−5**	**Sense (guide strand)**	**5′ GmUAAmCmCAAGAGmUAmUmUmCmCAmUdTdT 3′—OH**	**6761.087**	**21.8**	**17.17**
1441.236	−4	5′ N-3s	5′ AmCmCAAGAGmUAmUmUmCmCAmUdTdT 3′—OH	5766.896	22.71	17.03

2.2.1. The Chemistry behind the Origin of Impurities

Table 3 presents the most abundant ion of each impurity, its preferential charge state, deconvoluted mass, and annotated sequence, whereas the relative proportion for each impurity appointed as peak area and relative peak area for both MS and UV were collected in Table S1 Typically, impurities are formed as N-shortmers, but base mismatches are also possible. Additionally, at the 3′ end of the sequence the hydroxy (OH), phosphate (PO) or 2′,3′-cyclic phosphate (cyc) group may be present. Twenty-eight (28) impurities were annotated for the antisense strand of patisiran analogue, and twenty-two (22) for the sense strand. In both cases, a greater number of 5′-shortmers was found compared to 3′ ones (Table 3). In our study, we have only observed impurities formed as N-shortmer sequences of the main compound. Consequently, the failure sequences lacked various numbers of nucleotides from the 5′ and 3′ end of the target patisiran single nucleotide strands (Table 3). Similar types of impurities were already reported in the scientific literature [9,14]. The incomplete coupling (so-called coupling failures) of nucleotides during the synthesis leads to a number of impurities, which were presented in Table 3, e.g., coupling failure sequence formed in this way missing the last nine nucleotides from its 5′ end is described as the 5′ (N-9)as (for antisense strand of patisiran) or 5′ (N-9)s (for sense strand of patisiran analogue).

The results in Table S1 contain the relative and absolute signal values detected for each impurity and main compound. The absolute signal of the detected impurities is used only for relative comparisons, since direct use of these data for absolute quantification of impurities is not appropriate. The greatest relative and absolute signal values are attributed to 5′ end-missing early eluting impurities (Table S1). Moreover, the highest amount (relative to the main compound) was detected for impurities from 5′ N-18s to 5′ N-14s, as well as for 5′ N-18as and 5′ N-13as. These results suggest that coupling failures for the patisiran analogue are formed most significantly in the initial stages of synthesis.

2.2.2. Antisense Strand of Patisiran

Changes of the elution order of impurities were observed for the CHOL stationary phase when two different pH values of the salt in the mobile phase were compared (Table 3), e.g., for 5′ N-16as, 3′ N-15as, 3′ N-8as, 3′ N-6as, 3′ N-7as. The majority of impurities, for which the elution order has changed (at pH 7.5 compared to 6.3), possess the additional phosphate group at the 3′ end (Table 3). This effect may suggest that it has a significant impact on the retention of OGNs when near-neutral mobile phase conditions are applied.

Regarding the retention data for CHOL obtained for pH 6.3, it should be pointed out that there is no strict linear relationship between the MW of impurities and their retention. However, certain trends can nevertheless be observed. For the antisense strand, OGNs with low molecular masses between 650–2000 Da (charge state −1 and −2) are generally the first to elute from the CHOL column (Table 3). This is followed by the elution of impurities with higher masses in the range of 2100–6300 Da (charge state −3 and −4) in the elution window between 16 to 19.5 min. The retention of OGNs in the reversed-phase system is the result of their total negative charge, size, and the change in polarity determined by the nucleobases. For this reason, for example, 5′ N-19as is eluted after 3′ N-18as and 5′ N-18as, which are more polar (Table 3).

Different tendencies were noticed when the ammonium formate of pH 7.5 was used in the mobile phase. First, eight impurities of small size (below 2000 Da) (charge state −1, −2) are eluted from the column. Then, only OGNs that have a phosphate group at the 3′ end (8 compounds) are eluted (between 12 and 14 min). Next, impurities that have an OH group at the 3′ end (10 compounds) are eluted from the CHOL column. Apparently, changing the pH of the mobile phase for the CHOL column actually alters the interactions and their strength between the stationary phase ligands and the OGNs; introducing an additional phosphate group into the OGN structure reduces its retention. This remains in line with theoretical knowledge. Increasing the pH reduces the positive charge on the stationary phase, resulting in reduced electrostatic interactions. Therefore, any additional

ionized phosphate group will be stronger affected by this pH change and the cause of reduced OGN retention relative to impurities which miss this structural element.

These results clearly confirm that, in the case of mixed-mode stationary phases with hydrophilic-hydrophobic groups, the pH of the mobile phase is an additional parameter that can be changed to alter the separation selectivity by changing the retention of OGNs under RP conditions.

2.2.3. Sense Strand of Patisiran

The retention of impurities for sense strand and pH 6.3 is based on the following order: first, the five OGNs with the lowest masses are eluted between 11 and 15 min, followed by compounds with masses from 2000–3000 Da (between 15 and 19 min), whereas the OGNs with the highest masses and charge states are eluted last (Table 3). These tendencies are quite analogous to those of the antisense strand and are based on similar effects.

For the sense strand, the impurities are mainly OGNs with an -OH group at the 3′ end. Only seven compounds have a 3′ phosphate terminal group (Table 3). Three of them are lower molecular weight compounds that (irrespective of the strand and the pH of the mobile phase) elute early, in a short time. Thus, for pH 7.5, there is no very clear dependence of retention on the type of terminal group at the 3′ end. Neither was there such a dependence of the elution order on the molecular weight or the oligo length.

2.3. Closely Related Impurities in the Main Peak of Sense and Antisense Strands

The results summarized in Table 3 indicate that the complete separation of all impurities could not be achieved with CHOL. Some of them were eluted from the column together with the main compound (Table 3). Figure 3 presents the EIC for selected ions eluted from the CHOL column together with the antisense or sense strand. In the case of the antisense strand of patisiran, there are, in total, five N-1, N-2, N-3 shortmers differing in the 3′ end group (hydroxyl or phosphate) coeluting with the main compound: 5′ N-1as, 5′ N-2as, 5′ N-3as, 3′ N-2as, 3′ N-3as (Table 3). All of them are eluted in the front of the main peak (Figure 3A). Six impurities are eluted together with the main peak of patisiran sense strand, but one of them, 5′ N-3s, is eluted in the 'tail' of the main peak (Figure 3B). The other five impurities are the following shortmers: 3′ N-11s, 3′ N-10s, 5′ N-6s, 5′ N-4s, 5′ N-1s.

Although these structurally-related impurities were not able to be separated using the CHOL column, a characterization of those impurity species was still possible with a direct coupling with MS. To alleviate this selectivity problem, we decided to use 2D-LC in a selective comprehensive mode for this purpose to achieve a complete resolution.

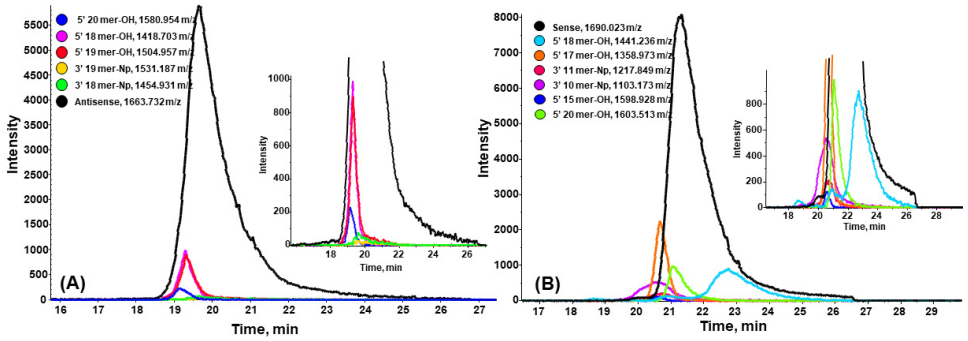

Figure 3. Extracted ion chromatograms (EIC) for selected ions eluted from CHOL column together with the main compound of: (**A**) antisense strand of patisiran analogue, (**B**) sense strand of patisiran analogue. Experimental LC conditions: MPA: 20 mM ammonium formate (pH 6.3); MPB: MeOH/20 mM ammonium formate (pH 6.3) 9:1 (*v*/*v*); 10–45 % MPB in 25 min (15 min re-equilibration); column temperature: 40 °C; autosampler temperature: 4 °C; flow rate: 0.3 mL/min; injection volume: 8 µL; MS parameters for nebulizer gas, heater gas, curtain gas, source temperature, ion spray voltage, declustering potential, and collision energy were set as follows: 90 psi, 90 psi, 35 psi, 550 °C, 4500 V, −150/−200/−150 V, −10 V.

2.4. Selective Comprehensive (High-Resolution Sampling) sRP × HILIC-2DLC for Patisiran

In our previous 2DLC experiments, reversed phase was employed as the second dimension for desalting before ESI-MS detection [22,23]. Hydrophilic interaction liquid chromatography (HILIC), which was shown to give enhanced separation under ion-pair free elution conditions, was envisaged as a second dimension for this 2DLC setup in combination with CHOL RP. We chose the previously developed HILIC method using a BEH Amide column for the present study [20]. The retention data are summarized in Table S2. Firstly, we have compared the normalized retention times (t_N) obtained for HILIC and RP using CHOL to check the orthogonality of the systems, as 2D-LC performance depends on the separation orthogonality. The t_N values were calculated by the use of the following formula:

$$t_N = \frac{t_R - t_0}{t_G - t_0} \quad (1)$$

wherein t_R is the retention time of the compound, t_G the gradient time, and t_0 is the void time.

The results on the orthogonality of the distinct LC modes are presented in Figure 4. The lower the determination coefficient (R^2) value, the higher the degree of orthogonality between columns (values lower than 0.5 are considered as indicating a high degree of scatter, which is desirable for 2DLC). The R^2 were equal to 0.5232 for the antisense strand and 0.6474 for the sense strand when the normalized retention time of corresponding impurities on the CHOL and BEH Amide columns were correlated (Figure 4). This indicates good orthogonality between both modes of LC and both columns, which is indispensable for a successful application of 2D-LC and can enable the selective separation of impurities in the second dimension.

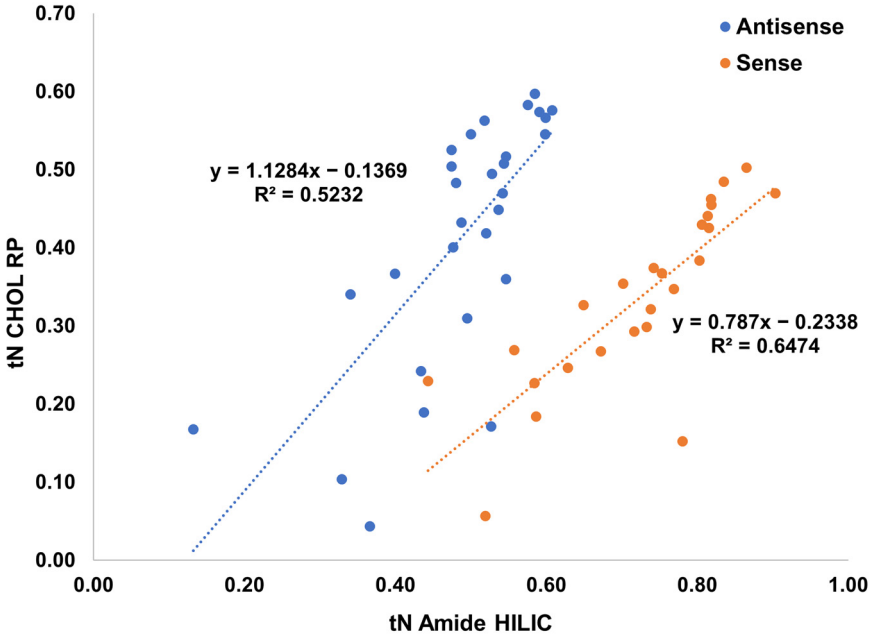

Figure 4. The correlation of normalized retention time (t_N) between identical impurities and main compounds detected by HILIC with Amide column and RP with CHOL column for two strands separately.

Finally, the RP method with the use of CHOL column was used in the first dimension, whereas HILIC with BEH Amide was used in the second dimension. Several groups have reported about the selectivity of BEH Amide towards different kind of OGNs [19,20,35]. For this study, we chose basic conditions at pH 9 to enhance the ionization of the OGNs. With 15 mM ammonium acetate, both MS compatibility and good chromatographical performance are given. The selective comprehensive mode of 2D-LC was used in order to improve the separation of closely related impurities. In this mode, a certain part of

the ^{1}D chromatogram, herein covering the main peak, is comprehensively sampled by a number of adjacent fractions and transferred into the second dimension. In this work, 10 fractions were stored in 40 µL sampling loops until analysis by the ^{2}D HILIC method. Due to the high aqueous content of the ^{1}D RP eluent and its high elution strength in the ^{2}D HILIC method, active solvent modulation was activated [36]. It allows dilution of the sampled fractions from ^{1}D by weak ^{2}D HILIC eluent before they are introduced onto the ^{2}D HILIC column. It avoids peak distortions and sample breakthrough effects. The exemplary results for the sense strand of patisiran are presented in Figures 5 and S11. Although it was not possible to obtain a full baseline separation of all six impurities eluted with the main peak in ^{1}D by this sRP × HILIC-2DLC, the partial separation was sufficient to provide the required information on impurity determination in good quality. The use of HILIC in ^{2}D allowed the separation of only three additional compounds (5′ N-4s, 5′ N-1s, 5′ N-3s) from the main sense strand (Figure 5). It is a limitation of the developed method that not all impurities could be fully baseline separated; yet, compared to a one-dimensional separation, an improved resolution could be achieved.

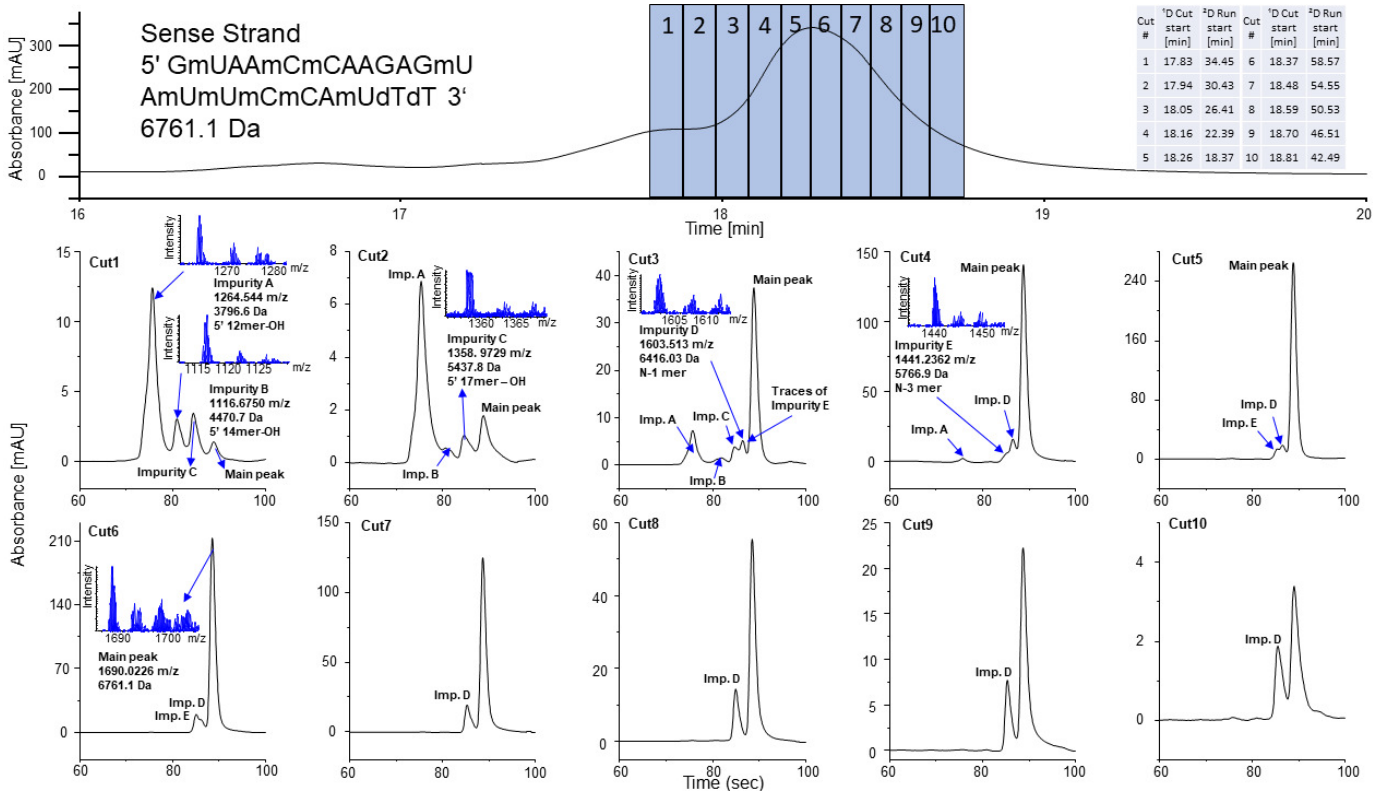

Cut #	^{1}D Cut start [min]	^{2}D Run start [min]	Cut #	^{1}D Cut start [min]	^{2}D Run start [min]
1	17.83	34.45	6	18.37	58.57
2	17.94	30.43	7	18.48	54.55
3	18.05	26.41	8	18.59	50.53
4	18.16	22.39	9	18.70	46.51
5	18.26	18.37	10	18.81	42.49

Figure 5. The UV chromatograms presenting the result of selective comprehensive 2D-LC analysis of sense strand of patisiran analogue. Upper chromatogram: ^{1}D LC with the use of CHOL in RP mode; lower chromatograms: ^{2}D LC with the use of Amide in HILIC mode. Detailed experimental conditions in Section 2.4.

A change in the elution order was observed. The 5′ N-3s in HILIC was eluted before the sense strand and before the 5′ N-1s impurity, whereas in ^{1}D, it was eluted after the main peak and other impurities. This effect is characteristic for these two chromatographic systems and further demonstrates the orthogonality of RP and HILIC.

Three of the impurities that were eluted together with the sense strand, 5′ N-6s (*m/z* 1598.9283), 3′ N-11s (*m/z* 1103.173), 3′ N-10s (*m/z* 1217.849), were not detected in the sRP × HILIC-2DLC approach due to their low concentration (100–500 cps in 1D-RPLC, see Figure 3B), splitting into multiple fractions and a further dilution effect upon injection into the ^{2}D. This is the drawback of our method. The new multi-inject software solution from

Agilent Technologies, which allows the transfer of the contents of the multiple loops of the multiple heartcutting loop decks at once before the entire deck is analyzed by a single ^{2}D analysis cycle, could solve this problem, but was not yet available in this work [37]. It not only overcomes the sensitivity problem, but also saves time, since only one ^{2}D analysis run needs to be carried out in contrast to the multiple injections of the different loops in the normal selective comprehensive 2DLC approach. This holds great promise for selective comprehensive sRP×HILIC-2DLC analysis of oligonucleotide pharmaceuticals, and will further empower the current selective comprehensive CHOL RP × BEH Amide HILIC-ESI-QTOF-MS approach in impurity profiling.

3. Materials and Methods

3.1. Materials

Acetic acid (ACS reagent, ≥99.8%), ammonium hydroxide (ACS reagent, 28–30%), ammonium acetate (LC-MS grade), and ammonium formate (LC-MS grade) were purchased from Sigma-Aldrich (Merck, Munich, Germany). LC-MS grade methanol (MeOH) and acetonitrile (ACN) were purchased from Carl Roth (Karlsruhe, Germany). Ultrapure water was obtained from Elga PurLab Ultra system (Celle, Germany). Both OGNs were purchased from Oligo Sigma (Merck, Munich, Germany) as desalted raw products without purification.

3.2. Oligonucleotides

Two OGNs were used during present study. Their sequences correspond to the sense and antisense strand of the patisiran, which is an active substance of a drug used for the treatment of polyneuropathy caused by hereditary transthyretin-mediated amyloidosis [38]. They were used as model compounds for the development of a method for the separation and identification of impurities. They were purchased as custom, synthesized, raw products, obtained as desalted, but non-purified, synthesis products from Oligo Sigma (Merck, Munich, Germany). Thus, they were not supposed to have drug quality, but were considered suitable test samples for our study. The sequence of passenger (sense) strand is as follows: 5′-G-Um-A-A-Cm-Cm-A-A-G-A-G-Um-A-Um-Um-Cm-Cm-A-Um-dT-dT-3′ with molecular mass of 6764 Da. The guide strand (antisense) has a sequence 5′-A-U-G-G-A-A-Um-A-C-U-C-U-U-G-G-U-Um-A-C-dT-dT-3′ and mass 6660 Da (dT stands for deoxyriboncleotide, whereas mU, mC stands for 2′-O-methylribonucleotide analogues).

3.3. Instrumentation

Preliminary, retention, and separation studies for cholesterol (CHOL) and alkylamide (AP) columns were performed with an Agilent 1290 Infinity II UHPLC system from Agilent Technologies (Waldbronn, Germany) equipped with a Multisampler (G7167B), binary High-Speed Pump (G7120A), column compartment (G7116B), and Diode Array Detector (DAD) (G7117B).

The 2D-LC experiments were carried out with the use of Agilent 1290 Infinity II 2D-LC Solution from Agilent Technologies, including a quaternary Flexible pump (G7104A), Multisampler (G7167B), and Variable Wavelength Detector (VWD) (G7114B) with 14 µL flow cell (G1314-60186) and a pressure relief valve (pressure release kit, G4236-600010) between the VWD and 2D-interface. The sampling frequency of the VWD was 5 Hz. In the second dimension, a binary High-Speed Pump (G7120A) and a Diode Array Detector (DAD) (G7117B) with 1 µL flow cell (G4212-60008) were employed. The sampling frequency of the DAD was 80 Hz. Two separate Infinity column compartments (G7116B) were used. Both dimensions were connected by a valve drive (G1170A) equipped with 5-position/10-port 2D-LC active solvent modulation (ASM) valve (#5067-4266) coupled to two 6-position/14-port valve heads (#5067-4142, multiple heart-cutting valves) equipped with six 40 µL loops each. The ASM valve contained the ASM capillary with dimensions of 85 × 0.12 mm (0.96 µL, #5500-1300) (ASM factor 5, ASM loop flushing: 3 times) [36]. The 2D-LC system

was controlled by Agilent OpenLab CDS ChemStation Rev. C.01.10 with 2D-LC add-on software.

MS detection was performed on a SCIEX Triple TOF 5600+ QTOF mass spectrometer with a Duospray ion source operating in negative ESI mode. The 2D-LC and MS instruments were coupled with a contact closure connection for peripheral devices from SCIEX, and the MS instrument was controlled with Analyst TF 1.7 software (AB SCIEX, Darmstadt, Germany).

3.4. LC-MS Conditions

Three different columns have been used in the present study: the home-made CHOL and AP columns (125 × 2.1 mm, 5 µm particle size, 100 Å), as well as Acquity UPLC BEH Amide for the second dimension (50 × 2.1 mm, 1.7 µm particle size, 130 Å). The structures of stationary phases are presented in Figure 1. CHOL and AP were synthesized according to a previously described synthesis method [29,30]. They were prepared from the same batch of 5 µm Kromasil® silica gel with 300 Å pore size. The CHOL stationary phase has 9.97% of carbon at the surface, whereas for AP, the carbon load is equal to 6.52%. The stationary phases were packed into stainless-steel columns with the use of a home-made apparatus with a Haskel pump (Burbank, CA, USA) under constant pressure (400 bars). Column void volume (t_0) was measured by injecting methanol.

For the retention and separation studies with CHOL and AP columns, similar elution conditions were used. The chromatographic parameters were as follows: mobile phase A (MPA) was composed of salt solution, whereas mobile phase B (MPB) contained MeOH/salt solution (9:1; v/v); gradient elution consisted in 10–45% MPB change in 25 min (with 15 min re-equilibration); column temperature: 40 °C; flow rate: 0.3 mL/min; injection volume: 8 µL; spectrophotometric UV detection was performed at λ = 254 nm. Four different parameters were tested during this stage of studies, namely the pH of salt (4.5–7.5), salt concentration (10–40 mM), salt type (ammonium formate and acetate), and organic solvent type (MeOH, ACN).

Finally, the optimized conditions used in the ^{1}D were as follows: column: CHOL; MPA: 20 mM ammonium formate (pH 6.3), MPB: MeOH/20 mM ammonium formate (pH 6.3) 9:1 (v/v); gradient elution: 10–45% MPB in 20 min (20 min re-equilibration); column temperature: 40 °C; autosampler temperature 10 °C; flow rate: 0.3 mL/min; injection volume: 8 µL.

The separation in the second dimension ^{2}D was performed in a HILIC mode with the following final conditions: column—Acquity UPLC BEH Amide, MPA: 15 mM ammonium acetate in ACN/water 7:3 (v/v) (pH 9), MPB: 15 mM ammonium acetate (pH 9), gradient elution: hold 0% MPB for 0.33 min (ASM), 0–60% MPB in 2.38 min, re-equilibration for 1.69 min, column temperature: 60 °C, flow rate: 1.0 mL/min.

MS detection was carried out in a negative polarity mode with an ESI source. The MS parameters for RP experiments with CHOL were as follows: nebulizer gas, 90 psi; heater gas, 90 psi; curtain gas, 35 psi; source temperature, 550 °C; ion spray voltage, 4500 V; declustering potential, 200 V; and collision energy, 10 V. In the case of 2D experiments, these parameters were: nebulizer gas, 80 psi; heater gas, 80 psi; curtain gas, 40 psi; source temperature, 450 °C; ion spray voltage, 4500 V; declustering potential, 150 V; and collision energy, 10 V. The data processing was accomplished by using PeakView (AB Sciex, Darmstadt, Germany).

The identification of impurities was performed by assigning charge states of the ions observed at the full scan spectra, calculation of masses, or application of deconvolution. The PeakView equipped with Bio Tool Kit Plug-in (Version 2 2 0.11391, SCIEX) was used during the deconvolution (Figure S7). When the molecular mass of impurities was determined, their identification (sequence assignment) was performed by mass calculation with the use of RoboOligo and the OMA/OPA program [33,34]. Moreover, the structural annotation of impurities was also performed based on their fragmentation.

4. Conclusions

The results obtained during the present study confirmed the high potential of mixed hydrophobic/hydrophilic stationary phases for the study of OGN impurities. The RP HPLC mode was successfully used for the separation of impurities with a cholesterol (CHOL)-based stationary phase, and no ion-pair reagents were needed for that purpose. This is one of the advantages of the method developed during the study. Because both the alkylamide and cholesterol phases possess surface chemistry capable of changing properties depending on the pH of the mobile phase, this parameter proved to be crucial in developing a method for separating impurities from the parent compound. In both cases, the best separation results were obtained for pH in the range 6.5–7.5. The type and concentration of salt used in the mobile phase had a lower impact on the retention and separation compared to pH. However, it should be underlined that 20 mM ammonium formate gave the best results in terms of resolution. When comparing the impurity separation between the two stationary phases, a significantly higher efficiency was obtained for the cholesterol stationary phase (less peak broadening and higher retention compared to the alkylamide column). Each of these chromatographic parameters has an impact on the intensity of the OGN-derived signals at the mass spectra. However, the pH of the mobile phase was again the most influential, and the highest intensities of impurities ions were observed for pH equal 6.5.

For the final chromatographic method developed in RP HPLC using CHOL, a good separation of most impurities was achieved within 25 min. A few structurally closely related impurities were coeluted with the main sense or antisense strand. For the characterization of the majority of impurities, the developed CHOL 1DLC separation was sufficient. Our plans for the future are to reduce the diameter of CHOL stationary phase particles to 3 µm or less, which will certainly lead to an increase in the efficiency of impurities separation. It may then be possible to use only RP HPLC and control pH to alter retention and separation.

The good orthogonality between RP HPLC with CHOL and HILIC with a commercially available amide column allowed us to use 2D-LC in a selective comprehensive mode for the separation of closely related impurities. We achieved the separation of several impurities eluted together with the main OGN. Some minor impurities could not be detected anymore in the selective comprehensive 2DLC analysis due to splitting of the ^{1}D peaks into several fractions and further dilution by ^{2}D eluent. The multi-inject approach, which allows analysis of the entire loop deck at once before ^{2}D analysis, has the potential to overcome this limitation and accelerate the entire analysis. With these further advancements, the developed 2D-LC method can be a successful tool for the separation and determination of impurities in oligonucleotide pharmaceuticals.

The main advantage of the developed method is the separation and identification of most impurities in 25 min using CHOL with RP HPLC. An advantage is the use of ion-pair-free or inorganic salts-free mobile phases. The use of 2D-LC leads to a further benefit: the increased resolution of compounds coeluted with the main OGN.

Supplementary Materials: The following supporting information can be downloaded at: https://www.mdpi.com/article/10.3390/ijms232314960/s1.

Author Contributions: Conceptualization, S.S., M.L. and F.L.; methodology, S.S., M.L. and F.L.; validation, S.S., M.L. and F.L.; investigation, S.S. and F.L.; data curation, S.S. and F.L.; writing—original draft preparation, S.S. and F.L.; writing—review and editing, S.S., M.L., F.L., M.S. and B.B.; visualization, S.S. and F.L. All authors have read and agreed to the published version of the manuscript.

Funding: This work was supported by Nicolaus Copernicus University in Toruń, *Mobilities for employee's* competition operating under Excellence Initiative-Research University. We are grateful to Agilent Technologies for the support of this research by an Agilent Research Award (#4068).

Institutional Review Board Statement: Not applicable.

Informed Consent Statement: Not applicable.

Data Availability Statement: Not applicable.

Acknowledgments: The authors thank Stephan Buckenmaier from Agilent Technologies, Waldbronn, Germany, for technical advice and valuable discussions.

Conflicts of Interest: The authors declare no conflict of interest.

References

1. Crooke, S.T.; Liang, X.H.; Baker, B.F.; Crooke, R.M. Antisense technology: A review. *J. Biol. Chem.* **2021**, *296*, 100416. [CrossRef] [PubMed]
2. Bennett, C.F. Therapeutic Antisense Oligonucleotides Are Coming of Age. *Ann. Rev. Med.* **2019**, *70*, 307–321. [CrossRef]
3. El Zahar, N.M.; Magdy, N.; El-Kosasy, A.M.; Bartlett, M.G. Chromatographic approaches for the characterization and quality control of therapeutic oligonucleotide impurities. *Biomed. Chromatogr.* **2017**, *32*, e4088. [CrossRef] [PubMed]
4. Crooke, S.T.; Witztum, J.L.; Bennett, C.F.; Baker, B.F. RNA-targeted therapeutics. *Cell Metab.* **2018**, *27*, 714–739. [CrossRef]
5. Deleavey, G.F.; Damha, M.J. Designing chemically modified oligonucleotides for targeted gene silencing. *Chem. Biol.* **2012**, *19*, 937–954. [CrossRef] [PubMed]
6. Shen, X.; Corey, D.R. Chemistry, mechanism and clinical status of antisense oligonucleotides and duplex RNAs. *Nucleic Acids Res.* **2018**, *46*, 1584–1600. [CrossRef] [PubMed]
7. Pourshahian, S. Therapeutic oligonucleotides, impurities, degradants, and their characterization by mass spectrometry. *Mass Spectrom. Rev.* **2021**, *40*, 75–109. [CrossRef]
8. Capaldi, D.; Teasdale, A.; Henry, S.; Akhtar, N.; den Besten, C.; Gao-Sheridan, S.; Kretschmer, M.; Sharpe, B.; Andrews, B.; Burm, B.; et al. Impurities in Oligonucleotide Drug Substances and Drug Products. *Nucleic Acid Ther.* **2017**, *27*, 1–14. [CrossRef]
9. Goyon, A.; Yehl, P.; Zhang, K. Characterization of therapeutic oligonucleotides by liquid chromatography. *J. Pharm. Biomed. Anal.* **2000**, *182*, 113105. [CrossRef]
10. Szekely, L.; Kiessig, S.; Schwarz, M.A.; Kalman, F. Capillary gel electrophoresis of therapeutic oligonucleotides–Analysis of single-and double-stranded forms. *Electrophoresis* **2009**, *30*, 1579–1586. [CrossRef]
11. Stilianos, G.; Roussis, A. Novel and Intuitive Method of Displaying and Interacting with Mass Difference Information: Application to Oligonucleotide Drug Impurities. *J. Am. Soc. Mass Spectrom.* **2015**, *26*, 1150–1164.
12. Elzahar, N.M.; Magdy, N.; El-Kosasy, A.M.; Bartlett, M.G. Degradation product characterization of therapeutic oligonucleotides using liquid chromatography mass spectrometry. *Anal. Bioanal. Chem.* **2018**, *410*, 3375–3384. [CrossRef]
13. Roussis, S.G.; Koch, C.; Capaldi, D.; Rentel, C. Rapid oligonucleotide drug impurity determination by direct spectral comparison of ion-pair reversed-phase high-performance liquid chromatography electrospray ionization mass spectrometry data. *Rapid Commun. Mass Spectrom.* **2018**, *32*, 1099–1106. [CrossRef]
14. Roussis, S.G.; Cedillo, I.; Rentel, C. Automated determination of early eluting oligonucleotide impurities using ion-pair reversed-phase liquid chromatography high resolution-mass spectrometry. *Anal. Biochem.* **2020**, *595*, 113623. [CrossRef] [PubMed]
15. Roussis, S.G.; Pearce, M.; Rentel, C. Small Alkyl Amines as Ion-Pair Reagents for the Separation of Positional Isomers of Impurities in Phosphate Diester Oligonucleotides. *J. Chromatogr. A* **2019**, *1594*, 105–111. [CrossRef] [PubMed]
16. Roussis, S.G.; Rodriguez, A.A.; Rentel, C. Determination of individual liogonucleotide impurities by small amine ion pair-RP HPLC MS and MS/MS: N-1 impurities. *J. Chromatogr. B* **2021**, *1169*, 122611. [CrossRef]
17. Rütters, H.; Möhring, T.; Rullkötter, J.; Griep-Raming, J.; Metzger, J.O. The persistent memory effect of triethylamine in the analysis of phospholipids by liquid chromatography/mass spectrometry. *Rapid Commun. Mass Spectrom.* **2000**, *14*, 122–123. [CrossRef]
18. Zimmermann, A.; Horak, J.; Sánchez-Muñoz, O.L.; Lämmerhofer, M. Surface charge fine tuning of reversed-phase/weak anion-exchange type mixed-mode stationary phases for milder elution conditions. *J. Chromatogr. A* **2015**, *1409*, 189–200. [CrossRef] [PubMed]
19. Lobue, P.A.; Jora, M.; Addepalli, B.; Limbach, P.A. Oligonucleotide analysis by hydrophilic interaction liquid chromatography-mass spectrometry in the absence of ion-pair reagents. *J. Chromatogr. A* **2019**, *1595*, 39–48. [CrossRef] [PubMed]
20. Huang, M.; Xu, X.; Qiu, H.; Li, N. Analytical characterization of DNA and RNA oligonucleotides by hydrophilic interaction liquid chromatography-tandem mass spectrometry. *J. Chromatogr. A* **2021**, *1648*, 462184. [CrossRef] [PubMed]
21. Kaczmarkiewicz, A.; Buszewski, B.; Studzińska, S. Application of hydrophilic interaction liquid chromatography coupled with tandem mass spectrometry for the retention and sensitivity studies of antisense oligonucleotides. *J. Chromatogr. A* **2020**, *1622*, 461100.
22. Li, F.; Su, X.; Bäurer, S.; Lämmerhofer, M. Multiple heart-cutting mixed-mode chromatography-reversed-phase 2D-liquid chromatography method for separation and mass spectrometric characterization of synthetic oligonucleotides. *J. Chromatogr. A* **2020**, *1625*, 461338. [CrossRef]
23. Li, F.; Lämmerhofer, M. Impurity profiling of siRNA by two-dimensional liquid chromatography-mass spectrometry with quinine carbamate anion-exchanger and ion-pair reversed-phase chromatography. *J. Chromatogr. A* **2021**, *1643*, 462065. [CrossRef] [PubMed]
24. Roussis, S.G.; Cedillo, I.; Rentel, C. Two-dimensional liquid chromatography-mass spectrometry for the characterization of modified oligonucleotide impurities. *Anal. Biochem.* **2018**, *556*, 45–52. [CrossRef] [PubMed]

25. Li, Q.; Lynen, F.; Wang, J.; Li, H.; Xu, G.; Sandra, P. Comprehensive hydrophilic interaction and ion-pair reversed-phase liquid chromatography for analysis of di-to deca-oligonucleotides. *J. Chromatogr. A* **2012**, *1255*, 237–243. [CrossRef] [PubMed]
26. Goyon, A.; Zhang, K. Characterization of antisense oligonucleotide impurities by ion pairing reversed-phase and anion exchange chromatography coupled to hydrophilic interaction liquid chromatography/mass spectrometry using a versatile two-dimensional liquid chromatography setup. *Anal. Chem.* **2020**, *92*, 5944–5951.
27. Studzińska, S.; Pietrzak, L.; Buszewski, B. The effects of stationary phases on retention and selectivity of oligonucleotides in IP-RP-HPLC. *Chromatographia* **2014**, *77*, 1589–1596. [CrossRef] [PubMed]
28. Studzińska, S.; Krzemińska, K.; Szumski, M.; Buszewski, B. Application of a cholesterol stationary phase in the analysis of phosphorothioate oligonucleotides by means of ion pair chromatography coupled with tandem mass spectrometry. *Talanta* **2016**, *154*, 270–277. [CrossRef] [PubMed]
29. Buszewski, B.; Jezierska-Świtała, M.; Kaliszan, R.; Wojtczak, A.; Albert, K.; Bochmann, S.; Matyska, M.T.; Pesek, J.J. Selectivity tuning and molecular modeling of new generation packings for RP HPLC. *Chromatographia* **2001**, *53*, 204–212. [CrossRef]
30. Gadzała-Kopciuch, R.M.; Buszewski, B. A comparative study of hydrophobicity of octadecyl and alkylamide bonded phases based on methylene selectivity. *J. Sep. Sci.* **2003**, *26*, 1273–1283. [CrossRef]
31. Guimaraes, G.J.; Bartlet, M.G. The critical role of mobile phase pH in the performance of oligonucleotide ion-pair liquid chromatography–mass spectrometry methods. *Future Sci. OA* **2021**, *7*, FSO753. [CrossRef] [PubMed]
32. Sutton, J.M.; Guimaraes, G.J.; Annavarapu, V.; van Dongen, W.D.; Bartlett, M.G. Current state of oligonucleotide characterization using liquid chromatography-mass spectrometry: Insight into critical issues. *J. Am. Soc. Mass Spectrom.* **2020**, *31*, 1775–1782. [CrossRef] [PubMed]
33. Sample, P.J.; Gaston, W.K.; Alfonzo, D.; Limbach, P.A. RoboOligo: Software for mass spectrometry data to support manual and de novo sequencing of post-transcriptionally modified ribonucleic acids. *Nucleic Acids Res.* **2015**, *43*, e64. [CrossRef] [PubMed]
34. Nyakas, A.; Blum, L.C.; Stucki, S.R.; Reymond, J.-L.; Schürch, S. OMA and OPA—Software-supported mass spectra analysis of native and modified nucleic acids. *J. Am. Soc. Mass Spectrom.* **2013**, *24*, 249–256. [CrossRef] [PubMed]
35. Demelenne, A.; Nys, G.; Nix, C.; Fjeldsted, J.C.; Crommen, J.; Fillet, M. Separation of phosphorothioated oligonucleotide diastereomers using multiplexed drift tube ion mobility mass spectrometry. *Anal. Chim. Acta* **2022**, *1191*, 339297. [CrossRef] [PubMed]
36. Stoll, D.R.; Shoykhet, K.; Petersen, P.; Buckenmaier, S. Active Solvent Modulation: A valve-based approach to improve separation compatibility in two-dimensional liquid chromatography. *Anal. Chem.* **2017**, *89*, 9260–9267. [CrossRef] [PubMed]
37. Buckenmaier, S.; Petersson, P. *Analysis of Peptide/Protein-Related Impurities Using the Integrated Solution of Bio 2D-LC/Q-TOF in Agilent MassHunter Software*; 5994–4743EN; Agilent Technologies: Waldbronn, Germany, 2022.
38. Akinc, A.; Maier, M.A.; Manoharan, M.; Fitzgerald, K.; Jayaraman, M.; Barros, S.; Ansell, S.; Du, X.; Hope, M.J.; Madden, T.D.; et al. The Onpattro story and the clinical translation of nanomedicines containing nucleic acid-based drugs. *Nat. Nanotechnol.* **2019**, *14*, 1084–1087. [CrossRef] [PubMed]

Cholesterol stationary phase in the separation and identification of siRNA impurities by two-dimensional liquid chromatography-mass spectrometry

Sylwia Studzińska [1,2,*], Feiyang Li [2], Michał Szumski [1], Michael Lämmerhofer [2], Bogusław Buszewski [1]

[1] Chair of Environmental Chemistry and Bioanalytics, Faculty of Chemistry, Nicolaus Copernicus University in Toruń, 7 Gagarin Str., PL-87-100 Toruń, Poland

[2] Institute of Pharmaceutical Sciences, Pharmaceutical (Bio-)Analysis, University of Tübingen, Auf der Morgenstelle 8, 72076 Tübingen, Germany

[3] Centre for Modern Interdisciplinary Technologies, Nicolaus Copernicus University in Toruń, 4 Wilenska St., 87-100 Toruń, Poland

***** Correspondence: kowalska@chem.umk.pl; Tel.: +48 56 6114753

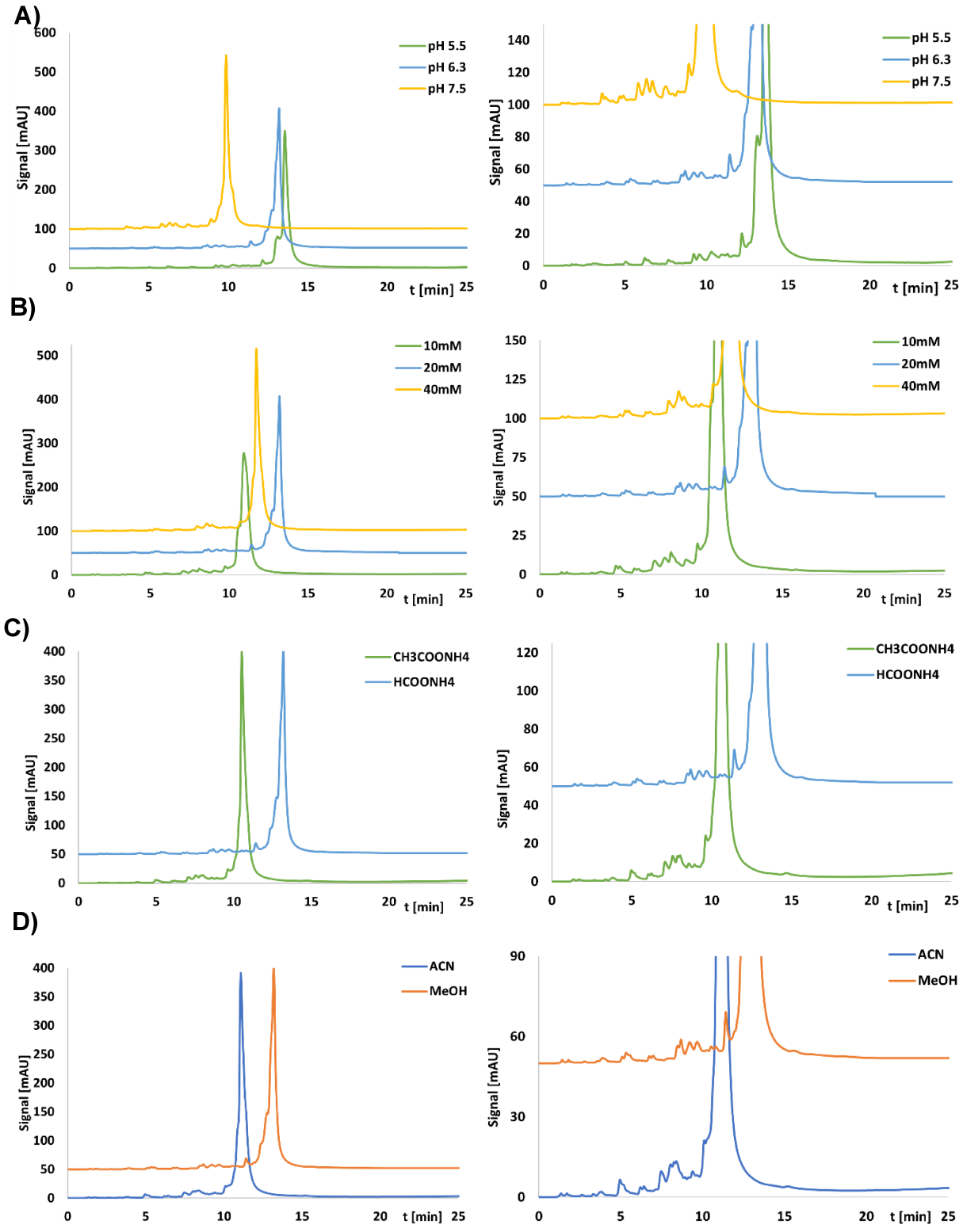

Figure S1. Exemplary chromatograms (left side) with enlarged view (right side) for sense strand of patisiran analogue for AP stationary phase obtained for: A) different pH values (for 20mM ammonium formate), B) different salt concentration (for ammonium formate); C) two different salts (both of them were 20mM solutions); D) two different organic solvents. Experimental conditions: MPA: salt solution, MPB: MeOH/salt solution 9:1 (v/v); gradient elution: 10-45% MPB in 20 minutes (20 minutes re-equilibration); column temperature: 40 °C; autosampler temperature 10 °C; flow rate: 0.3 mL/min; injection volume 8µL.

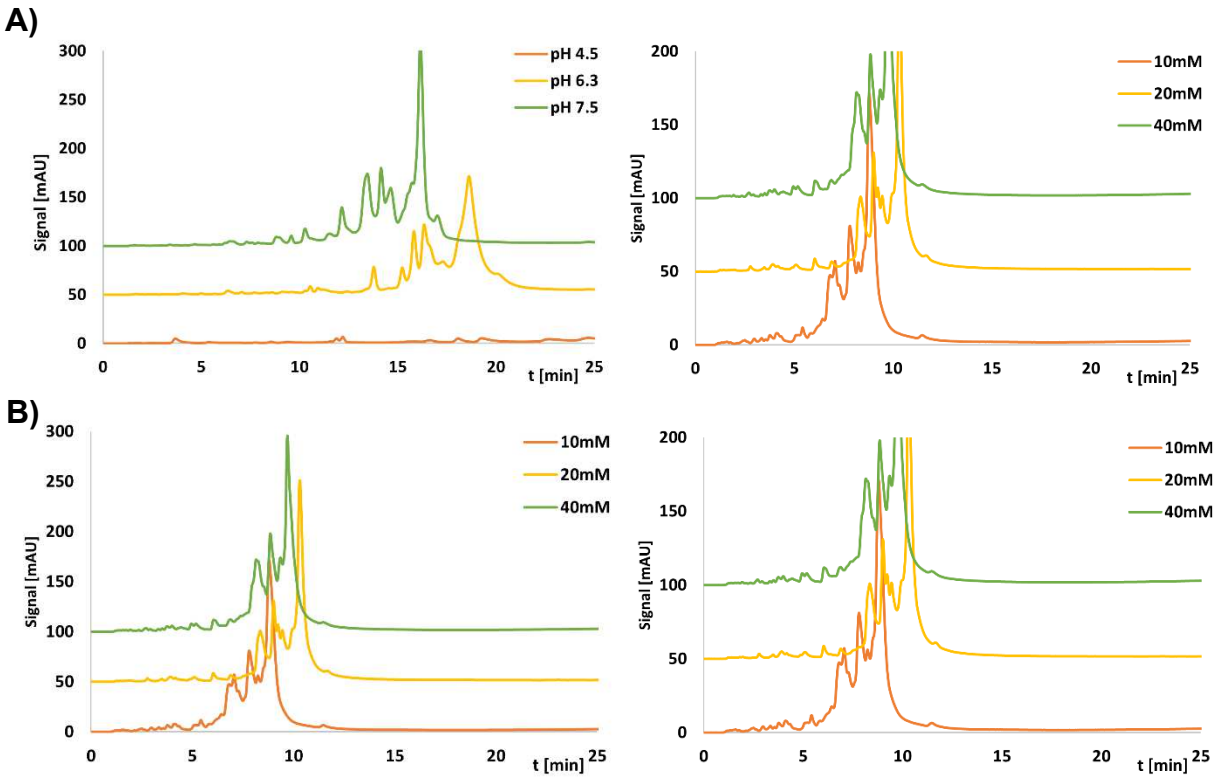

Figure S2. Exemplary chromatograms (left side) with enlarged view (right side) for antisense strand of patisiran analogue for: A) CHOL, different pH values (for 20mM ammonium formate), B) AP, different salt concentration (for ammonium formate, pH 6.3). Experimental conditions: MPA: ammonium formate, MPB: MeOH/20 mM ammonium formate 9:1 (v/v); gradient elution: 10-45% MPB in 20 minutes (20 minutes re-equilibration); column temperature: 40 °C; autosampler temperature 10 °C; flow rate: 0.3 mL/min; injection volume 8µL.

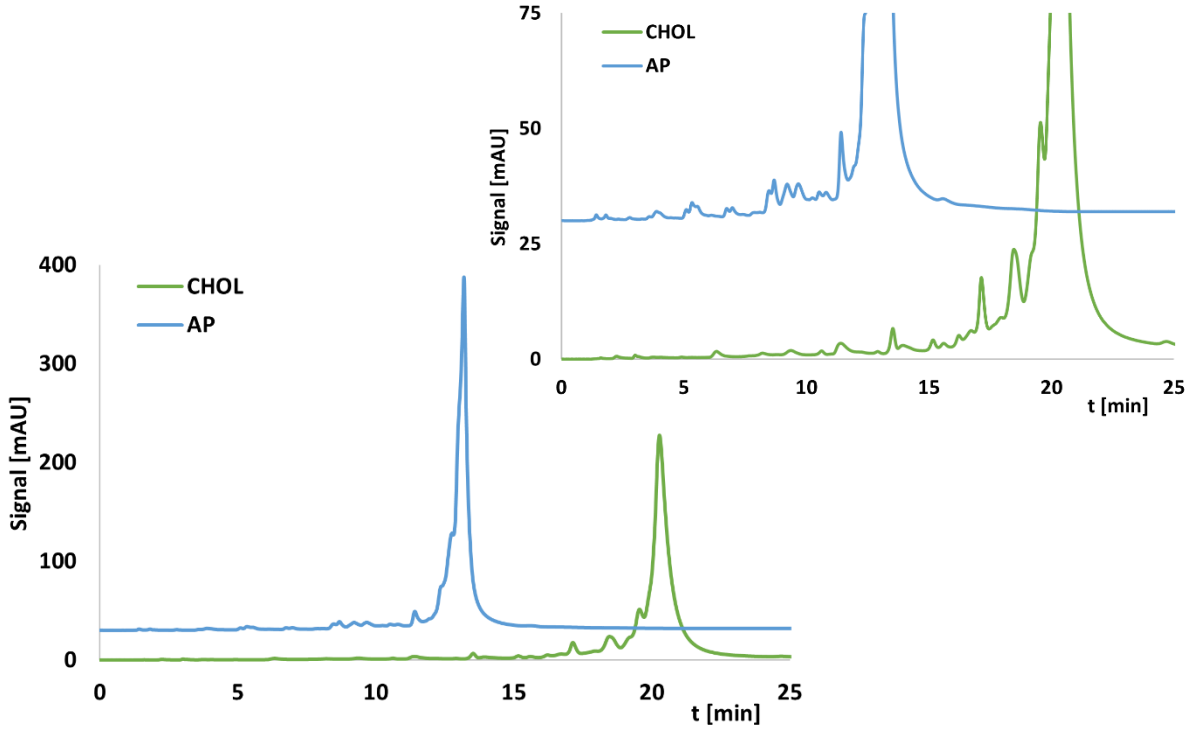

Figure S3. Chromatograms of the separation of the sense strand oligonucleotide and its impurities for two different columns and optimized conditions. Experimental conditions: MPA: 20 mM ammonium formate (pH 6.3), MPB: MeOH/20 mM ammonium formate (pH 6.3) 9:1 (v/v); gradient elution: 20 mM ammonium formate (pH 6.3); column temperature: 40 °C; autosampler temperature 10 °C; flow rate: 0.3 mL/min; injection volume 8 µL; UV detection with λ=254nm.

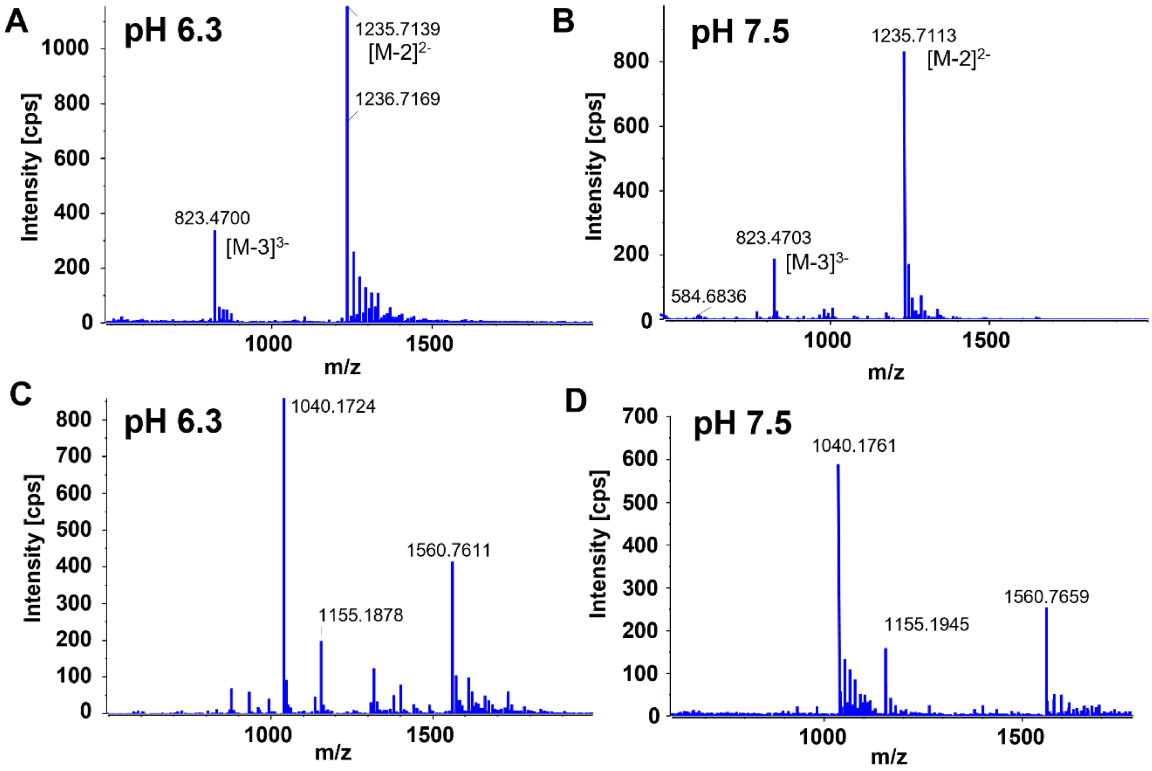

Figure S4. The full scan MS spectra for two impurities 5' N-13 (A, B) and 5' N-11 (C, D) and mobile phases of pH = 6.3 (A, C) and 7.5 (B, D). Experimental conditions: MPA: 20 mM ammonium formate (pH 6.3), MPB: MeOH/20 mM ammonium formate (pH 6.3) 9:1 (v/v); gradient elution: 10-45% MPB in 20 minutes (20 minutes re-equilibration); column temperature: 40°C; autosampler temperature 10°C; flow rate: 0.3 mL/min; injection volume 8µL; Q-TOF-MS conditions: nebulizer gas 90 psi, heater gas 90 psi, curtain gas 35 psi, source temperature 550 °C, ion spray voltage 4500 V, declustering potential -200 V and collision energy -10 V.

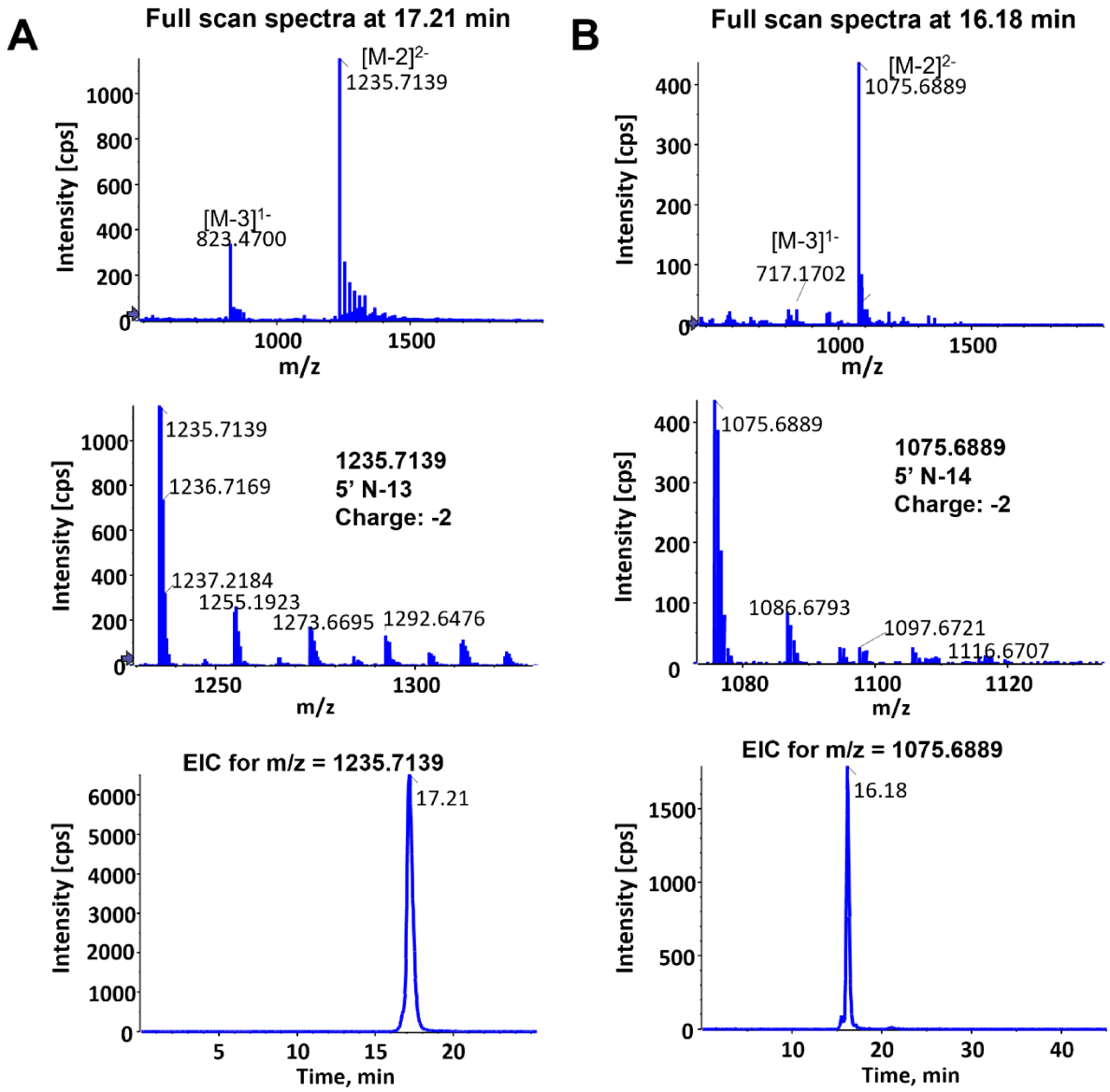

Figure S5. RP-LC-MS spectra and EIC of two selected impurity species from sense strand of Patisiran analogue: A) 5' N-13 at 17.21 min., B) 5' N-14 at 16.18 min. Experimental conditions: column: CHOL; MPA: 20 mM ammonium formate (pH 6.3), MPB: MeOH/20 mM ammonium formate (pH 6.3) 9:1 (v/v); gradient elution: 10-45% MPB in 20 minutes (20 minutes re-equilibration); column temperature: 40 °C; autosampler temperature 10 °C; flow rate: 0.3 mL/min; injection volume 8µL; MS parameters: nebulizer gas 90 psi, heater gas 90 psi, curtain gas 35 psi, source temperature 550 °C, ion spray voltage 4500 V, declustering potential -200 V and collision energy -10 V.

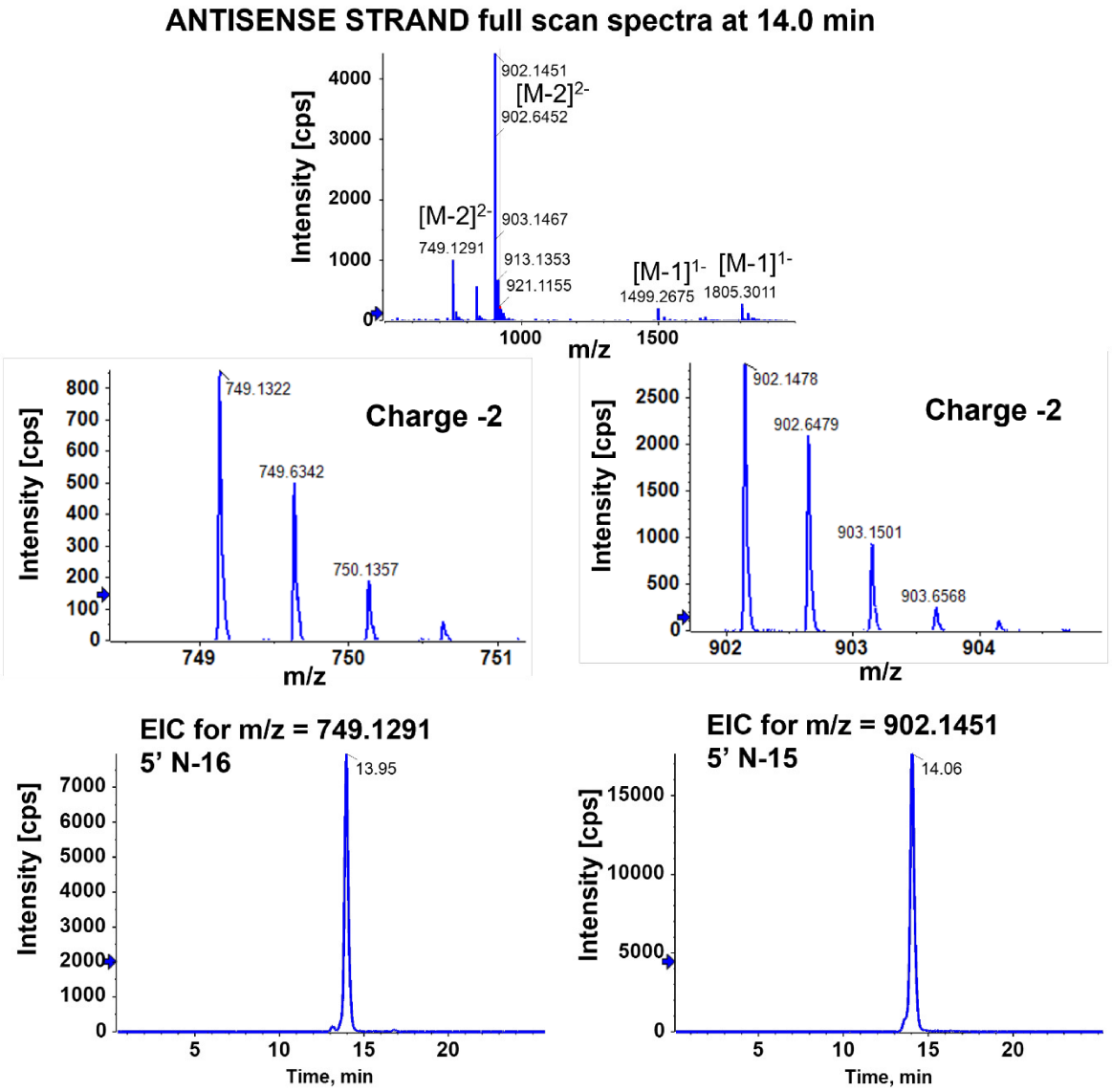

Figure S6. RP-LC-MS spectra and EIC of two selected impurity species from antisense strand of patisiran analogue. Experimental conditions: column: CHOL; MPA: 20 mM ammonium formate (pH 6.3), MPB: MeOH/20 mM ammonium formate (pH 6.3) 9:1 (v/v); gradient elution: 10-45% MPB in 20 minutes (20 minutes re-equilibration); column temperature: 40 °C; autosampler temperature 10 °C; flow rate: 0.3 mL/min; injection volume 8µL; MS parameters: nebulizer gas 90 psi, heater gas 90 psi, curtain gas 35 psi, source temperature 550 °C, ion spray voltage 4500 V, declustering potential -200 V and collision energy -10 V.

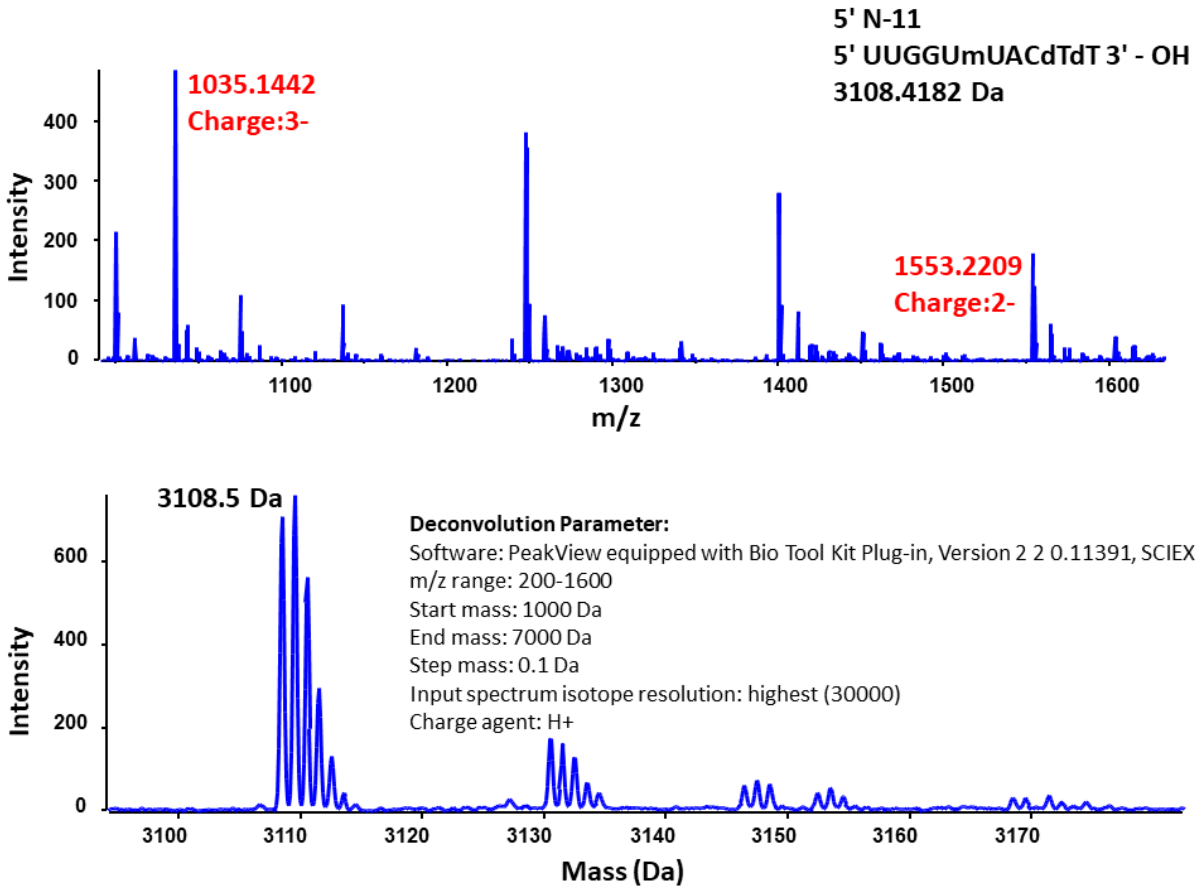

Figure S7. The scheme of deconvolution procedure used during impurities identification.

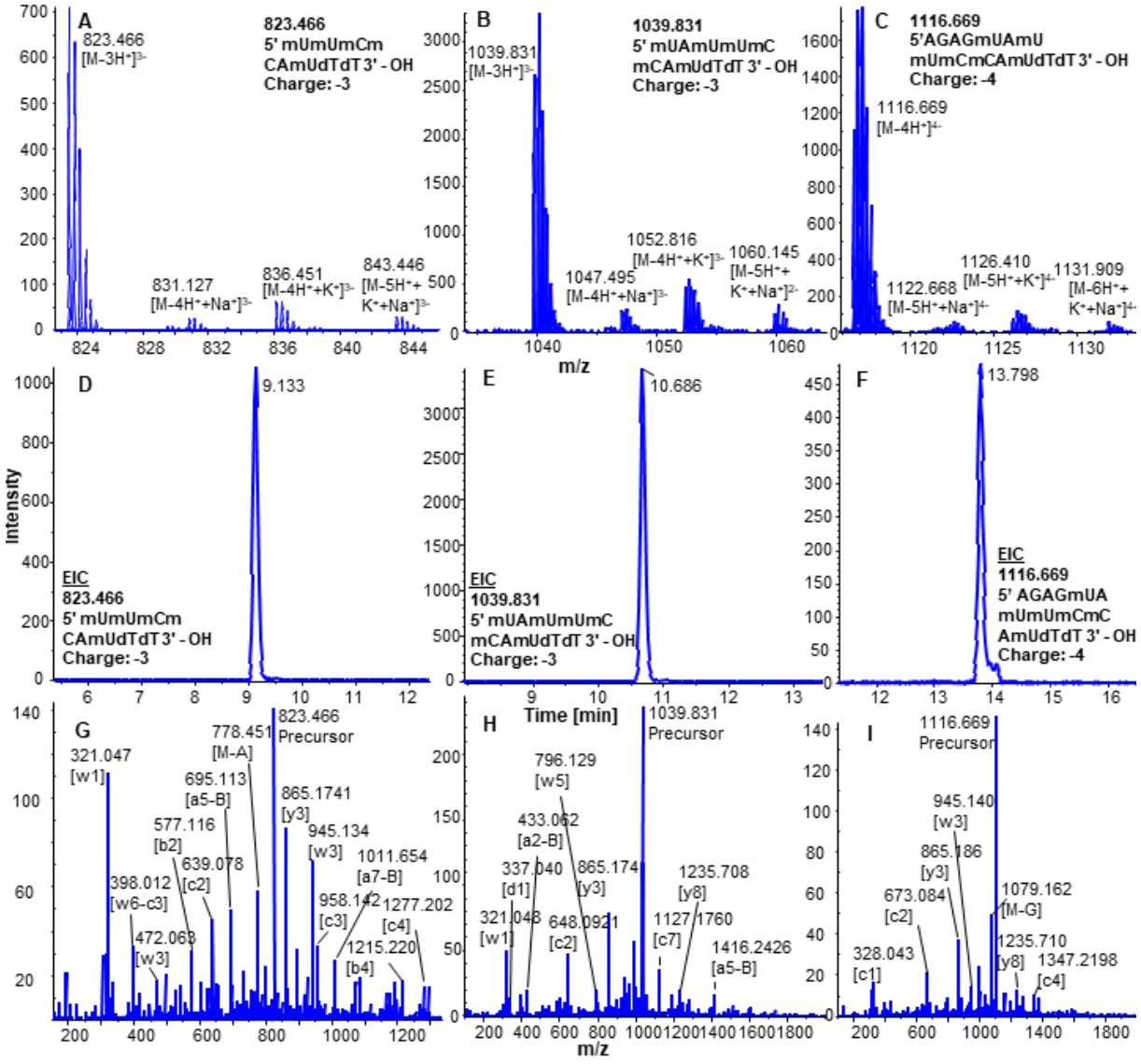

Figure S8. HILIC-LC-MS/MS spectra and extracted ion chromatogram of selected impurity species from sense strand of patisiran analogue. (A-C): MS spectra of impurity species with the most abundant charge states; (D-F): Extracted ion chromatograms of the monoisotopic mass; (G-I): MS^2 spectra of the corresponding precursor ion.

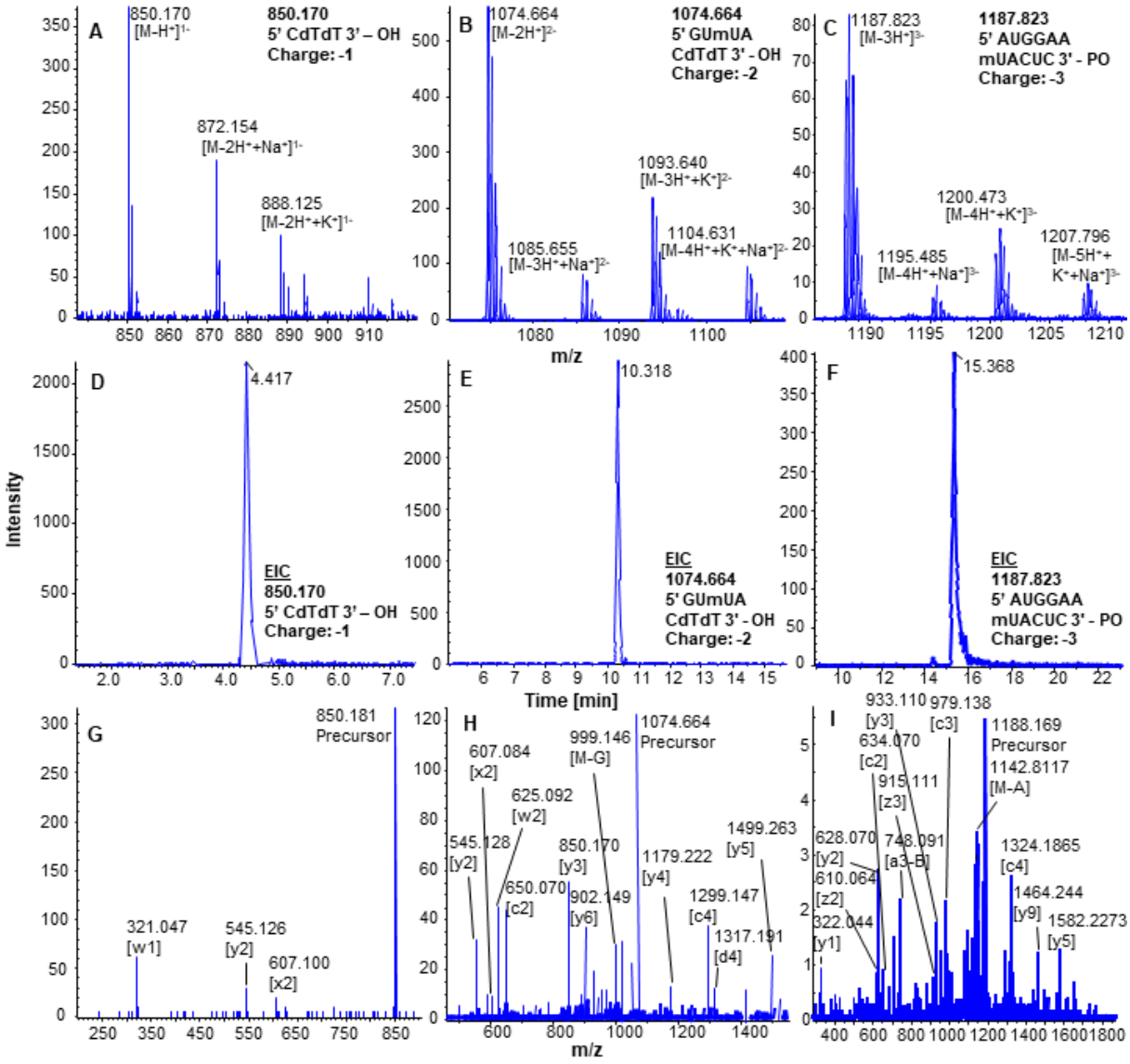

Figure S9. HILIC-LC-MS/MS spectra and extracted ion chromatogram of selected impurity species from antisense strand of patisiran analogue. (A-C): MS spectra of impurity species with the most abundant charge states; (D-F): Extracted ion chromatograms of the monoisotopic mass; (G-I): MS^2 spectra of the corresponding precursor ion.

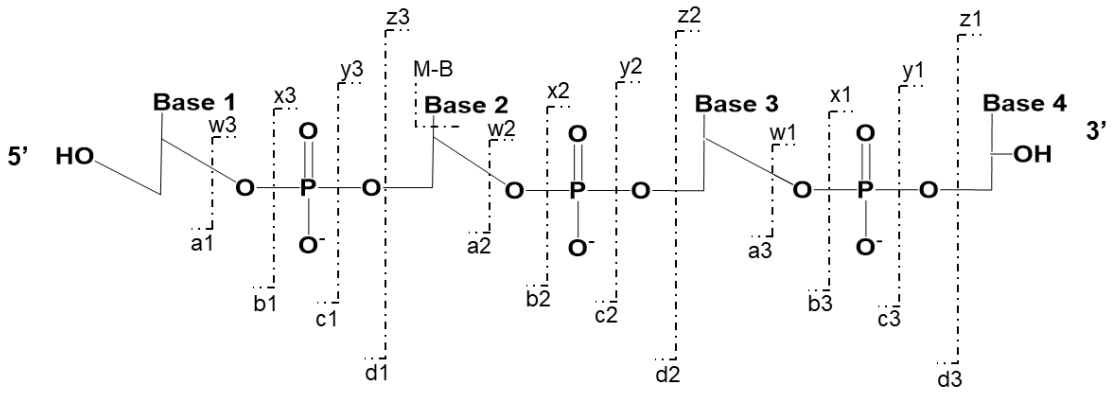

Figure S10. The standard nomenclature for oligonucleotide fragmentation during in mass spectrometry. The numbering of a-B, b, c, d and w, y fragments starts from the 5’ end and 3’ end.

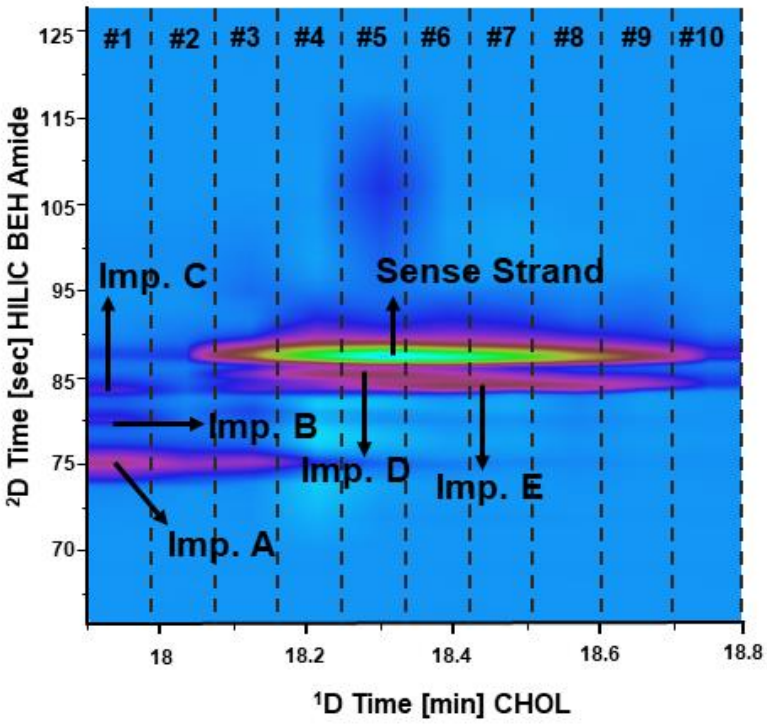

Figure S11. Heat map of the high-resolution sampling 2D-LC of the sense strand with ESI-MS detection.

Table S1. The relative proportion for each impurity sequence determined as peak area and relative peak area for both MS and UV detection and CHOL column (with mobile phase of pH 6.3).

The *m/z* values for most abundant ion	Charge	Impurity	Deconvoluted mass [Da]	Retention time CHOL pH 6.3 [min]	Peak number	MS detection		UV detection	
						Peak area	Relative to main [%]	Peak Area	Relative to main [%]
ANTISENSE STRAND									
652.082	-1	3' N-19as	653.082	8.46	1	12183	8.30	26.8	4.38
979.118	-1	3' N-18as	980.118	8.68	2	1245	0.85	20.5	3.35
850.170	-1	5' N-18as	851.170	10.73	3	5.60E+04	38.19	33.2	5.42
545.130	-1	5' N-19as	546.129	11.15	4	6.54E+04	44.61	32.4	5.29
749.128	-2	5' N-16as	1500.257	13.95	5	44526	30.35	494.3	80.77
835.111	-2	3' N-16as	1672.221	14.03	6	49860	33.99	co-eluted with 5	-
902.141	-2	5' N-15as	1806.282	14.06	7	105901	72.19	co-eluted with 5	-
1074.665	-2	5' N-14as	2151.330	15.62	8	72189	49.21	515.9	84.30
999.632	-2	3' N-15as	2001.264	16.11	9	22658	15.45	2502.2	408.86
1035.139	-3	5' N-11as	3108.418	16.35	10	39532	26.95	co-eluted with 9	-
831.123	-3	5' N-13as	2496.368	16.8	11	18017	12.28	co-eluted with 9	-
1136.819	-3	5' N-10as	3413.459	17.04	12	22041	15.02	co-eluted with 9	-
967.374	-4	3' N-9as	3873.496	17.28	13	1089	0.74	co-eluted with 9	-
1043.630	-4	3' N-8as	4178.519	17.28	14	1191	0.81	co-eluted with 9	-
928.868	-4	5' N-9as	3719.470	17.46	15	358	0.24	co-eluted with 9	-
1005.132	-4	5' N-8as	4024.528	17.46	16	1020	0.70	co-eluted with 9	-
882.455	-3	3' N-13as	2650.364	17.66	17	5200	3.54	co-eluted with 9	-
1187.822	-3	3' N-10as	3566.466	17.94	18	10870	7.41	co-eluted with 9	-
1167.402	-4	5' N-6as	4673.609	18.21	19	2881	1.96	co-eluted with 9	-
984.136	-3	3' N-12as	2955.407	18.41	20	6696	4.56	1005.1	164.23
1129.893	-4	3' N-7as	4523.570	18.7	21	1804	1.23	co-eluted with 20	-
1249.665	-4	5' N-5as	5002.661	18.95	22	5223	3.56	co-eluted with 20	-
1216.152	-4	3' N-6as	4868.606	19.04	23	3009	2.05	co-eluted with 20	-

1580.954	-4	5' N-1as	6327.814	19.16	24	1965	1.34	co-eluted with 20	-
1418.703	-4	5' N-3as	5676.783	19.29	25	8383	5.71	co-eluted with 20	-
1504.96	-4	5' N-2as	6021.828	19.33	26	9110	6.21	co-eluted with main	-
1531.187	-4	3' N-2as	6128.748	19.54	27	417	0.28	co-eluted with main	-
1454.931	-4	3' N-3as	5823.723	19.74	28	612	0.42	co-eluted with main	-
1663.732	-4	**Antisense strand**	6656.866	20.03	29	146700	100.00	7503.4	1226.05
SENSE STRAND									
1011.145	-1	3' N-18s	1012.123	11.77	1	24971	11.67	85.4	6944.67
865.169	-1	5' N-18s	866.169	13.58	2	72256	33.77	166.7	13555.93
1340.212	-1	3' N-17s	1341.212	14.49	3	5581	2.61	29.3	2382.66
915.667	-2	5' N-15s	1833.337	15.12	4	9146	4.27	co-eluted with 3	-
756.134	-2	5' N-16s	1514.268	15.18	5	7261	3.39	co-eluted with 3	-
1075.689	-2	5' N-14 OHs	2153.353	16.18	6	13770	6.44	102.4	8327.10
1115.676	-2	5' N-14 POs	2233.352	16.67	7	1778	0.83	117.4	9546.88
1235.714	-2	5' N-13s	2473.396	17.21	8	57222	26.74	89.8	7302.47
1153.181	-2	3' N-14s	2308.362	17.92	9	22286	10.42	74.9	6090.81
1395.750	-2	5' N-12 (A-mU)	2793.442	18.26	10	1459	0.68	co-eluted with 9	-
933.14	-3	5' N-12s	2802.449	18.65	11	2346	1.10	103.8	8440.94
1039.831	-3	5' N-11s	3122.492	18.79	12	22268	10.41	co-eluted with 11	-
1317.703	-2	3' N-13s	2637.407	18.87	13	10246	4.79	co-eluted with 11	-
1154.857	-3	5' N-10s	3467.530	19.14	14	27656	12.93	137.6	11189.53
1264.544	-3	5' N-9s	3796.590	20.31	15	32423	15.15	357.7	29087.91
1489.237	-3	5' N-7s	4470.688	20.4	16	18238	8.52	261.9	21297.52
1598.928	-3	5' N-6s	4799.718	20.58	17	988	0.46	794.3	64591.91
1103.173	-3	3' N-11s	3311.495	20.62	18	12452	5.82	co-eluted with 17	-
1358.973	-4	5' N-4s	5437.841	20.68	19	18992	8.88	co-eluted with 17	-
1217.849	-3	3' N-10s	3656.547	20.69	20	3450	1.61	co-eluted with 17	-
1603.513	-4	5' N-1s	6416.030	21.08	21	12325	5.76	co-eluted with 17	-
1690.023	-5	**Sense strand**	6761.087	21.8	22	213956	100.00	10316.5	838930.46
1441.236	-4	5' N-3s	5766.896	22.71	23	24133	11.28	1498.4	121848.82

Table S2. The impurities identified with the use of HILIC for sense and antisense strands of patisiran analogue together with the retention times used for orthogonality studies.

ANTISENSE				SENSE			
m/z	**Charge state of most abundant ion**	**Time [min]**	**Name**	***m/z***	**Charge state of most abundant ion**	**Time [min]**	**Name**
545.129	-1	2.696	5' N-19as	865.169	-1	3.082	5' N-18s
850.170	-1	4.424	5' N-18as	865.169	-1	3.31	5' N-18s
652.082	-1	6.266	3' N-19as	865.169	-1	3.704	5' N-18s
979.118	-1	6.37	3' N-18as	756.134	-2	6.73	5' N-16s
749.128	-2	6.888	5' N-16as	915.669	-2	7.969	5' N-15s
902.141	-2	8.41	5' N-15as	505.065	-2	8.045	3' N-18s
1074.665	-2	10.342	5' N-14as	716.784	-3	8.522	5' N-14s
835.110	-2	11.237	3' N-16as	823.466	-3	9.131	5' N-13s
831.126	-3	11.8	5' N-13as	669.593	-2	9.185	3' N-17s
999.632	-2	11.986	3' N-15as	930.147	-3	9.868	5' N-12s (mU-A)
882.455	-3	12.961	3' N-13as	933.150	-3	10.037	5' N-12s
1035.139	-3	13.481	5' N-11as	1039.831	-3	10.684	5' N-11s
984.136	-3	13.867	3' N-12as	1115.666	-2	10.839	5' N-14 POs
1136.820	-3	14.349	5' N-10as	1153.174	-2	11.621	3' N-14s
928.868	-4	14.958	5' N-9as	865.882	-4	12.005	5' N-10s
1187.822	-3	15.334	3' N-10as	878.131	-3	12.201	3' N-13s
1005.132	-4	15.66	5' N-8as	1264.53	-3	12.47	5' N-9s
967.374	-4	15.937	3' N-9as	1264.53	-3	12.8	5' N-9 (isomer)s
1167.403	-4	16.038	5' N-6as	1102.832	-3	13.669	3' N-11s
1249.665	-4	16.297	5' N-5as	1116.672	-4	13.796	5' N-7s
1043.630	-4	16.543	3' N-8as	1198.930	-4	14.117	5' N-6s

1418.196	-4	17.119	5' N-3as	1217.849	-3	14.53	3' N-10s
1129.893	-4	17.119	3' N-7as	1358.460	-4	14.737	5' N-4s
1216.152	-4	17.63	3' N-6as	1440.724	-4	14.945	5' N-3s
1504.457	-4	17.729	5' N-2as	1602.991	-4	15.375	5' N-1s
1580.954	-4	17.94	5' N-1as	1351.206	-5	15.898	Sense
1108.478	-6	18.009	Antisense				
1454.931	-4	18.198	3' N-3as				
1531.187	-4	18.609	3' N-2as				

6. Publication VI (Manuscript Only)

Two-dimensional reversed phase liquid chromatography of synthetic phosphorothioate oligonucleotides

Feiyang Li[a] , Cornelius Knappe[a], Enrico Favorat[a], Niklas Carstensen[a] Mimi Gao[b], Wiebke Holkenjans[b], Reinhard Pell[b], Michael Lämmerhofer*

[a, *]Institute of Pharmaceutical Sciences, Pharmaceutical (Bio-)Analysis, University of Tübingen, Auf der Morgenstelle 8, 72076 Tübingen, Germany

[b] Bayer AG, Research Center Aprath, Aprather Weg 18a, 42113 Wuppertal, Germany

*Author for correspondence:

Prof. Dr. Michael Lämmerhofer

Pharmaceutical (Bio-)Analysis

Institute of Pharmaceutical Sciences

University of Tübingen

Auf der Morgenstelle 8

72076 Tübingen, Germany

T +49 7071 29 78793, F +49 7071 29 4565

E-mail: michael.laemmerhofer@uni-tuebingen.de

Year 2023

Abstract

In recent years, many nucleic acid-based pharmaceuticals have been approved and entered the market, and even a larger number are in late stage clinical trials. Conventional oligonucleotides are facing issues in vivo like fast renal clearance and nuclease degradation. Therefore, to increase their stability, phosphorothioation is a frequent modification of therapeutic oligonucleotides (ONs) which also leads to improved binding affinity facilitating cell internalization and intracellular distribution. At the same time, by replacing a phosphodiester linkage with a phosphorothioate group, a phosphorous stereogenic center is generated which causes the formation of R_p- and S_p-diastereomers. It increases the structural diversity. For example, with 15 of those phosphorothioate (PS) linkages, 32,768 different diastereomers are expected. Since the phosphorothioate is introduced non-stereoselectively, the molecular complexity of the resultant phosphorothioate ON products is tremendously increased impeding the chromatographic separation in the course of quality control. Since distinct phosphorothioate diastereomers have different bioactivities and pharmacological properties, there is increasing interest in implications of stereoisomerism of phosphorothiate oligonucleotides. From a quality and regulatory viewpoint, batch-to-batch reproducibility of the diastereomer profile may be of concern. To address such a scientific question, in this study we investigated the stereoselectivity of LC methods for two phosphorothioate oligonucleotide (PSO) compounds differing in their molecular size and numbers of PS linkages. On the one hand, the diastereoselectivity of ion-pairing reversed-phase liquid chromatography (IP-RP LC), RPLC without ion-pairing agents and LC with chiral column based on polysaccharide chiral stationary phase were evaluated for model PSOs and an active pharmaceutical ingredient (API) of PSO with trivalent *N*-acetylgalactosamine (GalNAc) conjugate. Due to the structural complexity of PSOs, the separation power for the diastereomer mixture was increased

by using sequential selective comprehensive two-dimensional chromatography with an amylose tris(α-methylbenzylcarbamate)-immobilized chiral stationary phase (CSP) in the first dimension and ion-pair RPLC with ethylammonium acetate in the second dimension to achieve maximal diastereomer selectivity and a larger number of peaks separated.

Keywords

Phosphorothioate oligonucleotides, diastereomer separation, two-dimensional liquid chromatography, chiral stationary phase, amylose tris(α-methylbenzylcarbamate)

1 Introduction

Synthetic oligonucleotides (ONs), comprising antisense oligonucleotide (ASO) and small interfering RNA (siRNA), represent an emerging field of biopharmaceuticals to treat human diseases [1,2]. To improve the pharmacokinetic, pharmacodynamic and biodistribution properties of ONs, structural modifications of oligonucleotide base, sugar moieties and internucleotide linkages are commonly incorporated in therapeutic ONs [3]. To date, the phosphorothioation is the most common chemical modification of ONs. In the case of phosphorothioate oligonucleotides (PSO), one of the non-bridging oxygen atoms of the phosphate diester linkage is replaced by sulfur [4]. At the same time, this phosphorothioate (PS) linkage leads to a new stereogenic center at the phosphorous atom, having either Rp or Sp-configuration, resulting in 2^n diastereomers, with n being the number of PS linkages [5]. Theoretically, the proper Rp/Sp-design might lead to improved efficacy, lower toxicity, and enhanced delivery of PSOs [6,7]. An advantage of PS ASOs compared to PO ASOs is the strongly enhanced protein binding affinity, thereby facilitating ASO cell internalization and intracellular distribution [1]. Although certain synthesis parameters like activator used, nucleotide

getting coupled, and sequence dependency might impact the Rp/Sp ratio , in any case a complex mixture of diastereomers is usually obtained [8,9]. This circumstance will become a significant challenge when it comes to the chromatographic separation and analytical quality control of those oligonucleotide therapeutics. Not only from regulatory perspective, but also to ensure sufficient efficacy for the patient, a reproducible diastereomer profile during the synthesis is crucial [10]. It might be anticipated that stereoisomerically pure PSOs, i.e. single stereoisomers free of other diastereomers, are of advantage in this respect. However, they may also reveal weaknesses regarding bioactivity or bioavailability inside the human body: pure Rp-isomers of PSOs exhibit better binding affinity to their target, but show reduced nuclease stability [11]. Vice versa, fully-Sp configured PSOs are more resistant against nuclease degradation, yet reveal declined target affinity. Therefore, it is not straightforward to decide on a favorable PSO stereoisomer configuration for a stereoisomerically pure PSO therapeutics with optimal pharmacological properties [12]. To elucidate the role of stereochemistry of PSOs, efficient PSO diastereomer separation techniques are needed. Until today, numerous studies related to PSO LC separation have been published [13–19]. However, the majority of these reports do not aim at diastereomer separations of the PSOs, but their retention behavior and selectivity towards oligonucleotide impurities (desulfurization products with phosphate diester linkages and shortmer impurities). When it comes to the LC separation of these diastereomers, ion pairing reversed phase (IP-RP) chromatography and anion-exchange (AX) chromatography are still the dominating methods. *Wu et al.* used strong-anion exchange stationary phases based on monolith and polymer materials for the analysis of aptamer RNAs having incorporated two PS linkages [20]. Using elution conditions with chaotropic sodium perchlorate ($NaClO_4$) in the mobile phase, all four diastereomers were decently separated [20]. *Roussis et al.* used an RP-AX mixed-

mode stationary phase to investigate a 20-base DNA strand all with PS linkages. Despite the high number of chiral centres, only a slight diastereomeric selectivity was observed [21]. Besides of AX, the potential of IP-RP was thoroughly investigated for PSO diastereomer separations considering factors like temperature, buffer concentration or choice of the ion pair agent. *Kadlecová et al.* used conventional C18 phase for a diastereomeric separation of a 21-base DNA strand with 20 PS linkages. It was obvious that the diastereoselectivity is significantly suppressed with increasing temperature [22]. *Enmark et al.* systematically investigated factors influencing the separation of diastereomers of PSO under IP-RP conditions using triethylammonium acetate (TEAA). For a pentamer of deoxythymidine monophosphate with 2 PS linkages, the selectivity increased with decreased ion-pair concentration [23]. In another study, the same group used a fully phosphorothioated 16-mer deoxythymidine oligonucleotide as sample for further IP-RP experiments. When using more hydrophobic IP reagents like tributylamine, the diastereoselectivity was suppressed [24]. Besides, other techniques for the separation of the diastereomers were proposed as well. *Demelenne et al.* coupled hydrophilic interaction liquid chromatography (HILIC) to drift tube ion mobility spectrometry (DTIMS) to separate the diastereomers of a 5-base oligonucleotide with three PS linkages which was successful [11]. HILIC was used to characterize diastereomers of ASOs which were partly modified with PS linkages [25,26]. *Gilar et al.* evaluated capillary electrophoresis (CE) with polymer solutions as pseudostationary phase to separate DNA diastereomers [27].

In our study, liquid chromatographic methods have been optimized for maximal diastereoselectivity. On the one hand, nine short hexanucleotide PSOs (6-mers) with identical base sequence containing different number of PS linkages were employed as test substances (in **Figure 1**, the structure of one of the 6-mers is representatively illustrated; details about the other PSOs can be found in **Table 1)**.Additionally, a

phosphorothioate oligonucleotide-based active pharmaceutical ingredient (API) with 13 PS linkages conjugated with a trivalent *N*-acetylgalactosamine (GalNAc) residue was investigated as well in similar manner. Key factors affecting diastereoselectivity such as ion-pair hydrophobicity and concentration as well as column temperature were evaluated and optimized to achieve a maximal number of separated peaks. A complete separation of individual diastereomers by IP-RPLC is typically limited to PSOs that contain a low number of PS linkages (usually no more than three) [28]. Consequently, one-dimensional LC (1D-LC) is incapable of separating a large number of distinct diastereomers due to insufficient selectivity and limited peak capacity [14,29]. For this reason, two-dimensional LC (2D-LC) was considered as a more powerful tool enabling efficient separation of PSOs through higher peak capacity and combination of diastereoselectivities from two distinct LC dimensions. The enhanced separation capability of 2D-LC has been well reported for synthetic ONs [30–36]. Mostly, oligonucleotides with phosphodiester linkage were the target analytes. Only a few studies addressed the 2D-LC application for PSOs as samples. *Zhang et al.* combined IP-RP with HILIC to investigate 16-mer ASO with PS linkages concentrating on enhanced resolution of impurity species like shortmers, but not diastereomer separations [37]. In contrast, 2D-LC approaches targeting specifically the improvement of diastereomer separations for PSOs have not been reported yet. In this study, the goal was to elucidate the resolving power of above PSO diastereomers by the combination of RP-LC using a C18-based stationary phase with RP-LC using a polysaccharide-based chiral stationary phase in a sequential selective comprehensive 2D-LC (Seq-sLCxLC) setup. Seq-sLCxLC is a new form of comprehensive 2D-LC based on fully automated multiple selective comprehensive 2D-LC runs that can be reconstituted into a full comprehensive 2D-LC chromatogram for a specific region of the ^{1}D chromatogram but with extended coverage of the ^{1}D retention space than in

common selective comprehensive 2D-LC. Partially separated diastereomers from the ^{1}D were transferred into the second dimension to accomplish further resolution by the complementary retention principle-. With this novel approach using Seq-sLCxLC, a significantly higher stereoisomer separation power compared to conventional 1D-liquid chromatography can be expected.

2 Experimental

2.1 Chemicals

Acetic acid (AcOH) (ACS reagent, ≥ 99.8%), methylamine (MA) (40% in H_2O), ethylamine (EA) (66.0-72.0% in H_2O), propylamine (PA) (≥ 99%), diethylamine (EA) (≥ 99.5%), triethylamine (TEA) (≥ 99%), tripropylamine (TPA) (≥ 98%), ammonium hydroxide solution (NH_4OH) (28-30% NH_3 basis), ammonium acetate (AA) (HPLC grade) and methanol (MeOH) (HPLC grade) were purchased from Sigma-Aldrich (Merck, Munich, Germany). Acetonitrile (ACN) (HPLC grade) was obtained from Honeywell (Munich, Germany). Ultrapure water was obtained by purifying deionized water with an Elga PurLab Ultra purification system (Celle, Germany).

2.2 PSO Samples

The PSO model molecules (PSO-A, PSO-B, PSO-C, PSO-D, PSO-E, PSO-F, PSO-G, PSO-H, PSO-I) were synthesized by Oligo Sigma (Merck, Munich, Germany) and purchased as desalted raw products. The model PSO molecules A-I have identical base sequence. With PSO-A defined as original strand, it contains six DNA-based nucleotides with five PS linkages consisting of 32 potential diastereomers. Further, strands B-I carry less PS linkages in comparison to A. The replacement of PS by PO linkages took place from both 5’ – and 3’ end (see **Table 1**). The API was obtained by

Bayer AG (Wuppertal, Germany) which represents a 20mer Gapmer-based PSO containing 13 PS linkages leading to 8,192 potential diastereomers. Model molecules were stored at -20 °C as 100 mM aqueous solution. API was stored at -20 °C as lyophilisate. For LC experiments, the API solid was dissolved in water with a final concentration of 1 mg/mL.

2.3 Instruments

All one-dimensional LC experiments were performed with an Agilent 1290 Infinity II UHPLC system from Agilent Technologies (Waldbronn, Germany) equipped with Multisampler (G4226A), binary Pump (G4220A), column compartment (G1316C) and Diode Array Detector (DAD) (G4212A) with 1 µL flow cell (G4212-60008). Furthermore, both column compartment and multisampler were equipped with the Ultra-Low Dispersion Kit (5067-5963).

The 2D-LC experiments were carried out on the Agilent 1290 Infinity II 2D-LC Solution from Agilent Technologies including a binary High-Speed pump (G7120A), Multisampler (G7167B) and a Diode Array Detector (DAD) (G7117B) with 1 µL flow cell (G4212-60008) and a pressure relief valve (pressure release kit, G4236-600010) between the DAD and 2D-interface in the first dimension. In the second dimension, another binary High-Speed Pump and DAD of the identical type as in the ^{1}D were employed. Two separate Infinity column compartments (G7116B) were used for ^{1}D and ^{2}D. Both LC dimensions were connected by a valve drive (G1170A) equipped with 5-position/10-port 2D-LC active solvent modulation (ASM) valve (#5067-4266) coupled to two 6-position/14-port valve heads (#5067-4142, multiple heart-cutting valves) equipped with six 40 µL loops each. The ASM valve contained the ASM capillary of dimension 85 ×0.12 mm (0.96 µL, #5500-1300) (ASM factor 5, split ratio loop:ASM). The 2D-LC system was controlled by Agilent OpenLab CDS ChemStation Rev.

C.01.10 with 2D-LC add-on software. The contour plot resulting from the sequential selective comprehensive 2D-LC experiments were created by a self-developed script. This is described in chapter 2.6 under *Data processing*.

2.4 Mobile phase preparation

For all experiments, ion-pairing (IP) reagents were dissolved in water. Subsequently, the ${}^{w}_{w}pH$ values were adjusted to 9 by AcOH [38]. Finally, the aqueous solutions were 1:1 diluted by either ACN or MeOH. For AA solutions, buffer salts were dissolved in water. Afterwards, the ${}^{w}_{w}pH$ values were adjusted to 9 by NH_4OH. The aqueous solutions were eventually diluted by ACN or MeOH. For more details, see **Table 2**.

2.5 LC methods

An overview of all used LC methods can be found in **Table 3** and **Table 4**.

2.6 Data processing for sequential selective comprehensive 2D-LC

The reading, processing and plotting of the data were based on Python and Scipy in combination with Jupyter. The Jupyter notebooks are shown in the supplementary materials as PDF appendices. Signal data was converted and exported by GC Image and then imported into Pandas data frames. Cut times can be extracted by GC Image or “cuts.xml” files, which are stored in the data folder of the measurement. Both types of data are sorted via Pandas and Numpy. And finally, Matplotlib is used to plot and illustrate the data. This is step by step shown in the Jupyter Notebooks.

3 Results and Discussion

3.1 1D-LC-UV column screening experiments

In preliminary experiments (results not shown in this study), IP-RPLC (with BEH C18 column) [39], HILIC (with BEH Amide) [25,26], mixed-mode RP/WAX (with an in-house synthesized stationary phase) [32] and a number of chiral stationary phases (quinine carbamate and polysaccharide based) [30] were evaluated. For a better overview of those preliminary test columns, please see **Table 5**. Orthogonality evaluation of diastereoselectivity of two complementary chromatographic systems by 2D-LC was considered a method of first choice. From these scouting experiments, ion-pair RPLC and RP by polysaccharide-based column emerged as the most promising chromatographic modes.

3.1.1. Diastereoselectivity of BEH C18

In order to better understand how chromatographic parameters are affecting the diastereoselectivity under IP-RP conditions (using BEH C18, 130 Å, 1.7 µm), various series of 1D-LC-UV optimization experiments were conducted. The general LC conditions are summarized in **Table 3** (for all 1D experiments) and **Table 4** (for all 2D experiments). In particular, a MeOH gradient using a C18 column was carried out employing different type and concentration of IPs. For the model molecules, 25 °C and 60 °C as column temperatures were investigated for all experiments. In the case of API, a detailed temperature series (10-60 °C) was performed for all screening experiments.

Standard molecules PSO A-I

A series of hydrophilic IPs (ammonium acetate AA, methylammonium acetate AA, and ethylammonium acetate EAA) and IPs with intermediate lipophilicity (propylammonium acetate PAA, diethylammonium acetate DEAA, triethylammonium acetate TEAA, tripropylammonium acetate TPAA) were tested (all used IPs are listed in **Table 2**). The number of separated peaks served as a response factor for the optimization, whereby a clear shoulder was already counted as a separated peak. **Table S1** gives the number of separated peaks for the distinct ion-pairs for PSO-A (6-mer with 5 PS linkages which consists of a mixture of 32 diastereomers). A maximum of 14 peaks could be detected for the PSO-A with 20 mM ethylammonium acetate EAA at 60°C column temperature (14 out of 32 separated).

To study the effect of the number of phosphorothioate groups and their position, this model hexamer PSO-A was selected and a series of oxidation products in which 1-4 P=S group(s) were oxidized to P=O group(s) from either 3'-end PSO-B to PSO-E or 5'-end PSO-F to PSO-I (**Table 1**). For better illustration of the IP agent effects on the diastereomer separations of these phosphorothioates, a diastereomer coverage factor DCF (in %) was calculated as the ratio of diastereomer peaks separated and the total possible diastereomers in the respective PSO (2^n, whereby n is the number of PS linkages).

The results for the different IPs and PSOs are depicted in form of heat maps in **Figure 2A** for the column temperature of 60°C and in **Figure 2B** for 25°C. A diastereomer coverage of 100% means all diastereomers are separated, or more precisely, the number of peaks separated (including those with a shoulder) equals the theoretical number of diastereomers expected (**Figure 2**). It is obvious that the usage of TPAA caused very strong/total suppression of diastereoselectivity (**Figure 2A**). It was already previously reported that hydrophobic IPs, like tributylamine suppress

diastereoselectivity [23], while less hydrophobic IPs reveal superior selectivity [40]. Hydrophilic ion-pairs are less adsorbed to the C18 stationary phase and therefore PSOs can be eluted with less organic modifier. Under such conditions, hydrophobic interactions of the sulfur from the phosphorothioate bond with the alkyl strands of the RP18 phase are not supressed by the mobile phase due to its low organic solvent content. Due to overall distinct configurations of corresponding diastereomers resulting in different strength of C18/P=S interactions can lead to diastereoselectivity. This trend was confirmed in our study for the PSO A-I analytes (**Figure 2A**). The highest diastereomer coverage of PSO-A with its 5 phosphorothioate groups (32 possible diastereomers) was achieved with 20 mM EAA (approx. 44%). PSO-B and PSO-F, the phosphorothioates with 4 phosphorous stereogenic centers, were also best separated with EAA, especially at 100 mM (**Figure 2A**). **Figure 3** shows representative chromatograms of PSO-A and its oxidation product series with EAA as IP agent (the same series for AA as IP agent is illustrated on **Figure S1**). Up to 3 PS groups all, or almost all, stereoisomers can be resolved. With more PS groups the peak capacity and/or diastereoselectivity is insufficient to achieve a complete baseline separation and the diastereomer coverage drops quickly to about 30-40%. Another observation worth mentioning is the dependence of the diastereoselectivity on the PS position at the 3' or 5'-end. Comparing PSO-B (one PS linkage removed from 3' end) and PSO-F (one PS removed from 5' end), the diastereoselectivity was better under almost all conditions for PSO-B than for PSO-F, and a similar trend was observed for the corresponding PSOs with 2 P=S groups exchanged for P=O at either 3'-end (PSO-C) or 5'-end (PSO-G) as well as 3 P=S groups oxidized (PSO-D at 3'-end and PSO-H at 5'-end) (**Figure 2**).

It has been reported that column temperature also plays a significant role in PSO diastereomer separations under IP-RPLC conditions. According to literature reports,

lower column temperatures seem to be beneficial and lead to an increase of the diastereoselectivity [22]. For this purpose, relevant chromatographic attributeslike retention factor *k,* selectivity α (which is equivalent to diastereoselectivity) and resolution *Rs* have been calculated for PSO-D, PSO-E, PSO-H and PSO-I under chosen screening conditions (**Table S2**). For these PSOs, a low number of diastereomers are expected (four for PSO-D/H, two for PSO-H/I) allowing calculation of these chromatographic parameters. As shown in **Table S2**, α was not significantly increased at lower column temperature. On contrary, α even slightly declined in comparison to a column temperature of 60 °C. On the other hand, the resolution *Rs* between adjacent diastereomer peaks was overall improved at 25 °C due to extended retention time. **Figure 2B** shows another heat map generated for the results of all screening experiments under 25 °C instead of 60 °C. For PSO-C, -D, -E, -H and -I, the difference is marginal due to the high (mostly 100%) diastereomer coverage of these molecules containing low numbers of PS linkages. But for PSO-A, -B, -F and -G, it is obvious that the lower column temperature (25 °C) did not lead to better resolution. At 25°C, the number of diastereomers resolved is typically lower (**Figure 2B** and **Table S1**). The diastereomer coverage factor of these test standards decreased as visualized by “colder” colorization of the heat maps (**Figure 2A, 2B**). It has to be mentioned that the cited temperature study by *Gilar et al.* [22] was carried out by using larger test oligonucleotide strands (21-mer) which may behave differently. Indeed, in case of our experiments with the API (20-mer), the identical behaviour could be observed which will be discussed in the next subchapter.

In summary, the setup of 25 °C as column temperature and the usage of 20 mM EAA as IP turned out to be the best condition for PSO-A as the original test strand leading to 14 of 32 separated diastereomers. For the other test strands, the effect of the column

temperature is similar. The trend that an elevated column temperature is favourable for better separation of diastereomers, as reported in the literature, cannot be confirmed for the investigated test molecules. For PSO-F, PSO-G, PSO-H and PSO-I where the oxidation of the sulfur occurred from the 5' end, 100 mM instead of 20 mM IP provided better resolution power.

Authentic API sample

Therapeutically relevant phosphorothioates are typically larger than the 6-mer PSO model analyte. Herein, a 20-mer with 13 PS groups and a 5'-terminal GalNAc residue was investigated. The chromatographic results achieved for this API with the distinct IP reagents and at different column temperatures are summarized in form of a heat map in **Figure 4**. Four conclusions can be derived from this heat map: i) The diastereomer separation achieved poorly, i.e. only 5 of 8192 possible diastereomers could be separated to some degree. ii) With regard to the effect of hydrophobicity of the IPs, similar trends as for the PSOs were observed. However, the best result was achieved with the most hydrophilic ammonium ion (AA) (instead of ethylammonium ion, EAA for PSO-A) and with increasing lipophilicity the diastereomer coverage further declined, i.e. even less diastereomer peaks separated. iii) In all cases, the higher IP concentration (100 mM) yielded the better separations than low concentration (20 mM). A similar trend was described by *Gilar et al.* for 21-mer PSOs [22]. For longer PSOs, higher buffer concentrations provide better potential to achieve improved diastereoselectivity. iv) As mentioned above, column temperature has a significant impact on the diastereoselectivity. For this API, lower column temperature is necessary to generate diastereoselectivity at all (**Figure 4**). At 10 °C, the negative effect of highly hydrophobic IP reagents could even be partly compensated as shown by 100 mM

DEAA (**Figure 4**). With decreasing temperature, the resolution gradually becomes better (**Figure S2**, **Table S1**).

Effect of pore size

For biomolecules like nucleic acids and proteins with large hydrodynamic radius, stationary phases with bigger pore size provide better diffusion into the pores and hence higher efficiency. Therefore, the best run from the screening experiments was repeated on the same type of stationary phase (BEH C18) with 300 Å instead of 130 Å pore size using 20 mM AA at 10 °C (see **Table 3, Method C**). The chromatograms are illustrated in **Figure S3**. Due to enhanced diffusion of the analytes into the pores, the resolution was slightly improved with the wide pore material, but the effect was not ground-breaking for which reason the 130 Å column was further used

Effect of column length

In a few further 1D-LC experiments, the best conditions of the (IP-)RPLC method on BEH C18 for both API and PSO-A were transferred to a longer column (100 mm instead of 50 mm length) providing higher peak capacity improved separation power (although it was demonstrated recently that for most linear gradient separations of oligonucleotides a column length between 5 and 35 mm may be appropriate [41]). The gradient time has been extended (see **Table 3, Method B**). The results for both analytes are illustrated in **Figure S4**. For API (**Figure S4A and S4B**), the resolution between the separated peaks has been slightly increased, but in general, the total number of separated diastereomer peaks was unchanged (5 of 8192). In the case of PSO-A (**Figure S4C and S4D**), 19 of 32 possible diastereomers were separated using the longer 10 cm column instead of 14 with the shorter 5 cm long column. In other

words, the diastereomer coverage rate for PSO-A could be increased to 59% with the longer 10 cm column instead of 44% with the short 5 cm column. Nonetheless, it is evident that the limitation of 1D-LC has been reached for PSOs with four or five PS linkages [14,29]. Simple 1D-LC is not able to deliver higher diastereomer coverage factors for API and PSO-A. Consequently, the application of 2D-LC was envisioned to be advantageous.

3.1.2. Diastereoselectivity of polysaccharide-based stationary phase

Polysaccharide-based chiral stationary phases (CSPs) have been developed for HPLC enantiomer separation. Although this is their dedicated application, they may be valuable orthogonal stationary phases in other chromatographic LC separations including phosphorothioate oligonucleotide diastereomer separations. Polysaccharide CSPs are either based on cellulose or amylose derivatives which are coated or immobilized on wide pore silica. The polysaccharide backbones are derivatized to aryl ester, arylcarbamate or aralkylcarbamate derivatives at their 2, 3, and 6 hydroxyl groups. This offers a wealth of interaction sites (H-donor and H-acceptors for H-bonding, dipoles for dipole-dipole interactions, aromatic moieties for hydrophobic and π-π-interactions). Pending perpendicularly from the polysaccharide backbone, the aromatic residues are forming cavities for stereoselective analyte insertion. For accommodating a large oligonucleotide, these cavities appear too small and it can be assumed that only parts of the PSO would be inserted (e.g. bases, phosphorothioate loops). In general, it can be envisioned that this binding into the chiral cavities or onto the chiral polysaccharide derivatives may promote diastereoselectively which makes these stationary phases a promising tool for PSO diastereomer separations as then indicated by the preliminary screening test described above.

Herein, Chiralpak IH-U with an immobilized amylose tris[(S)-α-methylbenzylcarbamate] bonding chemistry (see suppl. **Figure S5**) based on 1.6 µm fully porous silica particles was selected as column for PSO diastereomer separations. It can be employed under typical reversed phase conditions. After a preliminary evaluation of some distinct elution conditions, ammonium acetate was finally selected as additive to aqueous-organic eluents with acetonitrile as organic modifier. The chromatographic separation of the PSO-A model diastereomer mixture is shown in **Figure 5A** in comparison to the IP-RPLC separation on BEH C18 with ethylammonium acetate in **Figure 5B**. It can be seen that a large number of diastereomer peaks can be obtained with the chiral column. The diastereomer coverage with the IH-U column under these conditions was about 44% (in comparison to 53% by above IP-RPLC method). Unfortunately, orthogonality of the diastereomer separation by IP-RPLC with BEH C18 cannot be assessed as all diastereomer peaks have the same mass precluding MS detection for peak assignment between the two runs and individual diastereomer standards were not available.

3.2 Sequential selective comprehensive 2D-LC experiments

2D-LC was considered a viable option not only to increase the number of separated diastereomers, but also to assess retention orthogonality [42] of the stereoisomers on the two chromatographic systems, IH-U and IP-RPLC. The 2D-LC arrangement maintains the correlation between the retentions in the two columns. A challenge in 2D-LC is to maintain the same peak capacity in the ^{2}D LC separation as achieved by a 1D-LC separation on the same column. For full comprehensive 2D-LC, column length and run times need to be kept short, to allow a comprehensive transfer of all fractions from the ^{1}D. Peak capacity (calculated just for the single column) may be compromised

for such fast separations. On the other hand, the current separation is also not a typical multiple heart cutting application. All peaks elute in a relatively narrow elution window, yet it is also not possible to cover the entire ^{1}D elution window of the diastereomers by a single selective comprehensive 2D-LC run with the 2 available loop decks with 10 loops for sample storage. For this reason, another 2D-LC modality was selected which we call sequential selective comprehensive 2D-LC. In this 2D-LC mode, multiple selective comprehensive 2D-LC runs are performed subsequently in an analytical batch. It allows an extended elution window of the ^{1}D to be sampled into the ^{2}D without making compromises in terms of ^{2}D run time, peak capacity (of this ^{2}D) and resolution. In this study, the IH-U column was selected in the ^{1}D and BEH C18 in the ^{2}D using conditions as summarized in **Table 4**. As discussed and shown above, the employed polysaccharide-based CSP should be able to separate PSO stereoisomers due to a combination of attractive forces such as hydrogen bonding, hydrophobic interactions, dipole–dipole interactions and charge transfer complex (π–π) formation [43]. A mixed-mode retention mechanism through hydrophobic interactions and additional π-π-interactions, hydrogen bonding, as well as dipole-dipole interactions was supposed to be orthogonal to ion-pairing and hydrophobic interactions on C18 in the ^{2}D. In combination with steric barriers towards these interactions, diastereoselectivity might be different in comparison to IP-RPLC since the fundamental retention mechanisms are different. BEH C18 IP-RPLC was selected in the ^{2}D as it exhibits better efficiency and also slightly better resolution compared to the chiral stationary phase IH-U. If peaks already resolved in the ^{1}D are remixed in the loops of the interface, there is a better chance to get resolved with the more efficient separation system in the ^{2}D. So, the LC system which gives the overall highest resolution should be used in the ^{2}D in sequential selective comprehensive 2D-LC. This specific 2D-LC mode was selected

for its significantly reduced time of complicated method development without compromising chromatographic separation power for both dimensions.

The analytical batch of the sequential selective comprehensive 2D-LC experiment of consisted of 4 consecutive injections for the PSO-A sample (see **Figure S6**) and of 2 consecutive injections for the API sample (see **Figure S7**). In each injection, 10 adjacent cuts were sampled from the ^{1}D into the loops of 2 loop decks (each equipped with six 40 µL loops). A detailed sampling table is given in **Figure S6** for PSO-A and in **Figure S7** for the API. The entire batch was running in fully automated manner. The sampling time was 7s (keeping undersampling relatively low) and loop filling was 58%. Since the ^{1}D LC eluent contained acetonitrile, the ASM valve was activated. It means the fractions were diluted with weak ^{2}D eluent before they were transferred onto the ^{2}D column.

The final 2D-LC results of these experiments are presented in **Figure S8** (PSO-A) and **Figure S9** (API) which show all ^{2}D chromatograms. These ^{2}D chromatograms were then reconstituted into 2D contour plots (2D chromatograms) shown in **Figure 5C** for PSO-A and in **Figure 6C** for API. **Figure 5C** depicts a significant spread of the diastereomers of PSO-A around the diagonal line in the 2D contour plot indicating some orthogonality between the two stationary phase systems. Hence, additional peaks could be resolved in the ^{2}D as compared to the ^{1}D. In particular in the second part of the 2D chromatogram, several diastereomer peak pairs were resolved in the ^{2}D which is only possible due to orthogonality in the ^{1}D and ^{2}D phase systems. Overall, for PSO-A, a larger number of peaks was detected than by 1D-LC of either phase system, the IH-U and IP-RPLC with BEH C18 (**Figure 5A and 5B**). The number of peaks counted in the 2D-plot exceeded 32 distinguished diastereomers. It can be assumed that some of the peaks originated from possible impurities (**Figure 5C**).

However, in general it is obvious that the 2D-LC run separated most of the 32 diastereomers clearly impossible by any of the two orthogonal 1D-LC phase systems.

As far as the API is concerned, the sequential selective comprehensive 2D-LC experiment enabled the separation and the detection of 21 peaks (**Figure 6C**). With more than 8000 expected diastereomers, it is unrealistic to separate all of them. However, the resultant 2D-contour plot can be regarded as a representative partial diastereomer profile and molecular “finger print” of an PSO API which can be helpful for quality control purposes. The improvement from 5 (Fig. 6A and 6B) up to 21 peaks (**Figure 6C**) with the current 2D-LC is significant.

Conclusion

For the separation of PSO diastereomers, IP-RPLC is still the method of choice. In this study, a series of model PSO (6-mers) with different number and position of PS linkages and a 20-mer API with a conjugated GalNAc-residue has been investigated by IP-RPLC under multiple conditions to maximize the number of resolved diastereomers. For the PSO-6mers, a low concentration of hydrophilic IP reagents and ammonium acetate buffer provided better diastereoselectivity. Due to the numerous PS linkages, 1D-LC experiments were not able to separate all possible diastereomers from each other once the number of PS linkages was larger than 3. For this reason, a number of orthogonal stationary phases comprising HILIC, mixed-mode and chiral stationary phases were evaluated. It was found that a polysaccharide based chiral stationary phase based on amylose tris(α-methylbenzylcarbamate) shows distinct diastereoselectivity for PSO oligonucleotides. It was not straightforward to assess orthogonality if IP-RPLC and chiral column based diastereoselective LC because peak

annotation by MS fails due to identical masses of diastereomers and individual stereoisomer standards were not available. Thus, 2D-LC using a sequential selective comprehensive modality was selected to document orthogonality between the two chromatographic phases systems. With sequential selective comprehensive 2D-LC experiments, the relevant part of the chromatogram of the ^{1}D with the amylose-based chiral stationary phase leading to partially separated diastereomer peaks was completely transferred into the ^{2}D with IP-RPLC with hydrophilic ion-pair agent and BEH C18, thus receiving increased separation power. By doing so, almost all of the 32 diastereomers of PSO-A were separated. For the 20-mer conjugated API, the number of separated diastereomers could also be significantly increased. The resultant 2D-contour plot therefore might be considered as a possibility to create a finger print profiling of the diastereomer mixtures for quality control aspects to study batch-to-batch reproducibility effects. Furthermore, the 2D-LC setup could also be hyphenated with MS to identify and distinguish chemical impurities from the diastereomers due to relatively MS-friendly conditions. It is also possible to further evaluate the orthogonality of diastereomers by investigating other chromatography types like HILIC or ion-exchange chromatography.

Acknowledgements

This project was financially supported by Bayer AG through research funding based on a research agreement. We are also grateful to Agilent Technologies for support of this research by 2DLC instrumentation through an Agilent Research Award (#4068). The authors thank Dr. Stephan Buckenmaier from Agilent Technologies, Waldbronn, Germany, for technical advice and valuable discussions.

Conflict of interest statement

The authors declare no conflict of interests.

References

[1] S.T. Crooke, X. Liang, R.M. Crooke, B.F. Baker, R.S. Geary, Antisense drug discovery and development technology considered in a pharmacological context, Biochem. Pharmacol. 189 (2021) 114196. https://doi.org/https://doi.org/10.1016/j.bcp.2020.114196.

[2] D.G. Brown, H.J. Wobst, A Decade of FDA-Approved Drugs (2010-2019): Trends and Future Directions, J. Med. Chem. 64 (2021) 2312–2338. https://doi.org/10.1021/acs.jmedchem.0c01516.

[3] T.C. Roberts, R. Langer, M.J.A. Wood, Advances in oligonucleotide drug delivery, Nat. Rev. Drug Discov. 19 (2020) 673–694. https://doi.org/10.1038/s41573-020-0075-7.

[4] M. Matsukura, K. Shinozuka, G. Zon, H. Mitsuya, M. Reitz, J.S. Cohen, S. Broder, Phosphorothioate analogs of oligodeoxynucleotides: inhibitors of replication and cytopathic effects of human immunodeficiency virus., Proc. Natl. Acad. Sci. U. S. A. 84 (1987) 7706–7710. https://doi.org/10.1073/pnas.84.21.7706.

[5] R.I. Hara, R. Yoshino, Y. Nukaga, Y. Maeda, K. Sato, T. Wada, Synthesis and properties of DNA oligomers containing stereopure phosphorothioate linkages and C-5 modified deoxyuridine derivatives, RSC Adv. 10 (2020) 34006–34013. https://doi.org/10.1039/d0ra06970a.

[6] P. Rosenqvist, V. Saari, E. Pajuniemi, A. Gimenez Molina, M. Ora, A. Horvath,

P. Virta, Stereo-Controlled Liquid Phase Synthesis of Phosphorothioate Oligonucleotides on a Soluble Support, J. Org. Chem. 88 (2023) 10156–10163. https://doi.org/10.1021/acs.joc.3c01006.

[7] K.W. Knouse, J.N. deGruyter, M.A. Schmidt, B. Zheng, J.C. Vantourout, C. Kingston, S.E. Mercer, I.M. Mcdonald, R.E. Olson, Y. Zhu, C. Hang, J. Zhu, C. Yuan, Q. Wang, P. Park, M.D. Eastgate, P.S. Baran, Unlocking P(V): Reagents for chiral phosphorothioate synthesis, Science (80-.). 361 (2018) 1234–1238. https://doi.org/10.1126/science.aau3369.

[8] N. Iwamoto, D.C.D. Butler, N. Svrzikapa, S. Mohapatra, I. Zlatev, Di.W.Y. Sah, Meena, S.M. Standley, G. Lu, L.H. Apponi, M. Frank-Kamenetsky, J.J. Zhang, C. Vargeese, G.L. Verdine, Control of phosphorothioate stereochemistry substantially increases the efficacy of antisense oligonucleotides, Nat. Biotechnol. 35 (2017) 845–851. https://doi.org/10.1038/nbt.3948.

[9] H. Jahns, M. Roos, J. Imig, F. Baumann, Y. Wang, R. Gilmour, J. Hall, Stereochemical bias introduced during RNA synthesis modulates the activity of phosphorothioate siRNAs, Nat. Commun. 6 (2015) 6317. https://doi.org/10.1038/ncomms7317.

[10] D. Capaldi, N. Akhtar, T. Atherton, D. Benstead, A. Charaf, T. De Vijlder, C. Heatherington, J. Hoernschemeyer, H. Jiang, U. Rieder, F. Ring, R. Peter, J.A. Stolee, R. Wechselberger, Strategies for Identity Testing of Therapeutic Oligonucleotide Drug Substances and Drug Products, Nucleic Acid Ther. 30 (2020) 249–264. https://doi.org/10.1089/nat.2020.0878.

[11] A. Demelenne, G. Nys, C. Nix, J.C. Fjeldsted, J. Crommen, M. Fillet, Separation of phosphorothioated oligonucleotide diastereomers using multiplexed drift tube ion mobility mass spectrometry, Anal. Chim. Acta. 1191 (2022) 339297.

https://doi.org/10.1016/j.aca.2021.339297.

[12] V.K. Sharma, J.K. Watts, Oligonucleotide therapeutics: chemistry, delivery and clinical progress, Future Med. Chem. 7 (2015) 2221–2242. https://doi.org/10.4155/fmc.15.144.

[13] T. Chen, S. Tang, Y. Fu, J.G. Napolitano, K. Zhang, Analytical techniques for characterizing diastereomers of phosphorothioated oligonucleotides, J. Chromatogr. A. 1678 (2022) 463349. https://doi.org/10.1016/j.chroma.2022.463349.

[14] N.M. El Zahar, N. Magdy, A.M. El-Kosasy, M.G. Bartlett, Chromatographic approaches for the characterization and quality control of therapeutic oligonucleotide impurities, Biomed. Chromatogr. 32 (2018). https://doi.org/10.1002/bmc.4088.

[15] M. Huang, X. Xu, H. Qiu, N. Li, Analytical characterization of DNA and RNA oligonucleotides by hydrophilic interaction liquid chromatography-tandem mass spectrometry, J. Chromatogr. A. 1648 (2021) 462184. https://doi.org/10.1016/j.chroma.2021.462184.

[16] A. Shimoyama, A. Fujisaka, S. Obika, Evaluation of size-exclusion chromatography for the analysis of phosphorothioate oligonucleotides, J. Pharm. Biomed. Anal. 136 (2017) 55–65. https://doi.org/10.1016/j.jpba.2016.12.036.

[17] S. Studzińska, K. Krzemińska, M. Szumski, B. Buszewski, Application of a cholesterol stationary phase in the analysis of phosphorothioate oligonucleotides by means of ion pair chromatography coupled with tandem mass spectrometry, Talanta. 154 (2016) 270–277. https://doi.org/10.1016/j.talanta.2016.03.082.

[18] S. Studzińska, F. Łobodziński, B. Buszewski, Application of hydrophilic

interaction liquid chromatography coupled with mass spectrometry in the analysis of phosphorothioate oligonucleotides in serum, J. Chromatogr. B. 1040 (2017) 282–288. https://doi.org/https://doi.org/10.1016/j.jchromb.2016.11.001.

[19] R. Easter, C. Barry, J. Caruso, P. Limbach, Separation and identification of phosphorothioate oligonucleotides by HILIC-ESIMS, Anal. Methods. 5 (2013) 2657–2659. https://doi.org/10.1039/c3ay26519f.

[20] J.R. Thayer, Y. Wu, E. Hansen, M.D. Angelino, S. Rao, Separation of oligonucleotide phosphorothioate diastereoisomers by pellicular anion-exchange chromatography, J. Chromatogr. A. 1218 (2011) 802–808. https://doi.org/https://doi.org/10.1016/j.chroma.2010.12.051.

[21] S.G. Roussis, I. Cedillo, C. Rentel, Characterizing the Diastereoisomeric Distribution of Phosphorothioate Oligonucleotides by Metal Ion Complexation Chromatography, In-Series Reversed Phase-Strong Anion Exchange Chromatography, and31P NMR, Anal. Chem. 93 (2021) 16035–16042. https://doi.org/10.1021/acs.analchem.1c03593.

[22] Z. Kadlecová, K. Kalíková, E. Tesařová, M. Gilar, Phosphorothioate oligonucleotides separation in ion-pairing reversed-phase liquid chromatography: Effect of ion-pairing system, J. Chromatogr. A. 1676 (2022) 463201. https://doi.org/https://doi.org/10.1016/j.chroma.2022.463201.

[23] M. Enmark, M. Rova, J. Samuelsson, E. Örnskov, F. Schweikart, T. Fornstedt, Investigation of factors influencing the separation of diastereomers of phosphorothioated oligonucleotides, Anal. Bioanal. Chem. 411 (2019) 3383–3394. https://doi.org/10.1007/s00216-019-01813-2.

[24] M. Enmark, J. Bagge, J. Samuelsson, L. Thunberg, E. Örnskov, H. Leek, F. Limé, T. Fornstedt, Analytical and preparative separation of phosphorothioated

oligonucleotides: columns and ion-pair reagents, Anal. Bioanal. Chem. 412 (2020) 299–309. https://doi.org/10.1007/s00216-019-02236-9.

[25] A. Goyon, M.S. Blevins, J.G. Napolitano, D. Nguyen, M. Goel, B. Scott, J. Wang, S.G. Koenig, T. Chen, K. Zhang, Characterization of antisense oligonucleotide and guide ribonucleic acid diastereomers by hydrophilic interaction liquid chromatography coupled to mass spectrometry, J. Chromatogr. A. 1708 (2023) 464327. https://doi.org/https://doi.org/10.1016/j.chroma.2023.464327.

[26] M. Gilar, B.M. Koshel, R.E. Birdsall, Ion-pair reversed-phase and hydrophilic interaction chromatography methods for analysis of phosphorothioate oligonucleotides, J. Chromatogr. A. 1712 (2023) 464475. https://doi.org/10.1016/j.chroma.2023.464475.

[27] M. Gilar, A. Belenky, A.S. Cohen, Polymer solutions as a pseudostationary phase for capillary electrochromatographic separation of DNA diastereomers, Electrophoresis. 21 (2000) 2999–3009. https://doi.org/https://doi.org/10.1002/1522-2683(20000801)21:14<2999::AID-ELPS2999>3.0.CO;2-1.

[28] A. Goyon, M.S. Blevins, J.G. Napolitano, D. Nguyen, M. Goel, B. Scott, J. Wang, S.G. Koenig, T. Chen, K. Zhang, Characterization of antisense oligonucleotide and guide ribonucleic acid diastereomers by hydrophilic interaction liquid chromatography coupled to mass spectrometry, J. Chromatogr. A. 1708 (2023). https://doi.org/10.1016/j.chroma.2023.464327.

[29] S.G. Roussis, C. Rentel, Separation of phosphorothioate oligonucleotide impurities by WAX HPLC under high organic content elution conditions, Anal. Biochem. 659 (2022) 114956. https://doi.org/https://doi.org/10.1016/j.ab.2022.114956.

[30] F. Li, M. Lämmerhofer, Impurity profiling of siRNA by two-dimensional liquid chromatography-mass spectrometry with quinine carbamate anion-exchanger and ion-pair reversed-phase chromatography, J. Chromatogr. A. 1643 (2021) 462065. https://doi.org/10.1016/j.chroma.2021.462065.

[31] S. Studzińska, F. Li, M. Szumski, B. Buszewski, M. Lämmerhofer, Cholesterol Stationary Phase in the Separation and Identification of siRNA Impurities by Two-Dimensional Liquid Chromatography-Mass Spectrometry, Int. J. Mol. Sci. 23 (2022). https://doi.org/10.3390/ijms232314960.

[32] F. Li, X. Su, S. Bäurer, M. Lämmerhofer, Multiple heart-cutting mixed-mode chromatography-reversed-phase 2D-liquid chromatography method for separation and mass spectrometric characterization of synthetic oligonucleotides, J. Chromatogr. A. 1625 (2020) 461338. https://doi.org/https://doi.org/10.1016/j.chroma.2020.461338.

[33] B.W.J. Pirok, D.R. Stoll, P.J. Schoenmakers, Recent Developments in Two-Dimensional Liquid Chromatography: Fundamental Improvements for Practical Applications, Anal. Chem. 91 (2019) 240–263. https://doi.org/10.1021/acs.analchem.8b04841.

[34] S. Studzińska, Ł. Nuckowski, B. Buszewski, Oligonucleotides Isolation and Separation—A Review on Adsorbent Selection, Int. J. Mol. Sci. 23 (2022). https://doi.org/10.3390/ijms23179546.

[35] Q. Li, F. Lynen, J. Wang, H. Li, G. Xu, P. Sandra, Comprehensive hydrophilic interaction and ion-pair reversed-phase liquid chromatography for analysis of di- to deca-oligonucleotides, J. Chromatogr. A. 1255 (2012) 237–243. https://doi.org/10.1016/j.chroma.2011.11.062.

[36] C. Vanhinsbergh, E.C. Hook, N. Oxby, M.J. Dickman, Optimization of orthogonal

separations for the analysis of oligonucleotides using 2D-LC, J. Chromatogr. B Anal. Technol. Biomed. Life Sci. 1227 (2023) 123812. https://doi.org/10.1016/j.jchromb.2023.123812.

[37] A. Goyon, K. Zhang, Characterization of antisense oligonucleotide impurities by ion-pairing reversed-phase and anion exchange chromatography coupled to HILIC/MS using a versatile 2D-LC setup, Anal. Chem. (2020). https://doi.org/10.1021/acs.analchem.0c00114.

[38] M. Rosés, X. Subirats, E. Bosch, Retention models for ionizable compounds in reversed-phase liquid chromatography. Effect of variation of mobile phase composition and temperature, J. Chromatogr. A. 1216 (2009) 1756–1775. https://doi.org/10.1016/j.chroma.2008.12.042.

[39] M. Donegan, J.M. Nguyen, M. Gilar, Effect of ion-pairing reagent hydrophobicity on liquid chromatography and mass spectrometry analysis of oligonucleotides, J. Chromatogr. A. 1666 (2022) 462860. https://doi.org/10.1016/j.chroma.2022.462860.

[40] M. Donegan, J.M. Nguyen, M. Gilar, Effect of ion-pairing reagent hydrophobicity on liquid chromatography and mass spectrometry analysis of oligonucleotides, J. Chromatogr. A. 1666 (2022) 462860. https://doi.org/10.1016/j.chroma.2022.462860.

[41] H. Lardeux, S. Fekete, M. Lauber, V. D'Atri, D. Guillarme, High-Throughput Chromatographic Separation of Oligonucleotides: A Proof of Concept Using Ultra-Short Columns, Anal. Chem. 95 (2023) 10448–10456. https://doi.org/10.1021/acs.analchem.3c01934.

[42] M. Gilar, P. Olivova, A.E. Daly, J.C. Gebler, Orthogonality of separation in two-dimensional liquid chromatography, Anal. Chem. 77 (2005) 6426–6434.

https://doi.org/10.1021/ac050923i.

[43] C.L. Barhate, E.L. Regalado, N.D. Contrella, J. Lee, J. Jo, A.A. Makarov, D.W. Armstrong, C.J. Welch, Ultrafast Chiral Chromatography as the Second Dimension in Two-Dimensional Liquid Chromatography Experiments, Anal. Chem. 89 (2017) 3545–3553. https://doi.org/10.1021/acs.analchem.6b04834.

Figure Captions

Figure. 1. Chemical structures of test analytes used for this study. A: PSO-A and B: API. Nucleobases not disclosed due to secrecy agreement.

Figure. 2. Heat maps of diastereomer coverages as overview for all 1D IP-RPLC experiments for PSO-A for column temperature of 60 °C (A) and 25 °C (B). For method details see **Table 3, Method A**.

Figure. 3. IP-RPLC-UV-chromatograms of all model PSO molecules generated by obtained with EAA as IP reagent. A: 20 mM EAA, 60 °C; B: 100 mM EAA, 60 °C; C: 20 mM EAA, 25 °C; D: 100 mM EAA, 25 °C. For method details see **Table 3, Method A**.

Figure. 4. Heat map demonstrating numbers of separated diastereomer for all 1D-IP-RPLC experiments of the API. For method details see **Table 3, Method A**.

Figure. 5. LC-UV-chromatograms of PSO-A on IH-U under RP (A) and C18 under IP-RP conditions (B). Both methods were eventually combined in the final sequential selective comprehensive 2D-LC method as illustrated in form of a contour plot in (C). For method details see **Table 4**, **Method A**.

Figure. 6. UV-chromatograms of API on IH-U under RP (A) and C18 under IPRP (B). Both methods were eventually combined in the final 2D-LC method. The 2D-LC result

is illustrated in form of a topographical plot on (C). For methods details see **Table 4**, **Method B**.

Table 1. Overview of investigated DNA-PSO standards.

Name	Sequence
PSO-A	5' dT*dT*dG*dG*dT*dG 3'
PSO-B	5' dT*dT*dG*dG*dT dG 3'
PSO-C	5' dT*dT*dG*dG dT dG 3'
PSO-D	5' dT*dT*dG dG dT dG 3'
PSO-E	5' dT*dT dG dG dT dG 3'
PSO-F	5' dT dT*dG*dG*dT*dG 3'
PSO-G	5' dT dT dG*dG*dT*dG 3'
PSO-H	5' dT dT dG dG*dT*dG 3'
PSO-I	5' dT dT dG dG dT*dG 3'

Table 2. Overview of used mobile phases for the screening 1D-LC IP-RP experiments.

Mobile Phase	IP agent	IP conc. [mM]	MeOH [%]	pH ($^{w}_{w}pH$)[a]
A1	TPAA	20	10	9
B1	TPAA	20	50	9
A2	TPAA	100	10	9
B2	TPAA	100	50	9
A3	TEAA	20	10	9
B3	TEAA	20	50	9
A4	TEAA	100	10	9
B4	TEAA	100	50	9
A5	DEAA	20	10	9
B5	DEAA	20	50	9
A6	DEAA	100	10	9
B6	DEAA	100	50	9
A7	PAA	20	10	9
B7	PAA	20	50	9
A8	PAA	100	10	9
B8	PAA	100	50	9
A9	EAA	20	10	9
B9	EAA	20	50	9
A10	EAA	100	10	9
B10	EAA	100	50	9
A11	MAA	20	10	9
B11	MAA	20	50	9
A12	MAA	100	10	9
B12	MAA	100	50	9
A13	AA	20	10	9
B13	AA	20	50	9
A14	AA	100	10	9
B14	AA	100	50	9

[a] pH-values defined according to *Rosés* [28].

All screening experiments were carried out under 25 and 60 °C

TPAA: Tripropylammonium acetate; TEAA: Triethylammonium acetate; DEAA: Diethylammonium acetate; PAA: Pentylammonium acetate;

EAA: Ethylammonium acetate; MAA: Methylammonium acetate; AA: Ammonium acetate

Table 3. Overview of all evaluated LC methods for 1D-LC experiments.

	1D-LC Method A	1D-LC Method B	1D-LC Method C
Column Dimension	BEH C18 50x2.1 mm, 130 Å, 1.7 µm	BEH C18 100x2.1 mm, 130 Å, 1.7 µm	BEH C18 50x2.1 mm, 300 Å, 1.7 µm
Mobile Phase A	20/100 mM[1] IP in 10% MeOH, $^{w}_{w}p\mathrm{H}$ 9	20/100 mM EAA/AA[2] in 10% MeOH, $^{w}_{w}p\mathrm{H}$ 9	20/100 mM EAA/AA[3] in 10% MeOH, $^{w}_{w}p\mathrm{H}$ 9
Mobile Phase B	20/100 mM[1] IP in 90% MeOH, $^{w}_{w}p\mathrm{H}$ 9	20/100 mM EAA/AA[2] in 90% MeOH, $^{w}_{w}p\mathrm{H}$ 9	20/100 mM EAA/AA[3] in 90% MeOH, $^{w}_{w}p\mathrm{H}$ 9
Gradient	0-50% B in 10 min; 0% B for 10 min	0-50% B in 27.3 min; 0% B for 15 min	0-50% B in 10 min; 0% B for 10 min
Column Temperature	10/20/25/30/40/50/60 °C[1]	10/60 °C[2]	10/60 °C[3]
Flow rate	0.3 mL/min	0.3 mL/min	0.3 mL/min
Injection Volume	5 µL	5 µL	5 µL
Detection	UV, 254 nm, 10 Hz	UV, 254 nm, 10 Hz	UV, 254 nm, 10 Hz

[1]: Buffer type, buffer concentration and different column temperatures were investigated for model molecules and API. For model PSO-A-I molecules, only 25 °C and 60 °C were investigated. For API, the temperature series was carried out. pH values defined after *Rosés* [28].
[2]: 20 mM EAA, 60 °C for model molecules, 100 mM AA, 10 °C for API.
[3]: 20 mM EAA, 60 °C for model molecules, 100 mM AA, 10 °C for API.

Table 4. Overview of employed 2D-LC methods.

	2D-LC Method A		2D-LC Method B	
Column Dimension (^{1}D/^{2}D)	Chiralpak IH-U 100x2.1 mm, 3 µm	BEH C18 100x2.1 mm, 130 Å, 1.7 µm	Chiralpak IH-U 100x2.1 mm, 3 µm	BEH C18 50x2.1 mm, 300 Å, 1.7 µm
Mobile Phase A (^{1}D/^{2}D)	20 mM AA, pH not adjusted	20 mM EAA in 10% MeOH, $^{w}_{w}p\mathrm{H}$ 9	100 mM AA, pH not adjusted	100 mM EAA in 10% MeOH, $^{w}_{w}p\mathrm{H}$ 9
Mobile Phase B (^{1}D/^{2}D)	20 mM AA in 50% ACN, pH not adjusted	20 mM EAA in 90% MeOH, $^{w}_{w}p\mathrm{H}$ 9	100 mM AA in 50% ACN, pH not adjusted	100 mM EAA in 90% MeOH, $^{w}_{w}p\mathrm{H}$ 9
Gradient (^{1}D/^{2}D)	10-20% B in 15 min	Hold 20% B for 2.22 min; 20-40% B in 7.78 min; 20% B for 5 min	25-50% in 15 min	Hold 30% B for 2.22 min; 30-45% B in 7.78 min, 30% B for 5 min
Column Temperature (^{1}D/^{2}D)	25 °C	60 °C	10 °C	10 °C
Flow rate (^{1}D/^{2}D)	0.2 mL/min	0.3 mL/min	0.2 mL/min	0.3 mL/min
^{1}D Injection Volume ^{2}D Transfer Amounts	8 µL	Loop filling: 58%; Sampling Time: 7s	8 µL	Loop filling: 58%; Sampling Time: 7s
Detection	UV, 254 nm, 10 Hz	UV, 254 nm, 20 Hz	UV, 254 nm, 10 Hz	UV, 254 nm, 20 Hz
2D-LC Mode	Sequential selective comprehensive 2D-LC Counter-current		Sequential selective comprehensive 2D-LC Counter-current	
ASM[1]	Activated, 2.22 min		Activated, 2.22 min	
Number of Runs[2]	Four, 700 min total analysis time		Two, 350 min total analysis time	

[1]: Factor 5, loop flushing: 3 times
[2]: For detailed sampling tables and illustrations of cut distribution of the 2D-LC methods, see Figure S6 and Figure S7.

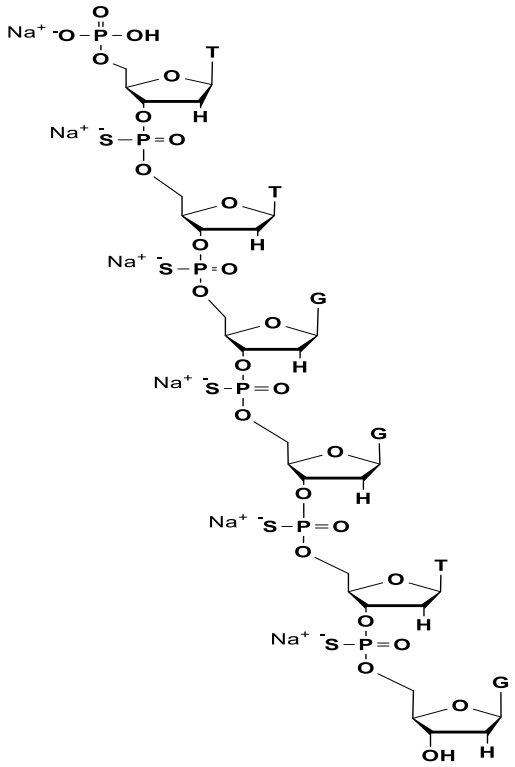

PSO-A, 5 PS, 32 Diastereomers

Figure 1

Figure 2

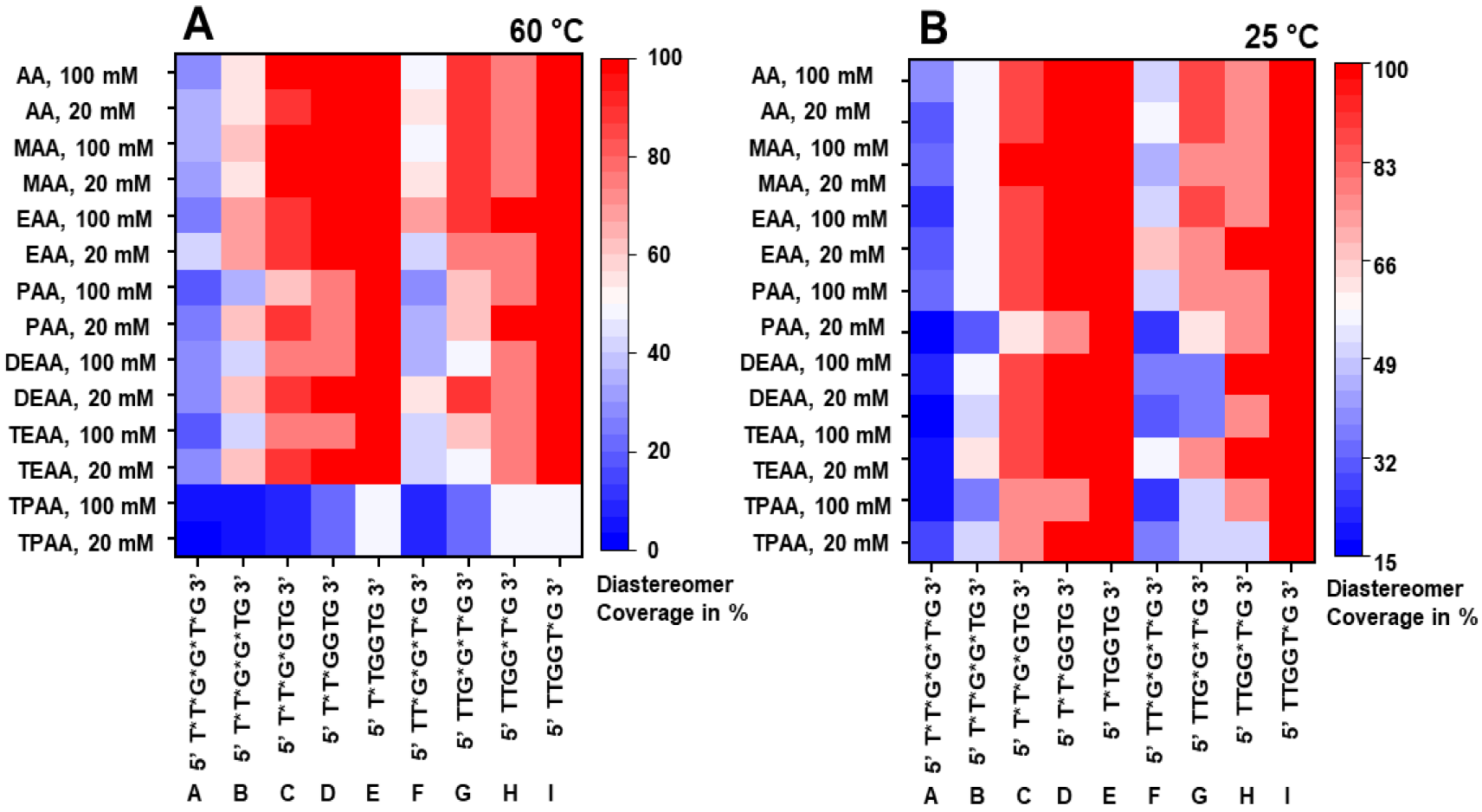
A
60 °C
AA, 100 mM
AA, 20 mM
MAA, 100 mM
MAA, 20 mM
EAA, 100 mM
EAA, 20 mM
PAA, 100 mM
PAA, 20 mM
DEAA, 100 mM
DEAA, 20 mM
TEAA, 100 mM
TEAA, 20 mM
TPAA, 100 mM
TPAA, 20 mM
100
80
60
40
20
0
Diastereomer Coverage in %
5' T*T*G*G*T*G 3'
5' T*T*G*G*TG 3'
5' T*T*G*GTG 3'
5' T*T*GGTG 3'
5' T*TGGTG 3'
5' TT*G*G*T*G 3'
5' TTG*G*T*G 3'
5' TTGG*T*G 3'
5' TTGGT*G 3'
A
B
C
D
E
F
G
H
I
B
25 °C
100
83
66
49
32
15
Diastereomer Coverage in %

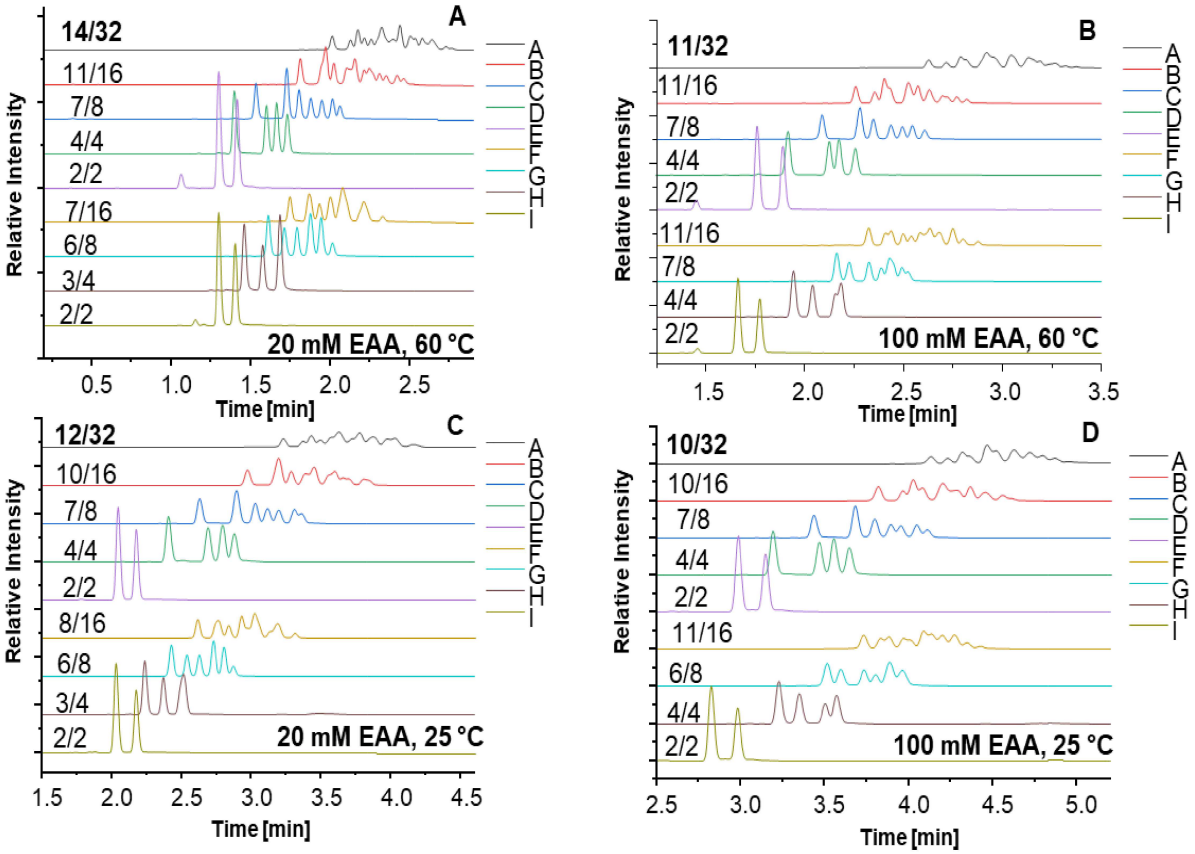

Figure 3

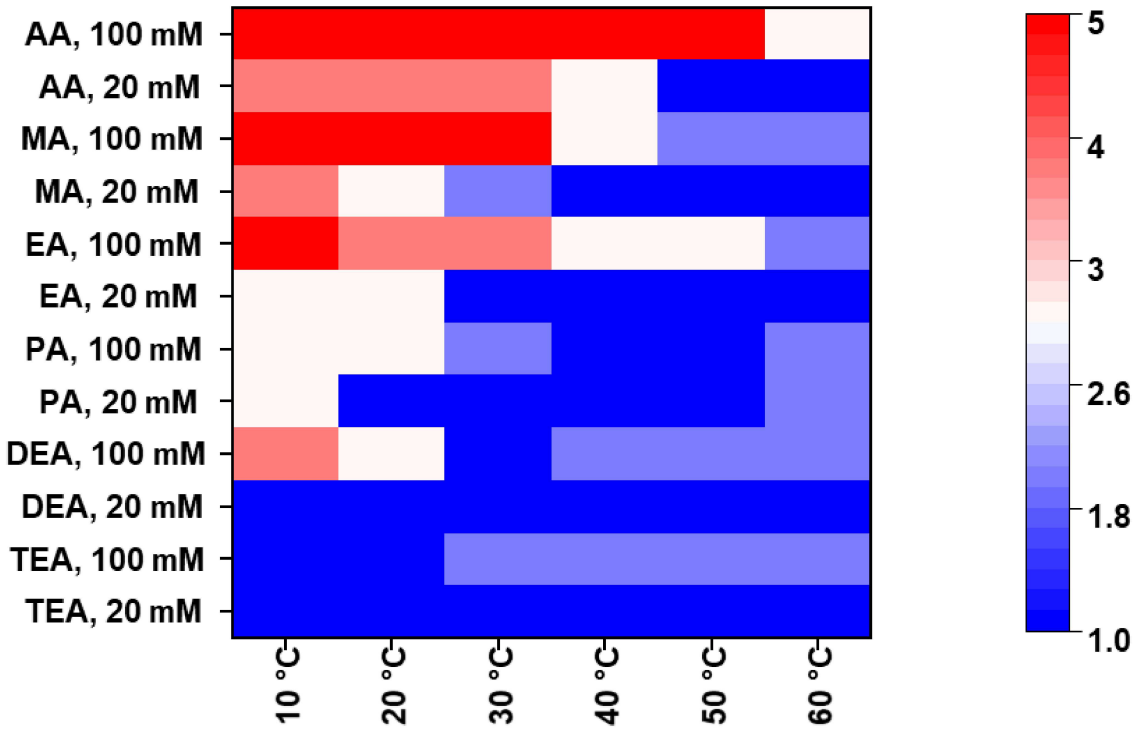

Figure 4

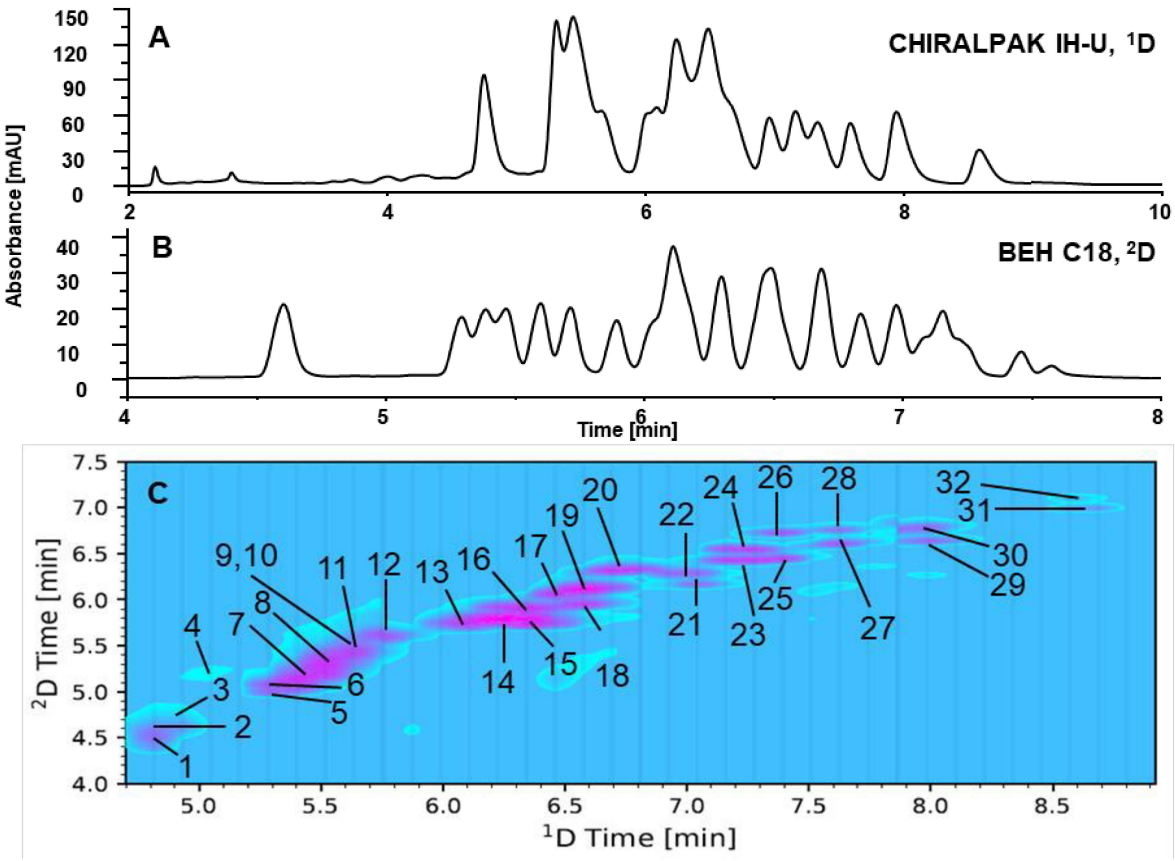

Figure 5

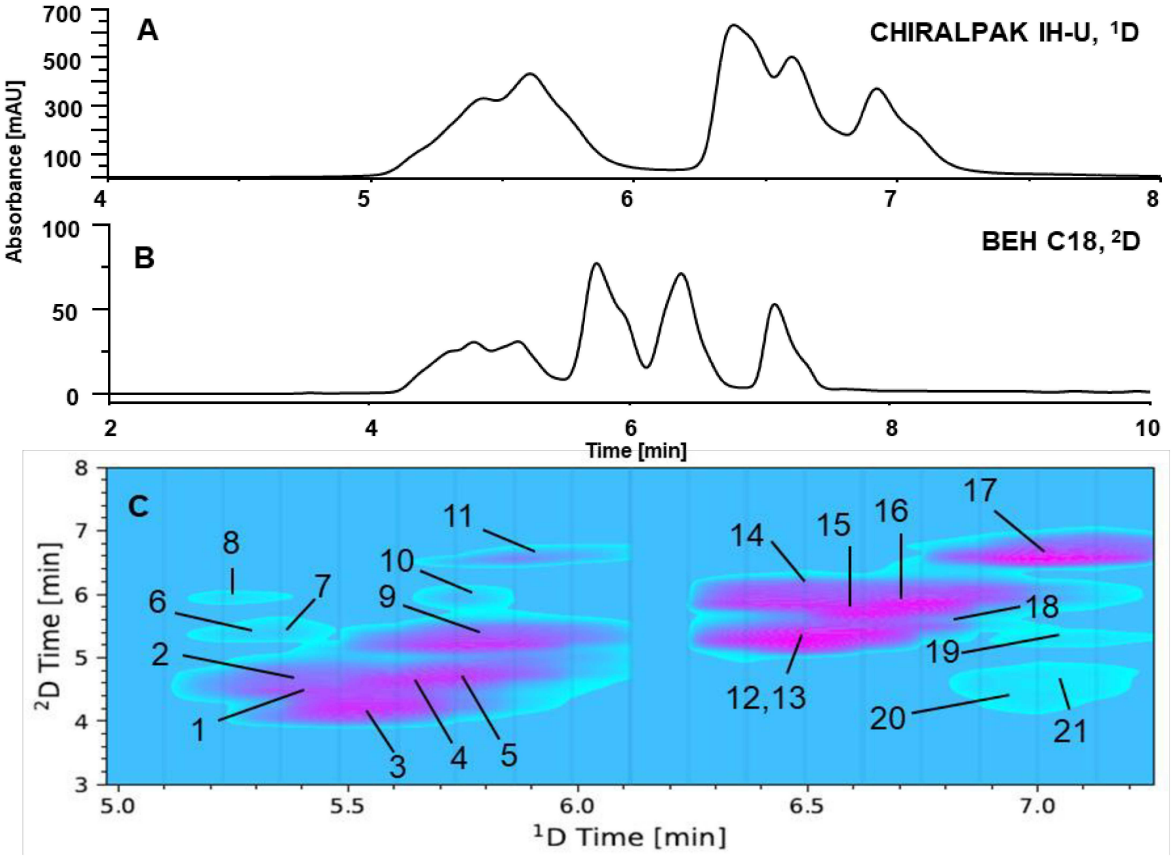

Figure 6

Supplementary Material

Two-dimensional sequential selective comprehensive chiral×reversed-phase liquid chromatography of synthetic phosphorothioate oligonucleotide diastereomers

Feiyang Li[a], Cornelius Knappe[a], Enrico Favorat[a], Niklas Carstensen[a] Mimi Gao[b], Wiebke Holkenjans[b], Terence Hetzel[b], Reinhard Pell[b], Michael Lämmerhofer[a]*

[a] *Institute of Pharmaceutical Sciences, Pharmaceutical (Bio-)Analysis, University of Tübingen, Auf der Morgenstelle 8, 72076 Tübingen, Germany

[b] Bayer AG, Research Center Aprath, Aprather Weg 18a, 42113 Wuppertal, Germany

*Author for correspondence:

Prof. Dr. Michael Lämmerhofer

Pharmaceutical (Bio-)Analysis

Institute of Pharmaceutical Sciences

University of Tübingen

Auf der Morgenstelle 8

72076 Tübingen, Germany

T +49 7071 29 78793, F +49 7071 29 4565

E-mail: michael.laemmerhofer@uni-tuebingen.de

Table S1. Overview of the numbers of diastereomer peaks separated for PSO-A and API with column temperature of 25 °C and 60 °C with the usage of different IP reagents. Number of detected peaks are listed under “Peak No.”. The difference of detected peaks between 25 °C and 60 °C are shown in the parenthesis.

60 °C

Sample	IP	IP conc. [mM]	Peak No.
Standard (32 Diast.)	TPAA	20	1
	TEAA		8
	DEAA		10
	PAA		9
	EAA		14
	MAA		11
	AA		12
	TPAA	100	2
	TEAA		7
	DEAA		10
	PAA		7
	EAA		9
	MAA		12
	AA		10
API (> 8000 Diast.)	TPAA	20	1
	TEAA		1
	DEAA		1
	PAA		2
	EAA		1
	MAA		1
	AA		1
	TPAA	100	1
	TEAA		2
	DEAA		2
	PAA		2
	EAA		2
	MAA		2
	AA		3

25 °C

Sample	IP	IP conc. [mM]	Peak No. (diff. to 60 °C)
Standard (32 Diast.)	TPAA	20	-
	TEAA		9 (+1)
	DEAA		6 (-4)
	PAA		7 (-2)
	EAA		11 (-3)
	MAA		8 (-3)
	AA		10 (-2)
	TPAA	100	-
	TEAA		6 (-1)
	DEAA		5 (-5)
	PAA		5 (-2)
	EAA		10 (+1)
	MAA		11 (-1)
	AA		13 (+3)
API (> 8000 Diast.)	TPAA	20	-
	TEAA		1
	DEAA		1
	PAA		1 (-1)
	EAA		3 (+2)
	MAA		3 (+2)
	AA		4 (+3)
	TPAA	100	-
	TEAA		1 (-1)
	DEAA		1 (-1)
	PAA		3 (+1)
	EAA		4 (+2)
	MAA		5 (+3)
	AA		5 (+2)

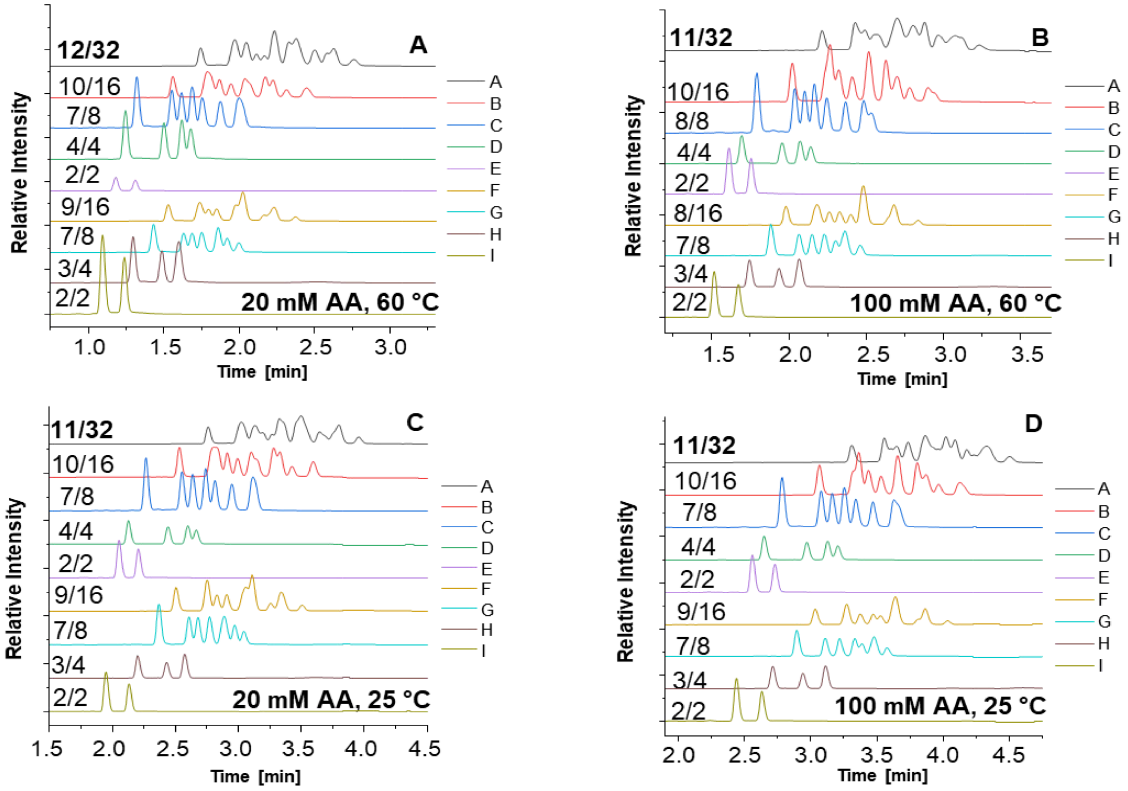

Figure S1. IP-RPLC-UV-chromatograms of all model PSO molecules obtained with AA as IP reagent. A: 20 mM AA, 60 °C; B: 100 mM AA, 60 °C; C: 20 mM AA, 25 °C; D: 100 mM AA, 25 °C. For method details see **Table 3**, **Method A**.

Table S2. Chromatographic results of chosen screening conditions (see **Table 2** for the used IPs and **Table 3**, **Method A**) for PSO-D, PSO-E, PSO-H and PSO-I.

Mobile Phase	Temp.	Sample	Peak No.	t_R [min]	$w_{1/2}$ [min]	t'_R [min]	R
20 mM AA	25 °C	PSO-D	1	2.13	0.04	1.680	
			2	2.44	0.04	1.990	4.57
			3	2.60	0.04	2.150	2.36
			4	2.67	0.04	2.220	1.03
20 mM AA	60 °C	PSO-D	1	1.24	0.04	0.790	
			2	1.50	0.04	1.050	3.84
			3	1.62	0.04	1.170	1.77
			4	1.68	0.04	1.230	0.88
20 mM AA	25 °C	PSO-E	1	2.05	0.04	1.600	
			2	2.21	0.04	1.760	2.36
20 mM AA	60 °C	PSO-E	1	1.18	0.03	0.730	
			2	1.31	0.04	0.860	2.19
20 mM AA	25 °C	PSO-H	1	2.20	0.04	1.750	
			2	2.43	0.04	1.980	3.39
			3	2.58	0.04	2.130	2.21
			4	n.a.	n.a.	n.a.	n.a.
20 mM AA	60 °C	PSO-H	1	1.29	0.03	0.840	
			2	1.49	0.04	1.040	3.19
			3	1.60	0.05	1.151	1.46
			4	n.a.	n.a.	n.a.	n.a.
20 mM AA	25 °C	PSO-I	1	1.95	0.04	1.500	
			2	2.14	0.04	1.690	2.80
20 mM AA	60 °C	PSO-I	1	1.09	0.04	0.640	
			2	1.24	0.04	0.790	2.53
20 mM PAA	25 °C	PSO-D	1	3.31	0.05	2.860	
			2	3.55	0.05	3.100	2.83
			3	3.61	0.06	3.160	0.64
			4	3.70	0.05	3.250	0.97
20 mM PAA	60 °C	PSO-D	1	2.08	0.03	1.630	
			2	2.28	0.05	1.830	2.95
			3	2.37	0.03	1.920	1.33
			4	n.a	n.a	n.a	n.a

20 mM PAA	25 °C	PSO-E	1	3.08	0.05	2.630	
			2	3.22	0.05	2.770	1.65
20 mM PAA	60 °C	PSO-E	1	1.89	0.03	1.440	
			2	2.01	0.03	1.560	2.36
20 mM PAA	25 °C	PSO-H	1	3.40	0.05	2.950	
			2	3.45	0.05	3.000	0.59
			3	3.58	0.05	3.130	1.53
			4	3.67	0.05	3.220	1.06
20 mM PAA	60 °C	PSO-H	1	2.12	0.03	1.670	
			2	2.16	0.03	1.710	0.79
			3	2.25	0.03	1.800	1.77
			4	2.30	0.03	1.850	0.98
20 mM PAA	25 °C	PSO-I	1	2.96	0.04	2.510	
			2	3.08	0.04	2.630	1.77
20 mM PAA	60 °C	PSO-I	1	1.80	0.03	1.350	
			2	1.89	0.03	1.440	1.77
20 mM MAA	25 °C	PSO-D	1	2.07	0.05	1.620	
			2	2.36	0.05	1.910	3.42
			3	2.49	0.05	2.040	1.53
			4	2.57	0.05	2.120	0.94
20 mM MAA	60 °C	PSO-D	1	1.18	0.03	0.730	
			2	1.40	0.04	0.950	3.71
			3	1.50	0.04	1.050	1.48
			4	1.56	0.04	1.110	0.89
20 mM MAA	25 °C	PSO-E	1	1.96	0.04	1.510	
			2	2.11	0.04	1.660	2.21
20 mM MAA	60 °C	PSO-E	1	1.10	0.03	0.650	
			2	1.22	0.04	0.770	2.02
20 mM MAA	25 °C	PSO-H	1	2.10	0.04	1.650	
			2	2.31	0.04	1.860	3.10
			3	2.46	0.04	2.010	2.21
			4	n.a.	n.a.	n.a.	n.a.
20 mM MAA	60 °C	PSO-H	1	1.23	0.03	0.780	
			2	1.39	0.04	0.940	2.55
			3	1.50	0.05	1.050	1.44
			4	n.a.	n.a.	n.a.	n.a.
20 mM MAA	25 °C	PSO-I	1	1.85	0.04	1.400	
			2	2.03	0.04	1.580	2.66

20 mM MAA	60 °C	PSO-I	1	1.04	0.04	0.590	
			2	1.16	0.04	0.710	2.02
20 mM EAA	25 °C	PSO-D	1	2.41	0.04	1.960	
			2	2.69	0.04	2.240	4.13
			3	2.80	0.05	2.350	1.44
			4	2.88	0.05	2.430	0.94
20 mM EAA	60 °C	PSO-D	1	1.40	0.03	0.950	
			2	1.60	0.03	1.150	3.93
			3	1.66	0.03	1.210	1.18
			4	1.73	0.03	1.280	1.38
20 mM EAA	25 °C	PSO-E	1	2.04	0.03	1.590	
			2	2.17	0.03	1.720	2.56
20 mM EAA	60 °C	PSO-E	1	1.30	0.03	0.850	
			2	1.41	0.03	0.960	2.16
20 mM EAA	25 °C	PSO-H	1	2.24	0.03	1.790	
			2	2.37	0.03	1.920	2.56
			3	2.51	0.05	2.060	2.07
			4	n.a.	n.a.	n.a.	n.a.
20 mM EAA	60 °C	PSO-H	1	1.46	0.03	1.010	
			2	1.58	0.03	1.130	2.36
			3	1.68	0.03	1.230	1.97
			4	n.a.	n.a.	n.a.	n.a.
20 mM EAA	25 °C	PSO-I	1	2.03	0.03	1.580	
			2	2.17	0.03	1.720	2.75
20 mM EAA	60 °C	PSO-I	1	1.30	0.03	0.850	
			2	1.40	0.03	0.950	1.97
20 mM DEAA	25 °C	PSO-D	1	3.18	0.03	2.730	
			2	3.34	0.02	2.890	3.78
			3	3.37	0.03	2.920	0.71
			4	3.44	0.03	2.990	1.38
20 mM DEAA	60 °C	PSO-D	1	2.54	0.04	2.090	
			2	2.76	0.04	2.310	3.25
			3	2.82	0.04	2.370	0.89
			4	2.90	0.04	2.450	1.18
20 mM DEAA	25 °C	PSO-E	1	2.96	0.03	2.510	
			2	3.07	0.03	2.620	2.16
20 mM DEAA	60 °C	PSO-E	1	2.44	0.04	1.990	
			2	2.58	0.04	2.130	2.07

20 mM DEAA	25 °C	PSO-H	1	2.95	0.03	2.500	
			2	3.01	0.03	2.560	1.18
			3	3.12	0.04	2.670	1.85
			4	n.a.	n.a.	n.a.	n.a.
20 mM DEAA	60 °C	PSO-H	1	2.88	0.04	2.430	
			2	2.98	0.04	2.530	1.48
			3	3.12	0.03	2.670	2.36
			4	3.16	0.05	2.710	0.59
20 mM DEAA	25 °C	PSO-I	1	2.56	0.03	2.110	
			2	2.64	0.03	2.190	1.57
20 mM DEAA	60 °C	PSO-I	1	2.49	0.03	2.040	
			2	2.63	0.03	2.180	2.75
20 mM TEAA	25 °C	PSO-D	1	2.93	0.05	2.480	
			2	3.13	0.04	2.680	2.74
			3	3.18	0.05	2.730	0.66
			4	3.28	0.05	2.830	1.18
20 mM TEAA	60 °C	PSO-D	1	2.22	0.03	1.770	
			2	2.40	0.05	1.950	2.66
			3	2.49	0.03	2.040	1.33
			4	n.a.	n.a.	n.a.	n.a.
20 mM TEAA	25 °C	PSO-E	1	2.67	0.05	2.220	
			2	2.81	0.05	2.360	1.65
20 mM TEAA	60 °C	PSO-E	1	1.99	0.03	1.540	
			2	2.11	0.03	1.660	2.36
20 mM TEAA	25 °C	PSO-H	1	2.95	0.09	2.500	
			2	3.13	0.07	2.680	1.33
			3	n.a.	n.a.	n.a.	n.a.
			4	n.a.	n.a.	n.a.	n.a.
20 mM TEAA	60 °C	PSO-H	1	1.91	0.03	1.460	
			2	1.98	0.03	1.530	1.38
			3	n.a.	n.a.	n.a.	n.a.
			4	n.a.	n.a.	n.a.	n.a.
20 mM TEAA	25 °C	PSO-I	1	2.55	0.04	2.100	
			2	2.64	0.04	2.190	1.33
20 mM TEAA	60 °C	PSO-I	1	2.26	0.03	1.810	
			2	2.39	0.04	1.940	2.19

Void time: 0.45 minute, n.a.: not available due to co-elution, Temp.: column temperature in °C.

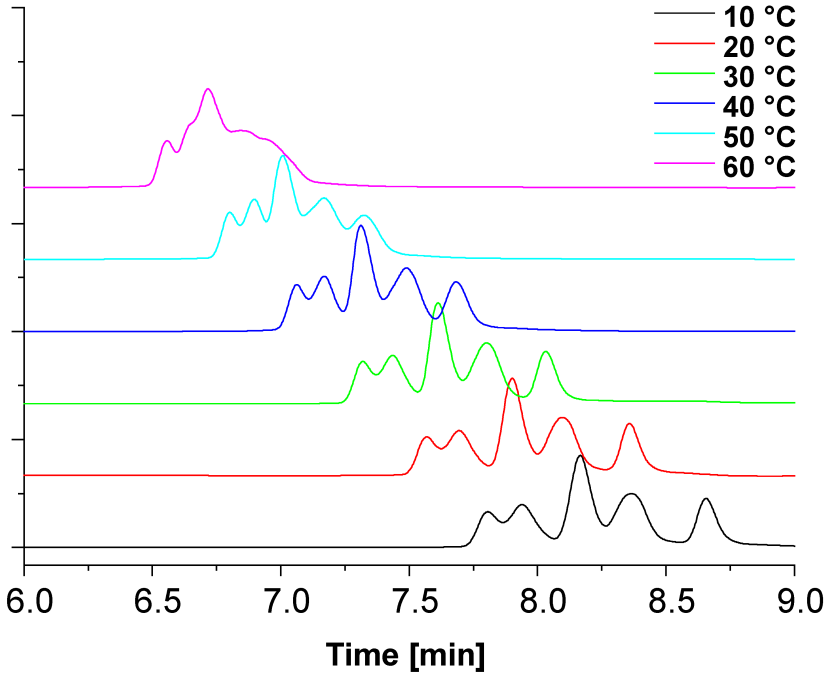

Figure S2. RP-HPLC-UV chromatograms of a temperature series for API using 100 mM AA. For more method details see **Table 3, Method A**.

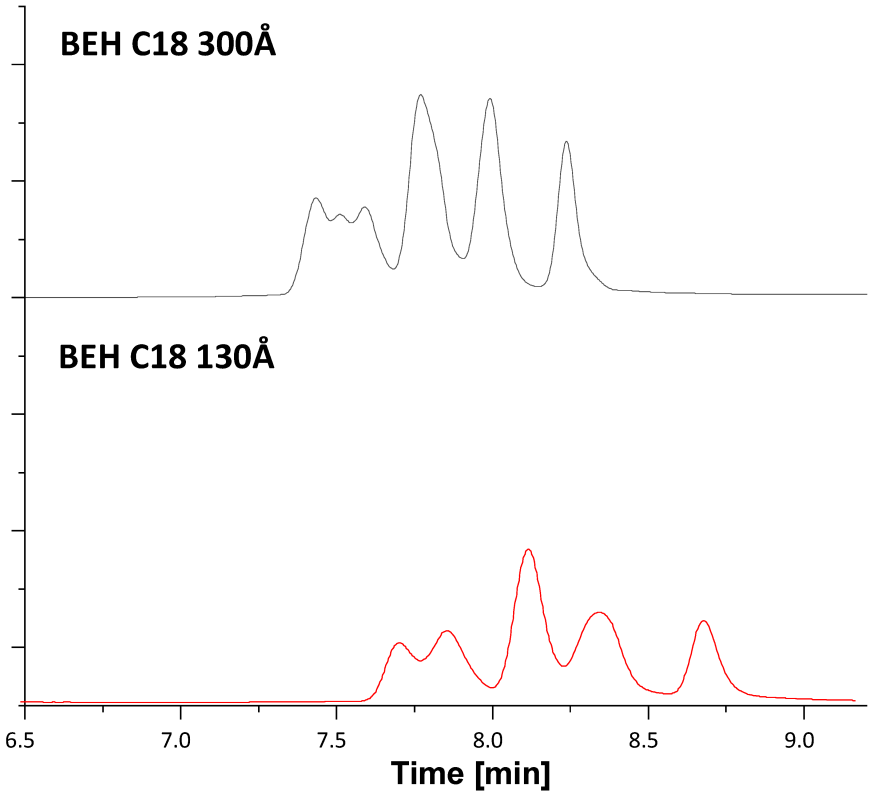

Figure S3. RPLC-UV chromatograms of API using 100 mM AA with BEH C18 columns of two different pore sizes. For more details see **Table 3, Method C**.

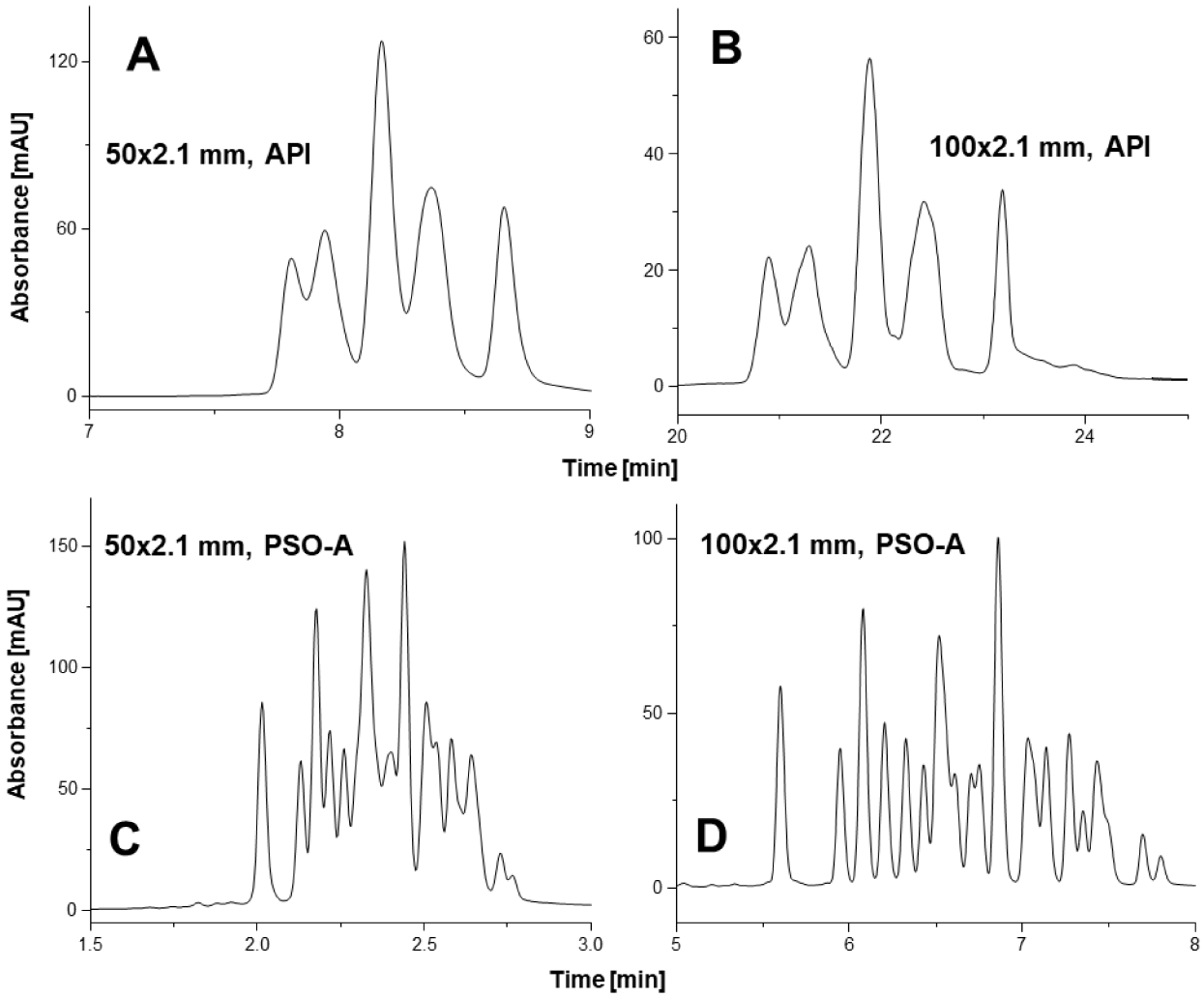

Figure S4. 1D-IP-RPLC-UV chromatograms of API and PSO-A using two different column dimensions of BEH C18. (A): API with 50x2.1 mm column, **Table 3**, **Method C**; (B): API with 100x2.1 mm column, **Table 3**, **Method B**; (C): PSO-A with 50x2.1 mm column, **Table 3**, **Method C**; (D): PSO-A with 100x2.1 mm, **Table 3**, **Method B**.

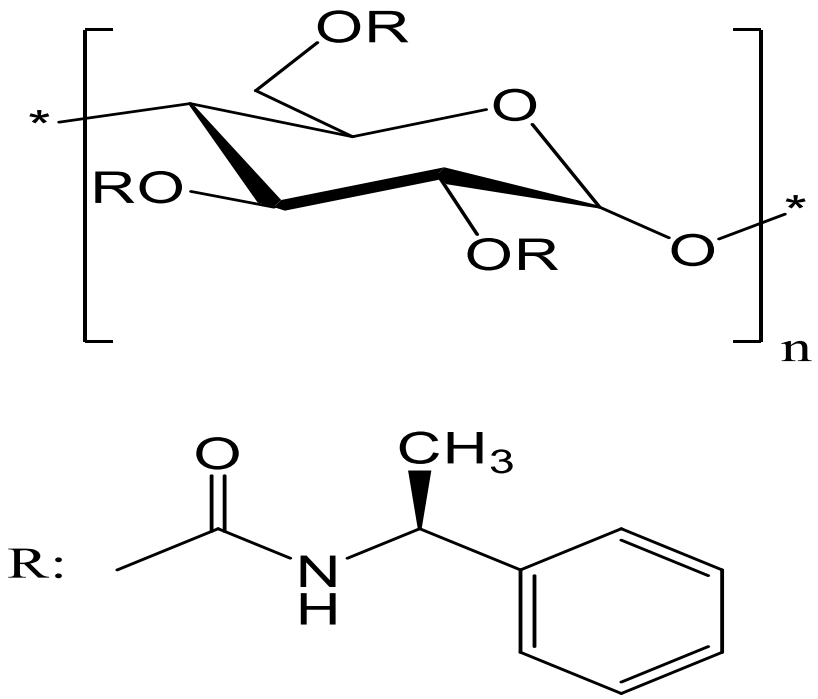

Figure S5. Chemical structure of Chiralpak IH-U. Amylose-tris[(S)-α-methylbenzylcarbamate] is immobilized on the surface of silica gel (1.6 μm).

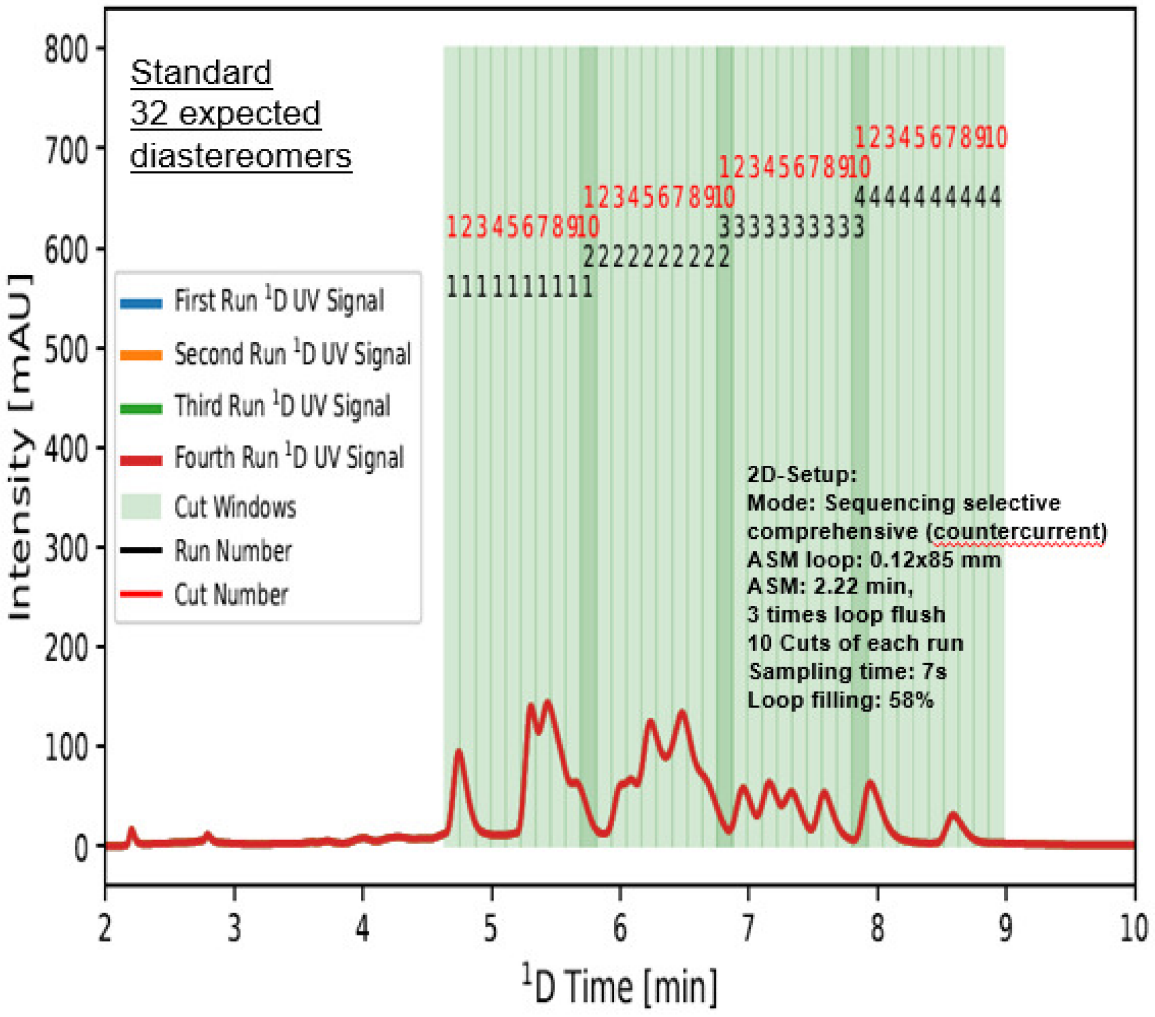

Cut #	¹D Cut start [min]	²D Run start [min]	Cut #	¹D Cut start [min]	²D Run start [min]
1	4.64	65.82	11	5.70	66.89
2	4.76	50.68	12	5.82	51.74
3	4.87	35.53	13	5.93	36.59
4	4.99	20.38	14	6.05	21.44
5	5.11	5.22	15	6.17	6.29
6	5.22	156.73	16	6.28	157.79
7	5.34	141.58	17	6.40	142.64
8	5.46	126.43	18	6.52	127.49
9	5.57	111.28	19	6.63	112.34
10	5.69	96.13	20	6.75	97.19

Cut #	¹D Cut start [min]	²D Run start [min]	Cut #	¹D Cut start [min]	²D Run start [min]
21	6.75	67.93	31	7.81	69.00
22	6.87	52.79	32	7.93	53.85
23	6.98	37.64	33	8.04	38.70
24	7.10	22.49	34	8.16	23.55
25	7.22	7.34	35	8.28	8.40
26	7.33	158.84	36	8.39	159.90
27	7.45	143.69	37	8.51	144.75
28	7.57	128.54	38	8.63	129.60
29	7.68	113.39	39	8.74	114.45
30	7.80	98.24	40	8.86	99.30

Figure S6. Sampling table and cut numbering of sequential selective comprehensive 2D-LC for PSO-A (see **Table 4, Method A**).

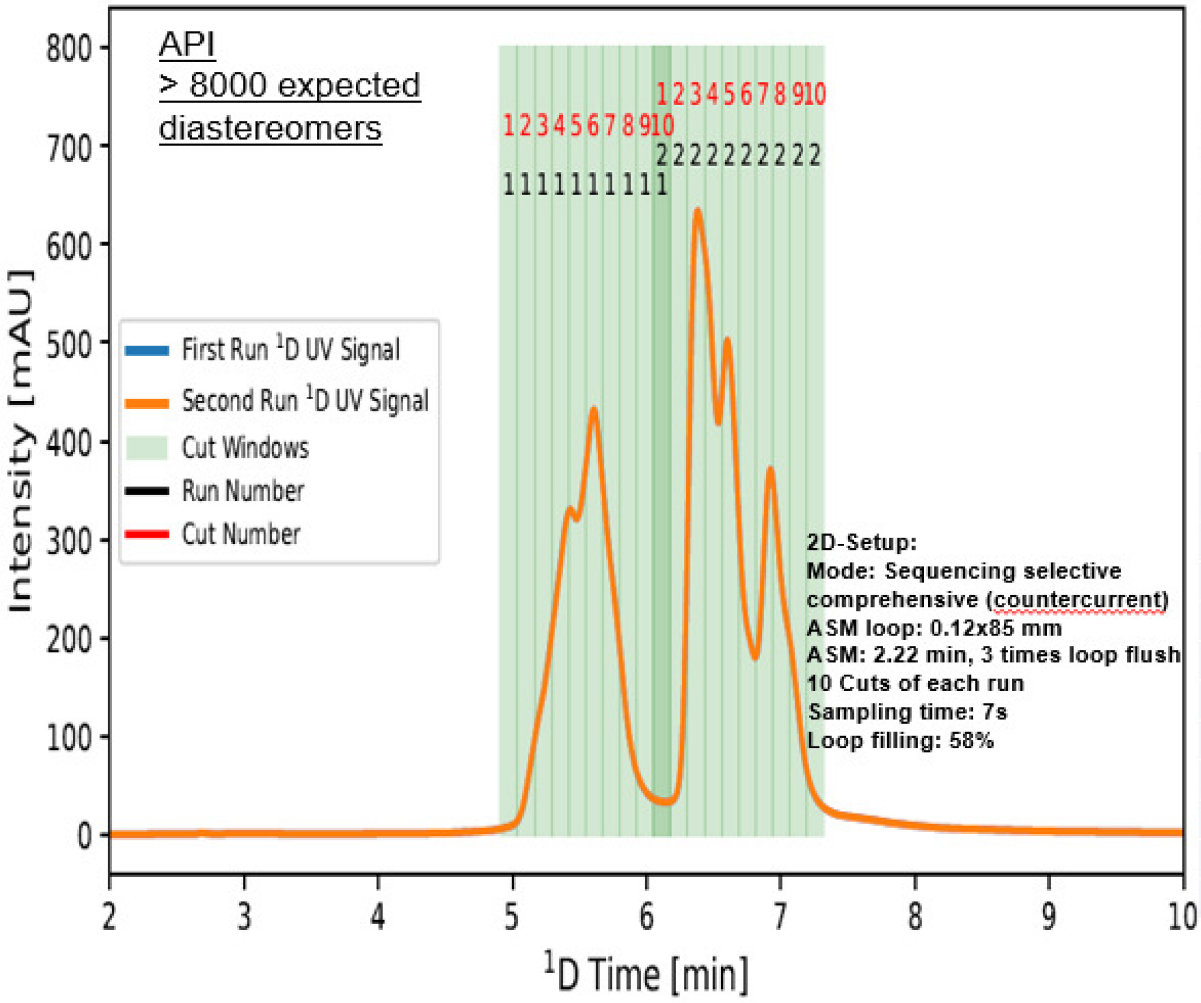

Cut #	¹D Cut start [min]	²D Run start [min]
1	4.91	66.15
2	5.04	51.00
3	5.16	35.85
4	5.29	20.70
5	5.42	5.55
6	5.54	157.05
7	5.67	141.90
8	5.80	126.75
9	5.92	111.60
10	6.05	96.45

Cut #	¹D Cut start [min]	²D Run start [min]
1	6.05	67.29
2	6.18	52.14
3	6.30	36.99
4	6.43	21.84
5	6.56	6.69
6	6.68	158.19
7	6.81	143.04
8	6.94	127.89
9	7.06	112.74
10	7.19	97.59

Figure S7. Sampling table and cut numbering of sequential selective comprehensive 2D-LC for API (see **Table 4, Method B**).

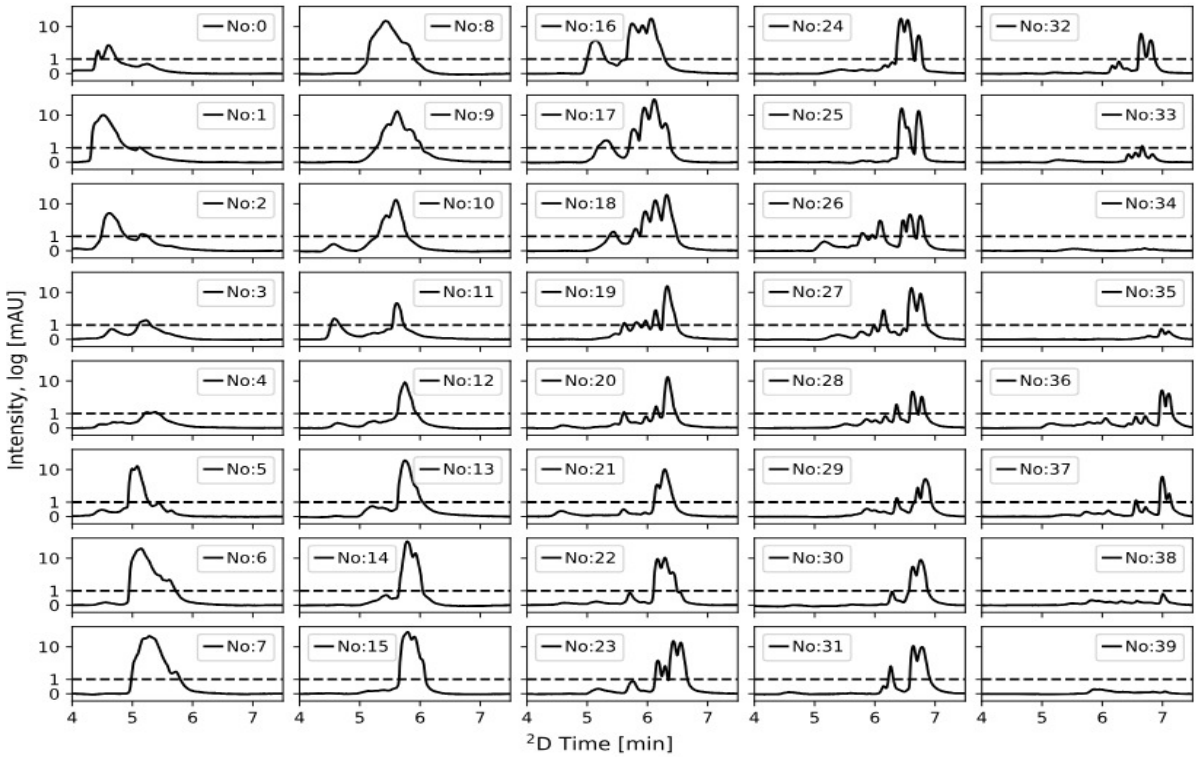

Figure S8. All 40 cuts in form of single 1D-UV chromatogram from the sequential selective comprehensive experiments for PSO-A. For more details see **Table 4**, **Method A**. Dashed line: threshold limit. Peaks below the threshold are not visible in the contour plot of Figure 5C.

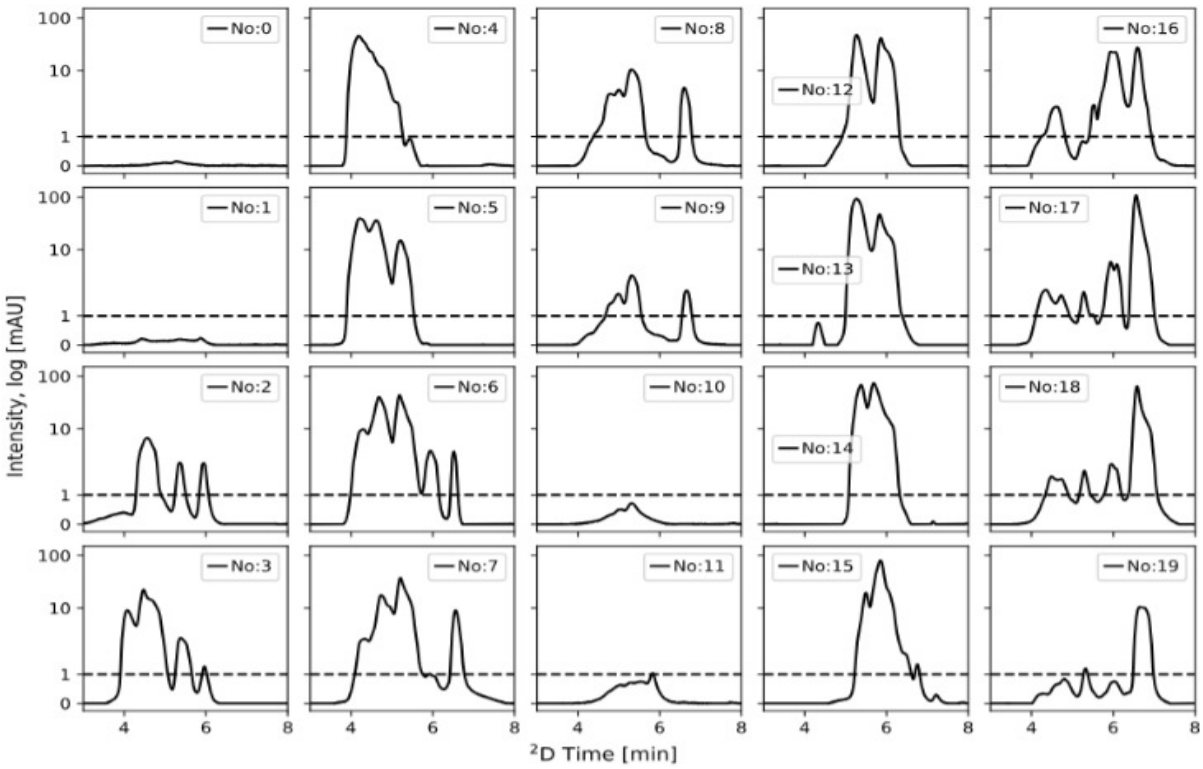

Figure S9. All 20 cuts in form of single 1D-UV chromatogram from the sequential selective comprehensive experiments for API. For more details see **Table 4**, **Method B**. Dashed line: threshold limit. Peaks below the threshold are not visible in the contour plot of Figure 6C.

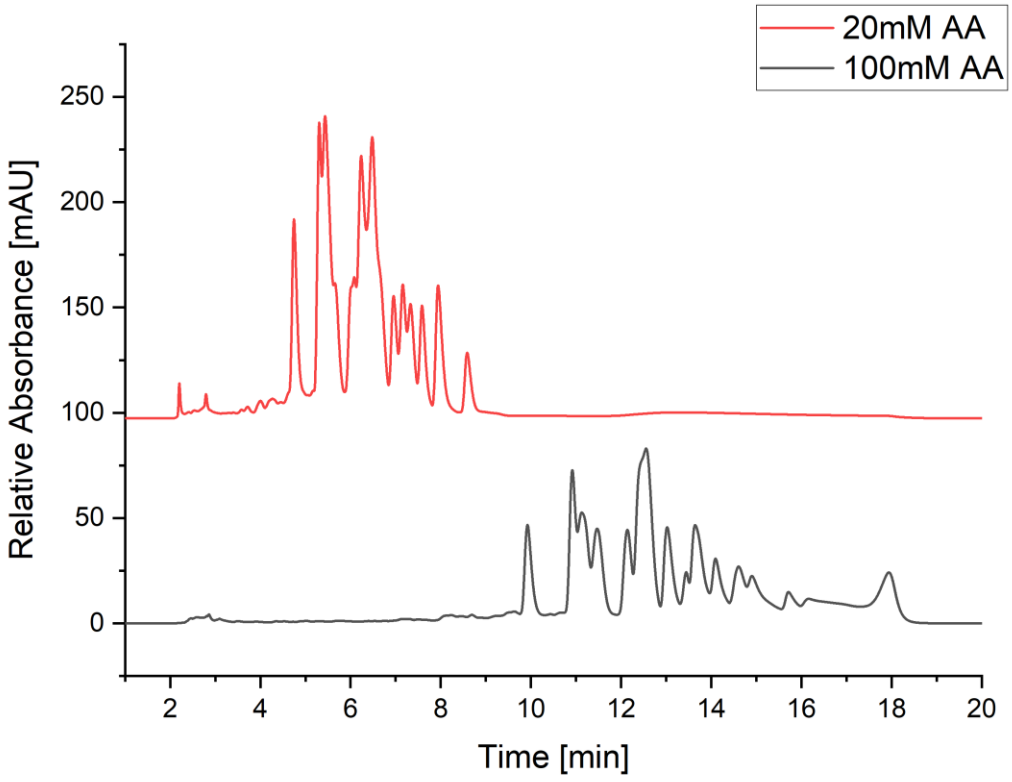

Figure S10. *Chiral Technologies IH-U (100mm x 3.0mm, 1.6µm), 0.2ml/min, 25°C, 10-*

20%B; A:10% MeOH + 20/100mM AA, B: 50% MeOH + 20/100mM AA, pH 6.7; Effect of buffer concentration on the amount of resolved peaks (PSO-A)

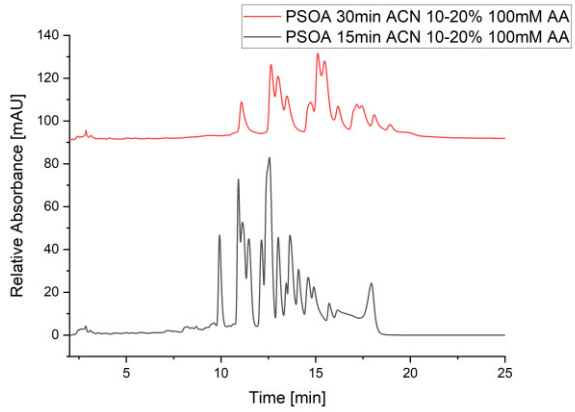

Figure S11. *Chiral Technologies IH-U (100mm x 3.0mm, 1.6µm); 0.2ml/min, 25°C, 10-20%B; A:10% ACN + 100mM AA, B: 50% ACN + 100mM AA; pH 6.7;* Comparison of 15min and 30min gradient time at 0.2ml/min

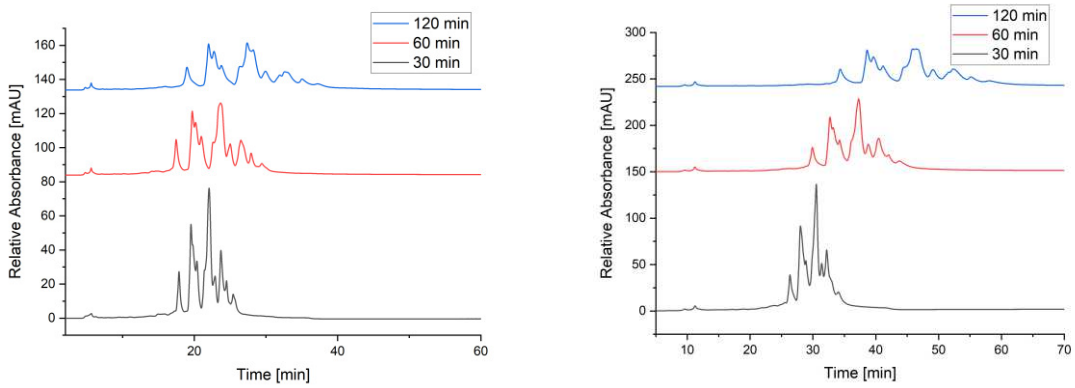

Figure S12. *Chiral Technologies IH-U (100mm x 3.0mm, 1.6µm); 0.2ml/min, 25°C; A:10% ACN + 100mM AA, B: 50% ACN + 100mM AA; pH 6.7;* Comparison of different gradient times at lower flow rates (PSO-A): (left) **0.1ml/min** 100mM AA 10-20% B pH 6.7; (right) **0.05ml/min** 100mM AA 10-20% B

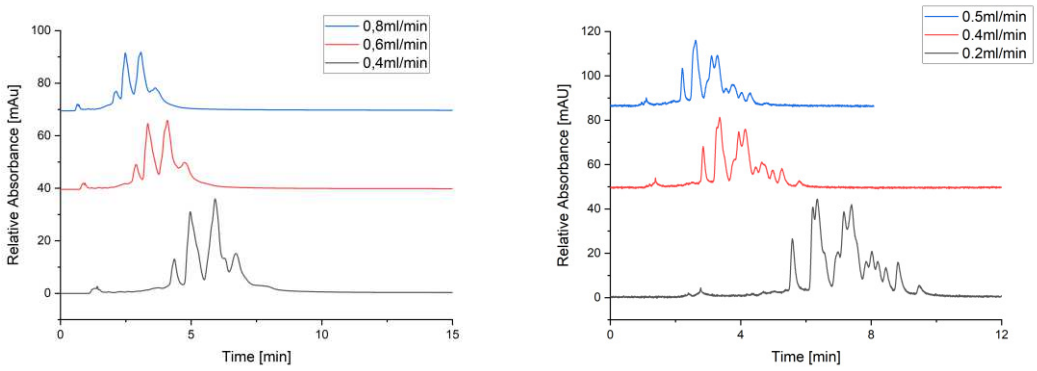

Figure S13. *Chiral Technologies IH-U (100mm x 3.0mm, 1.6µm); 25°C; 10-20%B; A:10% ACN + 100mM AA, B: 50% ACN + 100mM AA; pH 6.7;* Comparison of different flow rates (PSO-A): (left) gradient time: 15min; (right) gradient time: 25min,

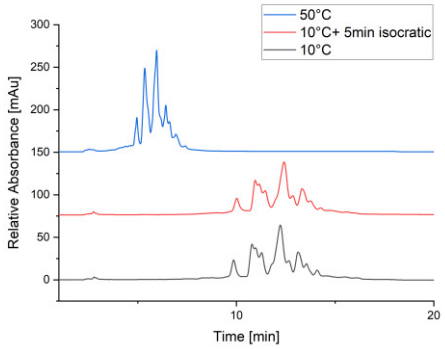

Figure S14. *Chiral Technologies IH-U (100mm x 3.0mm, 1.6µm); 10-20%B, isocratic step at 20%B; A:10% ACN + 100mM AA, B: 50% ACN + 100mM AA;* PSO-A Effects of Temperature;100mM AA,10-20% B in 15min, pH 6.7

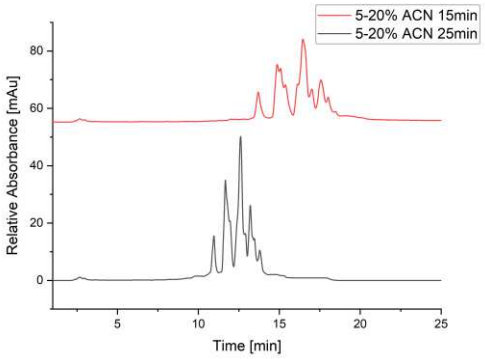

Figure S15. *Chiral Technologies IH-U (100mm x 3.0mm, 1.6µm); 25°C; 5-20%B; A:10% ACN + 100mM AA, B: 50% ACN + 100mM AA; pH 6.7;* PSO-A Effects of different gradient at different gradient times;

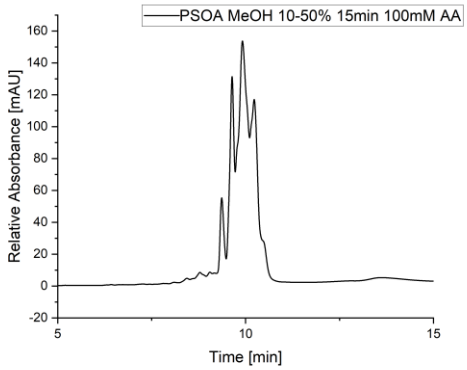

Figure S16. *Chiral Technologies IH-U (100mm x 3.0mm, 1.6µm); 25°C; 10-50%B; A:10% MeOH + 100mM AA, B:50% MeOH + 100mM AA;* Effect of MeOH as org. modifier, 10-50% B in 15min

XI. Acknowledgement

At the end of this thesis, I would like to thank a few important people.

First and foremost, of course, I would like to thank Prof. Dr. Michael Lämmerhofer, who has been my doctoral thesis supervisor for the past 4.5 years. His expertise and commitment have made a significant contribution to the success of this thesis and the stimulating discussions have not only challenged and encouraged me academically, but also personally.

Many thanks to Prof. Dr. Carolin Huhn for her support as my second supervisor during this thesis. I would also like to take this opportunity to mention that it was her excellent lectures that sparked my interest in analytical chemistry. I would also like to thank her for this.

I would also like to thank my parents and my family, who have always stood by my side and given me support and strength. Without my parents, I would not be where I am today and I am infinitely grateful to them for that. They had the courage to decide to start a new life in Germany. The years that followed were challenging, but my parents always exuded confidence and tried to give me the best possible chance. I dedicate this work to them for their love and support.

I would like to thank Dr. Katharina Fezer, who has accompanied me through this important phase of my life as my partner. 2023 was also a very important year for her in that she also successfully completed her dissertation. Despite this, she was always an important support for me and helped me to overcome the difficult moments.

Many thanks to Benjamin, Christina, Frank, Immanuel, John, Josua, Lisa, Steffen and all my fellow students. The time I spent with them was unforgettable and had a huge impact on me. These people in particular are not only good friends to me, but also important companions. I am lucky and privileged to have found these people.

Of course, a big thank you also goes to the entire Lämmerhofer working group. Thanks to Adrian B., Adrian SE., Bernie, Carlos, Christian, Corni, Ece, Eveline, Franz, Ingrid, Jeannie, Jörg, Kristian, Kristina, Maggie, Marc, Matthias, Michaela, Min, Mirna, Peng, Ryan, Simon, Siyao, Stefan, Steffi, Tamara and Xiaoqing. Without the help of this team, my work would not have been possible. Thanks to all the second authors for their

contribution to the publications. I wish the new colleagues Benedikt, Niklas and Yachao every success with their doctoral projects. Many thanks also to Enrico, Shenkai and Xiaoli for their work under my supervision. The results of their Master's theses were essential for my dissertation.

Last but not least, I would also like to thank external partners. Thanks to Prof. Dr. Sylwia Studzińska from the University of Toruń. We have achieved many good research results together and her guest stay in our working group was invaluable for me. Many thanks to Dr. Mimi Gao, Dr. Terence Hetzel, Dr. Reinhard Pell and Dr. Wiebke Holkenjans from Bayer AG. They trusted me to work with them in a scientific collaboration. That was a great experience and an important part of this work.

Certainly not all names have been explicitly mentioned in this acknowledgement, but in my mind, I remain endlessly grateful to everyone who has been involved in any way in the completion of this work.

Feiyang

Autumn, 2023, Tübingen

Deutsche Fassung:

Am Ende der vorgelegten Arbeit möchte ich noch ein paar wichtigen Mitmenschen meinen Dank aussprechen.

An erster Linie gilt mein Dank natürlich Prof. Dr. Michael Lämmerhofer, der mich als Betreuer der Promotionsarbeit in den letzten 4.5 Jahren begleitet hat. Seine Expertise und sein Engagement haben maßgeblich zum Gelingen dieser Arbeit beigetragen und die anregenden Diskussionen haben mich nicht nur wissenschaftlich, sondern auch menschlich sehr gefordert und gefördert.

Vielen Dank Prof. Dr. Carolin Huhn für ihren Einsatz als meine Zweitbetreuerin während dieser Arbeit. An dieser Stelle möchte ich auch erwähnen, dass es schließlich ihre exzellenten Lehrveranstaltungen gewesen sind, die mein Interesse für die analytische Chemie geweckt haben. Auch dafür gebührt ihr Dank.

Ich möchte mich auch an dieser Stelle bei meinen Eltern und meiner Familie bedanken, die mir immer zur Seite standen und Zuwendung sowie Kraft schenkten. Ohne meine Eltern wäre ich nicht hier, wo ich heute stehe, und dafür bin ich ihnen unendlich dankbar. Sie haben damals den großen Mut aufgebracht, sich für ein neues Leben in Deutschland zu entscheiden. Die darauffolgenden Jahre waren herausfordernd, aber meine Eltern haben immer Zuversicht ausgestrahlt und versucht, mir das Bestmögliche zu ermöglichen. Diese Arbeit widme ich ihnen für ihre Liebe und Unterstützung.

Ich bedanke mich bei Dr. Katharina Fezer, die mit mir als meine Lebensgefährtin durch diesen wichtigen Lebensabschnitt gegangen ist. 2023 war für sie auch ein sehr bedeutendes Jahr, in dem sie ihre Dissertation ebenfalls erfolgreich abgeschlossen hat. Trotz dieses Umstands war sie für mich immer eine wichtige Stütze und half mir dabei, die schweren Momente zu überwinden.

Großer Dank an Benjamin, Christina, Frank, Immanuel, John, Josua, Lisa, Steffen sowie an all meine Kommilitoninnen und Kommilitonen. Die gemeinsame Zeit mit ihnen war unvergesslich und hat mich sehr geprägt. Besonders die genannten Personen sind für mich nicht nur gute Freunde, sondern auch wichtige Weggefährten. Ich habe das Glück und das Privileg, diese Menschen gefunden zu haben.

Ein großer Dank geht selbstverständlich auch an den gesamten Arbeitskreis Lämmerhofer. Danke an Adrian B., Adrian SE., Bernie, Carlos, Christian, Corni, Ece, Eveline, Franz, Ingrid, Jeannie, Jörg, Kristian, Kristina, Maggie, Marc, Matthias, Michaela, Min, Mirna, Peng, Ryan, Simon, Siyao, Stefan, Steffi, Tamara und Xiaoqing. Ohne die Hilfe dieses Teams wäre meine Arbeit nicht möglich gewesen. Danke an alle Zweitautoren und Zweitautorinnen für ihre Mitarbeit bei den Publikationen. Den neuen Kolleginnen Benedikt, Niklas und Yachao wünsche ich viel Erfolg bei ihren Promotionsvorhaben. Ebenfalls vielen Dank an Enrico, Shenkai und Xiaoli für ihre Mitarbeit unter meiner Betreuung. Die Ergebnisse im Rahmen ihrer jeweiligen Masterarbeit waren essentiell für meine Dissertation.

Zu guter Letzt möchte ich mich auch bei externen Partnern bedanken. Danke an Prof. Dr. Sylwia Studzińska von der Universität Toruń. Wir haben gemeinsam viele gute Forschungsergebnisse erzielt und ihr Gastaufenthalt in unserem Arbeitskreis war von unschätzbarem Wert für mich. Vielen Dank an Dr. Mimi Gao, Dr. Terence Hetzel, Dr. Reinhard Pell und Dr. Wiebke Holkenjans von der Bayer AG. Sie haben mir das Vertrauen geschenkt, mit ihnen gemeinsam in einer wissenschaftlichen Kooperation zusammenarbeiten zu dürfen. Das war eine tolle Erfahrung und ein wichtiger Bestandteil dieser Arbeit.

Es wurden mit Sicherheit nicht alle Namen in dieser Danksagung explizit erwähnt, aber im Gedanken verbleibe ich mit endloser Dankbarkeit allen gegenüber, die in irgendeiner Form beim Anfertigen dieser Arbeit mit involviert waren.

Feiyang

Herbst, 2023, Tübingen